

CORRELATING LIGHT SIGNALING AND GIGANTEA WITH AUXIN IN PATTERNING THE ROOT AND SHOOT DEVELOPMENT IN PLANTS

By

ALENA PATNAIK

LIFE11201804022

**NATIONAL INSTITUTE OF SCIENCE EDUCATION AND RESEARCH
BHUBANESWAR**

A thesis submitted to the

Board of Studies in Life Sciences

In partial fulfillment of the requirements

for the Degree of

DOCTOR OF PHILOSOPHY

of

HOMI BHABHA NATIONAL INSTITUTE




MAY, 2024

Homi Bhabha National Institute¹


1. Recommendations of the Viva Voce Committee

As members of the Viva Voce Committee, we certify that we have read the dissertation prepared by **Ms. Alena Patnaik** entitled "**Correlating Light Signaling and GIGANTEA with Auxin in Patterning the Root and Shoot Development in Plants**" and recommend that it may be accepted as fulfilling the thesis requirement for the award of Degree of Doctor of Philosophy.

Chairman – Prof. Chandan Goswami



21/05/2024

Guide / Convener – Prof. Kishore Chandrasekhar Panigrahi

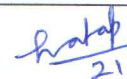

21/5/24

Co-guide - NA

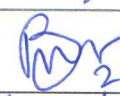
Examiner – Prof. Ananda Sarkar


21/5/2024

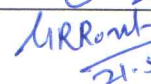
Member 1- Prof. Pratap Sahoo


21/05/2024

Member 2- Prof. Praful Singru


21/05/24

Member 3- Prof. Gyana Ranjan Rout


21.5.2024

Final approval and acceptance of this thesis is contingent upon the candidate's submission of the final copies of the thesis to HBNI.

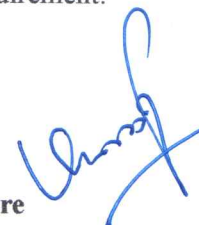
I/We hereby certify that I/we have read this thesis prepared under my/our direction and recommend that it may be accepted as fulfilling the thesis requirement.

Date: 21/5/24

Place: NISER, Jatni

Signature

Guide



¹ This page is to be included only for final submission after successful completion of viva voce.

STATEMENT BY AUTHOR

This dissertation has been submitted in partial fulfillment of requirements for an advanced degree at Homi Bhabha National Institute (HBNI) and is deposited in the library to be made available to borrowers under the rules of the HBNI.

Brief quotations from this dissertation are allowable without special permission, provided that accurate acknowledgment of the source is made. Requests for permission for extended quotation from or reproduction of this manuscript in whole or in part may be granted by the Competent Authority of HBNI when in his or her judgment the proposed use of the material is in the interests of scholarship. In all other instances, however, permission must be obtained from the author.

Alena Patnaik
NISER, Bhubaneswar

DECLARATION

I, hereby declare that the investigation presented in the thesis has been carried out by me. The work is original and has not been submitted earlier as a whole or in part for a degree/diploma at this or any other Institution / University.

Alena Patnaik
NISER, Bhubaneswar

LIST OF PUBLICATIONS ARISING FROM THE THESIS

Publications in Refereed Journal:

a) Published:

1. **Patnaik, A.**, Alavilli, H., Rath, J., Panigrahi, K., & Panigrahy, M*. (2022). Variations in Circadian Clock Organization & Function: A Journey from Ancient to Recent. *Planta*, 256(5), 1-21
2. **Patnaik, A.**, Kumar, A., Behera, A., Mishra, G., Dehery, S. K., Panigrahy, M., ... & Panigrahi, K. C*. (2023). GIGANTEA suppresses wilt disease resistance by down-regulating the jasmonate signaling in *Arabidopsis thaliana*. *Frontiers in Plant Science*, 14.

b) Communicated:

3. **Patnaik, A.**, Panigrahy, M., Behera, A., Kumar, A., Dalai, A., S, Mukundan, Priyadarshini, N., & Panigrahi, K. C*. Unraveling the multifaceted role of Auxin Binding Protein 1 (ABP1): Navigating plant development in challenging environments (Communicated and available in BioRxiv: doi.org/10.1101/2024.01.03.574050)
4. **Patnaik, A.**[#], Mishra, P.[#], Dash, A., Panigrahy, M.*[#], & Panigrahi, K. C*. Evolution of light dependent functions of GIGANTEA during terrestrialisation (Communicated and under revision) [#]Equal Contribution
5. **Patnaik, A.**, Mohanta, S., Kacchap, D., Dash, A., Das, N., Kumar S., Singh, K., Goswami, C.*[#], & Panigrahi, K. C*. Effect of temperature and Ca²⁺ on tubulin modification and organization in *Physcomitrella patens* (To be Communicated)

c) Under Preparation:

6. **Patnaik, A.**, Dash, L., Singh, K., Saha, B., Panigrahy, M., & Panigrahi, K*. C. Re-evaluating the role of GIGANTEA by CRISPR-Cas9 technology in *Arabidopsis thaliana* (MS under preparation)

OTHER PUBLICATIONS

7. Mishra, G., Yadav, N., Manasa, L., Kumar, A., **Patnaik, A.**, Panigrahy, M., Biswal, D.P., Rout, G.R. and Panigrahi, K.C., 2024. Chromium stress influences several parameters of leaf dynamics and morphology in *Oryza sativa* L. genotypes. *Plant Stress*, 12, p.100449.

CONFERENCE ATTENDED

1. 2024: 11th International Symposium on Plant Photobiology held at NISER, Bhubaneswar, India from 9th-12th January, 2024 (**Oral Presentation**)
2. **2023:** 24th International Conference on Plant Growth Substances held on 4th -8th July 2023 at HICO, Gyeongju, Republic of South Korea (**Poster Presentation**)
3. **2023:** National Science Day Celebration during March 03- 05, 2023, Theme: Global Science for Global Well-being – Lab to the Land organized by Indian Photobiology Society, Kolkata, India (**Oral presentation**)
4. **2023:** International Conference on Food and Nutritional Security 2023 held on 6-9th January 2023 organized by NABI, Mohali, Punjab, India (**Poster Presentation**)
5. **2022:** EMBO workshop “An Integrated View of Early Land Plant Evolution” held on 8-11th November 2022 organized by NISER, Bhubaneswar, India (**Poster Presentation**)
6. **2022:** 3rd National Conference Realigning Indian Agriculture for a Sustainable Future held on March 2022 at Bhubaneswar, Odisha organized by ATPBR in association with KIIT, OUAT, and ILS (**Poster Presentation**)
7. **2019:** 4th National *Arabidopsis* Meeting held between 29th -31st December 2019 at NISER, Bhubaneswar (**Poster presentation**)
8. **2018:** International Conference on Microscope and XXXIX Annual Meeting of Electron Microscope Society of India, Bhubaneswar

Alena Patnaik
NISER, Bhubaneswar

DEDICATED TO MY PARENTS

ACKNOWLEDGMENT

I would like to thank my supervisor Dr. Kishore CS Panigrahi for giving me the opportunity to work on this exciting and innovative project. As well, I would like to thank him for his guidance, patience, knowledge, advice, and support whenever the chips were down.

I would also like to thank the members of my doctoral committee: Prof. Chandan Goswami (Chairman), Dr. Kishore CS Panigrahi, Dr. Praful Singru, Dr. Pratap Kumar Sahu and Prof. Gyana Ranjan Rout (External, Odisha University of Agriculture and Technology, Bhubaneswar) for the valuable comments and suggestions. I thank Prof. Chandan Goswami and Prof. Gyana Ranjan Rout for always supporting me in all my hard times and boosting me up whenever required.

I would like to thank Dr. Madhusmita Panigrahy for her valuable advice, support, and help throughout my PhD tenure. This work would not have come to an end without the guidance and help of her. I am indebted to her. I am grateful to Prof. Dr. Anath Bandhu Das, Utkal University, Bhubaneswar for his advice from time to time which helped me a lot to complete the projects timely. I thank all our collaborators (Prof. Mitsuyasu Hasebe, Prof. A. B. Das, Prof. Klaus Palme, Prof. Mark Estelle and Prof. Jiri Friml) for providing GCaMP moss lines, *Fusarium* strain, auxin sensor constructs and *abp1* mutant lines used in this study.

This thesis work would not have been possible without the help of all my lab mates, especially Mr. Aman Kumar, Mr. Anshuman Behera, Mr. Loknath Behera, Ms. Aadishakti Dalai, Ms. Dipanjali Kachhap, Mr. Anish Dash, Mr. Soumyaranjan Barik and Mr. Soubhagya Ranjan Bastia for their timely and unconditional support in my professional and personal life. I am grateful to all lab members of CG lab especially Sushama, Nilesh, Dr. Satish Kumar and Dr. Ram Prasad Sahu for their constant help and support.

My heartfelt thanks go to my seniors and previous lab members especially Dr. Sony Kumari, Dr. Linkan Dash, Dr. Khusboo Singh, and Mr. Kishan Singh for providing the initial findings

for this project. I would like to thank Ms. Preeti Prava Sahu, Mr. Mukundan and Dr. Bedabrata Saha, whose assistance and help throughout this project were invaluable. Their help and support helped me a lot learn new techniques. Furthermore, I would like to express my gratitude to all the greenhouse staff, the SBS office and the teaching staff for helping me during the project.

I would also like to thank my dear friends Ms. Sushama Mohanta, Ms. Ananya Palo, Mr. Sakti Ranjan Rout, Ms. Sakshi Poddar, Ms. Nivedita Mitra, Mr. Saket Awadhesbhai Patel, and Mr. Aranyadip Gayen for their support throughout the project. Not only in my professional life, but Sushama, Sakti, Ananya, and Aranya were also always there behind me like a pillar in all my hard times.

I would also like to extend my sincere gratitude to my parents Mr. Anup Kumar Patnaik and Mrs. Renubala Patnaik and my younger brother Mr. Archit Patnaik for always having faith in me and driving me to achieve greater things in life. None of this would have been possible without the unconditional support of Mr. Arun Kumar Ray, who was a constant source of energy, love, and motivation even from afar.

Finally, I would like to thank myself for being able to complete this project in time. The journey to a Ph.D. was not at all easy and smooth. It included so many emotional and mental breakdowns, failures, and a lot more. Still, I was able to gather myself up and motivate myself to complete the task that I had taken up.

Alena Patnaik
NISER, Bhubaneswar

SUMMARY

All organisms on Earth possess the inherent ability to measure time through diurnal rhythms driven by the planet's 24-hour rotation. The fundamental periodicity, entrainment, temperature compensation, and oscillator mechanisms conveyed by the circadian clock which controls these rhythms are essential to its function. Although extensive research on *Arabidopsis thaliana* (*A. thaliana*) along with many crop plants has elucidated many aspects of the circadian clock, numerous variations in clock component organization and function remain to be deciphered. These variations are vital for plant sustainability and adaptation to diverse environmental conditions. Furthermore, the circadian clock's functions vary significantly during various abiotic and biotic stress conditions. In this study, we have tried to uncover the correlation between light signaling and auxin homeostasis with GIGANTEA (GI) influencing plant development. Light signal absorbed by phytochromes entrains the biological clock where a plant-specific nuclear protein, GI plays a role in integrating it. GI's involvement in circadian clock function, flowering time regulation, and various types of abiotic stress tolerance have been well-documented in recent years. However, the role of GI and its mechanism of interaction with other proteins regulating the overall growth and development of plants is yet to be understood. This study elucidates the evolutionary origin of GI from unicellular cyanobacteria to multicellular flowering plants by using an *in-silico* approach. Here, the role of GI in response to biotic stress with a hemi biotrophic pathogen i.e., *Fusarium oxysporum* (*F. oxysporum*) causing wilt disease in the plant is investigated at the molecular level comparing Col-0 WT with the *gi-100* mutant in *A. thaliana*. Disease progression, photosynthetic parameters, and comparative anatomy confirmed that the spread and damage caused by pathogen infection were less severe in *gi-100* than in Col-0 WT plants. Estimation of defense hormone after infection showed that jasmonic acid (JA) level was higher and salicylic acid (SA) level was lower in *gi-100* compared to Col-0 WT. The study shows that the relative transcript expression of *CORONATINE INSENSITIVE1 (COI1)* and *PLANT*

DEFENSIN1.2 (PDF1.2) as a marker of the JA pathway is significantly higher while *ISOCHORISMATE SYNTHASE1 (ICS1)* and *NON-EXPRESSOR OF PATHOGENESIS-RELATED GENES1 (NPR1)*, the markers of the SA pathway, are downregulated in the *gi-100* mutants compared to Col-0 plants. The present study convincingly suggests that the GI module promotes susceptibility to *F. oxysporum* infection by inducing the SA pathway and inhibiting JA signaling in *A. thaliana*. This project also investigates GI using the advanced error-free gene editing technique CRISPR-Cas9, aiming to eliminate off-target effects associated with traditional T-DNA mutants. The study evaluates GI's role in flowering and stress tolerance, revealing that CRISPR-generated *gi* mutants exhibit similar phenotypes to wild-type plants under short-day conditions. Furthermore, we have also tried to design some possible candidate antibodies which are based on the hydrophilicity of GI and can detect the endogenous level of the protein. This research extends our understanding of GI's functions and its potential role in stress tolerance. The role of Auxin Binding Protein 1 (ABP1) is re-evaluated using CRISPR-based mutants, demonstrating its involvement in root architecture, hypocotyl growth inhibition, and flowering time regulation under red light and other specific environmental conditions. ABP1's impact on phytochrome B (phyB) and GI transcript levels is also explored, shedding light on its role in stress tolerance, particularly in low-temperature conditions. Moreover, the correlation between red light signaling, auxin homeostasis, and root patterning is investigated by generating EMS mutagenized chemiluminescent ratio metric auxin sensor line and DR5::GFF line of *A. thaliana*. Finally, the functional significance of microtubule dynamics in stress adaptation is explored using the model plant *Physcomitrella patens*. This study uncovers the role of microtubule dynamics in response to auxin, temperature stress, and calcium variations, highlighting its importance in stress adaptation. These collective findings provide valuable insights into plant circadian clocks, stress responses, and the evolutionary adaptation of plants, providing valuable insights for further research and potential agricultural advancements.

CONTENTS

LIST OF FIGURES	17
LIST OF TABLES.....	22
LIST OF PRIMERS.....	23
CHAPTER 1	29
INTRODUCTION.....	29
1.1. Components of the Circadian Clock	31
1.2. GIGANTEA (GI)-A Major Component of Plant Circadian Clock	33
1.3. The Cellular Localisation of GIGANTEA	34
1.4. Flowering Time and Photoperiod-Related Molecular Functions of GIGANTEA	35
1.5. Light signalling Related Molecular Functions of GIGANTEA	38
1.6. Translational Regulation of GIGANTEA in Circadian Clock Control	39
1.7. Stress Response Related Molecular Functions of GIGANTEA	41
1.8. Phytohormones in plants	47
1.9. A Brief Overview of Auxin Synthesis, Signalling and Transport	51
1.10. Auxin signalling and involvement of clock components	53
1.11. Microtubules in response to phytohormones.....	55
1.12. Tubulin heterogeneity.....	58
1.13. Post-translational modifications of tubulin.....	58
1.14. Role of tubulin in stress conditions	59
1.15. Role of Ca ²⁺ in Microtubule Dynamics in <i>P. patens</i>	61
OBJECTIVES	63
CHAPTER 2	65
MATERIALS AND METHODS.....	65
CHAPTER 2: MATERIALS AND METHODS.....	66
2.1. <i>In-silco</i> Analysis of GIGANTEA from an Evolutionary Perspective	66
2.1.1. Protein sequence recovery	66
2.1.2. Construction of phylogenetic tree.....	69
2.1.3. Multiple sequence alignment.....	69
2.1.4. Identification of coding region for conserved amino acid.....	69
2.1.5. Identification of conserved motifs and domains.....	70
2.1.6. Prediction of Protein Secondary Structures and 3-D Modelling	70
2.2. Roles of GIGANTEA in Abiotic and Biotic Stress Tolerance	71

2.2.1. To Re-evaluate the role of GIGANTEA in drought and salinity stress using the CRISPR-Cas9 genome editing tool	71
2.2.1.1. Generation of null mutant seed line of GI using CRISPR-Cas9 genome editing tool	71
a. Preparation of DH5α super-competent cells by Inoue method	71
c. Methodology for using CRISPR-Cas9 system: gRNA spacers and primer design	72
d. Cloning procedure	73
e. Colony PCR using Taq Polymerase	74
f. Cloning of multiple guides	75
g. Final ligation in pGreen CRISPR	76
h. Agrobacterium Transformation Protocol	77
i. Floral dip methods of transformation	78
j. Selection of positive seeds by sorting under Fluorescence microscope	79
2.2.1.2. Genotyping and generation of homozygous lines	79
2.2.1.3. Plant materials and growth conditions	81
2.2.1.4. Next-generation sequencing	82
2.2.1.5. Phenotypic measurements	85
2.2.1.6. Generation of antibody	86
2.2.1.7. Protein extraction	86
2.2.1.8. Protein Quantification	87
2.2.1.9. Western Blotting	88
2.2.1.10. Soil stress assay	88
2.2.1.11. Histochemical and quantitative detection of O ₂ ⁻	89
2.2.1.12. Relative water content (RWC)	89
2.2.1.13. Lipid peroxidation assay	89
2.2.1.14. Anti-oxidative enzyme assays to determine ROS scavenging activity	90
2.2.1.15. Catalase (EC. 1. 11. 1. 6)	90
2.2.1.16. Guaiacol peroxidase (EC. 1.11.1.7)	90
2.2.1.17. Statistical analysis	91
2.2.2. To evaluate the role of GIGANTEA in biotic stress i.e., <i>Fusarium oxysporum</i> infection	91
2.2.2.1. Plant growth conditions	91
2.2.2.2. <i>F. oxysporum</i> infection and pathogenesis	92
2.2.2.3. RNA Extraction and Transcript Level Validation	93
2.2.2.3. Immuno-blotting and detection of GIGANTEA protein levels	93
2.2.2.4. Tissue fixation and histochemistry	94
2.2.2.5. Light and confocal microscopy	94

2.2.2.6. Chlorophyll fluorescence assessment.....	95
2.2.2.7. Leaf temperature analysis	96
2.2.2.8. Phytohormones estimation	97
2.2.2.9. Statistical analysis.....	98
2.3. Novel Role of Auxin Binding Protein1 (ABP1) in Plant Development and Abiotic Stress Tolerance.....	99
2.3.1. Plant growth conditions and treatments.....	99
2.3.2. Physiological and Biochemical tests	100
2.3.3. Carotenoid content.....	100
2.3.4. Relative water content (RWC).....	100
2.3.5. Leaf temperature analysis	101
2.3.6. Lipid peroxidation assay.....	101
2.3.7. Histochemical detection of superoxide radical.....	101
2.3.8. Antioxidative enzyme assays.....	102
2.3.9. RNA extraction and gene expression study	103
2.3.10. Scanning Electron Microscopy.....	103
2.3.11. Phytohormone estimation	104
2.3.12. Statistical analysis.....	104
2.4. Effect of Temperature and Calcium on Tubulin Modification and Organisation in <i>Physcomitrella patens</i>	106
2.4.1. <i>In silico</i> analysis and construction of cladograms	106
2.4.2. Plant growth conditions and treatments.....	106
2.4.3. Extraction and estimation of proteins	108
2.4.3. Western blotting.....	109
2.4.4. Ca ²⁺ imaging and quantification	109
2.4.5. Immunofluorescence, Confocal and Super resolution microscopy	110
2.4.6. Quantitative analysis.....	111
2.4.7. Statistical analysis.....	111
2.5. Correlation of Phytochrome B and Auxin in Patterning the Root Development in <i>Arabidopsis thaliana</i>	112
2.5.1. Generation and cloning of fluorescent/luciferase-based auxin sensor constructs in gateway cassette	112
2.5.2. EMS mutagenesis of auxin sensor and DR5:: GFP expressing Col-0 WT lines and bulking of seeds	115
2.5.3. Screening for hypo and hyper-sensitive mutants under saturating RG9 red light field.....	115
CHAPTER 3	117

IN-SILCO ANALYSIS OF GIGANTEA FROM AN EVOLUTIONARY PERSPECTIVE	117
CHAPTER 3: IN-SILCO ANALYSIS OF GIGANTEA FROM AN EVOLUTIONARY PERSPECTIVE	118
3.1. BACKGROUND	118
3.2. RESULTS	125
3.2.1. Retrieval of sequences	125
3.2.2. Assessment of Cladogram	128
3.2.3. Assessment of Multiple Sequence Alignment	129
3.2.4. Motif and domain identification	131
3.2.3. Prediction of Protein Model	132
3.3. DISCUSSION	135
CHAPTER-4	141
ROLES OF GIGANTEA IN ABIOTIC AND BIOTIC STRESS TOLERANCE	141
CHAPTER 4: ROLES OF GIGANTEA IN ABIOTIC AND BIOTIC STRESS TOLERANCE	142
4.1. TO RE-EVALUATE THE ROLE OF GIGANTEA IN DROUGHT AND SALINITY STRESS USING THE CRISPR-CAS9 GENOME EDITING TOOL	142
4.1.1. BACKGROUND	142
4.1.2. RESULTS	145
4.1.2.1. Genotyping for the confirmation of mutation	145
5.1.2.2. Characterization and detection of endogenous GI of expected molecular weight	148
5.1.2.3. Re-evaluating the role of GIGANTEA using CRISPR Cas9 technology	152
5.1.2.3.1 Characterizing hypocotyl and root development in CRISPR edited <i>gi</i> mutants of <i>Arabidopsis thaliana</i>	152
5.1.2.3.2. Photoperiodic Flowering of CRISPR mutant of GI in <i>Arabidopsis thaliana</i>	162
5.1.2.3.3. Effect of drought stress on CRISPR mutant of GI in <i>Arabidopsis thaliana</i>	164
5.1.2.3.4. Role of GI in salt stress	173
4.1.3. DISCUSSION	183
5.2. To evaluate the role of GIGANTEA in biotic stress i.e., <i>Fusarium oxysporum</i> infection	186
5.2.1. BACKGROUND	186
5.2.2. RESULTS	190
5.2.2.1. Severity of wilt disease due to <i>F. oxysporum</i> in Col-0 and <i>gi-100</i> plants	190
5.2.2.2. Effect of <i>F. oxysporum</i> infection on GIGANTEA transcript and protein levels	191
5.2.2.3. Effect of <i>Fusarium</i> infection on flowering time	193
5.2.2.4. Involvement of salicylic acid (SA) and jasmonic acid (JA) pathway during <i>F. oxysporum</i> infection in <i>gi-100</i> plants	194

5.2.2.5. Comparative anatomy of the effect of <i>F. oxysporum</i> infection on root cell structure in Col-0 and <i>gi-100</i> plants	198
5.2.2.6. Effect of <i>F. oxysporum</i> infection on stomatal density and integrity in Col-0 and <i>gi-100</i> plants	200
5.2.2.7. Effect of <i>F. oxysporum</i> infection on Chlorophyll A fluorescence and photosynthetic electron transport.....	201
5.2.2.8. Leaf internal temperature after <i>F. oxysporum</i> infection	202
5.2.3. DISCUSSION	204
CHAPTER-5.....	211
NOVEL ROLE OF AUXIN BINDING PROTEIN1 (ABP1) IN PLANT DEVELOPMENT AND ABIOTIC STRESS TOLERANCE.....	211
CHAPTER-5: Novel Role of Auxin Binding Protein1 (ABP1) in Plant Development and Abiotic Stress Tolerance	212
5.1. BACKGROUND.....	212
5.2. RESULTS	215
5.2.1. ABP1 affects seedling root phenotype under red and blue light	215
5.2.2. ABP1 mediates hypocotyl elongation under diurnal red rhythm along with low temperature	218
5.2.3. Synthetic auxin 1-NAA can rescue <i>abp1</i> mutant root phenotype under red light	222
5.2.4. ABP1 mutation delayed timing to flower at low temperature irrespective of photoperiod.....	224
5.2.5. Role of defense hormones in mediating low-temperature response in <i>abp1</i> mutant lines.....	226
5.2.6. Altered trichome morphology contributes to cold resistance in <i>abp1</i> mutants	228
5.2.7. ABP1 mutation positively affects dehydration tolerance	230
5.2.7.1. Physiological parametric confirmation of dehydration tolerance.....	230
5.2.7.2. Biochemical parametric confirmation of dehydration tolerance	232
5.3. DISCUSSION	235
CHAPTER 6.....	239
EFFECT OF MONOCHROMATIC LIGHT, PHYTOHORMONES, TEMPERATURE, AND Ca²⁺ ON TUBULIN MODIFICATION AND ORGANISATION IN <i>Physcomitrella patens</i>.....	239
CHAPTER 6: EFFECT OF MONOCHROMATIC LIGHT, PHYTOHORMONES, TEMPERATURE, AND Ca²⁺ ON TUBULIN MODIFICATION AND ORGANISATION IN <i>Physcomitrella patens</i>.....	240
6.1. BACKGROUND.....	240
6.2. RESULT	245
6.2.1. Post-translational modifications of tubulin are likely to occur in <i>Physcomitrella patens</i>	245

6.2.2. Validation of the presence of post-translational modifications of tubulin in <i>Physcomitrella patens</i>	252
6.2.3. Light-dependent post-translation modifications in <i>Physcomitrella patens</i>	252
6.2.4. Hormone-dependent post-translational modifications.....	271
6.2.5. Temperature and Calcium-dependent post-translational modifications.	273
6.2.6. Validation of a Sensor in <i>Physcomitrella patens</i> and Insights into Ca ²⁺ and Temperature-Dependent Post-Translational Modifications in GCamp	276
6.2.7. Gametophore development is dependent on extracellular Ca ²⁺ levels in <i>P. patens</i> at ambient and higher temperature	279
6.3. DISCUSSION	281
CHAPTER-7	289
CORRELATION OF PHYTOCHROME B AND AUXIN IN PATTERNING THE ROOT DEVELOPMENT IN	289
<i>Arabidopsis thaliana</i>	289
CHAPTER-7: Correlation of Phytochrome B and Auxin in Patterning the Root Development in <i>Arabidopsis thaliana</i>	290
7.1. BACKGROUND.....	290
7.2. RESULTS	293
7.2.1. Generation and cloning of fluorescent/luciferase-based auxin sensor constructs in gateway cassette	293
7.2.2. EMS mutagenesis of auxin sensor and DR5:: GFP expressing Col-0 WT lines and bulking of seeds.	295
7.2.3. Screening for hypo and hyper-sensitive mutants under saturating RG9 red light field.....	296
7.2.4. From the pool of defective in red light, further screening for mutants showing root patterning	298
7.3. DISCUSSION	300
CHAPTER 8	302
CONCLUSION AND FUTURE PERSPECTIVE	302
CHAPTER 8: CONCLUSION AND FUTURE PERSPECTIVE	303
CHAPTER 9	306
BIBLIOGRAPHY	306
CHAPTER 9: BIBLIOGRAPHY	307
ANNEXURE	344
ANNEXURE 1	345
ANNEXURE 2	352

LIST OF FIGURES

FIGURE NO.	DESCRIPTION	PAGE NO.
Figure 1.	Variations in the circadian clock components in different plant systems	32
Figure 2.	GI-FKF1 COMPLEX REGULATES THE PHOTOPERIODIC FLOWERING TIME	36
Figure 3.	Model of GIGANTEA (GI) dependent flowering time regulation in <i>A. thaliana</i>	37
Figure 4.	GIGANTEA interactions during the night (a) and day (b) to control flowering and circadian clock pathways	39
Figure 5.	Diagrammatic representation of the clock model showcasing autoregulatory feedback loops facilitated by transcriptional and post-translational mechanisms	40
Figure 6.	Schematic diagram depicting GI-EEL regulation of the ABA biosynthesis pathway	42
Figure 7.	Pleiotropic functions of GIGANTEA (GI) in plant growth and development	47
Figure 8.	A simplified cellular model for auxin biosynthesis, transport, and signalling	53
Figure 9.	Molecular localization of tubulin posttranslational modifications	59
Figure 10.	Microtubules serve various functions in plant morphogenesis and response to abiotic and biotic stresses	60
Figure 11.	<i>In vivo</i> analysis of Ca^{2+} dynamics in response to osmotic stress throughout <i>P. patens</i> gametophores expressing CYT-YC3.60	62
Figure 12.	Workflow for QIASeq FX DNA Library Preparation	83
Figure 13.	WGS bioinformatics workflow	85
Figure 14.	Circular cladogram of GIGANTEA protein	129
Figure 15.	Multiple sequence alignment of GIGANTEA domains	131
Figure 16.	Motif analysis of GIGANTEA protein	132
Figure 17.	Predicted models of GIGANTEA using i-TASSER web server	134
Figure 18.	Distribution of GI protein in the plant kingdom.	140
Figure 19.	Generation and screening of CRISPR mutants of GIGANTEA	145
Figure 20.	Flowchart depicting the genetic screening of <i>gi</i> mutant line generated by CRISPR-Cas9 technology.	146
Figure 21.	Genetic Screening of <i>gi-C27</i> .	147
Figure 22.	<i>In silico</i> analysis and topology of GIGANTEA epitopes	148
Figure 23.	Characterization of all the probable GI antibodies	149
Figure 24.	Specific binding of Ab04 to endogenous GI of <i>Arabidopsis thaliana</i>	150
Figure 25.	CDS sequence of GI translating the GI protein at Exon-2 (A) and Exon-7 (B)	151

Figure 26.	Comparison of <i>A. thaliana</i> hypocotyl development between wild-type Col-0 ecotype, 35S::GI, <i>gi-100</i> , <i>gi-C27</i> and <i>gi-1</i> mutants under <u>dark</u> in MS, half MS without sucrose and half MS with 1% sucrose growth media.	152
Figure 27.	Comparison of <i>A. thaliana</i> root development between wild-type Col-0 ecotype, 35S::GI, <i>gi-100</i> , <i>gi-C27</i> , and <i>gi-1</i> mutants under <u>dark</u> in MS, half MS without sucrose and half MS with 1% sucrose growth media.	153
Figure 28.	Comparison of <i>A. thaliana</i> hypocotyl development between wild-type Col-0 ecotype, 35S::GI, <i>gi-100</i> , <i>gi-C27</i> , and <i>gi-1</i> mutants under <u>white light</u> in MS, half MS without sucrose and half MS with 1% sucrose growth media.	154
Figure 29.	Comparison of <i>A. thaliana</i> root development between wild-type Col-0 ecotype, 35S::GI, <i>gi-100</i> , <i>gi-C27</i> , and <i>gi-1</i> mutants under <u>white light</u> in MS, half MS without sucrose and half MS with 1% sucrose growth media.	155
Figure 30.	Comparison of <i>A. thaliana</i> hypocotyl development between wild-type Col-0 ecotype, 35S::GI, <i>gi-100</i> , <i>gi-C27</i> and <i>gi-1</i> mutants under <u>red light</u> in MS, half MS without sucrose and half MS with 1% sucrose growth media.	156
Figure 31.	Comparison of <i>A. thaliana</i> root development between wild-type Col-0 ecotype, 35S::GI, <i>gi-100</i> , <i>gi-C27</i> , and <i>gi-1</i> mutants under <u>red light</u> in MS, half MS without sucrose and half MS with 1% sucrose growth media.	157
Figure 32.	Comparison of <i>A. thaliana</i> hypocotyl development between wild-type Col-0 ecotype, 35S::GI, <i>gi-100</i> , <i>gi-C27</i> , and <i>gi-1</i> mutants under <u>far-red light</u> in MS, half MS without sucrose and half MS with 1% sucrose growth media.	158
Figure 33.	Comparison of <i>A. thaliana</i> root development between wild-type Col-0 ecotype, 35S::GI, <i>gi-100</i> , <i>gi-C27</i> , and <i>gi-1</i> mutants under <u>far-red light</u> in MS, half MS without sucrose and half MS with 1% sucrose growth media.	159
Figure 34.	Comparison of <i>A. thaliana</i> hypocotyl development between wild-type Col-0 ecotype, 35S::GI, <i>gi-100</i> , <i>gi-C27</i> , and <i>gi-1</i> mutants under <u>blue light</u> in MS, half MS without sucrose and half MS with 1% sucrose growth media.	160
Figure 35.	Comparison of <i>A. thaliana</i> root development between wild-type Col-0 ecotype, 35S::GI, <i>gi-100</i> , <i>gi-C27</i> and <i>gi-1</i> mutants under <u>blue light</u> in MS, half MS without sucrose and half MS with 1% sucrose growth media.	161

Figure 36.	Analysis of flowering time phenotype in Col-0, <i>gi-100</i> , and <i>gi-C27</i> under long day (LD) and short day (SD) conditions at 18 °C and 22 °C	162
Figure 37.	Effect of drought stress under long-day conditions on the <i>gi</i> mutants in <i>Arabidopsis thaliana</i>	164
Figure 38.	Effect of drought stress under short-day conditions on the <i>gi</i> mutants in <i>Arabidopsis thaliana</i>	165
Figure 39.	Effect of drought stress on the endogenous temperature on leaves under short-day conditions on the <i>gi</i> mutants in <i>Arabidopsis thaliana</i>	166
Figure 40.	Histochemical detection of oxygen radical during dehydration stress	167
Figure 41.	Histochemical detection of oxygen radical during dehydration stress	169
Figure 42.	Test of physiological and biochemical parameters during dehydration stress	169
Figure 43.	Effect of salinity stress under long-day conditions on the <i>gi</i> mutants in <i>Arabidopsis thaliana</i>	172
Figure 44.	Effect of salinity stress under short-day conditions on the <i>gi</i> mutants in <i>Arabidopsis thaliana</i> .	174
Figure 45.	Effect of salinity stress on the endogenous temperature on leaves under short-day conditions on the <i>gi</i> mutants in <i>Arabidopsis thaliana</i> .	175
Figure 46.	Histochemical detection of oxygen radical during salinity stress	176
Figure 47.	Histochemical detection of oxygen radical during salinity stress	177
Figure 48.	Test of physiological and biochemical parameters during salinity stress	178
Figure 49.	Effect of <i>F. oxysporum</i> infection on GIGANTEA (GI) in <i>Arabidopsis thaliana</i>	181
Figure 50.	Transcript and protein levels of GIGANTEA after <i>F. oxysporum</i> infection	191
Figure 51.	Analysis of flowering time phenotype in the <i>F. oxysporum</i> infected Col-0 plants	192
Figure 52.	Involvement of salicylic acid pathway during <i>F. oxysporum</i> infection in <i>gi-100</i> plants infection	194
Figure 53.	Involvement of jasmonic acid pathway during <i>F. oxysporum</i> infection in <i>gi-100</i> plants	196
Figure 54.	Determination of Absciscic acid and Oxylipins after <i>F. oxysporum</i> in Col 0 and <i>gi-100</i> plants	197
Figure 55.	Effect of <i>F. oxysporum</i> infection on root cell morphology	198
Figure 56.	Effect of <i>F. oxysporum</i> infection on root cells in <i>Arabidopsis thaliana</i> using propidium iodide	199
Figure 57.	Effect of <i>F. oxysporum</i> infection on stomatal density and integrity in Col-0 and <i>gi-100</i> plants	200
Figure 58.	Effect of <i>F. oxysporum</i> infection on stomatal number and integrity in Col-0 and <i>gi-100</i> plants	201
Figure 59.	Effect of <i>F. oxysporum</i> on Chl a fluorescence	201
Figure 60.	Leaf internal temperature analysis in Col-0 and <i>gi-100</i>	202

Figure 61.	Diagrammatic representation of involvement of GIGENTEA, jasmonic acid, and salicylic acid pathway genes for eliciting pathogen response to <i>F. oxysporum</i> infection in <i>Arabidopsis thaliana</i>	203
Figure 62.	Seedling growth parameters were non-significant under different monochromatic lights at 22 °C	209
Figure 62.	Seedlings under diurnal monochromatic red light at 22 °C	216
Figure 64.	Seedling phenotype at low temperature i.e., 18 °C	218
Figure 65.	Hypocotyl growth inhibition under monochromatic red light and lower temperature (18 °C).	220
Figure 66.	Complementation of root growth phenotype with external application of synthetic auxin	222
Figure 67.	Flowering phenotype under LD and SD conditions at 22 °C	223
Figure 68.	Flowering phenotype at low temperature (18 °C).	224
Figure 69.	Estimation of endogenous contents of defense hormones (abscisic acid, salicylic acid, and jasmonic acid)	226
Figure 70.	Molecular analysis of trichome morphology	227
Figure 71.	Analysis of dehydration stress tolerance	229
Figure 72.	Plant leaf Temperature analysis	231
Figure 73.	Test of biochemical parameters during dehydration stress	232
Figure 74.	<i>In-silico</i> analysis of enzymes involved in PTMs of tubulin in <i>P. patens</i>	234
Figure 75.	Presence of post-translationally modified tubulins in <i>P. patens</i> at the cellular level.	251
Figure 76.	Effect of different lights on the post-translationally modified tubulins in <i>P. patens</i>	252
Figure 77.	Effect of phytohormones on immunodetection of tubulin modifications in <i>Physcomitrella patens</i>	253
Figure 78.	Effect of phytohormones on Ca ²⁺ in <i>Physcomitrella patens</i>	272
Figure 79.	Effect of temperature on immunodetection of tubulin modifications in <i>Physcomitrella patens</i> .	273
Figure 80.	Validation of a Ca ²⁺ Sensor and effect of varying exogenous Ca ²⁺ and temperatures on Post-Translational Modifications in <i>Physcomitrella patens</i> .	276
Figure 81.	Effect of varying Ca ²⁺ concentration and temperature on protonema to gametophyte transition	278
Figure 82.	Correlation plot between Endogenous Ca ²⁺ levels and tubulin modifications at varying extracellular Ca ²⁺ concentrations in <i>P. patens</i>	280
Figure 83.	Correlation plot between Endogenous Ca ²⁺ levels and tubulin modifications at varying temperatures in <i>P. patens</i> .	285
Figure 84.	Correlation plot between tubulin modifications at varying temperature treatments in <i>P. patens</i> .	286
Figure 85.	Correlation plot between tubulin modifications at varying extracellular Ca ²⁺ treatments in <i>P. patens</i>	287

Figure 86.	PCR screening after (a) BP and (b) LR reaction for positive cloning with luciferase auxin sensor	288
Figure 87.	Colony PCR for positive transformed <i>Agrobacterium</i> with luciferase auxin sensor	293
Figure 88.	PCR for transgenic Col-0 plants with luciferase auxin sensor	293
Figure 89.	PCR analysis of transformed seeds (F3 generation). Lanes 1 to 10 indicate transformed lines of different pools.	294
Figure 90.	DR5::GFP expression in the root tip of transgenic DR5::GFP plants	294
Figure 91.	EMS mutagenesis and bulking of Col-0 Luc and DR5::GFP lines in different pools	295
Figure 92.	Screening of mutants based on their hypocotyl lengths	296
Figure 93.	Summary of EMS mutagenized Col-0 Luc and DR5::GFP mutants generated and screened based on hypo and hypersensitive hypocotyl lengths	297
Figure 94.	The pGreen CRISPR plasmid was digested with EcoRI and KpnI, then electrophoresed in a 1% gel.	298
Figure 95.	Cloning of gRNA into the pBSK vector	345
Figure 96.	Cloning of multiple guides	347
Figure 97.	Ligation of the dual-guide cassette in pGreen CRISPR plasmid	348
Figure 98.	<i>Agrobacterium</i> transformation.	350
Figure 99.	The genomic locus of GI where the genomic targets in exon 2 and exon 7 have been shown	351
Figure 100.	Presence of post-translationally modified tubulins in <i>P. patens</i> .	353

LIST OF TABLES

TABLE NO.	DESCRIPTION	PAGE NO.
Table 1.	Accession numbers of GIGANTEA were obtained from different species. The datasets are derived from different sources like NCBI and the OneKP database.	66
Table 2.	Components used in the master mix preparation for colony PCR	74
Table 3.	Thermocycling conditions in the PCR machine for colony PCR.	74
Table 4.	Estimated DNA Concentration and Purity	83
Table 5.	Description of libraries	84
Table 6.	The definition of energy fluxes and fluorescence transients' parameters were used in OJIP test.	96
Table 7.	Accession numbers of GIGANTEA were obtained from different species	125
Table 8.	Details of positions of conserved amino acid in the exon lengths of GIGANTEA	131
Table 9.	Phytozome IDs of organisms used in the phylogenetic tree construction of ELP3, TTLL6, TTLL9, TTLL12, and ATAT.	249
Table 10.	List of proteins identified in PHYTOZOME and sorted in alphabetical order by protein name.	251
Table 11.	Responsive elements detected in tubulin modifying enzymes using PLANTCARE web server.	271
Table 12.	Hypocotyl lengths (average) of 7 d old seedlings of Col-0, Col-0 Luc, and DR5::GFP lines grown under dark, white, red, far-red, and blue light at 22 °C	295
Table 13.	Primary root and hypocotyl length measurements of EMS mutagenized DR5::GFP and Col-0 Luc seed lines.	299
Table 14.	Top six guide sequences that were predicted by CHOP-CHOP for the genomic locus of GI	346

LIST OF PRIMERS

SERIAL NO.	GENE NAME	PRIMER SEQUENCE
1	<i>GI</i> FORWARD	GCTTCTCGAGGATCTGGT
2	<i>GI</i> REVERSE	GTCAGCGTAGCAGTCTCA
3	<i>FT</i> FORWARD	CGAGTAACGAACGGTGA
4	<i>FT</i> REVERSE	CGCATCACACACTATATAAGTAAAACA
5	<i>ICSI</i> FORWARD	TAACGAGAACGGAAACGGAAA
6	<i>ICSI</i> REVERSE	GGATCAAGGTCACGGAAGAAA
7	<i>NPRI</i> FORWARD	CACTGCTGAGAAACGACTACA
8	<i>NPRI</i> REVERSE	CTGTCAGGGACGAATTCCTAA
9	<i>PRI</i> FORWARD	GGTTAGCGAGAAGGCTAACTAC
10	<i>PRI</i> REVERSE	CATCCGAGTCTCACTGACTTTC
11	<i>TGA2</i> FORWARD	CAGGGCGTCTTCATTTTCAGG
12	<i>TGA2</i> REVERSE	GACCTCAGCTCGTTCATTTGC
13	<i>PAD4</i> FORWARD	CCGCACTTTGGCTTCTATCT
14	<i>PAD4</i> REVERSE	GAGGTGGAGAGAGATTGGTTTC
15	<i>COII</i> FORWARD	GAAGCTAGACAAGTGTTCTGG
16	<i>COII</i> REVERSE	GCCACTTACCATCCTTTTCAC
17	<i>PDF1.2</i> FORWARD	GCTTCCATCATCACCCTTATCT
18	<i>PDF1.2</i> REVERSE	CATGTCCCACTTGGCTTCT
19	<i>ACT8</i> FORWARD	GGAATGGTTAAGGCTGGATTC
20	<i>ACT8</i> REVERSE	GTCGACCAACAACACTGGGG
21	<i>PHY B</i> FORWARD	TCCTGGCTGAGTTTCTGCTG
22	<i>PHYB</i> REVERSE	ACGCCATTCTGAATTCTGTGC
23	<i>YUCCA 2</i> FORWARD	GGAACCTTACATAAATGCATCCACTA
24	<i>YUCCA 2</i> REVERSE	CGATTTGGCAAGTTTGGATTG
25	<i>GI</i> (CRISPR) FORWARD	GATTCCGCCACGAGATCCTCAACA
26	<i>GI</i> (CRISPR) REVERSE	AAACTCTAAGGATGTCGTTGGCGG
27	<i>CPC</i> FORWARD	TGAGTAGTATCGAATGGGAAGC
28	<i>CPC</i> REVERSE	GCCGTGTTTCATAAGCCAATAT
29	<i>TRY</i> FORWARD	CGGTGATAGGTGGGATTTGATA
30	<i>TRY</i> REVERSE	TGGTATGTTTGTGGGAAGATGA

ABBREVIATIONS

GI	GIGANTEA
JA	JASMONIC ACID
SA	SALICYLIC ACID
COI1	CORONATINE INSENSITIVE1
PDF1.2	PLANT DEFENSIN1.2
ICS1	ISOCHORISMATE SYNTHASE1
NPR1	NON-EXPRESSOR OF PATHOGENESIS-RELATED GENES1
h	HOUR
At	<i>ARABIDOPSIS THALIANA</i>
TF	TRANSCRIPTION FACTORS
CCA1	CIRCADIAN CLOCK ASSOCIATED1
LHY	LATE ELONGATED HYPOCOTYL
TOC1	TIMING OF CAB EXPRESSION1
PRR5, PRR7, PRR9	PSEUDORESPONSE REGULATORS
LUX	LUX ARRHYTHMO
EFL3/ ELF4	EARLY FLOWERING3
RVE4, RVE6, RVE8	REVELLE
LNK1, LNK2	NIGHT LIGHT-INDUCIBLE AND CLOCK-REGULATED
ZTL	ZEITLUPE
SDs	SHORT DAYS
LDs	LONG DAYS
ZTL	ZEITLUPE
COP1	CONSTITUTIVE PHOTOMORPHOGENIC 1
<i>CO</i>	CONSTANS
<i>FT</i>	FLOWERING LOCUS T
CDFs	CYCLING DOF FACTORS
FKF1	FLAVIN-BINDING KELCH REPEAT F-BOX 1
CDF1	CYCLING DOF FACTOR 1
LOV	LIGHT, OXYGEN, OR VOLTAGE
LKP2	LOV KELCH PROTEIN 2
<i>SPY</i>	SPINDLY
<i>SVP</i>	SHORT VEGETATIVE PHASE
<i>TEM1</i>	TEMPRANILLO 1
<i>TEM2</i>	TEMPRANILLO 2
UVR-8	UVB-RESISTANCE 8
PHOTs	PHOTOTROPINS
CRYs	CRYPTOCHROMES
PHYs	PHYTOCHROMES
VLFR	VERY LOW FLUENCE RESPONSE
HY5	ELONGATED HYPOCOTYL
DDB1	DAMAGED DNA BINDING PROTEIN 1
WRKY44	WRKY DNA BINDING PROTEIN 44

ABA	ABSCISIC ACID
NCED3	9-CIS-EPOXYCAROTENOID DIOXYGENASE 3
EEL	ENHANCED EM LEVEL
SOS	SALT OVERLY SENSITIVE
CK2	CASEIN KINASE 2
CBF	C-REPEAT BINDING FACTORS
DREB1	DEHYDRATION-RESPONSIVE ELEMENT BINDING FACTOR 1
COR	COLD-REGULATED
GCN1	GENERAL CONTROL NONREPRESSIBLE
HSFs	HEAT SHOCK TRANSCRIPTION FACTORS
CK	CYTOKININ
ET	ETHYLENE
GA	GIBBERELIC ACID
SL	STRIGOLACTONE
BR	BRASSINOSTEROID
IAA	INDOLE-3-ACETIC ACID
PIN	PIN-FORMED
RAG1	RECOMBINATION-ACTIVATING GENE 1
SAUR36	SMALL AUXIN UPREGULATED RNA 36
JAZ	JASMONATE ZIM DOMAIN
JA-Ile	JASMONOYL-L-ISOLEUCINE
BZR1	BRASSINAZOLE-RESISTANT 1
TAA/YUC	TRYPTOPHAN AMINOTRANSFER-ASE OF <i>ARABIDOPSIS</i> /YUCCA
IPyA	INDOLE-3-PYRUVATE
Trp	TRYPTOPHAN
GH3	GRETCHEN HAGEN 3
ARF	AUXIN RESPONSE FACTOR
PAT	POLAR AUXIN TRANSPORT
ABCB/MDR/PGP	ATP BINDING CASSETTE B/MULTIDRUG-RESISTANCE/P-GLYCOPROTEIN
RVE1	REVEILLE 1
YUC8	YUCCA8
TIC	TIME FOR COFFEE
PKL	PICKLE
H3K27me3	TRIMETHYLATION OF H3 LYSINE 27
IAA19	INDOLE-3-ACETIC ACID INDUCIBLE 19
EMS	ETHYL METHANESULPHONATE
son1	OVERSENSITIVE TO NICOTINAMIDE
MTs	MICROTUBULES
MFs	MICROFILAMENTS
PTMs	POST-TRANSLATIONAL MODIFICATIONS
Ca ²⁺	CALCIUM ION
ABP1	AUXIN BINDING PROTEIN 1

NCBI	NATIONAL CENTRE FOR BIOTECHNOLOGY INFORMATION
MAFFT	MULTIPLE ALIGNMENT USING THE FAST FOURIER TRANSFORM
CDS	CODING DNA SEQUENCE
GSDS	GENE STRUCTURE DISPLAY SERVER
CDD	CONSERVED DOMAIN DATABASE
h	HOURS
OD	OPTICAL DENSITY
Min	MINUTES
DMSO	DIMETHYL SULFOXIDE
LB	LYSOGENY BROTH
MgCl ₂	MAGNESIUM CHLORIDE
CaCl ₂	CALCIUM CHLORIDE
AGI	<i>ARABIDOPSIS</i> GENOME INITIATIVE
gRNA	GUIDE RNA
G	GUANINE
NaCl	SODIUM CHLORIDE
PCR	POLYMERASE CHAIN REACTION
TAE	TRIS ACETATE EDTA
EtBr	ETHIDIUM BROMIDE
°C	DEGREE CELCIUS
mL	MILI LITRE
EDTA	ETHYLENEDIAMINETETRAACETIC ACID
μL	MICRO LITRE
μg	MICRO GRAM
d	DAYS
MS media	MURASHIG AND SKOOG MEDIA
WL	WHITE LIGHT
R	RED
FR	FAR-RED
B	BLUE
D	DARK
SDS	SODIUM DODECYL SULFATE
NaF	SODIUM FLUORIDE
PIC	PROTEASE INHIBITOR COCKTAIL
PAGE	POLYACRYLAMIDE GEL ELECTROPHORESIS
rpm	REVOLUTIONS PER MINUTE
BSA	BOVINE SERUM ALBUMIN
V	VOLTAGE
PVDF	POLYVINYLIDENE DIFLUORIDE
HRP	HORSE REDOX PEROXIDASE
RWC	RELATIVE WATER CONTENT
MDA	MALONDIALDEHYDE
CAT	CATALASE
POX	GUAIACOL PEROXIDASE

H ₂ O ₂	HYDROGEN PEROXIDE
mM	MILI MOLAR
nM	NANO MOLAR
M	MOLAR
pH	PONDUS HYDROGENII (QUANTITY OF HYDROGEN)
NBT	NITRO-BLUE TETRAZOLIUM
NaN ₃	SODIUM AZIDE
FW	FRESH WEIGHT
TW	TURGID WEIGHT
DW	DRY WEIGHT
TBA	THIOBARBITURIC ACID
TCA	TRICHLOROACETIC ACID
PVP	POLYVINYLPIRROLIDONE
SEM	STANDARD ERROR OF THE MEAN
PDB	POTATO DEXTROSE BROTH
HPI	HOURS POST-INFECTION
DPI	DAYS POST-INFECTION
qRT-PCR	QUANTITATIVE RT-PCR
mg	MILLIGRAM
FAA	FORMALIN-ACETIC-ALCOHOL
O ₂ –	SUPEROXIDE
(w/v)	WEIGHT/ VOLUME
KOH	POTASSIUM HYDROXIDE
HCl	HYDROCHLORIC ACID
DAPI	4', 6-DIAMIDINO-2-PHENYLINDOLE
μmol	MICRO MOLE
nm	NANOMETERS
Sec/ s	SECOND
ng	NANO GRAM
KH ₂ PO ₄	MONOPOTASSIUM PHOSPHATE
KCl	POTASSIUM CHLORIDE
MgSO ₄ ·7H ₂ O	MAGNESIUM SULFATE HEPTAHYDRATE
Ca (NO ₃) ₂ ·4H ₂ O	CALCIUM NITRATE TETRAHYDRATE
FeSO ₄ ·7H ₂ O,	IRON(II) SULFATE HEPTAHYDRATE
H ₃ BO ₃	BORIC ACID
MnCl ₂ ·4H ₂ O	MANGANESE(II) CHLORIDE TETRAHYDRATE
Al ₂ (SO ₄) ₃ ·K ₂ SO ₄ ·24H ₂ O	POTASSIUM ALUMINIUM SULFATE OR POTASH ALUM
CoCl ₂ ·6H ₂ O	COBALT(II) CHLORIDE HEXAHYDRATE
CuSO ₄ ·5H ₂ O	COPPER(II) SULFATE PENTAHYDRATE
ZnSO ₄ ·7H ₂ O	ZINC SULFATE HEPTAHYDRATE
KBr	POTASSIUM BROMIDE
KI	POTASSIUM IODIDE
LiCl	LITHIUM CHLORIDE
SnCl ₂ ·2H ₂ O	STANNOUS CHLORIDE DIHYDRATE
Na ₂ MoO ₄ ·2H ₂ O	SODIUM MOLYBDATE DIHYDRATE
NiCl ₂ ·6H ₂ O	NICKEL(II) CHLORIDE HEXAHYDRATE.

$\mu\text{mol}\cdot\text{m}^{-2}\cdot\text{s}^{-1}$	MICROMOLE: PER SECOND AND SQUARE METER
PEB	PROTEIN EXTRACTION BUFFER
β -ME	B-MERCAPTOETHANOL
MeOH	METHANOL
NaOH	SODIUM HYDROXIDE
μM	MICRO MOLAR
MTSB	MICROTUBULE STABILIZING BUFFER
Na_2HPO_4	DISODIUM PHOSPHATE
KH_2PO_4	MONOPOTASSIUM PHOSPHATE
kb	KILOBASE
%	PERCENTAGE
GFEL	GENE EXPRESSION FEEDBACK LOOP
~	APPROXIMATELY/NEARLY
kbp	KILO BASE PAIR
DSB	DOUBLE-STRANDED BREAK
NHEJ	NON-HOMOLOGOUS END JOIN REPAIR
HDR	HOMOLOGY DIRECTED REPAIR
Ab	ANTIBODY
kDa	KILO DALTON
T	THYMINE
C	CYTOSINE
WW	WATER WITHHELD
<i>gi</i>	<i>Gigantea</i>
HIR	HIGH-IRRADIANCE RESPONSES
ELP3	ELONGATOR PROTEIN 3
CaCl_2	CALCIUM CHLORIDE
H3a	ANTI-HISTONE ANTIBODY
ATAT	ALPHA-TUBULIN ACETYLTRANSFERASE1
TTLL	TUBULIN TYROSINE LIGASE-LIKE
TTL	TUBULIN TYROSINE LIGASE
SEM	SCANNING ELECTRON MICROSCOPY
TRY	TRIPTYCHON
CPC	CAPRICE

CHAPTER 1

INTRODUCTION

CHAPTER 1: INTRODUCTION

The circadian clock operates in all domains of life, including archaea, bacteria, and eukaryotes (Wulund *et al.*, 2015). Circadian oscillations are fundamentally due to diurnal rhythms, which arise due to environmental fluctuations of day and night in a 24-hour (h) cycle. Time cues to these oscillations originate from light and temperature variations during the day and night. The three basic parameters of circadian rhythms are defined by entrainment, periodicity, and temperature compensation. However, in the absence of time cues, a free-running period of 24 hour is observed (McClung, 2006). Mechanisms and operations of the circadian clock, its components, and their interactions with components of several pathways downstream could be known with the advent of the updated knowledge as a result of several studies. Moreover, changes occurring in the above-mentioned operations in changed environmental conditions, as well as tissue-specific variations (McClung, 2001) have become much clearer due to recent scientific methods, and genomic technologies. Therefore, a revised definition of the circadian clock could be: it is the endogenous internal clock that anticipates and prepares the organism for seasonal and diurnal environmental changes, boosting plant fitness in changing environments. A plant's circadian clock assists in plant fitness and modulates/regulates the abiotic stress-responsive pathways to strengthen stress tolerance without any trade-off in plant growth and development (Sharma *et al.*, 2021; Wei *et al.*, 2021). Hence, addressing the reprogramming of clock regulations during various abiotic stresses (i.e., high/low light, high/low temperature, flooding/desiccation stress, salinity, and nutrient deficiency) along with natural variations existing in different plant systems (including marine, lower plants, dicots, monocots, and non-flowering plants) as well as recent advances on regulations due to non-coding and microRNA can clarify several aspects of the complexity of circadian clock organizations and functions in the current context.

1.1. Components of the Circadian Clock

The concept and discovery of the molecular mechanism of the circadian clock dates back to the 1990s when the *PER*, *TIM*, *dCLK*, and *CYC* clock proteins were reported in *Drosophila* (Lee *et al.*, 1998; Hardin *et al.*, 1990). This discovery becomes the basis for autoregulatory negative feedback loops for functioning in an oscillatory time cycle or circadian clock (Blau and Young, 1999). The fundamental building blocks of an endogenous clock are based on at least two interlocked feedback loops that operate with the components having both positive- and negative feedback functions. The positive components stimulate the transcription of the negative components, while the negative ones play dual roles. First, they inhibit their expression and promote the transcription of the positive components. Together, they create an interlocked transcriptional/translational feedback loop and result in oscillation.

The circadian clock in the model plant *Arabidopsis thaliana* (*At* or *A. thaliana*) is comprised of three interlocked groups of components. The primary interlocked loop consists of two Myb domain transcription factors (TF), *CIRCADIAN CLOCK ASSOCIATED1* (*CCA1*) and *LATE ELONGATED HYPOCOTYL* (*LHY*), which operate in each loop. The second interlocked loop is formed by *TIMING OF CAB EXPRESSION1* (*TOC1*), while three *PSEUDORESPONSE REGULATORS* (*PRR5*, *PRR7*, and *PRR9*) close the loop. The 3rd loop is formed by the Myb TF *LUX ARRHYTHMO* (*LUX*) along with *EARLY FLOWERING3* (*EFL3*) and *ELF4*. Each component and its associated activator and repressors peak at a specific time of day to regulate others' expressions. The *CCA1* and *LHY* of the morning-phased loop are associated with the dusk-phased pseudo-response regulator *TOC1*. *TOC1* is repressed by morning-expressed proteins *CCA1* and *LHY* by binding with its promoter, which leads to *TOC1* accumulation in the evening. *TOC1*, in turn, represses the transcription of *CCA1/LHY* (Pokhilko *et al.*, 2012), closing the feedback loop. *PRR7* and *PRR9* also add to this repression of *CCA1/LHY* during daylight (Pokhilko *et al.*, 2012). *CCA1/LHY* also represses the night-expressed genes *EARLY FLOWERING3* (*EFL3*), *ELF4*, and *LUX*, the evening complex (EC) members, by binding to

their cis-motif in their regulatory regions. These EC genes repress the morning and afternoon-expressed genes to close another feedback loop (Huang and Nusinow, 2016). The mid-day expressed genes add a second layer of positive feedback on the top of the expression of core circadian clock genes, including the Myb TF, (*REVELLE*) *RVE4*, *RVE6*, and *RVE8* (Rawat *et al.*, 2011; Farinas and Mas, 2011; Hsu *et al.*, 2013). These genes can activate the expressions of *TOC1* and the EC genes. *RVE8* [*NIGHT LIGHT-INDUCIBLE AND CLOCK-REGULATED (LNK1)*] and *LNK2* bind with the promoters of *TOC1* and *PRR5* (Xie *et al.*, 2014). The negative feedback is imposed by *TOC1*, which represses the *RVE8* expression. A blue-light receptor *ZEITLUPE (ZTL)* targets *PRR5* and *TOC1* for ubiquitination-mediated degradation after dusk (Más *et al.*, 2003a). Thus, the expression levels of these Myb TFs during different times of the day-night cycle reconfirm the stringency of the feedback loops (Shalit-Kaneh *et al.*, 2018). An excellent review of the basic functioning of the circadian clock in *A. thaliana* can be had in McClung (2019), also depicted in a simplified manner in the central part of Figure. 1.

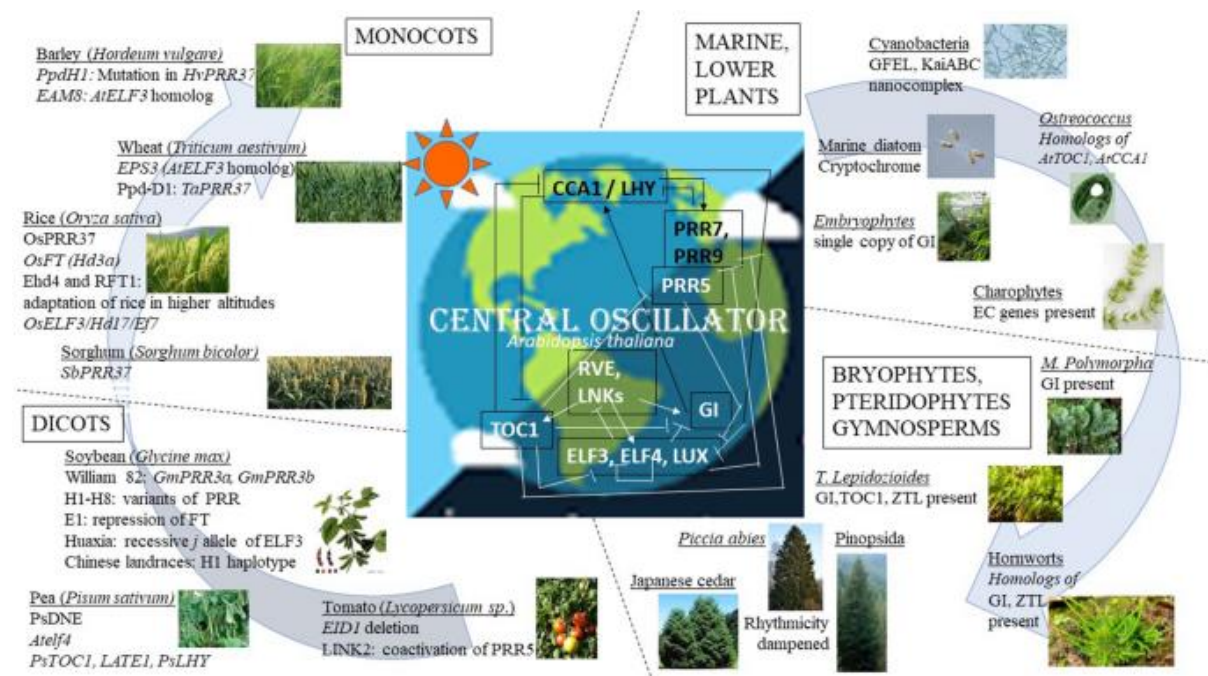


Figure 1. Variations in the circadian clock components in different plant systems. Diurnal rhythms on the earth arise due to 24 h day–night cycle. All plant systems on Earth roughly follow this rhythm to generate their endogenous circadian rhythms. The basic component of the circadian clock is the central oscillator and its function through interlocked loops of transcription is depicted here from *A. thaliana* at the center. Different plant systems with major variations in their circadian clock are indicated around with a sample picture of their appearance on the peripherals. The blue arrows on both sides indicate the complexity and position of the plant system in the course of evolution. The blue arrow is broken on the right side to indicate that monocots are more evolved than the dicots, but may not have evolved from them. GEFL: Gene Expression Feedback Loop, *TOC1* TIMING OF

CAB EXPRESSION1, *CCA1* CIRCADIAN CLOCK ASSOCIATED 1, *GI* GIGANTEA, *EC* evening complex, *ZTL* ZEITLUPE, *EID1* EMPFINDLICHER IM DUNKELROTEN LICHT, *LINK2* NIGHT LIGHT-INDUCIBLE AND CLOCK-REGULATED, *PsDNE* Die Neutrals, *ELF4* EARLY FLOWERING 4, *LATE1* LATE BLOOMER1, *LHY* LONG HYPOCOTYLE, *PRR* PSEUDO RESPONSE REGULATOR, *FT* FLOWERING TIME, *ELF3* EARLY FLOWERING 3, *Hd* HEADING DATE, *EF7* EARLY FLOWERING 7, *EHD1* EARLY HEADING DATE 1, *RFT1* RICE FLOWERING LOCUS T1, *EAM8* EARLY MATURITY 8, *PpdH1* PHOTOPERIOD-H1, *EPS3* EARLINESS PER SE D3. The figure is not to scale (Patnaik *et al.*, 2022)

1.2. GIGANTEA (GI)-A Major Component of Plant Circadian Clock

The transition from a vegetative to a reproductive phase in plants is influenced by several factors including light, temperature, age, and hormones. Photoperiodic flowering occurs when this transition is influenced by light and fine-tuned by diurnal and circadian regulatory mechanisms (de Montaigu *et al.*, 2010; Sanchez and Kay, 2016). GIGANTEA (GI) is one of the crucial circadian clock output components in plants (Fowler *et al.*, 1999; Kim *et al.*, 2013). GI gene was first discovered in *Arabidopsis* because mutations in it delayed flowering response to inductive photoperiods with little variation in short days (SDs) (Rédei, 1962; Fowler *et al.*, 1999). GI is a plant-specific nuclear protein that plays a pleiotropic role in the growth and development of plants. GI's involvement in circadian clock function, flowering time regulation, and various types of abiotic stress tolerance have been well-documented in recent years.

In *Arabidopsis thaliana*, a single copy of GI contains 14 exons that code for a 127-kDa protein with 1,173 amino acids (Park *et al.*, 1999). GI is reported to be a nuclear protein with a nuclear localization sequence between residues 543 and 783 in the core 241-amino-acid region (Huq *et al.*, 2000). GI structural homology reveals that it lacks any conserved protein domains (David *et al.*, 2006; Mishra and Panigrahi, 2015). GI is diurnally regulated, and its transcript and protein levels are strictly controlled by the circadian clock (Patnaik *et al.*, 2022). Any change in the components of the circadian clock has been demonstrated to alter the transcription of GI. Furthermore, despite overexpressing the GI protein with a constitutive promoter, its abundance follows a cyclic pattern of aggregation under long days (LDs) and SDs, indicating an additional layer of regulation on the protein expression at the post-transcriptional level (David *et al.*, 2006; Yu *et al.*, 2008).

1.3. The Cellular Localisation of GIGANTEA

The cellular localization of GI in *Arabidopsis* was determined through the constitutive expression of GI-GFP, both in transient protoplasts and transgenic plants. Analysis using fluorescent microscopy revealed that the GI protein predominantly resides in the nucleus of specific cell types, forming nuclear bodies (Mizoguchi *et al.*, 2005; Kim *et al.*, 2013). It is noteworthy that GI proteins do not possess a nuclear localization signal. To gain insights into the nature of these formations, specific sub-nuclear marker proteins targeting various compartments, such as nucleoli, spliceosomes, heterochromatin beams, and Cajal bodies, were employed. However, GI was not detected in any of these nuclear compartments, indicating that GI does not participate in processes such as protein degradation, pre-mRNA splicing, and the biogenesis of rRNA and snRNP.

EARLY FLOWERING 4 (ELF4) was identified as the evening complex gene responsible for relocating GI from the nucleoplasm, where it binds to the CO promoter, to discrete nuclear bodies (Kim *et al.*, 2013). In *Arabidopsis*, long days induce this relocation process. The synthesis of ELF4 protein and the formation of GI nuclear bodies oscillate daily, peaking at night. It is proposed that GI can be released without the need for de novo GI synthesis in the morning (Kim *et al.*, 2013).

In addition to its nuclear localization, GI is also found in the cytosol, where it plays a role in stabilizing the F-box protein ZEITLUPE (ZTL) through heterodimerization. When exposed to blue light, GI binds to the LOV (light, oxygen, or voltage sensing) domain of ZTL, ensuring a robust and accurate oscillation of its target proteins (Kim *et al.*, 2007). This interaction leads to the sequestration of GI by ZTL in the cytosol, which in turn regulates the nuclear pool of GI. This regulation controls the distribution of GI between the nucleus and cytosol, serving as a protective mechanism against degradation (Kim *et al.*, 2013).

The degradation of GI within the nucleus is closely associated with the high accumulation of

CONSTITUTIVE PHOTOMORPHOGENIC 1 (COP1) and the clock-associated protein ELF3. COP1 functions as an E3 ubiquitin ligase, and ELF3 facilitates the interaction between COP1 and GI, ultimately leading to the degradation of GI, particularly under short-day conditions. This process of destabilization mediated by COP1 and ELF3 plays a crucial role in the modulation of circadian rhythms and the regulation of the flowering transition in *Arabidopsis* (Yu *et al.*, 2008).

1.4. Flowering Time and Photoperiod-Related Molecular Functions of GIGANTEA

In vascular plants, GI is evolutionarily conserved and plays an important role in a variety of physiological responses. The role of GI in photoperiodic flowering has been thoroughly studied, where it is required to increase the transcription of *CONSTANS* (*CO*) and *FLOWERING LOCUS T* (*FT*) (Fornara *et al.*, 2009). The degradation of repressors from the DOF family of transcriptional regulators, known as CYCLING DOF FACTORS (CDFs), is necessary for the stimulation of CO and FT expression under LD conditions. In the afternoon, GI forms a complex with the blue light-absorbing FLAVIN-BINDING KELCH REPEAT F-BOX 1 (FKF1), an F-box protein, which degrades the DOF transcriptional repressors, allowing *CO* transcription leading to flowering under LD conditions (Imaizumi *et al.*, 2005; Sawa *et al.*, 2007; Kim *et al.*, 2013). Under short-day (SD) conditions, however, CO expression peaks after sunset since light does not sufficiently stabilize the CO protein (Valverde *et al.*, 2004). The CYCLING DOF FACTOR 1 (CDF1) transcriptional repressor, which binds to the CO promoter, represses CO transcription at sunrise.

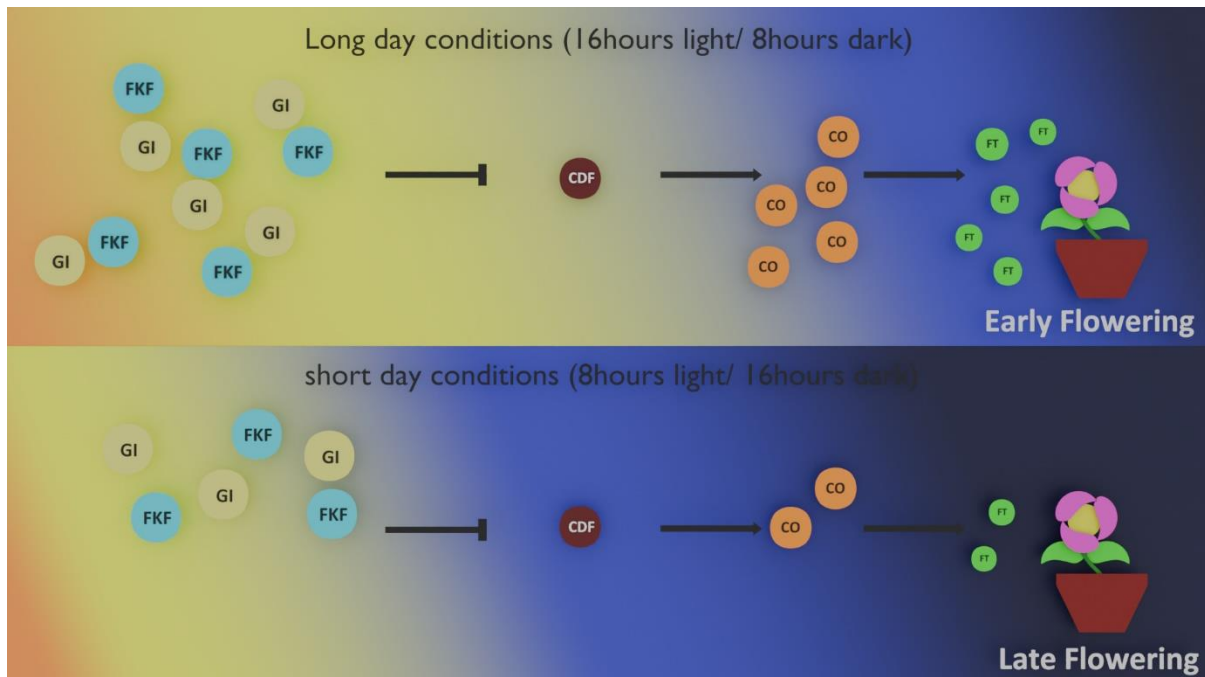


Figure 2. GI-FKF1 COMPLEX REGULATES THE PHOTOPERIODIC FLOWERING TIME. In LD, the peak expression of *GI* and *FLAVIN-BINDING KELCH REPEAT F-BOX 1 (FKF1)* coincide, leading to the accumulation of GI-FKF1 complex. The GI-FKF1 complex regulates the degradation of Cycling DOF factors (CDFs) bound to the *CONSTANS (CO)* promoter. In the absence of the inhibitor, *CO* transcription occurs resulting in the accumulation of CO protein that promotes flowering. While in SDs, less abundance of GI-FKF1 complex does not degrade CDFs repressing *CO* transcription (Mishra and Panigrahi, 2015)

In *Arabidopsis*, an enzymatic complex is established through a direct protein-protein interaction between GI and FLAVIN-BINDING, KELCH REPEAT, F BOX protein 1 (FKF1) via FKF1's LOV (Light, Oxygen, or Voltage) domain (Sawa *et al.*, 2007). This complex facilitates the degradation of CYCLING DOF FACTOR 1 (CDF1), a primary repressor of CONSTANS (CO). Its formation is intricately tied to light, as the expression of GI is regulated by the circadian clock. Consequently, around midday when both GI and FKF1 reach their peak accumulation, the DOF-degradation complex is inhibited, resulting in an upsurge in CO transcription and, subsequently, the transcription of FLOWERING LOCUS T (FT) (Sawa *et al.*, 2007; Imaizumi *et al.*, 2003). Notably, this regulatory mechanism is altered in short days in *Arabidopsis*, where the GI accumulation peak precedes that of FKF1 by approximately three hours. This temporal shift prevents the formation of the DOF-degradation complex, leading to a consequent reduction in the abundance of the CO transcript.

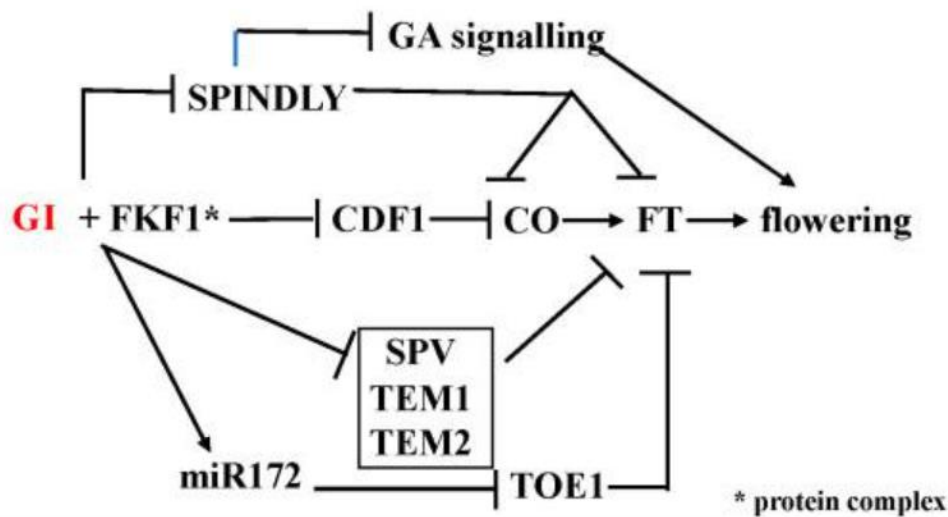


Figure 3. Model of GIGANTEA (GI) dependent flowering time regulation in *A. thaliana* (Adapted from Brandoli *et al.*, 2020).

Other blue light circadian photoreceptors like LOV KELCH protein 2 (LKP2) and ZEITLUPE (ZTL) interact and stabilize GI (Kim *et al.*, 2007). This regulates the appropriate development and resilience of the circadian clock in plants (Somers *et al.*, 2000; Kim *et al.*, 2007; Fornara *et al.*, 2009; Baudry *et al.*, 2010). In recent times, GI has been shown to act as a co-chaperone in *A. thaliana*'s circadian clock, facilitating the maturation of ZTL (Cha *et al.*, 2017).

Yet another light-dependent regulation of flowering in GIGANTEA is *SPINDLY* (*SPY*). GI regulates the photoperiodic flowering by inhibiting *SPY* in a light-dependent manner. Simultaneously *SPY* inhibits the expression of *CO* and *FT*, as seen in *spy-4* plants, where the late-flowering phenotype of *gi-2* plants was eliminated due to a partial suppression of abundance reduction in *CO* and *FT* RNA (Tseng *et al.*, 2004). Furthermore, *SPY* affects flowering by inhibiting GA signalling, which is necessary for flower promotion (Swain *et al.*, 2001). Furthermore, GI can modulate the expression of *FT* independently of *CO*. It restricts *FT* transcriptional repressors including *SHORT VEGETATIVE PHASE* (*SVP*), *TEMPRANILLO 1* (*TEM1*), and *TEMPRANILLO 2* (*TEM2*). GI affects their stability or neutralizes their repressor effect by preventing them from accessing the *FT* promoter region. Similarly, GI binds to particular target regions on the *FT* promoter (Sawa *et al.*, 2011), which affects the abundance of *FT* transcripts. GI regulates *FT* expression and photoperiodic flowering independently of *CO* through an interaction with a microRNA. The miRNA172 inhibits the expression of *FT*'s

main transcriptional repressors, TOE1 and APETALA 2. It was discovered that miRNA172 processing is positively regulated in the presence of GI protein via an unknown molecular interaction (Jung *et al.*, 2007). Growth of plants under natural conditions, i.e., photo and thermoperiod, demonstrates that it has a significant impact on FT coordination, implying that GI may play a role in temperature and light coordination (Song *et al.*, 2018).

1.5. Light signalling Related Molecular Functions of GIGANTEA

Plants deploy a variety of photoreceptors to perceive different light qualities as well as quantities. They have photoreceptors like UVB-resistance 8 (UVR-8), Phototropins (PHOTs), Cryptochromes (CRYs), and Phytochromes (PHYs) that function at various wavelengths (Griffin and Toledo-Ortiz, 2022). Photoreceptors are found throughout plants, primarily in the shoot region, but also in roots (Gelderen *et al.*, 2018). Phototropins and cryptochromes, which absorb primarily in the blue spectrum ($\lambda = 400$ to 499 nm), regulate flowering time, inhibit hypocotyl growth, and promote phototropism (Lin *et al.*, 2000). In *Arabidopsis*, five phytochromes (Phy) exist, ranging from PhyA to PhyE (Brandoli *et al.*, 2020). Mutations in GI have been reported to affect phytochrome signalling. The *gi-100* mutant exhibited late flowering and a longer hypocotyl phenotype only under red light. However, the effect was not observed under far-red light. The *gi-100* mutation does not affect the abundance of PhyA and PhyB proteins (Huq *et al.*, 2000). Thus, GI has been identified to be downstream of the PhyB signalling pathway. It was also observed that there was no interaction between GI and PhyA (Huq *et al.*, 2000). Several other reports also suggest that the *gi* mutation decreases the Very Low Fluence Response (VLFR) to FR, suggesting that it plays a positive role in Phytochrome A-mediated VLFR signalling (Oliverio *et al.*, 2007). Additionally, GI functions as an important part of blue light signalling. *gi* mutants have longer hypocotyls than WT under blue light. Previous work indicates the GI can either positively regulate TOC1 or function in parallel with it. In contrast, only *gi* mutants exhibited longer hypocotyls under blue light, while *toc1* mutants

did not. According to Martin-Tryon *et al.*, (2007), TOC1 and GI function independently under blue light conditions (Figure 4).

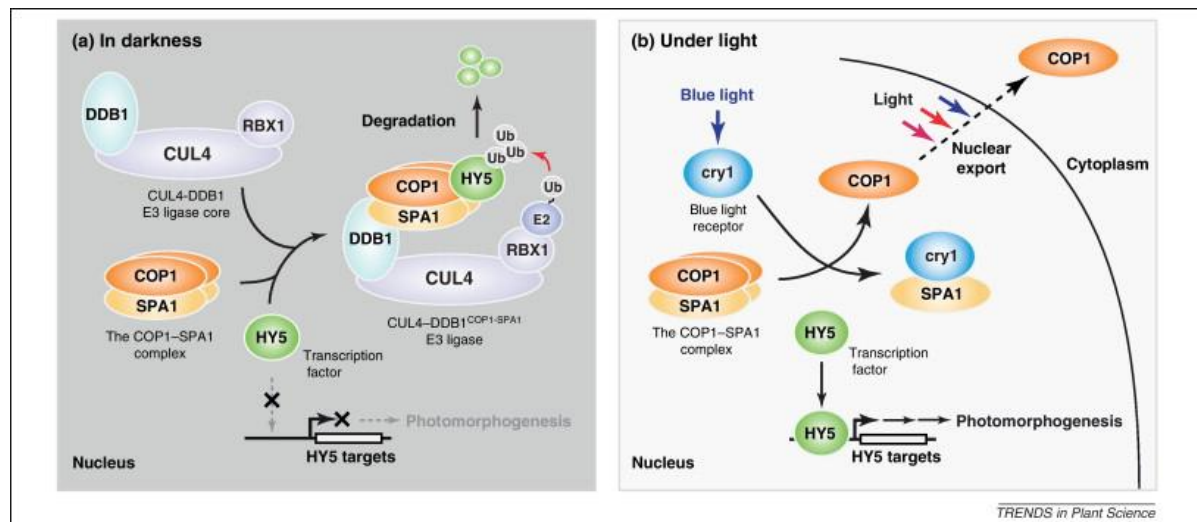


Figure 4. GIGANTEA interactions during the night (a) and day (b) to control flowering and circadian clock pathways. (a) At night, COP1 is in charge of the proteasome-mediated degradation of transcription factors like HY5, which promotes photomorphogenesis. COP1 forms a tetrameric complex with SPA family members (two COP1s and two SPAs) and interacts with the substrate, HY5. The interaction with the CUL4-DDB1 core is further mediated by the WDXR motifs on either COP1 or SPA, resulting in the multimeric CUL4-DDB1-COP1-SPA1 E3 ligase assembly. Activated E2s are recruited to the E3, resulting in HY5 polyubiquitination and degradation. Photomorphogenesis is suppressed. (b) During the day, activated photoreceptors inhibit COP1. In blue light, cry1 interacts with SPA1 and sequesters it from COP1, most likely disrupting the COP1-SPA1 complex, which is necessary for E3 function. Visible light promotes the nuclear export of COP1, resulting in long-term repression. Reduced COP1 activity causes HY5 to accumulate, bind to its targets, and promote photomorphogenesis. cry1, cryptochrome 1; COP1, CONSTITUTIVE PHOTOMORPHOGENIC 1; CUL4, CULLIN4; DDB1, DAMAGED DNA BINDING PROTEIN 1; HY5, ELONGATED HYPOCOTYL 5; RBX1, RING-BOX 1; SPA1, SUPPRESSOR OF PHYA-105 1; and Ub, ubiquitin. (Lau *et al.*, 2012)

1.6. Translational Regulation of GIGANTEA in Circadian Clock Control

The circadian clock in plants is responsible for controlling the changes that occur daily like cell growth, expression of genes, photosynthetic activities, etc (Johnson *et al.*, 1995; Carre, 1996; Kreps and Kay, 1997). The endogenous clock serves to be a complex mechanism in plants where proteins interact with each other in negative feedback loops through many transcriptional and post-translational repression and activation (Pokhilko *et al.*, 2012). The circadian clock consists of three loops (central loop, morning loop, and evening loop) which act in an autoregulatory negative feedback mechanism to control the plant's overall day and night cycle (Adams *et al.*, 2015). The central loop consists of LATE ELONGATED HYPOCOTYL (LHY) and CIRCADIAN CLOCK ASSOCIATED 1 (CCA1) along with TIMING OF CAB EXPRESSION 1 (TOC1), also known as PSEUDO- RESPONSE

REGULATOR 1 (PRR1) (Adams *et al.*, 2015). PSEUDO- RESPONSE REGULATORS (PRR9, PRR7 and PRR5) forms the morning loop. And, the evening loop is formed by ZEITLUPE (ZTL), LUX ARHYTHMO (LUX), EARLY FLOWERING 3, and EARLY FLOWERING 4 (ELF3 & ELF4) (Más *et al.*, 2003b). GI is found to interact with several of these clock genes ensuring GI transcript expression peak and amplitude of the different clock genes at specific times of the day (Fowler *et al.*, 1999). In *Arabidopsis thaliana*, alterations of circadian rhythm and photoperiod insensitive flowering are observed when the GI gene is mutated (Park *et al.*, 1999). The expression level of clock-associated genes like LHY and CCA1 along with GI are found to be altered in *gi* mutants. This indicates that GI plays an important role in maintaining the feedback loop of the circadian clock in plants (Park *et al.*, 1999). The morning elements, LHY and CCA1 form a complex and repress the TOC1 expression. And, the evening members like GI, PRRs, ELF3, ELF4, and LUX when expressed, repress the expression of LHY and CCA1. This repression feedback loop continues when in the evening, TOC1 represses all the components that are expressed previously in the plant system. The molecular functioning of GI with other circadian clock components in response to day and night is represented in Figure 5.

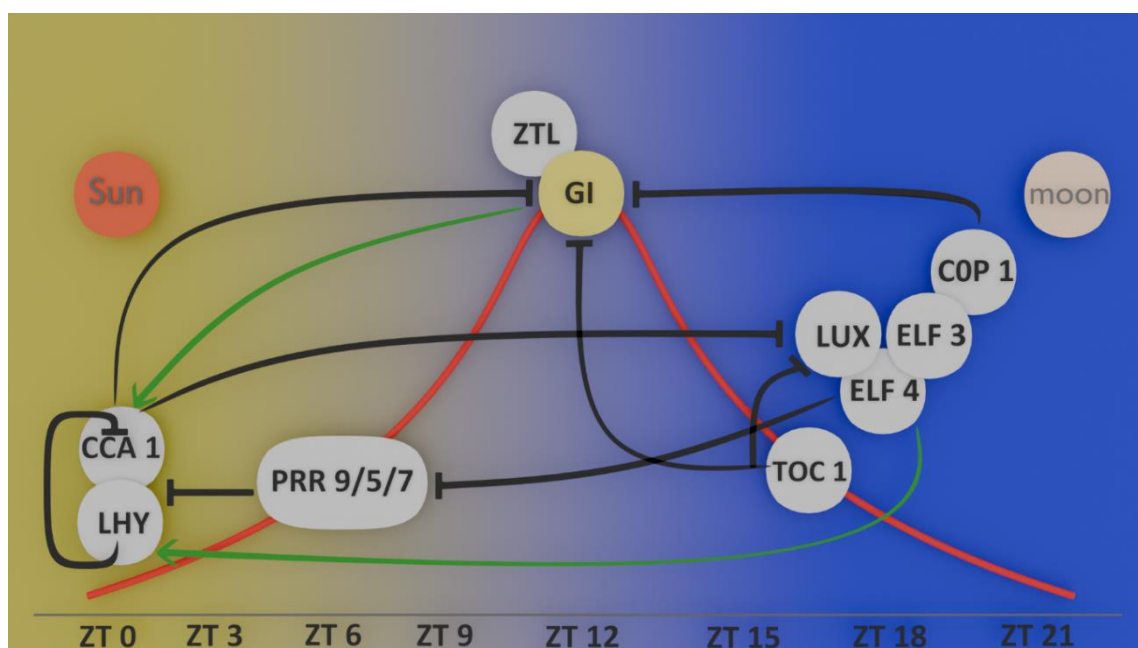


Figure 5. Diagrammatic representation of the clock model showcasing autoregulatory feedback loops facilitated by transcriptional and post-translational mechanisms. Clock components are arranged based on their peak-time expression, progressing from left to right. The red curve illustrates the daytime expression pattern of GI. During daylight hours, GI interacts directly with ZTL, shielding TOC1 from ZTL-mediated proteasomal

degradation. In the evening, ELF3 triggers GI degradation via its association with COP1, thereby facilitating ZTL-mediated TOC degradation. Boxed regions denote groups of genes operating synergistically. The PRR box includes PRR 5, 7, and 9, sequentially expressed throughout the day, collectively repressing LHY and CCA1. The GI-ZTL box signifies the protein-protein interaction essential for ZTL maturation. Lastly, the ELF3-ELF4-LUX complex box denotes the protein complex peaking at dusk.

1.7. Stress Response Related Molecular Functions of GIGANTEA

GI regulates multiple abiotic stress responses in plants, including cold, drought, heat, salt, and oxidative stress (Brandoli *et al.*, 2020; Mishra and Panigrahi, 2015).

a. Involvement of GI in Drought Tolerance

The circadian clock regulates several genes that respond to drought stress. Among them, GI contributes a role in drought escape tolerance that is Absciscic acid (ABA) dependent. Drought stress activates GI transcription, increasing the abundance of the miR172E variant (Mishra and Panigrahi, 2015; Han *et al.*, 2013). In drought stress, GI suppresses WRKY DNA binding protein 44 (WRKY44), which interacts with TOE1. GI-miR172-WRKY44 was proposed to be in the same pathway, possibly related to drought stress tolerance. Similarly, the light-dependent GI-mediated stomatal opening response may be mediated by ABA (Mishra and Panigrahi, 2015; Ando *et al.*, 2013). Furthermore, it has been reported that drought stress promotes flowering, and GI has been identified as a key component mediating drought response in *Arabidopsis*. According to one proposed mechanism of action, GI may regulate chromatin accessibility and/or interfere with repressor activity at florigen promoters via the plant stress hormone abscisic acid (ABA) (Riboni *et al.*, 2014; Brandoli *et al.*, 2020). However, during flowering in *Arabidopsis* under short-term drought stress, endogenous ABA levels increased and this phenomenon is referred to as the drought escape response (Bader *et al.*, 2023; Riboni *et al.*, 2013). Studies have shown that GI plays an important role in DE response by regulating ABA biosynthesis, implying that GI promotes flowering through both ABA synthesis and florigen gene regulation in response to drought stress. (Bader *et al.*, 2023; Baek *et al.*, 2020; Riboni *et al.*, 2013). In contrast, a recent study suggests that the highest accumulation of GI at

noon is critical in establishing a phase of decreased ABA concentration and is associated with negative regulation of ABA transcriptional responses and sensitivity (Siemiakowska *et al.*, 2022). Additionally, Bader and colleagues recently reported that, unlike wild-type plants, the *gi-1* mutant plants exhibited an ABA-insensitive phenotype, which provides additional evidence for the lower endogenous ABA concentration in *gi-1* measured previously by Beak *et al.* and explains the close relationship between GI and ABA. In conclusion, GI regulates flowering by binding to FKF1 and ZTL, whereas its association with ENHANCED EM LEVEL (EEL) promotes ABA biosynthesis and DE responses (Bader *et al.*, 2023).

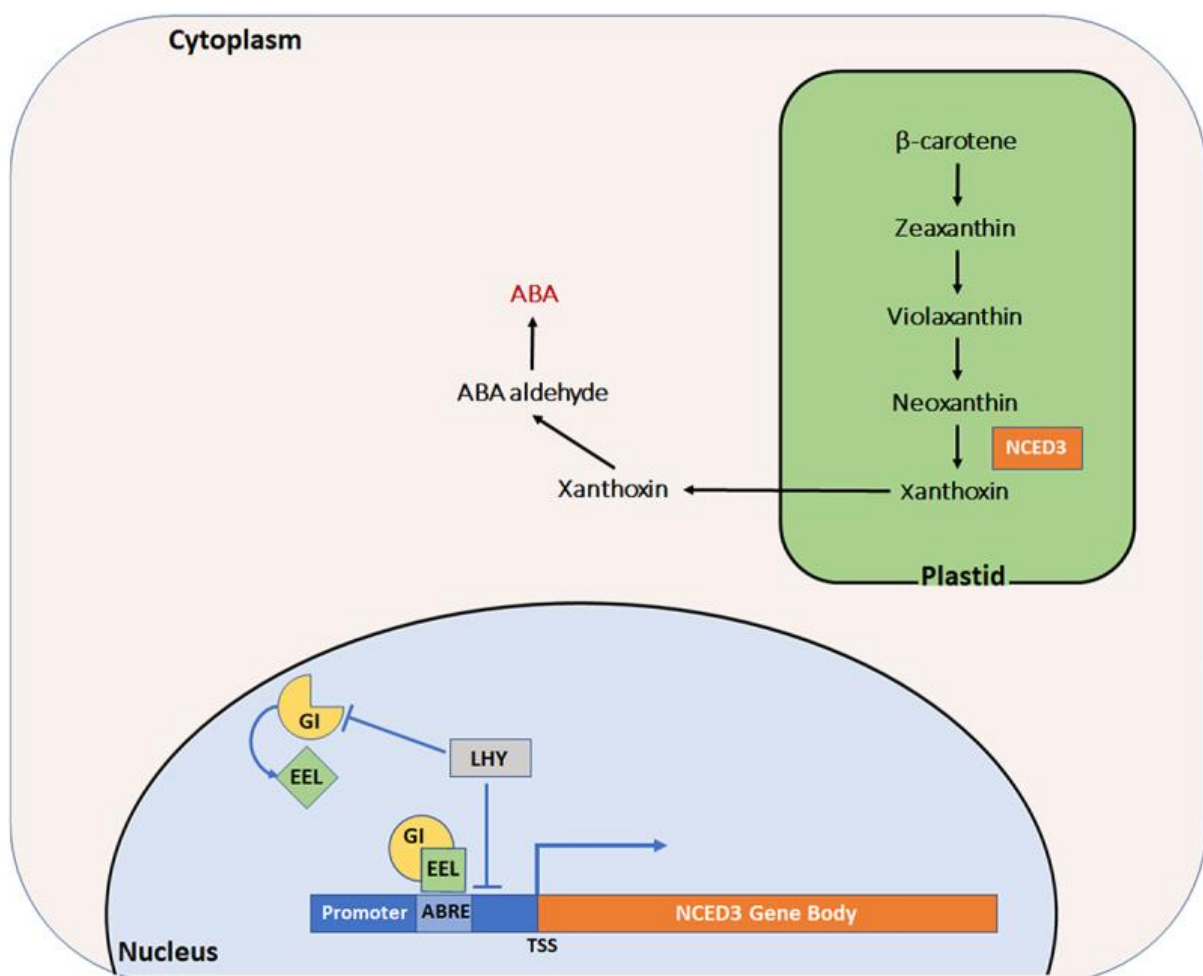


Figure 6. Schematic diagram depicting GI-EEL regulation of the ABA biosynthesis pathway. GI forms a complex with EEL on the 9-CIS-EPOXYCAROTENOID DIOXYGENASE 3 (NCED3) promoter in the nucleus, containing the ABRE motif, which positively regulates NCED3 expression. In plastids, the NCED3 enzyme converts neoxanthin to xanthoxin, which moves to the cytoplasm and undergoes catalytic reactions to produce ABA. (Adapted from Bader *et al.*, 2023)

b. *Involvement of GI in Salinity Tolerance*

GI plays a crucial role in enhancing salt tolerance in crops by regulating the Salt Overly Sensitive (SOS) signaling pathway. This pathway is responsible for maintaining ion homeostasis, a process conserved in dicot plants like *Arabidopsis* and *Brassica nigra*, as reported in studies by Zhu (2002) and Tang *et al.*, (2015). GI interacts with the SNF1-related protein kinase SOS2, a key component of the SOS pathway. This interaction significantly reduces or prevents the primary function of SOS2 by activating the SOS1 antiporter during normal, non-stressful growth conditions (Park *et al.*, 2016). Salt stress triggers proteasomal degradation of GI, releasing the SOS2 protein, which then interacts with the SOS3 protein. The process of SOS2 caging and release is reflected in the phenotypes. Plants that overexpress GI are more sensitive to salt compared to wild-type plants, while GI mutants are more salt tolerant. This observation supports the idea that salt activates the SOS2 kinase, which then activates the Na⁺/H⁺ antiporter SOS1 (Kim *et al.*, 2013; Park *et al.*, 2013). GI adds to the dynamic behavior of SOS2 by triggering stress-induced release through interaction. The presence of GI and its degradation link salt stress to clock functions, revealing previously unrelated pathways. Interestingly, it has been reported that under high salinity environments, *gi* mutant showed tolerance to high salt (Park *et al.*, 2016).

c. *Involvement of GI in Cold Tolerance*

Abiotic stress like cold stress which includes chilling temperatures ranging from 0 °C to 15 °C and freezing temperatures which is less than 0 °C, negatively impacts plant growth and agricultural productivity (Guo *et al.*, 2018; Liu J. *et al.*, 2018). The response to cold temperatures entails changes in gene expression, resulting in increases in metabolite levels, including those known to protect against the damaging effects of cold stress (Sanghera *et al.*, 2011). Plants can adapt to low temperatures by gradually increasing their freezing tolerance through prolonged exposure to low but non-freezing temperatures, a process known as cold

acclimation (Guy *et al.*, 1990). The resistance of plants to cold appears to be organ-specific (Weiss *et al.*, 2009). This process is distinguished by complex biochemical and physiological changes, such as changes in gene expression (Guy *et al.*, 1985; Thomashow, 1999), enzyme activities (Uemura *et al.*, 2003), lipid membrane composition (Miquel *et al.*, 1993), and leaf ultrastructure modification (Ristic *et al.*, 1993). Chilling injuries cause the collapse of deep cell layers and the disruption of antioxidant activity, among other things (Gomez *et al.*, 2009).

According to recent research, miR172 is likely to play a central coordinating role in response to cold stress, particularly in the regulation of CK2 and the circadian rhythm in cold-resistant wild bananas, *Musa itinerans*, from China (Liu *et al.*, 2018). The *gi* mutants have increased freezing tolerance and up-regulation of cold-responsive genes. The freezing tolerance phenotype in *gi* mutants is dependent on CDF transcription. Bánfalvi *et al.*, (2019) and Fornara *et al.*, (2015) found that the *gi*, *cdf* double mutants exhibit cold sensitivity. A heat map analysis revealed that freezing stress induces GI (Xin *et al.*, 2019). Freezing tolerance causes an increase in GI abundance via a pathway independent of C-repeat binding factors (CBF) (Cao *et al.*, 2005). C-repeat binding factors (CBF) transcription factors, also known as dehydration-responsive element binding factor 1 (DREB1) proteins, could bind directly to the CRT/DRE cis-element in the promoters of cold-regulated (COR) genes, thereby inducing COR gene expression (Jaglo-Ottosen *et al.*, 1998; Liu *et al.*, 2018). The COR genes, which encode cryoprotective proteins and key enzymes for osmolyte biosynthesis, protected plant cells from cold-induced damage, repaired cold-rigidified membranes, and stabilized cellular osmotic potential (Chinnusamy *et al.*, 2007). Two candidate interactors, REI1-LIKE and GENERAL CONTROL NONREPRESSIBLE (GCN1) have been linked to cold tolerance via ribosome maturation and translation initiation regulation, respectively (Schmidt *et al.*, 2013; Wang *et al.*, 2017). These potential interactors could be useful in developing hypotheses about how GI regulates cold tolerance (Krahmer *et al.*, 2018). The *gi* mutant is sensitive to cold and freezing, with lower levels of cold-induced sugars and increased accumulation of starch (Cao *et al.*,

2005; 2007; Eimert *et al.*, 1995). GI has been shown to independently mediate a cold stress response via the CBF-mediated cold stress pathway (Cao *et al.*, 2005). The *prp5,7,9* and *toc1* mutants show significantly increased freezing survival (Jang *et al.*, 2024; Nakamichi *et al.*, 2009; Keily *et al.*, 2013). However, *gi*, *lux*, *lhy*, *cca1*, and *lhy cca1* mutants exhibit decreased constitutive and acclimated freezing tolerance (Jang *et al.*, 2024; Cao *et al.*, 2005; Espinoza *et al.*, 2010; Dong *et al.*, 2011; Chow *et al.*, 2014).

GI promotes the degradation of a family of CDF1 transcriptional repressors, thereby activating the expression of CO and FT, the key floral regulators. In *Arabidopsis* and tomato, a *gi*-mutant background resulted in increased CDF protein stability and accumulation, as well as higher transcript levels of stress-responsive genes such as COR15a, RD29A, and ERD1, as well as improved cold stress resistance (Brandoli *et al.*, 2020; Corrales *et al.*, 2014; Fornara *et al.*, 2009). As a result, it has been proposed that, in addition to flowering, CDF regulation via GI influences freezing temperature responses (Brandoli *et al.*, 2020; Fornara *et al.*, 2009).

d. Involvement of GI in Heat Tolerance

Temperature compensation is an important feature of the circadian clock because it allows it to maintain its rhythm across a wide range of environmental temperatures. GI was identified as a candidate for regulating the temperature compensation effect, particularly at higher temperatures (Edwards *et al.*, 2005; Gould *et al.*, 2006; Mishra and Panigrahi, 2015). Because temperature fluctuations regulate the abundance of GI transcripts, the GI and temperature sensing mechanisms may communicate and feedback to one another. Emerging transcriptome datasets demonstrate that the transcriptional response to heat stress is highly dynamic (Blair *et al.*, 2019; Li *et al.*, 2019). In *Arabidopsis*, the transcript abundance of core clock genes changes in response to daytime heat stress (Blair *et al.*, 2019). At higher temperatures, the transcript levels of circadian clock core genes in barley (*Hordeum vulgare*) increase, including CIRCADIAN CLOCK ASSOCIATED 1 (CCA1), GI, PSEUDO RESPONSE REGULATOR

59 (PRR59), PSEUDO RESPONSE REGULATOR 73 (PRR73), PSEUDO RESPONSE REGULATOR 95 (PRR95), and LUX. Furthermore, the *elf3* mutant loses the response of GI and *PRR* genes to temperature stress, implying that their response to temperature cues is dependent on ELF3 (Ford *et al.*, 2016). In soybeans, heat stress causes a milder disruption in the global circadian rhythm (Li *et al.*, 2019). In rice, 17 of the 25 known heat shock transcription factors (HSFs) exhibit rhythmic expression under diel conditions, with 11 of those 17 being induced by heat stress (Mockler *et al.*, 2007; Mittal *et al.*, 2009). These datasets show a strong link between the circadian clock and heat responses, though the direct mechanisms of crop circadian clock component responses to heat stress are not fully understood (Xu *et al.*, 2023).

e. Involvement of GI in Oxidative Stress

The *gi-3* mutants demonstrated increased tolerance to the redox cycling agent paraquat and H₂O₂ (Kurepa *et al.*, 1998a). Exogenous polyamines such as putrescine, spermine, and spermidine reduce paraquat tolerance (Kurepa *et al.*, 1998b). Endogenous putrescine levels were increased by paraquat treatment in *gi-3* and WT cells. Analysis of endogenous H₂O₂ and superoxide anion radicals, as well as lipid peroxidation, showed that *gi-3* mutant plants were more resistant to oxidative stress. This was not due to defects in PQ uptake or sequestration from its site of action. Instead, the *gi-3* mutation reduced oxidative damage to plant cells caused by PQ stress. The *gi-3* mutant activated cytosolic Cu/Zn SOD, plastidic Fe SOD, cytosolic APX1, and stromal APX genes, leading to increased anti-oxidative enzyme activity (SOD and APX, respectively) (Cao *et al.*, 2006). The exogenous application of polyamines is effective for resistance, but the mechanism of transporters during this stress requires investigation (Mishra and Panigrahi, 2015). Imazethapyr herbicide has been linked to increased GI abundance and earlier flowering by ~4 days (Qian *et al.*, 2014). The mechanism underlying higher tolerance to oxidative stress via GI is still unknown.

GI expression is present at all stages of plant development, indicating its involvement in various functions as shown in Figure 6. It is interesting to note the ubiquitous expression of GI, which reflects its pleiotropic roles in a wide range of responses, from seed dormancy breaking to hypocotyl elongation, initiating the circadian rhythm in seeds, and fruit setting in the adult plant. Many of the above-mentioned outcomes incorporate information from light input and external temperature, making this an intriguing but complex area of plant science.

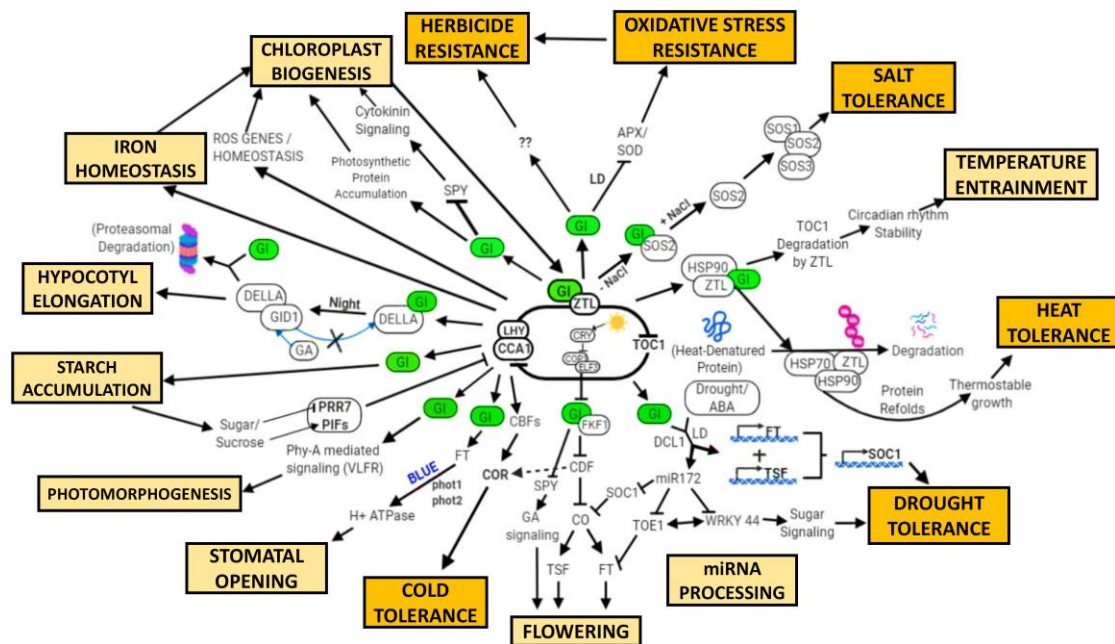


Figure 7. Pleiotropic functions of GIGANTEA (GI) in plant growth and development. GI is known to be involved in drought tolerance and escape (Han *et al.*, 2013), miRNA processing (Morris *et al.*, 2010; Han *et al.*, 2013), flowering time regulation (Park *et al.*, 2016), cold tolerance Brandoli *et al.*, 2020), stomatal opening (Ando *et al.*, 2013), photomorphogenesis (Huq *et al.*, 2000; Martin-Tryon *et al.*, 2007; Oliverio *et al.*, 2007), starch accumulation (Kim *et al.*, 2017), hypocotyl elongation (Nohales *et al.*, 2019), iron homeostasis (Tissot *et al.*, 2014), chloroplast biogenesis (Cha *et al.*, 2019;), herbicide resistance (Cha *et al.*, 2019), oxidative stress tolerance (Cha *et al.*, 2022), salt tolerance (Park *et al.*, 2016), temperature entrainment (Gil *et al.*, 2019), heat tolerance (Gil and Park (2019), circadian clock control and light signalling (Mishra and Panigrahi, 2015). (Adapted from Behera. A., 2022)

1.8. Phytohormones in plants

Plants use a variety of signalling factors, including phytohormones, to regulate their growth. There are several types of phytohormones, including Auxin, Cytokinin (CK), Ethylene (ET), Gibberellic acid (GA), Absciscic acid (ABA), Jasmonic acid (JA), Brassinosteroid (BR), and Salicylic acid (SA) (Taiz and Zeiger, 2002; Wani *et al.*, 2016; Marzec, 2017). Phytohormones are crucial for plant development throughout the life cycle.

a. *Auxin*

Auxin is the first and most widely studied phytohormone in plants. Indole-3-acetic acid (IAA) is a naturally occurring auxin. It contributes to various aspects of plant development. It promotes hypocotyl growth, vascular patterning, primary root development, and lateral root branching, and regulates root movement (Aloni *et al.*, 2006; Chae *et al.*, 2012). It regulates multiple processes or works with other phytohormones to enhance plant functions. It increases hypocotyl elongation and promotes apical dominance (Moore and Moore, 1974). Apical dominance refers to the growth of the main shoot over the lateral branches. It also improves shoot vascular differentiation. Auxin influx and efflux play a significant role in vascular patterning (Fàbregas *et al.*, 2015). IAA promotes lateral branching while inhibiting primary root elongation. Auxin efflux is carried by PIN-FORMED (PIN) proteins, and PIN3-dependent auxin transport promotes both hypocotyl and root gravitropism (Rakusová *et al.*, 2011).

b. *Cytokinin*

Cytokinin (CK) regulates apical dominance, phyllotaxis, leaf senescence, and root growth (Werner *et al.*, 2003). It works alongside auxin to regulate root-shoot ratio, apical dominance, phyllotaxis, and root architecture. It inhibits the growth of the main shoot by competing with auxin in apical dominance (Moore and Moore, 1974). It promotes root hair formation but inhibits primary root growth and lateral root initiation. It promotes phyllotaxis and slows down leaf senescence (Pua and Davey, 2010; Kieber and Schaller 2018). CK helps reduce leaf and flower senescence and balances the effects of ET.

c. *Gibberellic Acid*

Gibberellic acid (GA) falls under the terpenoid family and is found in plants as well as many fungi. It contributes to seed germination, flowering, stem elongation, root phenotype, and so on. It promotes seed germination and helps to maintain flowering uniformity (Hedden and Sponsel, 2015). GA promotes skotomorphogenesis, which positively controls stem elongation in darkness. It regulates stem elongation by minimizing HY5 stability and enhancing PIFs.

Therefore, GA-mediated stem elongation in the dark depends on HY5 and PIF stability (Alabadi, 2004; Alabadí *et al.*, 2008). The RAG1 gene links the auxin and gibberellin signaling pathways. It is a SMALL AUXIN UPREGULATED RNA 36 (SAUR36) gene that has been shown to promote hypocotyl elongation in the dark. However, Light inhibits hypocotyl growth by reducing RAG1 expression (Stamm and Kumar, 2013).

d. *Abscisic acid*

Abscisic acid (ABA) is primarily known as a stress hormone; it controls plant physiology during stress while offering resistance to abiotic stress (Lim *et al.*, 2015). It regulates seed germination, dormancy, hypocotyl growth, and root morphology. It protects plants from both biotic and abiotic stress and typically functions in adverse conditions. It promotes de-etiolation and inhibits hypocotyl growth via HY5 accumulation. ABI5 also plays an important role in growth control (Chen *et al.*, 2008). ABI5 encodes the basic leucine zipper transcription factor, which participates in ABA signaling during seed development. It inhibits primary and lateral root growth, and the Root growth is affected by ABA concentration (Sharp *et al.*, 2002).

e. *Jasmonic acid*

JA is an organic compound that primarily aids in plant defense and abiotic stress tolerance. It controls root growth and hypocotyl elongation (Robson *et al.*, 2010). In general, it retards or suppresses plant growth while promoting defense-related responses in stressful conditions. This improves plant survival during both pathogen infection and herbivore attack (Wang and Wu, 2013). It protects plants from a variety of stressors such as cold, salt, drought, and heat by involving JA signaling genes like Jasmonate ZIM domain (JAZ) and MYC2 (Ahmad *et al.*, 2016). JAZ serves as a transcriptional repressor in JA signalling. COI1 degrades JAZ in the presence of Jasmonoyl-L-isoleucine (JA-Ile), a type of JA, through a ubiquitin-mediated pathway. CORONATINE INSENSITIVE 1 is an E3-ubiquitin ligase (Pauwels and Goossens, 2011). MYC2 is a transcriptional activator that promotes JA-responsive genes and signalling (Liu *et al.*, 2019). JA has been demonstrated to inhibit primary and lateral root growth.

Oxylipin, a JA, causes root waving and apical dominance failure. In the dark, JA inhibits hypocotyl growth via MYC2 (Chen *et al.*, 2013).

f. Salicylic acid

Unlike JA and ABA, Salicylic acid (SA), is also an essential phytohormone for plant defense and survival during abiotic stress. It also regulates various physiological and morphological aspects of plant development. It controls photosynthesis, seed germination, thermogenesis, and flower development. It has been shown to promote root and hypocotyl growth (Rivas-San and Plasencia, 2001). SA interacts with other phytohormones to control plant stress, both biotic and abiotic.

g. Brassinosteroids

Brassinosteroids (BRs) are polyhydroxylated steroid hormones that regulate plant development, including photomorphogenesis, cell division, and root growth (Wei and Li, 2016). BRASSINAZOLE-RESISTANT 1 (BZR1) positively regulates BR signalling and promotes skotomorphogenesis. It inhibits photomorphogenesis by suppressing GATA2 transcription (Luo *et al.*, 2010). GATA2 is a transcription factor that regulates light signalling. BZR1 promotes hypocotyl growth by interacting with PIF4 and COP1 (Oh *et al.*, 2012; Kim *et al.*, 2014). BR regulates root growth by elongating and organizing cells. It controls root growth in a concentration-dependent manner (Wei and Li, 2016). Higher concentrations of BR inhibit root growth, while lower concentrations promote it.

h. Ethylene

Ethylene (ET) is a gaseous plant regulator known for its significant contribution to fruit ripening. It regulates hypocotyl growth, abscission control, leaf development, and root phenotype (Schaller, 2012). It works alongside other phytohormone signalling pathways to regulate plant growth and development (Iqbal *et al.*, 2017). It promotes fruit ripening, softening, and maturity. It also positively regulates hypocotyl elongation, which is influenced by light fluence and quality (Smalle *et al.*, 1997; Yu *et al.*, 2013). ET encourages the abscission

of fruits, flowers, and leaves. Leaf growth and development depend on both ET concentration and plant species. It suppresses root growth by inhibiting root cell elongation (Schaller, 2012). ET-dependent root inhibition occurs due to changes in auxin synthesis and transport (Ruzicka *et al.*, 2007).

1.9. A Brief Overview of Auxin Synthesis, Signalling and Transport

Auxin activity in various physiological processes can be spatiotemporally controlled by three major regulatory mechanisms: auxin biosynthesis and inactivation, auxin-directed transport, and signal transduction. IAA (Indole-3-Acetic Acid) is a ubiquitous endogenous auxin in plants, produced through both Trp (Tryptophan)-independent and Trp-dependent pathways (Zhao *et al.*, 2012; Korasick *et al.*, 2013). Presently, the only complete auxin biosynthetic pathway that has been identified in plants is TAA/YUC (TRYPTOPHAN AMINOTRANSFER-ASE OF *ARABIDOPSIS*/YUCCA) (Stepanova *et al.*, 2011; Dai *et al.*, 2013). The TAA/YUC pathway converts Trp to IAA through two sequential chemical steps. Initially, the TAA family of aminotransferases converts Trp to IPyA (Indole-3-Pyruvate). The YUC family of flavin-containing monooxygenases then catalyzes the oxidative decarboxylation of IPyA, resulting in IAA. It is the primary auxin biosynthesis pathway and is required for all major developmental processes (Zhao *et al.*, 2018).

The auxin response is concentration-dependent across the majority of tissues, with various tissues responding distinctly to different levels of exogenous auxin (Thimann *et al.*, 1937). Higher auxin concentrations are inhibitory; therefore, the optimum endogenous levels must be precisely maintained in the plants for its function. There are several mechanisms for regulating auxin homeostasis, including dynamic biosynthesis, degradation, transport, and conjugate formation of free IAA (Zhang *et al.*, 2009). IAA is the plant's primary source of active auxin (Woodward *et al.*, 2005, Paciorek *et al.*, 2006). Monocotyledonous and dicotyledonous plants maintain IAA homeostasis through the breakdown of free IAA to its conjugated form, which

is a conserved mechanism. The GH3 (Gretchen Hagen 3) protein family is capable of synthesizing auxin amino acids. It binds free IAA to amino acids, converting it from active to inactive. The combination and degradation of amino acid molecules and IAA contribute to IAA homeostasis in plants (Staswick *et al.*, 2005). GH3 contributes to the negative feedback regulation of IAA concentration, and excess IAA stimulates GH3 expression, resulting in the storage or degradation of amino-acid-bound IAA. The GH3 gene is required for normal plant growth and resistance to environmental stress (Zhang *et al.*, 2009; Ludwig-Müller *et al.*, 2011).

Auxin affects numerous physiological processes by regulating gene transcription via the SCFTIR1/AFB-Aux/IAA-ARF nuclear signaling module. The module requires a combination of three key components. The F-box proteins AFB1-5/TIR1 are auxin receptor subunits of the SCF-Family E3 ubiquitin, which bind to the activator class of ARF (AUXIN RESPONSE FACTOR) transcription factors and the transcriptional repressors Aux/IAA (Weijers *et al.*, 2016). Auxin perception begins with the binding of auxin to TIR1/AFB receptors. It causes the degradation of Aux/IAA proteins, which physically interact with ARF transcription factors and suppress auxin signaling (Mockaitis and Estelle, 2008). Auxin promotes the ubiquitination and degradation of the Aux/IAA protein, as well as the release of ARF's transcriptional activity, which activates the transcription of downstream auxin-responsive genes. Aux/IAA-ARF modules and auxin response genes regulate various developmental processes (Vanneste *et al.*, 2009).

In higher plants, auxin is transported in two distinct but interconnected systems: a fast, non-directional flow with photoassimilates in the phloem, and a slow, directed intercellular polar auxin transport (PAT) (Adamowski and Friml, 2015). Polar transportation is the directional active movement of auxin molecules in plant tissues, which requires specific carrier proteins to complete. The combined activity of auxin influx and efflux carrier proteins results in local hormone maxima. Directional auxin gradients are required for essential plant developmental processes such as organ development, apical hook formation, gravitropism, hydrotropism

(bending to directional root growth), and phototropism (Enders *et al.*, 2015). Auxin polar transport is dependent on three transport proteins: the import carrier protein AUX/LAX (AUXIN1/LIKE-AUX1) family, the export carrier protein PIN (pin-formed) family, and the ABCB/MDR/PGP (ATP binding cassette B/Multidrug-resistance/p-glycoprotein) family, which performs both import and export functions (Blakeslee *et al.*, 2005).

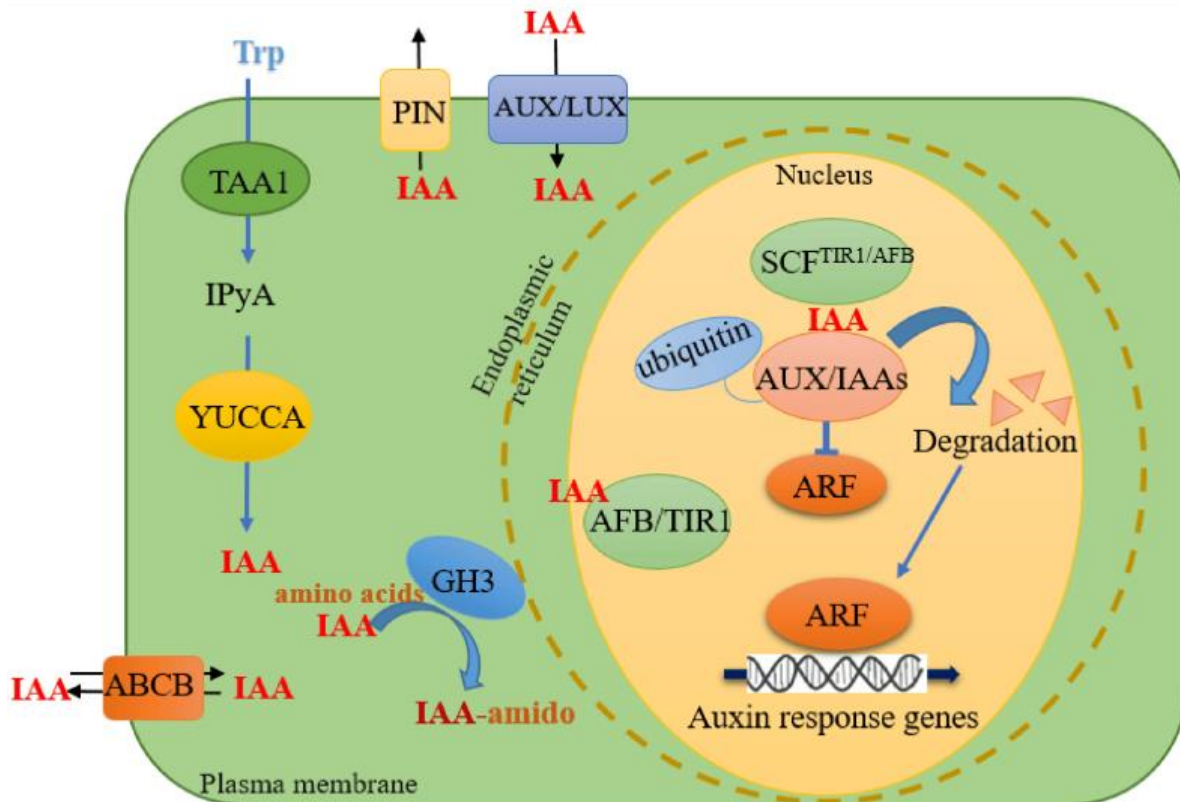


Figure 8. A simplified cellular model for auxin biosynthesis, transport, and signalling. TAA1 and YUCCA in the TAA/YUC pathway use IPyA to biosynthesize IAA from Trp. IAA is transported by the AUX1/LAX1, PIN, and ABCB proteins. The auxin-induced GH3 enzyme turns active IAA into inactive IAA-amido. Auxin causes ubiquitination and degradation of Aux/IAA proteins through SCFTIR1/AFB. The degradation of the Aux/IAA repressor restores ARF activity and activates the transcription of auxin-responsive genes. (Adapted from Zhang *et al.*, 2022)

1.10. Auxin signalling and involvement of clock components

Early studies suggesting the potential significance of circadian rhythmicity in polar transport in addition to endogenous auxin accumulation provided evidence for the link between auxin and the circadian clock (Shen-Miller *et al.*, 1973; Jouve *et al.*, 1999). Later genome-wide transcriptomic studies revealed that a particular group of genes involved in auxin biosynthesis, perception, and signalling were modulated by the clock (Covington *et al.*, 2007). It is worth noting that the transcriptional repressors AUX/IAAs and activators ARFs exhibit anti-phasic

oscillations. These anti-phasic transcriptional rhythms indicate that the circadian clock specifically times the activity of antagonistic auxin-related components. Later studies revealed a possible molecular link between the clock and auxin. Indeed, the clock-regulated MYB-like transcription factor REVEILLE 1 (RVE1) promotes auxin accumulation during the day by activating the expression of the auxin biosynthesis gene YUCCA8 (YUC8). This regulation is consistent with the circadian-gated enhancement of hypocotyl growth and development (Rawat *et al.*, 2009). Recent research also found that lateral root emergence varies in plants where the clock is not functioning properly or when the rhythmic expression of auxin-related targets is interrupted. In addition, recent findings have suggested that the circadian clock re-phases during lateral root emergence, regulating the expression of auxin-related genes (Voß *et al.*, 2015). TIME FOR COFFEE (TIC), a clock-related component, also regulates root meristem size (Hong *et al.*, 2013). The regulation is based on controlling the expression of the PIN-FORMED (PIN) genes, which are involved in auxin distribution, resulting in low auxin accumulation in *tic* mutant plant roots. The clock-auxin connection has been further elucidated by the discovery that the clock component CCA1 directly binds to the promoter of the ATP-dependent chromatin remodeling gene PICKLE (PKL), positively regulating its expression (Zha *et al.*, 2017). PKL regulates the trimethylation of H3 lysine 27 (H3K27me3) and activates the expression of INDOLE-3-ACETIC ACID INDUCIBLE 19 (IAA19) and IAA29, which are required for hypocotyl growth at 28 °C (Zha *et al.*, 2017). ELF3 most likely interacts with CCA1 to prevent binding to the PKL promoter, inhibiting CCA1-dependent activation of PKL expression (Zha *et al.*, 2017). Exogenous auxin treatment has only a minor effect on clock function, indicating that auxin signaling does not provide strong feedback to the clock (Covington *et al.*, 2007). However, auxin is essential for maintaining clock precision, particularly under constant light conditions (Hanano *et al.*, 2006). A further link between the circadian clock and auxin emerged from studies looking for factors important for the dynamic control of the circadian period and phase entrainment (Hearn *et al.*, 2018). An Ethyl

Methanesulphonate (EMS) mutagenesis screen discovered a period oversensitive to nicotinamide (*SONI*), which corresponded to the BIG gene, which encodes a Calossin-like protein required for normal auxin efflux (Gil *et al.*, 2001). In response to nicotinamide, the *sonI* mutant changes its ability to adjust to the circadian period (Hearn *et al.*, 2018).

1.11. Microtubules in response to phytohormones

Microtubules (MTs) are hollow tube-like structures discovered in dividing eukaryotic cells in the early 20th century and confirmed by high-resolution transmission electron microscopy images in 1963 (Slautterback *et al.*, 1963; Ledbetter *et al.*, 1963). MTs are hollow cylinders with a diameter of about 24 nm that are made up of β - and α -tubulin heterodimers that are not covalently linked and have a molecular mass of about 50 kDa each. Heterodimers align head-to-tail in 13 protofilaments, which make up the majority of MTs in eukaryotes and engage in lateral interaction. Every subunit has two GTP-binding sites. The non-exchangeable N-site of α -tubulin is buried longitudinally inside the tubulin dimer and cannot be hydrolyzed. In contrast, the E-site of β -tubulin can be exchanged because it is exposed on the terminal tubulin dimer surfaces of the MT plus end, which helps with the MT dynamics (Fosket *et al.*, 1992). MTs display two types of dynamic behavioral traits: dynamic instability and tread-milling. Tread-milling is a kind of directed growth in which tubulin dimers are specifically added at one end of the MT and gradually lost at the other, known as the plus and minus ends, respectively (Bisgrove *et al.*, 2004). The variability of MT plus end dynamics is referred to as dynamic instability. Whereas its stochastic loss destabilizes the end structure and causes a phenomenon of rapid shrinkage known as catastrophe, the presence of a GTP cap ensures steady MT growth. Following the so-called rescue (Sedbrook *et al.*, 2004) of restoring the GTP cap, the MT grows once more. Animal MT dynamics differ greatly from those of plants. While animal MTs reach the pause state for 60% of their lifetime, plant MTs are always in motion, and their moderately fixed interphase MTs only pause for about 10 % of the time (Shaw *et al.*,

2003; Ehrhardt *et al.*, 2006). During cell growth and development, MT and MF orientation can change due to abiotic (photoperiod, mechanical stimuli, temperature changes) and biotic (pathogen infection) factors.

Phytohormones play a crucial role in plant development by coordinating genetically programmed growth and cell division, ultimately determining the plant's phenotype. Molecular physiology focuses on establishing signalling cascade components, including signal generators, receptors, messengers, and intracellular targets, as well as signal transduction pathways. Plant cytoskeleton components, including microtubules (MTs), microfilaments (MFs), and associated proteins, play a crucial role in signal transduction. Intracellular stimuli cause rapid cytoskeleton reorganization, which impacts the activity of other signalling molecules (Chilley *et al.*, 2006). Plant organs, especially flowers and leaves, require localized growth controlled by auxins and directed growth dependent on MTs (Heisler *et al.*, 2010). Several research indicate that auxin-induced root organogenesis is preceded by MT rearrangement necessary for polar cell growth (Baluška *et al.*, 1996; Verbelen *et al.*, 2008). Transverse MT orientation is preferred for cell growth in favorable conditions, such as the presence of auxins or gibberellins, while longitudinal MT orientation is preferred in unfavorable conditions, such as long-term plant irradiation with visible light, late senescence, or growth inhibitors (Shibaoka, 1994). Cytokinins regulate plant, algae, and moss development. Cytokinins disrupt actin polymerization during root formation and plant gravitropic response (Kushwah *et al.*, 2011). Cytokines, auxins, and brassinosteroids promote differentiation of tracheary elements, leading to programmed cell death and lignification of secondary cell walls (Fukuda *et al.*, 2000). Secondary cell wall structure is influenced by MTs and MFs, which reorient the cellulose synthase complex in the plasmalemma from longitudinal to transverse in *Zinnia* xylogenic cells (Fukuda *et al.*, 2000). Cytokines can impact lignification and programmed cell death, which rely on cytoskeletal components.

ABA inhibited the growth of dwarf pea epicotyls and maize hypocotyls by causing MT orientation to change to longitudinal (Shibaoka, 1994). ABA treatment reduced the cell wall extensibility of maize coleoptiles by causing longitudinal deposition of cellulose microfibrils after cortical MT orientation (Shibaoka, 1994). ABA reduced MT abundance, suppressed coffee embryo cell growth, caused MT randomization, reduced DNA replication activity in the embryo axis, prevented β tubulin transcript accumulation, and impacted seed maturation (Da *et al.*, 2008). Additionally, ABA delayed the G2 transition of apple meristematic cells (Da *et al.*, 2008).

Ethylene is known to cause MT reorientation (Shibaoka, 1994; Baluška *et al.*, 1993; Roberts, *et al.*, 1985). Immunofluorescence was found in the epidermis and outer cortex of pea epicotyls and mungbean hypocotyls, marking the first instance. The majority of MTs were oriented transversely to the cell axis, with some oriented obliquely, helically, and rarely longitudinally. After treatment with ethylene, most MTs exhibited longitudinal or oblique orientation (Roberts, *et al.*, 1985). The study found that disrupting the parallel orientation of cortical MTs and cellulose microfibrils inhibited longitudinal elongation in pea epicotyls and mungbean hypocotyls while activating lateral expansion (Roberts, *et al.*, 1985). Jasmonic acid, ethylene, and salicylic acid trigger programmed cell death during the hypersensitive response. Pathogens on plant cell surfaces trigger jasmonate synthesis, which can reorganize cortical and transvascular MFs, transport secreted compounds to infection sites, and activate callose synthesis (Hardham *et al.*, 2007).

The cytoskeleton mediates phytohormone action on plant growth and development at the cellular and tissue levels. Plant growth regulators, including phytohormones, impact the organization of microtubules and actin microfilaments, which play a crucial role in coordinating cell division, growth, and differentiation. Additionally, phytohormones affect the expression of tubulin and actin genes.

1.12. Tubulin heterogeneity

Plants exhibit an extensive degree of functional diversity, building a variety of microtubule structures to enable them to adapt to different environmental conditions and developmental stages. Post-translational modifications (PTMs) and differential gene transcriptions that are coordinated both spatially and temporally are responsible for this tubulin heterogeneity.

1.13. Post-translational modifications of tubulin

Post-translational addition or removal of specific chemical groups produces tubulin isoforms. Tyrosination, acetylation, phosphorylation, poly-glutamylation, poly-glycylation, transamidation, and the inverse reactions have all been documented in plant systems. Tubulin's post-translational modifications are essential for controlling the stability, organization, and function of microtubules. This outlines the recent findings regarding the functional significance of tubulin PTMs and emphasizes the numerous cellular processes in which they are involved. Further studies on the interactions between various modifications and the regulatory mechanisms governing them will shed light on the intricate functions of tubulin PTMs in cellular physiology and pathology.

Plant tyrosination is by far the most common isoform (MacRae *et al.*, 1997). The last C-terminal amino acid in tubulins is tyrosine which is widely conserved. The enzymatic elimination of carboxypeptidase residue results in stable, long-lasting MTs, whereas tyrosinated MTs indicate the MT is relatively new (Aström *et al.*, 1992; Smertenko *et al.*, 1997). There are only a few tissue-specific detyrosinated tubulins. Detyrosination of tubulin is further brought on by auxin depletion, most likely by activating a tubulin tyrosine carboxypeptidase, which in turn affects the way a specific tubulin isoform accumulates (Wiesler *et al.*, 2002). The interaction between Lys60 and His283 can be disrupted by acetylation changes in Lys40 in α -tubulin. The stiffness of the MTs is decreased by the weakening of inter-protofilament contacts. In the end, they are increasing their resistance to

bending by mechanical means (Janke and Magiera, 2020). When compared to unmodified MTs, acetylated MTs exhibit greater stability. They are tolerant to drugs such as colchicine (LeDizet and Piperno, 1986; Piperno *et al.*, 1987) and nocodazole (De Brabander *et al.*, 1986). Recent studies have also reported that PTMs can occasionally interfere with MT-associated protein (MAP) binding (Howes *et al.*, 2014).

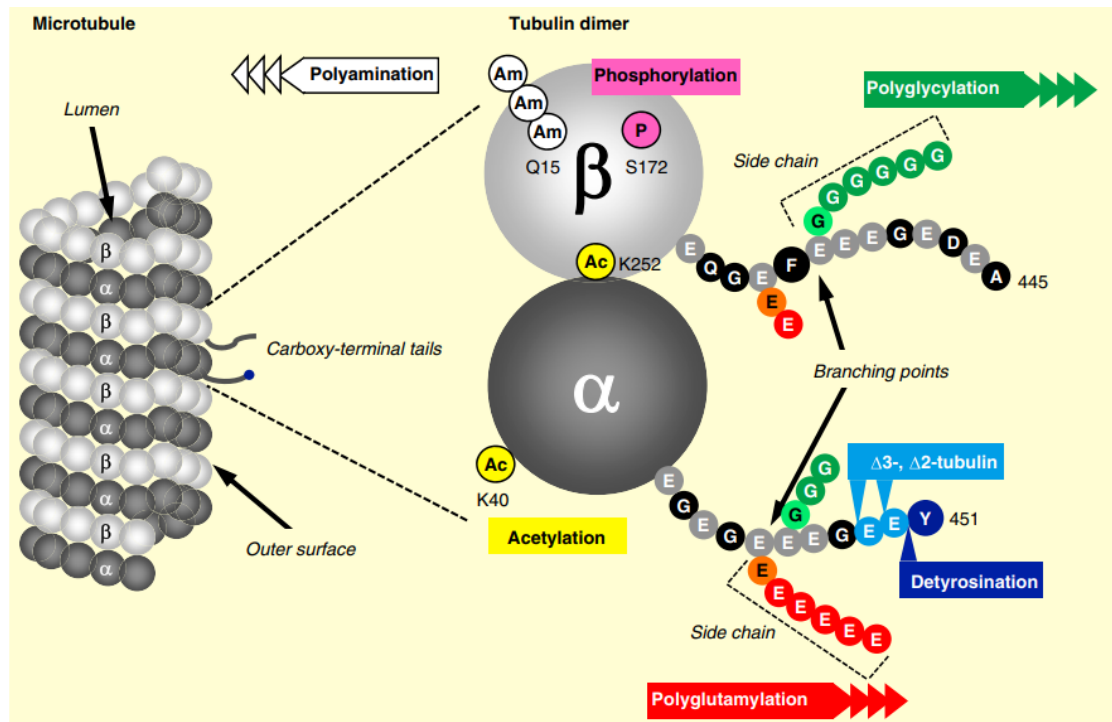


Figure 9. Molecular localization of tubulin posttranslational modifications. Dimers of α - and β -tubulin combine to form hollow tubes made up of thirteen protofilaments, which are the building blocks of microtubules. The luminal surface and the walls of microtubules are formed by the globular tubulin parts, and the outer surface of microtubules, which is the site of numerous MAP and motor binding, is ornamented by the carboxy-terminal tails. PTMs are located on different parts of the tubulin dimer: the K40 acetylation site of α -tubulin is located at the luminal surface of microtubules, and the K252 acetylation site of β -tubulin is located on the tubulin- α - β boundary. In the globular, folded region of β -tubulin, polyamination at Q15 and phosphorylation at S172 are present. These modifications may have an impact on the microtubule assembly and stability rates. The carboxy-terminal tails of α -tubulins are modulated by detyrosination/tyrosination, D2- and D3-tubulin, and both α - and β -tubulin's carboxy-terminal tails contain polyglutamylation and polyglycylation. The interactions between microtubules and related proteins are probably regulated by all changes to the carboxy-terminal tails. (Adapted from Magiera and Janke, 2020).

1.14. Role of tubulin in stress conditions

Plant MTs serve multiple functions beyond establishing and moving the division spindles. Plants have microtubule arrays that control cell shape based on external signals like light, gravity, and mechanical strains, as well as internal signals like hormones and developmental state (Nick, 1998). The microtubular response is a crucial step in plant morphogenesis, ensuring flexibility. Cortical microtubules in interphase cells direct the deposition of new cellulose

microfibrils, affecting the mechanics of the expanding cell wall (Giddings & Staehelin, 1991). Cell shape can be changed by manipulating cortical microtubules. The preprophase band marks the axis and symmetry of plant cell division, while the phragmoplast organizes the formation of the new cell plate after nuclear division (Breviario and Nick, 2000). MTs play a role in both cellular morphogenesis and stress response. Low temperature can cause disassembly, affecting the sensitivity of cold-sensitive calcium channels found that they play a crucial role in defending against fungal pathogens by directing secretion toward the penetration site (Mazars *et al.*, 1997; Kobayashi *et al.*, 1997). Whereas, microtubules are usurped by certain viruses as guiding tracks for cell–cell movement (Heinlein *et al.*, 1995).

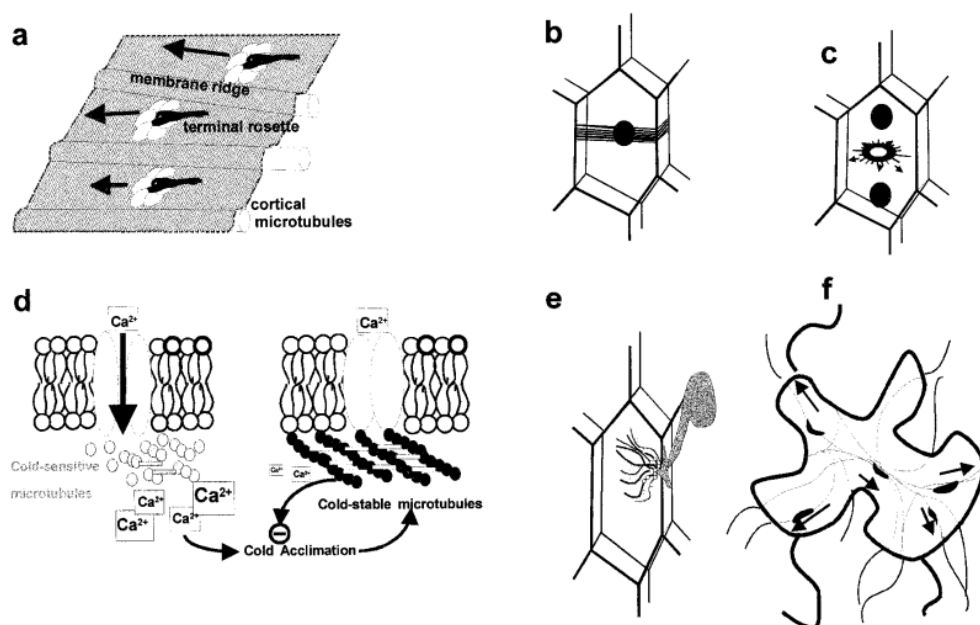


Figure 10. Microtubules serve various functions in plant morphogenesis and response to abiotic and biotic stresses. (a) Cortical microtubules regulate cellulose deposition. Cortical microtubules guide terminal rosettes of cellulose-synthesizing enzymes through the plasma membrane, forming microfibrils parallel to them. The transverse orientation of microtubules causes the transverse orientation of microfibrils, resulting in cell elongation. (b) The spindle is organized perpendicular to the microtubular preprophase band, which defines the axis of cell division. (c) The microtubular phragmoplast directs the transport of vesicles containing cell-wall matrix, regulating the formation of the new cell plate after mitosis. (d) Microtubules disassemble in response to cold, which increases the activity of cold-sensitive calcium channels. Cold-stable microtubule formation may modulate these channels' activity, resulting in a balanced cold response. (e) Microtubules, along with actin microfilaments, prevent fungal attack in resistant cultivars by directing vesicles containing callose and antifungal compounds to the penetration site. (f) Plant viruses use microtubules to guide cell-cell movement through the plasmodesmata. (Adapted from Breviario and Nick, 2000)

Research suggests that MTs, MAPs, and motor proteins rely on PTMs triggered by hormones, external stimuli, and developmental stages to function (Smertenko *et al.*, 2004; Del Duca *et al.*, 2009). PTM signatures function as 'molecular markers', becoming part of the tubulin code and

regulating a variety of local cellular functions. In plants, the cytoskeleton serves as a ‘low-temperature sensor’ (Mazars *et al.*, 1997; Abdrakhamanova *et al.*, 2003). Plant cellular mechanics is characterized by an extracellular signal that travels from the cell wall to the plasma membrane and then to the cytoskeleton (Akashi, *et al.*, 1990; Nguema-Ona *et al.*, 2007). A decrease in membrane fluidity caused by cold stress causes MT to disassemble and reorganize using cell wall proteins like xyloglycans (Akashi, *et al.*, 1990; Takeda *et al.*, 2002). Although the relationship between Ca^{2+} influx and MT depolymerization is complex, MT activity mediates Ca^{2+} channel activation, which leads to a brief increase in intracellular Ca^{2+} ion levels and downstream signaling events to express cold-induced genes (Mazars *et al.*, 1997; Breviario *et al.*, 2000). Additionally, MAPKs modify cortical MT organization by phosphorylating either tubulin or MAPs during the cold acclimation process (Koontz *et al.*, 1993; Durso *et al.*, 1994; Šamaj *et al.*, 2004).

1.15. Role of Ca^{2+} in Microtubule Dynamics in *P. patens*

Stresses such as drought, cold, and dehydration can cause an increase in calcium waves in vascular plant cells. However, it also affects lower plants such as *Physcomitrella patens*. Observing the entire plant in a single time-series acquisition revealed that different cell types were sensitive to osmotic stress, and Ca^{2+} waves originated from the basal part of the gametophore and propagated directionally to the top of the plant. Under similar conditions, the vascular plant *Arabidopsis thaliana* produced Ca^{2+} waves that propagated more quickly than those of *P. patens*. These findings indicated that systemic Ca^{2+} propagation occurs in plants even in the absence of vascular tissue, though the rates may differ (Storti *et al.*, 2018).

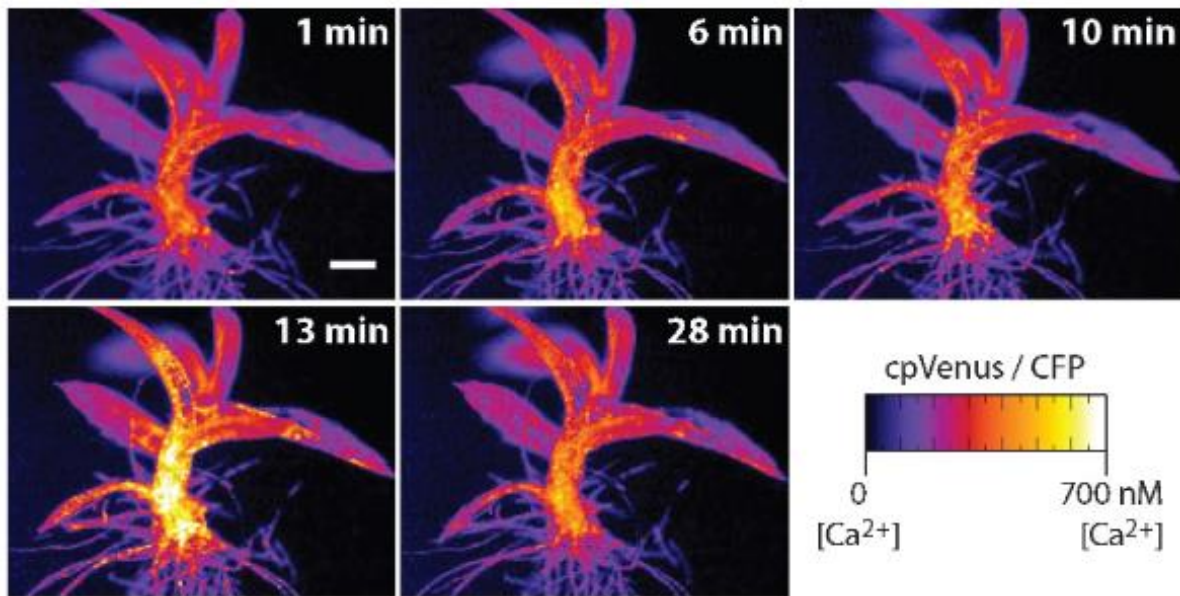


Figure 11. *In vivo* analysis of Ca²⁺ dynamics in response to osmotic stress throughout *P. patens* gametophores expressing CYT-YC3.60. Fluorescence ratio imaging was acquired during continuous perfusion with hyperosmotic (6 and 10 min) and hypoosmotic (1, 13, and 28 min) solutions. False colors represent the ratio of CP Venus fluorescence emission to CFP fluorescence emission at a given time point (Adapted from Storti *et al.*, 2018).

Studies also suggest that when the cell's calcium level increased, several proteins were activated. Proteins such as MDP-25 can destabilize the mitochondrial membrane. As a result, hypocotyl cell elongation inhibits growth. MDP-25 is primarily found in the plasma membrane, but when calcium levels rise, it dissociates and moves to the cytosol. It binds and destabilizes cortical MTs (Li *et al.*, 2011).

OBJECTIVES

All organisms on Earth possess the inherent ability to measure time through diurnal rhythms driven by the planet's 24-hour rotation. The fundamental periodicity, entrainment, temperature compensation, and oscillator mechanisms conveyed by the circadian clock which controls these rhythms are essential to its function. Although extensive research on *Arabidopsis thaliana* (*A. thaliana*) along with many crop plants has elucidated many aspects of the circadian clock, numerous variations in clock component organization and function remain to be deciphered. These variations are vital for plant sustainability and adaptation to diverse environmental conditions. Furthermore, the circadian clock's functions vary significantly during various abiotic and biotic stress conditions. In this study, we have tried to uncover the correlation between light signaling and auxin homeostasis with GIGANTEA (GI) influencing plant development. Light signal absorbed by phytochromes entrains the biological clock where a plant-specific nuclear protein, GI plays a role in integrating it. GI's involvement in circadian clock function, flowering time regulation, and various types of abiotic stress tolerance have been well-documented in recent years. However, the role of GI and its mechanism of interaction with other proteins regulating the overall growth and development of plants is yet to be understood. This study elucidates the evolutionary origin of GI from unicellular cyanobacteria to multicellular flowering plants by using an *in-silico* approach. Here, the role of GI in response to biotic stress with a hemi biotrophic pathogen i.e., *Fusarium oxysporum* (*F. oxysporum*) causing wilt disease in the plant is investigated at the molecular level comparing Col-0 WT with the *gi-100* mutant in *A. thaliana*. This project also investigates GI using the advanced error-free gene editing technique CRISPR-Cas9, aiming to eliminate off-target effects associated with traditional T-DNA mutants. The study re-evaluates GI's role in flowering and stress tolerance. Furthermore, we have also tried to design some possible candidate antibodies that are based on the hydrophilicity of GI and can detect the endogenous level of the protein. This research extends our understanding of GI's functions and its potential

role in stress tolerance. The role of Auxin Binding Protein 1 (ABP1) is re-evaluated using CRISPR-based mutants, demonstrating its involvement in root architecture, hypocotyl growth inhibition, and flowering time regulation under red light and other specific environmental conditions. ABP1's impact on phytochrome B (phyB) and GI transcript levels is also explored, shedding light on its role in stress tolerance, particularly in low-temperature conditions. Moreover, the correlation between red light signaling, auxin homeostasis, and root patterning is investigated by generating EMS mutagenized chemiluminescent ratio metric auxin sensor line and DR5::GFF line of *A. thaliana*. Finally, the functional significance of microtubule dynamics in stress adaptation is explored using the model plant *Physcomitrella patens* which lacks GI, a major clock component in higher plants. This study uncovers the role of microtubule dynamics in response to auxin, temperature stress, and calcium variations, highlighting its importance in stress adaptation. These collective findings provide valuable insights into plant circadian clocks, stress responses, and the evolutionary adaptation of plants, providing valuable insights for further research and potential agricultural advancements.

In this thesis, we have tried to focus on the following objectives:

1. *In-silco* analysis of GIGANTEA from an Evolutionary Perspective
2. Roles of GIGANTEA in Abiotic and Biotic Stress Tolerance
 - 2.1. To Re-evaluate the role of GIGANTEA in drought and salinity stress using the CRISPR-Cas9 genome editing tool
 - 2.2. To evaluate the role of GIGANTEA in biotic stress i.e., *Fusarium oxysporum* infection
3. Novel Role of Auxin Binding Protein1 (ABP1) in Plant Development and Abiotic Stress Tolerance
4. Effect of Monochromatic Light, Phytohormones, Temperature, and Ca²⁺ on Tubulin Modification and Organisation in *Physcomitrella patens*
5. Correlation of Phytochrome B and Auxin in Patterning the Root Development in *Arabidopsis thaliana*

CHAPTER 2

MATERIALS AND METHODS

CHAPTER 2: MATERIALS AND METHODS

2.1. *In-silco* Analysis of GIGANTEA from an Evolutionary Perspective

2.1.1. Protein sequence recovery

For various computational analyses, 123 full-length GIGANTEA (GI) protein sequences from various plant species were obtained in FASTA format from the NCBI (National Centre for Biotechnology Information) and OneKP databases. The study focused on analyzing GI at the protein level due to the unavailability of GI mRNA sequences of all the selected species in the different databases. Consequently, the investigation was conducted exclusively with protein sequences to facilitate the *in-silco* analysis of GI. The number of protein sequences with accession numbers and source organisms is given in Table 1.

SPECIES	ACCESSION NUMBER
<i>Abrus precatorius isoX1</i>	XP_027367356.1
<i>Abrus precatorius isoX2</i>	XP_027367357.1
<i>Abrus precatorius isoX3</i>	XP_027367360.1
<i>Aegilops tauschii</i>	XP_020192041.1
<i>Amborella trichopoda isoX1</i>	XP_020521564.1
<i>Amborella trichopoda isoX2</i>	XP_020521567.1
<i>Ananas comosus</i>	XP_020088620.1
<i>Anthoceros agrestis</i>	Data from oneKP database (Linde <i>et al.</i> , 2017)
<i>Arabidopsis lyrata</i>	AKX69184.1
<i>Arabidopsis thaliana</i>	NP_564180.1
<i>Arachis duranensis</i>	XP_015942477.1
<i>Arachis duranensis*</i>	XP_015967961.1
<i>Arachis hypogaea</i>	XP_025621154.1
<i>Arachis hypogaea*</i>	XP_025702258.1
<i>Arachis hypogaea isoX2</i>	XP_029148589.1
<i>Arachis hypogaea isoX2*</i>	XP_029151850.1
<i>Arachis hypogaea isoX3</i>	XP_025657109.1
<i>Arachis ipaensis</i>	XP_016174692.1
<i>Arachis ipaensis*</i>	XP_016204447.1
<i>Brachypodium distachyon</i>	XP_010230544.1
<i>Brassica napus</i>	XP_013696193.2
<i>Brassica rapa</i>	NP_001288824.1
<i>Brassica rapa isoX1</i>	XP_009115601.1
<i>Cajanus cajan</i>	XP_020224531.1
<i>Cajanus cajan isoX1</i>	XP_020239412.1

<i>Cajanus cajan isoX2</i>	XP_020239416.1
<i>Cajanus cajan isoX3</i>	XP_029124666.1
<i>Cannabis sativa</i>	XP_030492608.1
<i>Cannabis sativa*</i>	XP_030507774.1
<i>Capsella rubella</i>	XP_006306336.1
<i>Carica papaya</i>	XP_021902416.1
<i>Cicer arietinum isoX1</i>	XP_004496435.1
<i>Cicer arietinum isoX2</i>	XP_027189172.1
<i>Citrus sinensis</i>	XP_006473104.1
<i>Coffea eugenoides</i>	XP_027148263.1
<i>Coleochaete irregularis</i>	gnl onekp QPDY_scaffold_2006257
<i>Cucumis sativus</i>	XP_031743418.1
<i>Cucumis sativus isoX1</i>	XP_011659108.1
<i>Cucumis sativus isoX2</i>	XP_031744582.1
<i>Cucumis sativus isoX3</i>	XP_031744584.1
<i>Cucurbita pepo</i>	XP_023549953.1
<i>Cylindrocystis cushleackae</i>	gnl onekp JOJQ_scaffold_2008725
<i>Dendrobium catenatum</i>	XP_020681376.1
<i>Elaeis guineensis</i>	XP_010915066.1
<i>Elaeis guineensis*</i>	XP_010925341.1
<i>Eutrema salsugineum</i>	XP_006416160.1
<i>Glycine max</i>	NP_001239995.2
<i>Glycine max*</i>	XP_014624480.1
<i>Helianthus annuus isoX1</i>	XP_021992239.1
<i>Helianthus annuus isoX2</i>	XP_021992244.1
<i>Herrania umbratical</i>	XP_021285158.1
<i>Hevea brasiliensis</i>	XP_021644050.1
<i>Jatropha curcas</i>	XP_012073938.1
<i>Jatropha curcas isoX2</i>	XP_020535511.1
<i>Malus domestica</i>	XP_028957741.1
<i>Manihot esculenta</i>	XP_021601157.1
<i>Marchantia polymorpha</i>	BAO66507.1
<i>Medicago truncatula isoX2</i>	XP_024641844.1
<i>Medicago truncatula isoX1</i>	XP_003592048.2
<i>Medicago truncatula isoX3</i>	XP_024641850.1
<i>Morus notabilis</i>	XP_024022247.1
<i>Oryza sativa</i>	XP_015649578.1
<i>Panicum hallii</i>	XP_025816790.1
<i>Phalaenopsis equestris</i>	XP_020572459.1
<i>Picea abies</i>	AGH20049.1
<i>Picea asperata</i>	ANS12856.1
<i>Picea breweriana</i>	AND98324.1
<i>Picea glauca</i>	AND98320.1
<i>Picea jezoensis</i>	AND98247.1
<i>Picea likiangensis</i>	ADE32551.1
<i>Picea meyeri</i>	ANB44963.1
<i>Picea morrisonicola</i>	AHC92686.1
<i>Picea obovate</i>	AND98240.1

<i>Picea purpurea</i>	ADE32592.1
<i>Picea schrenkiana</i>	ADE32606.1
<i>Picea sitchensis</i>	ADM74041.1
<i>Picea smithiana</i>	AIE55309.1
<i>Picea wilsonii</i>	AGK38575.1
<i>Pinus hwangshanensis</i>	AIF76061.1
<i>Pinus massoniana</i>	AIF76056.1
<i>Pinus pinaster</i>	ATP62246.1
<i>Pinus sylvestris</i>	AFV79206.1
<i>Pinus taeda</i>	ATP62296.1
<i>Pistacia vera isoX1</i>	XP_031251681.1
<i>Pistacia vera isoX2</i>	XP_031251690.1
<i>Populus trichocarpa</i>	XP_002307516.2
<i>Populus trichocarpa*</i>	XP_006386299.2
<i>Prosopis alba isoX1</i>	XP_028763906.1
<i>Prosopis alba isoX2</i>	XP_028763910.1
<i>Prunus avium isoX1</i>	XP_021818210.1
<i>Prunus avium isoX2</i>	XP_021818214.1
<i>Prunus avium isoX3</i>	XP_021818215.1
<i>Prunus dulcis isoX1</i>	XP_034196939.1
<i>Prunus dulcis isoX2</i>	XP_034196940.1
<i>Prunus dulcis isoX3</i>	XP_034196942.1
<i>Prunus dulcis isoX4</i>	XP_034196943.1
<i>Prunus dulcis IsoX5</i>	XP_034196944.1
<i>Prunus dulcis isoX6</i>	XP_034196945.1
<i>Prunus persica isoX1</i>	XP_007199688.2
<i>Prunus persica isoX2</i>	XP_020426395.1
<i>Punica granatum</i>	XP_031394148.1
<i>Quercus suber</i>	XP_023907641.1
<i>Rhodamnia argentea</i>	XP_030549673.1
<i>Ricinus communis</i>	XP_025014064.1
<i>Rosa chinensis isoX1</i>	XP_024166286.1
<i>Rosa chinensis isoX2</i>	XP_024166288.1
<i>Selaginella moellendorffii</i>	XP_024528715.1
<i>Setaria italica isoX1</i>	XP_004968438.1
<i>Setaria italica isoX2</i>	XP_022682651.1
<i>Setaria viridis isoX1</i>	XP_034596606.1
<i>Setaria viridis isoX2</i>	XP_034596610.1
<i>Solanum lycopersicum</i>	XP_004237832.1
<i>Sorghum bicolor</i>	XP_021312623.1
<i>Spinacia oleracea</i>	XP_021849292.1
<i>Syzygium oleosum isoX1</i>	XP_030465408.1
<i>Syzygium oleosum isoX2</i>	XP_030465409.1
<i>Takakia lepidozoides</i>	gnl onekp SKQD_scaffold_2004946
<i>Vigna radiata</i>	XP_014513458.1
<i>Vigna radiata isoX1</i>	XP_014514134.1
<i>Vigna radiata isoX2</i>	XP_014514153.1
<i>Vigna unguiculata isoX1</i>	XP_027935547.1

<i>Vigna unguiculata isoX2</i>	XP_027935549.1
<i>Ziziphus jujuba</i>	XP_015886353.1

Table 1. Accession numbers of GIGANTEA were obtained from different species. The datasets are derived from different sources like NCBI and the OneKP database.

2.1.2. Construction of phylogenetic tree

Through the application of cladistic analysis, the hypothetical distribution of GI was identified across the plant kingdom. MSA was performed for the protein sequence listed in Table 1 by using Multiple Alignment using the Fast Fourier Transform (MAFFT) method in the MAFFT version 7 online web server. This server is used to execute multiple alignment programs for amino acid or nucleotide sequences. The maximum likelihood tree was constructed using the software IQ-TREE version 1.6.12 with a bootstrap value of 1000. The cladogram was visualized and extracted from i-TOL version 6 online software.

2.1.3. Multiple sequence alignment

The multiple sequence alignment of selected protein sequences *C. cushleackae*, *C. irregularis*, *M. polymorpha*, *A. agrestis*, *T. lepidozoides*, and *A. thaliana* was done using MEGA 11 software. The ClustalW program was used to perform multiple alignments of sequences.

2.1.4. Identification of coding region for conserved amino acid

Stretches of amino acids were manually selected from the MSA which showed conservation across the selected GI sequences. The Coding DNA Sequence (CDS) of GI in *A. thaliana* was obtained from NCBI with the accession number AF105064.1. The nucleotide sequence was then converted to amino acid sequence in MEGA 11. The corresponding coding region of the conserved stretches of amino acids was manually identified. The intron and exon sequences on the *GI* gene in *A. thaliana* were obtained from TAIR. The identified coding region of the conserved stretches of amino acids was traced back to respective exons. The gene structure was illustrated using Gene Structure Display Server (GSDS) version 2.0. GSDS is used for the

visualization of gene features such as the composition and position of introns, exons, and conserved elements.

2.1.5. Identification of conserved motifs and domains

The analysis of motifs was done using the MEME tool (<http://meme.sdsc.edu/meme/meme.html>), which was also used to search their protein family using the NCBI conserved domain database (CDD) (<https://www.ncbi.nlm.nih.gov/Structure/cdd/wrpsb.cgi>).

2.1.6. Prediction of Protein Secondary Structures and 3-D Modelling

The protein sequence of GI from *A. thaliana* (accession number NP_564180.1) was obtained from NCBI and was given as input in an online server like i-TASSER for 3-D model prediction.

The predicted secondary structures and 3-D model of GI were obtained.

2.2. Roles of GIGANTEA in Abiotic and Biotic Stress Tolerance

2.2.1. To Re-evaluate the role of GIGANTEA in drought and salinity stress using the CRISPR-Cas9 genome editing tool

2.2.1.1. Generation of null mutant seed line of GI using CRISPR-Cas9 genome editing tool

The null mutant of GI using the CRISPR-Cas9 genome editing tool is generated according to Dash. L., 2018. The method used in the generation of the *gi-C27* seed line, CRISPR mutant of GI is adapted from Dash. L., 2018, and is described briefly below.

a. Preparation of DH5α super-competent cells by Inoue method

DH5α bacteria obtained from glycerol stock were streaked onto LB-Agar plates devoid of any antibiotics and were then incubated at 37 °C for 12 hours (h). Following incubation, a single colony was selected after 24 h and introduced into 25 mL of LB broth, where it was allowed to proliferate for 6-8 hours at 37 °C with agitation at 220 rpm, constituting the primary culture. Strict sterile procedures were followed throughout, including the use of autoclaved solutions. Subsequently, aliquots of 10 mL, 4 mL, and 2 mL from the primary cultures were transferred into three separate 1 L flasks containing 250 mL of LB broth, and allowed to grow overnight (12 hours) at 18 °C. The following morning, the optical density (OD) of the cultures was assessed, and those with an OD₆₀₀ of approximately 0.55 were selected for further processing. The cultures were then centrifuged at 2500 g for 10 minutes (min) at 4 °C, the supernatant was discarded, and the pellet was resuspended in a pre-chilled Inoue transformation buffer. After centrifugation and resuspension, the cells were diluted in 20 mL of pre-chilled Inoue transformation buffer, and 1.5 mL of dimethyl sulfoxide (DMSO) was added to the culture. The mixture was dispensed into chilled microfuge tubes and subjected to rapid freezing in

liquid nitrogen, thus generating the frozen competent cells, which were subsequently stored in an -80 °C freezer.

b. Preparation of competent cells by CaCl₂ method

Freshly streaked colonies were initially introduced into a 10 mL LB broth devoid of antibiotics, followed by incubation at 37 °C overnight with agitation at 220 rpm. Subsequently, 10 mL of a starter culture was used to inoculate 1 L of LB medium, permitting growth until the optical density at 600 nm (OD₆₀₀) reached 0.3-0.4. The culture was promptly transferred to an ice bath and then dispensed into prechilled 250 mL centrifuge tubes. Following centrifugation at 3000 g for 15 mins at 4 °C, the supernatant was carefully removed, and the pellet was resuspended in 100 mL of ice-cold MgCl₂. The centrifugation step was repeated. After the second centrifugation step, the MgCl₂ solution was decanted, and the cells were resuspended in 200 mL of ice-cold CaCl₂. Subsequent centrifugation and resuspension steps were conducted, with the cells finally suspended in an 85 mM, 15 % glycerol solution. The culture was then aliquoted into microcentrifuge tubes and promptly frozen using liquid nitrogen before storage at -80 °C freezer.

c. Methodology for using CRISPR-Cas9 system: gRNA spacers and primer design

Upon accessing the CHOPCHOP welcome page (<https://chopchop.cbu.uib.no/>), the model organism *Arabidopsis thaliana* (*A. thaliana*) was selected and AGI (*Arabidopsis* Genome Initiative) identifier corresponding to the target gene, in this instance *GIGANTEA*, was inputted for editing. The results page provided a genome browser visualization of the queried region, illustrating gene models and potential guide RNA (gRNA) spacers. Beneath this visualization, a table listed all potential gRNA spacers in the region, ordered from optimal to suboptimal, based on various criteria. The ranking of spacers considered parameters such as GC content, the presence of a guanine (G) at the first position (required for transcription initiation), the number of mismatches with off-target sequences, and the number of predicted off-targets.

Spacers were scored based on these criteria, with penalties applied for deviations from optimal conditions. Spacers with scores below 20 were favored, with a preference for those starting with a G if necessary. Upon selection of a spacer, its reverse complement sequence was provided. Additionally, specific overhangs for primer ligation were recommended, with distinct sequences for the forward and reverse primers, facilitating subsequent molecular manipulations.

d. Cloning procedure

Primer annealing commenced with the preparation of a 10X annealing buffer containing 100 mM Tris- HCl (pH 7.5), 1.5 M NaCl, and water up to 10 mL. A master mix was then prepared by combining 100 μ M oligo Forward and 100 μ M oligo Reverse stocks with 5 μ L annealing buffer and 35 μ L water, resulting in a final concentration of 10uM for annealed oligos. The master mix underwent incubation at 95 °C for 3-4 min followed by gradual cooling overnight using a heat block.

Subsequent ligation of spacers into the pAtU6-26: gRNA plasmid involved its digestion using the BbsI restriction enzyme, facilitated by a digestion mix comprising plasmid DNA, NEB 2.1 buffer, and BbsI enzyme. After a 1.5-hour incubation at 37 °C, the digested products were visualized on a 1 % agarose gel and purified using a mini-column.

For ligation, a mixture containing plasmid DNA (150 ng), annealed spacer (0.5 μ L), T4 ligase buffer (1 μ L), T4 ligase (1 μ L), and water were prepared. This ligation mix underwent incubation either at room temperature for 2 hours or overnight at 4 °C. The ligated product was subsequently transformed into competent bacteria.

Colonies resulting from transformation were subjected to colony PCR using RNA spacer-specific primers to amplify an approximate 670 bp amplicon. Plasmids were further verified

for spacer insertion by BbsI digestion, which abolishes cleavage sites upon spacer integration, thereby impeding plasmid opening upon digestion.

e. Colony PCR using Taq Polymerase

For colony PCR, a master mix was prepared according to the specifications outlined below (Table 2). Individual bacterial colonies were selected and suspended in the master mix using a sterile toothpick within a sterile environment. Following the suspension, the same toothpick was utilized to streak the colonies onto fresh LB agar plates supplemented with appropriate antibiotics. Each streak was meticulously labeled and incubated at 37 °C for bacterial growth spanning 4-5 h. Thermocycling conditions were established in the PCR machine according to predefined parameters (Table 3). Following the PCR completion, the samples were mixed with 2 µL of NEB's 10X violet gel loading dye and subsequently loaded into wells of a 1 % agarose gel prepared with 1X TAE buffer containing 1X EtBr. This procedure enabled the visualization of PCR products for subsequent analysis.

Component	25 µL Reaction	Final Concentration
Standard Taq Reaction Buffer 10X	2.5 µL	1X
10 mM dNTPs	0.5 µL	200 µM
10 µM Forward Primer	0.5 µL	0.2 µM
10 µM Reverse Primer	0.5 µL	0.2 µM
Template DNA	variable	<1,000 ng
Taq DNA Polymerase	0.125 µL	1.25 units/50 µl PCR
Nuclease-free water	to 25 µL	

Table 2. Components used in the master mix preparation for colony PCR

STEP		TEMP	TIME
35 cycles	INITIAL DENATURATION	95 °C	3 minutes
	DENATURATION	95 °C	30 seconds
	ANNEALING	45 °C	60 seconds
	EXTENSION	68 °C	2 minute/kb
	FINAL EXTENSION	68 °C	10 minutes
	HOLD	4 °C	

Table 3. Thermocycling conditions in the PCR machine for colony PCR.

f. Cloning of multiple guides

To target multiple sequences simultaneously, a strategy was employed wherein several spacers were cloned onto the same T-DNA. This involved the digestion of the plasmid containing guide1 with SpeI and KpnI, while the plasmid containing guide2 was digested with XbaI and KpnI.

For Digestion Mix 1: 2ug of plasmid containing the RNA guide 1 (pAtU6-26: spacer1-gRNA), 2 uL of Cutsmart Buffer, 1 µL of KpnI-HF, 1 µL of SpeI, 1uL of rSAP and water up to 20 µL

For Digestion Mix 2: 2ug of plasmid containing the RNA guide 2 (pAtU6-26: spacer2-gRNA), 2 µL of buffer CutSmart, 1 µL of KpnI-HF, 1 µL of XbaI

Both mixes were incubated for approximately 1.5 hour at 37 °C. The resulting digests were then analyzed on a 1 % agarose gel, with the desired bands excised and purified using a QIAGEN mini-column.

A ligation mix was subsequently prepared using the purified linearized plasmid, comprising approximately 150 ng of opened plasmid (KpnI/SpeI), a molecular ratio of 1:3 for guide2 (KpnI/XbaI), T4 ligase buffer (1 µL), T4 ligase (1 µL), and water, to reach a total volume of 10 µL. The ligation mixture underwent incubation either at room temperature for 2 hours or overnight at 4 °C, after which it was transformed into competent bacterial cells. Colonies resulting from transformation were screened by PCR using spacer1 sense and spacer2 antisense primers, with an expected amplicon size of approximately 670 base pairs. Plasmids were further validated through restriction digestion with SacI, which excised the guides from the plasmid, resulting in fragments of around 700 base pairs per guide. In cases involving a plasmid containing four guide cassettes, additional digestion with PvuI-HF was necessary alongside SacI to aid in the separation of the insert band (approximately 2500 base pairs) from the plasmid

(approximately 2900 base pairs). This process could be iterated to facilitate the cloning of multiple guides into the same plasmid.

g. Final ligation in pGreen CRISPR

The cassette containing the guide(s) RNA(s) from pBSK: AtU6-26: gRNA was finally cloned in pGreen CRISPR (a gift from Dr. Chloe-Zubieta's lab, European Synchrotron Radiation Facility, Grenoble, France) together with the cassette containing Cas9 sequence from pGreen: CamV: CoCas9 in one cloning step.

pBSK: AtU6-26: gRNA(s) digestion: 2 µg of plasmid 2 µL of buffer CutSmart, 1 µL of either KpnI-HF, 1 µL of SbfI and water up to 20 µL

pGreen CRISPR digestion mix 1: 2 µg of plasmid, 2 µL of buffer CutSmart, 1 µL of either EcoRI-HF, 1 µL of SbfI and water up to 20 µL

pGreen CRISPR digestion mix 2: 2 µg of plasmid, 2 µL of buffer CutSmart, 1 µL of either KpnI-HF, 1 µL of EcoRI-HF, 1 µL of rSAP, and water up to 20 µL

The digestion mixtures were incubated for ~ 1.5 h at 37 °C. The digestion was checked on 1 % agarose gel, and the band was cut out and purified on a mini-column. gRNA cassette was around 700 bp per guide, Cas9 cassette was 5.5 kb.

Ligation mix: ~ 150 ng of opened plasmid, 1:3 molecular ratio of gRNA cassette, 1:3 molecular ratio of Cas9 cassette, 1.5 µL T4 ligase buffer, 1 µL T4 ligase and water up to 15 µL

The ligation mix was incubated at room temperature for 2 hours or overnight at 4 °C followed by transformation in competent bacterial cells. Plasmids were verified by restriction with SalI and EcoRI, cutting out both cassettes. Plasmids were now ready to be transformed into competent *Agrobacterium* cells.

h. Agrobacterium Transformation Protocol

Preparation of Competent Cells:

A 200 mL volume of Luria-Bertani (LB) broth was inoculated with 1 mL of an overnight culture of the designated strain of *Agrobacterium*. Subsequently, the inoculated broth was incubated at 28 °C with vigorous agitation until the cells reached the logarithmic growth phase, as indicated by an optical density at 550 nm (OD₅₅₀) ranging between 0.5 and 0.8 nm. Following growth, the cells were sedimented via centrifugation at 5000 rpm for 10 minutes at room temperature. It is noteworthy that *Agrobacterium* exhibits a longer sedimentation time compared to *Escherichia coli*. The resulting cell pellet was subjected to a wash procedure using sterile 1X Tris-EDTA (TE) buffer. Following washing, the cells were resuspended in a volume equivalent to 0.1X of the original LB culture volume. Subsequently, aliquots of either 250 µL or 500 µL were dispensed into microcentrifuge tubes. These aliquots were promptly snap-frozen in liquid nitrogen and subsequently stored at -70 °C for future use.

Transformation and Recovery:

Upon thawing on ice, competent *Agrobacterium* cells (utilizing 250 µL per transformation reaction) were combined with DNA, comprising either 10 µL of standard *E. coli* miniprep DNA or 1-5 µg of CsCl-purified DNA. Following a 5 mins incubation on ice, the mixture was briefly immersed in liquid nitrogen for 5 mins, then incubated for an additional 5 mins in a 37 °C water bath. Subsequently, 1 mL of Luria-Bertani (LB) medium was added to each tube, thoroughly sealed, and placed on a rocking table at room temperature for 2 to 4 hours. After incubation, the cells were promptly collected via brief centrifugation in a microcentrifuge, and then evenly spread onto two LB agar plates supplemented with the appropriate antibiotic for the T-DNA vector. The plates were then incubated for 2 days (d) at 28 °C. Following colony growth, the colonies were subjected to re-streaking onto new

plates, which were further incubated for 2 days at 28 °C. The resultant plate was sealed with Parafilm in a sterile environment and preserved as a stock plate. Subsequent steps involved the growing of small liquid cultures derived from the re-streaked colonies, followed by miniprep procedures coupled with Polymerase Chain Reaction (PCR) to confirm the presence of the plasmid DNA. Finally, glycerol stocks were prepared from the selected clones and maintained at -20 °C for long-term storage.

i. Floral dip methods of transformation

The growth protocol for *Arabidopsis thaliana* involved planting 10-15 plants per 4-inch pot and subjecting them to long-day conditions with 16 hours of light exposure per day. Adequate fertilization was provided to promote the development of large rosettes. To encourage further inflorescence growth, initial inflorescence shoots were promptly removed upon emergence. Transformation readiness was typically achieved within one week when secondary inflorescence shoots reached approximately 3 inches in height, signaling the optimal stage for floral dip transformation.

For the floral dip method, a liquid culture of *Agrobacterium* carrying a suitable binary vector was prepared three days before plant transformation. The culture, cultivated in LB medium supplemented with antibiotics targeting both Ti and T-DNA plasmids (Rifampicin and Kanamycin), was incubated at 28 °C with vigorous agitation. Subsequently, a 200 mL volume of YESB medium was inoculated with 1 mL of the preculture and incubated for an additional 24 hour under similar conditions. Before dipping, plant watering was ceased to allow the soil to partially dry, reducing the risk of soil displacement during the process. *Agrobacterium* cells were pelleted by centrifugation at 6000 rpm for 10 mins at room temperature, yielding a distinctive pink cell pellet. The pellet was resuspended in 400 mL of infiltration medium, followed by the addition of 200 µL of Silwet L-77 (0.02 %) to the culture. The suspension was then transferred to a suitable vessel for plant dipping, such as a lid from a disposable pipette

tip box or a 100 mL beaker. Inflorescence shoots of plants, inverted within their pots, were immersed in the suspension for approximately 30 seconds to ensure adequate coverage. Contamination of soil with *Agrobacterium*, characterized by an unpleasant odor, was carefully avoided. Following dipping, pots were placed on their sides in a plastic nursery flat and covered with a transparent lid for 24 hours. After this period, the cover was removed, and plants were returned to their normal growth conditions. Approximately three weeks post-transformation, seeds were harvested for further analysis.

j. Selection of positive seeds by sorting under Fluorescence microscope

Upon seed harvest, meticulous segregation into individual tubes was conducted to prevent seed mixing. Subsequently, either a glass petri plate or a cavity slide was selected, and seeds were meticulously dispersed across its surface. Utilizing a toothpick or dissection needle, the seeds were arranged to form a single layer. The container was then cautiously positioned over an inverted fluorescence microscope configured with a Fit-C filter set at an intensity of 50/100. Seeds emitting a GFP signal were discerned and delicately isolated using a toothpick, which was moistened with water before seed segregation. The positive glowing seeds were carefully selected using the dampened tip of the toothpick, ensuring exclusive picking of glowing seeds while avoiding non-glowing ones. This approach obviated the need for a laborious BASTA/Hygromycin selection step, thereby streamlining the seed selection process. Such precision in seed selection facilitated efficient identification and isolation of GFP-expressing seeds for further experimentation and analysis.

2.2.1.2. Genotyping and generation of homozygous lines

Fifty seeds exhibiting eGFP expression were selected, planted on soil pots, and subjected to vernalization for 48 hours at 4 °C under dark conditions. The pots were shifted to white light Long Day conditions (LD), i.e., 16-hour light and 8-hour dark. The germinated seedlings were

further used to isolate DNA (DNeasy Plant Mini kit from Qiagen) from the leaves of these transformant plants. PCR was performed using primers complementary to the genomic targets. The PCR product was further visualized in the 1% electrophoresis gel. The seed lines that showed the successful mutation in exon 2 and exon 7 were further selected and named according to the exons targeted for the mutation and pots namely *gi-C272*, *gi-C278*, and *gi-C2710*.

Following the selection of transformed seeds from the F₀ generation, which were hemizygous, they were planted in soil to generate homozygous GI-CRISPR mutant lines. The resulting transgenic plants from the F₀ seeds were designated as the F₁ generation (F₁ transgenic plants). Seeds obtained from the F₁ transgenic plants exhibiting eGFP signals were specifically chosen and labeled as F₁ generation seeds with a hemizygous genotype (R/0). Subsequently, F₂ generation plants were grown from the F₁ generation seeds sown in the soil, allowing for self-pollination and subsequent seed harvest, named the F₂ generation seeds. To confirm the homozygosity of the seedlings, a random selection of 100 seeds from F₂ generation plants was observed under a fluorescent microscope. The phenotype of the F₂ generation seedcoats was categorized as either eGFP positive or eGFP negative. Among the observed seedcoats, approximately 74 exhibited eGFP signals (glowing seeds), while the remaining 26 did not display eGFP signals (non-glowing seeds). The observed ratio of eGFP positive to eGFP negative seedcoats was determined to be 3:1, consistent with Mendel's law of segregation, supporting a phenotypic ratio of 3:1 (homozygous dominant: heterozygous recessive). Consequently, the homozygous glowing seeds identified through the screening process were further selected and allowed to undergo self-pollination. The resultant bulked seeds were designated as the F₃ generation seeds, ensuring that all seeds within this generation were homozygous for the desired trait.

Further to confirm the mutation in the homozygous lines of *gi* mutants generated from CRISPR-Cas9 technology, a genetic screening was performed. For this study, a T-DNA insertional mutant of *GI* i.e., *gi-100*, and the newly developed CRISPR mutants of *GI* i.e., *gi-C272*, *gi-C278* and

gi-C2710 along with the wildtype Col-0 was used. Since all the CRISPR mutants of *gi* showed similar phenotype and genotype, we proceeded with only *gi-C2710* (which is further called *gi-C27* based on its position of mutation only) mutant for further studies. RNA was extracted from the 7-day-old seedlings of Col-0, *gi-100*, and *gi-C27* according to the standardized protocol in the RNeasy Plant Mini Kit by Qiagen. The RNA was quantified in a nanodrop (Thermo Fisher) and calculated accordingly for cDNA synthesis. 1000 ng of synthesized RNA, 4 μ L of Buffer RT mix, 1 μ L of RT enzyme, and water up to 20 μ L were used to prepare the cDNA mix. The cDNA synthesis of these lines was done using an iScript cDNA synthesis kit by Biorad (Catalog No: 1708890) according to the protocol mentioned in the kit. PCR was performed using the synthesized cDNA of these lines and the resultant PCR product was run on 1 % electrophoresis gel.

2.2.1.3. Plant materials and growth conditions

Seeds of *Arabidopsis thaliana* was surface sterilized using 70 % and 100 % ethanol for 5 mins each respectively followed by air drying for 2 hours inside the laminar hood. The sterilized seeds were sown on MS media (Himedia: Catalog No: PT100-1L). For adult plant phenotyping and stress physiology, unsterilized seeds were sown on sterilized soil. Both the plates and soil pots were subjected to cold stratification (4 °C, dark) for 48 hours. The plates or pots were then shifted to white light (WL) plant growth chambers (model-AR36, Percival, USA) set to 18 °C or 22 °C and 70 % relative humidity. The growth chambers were programmed to provide cycles of 16 hours light and 8 hours dark (LDs) or 8 hours light and 16 hours dark (SDs). For monochromatic red (R), far-red (FR), and blue (B) light irradiation, seedlings were grown in E-30 LED chambers (Percival, USA) maintained at 22 °C temperature and with 70 % relative humidity. For Dark experiments, the plates were covered with aluminum foil after the germination induction and kept in the WL Percival chamber. The intensities of incident lights were 80 μ mol/m²/s for WL, 50 μ mol/m²/s for R, 6 μ mol/m²/s for FR and 30 μ mol/m²/s for B.

2.2.1.4. Next-generation sequencing

7-day old seedlings of *gi-C27* grown under LD conditions were harvested using liquid nitrogen and stored at -80 °C till the samples were sent to Genotypic company (<https://www.genotypic.co.in/>) for whole genome sequencing. The protocol followed in the company is as follows

- DNA was extracted from the plant tissue using a Qiagen DNeasy Plant mini kit (Cat no. 69104). The plant sample (~ 100 mg) was disrupted to a fine powder in liquid nitrogen using a pestle and mortar. The cells were lysed by adding AP1 buffer and incubated at 65 °C for 30 mins. The lysate treated with RNase A (Catalog No: 210107683; MP Biomedicals) was incubated at 65 °C for 20 mins. Buffer P3 was added to the lysate, inverted mixed, and incubated on ice for 10 mins. The lysate was transferred to a QIA shredder spin column placed in a 2 mL collection tube and centrifuged at 10,000 rpm for 2 mins. The filtrate was transferred to a new microcentrifuge tube and 1.5 volumes of buffer AW1 was added. The lysate mixture was loaded into a DNeasy mini spin column placed in a 2 mL collection tube and centrifuged at 10,000 rpm for 1 min. The remaining column wash steps were performed according to the manufacturer's protocol. DNA was eluted from the column with 10 mM Tris-Cl pH 8.0. The concentration and purity of genomic DNA were quantified using a Nanodrop Spectrophotometer (Thermo Scientific; 2000) while the integrity of DNA was observed on agarose gel electrophoresis. DNA concentration was quantified using the Qubit dsDNA HS assay kit (Catalog No: Q32854). The samples that passed the quality assessment with optimal yield and concentration were deemed suitable for Illumina and Nanopore library preparation (Table 4).

Sample ID	Nanodrop QC						Qubit QC					
	ng/ul	260/280	260/230	Volume (μl)	Yield (ng)	Volume loaded on gel (μl)	Qubit Conc. (ng/ul)	Volume (μl)	Yield (ng)	QC Purity	QC Yield	QC Integrity
SO_9677_B_giC27	55.2	1.92	2.04	50	2760	2	40.2	50	2010	Optimal	Optimal	Intact band + smear

Table 4. Estimated DNA Concentration and Purity

- Library construction was carried out at Genotypic Technology using QIASeq FX DNA Library Preparation protocol1 (Catalog No: 180475) following the manufacturer's instructions.

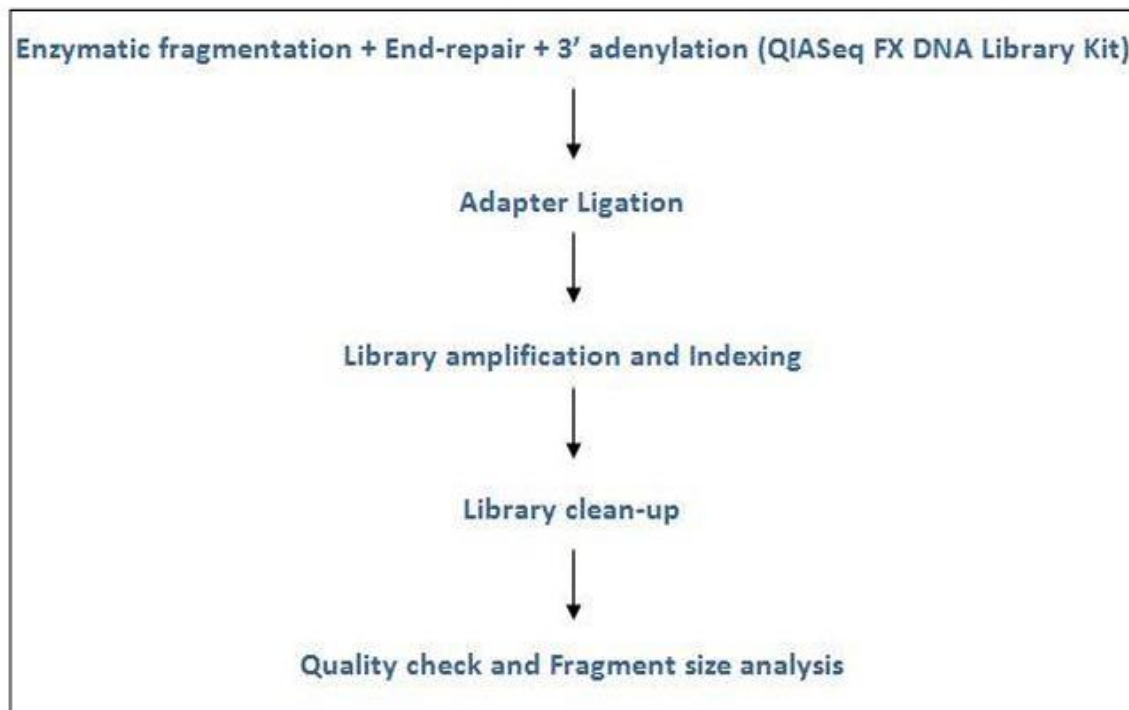


Figure 12. Workflow for QIASeq FX DNA Library Preparation

The FX Enzyme Mix provided in the QIASeq FX DNA kit was used to enzymatically fragment, end-repair, and A-tail 50 ng of Qubit quantified DNA in a one-tube reaction. The end-repaired and adenylated fragments were subjected to adapter ligation, whereby index incorporated Illumina adapter was ligated, to generate a sequencing library. The library was subjected to 6 cycles of Indexing-PCR (Initial Denaturation at 98 °C for 2 min, cycling (at 98 °C for 20 sec, 60 °C for 30 sec, 72 °C for 30 sec) and final extension at 72 °C for 1 min) to enrich the adapter-tagged fragments. Finally, the amplified libraries were purified using Sera-MagTM Select

beads (Cytiva, Catalog No: 29343057) followed by a library quality control check. Illumina-compatible sequencing libraries were quantified by Qubit fluorometer (Thermo Fisher Scientific, MA, USA) and its fragment size distribution was analyzed on Agilent 2200 TapeStation. The Illumina-compatible sequencing libraries for the samples showed an average fragment size of 394 bp and sufficient concentration for obtaining desired sequencing data. Table 5 mentions the concentration obtained for each library and index used.

Sample ID	Qubit Conc. (ng/ul)	Vol (ul)	Yield (ng)	Barcode 1	Index Sequence 1	Barcode 2	Index Sequence 2
SO_9677_B_giC27	32	10	320	UDI046	CCTCCGGTT	UDI046	AGCTCAG ATA

Table 5. Description of libraries

- The libraries were sequenced on Illumina NovaSeq 6000 (Illumina, San Diego, USA) using 150 bp paired-end chemistry following the manufacturer's instructions. The data obtained from the sequencing run was de-multiplexed using Bcl2fastq2 software v2.20 and FastQ files were generated based on the unique dual barcode sequences. The sequencing quality was assessed using Commander3 v2.0.20 software. The adapter sequences were trimmed and bases above Q30 were considered. Low-quality bases were filtered off during read pre-processing and used for downstream analysis.
- A total of ~22 million Illumina sequenced paired-end reads were generated for plant samples i.e., SO_9677_B_giC27. The raw Illumina reads were trimmed for adapter removal and filtered to retain high-quality reads using the Trimalore-v0.4.04 tool. The adapter clipped, high-quality reads were mapped against reference *Arabidopsis thaliana* genome sequence (*Arabidopsis thaliana* Refseq Assembly accession: GCF_000001735.4) using BWA-v0.7.55 aligner. Processing of the alignment data was performed using Samtools-v1.9.6. The PCR duplicate reads were removed from aligned data using the PICARD-v1.1027 tool. Variant

identification was carried out using the bcftools 1.128 pipeline composed of a set of utilities that can call and manipulate variant calls in the Variant Call Format (VCF). Finally, the annotation was carried out for all the identified variants using SnpEff-v3.3h9, which can quickly identify and classify disease-relevant variants. The complete bioinformatics workflow is given in Figure 13 below

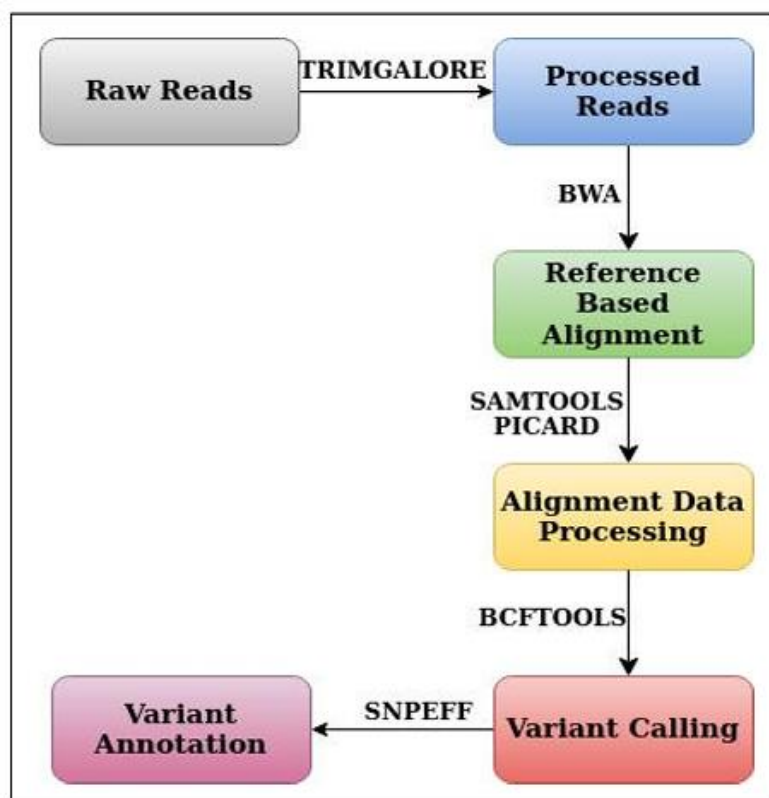


Figure 13. WGS bioinformatics workflow

- The result data was then accessed through the cloud and analyzed using the Snap gene software to identify the mutation that occurred in *gi-C27*.

2.2.1.5. Phenotypic measurements

Flowering time was evaluated as the number of days from germination to visible emergence of the bolt and the number of total rosette leaves at the bolting. The number of leaves in the plants was measured every 6 days intervals till it reached the adult stage. The experiment was conducted in 3 biological replicates and the mean of 10 individual plants were taken. For hypocotyl and root length measurement, the seedlings were allowed to grow in different light

conditions i.e. Dark, White, Red, Far-red, and Blue after 2 days of cold stratification followed by 6 hours of germination induction. The plates were then transferred to different light chambers (WL, D, R, FR, and B) for light treatment at 22 °C for 7 days. The seedlings were grown in filter papers or MS media, depending on the experiment. A vertical position was maintained for studying the root length of the seedlings. The seedlings were scanned and hypocotyl as well as the root length was measured using ImageJ software. The experiment was done in 3 biological replicates and the mean of 20 individual seedlings were taken.

2.2.1.6. Generation of antibody

A new method was adopted to make GI antibodies which include hydropathy index, primary sequence blast, and based finding tools as described in Singh K., 2017. The peptide having a single post-translational modification was eliminated. Based on these 6 candidate antisera against GI protein were made. Hydrophilic stretches are the most accessible epitope of protein molecules and they are in contact with the aqueous region. The epitope sites were designed from a web-based software tool called NHLBI-AbDesigner6 by selecting the above-mentioned criteria and were sent to Euro-Gene for antibodies developed in rabbits and guinea pigs.

2.2.1.7. Protein extraction

Protein extraction was done from different seed lines: Col-0, *gi-100*, 35S::GI, GI::GI-TAP, and *gi-C27*. Seeds were surface sterilized and sown on an MS media plate, then cold stratification was given for 48 hours. The plates were then transferred to WL Percival cabinets under diurnal LD conditions and allowed to grow for 7 days. The samples were harvested after 7 days at ZT 12 using liquid nitrogen and kept at a -80 °C freezer for further use. The samples were then ground in a chilled mortar and pestle using liquid nitrogen. The ground samples were subjected to protein extraction buffer [100 mM Tris-Cl pH 6.8 (Catalog No: 1610716, Biorad), 1 mM Ethylenediaminetetraacetic acid (EDTA, Catalog No: 4005-OP, Sigma-Aldrich), 8 M Urea

(Catalog No: U5378, Sigma-Aldrich), 5 % Sodium dodecyl sulfate (SDS, Catalog No: GRM6218, Himedia), 0.00125 % Bromophenol blue (Catalog No: MB123, Himedia), 2 % β -Mercaptoethanol (Catalog No: 516732, Sigma-Aldrich), 2 mM Sodium Orthovanadate (Catalog No: S6508, Sigma-Aldrich), 2 mM Sodium Fluoride (NaF, Catalog No: GRM7502, Himedia), 1:200 Protease Inhibitor Cocktail (PIC, Catalog No: P9599, Sigma-Aldrich) and 50 μ M MG-132 (Catalog No: 474791, Sigma-Aldrich)] by vortexing them for 10-15 mins. Pre-heated (98 °C) 5X laemmli buffer was added to the ground sample containing extraction buffers and boiled on a thermomixer at 14000 rpm for 10 mins at 98 °C. Centrifugation was done at 13,000 rpm for 5 mins at room temperature, supernatant was taken and pellets were discarded. This step was repeated two times. The produced supernatant was stored at a -20 °C freezer and used later for protein quantification by the Amido black method, SDS PAGE, and Western blotting.

2.2.1.8. Protein Quantification

The protein was quantified using the amido black method by preparing amido black solution using 0.1 % Amido Black 10B dye, 45 % water, 10 % acetic acid, and 45 % methanol. A standard curve was prepared using serial dilution of BSA. 10 μ L of extracted protein along with 250 μ L of amido black dye was taken in a 1.5 mL Eppendorf tube and vortexed for 1 min. the solution was incubated for 10 minutes at room temperature. The solution was then centrifuged at 13000 rpm for 10 mins at room temperature. The supernatant was discarded and the pellet was washed with 250 μ L of washing solution (90 % Methanol and 10 % acetic acid) by vortexing and centrifuging at 13000 rpm for 5 mins. The washing step is repeated until the solution appears clear (devoid of any blue pigment). The supernatant was then discarded and the pellets were kept for air drying for ~1 hour. After the pellets were completely air-dried, 250 μ L of 0.2 M NaOH was added to the Eppendorf tubes and the solution was vortexed followed by centrifugation for 2 mins at 5000 rpm. OD was measured at 595 nm in an ELISA plate

reader (Biorad). The protein concentration of the unknown samples was calculated from the standard curve derived from the known BSA concentrations.

2.2.1.9. Western Blotting

SDS denaturing 8 % gels were prepared according to (Panigrahy, 2004). Nearly 25 µg of protein for each sample was loaded in acrylamide gels and run for approximately 2.5 hours at 80 V till the protein ladder was completely separated followed by transferring onto PVDF membranes (Immobilon-P; EMD Millipore) for western blotting using semi-dry transfer system (Bio-Rad, Model No: 1703940). The membrane was blotted against all the generated 6 possible anti-GI monoclonal primary antibodies (provided by the Euro gene company) overnight at 4 °C followed by incubation with secondary antibody anti-rabbit polyclonal HRP (supplied by Sigma Aldrich, Catalog No: A0545-1ML) for 2 hours at room temperature. Detection was done using an ECL substrate reagent (supplied by Bio-rad, Catalog No: 1705060). Coomassie brilliant blue staining was done and used as a loading control. The experiment was reproduced thrice with biological replicates.

2.2.1.10. Soil stress assay

Approximately 10 days before bolting the plants (Col-0, *gi-100*, *gi-C27*) grown in soil pots under LD and SD conditions were subjected to drought and salt stress. Drought stress was given with direct withdrawal of water for 10 days. Salt stress in the same number of plants was imposed by treating the plants with 200 mM saline water (NaCl) for 10 days. Control plants were kept for both drought and salt stress where normal watering was continued. The leaves of control and stressed plants were harvested randomly from the plants on the day of stress termination (10th day). Furthermore, relative water content (RWC), malondialdehyde (MDA), Chlorophyll estimation, carotenoid estimation, catalase (CAT), and guaiacol peroxidase (POX) activity was estimated along with the histochemical and quantitative detection of H₂O₂ and O₂⁻

in both stressed as well as unstressed plants.

2.2.1.11. Histochemical and quantitative detection of O_2^-

Detection of superoxide radical (O_2^-) was done by NBT staining following the modified method of Rao and Davis (1999) in leaf segments of both stressed and control plants. The leaf segments were immersed and infiltrated under vacuum with 3 mg/mL nitro-blue tetrazolium (NBT) staining solution in 10 mM potassium phosphate buffer (pH 7.0) staining solution containing 10 mM NaN_3 for 30 mins at room temperature. Stained leaves were bleached in acetic acid: glycerol: ethanol (1:1:3 v/v) solution at 100 °C for 5 mins, and stored in glycerol: ethanol (1:4 v/v) solution until photographed.

2.2.1.12. Relative water content (RWC)

Leaf segments were excised from fully expanded leaves and fresh weight (FW) was recorded. The segments were then allowed to float on deionized water for 3 hours and the turgid weight (TW) was recorded. The leaf segments were dried at 80 °C for 24 hours or the leaves were completely dried and dry weight (DW) was recorded. Finally, RWC was calculated according to Smart and Bingham (1974).

2.2.1.13. Lipid peroxidation assay

Lipid peroxidation was measured according to Heath and Packer (1968). In the whole process malondialdehyde (MDA) amount was determined by the thiobarbituric acid (TBA) reaction. 0.1 g of fresh leaf samples were homogenized with 2.5 mL of 0.25 % TBA containing 10% TCA (trichloroacetic acid). The homogenate was boiled for 30 min at 95 °C and centrifuged at 10,000 g for 10 mins. Absorbance was recorded at 532 nm and MDA content was thus calculated.

2.2.1.14. Anti-oxidative enzyme assays to determine ROS scavenging activity

The extraction of the enzymes was done as suggested by Larkindale and Huang (2004). 0.1 g leaves were harvested and ground to a fine powder in liquid nitrogen using a chilled mortar and pestle. The powder was homogenized in 2 mL of chilled phosphate buffer (100 mM, pH 7.0) containing 1 % polyvinylpyrrolidone (PVP) and 1 mM EDTA and centrifuged at 4 °C for 15 mins at 10,000 g. The above process was repeated twice and the supernatant was separated. The freshly collected supernatant was further used for the assay of enzyme activity.

2.2.1.15. Catalase (EC. 1. 11. 1. 6)

Catalase activity was estimated by the UV method of Aebi (1984). The reagents were 100 mM H₂O₂ and 50 mM potassium phosphate buffer (pH 7.0). For the assay, 100 µL of diluted enzyme extract was taken, and 1.0 mL of potassium phosphate buffer was added to it. The reaction was initiated by adding 100 µL of H₂O₂. The change in absorbance was recorded at 240 nm at an interval of 30 s for 2 mins. The enzyme activity was expressed as units mg⁻¹ protein min⁻¹. One unit can be defined as a 0.1 decrease in absorbance.

2.2.1.16. Guaiacol peroxidase (EC. 1.11.1.7)

Guaiacol peroxidase (POX) activity was measured by estimating the oxidation of guaiacol (Saha *et al.*, 2016; Rao *et al.*, 1996). The reagents were 100 mM potassium phosphate buffer (pH 7.0) containing 1 mM EDTA, 10 mM H₂O₂, and 10 mM guaiacol. For the assay, 100 µL diluted enzyme extract was taken and 0.9 mL of potassium phosphate buffer along with 0.1 mL of guaiacol were added. The reaction was initiated by adding 100 µL of H₂O₂. The change in absorbance was recorded at 30-seconds intervals for 2 mins at 470 nm. An increase of 0.1 absorbance has been taken as a unit. The enzyme activity was expressed as units mg⁻¹ protein min⁻¹.

2.2.1.17. Statistical analysis

All the statistical analyses used in this study were performed using GraphPad Prism version 8.0.1. A test of significance was performed to analyze grouped column graphs using two-way ANOVA analysis with multiple comparisons (Tukey and Sidak) and student's unpaired T-test. Error bars represent the standard error of the mean (SEM).

2.2.2. To evaluate the role of GIGANTEA in biotic stress i.e., *Fusarium oxysporum* infection.

2.2.2.1. Plant growth conditions

The seeds of *Arabidopsis thaliana* Columbia 0 (Col-0) ecotype, mutant and overexpressor lines of GIGANTEA i.e., *gi-100*, *gi-1*, GI::GI-TAP and 35S::GI (Berns *et al.*, 2014) respectively were vernalized at 4 °C for 48 hours in pots containing soil followed by growth under white light in controlled plant growth chambers (Model No: AR36, Percival, USA) till the end of the experiment. As all the genotypes used in this study vary substantially in their growth, morphology, and flowering time (Mishra and Panigrahi, 2015), an initial growth period of 15 days under LD conditions (i.e., 16h light and 8 h dark, 22 °C) was adapted (Figure 55A) to obtain a synchronized growth morphology among them with comparable number of rosette leaves (Figure 55B, upper panel) before fungal inoculation. On 16th day, plants were shifted to SD conditions (8-hour light and 16-hour dark, 22 °C) and all the sampling, as well as experiments, were done under SD conditions to focus the study mainly on the vegetative stage of the plant (Figure 55A). An entrainment period of 5 days was imposed immediately after shifting the plants to SD before the fungal inoculation on the 20th day. At the time of infection, all the 3 genotypes (Col-0, *gi-100*, *gi-1*) had nearly 14 ± 2 rosette leaves (Figure 55B).

2.2.2.2. *F. oxysporum* infection and pathogenesis

The pure culture of *F. oxysporum* was taken by aseptically punching out 5 mm of *F. oxysporum* fungal colony from stock. It was allowed to grow for 15 days in a 250 mL conical flask containing 100 mL of Potato Dextrose Broth (PDB) along with the inoculum, in a shaker maintained at 25 °C and 60 rpm (Rath and Patnaik, 2018). After the incubation period, the culture along with the fungal mycelia was separated using a sterile nylon cloth, and the density of the conidial suspension was counted using a hemocytometer till it attained the concentration of $\sim 6.5 \times 10^6$ spores / mL. A few drops of this suspension culture were taken and stained with trypan blue solution to ensure viability and to visualize the structure of fungal hyphae (Figure 55E).

Three weeks old plants were infected with the *F. oxysporum* culture either at the roots by dropping ~ 200 μ L of the conidial suspension in pots or ~ 10 μ L of inoculum on the adaxial surface of the leaves at dawn. Plants with a similar amount of PDB medium without fungal culture were used as the control. To better ensure the pathogenicity, the infection was induced both in the roots and leaves of the plant. A similar method of leaf infection caused due to *F. oxysporum* has already been reported (Wang *et al.*, 2021). The incidence of the spread of disease as necrotic lesions was first observed on the 5th day of infection (data not shown). Leaves from infected and uninfected plants were sampled 24 hours post-infection (HPI) and 9th days post-infection (DPI) at ZT-0, as many defense-related genes were highly induced in the dawn (de Leone *et al.*, 2020). The experiments were repeated three times with similar results.

The leaves of the infected and uninfected plants after 9-DPI were studied using a Carl Zeiss stereo microscope (Model No: Stereo Discovery. V20) equipped with a 5.8X magnification and Axiocam 305 camera to obtain the total area of infection. The disease severity percentage was calculated using Image J (version: ImageJ 1.53a). Ten different morphologically similar leaves were chosen from 6 plants of each category to analyze the disease severity. The experiment was repeated three individual times.

2.2.2.3. RNA Extraction and Transcript Level Validation

Plant tissues (roots and leaves) were snap-frozen with liquid nitrogen and immediately stored at -80 °C till further use. Total RNA was extracted from ~500 mg plant samples using RNeasy Plant Mini Kit (supplied by Qiagen, Catalog No: 74136). One µg of total RNA was used to obtain cDNA using Reverse Transcription Super-mix (supplied by Bio-Rad, Catalog No: 1708840). For relative transcript levels, quantitative RT-PCR (qRT-PCR) was carried out using the Bio-Rad laboratories' CFX384 Touch™ Real-time detection system, following the manufacturer's instructions and iTaq™ universal SYBR green super mix as done previously (Kumar, 2021). Primer Quest tool (Integrated DNA Technologies, Inc., USA) was used to design gene-specific primers used in the qRT-PCR (Refer Primer List). All reactions were carried out in hardshell 384-well PCR plates (supplied by Bio-Rad, Catalog No: HSP3805). ACTIN was used to normalize transcript levels. Absolute expression is calculated according to the $2^{-\Delta\Delta C_t}$ method (Pfaffl, 2001). Relative transcript levels are represented in the graph, which is obtained by normalizing the absolute values to 1 for the uninfected respective samples. The qRT-PCR reactions were done in triplicates from three biological replicates. Data represented as the mean \pm SEM.

2.2.2.3. Immuno-blotting and detection of GIGENTEA protein levels

For western analysis, the leaf samples of the GI::GI-TAP line were collected after 24-HPI at ZT-8 of the photoperiod. GI::GI-TAP transgenic line has an endogenous GI promoter tagged with a Tandem Affinity Purification reporter (David *et al.*, 2006). For the detection of GI protein, the above-mentioned line was taken instead of Col-0, as GI protein levels at ZT-8 under SD conditions in Col-0 were barely detectable. The leaves were crushed in a mortar and pestle using liquid nitrogen. Total protein was extracted from 100 mg of leaf sample using protocol according to Khaleda *et al.*, (2017). and further used for quantification, SDS-PAGE, and western blotting. The quantification of the protein was done by Amido black assay (Panigrahy,

2004). SDS denaturing 8 % gels were prepared according to (Panigrahy, 2004). Nearly 25 µg of protein for each sample was loaded in acrylamide gels and run for approximately 2.5 hours at 80V till the protein ladder was completely separated followed by transferring onto PVDF membranes (Immobilon-P; EMD Millipore) for western blotting using semi-dry transfer system (Bio-Rad, Model No: 1703940). The membrane was blotted against anti-GI monoclonal primary antibody (unpublished data) overnight at 4 °C followed by incubation with secondary antibody anti-rabbit polyclonal HRP (supplied by Sigma Aldrich, Catalog No: A0545-1ML) for 2 hours at room temperature. Detection was done using an ECL substrate reagent (supplied by Bio-rad, Catalog No: 1705060). ImageJ software was used for densitometric quantification of western blot and normalization with the loading controls against Coomassie brilliant blue staining. The experiment was reproduced thrice with biological replicates.

2.2.2.4. Tissue fixation and histochemistry

Leaves were fixed with FAA (Formalin-Acetic-Alcohol) substituted with methanol (45 % methanol, 10 % formaldehyde, 5 % Glacial acetic acid, and 40 % distilled water) using a portable vacuum pump for 15-20 mins. During the initial 15 minutes of fixation, the vacuum was drawn and released several times to preserve the cell organelles properly. Roots were incubated at 96 °C for 1 min in 10 % (w/v) KOH (Banhara *et al.*, 2015; Mishra *et al.*, 2018). Roots were stained with propidium iodide (1:1000 c phosphate buffer). The plant tissues were incubated with 10% KOH for 30 minutes followed by 15 minutes of incubation with alkaline H₂O₂. The tissues were then exposed to 2 % HCl for 2 mins. Trypan blue (0.1 %) visualized root cell wall morphology after fungal invasion. Fluorescent DNA stains such as DAPI (4', 6-diamidino-2-phenylindole) (1:1000 v/v phosphate buffer) and Acridine orange (0.1 %) were used for staining the viable nuclei of stomatal guard cells.

2.2.2.5. Light and confocal microscopy

A phase contrast microscope (Model No: 59556, Nikon, Japan) equipped with a digital sight DS-Fi1 camera (Nikon) was used for imaging. For confocal microscopy, a confocal microscope system (Leica SP8, Leica Application Suite*3.5.5.19976) operating on an inverted microscope (DMI8), equipped with 63× NA 1.3 glycerol immersion lenses (Leica, Wetzlar, Germany), was used for imaging. High-resolution Z stack images were recorded with 4-fold line averaging and a 1.00 μm step size. Along with concurrent transmitted light images, fluorescence images were collected from 420-500, 500–550, and 620-650 nm using excitation at 405, 488, and 552 nm. All image series were captured with the same imaging conditions. Image intensities were quantified from image stacks in ImageJ (FIJI installation of version 1.47v, National Institute of Health, Bethesda, MD, USA). Images were prepared according to standard brightness and contrast settings in Photoshop (version CS4, Adobe Systems, San Jose, CA, USA) and ImageJ.

2.2.2.6. Chlorophyll fluorescence assessment

The effect of *F. oxysporum* on photosynthetic electron transport in Col-0 and *gi-100* mutant lines of *A. thaliana* was estimated through OJIP transient analysis to analyze the photosystem activities in stress conditions. The chlorophyll fluorescence was measured in the top 3rd leaf using a Multifunction Plant Efficiency Analyzer (M-PEA, Hansatech Instruments Ltd, UK). White actinic light of 3000 $\mu\text{mol photons m}^{-2} \text{s}^{-1}$ was used for the fluorescence induction, which was recorded at wavelengths around 685 nm. The energy fluxes were calculated as per the equations of the JIP test using Image Lab Biolyzer HP3 software. The plant leaves were allowed to acclimatize to dark conditions for at least 30 min before the fluorescence signal was measured. The measurements were taken in the middle of the upper surface of fully developed leaves. The translated values of biophysical parameters of OJIP transients like the quantum yields (ϕPo , ϕRo , ϕDo , ψEo); specific activities per reaction center (ABS/RC, DIO/RC, TRO/RC, ETO/RC, REO/RC); performance indexes (PI) and structure-function indexes (VJ, SM and N) were plotted based on Strasser *et al.*, (2004). Abbreviations of the formulas used are

compiled in Table 6. Measurements were done in at least ten different plants for each treatment with three leaves from each plant. The OJIP curve was created using the mean values in each condition.

Technical fluorescence parameters	Meaning
$t_{max}=T_{Fm}$	Time needed to reach F_m
$F_0=F_{50\mu s}=O$	Minimum fluorescence intensity at 20-50 μs
$V_j=2ms=J$	Relative Variable Fluorescence At J Step; $V_j=(F_j-F_0)/F_m-F_0$
$V_i=30ms=I$	Relative Variable Fluorescence At I Step; $V_i=(F_i-F_0)/F_m-F_0$
$F_M=P$	Maximum fluorescence intensity
$FV = F_M-F_0$	Maximum variable fluorescence
$V_t = (F_t-F_0)/FV$	Relative variable fluorescence
$M_0 = (\Delta V/\Delta t) 0 \approx 4(F_{0.3ms}-F_{0.05ms})/FV$	Initial slope (in ms ⁻¹) of the O-J fluorescence rise
$S_m = Area/FV$	Normalized area between the OJIP curve and the line $F = F_M$, which is a proxy of the number of electron carriers per electron transport chain
Efficiencies and quantum yields	
$\delta R_0 = \psi R_0/\psi E_0 = RE_0/ET_0$	Efficiency with which an electron from PQH ₂ is transferred to final PSI acceptors
$TR_0/ABS = \phi P_0 = FV/FM$	Maximum quantum yield of primary PSII photochemistry
$\phi E_0 = ET_0/ABS = \phi P_0 \times \psi E_0$	Quantum yield of electron transport from QA to PQ
Specific energy fluxes (per active PSII)	
$ABS/RC = (M_0/VJ)/\phi P_0$	Apparent antenna size of an active PSII
$TR_0/RC = M_0/VJ$	Maximum trapped excitation flux per active PSII
$ET_0/RC = (M_0/VJ) \times \psi E_0$	The flux of electrons transferred from QA to PQ per active PSII
$RE_0/RC = (M_0/VJ) \times \psi R_0$	The flux of electrons transferred from QA to final PSI acceptors per active PSII
$DI_0/RC = ABS/RC - TR_0/RC$	The flux of energy dissipated in processes other than trapping per active PSII
Quantum efficiencies, flux ratios	
ϕP_0	Quantum yield of the QA reduction $\phi P_0 = (1-F_0)/FM = TR_0/ABS$
ϕE_0	Quantum yield of the electron transport beyond QA $\phi E_0 = (1-F_0/FM) \psi_0 = ET_0/ABS$
Ψ_0	Probability that a trapped excitation is used for electron transport beyond QA. $\psi_0 = 1-VJ = ET_0/TR_0$
Performance Index and derived parameters	
PIABS	Performance Index on absorption basis. $PI_{abs} = RC/ABS [\phi P_0/(1-\phi P_0)] [\psi_0/(1-\psi_0)]$
$PI_{ABS,total} = PI_{ABS} \times [\delta R_0/(1-\delta R_0)]$	Total performance index on absorption basis

Table 6. The definition of energy fluxes and fluorescence transients' parameters were used in the OJIP test. These parameters are used to analyze the 'test' (<1 s) chlorophyll a fluorescence transient (Strasser *et al.*, 2004, Stirbet *et al.*, 2018)

2.2.2.7. Leaf temperature analysis

The uninfected and infected plants post 9-DPI were used for studying the plant temperature. The plants were kept in a dark room keeping the FLUKE Infra-red Camera (Model No: Ti450 PRO) equidistant i.e., 40 cm away from the plants. The thermal images were analyzed using the SMART VIEW software version 4.8. 20 different parts of the plant showing the highest temperature were specifically selected using the software and the temperatures were noted down. Temperatures from a minimum of 10 plants from each biological replicate were analyzed and averaged to generate leaf temperature data.

2.2.2.8. Phytohormones estimation

The plant leaf samples (~300 mg) were collected at 24-HPI using liquid nitrogen and grounded using tissue-lyser (Tissuelyser II manufactured by Retsch, Qiagen) and kept in lyophiliser overnight. Defense phytohormones were estimated according to (Vadassery *et al.*, 2012) with some modifications. Briefly, lyophilized samples (~ 20 mg) were extracted in 1 mL of methanol containing 40 ng mL⁻¹ of D6-jasmonic acid, (HPC Standards GmbH, Cunnors dorf, Germany), 40 ng mL⁻¹ D4-salicylic acid, 40 ng mL⁻¹ D6-abscisic acid, and 8 ng mL⁻¹ of jasmonic acid [13C6] isoleucine conjugate as internal standards. The homogenized samples were mixed in a shaker for 30 mins and centrifuged at 14,000 rpm for 20 mins at 4 °C. The supernatants were collected, and the homogenates were again extracted with 500 µL methanol and centrifuged. The supernatants were taken out and mixed with the previous extracts. All steps were performed at 4 °C. The combined extracts were subjected to vacuum evaporation at ambient temperature and re-suspended in 500 µL of methanol. Samples were analyzed on Exion LC (Sciex ®) UHPLC system using formic acid (0.05 %) in water as mobile phase A and acetonitrile as mobile phase B. Separation was attained on a Zorbax Eclipse XDB-C 18 column (50 x 4.6 mm, 1.8 µm, Agilent) coupled with a triple Quadrupole-trap MS/MS system (Sciex 6500+) in negative ionization mode. The flow rate was 1 mL min⁻¹ and elution profile was as follows: 0-0.5 min: 5 % B; 0.5-9.5 min: 5 to 42 % B; 9.5-9.51 min: 42 to 100 % B; 9.51-12 min: 100 % B and 12.1-

15 min: 5% B. Scheduled Multiple-reaction monitoring (MRM) is used to precisely observe analyte parent ion → product ion with detection window of 60 sec according to Vadassery *et al.*, 2012. Phytohormones were quantified relative to the signal of their corresponding internal standard concentrations.

2.2.2.9. Statistical analysis

All the statistical analyses used in this study were performed using GraphPad Prism version 8.0.1. For the test of significant differences, two-way ANOVA analysis with multiple comparisons (Tukey and Sidak) and student's unpaired T-test were used to analyze grouped column graphs. Error bars represent the standard error of the mean (SEM).

2.3. Novel Role of Auxin Binding Protein1 (ABP1) in Plant Development and Abiotic Stress Tolerance

2.3.1. Plant growth conditions and treatments

Two *abp1* CRISPR-Cas9 generated knockout lines of ABP1, namely *abp1-C1* (Gao *et al.*, 2015) and *abp1-C2* in Col-0 background were used in this study. The *abp1-C1* line harbored a 5-bp deletion in the first exon of ABP1 and resulted in a frameshift with the introduction of a stop codon (Gao *et al.*, 2015). The *abp1-C2* line was received from Professor Klaus Palme's group, generated using CRISPR technology, and was shown to be a functional null for ABP1 (unpublished data). Surface sterilized seeds of *Arabidopsis thaliana* Columbia 0 (Col-0) ecotype, *abp1* mutant lines i.e. *abp1-C1* and *abp1-C2* were sown on square plates with full Murashige and Skoog (MS) medium supplemented with 1 % (w/v) sucrose and 0.8 % (w/v) Phytoagar (pH 5.9) and vernalized at 4 °C for 48 hours. Seeds were germinated and grown either at 22 °C or at 18 °C under a long day (LD, 16 hours light and 8 hours dark) or short day (SD, 8 hours light and 16 hours dark) photoperiod conditions and irradiated with different light conditions (dark, white, red, far-red, blue). For exogenous auxin treatment, seeds were directly germinated on MS medium supplemented with 10 mM of 1-Naphthaleneacetic acid (1-NAA, active form of auxin) (Catalog No: PCT0809, Himedia), 10 mM of 2-Naphthaleneacetic acid (2-NAA, inactive form of auxin) (Catalog No: N4002, Sigma) and 20 nM of synthetic auxin 2,4-Dichlorophenoxyacetic acid (2,4-D) (Catalog No: PCT0825, Himedia) and grown for 7 days followed by seedling phenotype analysis. LED chambers (Percival Scientific Inc. Model No. E-30LEDL3) were used with red ($30 \mu\text{mol m}^{-2} \text{s}^{-1}$, 660 nm), far-red ($30 \mu\text{mol m}^{-2} \text{s}^{-1}$, 730 nm) and blue ($30 \mu\text{mol m}^{-2} \text{s}^{-1}$, 460 nm). Simultaneous irradiations of blue and red light were also done using the above two monochromatic light panels. LED chambers were maintained at 22 °C in the LD or SD cycle. Light intensity and wavelength were measured by SpectraPen LM 510 (PSI Instruments, Drásov, Czech Republic). For pot experiments, after 2-days of the

vernalization period, the soil pots containing seeds were transferred to either LD or SD conditions in controlled plant growth chambers (Model No: AR36, Percival, USA) irradiated with white light ($50 \mu\text{mol m}^{-2}\text{s}^{-1}$) at 18 °C and 22 °C till the end of the experiment. The flatness of the leaves (leaf epinasty) was determined as discussed earlier by Kozuka *et al.*, 2013. The ratio of the straight-line distance between the two edges of the leaf blade to the actual width of the leaf blade along the curved surface was then determined. For seedling phenotype analysis, 7 days old seedlings were used for scanning as described in (Kumari *et al.*, 2019) using an HP Scanjet G4010 Flatbed scanner. The root and hypocotyl lengths were measured using ImageJ software (<https://github.com/imagej/ImageJ>). To impose dehydration stress, plants were exposed to water withheld (WW) differently at 22 °C or 18 °C. Plants grown at 22 °C were subjected to WW for 5 days at 15 days after germination. In parallel, plants grown at 18 °C were subjected to WW for 10 days at 40-day old stage. The difference in the pattern of WW and age of the plant at 22 °C and 18 °C was done due to the slower metabolism rate and longer flowering time in case of low-temperature conditions. Leaves of stressed and unstressed plants were sampled for physiological and biochemical analyses (i.e., relative water content (RWC), leaf temperature analysis, lipid peroxidation assay, carotenoid estimation, enzyme assays, and histochemical detection of superoxide radicals).

2.3.2. Physiological and Biochemical tests

2.3.3. Carotenoid content

Leaf samples (~25 mg) were incubated with 3 mL of 80 % acetone for 48 hours at 4 °C in the dark followed by centrifugation at 13000 rpm for 5 mins. The absorbance (A) of supernatants was recorded at 645 nm, 663 nm, and 480 nm. Estimation of carotenoids was done according to Manasa *et al.*, (2023).

2.3.4. Relative water content (RWC)

Leaf segments were excised from the top 4th expanded leaves and fresh weight (FW) was recorded. The segments were floated on deionized water for about 3 hours and turgid weight (TW) was recorded. The leaf segments were dried at 60 °C for 24 hours and dry weight (DW) was recorded. RWC was calculated using the formula

$$\text{RWC} = \{(\text{FW}-\text{DW}) / (\text{TW}-\text{DW})\} \times 100; \text{Where: FW} = \text{Fresh weight; TW} = \text{turgid weight}$$

2.3.5. Leaf temperature analysis

Plants were used for studying the leaf temperature as described by Patnaik *et al.*, (2023). Briefly, thermal images from plants were captured after keeping them in a dark room with the FLUKE Infra-red Camera (Model No: Ti450 PRO) equidistantly placed 40 cm away. The images were processed using the SMART VIEW software version 4.8.20 and different parts of the plant showing the highest temperature were selected. Temperature from a minimum of 20 plants with 3 biological replicates was analyzed to obtain average leaf temperature data.

2.3.6. Lipid peroxidation assay

Lipid peroxidation was measured according to Heath and Packer (1968). Malondialdehyde (MDA) amount was determined by the thiobarbituric acid (TBA) reaction. Fresh leaf samples (~100 mg) were homogenized with 2 mL of 0.25 % TBA containing 10 % trichloroacetic acid (TCA). The homogenate was incubated at 95 °C for 30 mins and centrifuged at 10,000g for 10 mins. Absorbance was recorded at 532 nm and nonspecific absorption measured at 600 nm was subtracted.

2.3.7. Histochemical detection of superoxide radical

Nitro-blue tetrazolium (NBT) staining of stressed and unstressed leaves was done to detect the superoxide radical (O_2^-) using the method of Rao and Davis (1999) with some modifications according to Manasa *et al.*, (2023). The leaves were immersed in a 10 mM sodium phosphate

buffer maintained at pH 7.0 containing 3 mg / mL nitro-blue tetrazolium (NBT) and 10 mM sodium azide (NaN₃). The immersed leaves were subjected to vacuum infiltration at 80 kPa for 12 hours at room temperature in the dark. Acetic acid: glycerol: ethanol (1:1:3 v/v) solution was used to bleach the stained leaves at 100 °C for 30 mins in a water bath. The leaf samples were then stored at 4 °C in a storage solution containing glycerol: ethanol (1:4 v/v). The leaves of the stressed and unstressed plants were imaged using a Carl Zeiss stereo microscope (Model No: Stereo Discovery. V20) equipped with 5.8X magnification and an Axiocam 305 camera to obtain the total area of the NBT stain. The O₂⁻ accumulation in the leaves was interpreted in terms of the percentage of stained area. The percentage of stained area in the leaves was calculated using Image J (version: ImageJ 1.53a). Ten different morphologically similar leaves were chosen from five plants of each category to estimate the O₂⁻ accumulation. The experiment was repeated thrice with two biological replicates each time.

2.3.8. Antioxidative enzyme assays

For all enzyme assays done for this study (Saha *et al.*, 2016), ~100 mg of leaf extracts was prepared with 2 mL of 100 mM sodium phosphate buffer, pH 7.0 containing 1 % PVP (polyvinylpyrrolidone) and 1 mM EDTA (Ethylenediaminetetraacetic acid) on ice. The homogenate was centrifuged at 4 °C for 20 mins at 14000 rpm. The supernatant was used for the enzyme assays.

- Catalase (CAT): Catalase (EC 1.11.1.6) activity was measured according to Aebi (1984). Briefly, 0.1 mL of enzyme extract was added to 1 mL of 50 mM sodium phosphate buffer maintained at pH 7.0. The reaction was initiated by adding 0.1 mL of 100 mM hydrogen peroxide (H₂O₂). A decrease in absorbance was recorded at intervals of 30 seconds (s) for 2 mins at 240 nm.
- Guaiacol peroxidase (POX): Guaiacol peroxidase (EC 1.11.1.7) activity was measured according to Rao *et al.*, (1996). Briefly, 100 µL of enzyme extract was taken for the assay and

0.7 mL of sodium phosphate buffer, pH 7.0, and 0.1 mL of 1% guaiacol solution were added. 0.1 mL of 10 mM H₂O₂ was added to initiate the reaction. The mixture was incubated for 5 mins at room temperature and a change in absorbance was recorded at 470 nm.

- Superoxide dismutase (SOD): The activity of Superoxide dismutase (EC 1.15.1.1) activity was determined using 0.1 mL of enzyme extract as described in Panigrahy *et al.*, (2019). Briefly, SOD activity was determined by measuring the decrease in the absorbance of blue-colored formazone and O₂⁻ at 560 nm.

2.3.9. RNA extraction and gene expression study

Total RNA was extracted from 7-d-old seedlings grown in different light conditions. Hypocotyl, root samples, or 3rd and 4th leaf samples were separately harvested and ~500 mg of samples were used for total RNA extraction using RNeasy Plant Mini Kit (supplied by Qiagen, Catalog No: 74136). One µg of total RNA was used to obtain cDNA using Reverse Transcription Supermix (supplied by Bio-Rad, Catalog No: 1708840). For quantitative RT-PCR (qRT-PCR), the Primer Quest tool (Integrated DNA Technologies, Inc., USA) was used to design gene-specific primers used in the qRT-PCR. All reactions were carried out in hardshell 384-well PCR plates (Bio-Rad, Catalog No: HSP3805) in Bio-Rad laboratories' CFX384 TouchTM Real-time detection system, following the manufacturer's instructions and iTaqTM universal SYBR green super mix as described recently (Patnaik *et al.*, 2023). ACTIN was used to normalize transcript levels. Relative expression levels of the genes were calculated using 2^{-ΔΔCt} method (Pfaffl, 2001). The qRT-PCR reactions were done in triplicates from three biological replicates. Data represented as the mean ±SEM.

2.3.10. Scanning Electron Microscopy

2nd and 4th leaf samples were collected from Col-0 and *abp1* mutant plants at the bolting stage grown on soil under LD conditions at 22 °C. The leaf samples were cleaned properly, placed

on glass coverslips with a drop of water, and dehydrated at 60 °C for 12 hours. The leaves facing upward (adaxial side) were placed on the carbon tape and the surface of the leaf samples was coated with heavy metal platinum before imaging (Pathan *et al.*, 2010) using Carl Zeiss Field Emission Scanning Electron Microscopy (Model-ZEISS GeminiSEM 450). An accelerating voltage of 3-5c was applied for imaging at different magnifications. The experiment was repeated in three biological replicates.

2.3.11. Phytohormone estimation

Defense phytohormones (Jasmonic acid, salicylic acid) were estimated at the metabolite estimation facility of NIPGR, New Delhi as described by Patnaik *et al.*, (2023) and Vadassery *et al.*, (2012) with some minor modifications. Briefly, leaf samples (~300 mg) were harvested at the bolting stage using liquid nitrogen and ground to powder form using tissue lyser (Tissuelyser II, Retsch, Qiagen) at 30 frequency/ s for 2 mins and lyophilized overnight. Nearly 20 mg of lyophilized samples were extracted in 1 mL of methanol. Forty ng mL⁻¹ of D6-jasmonic acid (HPC Standards GmbH, Cunnerns dorf, Germany), 40 ng mL⁻¹ of D4-salicylic acid, 40 ng mL⁻¹ of D6-abscisic acid, and 8 ng mL⁻¹ of jasmonic acid- [13C6] isoleucine conjugate were used as internal standards. The homogenized samples were centrifuged at 14,000 rpm for 20 mins at 4 °C after shaking for 30 mins. The above step is repeated to pool the supernatants, followed by vacuum evaporation and re-suspension in 500 µL of methanol. Samples were analyzed on Exion LC (Sciex ®) UHPLC system using formic acid (0.05%) in water as mobile phase A and acetonitrile as mobile phase B. The column and separation protocols were done as described by Patnaik *et al.*, (2023).

2.3.12. Statistical analysis

All the statistical analyses used in this study were performed using GraphPad Prism version 8.0.1. A test of significance was performed to analyze grouped column graphs using two-way

ANOVA analysis with multiple comparisons (Tukey and Sidak) and student's unpaired T-test.

Error bars represent the standard error of the mean (SEM).

2.4. Effect of Temperature and Calcium on Tubulin Modification and Organisation in *Physcomitrella patens*

2.4.1. *In silico* analysis and construction of cladograms

In this study, using *in silico* approaches, we investigated the presence of enzymes responsible for catalyzing post-translational modifications of tubulin in plants. Through the application of cladistic analysis, we tested the hypothesized distribution of enzymes responsible for tubulin PTMs across the plant kingdom.

The proteins involved in most likely occurring post-translational modification (viz., tyrosination, acetylation, polyglutamylation) in *Mus musculus* were compared with Basic Local Alignment Search Tool (BLASTP) using NCBI (<https://blast.ncbi.nlm.nih.gov/>) and Phytozome 13 (<https://phytozome-next.jgi.doe.gov/>) against the proteome of *Tetrahymena thermophila*, *Chlamydomonas reinhardtii* and *Physcomitrella patens*. The top hit (which had to have an E value $< 1 \times 10^{-05}$ to discount random matches) was selected. Further, protein sequences homologous to *P. patens* were obtained from NCBI and Phytozome 13. Subsequently, Multiple Sequence Alignment was performed using MAFFT at <https://mafft.cbrc.jp/alignment/server/index.html>. The Maximum Likelihood Trees were constructed using the software IQ-tree version 1.6.12 with bootstrap values of 1000. The cladogram was visualized and extracted from the software FigTree v1.4.4.

The sequences of ATAT, ELP3, TTLL6, TTLL9 and TTLL12 from *P. patens* were further used in the PLANTCARE web server (<https://bioinformatics.psb.ugent.be/webtools/plantcare/html/>) to identify the light, hormone, temperature and stress-responsive elements.

2.4.2. Plant growth conditions and treatments

The WT strain of *Physcomitrium patens* (*P. patens*) (Hedw.) Mitt and the calcium sensor line transformed in *P. patens*, i.e., the GCaMP 6f line (obtained from Prof. Dr. Mitsuyasu Hasebe,

National Institute of Basic Biology, Japan) were used as this study's plant material. Protonema cultures were consistently maintained in a modified Knop solid medium (comprising 250 mg KH_2PO_4 , 250 mg KCl , 250 mg $\text{MgSO}_4 \cdot 7\text{H}_2\text{O}$, 1000 mg $\text{Ca}(\text{NO}_3)_2 \cdot 4\text{H}_2\text{O}$, 12.5 mg $\text{FeSO}_4 \cdot 7\text{H}_2\text{O}$, and 12 g agar in 1000 mL, with a pH of 4.5) (Biswal and Panigrahi, 2022). These cultures were placed in 9 cm Petri dishes and subjected to weekly sub-culturing, with each dish overlaid with a cellophane disk (80 mm in diameter, type 325 P, AA Packaging, Preston, UK). Hogland's A-Z trace element solution (1 mL/1000 mL Knop medium) (614 mg H_3BO_3 , 389 mg $\text{MnCl}_2 \cdot 4\text{H}_2\text{O}$, 110 mg $\text{Al}_2(\text{SO}_4)_3 \cdot \text{K}_2\text{SO}_4 \cdot 24\text{H}_2\text{O}$, 55 mg $\text{CoCl}_2 \cdot 6\text{H}_2\text{O}$, 55 mg $\text{CuSO}_4 \cdot 5\text{H}_2\text{O}$, 55 mg $\text{ZnSO}_4 \cdot 7\text{H}_2\text{O}$, 28 mg KBr , 28 mg KI , 28 mg LiCl , 28 mg $\text{SnCl}_2 \cdot 2\text{H}_2\text{O}$, 25 mg $\text{Na}_2\text{MoO}_4 \cdot 2\text{H}_2\text{O}$, 59 mg $\text{NiCl}_2 \cdot 6\text{H}_2\text{O}$ in 1000 mL) (Ashton *et al.*, 1997). The protonema tissues, which were one week old (7 days), were ground using a tissue homogenizer (Omni International, Kennesaw, GE, USA) and then transferred to a fresh Knop solid medium overlaid with a cellophane disk every week. The protonema plates were allowed to grow in controlled growth cabinets (Percival Scientific Inc. Perry, USA, Model No: CU36L6) equipped with white fluorescent light ($50 \mu\text{mol m}^{-2} \text{s}^{-1}$), maintained at 25 °C.

For calcium treatment, protonema tissue was grown under standard conditions in Knop solid medium with different CaCl_2 concentrations using (10 mM, 100 mM, and control at 0 mM) and allowed to grow for 8 or 15 days. Moss tissues were either used at 8 days for immunofluorescence or harvested after 15 days and stored at -80 °C for protein extraction.

For temperature treatment, the 7 days old protonema tissues were kept at 18 °C (low temperature) and 38 °C (high temperature) and controlled at 25 °C in controlled growth cabinets for 24 hours and hence used for immunofluorescence.

For light treatment, protonema tissue was grown under standard conditions in Knop solid medium at 22 °C under diurnal red (R, $30 \mu\text{mol m}^{-2} \text{s}^{-1}$, 660 nm), far-red (FR, $30 \mu\text{mol m}^{-2} \text{s}^{-1}$, 730 nm) and blue (B, $30 \mu\text{mol m}^{-2} \text{s}^{-1}$, 460 nm) light fitted in the Percival LED chambers for 7 days. Positive and negative controls were also taken where protonema culture was grown in

white (WL) and Dark (D) for 7 days. The samples were fixed for imaging or live cell imaging was done post 7 days of growth.

For phytohormone treatment, filter sterile 1 nM auxin i.e., Indole-3-acetic acid (IAA, Catalog No: PCT0803, Himedia) and 1 nM cytokinin i.e., Kinetin (Catalog No: PCT0806, Himedia) were added to the Knop solid medium. The protonema tissue was allowed to grow in the Knop media at 22 °C for 7 days under diurnal WL in a Percival chamber. The samples were fixed for imaging or live cell imaging was done post 7 days of growth.

2.4.3. Extraction and estimation of proteins

Moss tissues (1 gms) grown in different conditions were collected and ground in liquid nitrogen using a mortar and pestle. 3 mL of protein extraction buffer (PEB) containing 25 mM Tris-HCl buffer (pH 7.5), 50 mM KCl, 5 mM MgCl₂, and 5 mM β-mercaptoethanol were added to each of the homogenized tissues on ice. The homogenate was mixed properly using a vortex for 10 mins and centrifuged at 13500 rpm for 10 mins at 4 °C (Patnaik *et al.*, 2023). The supernatant was collected in separate tubes. 500 µL of extraction buffer was added to the remaining pellet to extract the nucleoplasmic protein followed by vortexing for 2 mins. The protein extracts were used directly for protein estimation, SDS-PAGE, or stored at -80 °C until further use. Protein estimation of the extracted proteins was done by the Amido Black method, according to Patnaik *et al.*, 2023. 500 µL of Amido Black staining solution (0.05 % w/v amido black, 10 % v/v acetic acid, 90 % v/v MeOH) was added to each pellet, and supernatant fraction (10 µL) and incubated for 15 mins at room temperature. The samples were then spun down at 13000 rpm for 15 mins. The supernatant was discarded, and the obtained pellet was washed with 1 mL wash solution (90 % methanol + 10 % acetic acid) till the solution appeared clear. Pellets were then allowed to dry for 10 mins at room temperature. 500 µL of 0.2 M NaOH solution was added to the dried pellet and vortexed properly. The absorbance was measured at 595 nm in an ELISA plate reader (Bio-Rad). An equal quantity of proteins was loaded in 10 % SDS-PAGE, and then western

blotting was performed using the Semi-Dry Transfer method.

2.4.3. Western blotting

Proteins were separated using a 10 % SDS-PAGE, and the gel was run for 2 hours at 50 V, followed by western blotting. The separated SDS-PAGE was transferred to the PVDF membrane by using a Bio-Rad semi-dry transfer system. The power supply was set to 22 V for 45 mins. The transferred PVDF membrane was blocked for 1 hour with 5 % skimmed milk TBST solution. The membranes were incubated with different primary antibodies like mouse anti-acetylated tubulin (Monoclonal Anti-Acetylated tubulin antibody produced in mouse, Catalog No: T741, SIGMA), mouse anti-tyrosinated tubulin (Rat mAb to tubulin, YL1/2, Catalog No: ab6160, Abcam), mouse anti-polyglutamated tubulin (Monoclonal Anti-Tubulin, Polyglutamylated antibody produced in mouse, Catalog No: T9822, SIGMA) and rabbit anti-histone in 1:1000 dilution respectively for 1 hour at room temperature. Secondary antibodies (anti-mouse HRP in 1:10,000 dilution and anti-rabbit HRP 1:10,000 dilution in MTBST) were added to respective blots and left for 1 hour at room temperature. Blots were developed using Super Signal West Femto Maximum Sensitivity substrate (Thermo Scientific) and detected with Bio-Rad Quantity One (Chemi Hi Sensitivity).

2.4.4. Ca²⁺ imaging and quantification

To check the efficiency of the Ca²⁺ sensor protein, 7 days old protonema of GCaMP 6f line of *P. patens* was taken and treated with 5 μ M of Ionomycin (Ca²⁺ activator) and 20 μ M BAPTA-AM (Ca²⁺ chelator) for nearly 12 hours. To further investigate the effect of temperature and exogenous Ca²⁺ on the Ca²⁺ sensor protein present in the GCaMP 6f line of *P. patens*, one-week-old protonema grown in KNOP media containing 0 mM, 10 mM, and 100 mM CaCl₂ was taken and was exposed to low (18 °C), high (38 °C) and control (25 °C) temperatures for 24 hours. Phytohormone-treated protonema culture (7 day old) was also used for live cell imaging

to quantify the endogenous Ca^{2+} levels present in the cell. After the treatment period, the protonema tissues were taken and imaged using an Olympus FV3000 confocal microscope. Snaps were acquired using a 488 nm laser. Time series of live cells were conducted using a 2% 488 nm laser, and images were acquired for a total of 217 sec at a rate of 1 frame/1.085 sec. The intensity of the ultrasensitive protein calcium sensor GCaMP6f changed over time in 200 frames. Each cell was treated as an individual ROI, and the intensity change was measured using Fiji software. The initial value was set to 1, and the changes were further determined, and graphs were plotted using the GraphPad Prism 8 software.

2.4.5. Immunofluorescence, Confocal and Super resolution microscopy

The 8-day-old treated protonema of *P. patens* was taken, and fixation was done using Microtubule Stabilizing Buffer (MTSB) consisting of 0.1 M PIPES-KOH (pH-6.8), 1 mM MgCl_2 , 5 mM and 0.01 % of Triton X-100 for 1 min. The tissues were then transferred and incubated in MTSB containing 8 % (w/v) and 1 % DMSO for 20-30 mins. The tissues were further stored at 4 °C with 2 % Sodium Azide in 1 % PBS (137 mM NaCl, 2.7 mM KCl, 10 mM Na_2HPO_4 , 1.8 mM KH_2PO_4) maintained at pH 7.4 till further use. To process the tissues for immunofluorescence, confocal and super resolution microscopy, the fixed tissues were taken and washed twice with MTSB-2 (50 mM PIPES, 5 mM EGTA, 1 mM MgSO_4 , 1 % glycerol, and 2 % Triton X-100) for 5 mins each. The tissues were then blocked with 5 % BSA in 1 % PBS for 1 hour. The tissues were incubated with different primary antibodies like mouse anti-acetylated tubulin, mouse anti-tyrosinated tubulin, mouse anti-polyglutamated tubulin, and rabbit anti-histone (Catalog No: SAB5700778, SIGMA) in 1:1000 dilution with 5 % BSA and 2 % Triton X-100 respectively for 12 hours at 4 °C. After the primary antibody incubation, the tissues were washed with MTSB-2 thrice for 5 mins each followed by secondary antibody incubation with anti-mouse IgG(H+L) F(ab')₂ CF488A produced in goat (Catalog No: SAB4600388, SIGMA) and anti-rabbit IgG(H+L) F(ab')₂ CF488A produced in goat (Catalog

No: SAB4600234, SIGMA) 1:10,000 dilution with 5 % BSA and 2 % Triton X-100 for 1 hour at room temperature. The tissues were again washed thrice with MTSB-2 for 5 mins each. The tissues were then mounted on a clean glass slide with glycerol and were imaged using an Olympus FV3000 confocal microscope. Snaps were acquired using a 488 nm laser. For super-resolution microscopy, after secondary antibody incubation and washing, the tissues were treated with 0.1 % DAPI (4',6-diamidino-2-phenylindole) (Catalog No: MBD0015, SIGMA) for 20 mins before mounting in glass slides with glycerol. The slides were then imaged and processed with a Zeiss elyra 7 sim square super-resolution microscope.

2.4.6. Quantitative analysis

All the microscopy and western blot images were reduced to 8-bit size, and calculations for fluorescence intensity and area were done using ImageJ software. Results were summarized to get the mean value and standard deviation, and then respective graphs were plotted in GraphPad Prism software.

2.4.7. Statistical analysis

GraphPad Prism 8.0.1 was used to create column graphs with only one variable for each construct based on these values. One-way ANOVA (and non-parametric) was used to compare the mean of each column to the mean of every other column, and P values were determined using Tukey's multiple comparison test. Fiji software was used for all intensity measurements, and the raw intensity values were plotted as arbitrary units in GraphPad Prism.

2.5. Correlation of Phytochrome B and Auxin in Patterning the Root Development in *Arabidopsis thaliana*

2.5.1. Generation and cloning of fluorescent/luciferase-based auxin sensor constructs in gateway cassette

The auxin sensor construct has renilla and firefly luciferases, 2A, and a short stretch of the AUX/IAA degron sequence. The order of this sequence is as such: Firefly-AUX/IAA-2A-Renilla and the length of this stretch is ~2.7 kb. It works on the principle that when auxin is present in the cell, it will go and bind to the AUX/IAA sequence and the AUX/IAA sequence degrade along with attached firefly luciferase. The degradation of AUX/IAA enhances with increasing concentration of auxin and hence firefly expression will go down. The expression of renilla will not change in this case and on this basis, the concentration of auxin in the cell can be evaluated. In this current work, we have amplified the firefly, AUX/IAA, 2A, and renilla in a single stretch and then cloned it in the pDONR201 vector by BP gateway cloning. After that, it was transformed into the DH5 α strain of *E. coli*, and the selection was performed in kanamycin. The antibiotic-resistant colonies were confirmed by PCR. Then, the plasmid of the positive colony was cloned in the pB2GW7 destination vector by LR gateway cloning despite 35S:CFP: GW vector as mentioned in the project proposal, and further transformation was done in DH5 α strain of *E. coli*. The selection was performed in spectinomycin antibiotic, the resistant colonies were screened through colony PCR. The plasmid of the positive colony was transformed into *Agrobacterium tumefaciens* by the heat shock method. The selection was done in the presence of spectinomycin and rifampicin, the resistant *Agrobacteria* colonies were further screened by colony PCR. The positive colonies were used to transform Col-0 plants via the floral dip method. The transgenic lines were generated, bulked, and screened through PCR for three generations.

BP Gateway Cloning: The amplified product was combined with pDONR201, BP Clonase mix, and TE buffer, resulting in a total volume of 10 μ L. The mixture was then incubated overnight at 25 °C. Following incubation, Proteinase K was introduced and the mixture was maintained at 37 °C for 10 mins. Subsequently, the BP mix obtained was utilized for the transformation of *E. coli*. The colonies resulting from the transformation were subjected to examination via PCR and restriction digestion for further analysis.

LR Gateway Cloning: The colonies identified as positive following the BP reaction underwent miniprep to isolate plasmid DNA (entry clone), which served as the starting material for the LR reaction. The entry clone was combined with the destination vector (pB2GW7), LR Clonase, and TE buffer, and incubated at 25°C for 14 hours. Subsequently, the mixture was supplemented with Proteinase K and incubated at 37 °C for 10 mins. The LR mix obtained was then employed for transformation in *E. coli*. Verification of transformed colonies was performed through colony PCR and digestion with specific restriction enzymes for further validation.

E. coli Transformation: For *E. coli* transformation, 50 μ L of competent cells was combined with 1 μ L of plasmid and incubated for 30 mins on ice. Following incubation, the mixture underwent a heat shock treatment at 42 °C for 40 secs, followed by an additional 5-mins incubation on ice. LB media was then added to the mixture and allowed to incubate for 1 hour. Subsequently, centrifugation was carried out for 1 min at 6000 rpm, after which excess media was removed, and the pellet was resuspended in the remaining media. The suspended pellet was evenly spread onto a media plate and left to incubate.

Preparation of *Agrobacterium* competent cells: To prepare *Agrobacterium-competent* cells, a single colony from a bacterial culture was introduced into LB broth and left to incubate overnight at 28 °C with agitation at 220 rpm. The resulting overnight bacterial culture was then added to 100 mL of LB media containing rifamycin and cultivated until reaching an optical density (OD) of 0.5. Once the OD reached 0.5, the culture was cooled on ice for 25 mins, followed by centrifugation at 4 °C for 15 mins at 5000 rpm. After discarding the excess media,

the pellet was washed three times with 40 mL of 10 % glycerol. Subsequently, 1 mL of 10 % glycerol was added to the pellet, and aliquots were prepared for storage.

Agrobacterium transformation: For *Agrobacterium* transformation, 50 μ L of competent cells was combined with 1 μ L of plasmid on ice before being transferred to a pre-chilled electroporation cuvette. The cuvette was then placed in an adoration system where an electroporation shock was administered three times. Following electroporation, 1 mL of LB broth was added, and the mixture was incubated overnight at 28 °C with agitation at 220 rpm. After overnight incubation, the culture was subjected to centrifugation at room temperature for 1 min at 6000 rpm. The supernatant was carefully discarded, and the pellet was resuspended in the remaining media. The resuspended pellet was then spread evenly over an LB agar plate supplemented with the appropriate antibiotic selection marker and incubated for 2-3 days until colonies appeared.

Plant Transformation: To initiate plant transformation and mutant screening, the transformed *Agrobacterium* colony was cultured in YEBS media supplemented with streptomycin and rifamycin. The culture was incubated at 28 °C with agitation at 220 rpm, and the optical density at 600 nm (OD₆₀₀) was monitored at regular intervals until it reached 0.8. A portion of the culture, referred to as the feeder culture, was reserved for subsequent floral dip procedures. Upon reaching an OD of 0.8, Silwett L-77 was introduced into the culture, followed by the immersion of floral parts of plants at the bolting stage into the culture. Following dipping, the plants were maintained in darkness for 12 hours while slanted and covered with polybags. After this period, the polybags were removed, and the plants were transferred to growth rooms. For enhanced transformation efficiency, the floral dip process was repeated three times, with a 3days interval between each dip, utilizing the feeder culture. After the floral dip treatments, transformant seeds were harvested and sown in the soil. These seeds underwent treatment with BASTA on three separate occasions. Healthy seedlings surviving the BASTA treatment were then subjected to PCR screening to identify desired mutants.

PCR and Colony PCR: PCR and Colony PCR were conducted utilizing Taq polymerase and Phusion polymerase enzymes, respectively. The standard protocol provided by NEB (New England Biolabs) was adhered to for both procedures.

2.5.2. EMS mutagenesis of auxin sensor and DR5:: GFP expressing Col-0 WT lines and bulking of seeds

A 0.2 % EMS solution was created using water and subsequently applied to the seeds (Col-0 Luc and DR5::GFP). The seeds were adequately suspended and left overnight on a rotating mixer. Following this, excess EMS solution was removed, and the seeds were rinsed with water. Subsequently, the seeds were incubated with water for 1 hour. All procedures were conducted within a fume hood. The mutagenized seeds were then planted on soil in different pools for further bulking. The seeds were bulked and collected individually from different pools in separate vials. These vials were further named V 1, V 2, V 3.....V 50 and ED 1, ED 2, ED 3.....ED 50 for EMS mutagenized Col-0 Luc and DR5: GFP lines respectively.

2.5.3. Screening for hypo and hyper-sensitive mutants under saturating RG9 red light field

The obtained seeds from different pools were subsequently screened under continuous red light (saturating RG9 red light) at 22 °C based on the hypocotyl lengths as compared to their respective controls. The initial screening was done from the above pooled EMS mutagenized Col-0 Luc and EMS mutagenized DR5::GFP lines. The hypocotyls which were longer than the wild type was termed hypersensitive mutants. Similarly, the hypocotyls which were shorter than the wild type were named hyposensitive mutants. These mutants were considered as F₀ generation. The hypersensitive and hyposensitive mutants which retained the phenotype were further screened under continuous red light till F₃ generation by the selfing method and further bulking was done.

Mutant seed lines (F_3 generation) were further sterilized and sown on MS media. After cold stratification, seeds were grown under diurnal red light (16 hours light/ 8 hours dark) for root patterning study. Seedlings showing altered or defective root architecture were selected and bulked. Seedlings with defective in both red light signalling and root architecture were further checked for alteration in primary root and hypocotyl lengths.

CHAPTER 3

***IN-SILCO* ANALYSIS OF GIGANTEA FROM AN EVOLUTIONARY PERSPECTIVE**

CHAPTER 3: *IN-SILCO* ANALYSIS OF GIGANTEA FROM AN EVOLUTIONARY PERSPECTIVE

3.1. BACKGROUND

Plant plasticity strives to adapt to changing environmental conditions. The adaptability cues are based on the environmental stimulus perceived by the plant. Environmental changes ultimately trigger the reprogramming of transcriptional, post-transcriptional, translational, and post-translational events to attenuate the plant's metabolic balance accordingly. The expressions of many abiotic and biotic stress-responsive genes along with the biosynthesis and signalling components downstream of hormone pathways are revealed to be modulated by the circadian clock (Grundy *et al.*, 2015; Patnaik *et al.*, 2022). The circadian clock of plants anticipates and prepares them for seasonal, diurnal, and environmental changes. It helps boost plant plasticity and assists in plants' overall fitness to mediate stress tolerance without compromising plant growth and development (Patnaik *et al.*, 2022). The biological clock is ubiquitously found in cyanobacteria, fungi, insects, plants, and mammals (Young and Kay, 2001). Circadian oscillation is fundamentally due to the earth's rotation well-tuned to a 24-hour day-night cycle (Dodd *et al.*, 2005). In *Arabidopsis thaliana*, circadian oscillatory mechanisms are comprised of three loops: the morning loop, a central oscillator, and an evening loop. The central oscillator comprises two transcription factors i.e., CIRCADIAN CLOCK ASSOCIATED 1 (CCA1) and LATE ELONGATED HYPOCOTYL (LHY), and a member of the PSEUDO-RESPONSE REGULATOR (PRR) family TIMING OF CAB EXPRESSION 1 (TOC1/PRR1). The operation of the circadian clock is based on a dual negative feedback loop where the morning and evening expressions of *CCA1/LHY* and *TOC1* repress each other respectively. (Wang and Tobin, 1998; Alabadi *et al.*, 2001; Huang *et al.*, 2012). In the evening loop, the expression of *TOC1* represses *GIGANTEA* (GI) which in turn activates *TOC1* for further transcription and translation processes (Huang *et al.*, 2012; Kim *et al.*, 2007; Locke *et al.*, 2006).

Though the interlocked transcriptional/ transcriptional feedback loops can explain all the functional aspects of the circadian clock in most organisms to date, combinatorial variations are observed in several organismal model systems. Marine ecosystems are influenced by different environmental cycles due to periodic cycles of occurrence of the moon and sun, cycles of the shorter or longer periods due to tides, lunar/semi-lunar cycles, or the seasons. Accordingly, marine species exhibit a variety of biological rhythms, including circadian, circalunar, or circatidal rhythms (Tessmar-Raible *et al.*, 2011). Due to adaptation and synchronization to these rhythms, marine organisms have evolved over the centuries. However, in all known cases, the zeitgeber stimuli that serve as synchronization cues are directly or indirectly linked to sun and moon cycles. The study of marine unicellular green alga *Ostreococcus* presents a simpler context for studying circadian clock mechanisms as it reveals an ancient aspect of *A. thaliana* clock with the orthologs of the two core clock genes *TOC1* and *CCA1*, excluding other components, and aided with a micro-eukaryotic genome of only 13 Mbp (Corellou *et al.*, 2009). Unicellular marine organisms such as diatoms and green alga synchronize their cell divisions, and photosynthetic activity in a circadian pattern (Harding and Heinbokel, 1984). In marine diatom *Phaeodactylum tricornutum*, the photoreceptor cryptochrome is assigned for circadian regulation, evidenced by the diversified function and the missing link to a photolyase molecule (Coesel *et al.*, 2009). Seagrass has adopted marine environments and can survive in extreme underwater light and temperature with its critical physiological and biochemical changes by adding or deleting genes of circadian clock components, photoreceptors (Olsen *et al.*, 2016), and their regulation at daily and seasonal scales (Dattolo *et al.*, 2014). The cyanobacterial circadian clock describes a very different scheme of circadian regulation and is the signature of prokaryotic circadian regulation. The cyanobacterial prokaryotic circadian clock was first known in *Synechococcus elongatus* in 1997 (Sartor *et al.*, 2019). It consists of a post-translational feedback system, classified as a gene expression feedback loop (GFEL), in contrast to the transcriptional–translational feedback

loop of *A. thaliana*. Investigation of the clock components in the highly evolved Chlorophyta subdivision. Charophytes showed that the central clock components of the angiosperms, namely the EC genes, including *ELF3*, *ELF4*, *LUX*, and *GIGANTEA (GI)* and the genes of the *ZTL* family are present (Petersen *et al.*, 2022). However, the function of these EC genes is not described till now in charophytes.

Excellent shreds of evidence of alteration of the circadian clock in terms of the phase, amplitude, and period can be observed during domestication and crop improvement processes in many crops, such as tomato, barley, soybean, wheat, etc. *AtPRR3* is observed with two naturally occurring non-synonymous substitutions in the EAR motif and the CCT domain, which are ubiquitous in all *A. thaliana* ecotypes (Alonso-Blanco *et al.*, 2016). They have different roles from the standard role of transcript repression of the *PRRs*, which can be found in the soybean *GmPRR3* with functional EAR motif and CCT domain (Lu *et al.*, 2020). Furthermore, a genome-wide association mapping study identified *Tof11* and *Tof12* QTLs, which contain the *GmPRR3a* and *GmPRR3b* as the genes for flowering and maturity which are selected in the domestication process. They act as repressors of *GmLHY/CCA1* homologs, which are in turn repressors of the maturity gene (*E1*) (McBlain and Bernard, 1987). A series of repression of *GmFT* by *E1* delays flowering (Lu *et al.*, 2020). Studies on *ELF3* in soybeans have discovered the *J* locus in the LJ variety, a recessive *j* allele in the Huaxia parent background. *GmELF3* in the LJ variety is an Indel mutation resulting in loss of function and ultimately aberrations in durational oscillation. Moreover, *GmELF3* affects *GmPHYA3* and *A2* functions. It is not only a part of the evening complex, but its recessive *j* allele can suppress the *FLOWERING TIME (FT)* expression through *E1* to result in delayed flowering (Lu *et al.*, 2017). The *Pisum sativum* ortholog of *AtELF4*, *DIE NEUTRALS (PsDNE)* is involved in the circadian clock. The null allele of *dne* has perturbed expression of clock genes, such as *PsTOC1*, *LATE BLOOMER1 (LATE1)*, and *PsPRR59*, under the diurnal condition of LD, SD, L/L, and D/D and increased expression

of *FT*-like gene (*FTL*) (Liew *et al.*, 2009). However, the *DNE* involvement in the circadian clock has a minor role than *AtELF4*, since *elf4* mutants of *Arabidopsis* showed arrhythmicity and reduced accuracy in periodicity. The difference in the regulatory relationships between the EC genes in *A. thaliana* and *P. sativum* is evidenced by the *STERILE NODES* (SN) *sn* mutants in peas. They exhibit disrupted rhythmicity of *PsTOC1*, and *LATE1* along with dampened expressions of *PsLHY*. On the other hand, the SN in pea was reported to be an ortholog of *AtLUX*, and conserved regulation exists with its *A. thaliana* counterpart (Liew *et al.*, 2014).

Though several crop plants, such as rice, maize, wheat, barley, and sorghum, bear more agronomical importance, the understanding of their circadian regulation lags behind those of the dicot plants. Nevertheless, several orthologs of *A. thaliana* circadian clock are found in monocots, too (Murakami *et al.*, 2007, Patnaik *et al.*, 2022). It is also proved from the phylogenetic analysis that the evolution of the circadian clock components dates far before the divergence of monocots and dicots (Takata *et al.*, 2010). In *Lemna gibba*, any alteration due to over-expression or knock-down in an expression of genes such as *LgLHYH1*, *LgGIH1*, and *LgELF3H1* except *LgLHYH2* resulted in disrupted rhythms of the clock genes (Serikawa *et al.*, 2008). The set of clock-associated genes is highly conserved in rice. Loss-of-function of *OsPRR73*, a circadian clock component, results in an early heading date only under long day conditions. At the same time, improper expression of *OsPRR73* results in disturbed expression of several clock genes (Liang *et al.*, 2021). *OsPRR37*, a far homolog of *GmPRR3*, can affect the expression of *OsFT* (*Hd3a*), thus suppressing the flowering time in the absence of the E1-like protein. Trigenic interaction of *Ghd7*, *Ghd8*, and *PRR37* can contribute to significant variation in flowering and requires further study (Zhang *et al.*, 2019). *CO-FT* pathway in short-day crop plants like rice has a distinctly different alternate flowering mechanism to that of *A. thaliana*, which is clock-controlled. The *Ehd1*, a rice-specific B-type response regulator regulated the *Hd3a* expression and *Ghd7* to control flowering in inductive short days (Doi *et al.*, 2004; Matsubara *et al.*, 2012). *Ehd1*-induced repression of *Ghd7* is controlled by the

circadian clock (Xue *et al.*, 2008). *OsELF3/Hd17/Ef7* coordinates to repress *Ghd7* (Saito *et al.*, 2012) leading to decreased *Ehd1* and *Hd3a* levels (Matsubara *et al.*, 2012). *OsPRR37* acts as a transcriptional repressor of *Ehd1* (Liu *et al.*, 2018). Allelic variants of flowering genes such as *Ehd4* and *RFT1* have also been shown to be necessary for the adaptation of rice in higher altitudes (Zhao *et al.*, 2015). In Barley, multiple orthologs of *A. thaliana* *CCA1*, *RVE8*, *TOC1*, *GI*, and *LUX* exist. Functional variabilities of *HvPRR37* compared to *A. thaliana* proved that the evolution of the major determiners of flowering, the PRR genes, has followed diverse routes in grasses (Takata *et al.*, 2010). Mutation in *HvPRR37* (*PpdH1*) does not alter circadian clock genes' expression, indicating that *PpdH1* may not be involved in circadian clock function. Also, it was evidenced that the evolution of *HvPRR37* incorporated this loss of clock function which is retained by *HvPRR73* due to its functional redundancy with *PpdH1*. However, *HvPRR37* is the major effective factor for photoperiod responsiveness and has reduced expression due to mutation in the spring-sown varieties. This mutated version of *ppdH1* helps to delay the diurnal expression of *HvCO1* and *HvCO2* to peak in the dark, preventing their proteins from accumulating, and ultimately leading to reduced expression of *HvFT* (Turner *et al.*, 2005). *A. thaliana* *ELF3* homolog *EAM8* from Barley and *EPS3* from wheat has been shown to alter flowering time, phase, period, and amplitude of their circadian clock (Faure *et al.*, 2012; Gawroński *et al.*, 2014). Alteration in the gene sequence of wheat (*Triticum aestivum*) *TaPRR37*, a homolog of *HvPRR37*, the *Ppd-D1* results in photoperiodic insensitivity along with altered flowering time. The evidence for this was observed in the *Ppd-D1a* allele, which had a 2 kb deletion upstream of the *Ppd-D1* gene. The *Ppd-D1a* allele results in early flowering and photoperiod insensitivity by reducing *TaCO1* expression resulting in a shift in the peak of *Ppd-D1* and increased expression of *TaFT1* (Beales *et al.*, 2007). The sorghum (*Sorghum bicolor*) *SbPRR37* is circadian clock regulated and among the highly conserved in grasses. However, the evening peaked expression of *SbPRR37* is unique to

sorghum, which helps in the repression of flowering in LD through increased *SbCO* followed by repressed *SbFT* gene expression (Murphy *et al.*, 2011).

In addition, with the regulation of the circadian clock in plants, GIGANTEA (GI) has been reported to have a diverse pleiotropic function like drought tolerance and escape (Han *et al.*, 2013), miRNA processing (Morris *et al.*, 2010; Han *et al.*, 2013), flowering time regulation (Park *et al.*, 2016), cold tolerance Brandoli *et al.*, 2020), stomatal opening (Ando *et al.*, 2013), photomorphogenesis (Huq *et al.*, 2000; Martin-Tryon *et al.*, 2007; Oliverio *et al.*, 2007), starch accumulation (Kim *et al.*, 2017), hypocotyl elongation (Nohales *et al.*, 2019), iron homeostasis (Tissot *et al.*, 2014), chloroplast biogenesis (Cha *et al.*, 2019;), herbicide resistance (Cha *et al.*, 2019), oxidative stress tolerance (Cha *et al.*, 2022), salt tolerance (Park *et al.*, 2016), temperature entrainment (Gil *et al.*, 2019), heat tolerance (Gil and Park, 2019), circadian clock control and light signalling (Mishra and Panigrahi, 2015). GI is a unique plant-specific nuclear-localized protein identified way back in 1962 by György P. Rèdei. Even more than fifty years after its discovery, many questions regarding its biochemical functions, evolution, etc are still unclear. The genomic locus of GI consists of 14 exons and 1173 amino acids (Fowler *et al.*, 1999; Park *et al.*, 1999). The genomic location of GI mapped to chromosome 1 in *Arabidopsis thaliana* consists of 14 exons that transcribe to a full-length protein comprising 1173 amino acids (Fowler *et al.*, 1999a; Park *et al.*, 1999). Both the transcription and translation of GI are intricately regulated by diurnal cycles. The precise control over its transcriptional and post-translational processes, coupled with its transient expression, has posed challenges in unraveling the precise biochemical mechanisms and distinctive functions of GI. Despite being the major component of the circadian clock, the evolutionary history of GI is less understood thoroughly. Studying the evolutionary trajectory of GI will aim to dissect the evolutionary processes and physiological mechanisms by which GI diversified and to reveal how their physical architecture facilitates and constrains their evolution from water-dwelling lower plants to land-dwelling higher plants. To investigate the transition from a simple clock in algae to a

complex one in angiosperms, we aimed to understand the paradigm of the evolutionary conservancy of GI across the plant kingdom. This chapter will shed light on the evolutionary analysis of GI providing the ultimate explanation for ‘Why GI has the properties it has today’.

3.2. RESULTS

3.2.1. Retrieval of sequences

One twenty-three full-length GIGANTEA protein sequences from various plant species were obtained from the NCBI (National Centre for Biotechnology Information) and OneKP databases. Out of which, 2 green algae, 4 bryophytes, 19 gymnosperms, and 98 angiosperms (2 amborellales, 14 monocots, and 82 eudicots) were identified (Table 7). It was observed that homologs of GI were abundantly found in almost all the higher plants i.e., in 98 angiosperms. Interestingly, two isoforms of GI were also found in *Amborella trichopoda*, the basal angiosperms i.e., amborellales. This indicated that GI has evolved from basal angiosperms to mature angiosperms in the evolutionary trend. Sequences of GI were also found in 19 species of gymnosperms. In addition, sequences of GI were also found in a few lower plants like *M. polymorpha*, *A. agrestis*, *T. lepidozoides*, *S. moellendorffii*, *C. cushleackae*, and *C. irregularis*. However, homologs of GI were not yet found in other species of green algae, bryophytes, and pteridophytes. Thus, GI was found in higher plants, however, instances of the presence of GI in lower plant species and algae were rare.

SPECIES	ACCESSION NUMBER
<i>Abrus precatorius isoX1</i>	XP_027367356.1
<i>Abrus precatorius isoX2</i>	XP_027367357.1
<i>Abrus precatorius isoX3</i>	XP_027367360.1
<i>Aegilops tauschii</i>	XP_020192041.1
<i>Amborella trichopoda isoX1</i>	XP_020521564.1
<i>Amborella trichopoda isoX2</i>	XP_020521567.1
<i>Ananas comosus</i>	XP_020088620.1
<i>Anthoceros agrestis</i>	Data from oneKP database (Linde <i>et al.</i> , 2017)
<i>Arabidopsis lyrata</i>	AKX69184.1
<i>Arabidopsis thaliana</i>	NP_564180.1
<i>Arachis duranensis</i>	XP_015942477.1
<i>Arachis duranensis*</i>	XP_015967961.1
<i>Arachis hypogaea</i>	XP_025621154.1
<i>Arachis hypogaea*</i>	XP_025702258.1
<i>Arachis hypogaea isoX2</i>	XP_029148589.1
<i>Arachis hypogaea isoX2*</i>	XP_029151850.1

<i>Arachis hypogaea isoX3</i>	XP_025657109.1
<i>Arachis ipaensis</i>	XP_016174692.1
<i>Arachis ipaensis*</i>	XP_016204447.1
<i>Brachypodium distachyon</i>	XP_010230544.1
<i>Brassica napus</i>	XP_013696193.2
<i>Brassica rapa</i>	NP_001288824.1
<i>Brassica rapa isoX1</i>	XP_009115601.1
<i>Cajanus cajan</i>	XP_020224531.1
<i>Cajanus cajan isoX1</i>	XP_020239412.1
<i>Cajanus cajan isoX2</i>	XP_020239416.1
<i>Cajanus cajan isoX3</i>	XP_029124666.1
<i>Cannabis sativa</i>	XP_030492608.1
<i>Cannabis sativa*</i>	XP_030507774.1
<i>Capsella rubella</i>	XP_006306336.1
<i>Carica papaya</i>	XP_021902416.1
<i>Cicer arietinum isoX1</i>	XP_004496435.1
<i>Cicer arietinum isoX2</i>	XP_027189172.1
<i>Citrus sinensis</i>	XP_006473104.1
<i>Coffea eugenoides</i>	XP_027148263.1
<i>Coleochaete irregularis</i>	gnl onekp QPDY_scaffold_2006257
<i>Cucumis sativus</i>	XP_031743418.1
<i>Cucumis sativus isoX1</i>	XP_011659108.1
<i>Cucumis sativus isoX2</i>	XP_031744582.1
<i>Cucumis sativus isoX3</i>	XP_031744584.1
<i>Cucurbita pepo</i>	XP_023549953.1
<i>Cylindrocystis cushleckae</i>	gnl onekp JOJQ_scaffold_2008725
<i>Dendrobium catenatum</i>	XP_020681376.1
<i>Elaeis guineensis</i>	XP_010915066.1
<i>Elaeis guineensis*</i>	XP_010925341.1
<i>Eutrema salsugineum</i>	XP_006416160.1
<i>Glycine max</i>	NP_001239995.2
<i>Glycine max*</i>	XP_014624480.1
<i>Helianthus annuus isoX1</i>	XP_021992239.1
<i>Helianthus annuus isoX2</i>	XP_021992244.1
<i>Herrania umbratica</i>	XP_021285158.1
<i>Hevea brasiliensis</i>	XP_021644050.1
<i>Jatropha curcas</i>	XP_012073938.1
<i>Jatropha curcas isoX2</i>	XP_020535511.1
<i>Malus domestica</i>	XP_028957741.1
<i>Manihot esculenta</i>	XP_021601157.1
<i>Marchantia polymorpha</i>	BAO66507.1
<i>Medicago truncatula isoX2</i>	XP_024641844.1
<i>Medicago truncatula isoX1</i>	XP_003592048.2
<i>Medicago truncatula isoX3</i>	XP_024641850.1
<i>Morus notabilis</i>	XP_024022247.1
<i>Oryza sativa</i>	XP_015649578.1
<i>Panicum hallii</i>	XP_025816790.1
<i>Phalaenopsis equestris</i>	XP_020572459.1

<i>Picea abies</i>	AGH20049.1
<i>Picea asperata</i>	ANS12856.1
<i>Picea breweriana</i>	AND98324.1
<i>Picea glauca</i>	AND98320.1
<i>Picea jezoensis</i>	AND98247.1
<i>Picea likiangensis</i>	ADE32551.1
<i>Picea meyeri</i>	ANB44963.1
<i>Picea morrisonicola</i>	AHC92686.1
<i>Picea obovate</i>	AND98240.1
<i>Picea purpurea</i>	ADE32592.1
<i>Picea schrenkiana</i>	ADE32606.1
<i>Picea sitchensis</i>	ADM74041.1
<i>Picea smithiana</i>	AIE55309.1
<i>Picea wilsonii</i>	AGK38575.1
<i>Pinus hwangshanensis</i>	AIF76061.1
<i>Pinus massoniana</i>	AIF76056.1
<i>Pinus pinaster</i>	ATP62246.1
<i>Pinus sylvestris</i>	AFV79206.1
<i>Pinus taeda</i>	ATP62296.1
<i>Pistacia vera isoX1</i>	XP_031251681.1
<i>Pistacia vera isoX2</i>	XP_031251690.1
<i>Populus trichocarpa</i>	XP_002307516.2
<i>Populus trichocarpa*</i>	XP_006386299.2
<i>Prosopis alba isoX1</i>	XP_028763906.1
<i>Prosopis alba isoX2</i>	XP_028763910.1
<i>Prunus avium isoX1</i>	XP_021818210.1
<i>Prunus avium isoX2</i>	XP_021818214.1
<i>Prunus avium isoX3</i>	XP_021818215.1
<i>Prunus dulcis isoX1</i>	XP_034196939.1
<i>Prunus dulcis isoX2</i>	XP_034196940.1
<i>Prunus dulcis isoX3</i>	XP_034196942.1
<i>Prunus dulcis isoX4</i>	XP_034196943.1
<i>Prunus dulcis IsoX5</i>	XP_034196944.1
<i>Prunus dulcis isoX6</i>	XP_034196945.1
<i>Prunus persica isoX1</i>	XP_007199688.2
<i>Prunus persica isoX2</i>	XP_020426395.1
<i>Punica granatum</i>	XP_031394148.1
<i>Quercus suber</i>	XP_023907641.1
<i>Rhodamnia argentea</i>	XP_030549673.1
<i>Ricinus communis</i>	XP_025014064.1
<i>Rosa chinensis isoX1</i>	XP_024166286.1
<i>Rosa chinensis isoX2</i>	XP_024166288.1
<i>Selaginella moellendorffii</i>	XP_024528715.1
<i>Setaria italica isoX1</i>	XP_004968438.1
<i>Setaria italica isoX2</i>	XP_022682651.1
<i>Setaria viridis isoX1</i>	XP_034596606.1
<i>Setaria viridis isoX2</i>	XP_034596610.1
<i>Solanum lycopersicum</i>	XP_004237832.1

<i>Sorghum bicolor</i>	XP_021312623.1
<i>Spinacia oleracea</i>	XP_021849292.1
<i>Syzygium oleosum isoX1</i>	XP_030465408.1
<i>Syzygium oleosum isoX2</i>	XP_030465409.1
<i>Takakia lepidozoides</i>	gnl onekp SKQD_scaffold_2004946
<i>Vigna radiata</i>	XP_014513458.1
<i>Vigna radiata isoX1</i>	XP_014514134.1
<i>Vigna radiata isoX2</i>	XP_014514153.1
<i>Vigna unguiculata isoX1</i>	XP_027935547.1
<i>Vigna unguiculata isoX2</i>	XP_027935549.1
<i>Ziziphus jujuba</i>	XP_015886353.1

Table 7. Accession numbers of GIGANTEA were obtained from different species. The datasets are derived from different sources like NCBI and the OneKP database.

3.2.2. Assessment of Cladogram

To examine the ancestral relationships of the GIGANTEA protein and investigate the evolutionary history of this protein among the plants, a cladogram of GI was constructed using the IQ-TREE web server with 1000 bootstraps. Accordingly, analysis of GI protein sequences showed that the protein found in eudicots, monocots, amborales (basal angiosperms), gymnosperms, pteridophytes-bryophytes, and green algae formed distinct clades. The cladistic analysis revealed that the green algae were closely related to bryophytes. The GI of *A. agrestis* is more closely related to the GI protein of green algae than the GI protein of other mosses in the tree, which are more closely related to each other. The GI of pteridophyte i.e., *S. moellendorffii* is present in the same clade as of algae and bryophyte but is more distant. It is also observed that homologs of GI in all the species of green algae, bryophytes, pteridophytes, gymnosperm, and basal angiosperm belong to the same clade. Similarly, all the species of monocots were also found to be in the same clade. However, GI in angiosperms is present in several clades (Figure 14).

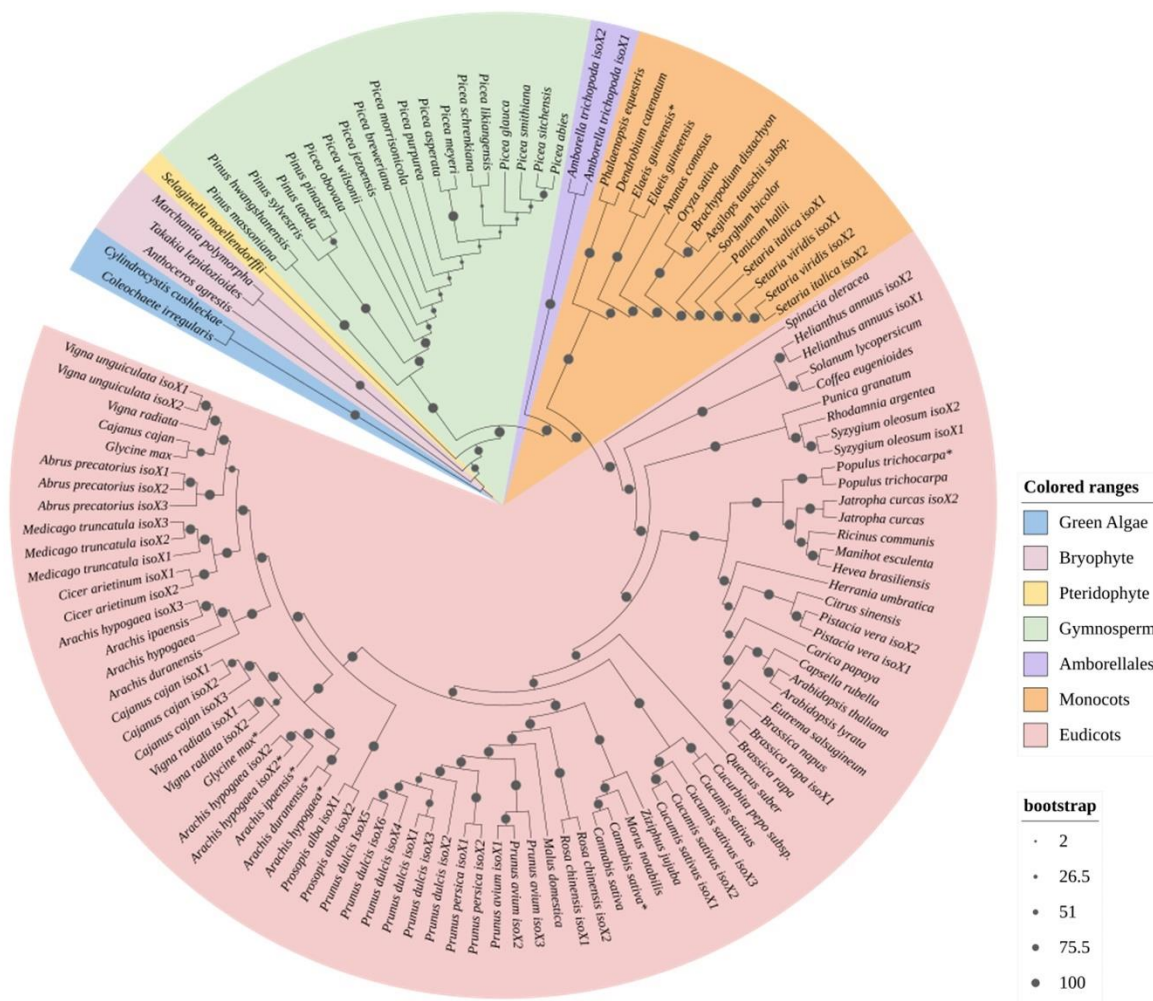


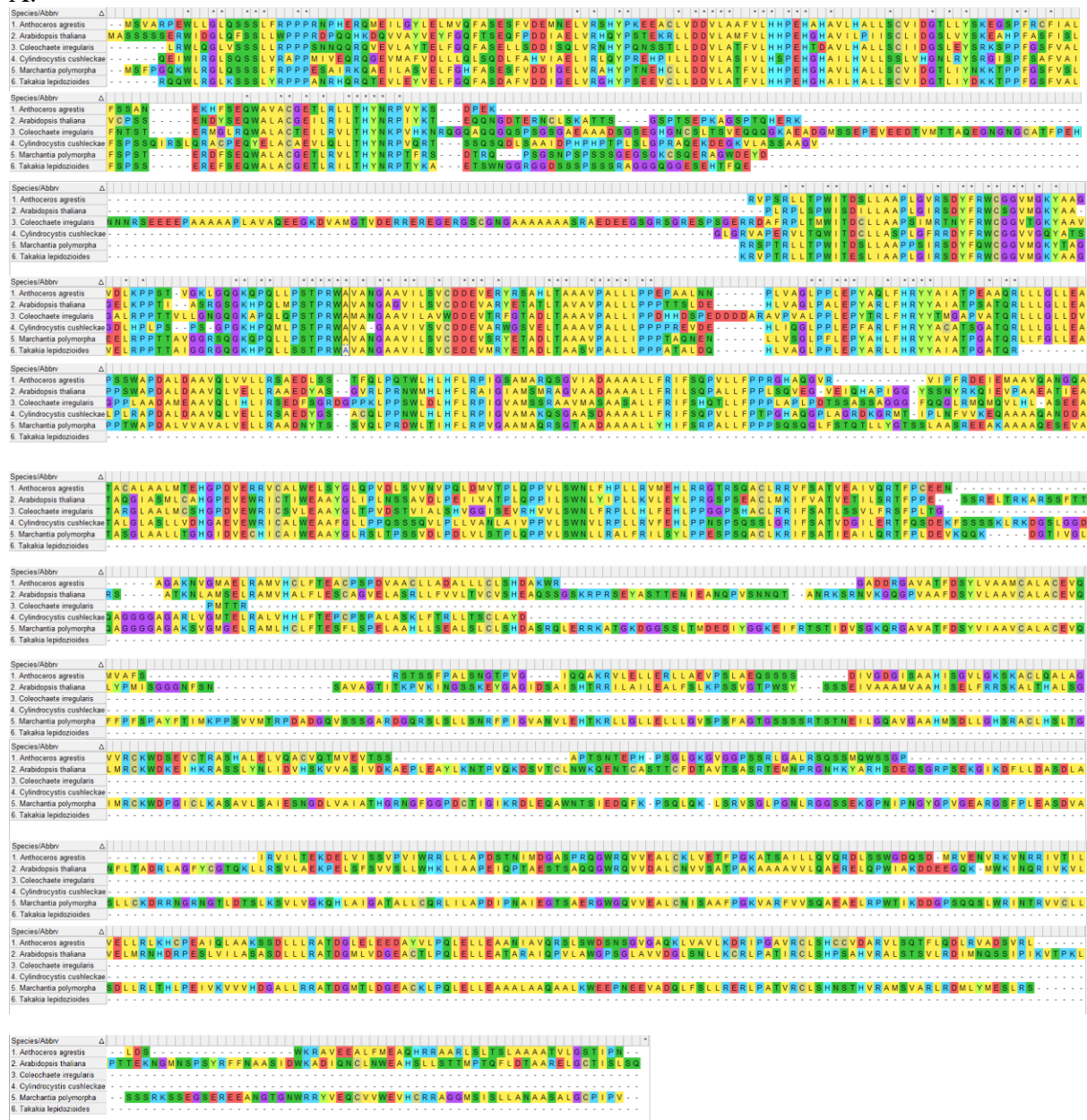
Figure 14. Circular cladogram of GIGANTEA protein. The tree was generated and viewed with IQ-TREE web server with 1000 bootstrap values with default settings. The genera are color-coded where: Peach- Eudicot, Yellow- Monocot, Blue- Amborallales, Purple- Bryophytes, Grey- Pteridophytes, Lime- Geen algae, and Green- Gymnosperms.

3.2.3. Assessment of Multiple Sequence Alignment

From a total of 123 species of plant kingdom, 6 species i.e., 2 algae and 3 bryophytes along with the sequence of *A. thaliana* which is the model organism of higher plants were selected to compare the GI sequences from lower to higher plants. The amino acid sequences of GI obtained from *C. cushlecae*, *C. irregularis*, *M. polymorpha*, *A. agrestis*, *T. lepidozoides*, and *A. thaliana* were aligned using the ClustalW program in MEGA version 11 software. The residue numbers of the conserved stretches of amino acids were identified from the protein

sequence of *GI* of *A. thaliana* based on MSA (Figure 15A). Five different conserved amino acid stretches (DDVLAM, LTHYNR, STPRWAV, VPALLLPPP, and LFHRYYA) were found in the MSA assessment. We identified the nucleotide sequences that code for these conserved amino acid stretches and located them on the exons of the *GI* gene of *A. thaliana*. According to the TAIR database, the *GI* gene lies in chromosome 1 stretching out from 8061751 bp to 8067790 bp in plus strand. We found the DDVLAM to be coded by exons 3 and 4, LTHYNR coded by exon 5, STPRWAV and VPALLLPPP to be coded by exons 7 and LFHRYYA to be coded in exons 7 and 8 (Figure 15B & Table 8).

A.



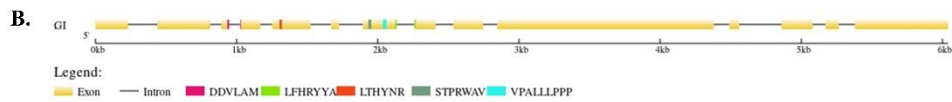


Figure 15. Multiple sequence alignment of GIGANTEA domains. Alignment was performed using the ClustalW program and is displayed using the MEGA version 11 tool (A). The amino acid residues which were highly conserved were aligned with the respective exons in the *GI* gene. The gene structure was illustrated using Gene Structure Display Server (GSDS) version 2.0 (B). The five different conserved amino acid sequences were traced in the gene structure and indicated with different colors. MSA analysis of DDVLAM, LTHYNR, STPRWAV, VPALLLPPP, and LFHRYYA conserved amino acid sequences was performed obtained from *C. cushleackae*, *C. irregularis*, *M. polymorpha*, *A. agrestis*, *T. lepidozoides* and *A. thaliana*. Maroon-DDVLAM, Green-LTHYNR, Red-STPRWAV, Grey-VPALLLPPP and Torquoise-LFHRYYA

Exon number	Number of Nucleotides	Position on Chromosome	Positions of Conserved Amino Acids
1	231	8061251-8061981	NA
2	372	8062191-8062562	NA
3	55	8062643-8062697	DDVLAM
4	143	8062776-8062918	
5	272	8063003-8063274	LTHYNR
6	56	8063421-8063476	NA
7	238	8063646-8063883	STPRWAV (7 th Exon) VPALLLPPP (7 th Exon)
8	151	8064010-8064160	LFHRYYA (7 th and 8 th Exon)
9	210	8064287-8064496	NA
10	1533	8064597-8066129	NA
11	69	8066242-8066310	NA
12	219	8066612-8066830	NA
13	93	8066923-8067015	NA
14	661	8067130-8067790	NA

Table 8. Details of positions of conserved amino acid in the exon lengths of GIGANTEA

3.2.4. Motif and domain identification

For further analysis of the similarity and diversity of motifs, MEME analysis of the above six amino acid sequences was performed. The MEME analysis provided with 15 motif consensus sequences. We found that all 15 motif consensus sequences were present in *A. thaliana*, *M. polymorpha*, and *A. agrestis*. In *T. lepidozoides* 6 motifs were found out of 15 motifs present

in *A. thaliana*. However, algae like *C. cushleackae* and *C. irregularis* have 11 and 10 motifs respectively out of 15 motifs present in *A. thaliana* (Figure 16). Upon analyzing these consensus sequence motifs in CDD NCBI, we found that these sequences do not correspond to any known protein domain. Therefore, the lack of any known conserved domain in GI protein makes it difficult to determine any functional conservation of the protein both in lower and higher plants despite knowing the conserved sequences.

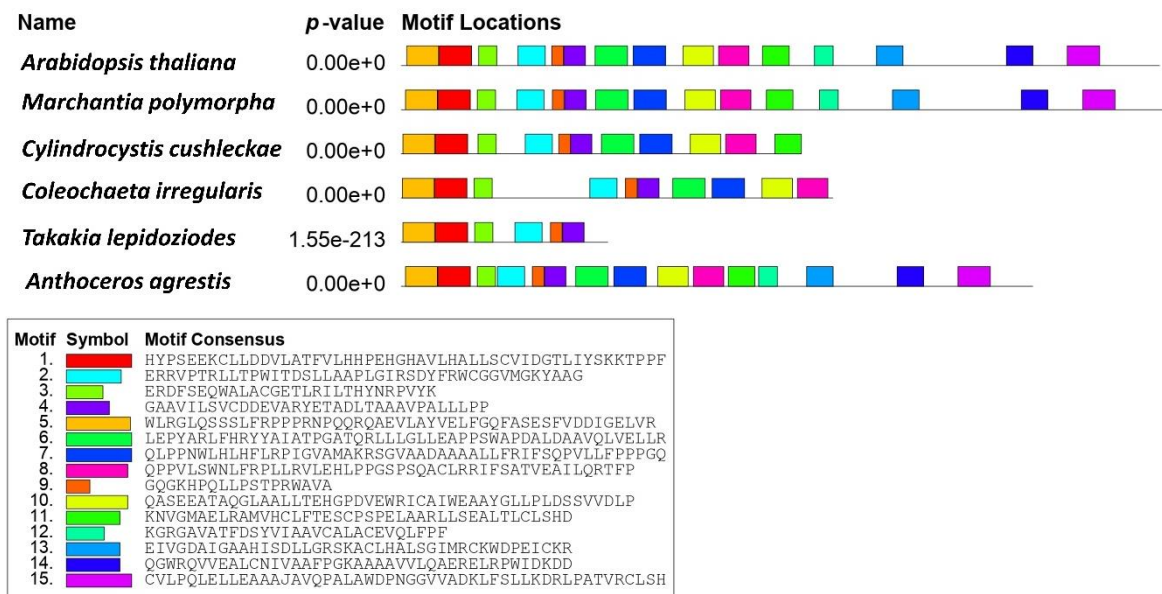


Figure 16. Motif analysis of GIGANTEA protein. The distribution of 15 motif consensus sequences in GI protein, identified by the MEME program, was shown as colored boxes. MEME analysis was performed of sequences obtained from *C. cushleackae*, *C. irregularis*, *M. polymorpha*, *A. agrestis*, *T. lepidozoiodes*, and *A. thaliana*.

3.2.3. Prediction of Protein Model

The 3D shape of a protein determines its biological function and provides essential details for modifying it to provide beneficial biotechnology tools or regulate its functionality. Even after many advancements over the decades in understanding the mechanism and function of GI protein in plant development, the structure of a protein is yet to be crystallized. The structural framework of GI is not known because of the absence of any homology and conserved domains. In this scenario, 3-D model prediction using different biotechnique tools serves as an important asset in solving the structure of proteins to have a deeper understanding of the functionality of the protein. Predicting the structure of GI will provide insight into understanding the precise

mechanism of interactions with its partner. In this study, i-TASSER web servers have been used for predicting the 3-D structure of the GI of *A. thaliana* along with its secondary structure. The predicted model obtained from i-TASSER revealed 51 α -helix and 15 β -sheet stretches. The software provided the 5 best models which correspond to the largest structure clusters of the decoy. For each target, I-TASSER simulations generate a large ensemble of structural conformations, called decoys. The final model is selected when i-TASSER uses the SPICKER program to cluster all the decoys based on the pair-wise structure similarity and reports up to five models that correspond to the five largest structure clusters. The confidence of each model is quantitatively measured by a C-score that is calculated based on the significance of threading template alignments and the convergence parameters of the structure assembly simulations. C-score is typically in the range of [-5, 2], where a C-score of a higher value signifies a model with a higher confidence and vice-versa. TM-score and RMSD are estimated based on C-score and protein length following the correlation observed between these qualities. Since the top 5 models are ranked by the cluster size, the lower-rank models may have a higher C-score in rare cases. Although the first model has a better quality in most cases, it is also possible that the lower-rank models have a better quality than the higher-rank models as seen in our benchmark tests. If the I-TASSER simulations converge, it is possible to have less than 5 clusters generated; this is usually an indication that the models have a good quality because of the converged simulations.

The 2-D images of the top 5 models thus obtained from I-TASSER are shown in Figure 17 with C-score values.

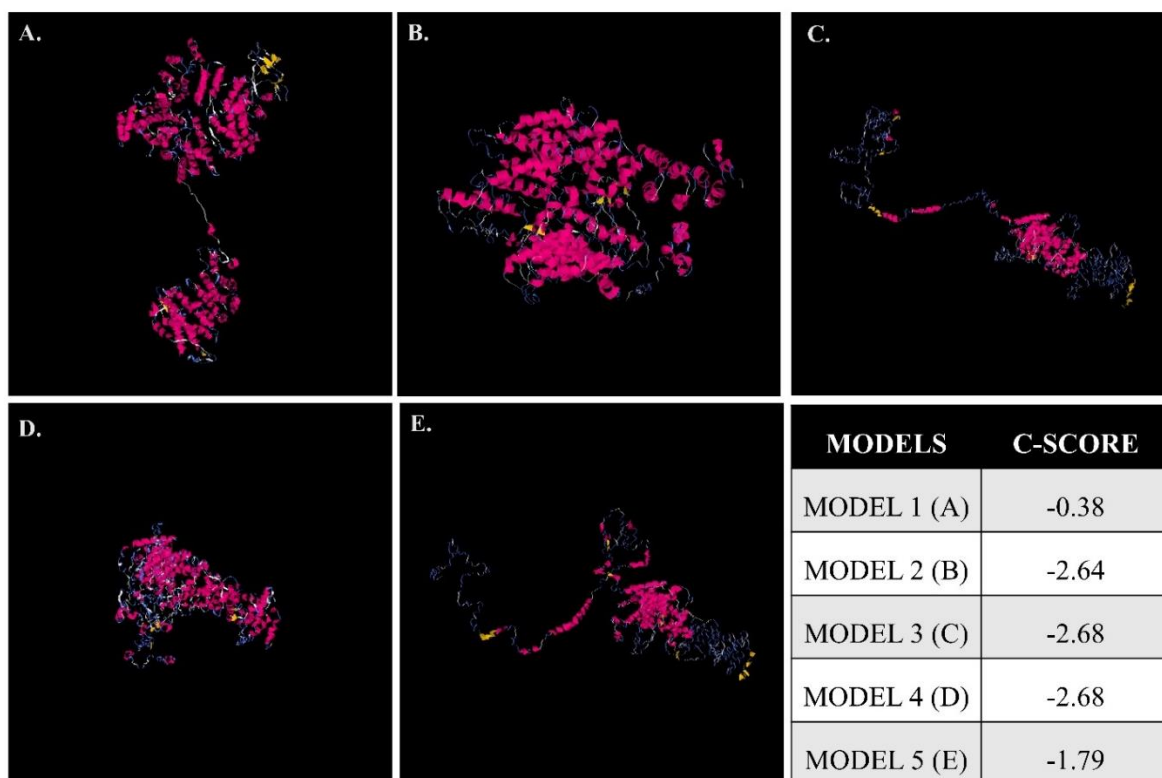


Figure 17. Predicted models of GIGANTEA using i-TASSER web server. The software provided the 5 best models which correspond to the largest structure clusters of the decoy.

3.3. DISCUSSION

A comprehensive analysis of the evolutionary trajectory of GI throughout the plant kingdom indicates its presence in angiosperms and recruitment in the ancestral lineages of land plants, especially charophytes (Linde *et al.*, 2017). GI exists as a single copy in most species, and its evolution is believed to have occurred concurrently with the emergence of land plants. The dynamics of GI evolution include critical events like gene duplication and loss, which shape the complexity of this essential protein. Despite its importance, GI is absent in lower plant species such as *Physcomitrella* and *Chlamydomonas*. Extensive research has been conducted on GI homologs from both flowering and non-flowering plants, providing a more detailed understanding of GI's evolution across various phyla (Linde *et al.*, 2017).

According to phylogenetic analyses, GI sequences are notably absent in most green algae. It has also been reported that there are no known GIGANTEA homologs in prokaryotes, fungi, mosses, or animals (Holm *et al.*, 2010). The green unicellular alga *Ostreococcus tauri* lacks a GI homolog (Corellou *et al.*, 2009). However, a single GI homolog has been discovered in more recently diverged charophytes, specifically Coleochaetales (*Coleochaete irregularis*) and Zygnematales (*Cylindrocystis cushleackae*) (Linde *et al.*, 2017). However, it is not found in *Klebsormidiales*. Thus, it is evident that the complexity of the circadian clock right from *Klebsormidium* is in line with the adaptation to terrestrial habits (Linde *et al.*, 2017). This observation supports the theory that Zygnematales or Coleochaetales, which are more closely related to land plants, witnessed the spontaneous emergence of GI concurrent with the transition to a terrestrial environment.

Bryophytes claim a vital position during evolution, being the first embryonic land plants, the first plants that colonized the land. Circadian rhythms in *Marchantia polymorpha* are weaker than those of angiosperms, while *Physcomitrella patens* are rhythmic in DD but not LL conditions. *M. polymorpha* lacked morning-phased genes responsible for the acute light

response. The interaction of *GI* in the liverwort, *M. polymorpha* for reproductive induction (Kubota *et al.*, 2014) is similar to that of *AtFKF1* for flower induction, however, it requires longer photoperiods. Nonetheless, the absence of the most fundamental component of the clock, *CCA1*, in liverworts warrants further study (Linde *et al.*, 2017). The lack of *GI*, *TOC1*, and *ZTL* homologs in the higher moss *P. patens* circadian clock is evidenced by gene loss and a comparatively more uncomplicated ancestral form (Holm *et al.*, 2010). The absence of *GI*, *TOC1*, and *ZTL* homologs in *P. patens* suggests a reduction in circadian clock components, implying a simpler ancestral state. *Takakia lepidozoides*, an early diverging moss, is an exception, expressing *GI* and *ZTL/FKF1* homologs, highlighting the nuanced evolution of *GI* in mosses as in a basal moss *T. lepidozoides*, homologs to these three genes are present and thus might have been lost soon after branching of mosses. Hornworts represent another kind of variation in which only the homolog of *TOC1* is absent, retaining the homologs of *GI* and *ZTL* (Linde *et al.*, 2017).

In pteridophytes, except for *Selaginella moellendorffii*, *GI* homologs are conspicuously absent in tested pteridophytes, indicating that gene loss was a critical aspect of *GI* evolution in early plants. The *FKF* homologs are also found to be present in the *S. moellendorffii* which indicates that the *GI-FKF1* module has been conserved since ancient times and may have played a role in shaping the evolution of higher plants (Kubota *et al.*, 2014; Mishar and Panigrahi, 2015). This light perception module must be thoroughly studied to comprehend the evolution of various functions and residues, as well as putative domains required to carry out these functions in plants.

The *GIGANTEA* ortholog in gymnosperms like *Picea abies*, *PaGI*, exhibits a 58 % identity and 72 % similarity with *AtGI*. Along with *GI*, in *P. abies*, *CCA* and *ZTL* were partly conserved, but under free-running conditions of both LL and DD conditions, the rhythmicity of the clock genes is dampened (Holm *et al.*, 2010). The observed natural variations in *GI* have been associated with clinal variations within distinct populations of the closely related Scandinavian

Norway spruce (Chen *et al.*, 2014; Mishra and Panigrahi, 2015). The ortholog *PaGI* shows functional conservation, rescuing the late-flowering phenotype and flowering synchronously with wild-type plants which again confirms that GI is a crucial clock component required for plant development. Circadian light-harvesting complex (LHC) expression was lacking in several members of Pinopsida, including *Picea*, *Pinus*, *Abies*, *Larix*, *Taxus*, and Ginkgopsida (Piechulla *et al.*, 2001). Dampening of *LHYa*, *LHYb*, *TOC1*, *GI*, and *ZTL* in the summer was observed from the diurnal transcriptomic analysis of Japanese cedar [*Cryptomeria japonica* (L.f.) D.Don] (Nose and Watanabe, 2014).

In angiosperms, GIGANTEA has been found in all higher plants studied so far. GI divergence is less pronounced in monocots than in dicots, implying that gene duplication in the GI lineage results in redundancy and functional diversification in higher plants. In dicots like soybean, *GIGENTIA* (*GmGI*) also presents an example of a variant as compared to *AtGI*. Out of the three copies of *GmGI*, *GmGIa* acts as a suppressor of flowering compared to its counterpart *A. thaliana* (Watanabe *et al.*, 2011). The H1 haplotype in the Chinese landraces bears sequence variations, including truncation, exerts early flowering and maturation phenotype (Wang *et al.*, 2016). The nucleotide diversity and polymorphism in the 47 haplotypes of *GmGIa* confer the potential to be exploited for clock (Hyten *et al.*, 2006) and abiotic stress tolerance studies (Simon *et al.*, 2020). Although several monocot crop plants, such as rice, maize, wheat, barley, and sorghum, are more important in agriculture, our understanding of their circadian regulation lags behind that of dicot plants. Nonetheless, monocots contain several orthologs of the *A. thaliana* circadian clock (Murakami *et al.*, 2007). The phylogenetic analysis also demonstrates that the evolution of circadian clock components occurred long before the divergence of monocots and dicots (Takata *et al.*, 2010). Any alteration in *Lemna gibba* due to over-expression or knock-down in an expression of genes *LgGIH1* resulted in disrupted rhythms of the clock genes (Serikawa *et al.*, 2008). *OsGI* functional knockouts in rice display reduced

adaptability to seasonal changes in field-grown conditions and disturbed diurnal gene expression up to 75 % (Izawa *et al.*, 2011).

The cladogram thus indicated that GI appeared in a common ancestor of algae and plants. However, the fact that GI is present in very few lower plants while being universally present in angiosperms indicates throughout evolution GI has become an integral part of the plant circadian clock and flowering time regulation pathways in higher plants, a role that has not yet been established in lower plants. The widespread distribution of GI homologs across various plant species aligns with the concept of gene conservation and functional significance in plant development. GI homologs are significantly present in higher plants, particularly in angiosperms. Several studies have highlighted the presence of GI orthologs in diverse angiosperms, including model plants like *Arabidopsis thaliana* and rice (Park *et al.*, 1999; Fowler *et al.*, 1999). The presence of GI in *Amborella trichopoda*, a basal angiosperm, suggests its evolutionary origin from basal to mature angiosperms, indicating its ancient role in plant development. The identification of GI in *Amborella trichopoda* supports the notion that GI has ancient origins predating the diversification of flowering plants (Mathews and Donoghue, 1999; Zeng *et al.*, 2014). While traces of GI were found in gymnosperms and a few lower plants, its presence in green algae, bryophytes, and pteridophytes is rare, indicating a more recent evolutionary acquisition or loss in these lineages which is consistent with previous genomic studies (Merchant *et al.*, 2007; Bowman *et al.*, 2017). Cladistic analyses have been instrumental in elucidating the evolutionary relationships among GI proteins across plant taxa. This reveals distinct clades formed by GI proteins across different plant groups, including eudicots, monocots, amborellales, gymnosperms, bryophytes, and green algae. Green algae are closely related to bryophytes, suggesting a shared evolutionary history. The close relationship between green algae and bryophytes inferred from cladistic analyses is consistent with the notion of shared ancestry between these groups, reflecting their evolutionary transition from aquatic to terrestrial environments (Delwiche and Cooper, 2015). The GI protein of *A. agrestis* shows a

closer relation to green algae than other mosses, indicating potential ancient connections between certain mosses and algae. The presence of GI homologs in these species of green algae, bryophytes, pteridophytes, gymnosperms, and basal angiosperms belonging to the same clade suggests a conserved role across these plant groups (Figure 18). The shared ancestry between these groups reflects their evolutionary transition from aquatic to terrestrial environments according to Delwiche and Cooper (2015). Previously it has been reported that the homologs from diverse plant lineages belong to the same clade suggesting functional conservation and possibly shared regulatory roles in plant biology (Song *et al.*, 2015). Multiple sequence alignment (MSA) revealed that the conserved amino acid stretches across GI sequences from different plant species, indicating functional constraints and the potential importance of these regions in protein function. These conserved motifs may play critical roles in protein-protein interactions, subcellular localization, or post-translational modifications (Fowler *et al.*, 1999; Huq *et al.*, 2000). The lack of known conserved domains in the GI protein despite the presence of conserved motifs suggests functional diversity and possibly novel functions in both lower and higher plants. In addition, Structural prediction of the GI protein provides insights into its potential 3D shape and secondary structure. The predicted models offer a basis for understanding potential interactions with partner molecules and can guide further experimental studies to elucidate the precise mechanisms of GI function in plant development and adaptation.

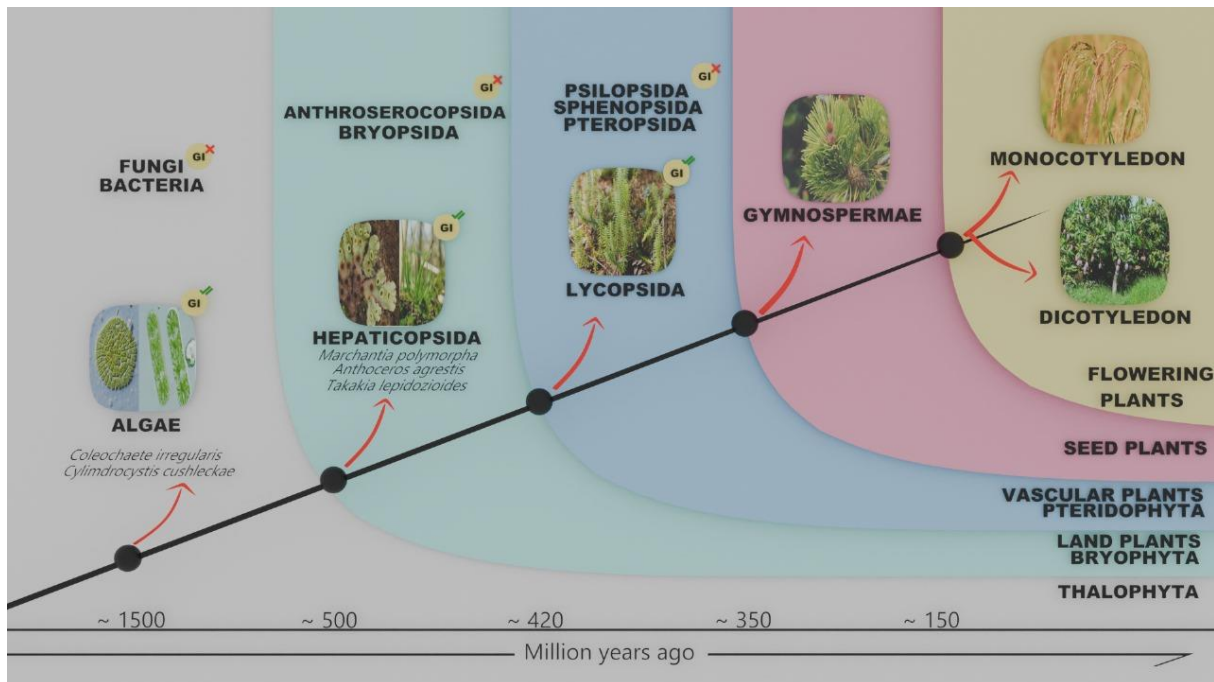


Figure 18. Distribution of GI protein in the plant kingdom.

In conclusion, the *in silico* analyses provide valuable insights into the evolutionary history, conservation patterns, and structural characteristics of the GIGANTEA protein across diverse plant taxa. Understanding the evolutionary dynamics and functional diversity of GI contributes to our knowledge of plant evolution and adaptation strategies, offering avenues for further experimental investigations into its biological roles and regulatory mechanisms in plant biology.

CHAPTER-4

ROLES OF GIGANTEA IN ABIOTIC AND BIOTIC STRESS TOLERANCE

CHAPTER 4: ROLES OF GIGANTEA IN ABIOTIC AND BIOTIC STRESS TOLERANCE

4.1. TO RE-EVALUATE THE ROLE OF GIGANTEA IN DROUGHT AND SALINITY STRESS USING THE CRISPR-CAS9 GENOME EDITING TOOL

4.1.1. BACKGROUND

Higher plants possess the ability to detect irregular variations in day length, a phenomenon known as photoperiodism, which influences the initiation of flowering and other developmental processes. In *Arabidopsis thaliana*, a model plant species, the circadian clock coordinates responses to changes in day length, with the GIGANTEA (GI) protein serving as a key regulator. The expression of GI, controlled by the circadian clock, exhibits diurnal oscillations, peaking at specific times of the day depending on the light-dark cycle. GI plays diverse roles in plant development, including regulation of flowering time, hypocotyl elongation, stress responses, and starch accumulation. Mutations in GI have been extensively studied, revealing various alleles with distinct phenotypic effects. These mutations, arising from irregular mutagenesis or T-DNA insertions, have provided insights into the multifaceted functions of GI. For instance, certain alleles introduce premature stop codons or alter protein structure, affecting GI expression levels or function. Notably, recent advancements in gene editing technologies like CRISPR-Cas9 have shed light on the limitations of traditional mutation methods, such as T-DNA insertion, in generating accurate mutant phenotypes.

Redei *et al.*, first depicted *gi* mutants as late-flowering mutants in 1962. Other *gi* mutants depicted in literature include *gi-1*, *gi-2*, *gi-3*, *gi-4*, *gi-5*, *gi-6*, *gi-11*, *gi-12*, *gi-100*, *gi-200*, *gi-201*, *gi-596*, and *gi-611*. Some of the *gi* mutants were found to influence the activity of the circadian clock, while others altered various responses. The alleles of *GI* are the result of irregular mutagenesis or T-DNA addition, which has helped us understand its various functions. Alleles such as *gi-1*, *gi-2*, *gi-3*, and *gi-6* introduce an untimely stop codon, whereas *gi-4* and *gi-*

5 most likely adjust the protein's C-end due to casing shift changes (Fowler *et al.*, 1999). The *gi-11* and *gi-201* alleles containing T-DNA insertion showed negligible to no *GI* expression (Martin-Tryon *et al.*, 2007). The *gi-100* mutation was initially identified in a red-light screen, and contained a T-DNA inclusion, but delivered a truncated transcript of approximately 2 kb due to the absence of the 3' end of *GI* (Huq *et al.*, 2000). The transcript levels in *gi-1*, *gi-2*, and *gi-3* are lower than those in *gi-4*, *gi-5*, *gi-6*, and *gi-100*, which have comparable or higher levels than their respective WT (Fowler *et al.*, 1999; Huq *et al.*, 2000). The role of *GI* in blue light-dependent hypocotyl elongation was discovered using the *gi-200* allele, which included a serine 932 substitution (Martin-Tryon *et al.*, 2007). Any deletion in *GI* for the most part causes defects in the flowering time, circadian clock, and control of hypocotyl elongation.

Studies on other genes, such as *ABP1* and *PSRP5*, have highlighted unexpected findings regarding the roles of these genes in plant development. CRISPR-generated mutants have revealed discrepancies compared to earlier conclusions drawn from T-DNA insertion lines, underscoring the importance of precise genetic manipulation techniques. *ABP1* was previously thought to play an important role in plant development and auxin signalling (Nishimasu *et al.*, 2014). Nonetheless, recent mutational studies based on CRISPR-generated mutants produced shocking results. Previous studies using antisense lines, antibody lines, and *Arabidopsis* mutant alleles have concluded that *ABP1* is required for embryogenesis, root development, and a variety of other developmental processes. The new *ABP1* CRISPR mutant lines were indistinguishable from wild-type (WT) plants at all developmental stages studied (Gao *et al.*, 2015). Furthermore, Tamura *et al.*, (2016) discovered that the embryo lethal phenotype of the T-DNA insertional mutant *abp1-1* was caused by a deletion in the neighboring *BELAYA SMERT* gene. According to Romani *et al.*, (2012) and Tiller *et al.*, (2012), the *PSRP5* T-DNA insertion line (SALK_051891) was the most severely affected mutant among *Arabidopsis psrp* mutants. These findings indicated that protein translation in plastids plays a critical role in plant growth. It is therefore possible that the knockdown of *PSRP5*, which is located next to *ALADIN*

on chromosome 3, is the cause of the *Aladin-1* mutant phenotype. It remains to be seen how the T-DNA insertion within *ALADIN* affects the nearby *PSRP5* gene. Previous research discovered that T-DNA insertion lines had unexpectedly high rates of inter-chromosomal rearrangements (Tax *et al.*, 2001). In those instances, mutants had single T-DNA inserts and segregated normally, but sequences from loci unrelated to the insertion site were found flanking the T-DNA border. *Aladin-1*'s genomic sequence between the T-DNA border and *PSRP5* was identical to that of the corresponding wild-type sequence (Tamura *et al.*, 2016). It is therefore unlikely that T-DNA integration in *Aladin-1* caused inter-chromosomal rearrangements that influenced *PSRP5* expression. However, we cannot rule out the possibility that genetic changes at different loci in the regions we sequenced influence *PSRP5* expression. Alternatively, even though the insertion occurred 2.2 kbp downstream of *PSRP5*, the T-DNA could have disrupted a cis-regulatory element that controls *PSRP5* expression (Tamura *et al.*, 2016).

Understanding the molecular mechanisms underlying GI function requires comprehensive investigation, including the development of specific antibodies tailored to plant GI. Additionally, unraveling the molecular basis of off-target effects associated with T-DNA mutants is crucial for refining genetic studies using CRISPR-Cas9 technology, ultimately enhancing the accuracy and reliability of genetic research in plants. GI plays a pleiotropic role in plant development, so understanding its mechanisms is crucial. To accomplish this, we have designed an antibody specific to the plant that would help us understand other biochemical functions of GI. Moreover, the exact molecular mechanism responsible for the off-target effects specific to T-DNA mutants in GI remains unclear. We aimed to eliminate such off-target effects of GI from our system using CRISPR-Cas9 technology by generating and characterizing CRISPR mutant line *gi* to achieve higher accuracy in the ongoing genetics research. The preliminary work from our lab (Dash L., 2018) involves generating GI null mutant using the CRISPR genome editing tool described in Annexure 1.

4.1.2. RESULTS

4.1.2.1. Genotyping for the confirmation of mutation

The Cas9 enzyme cleaves the spacer/guide sequence complementary region of the genomic DNA at the target site, causing a double-stranded break (DSB) within the nucleus. The cell initiates repair mechanisms, primarily Non-Homologous End Join Repair (NHEJ) and Homology Directed Repair (HDR). HDR requires a homologous sequence nearby and is slower, while NHEJ is faster but error-prone, often preferred by the cell. Targeting two sites approximately 1.3 kbp apart allows for the deletion of the intervening genomic sequence when both sites are cleaved. Figure 19 depicts the genomic locus of GI where the genomic targets in exon 2 and exon 7 have been shown.

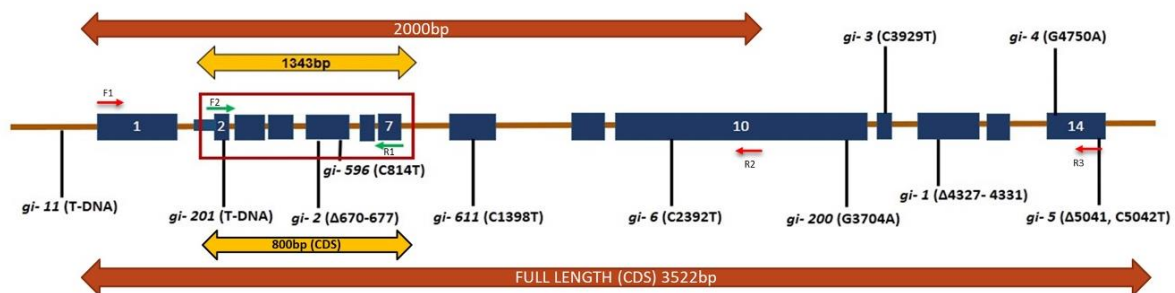


Figure 19. The genomic locus of GI where the genomic targets in exon 2 and exon 7 have been shown.

Fifty seeds exhibiting eGFP expression were selected, planted, and subjected to vernalization under LD conditions, resulting in 16 successful germinations. DNA was isolated from the leaves of these transformant plants. PCR was performed using primers complementary to the genomic targets. Expectedly, two amplicons were anticipated: a 670 bp amplicon from the construct inserted during floral dip transformation and a ~1.3 kbp amplicon from the genomic loci of the targets.

Plants with perturbed target sites would display only the construct amplicon (~670 bp), while those with intact targets would show the genomic amplicon (~1.3 kbp). Among the 16 positive transformants, three exhibited homozygous perturbation at their *GI* genomic loci (Figure 20).

The three lines that showed homozygous perturbation, were named according to the exons targeted for the mutation and pots namely *gi-C272*, *gi-C272(8)*, and *gi-C272(10)*.

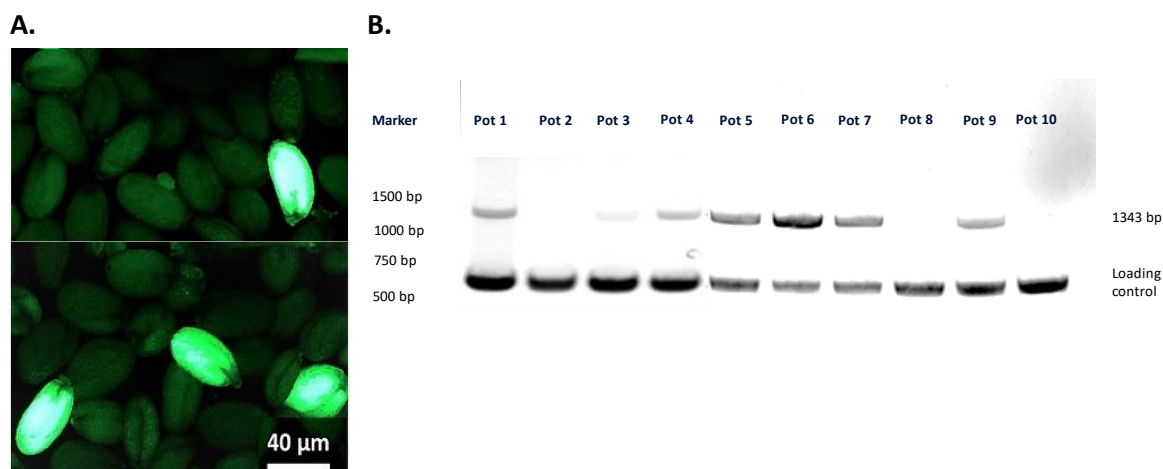


Figure 20. Generation and screening of CRISPR mutants of GIGANTEA. (A) Representative image of selected transformed seeds based on the absence and presence of eGFP signals on the seed coats in *A. thaliana*. (B) Gel picture of DNA samples extracted from the leaves of plants growing in different pots (pot 1, pot 2, pot 3, pot 4, pot 5, pot 6, pot 7, pot 8, pot 9 and pot 10)

The selected transformed seeds (F₀ generation, hemizygous) are then sown on the soil to generate homozygous GI-CRISPR mutant lines. The transgenic plants obtained from F₀ seeds were named F₁ generation (F₁ transgenic plants). The seeds from the F₁ transgenic plants that showed the eGFP signals were selected and named F₁ generation seeds where the genotype was hemizygous (R/0). The plants (F₂ generation plants) grown from F₁ generation seeds sown in soil were then allowed to self-pollinate and the seeds were harvested which were named as F₂ generation seeds. Randomly selected 100 seeds of F₂ generation plants were taken for observation under a fluorescent microscope to confirm the homozygosity of the seedlings. The phenotype of F₂ generation seedcoats was either eGFP positive or eGFP negative. Apart from that, nearly 74 seedcoats showed eGFP signals (glowing seeds) and the rest 26 seedcoats did not show eGFP signals (non-glowing seeds). The ratio of eGFP positive to eGFP negative seedcoats came out to be 3:1 which supports Mendel's law of segregation of phenotypic ratio, 3:1 (homozygous dominant: heterozygous recessive). Hence, the homozygous glowing seeds from the above screening processes were further selected and allowed to self-pollinate.

Therefore, the bulked seeds were named as F₃ generation seeds which were all homozygous.

The detailed flowchart of genetic screening is mentioned in Figure 21.

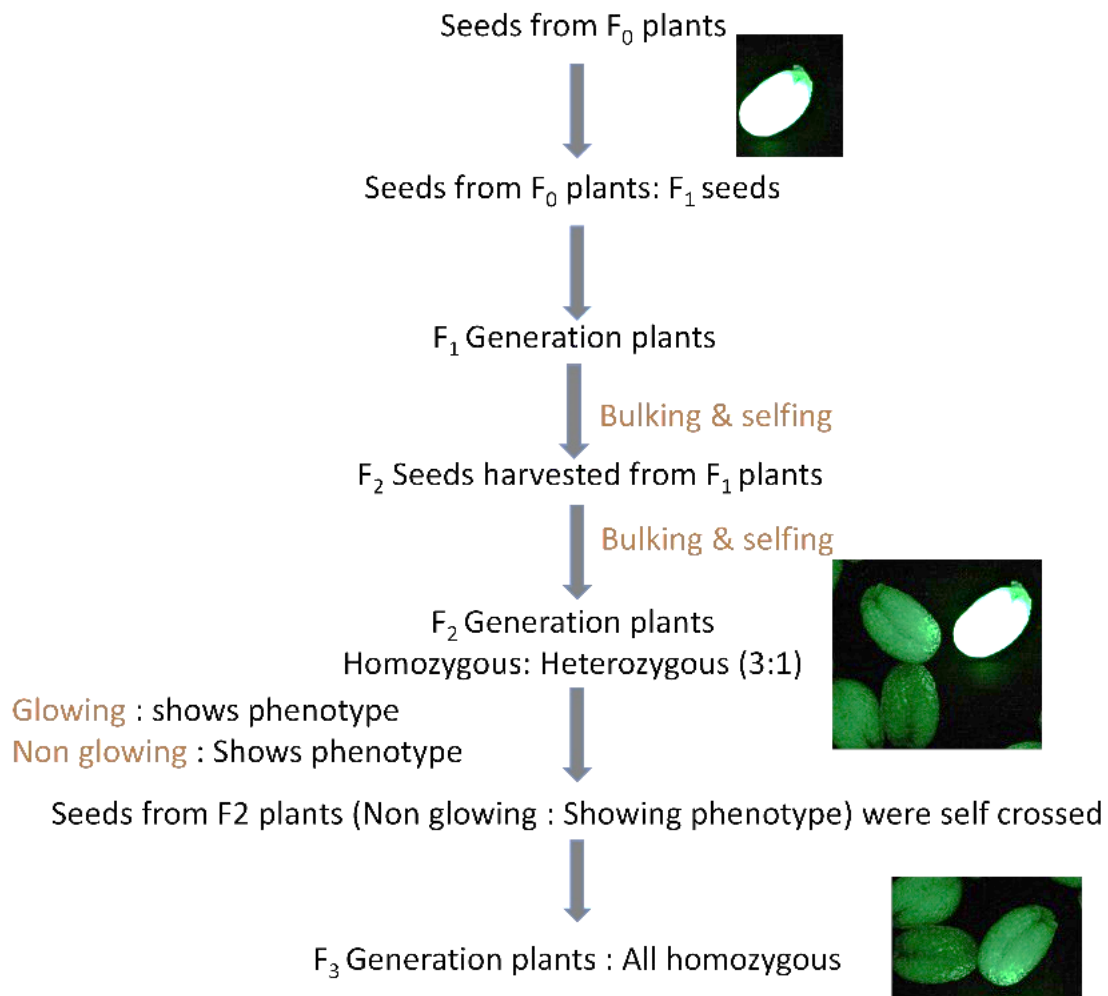


Figure 21. Flowchart depicting the genetic screening of *gi* mutant line generated by CRISPR-Cas9 technology.

Further to confirm the mutation in the homozygous lines of *gi* mutants generated from CRISPR-Cas9 technology, a genetic screening was performed. For this study, a T-DNA insertional mutant of *GI* i.e., *gi-100*, and the newly developed CRISPR mutants of *GI* i.e., *gi-C272*, *gi-C278* and *gi-C2710* along with the wildtype Col-0 were used. Since all the CRISPR mutants of *gi* showed similar phenotype and genotype, we proceeded with only *gi-C2710* (which is further called *gi-C27* based on its position of mutation only) mutant for further studies. RNA was extracted from the 7-day-old seedlings of Col-0, *gi-100*, and *gi-C27* followed by the cDNA synthesis of these lines. PCR was performed using the synthesized cDNA of these lines and the resultant PCR product was run on 1 % electrophoresis gel. The product of the expected mutation

site is ~800 bp which targets from exon 2 to exon 7. Convincingly from the electrophoresis gel, we found out that there was no 800 bp band detected in the *gi-C27* line whereas, Col-0 along with *gi-100* showed the presence of this 800 bp band in the gel (Figure 22). This experiment confirms the genotype of *gi-C27* to be a complete null mutant of *GI*.

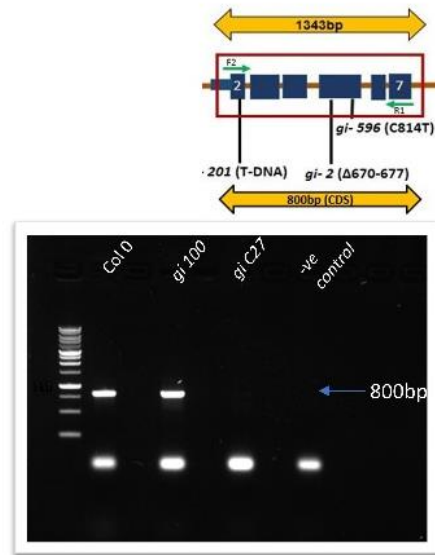


Figure 22. Genetic Screening of *gi-C27*. Gel picture of cDNA samples extracted from the leaves of *gi-C27*

Therefore, the seeds from these selected homozygous plants were used along with the traditional T-DNA insertion mutant lines for further analysis.

5.1.2.2. Characterization and detection of endogenous GI of expected molecular weight

Numerous efforts were made to develop antisera and antibodies that target the entire C-terminal domain of GI. Unfortunately, these attempts were ineffective in detecting the endogenous GI extracted from plants. Commercially available antibodies designed for GI exhibited reactivity with bacterially expressed GI protein but failed to detect plant GI. This discrepancy is likely attributed to post-translational modifications of plant proteins, rendering bacterially expressed antigens ineffective in detecting endogenous GI protein. Despite synthesizing various anti-peptide antibodies by many leading scientists in the field, none have successfully detected endogenous GI protein.

Therefore, we endeavoured to establish a novel method for generating GI antibodies, integrating hydropathy index analysis, primary sequence blast, and Expasy-based tools for the identification of peptides. Peptides bearing any post-translational modifications were excluded. Subsequently, six candidate antisera against GI protein were generated, emphasizing the presence of surface-exposed epitopes (Figure 23). Hydrophilic stretches, being accessible epitopes, were prioritized due to their aqueous region contact. These sequences were forwarded to Euro-Gene for antibody development in rabbits.

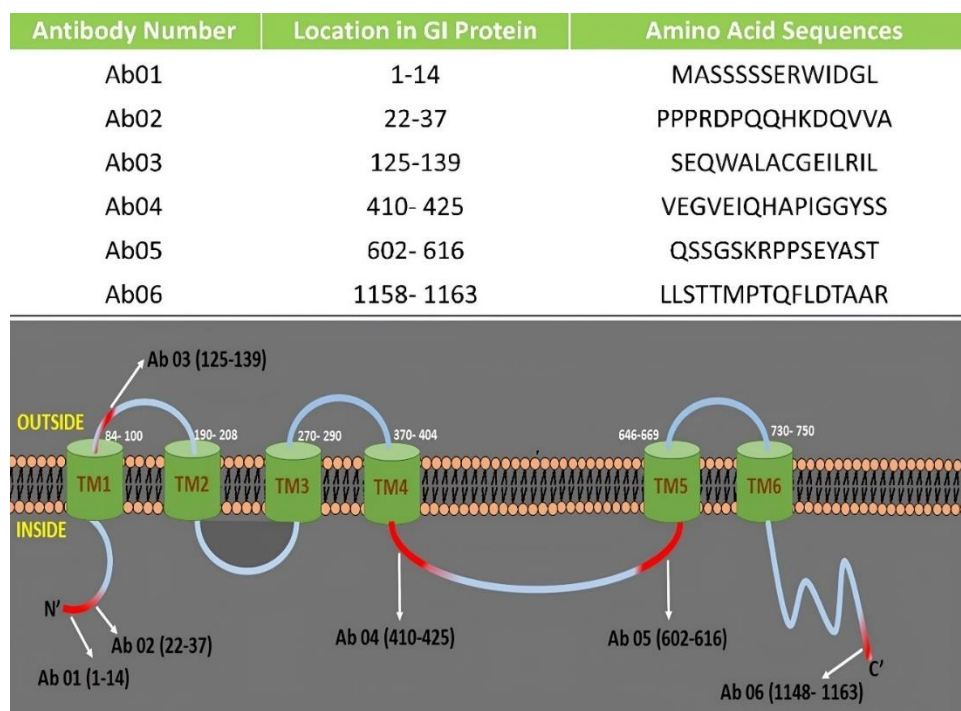


Figure 23. *Insilco* analysis and topology of GIGANTEA epitopes

Six different antibodies were generated against six different epitopes of the GI amino acid sequence (Figure 23). Antibody Ab01 was designed to specifically target the amino acid sequence MASSSSSERWIDGL located in the N-terminal region of the GI protein. Ab02 was developed to recognize the PPPRDPQQHKDVVA sequence found on the N-terminal portion of GI, which ranges from amino acid positions 22 to 37. Ab03 was designed to detect the SEQWALACCGILRIL sequence, found on the plasma membrane's extracellular side, and ranges from amino acid position 125 to 139. Ab04 has been developed to recognize the VEGVEIQHAPIGGYSS sequence found on the inner side of the plasma membrane, spanning

positions 410 to 425. Ab05 was created to target the QSSGSKRPPSEYAST sequence found on the inner side of the plasma membrane, which ranges from positions 602 to 616. Finally, Ab06 was designed to recognize the LLSTMPTQFLDTAAR amino acid sequence.

The total protein extracts were obtained from Col-0 wild type, 35S::GI overexpressing line, GI::GI-TAP tagged line, and the T-DNA insertional mutant of GI using the prescribed protocol outlined in the Materials and Methods section. Subsequent Western blot analysis was conducted to evaluate the efficacy of the generated GI antibodies in detecting endogenous GI protein. Notably, Ab01, Ab02, Ab03, Ab05, and Ab06 failed to produce bands corresponding to the expected molecular weight of 127 kDa in Col-0, 35S::GI, and GI::GI-TAP samples. Conversely, Ab04 successfully detected endogenous GI in Col-0, 35S::GI, and GI::GI-TAP samples, while no bands were observed in the *gi-100* mutant line (Figure 24).

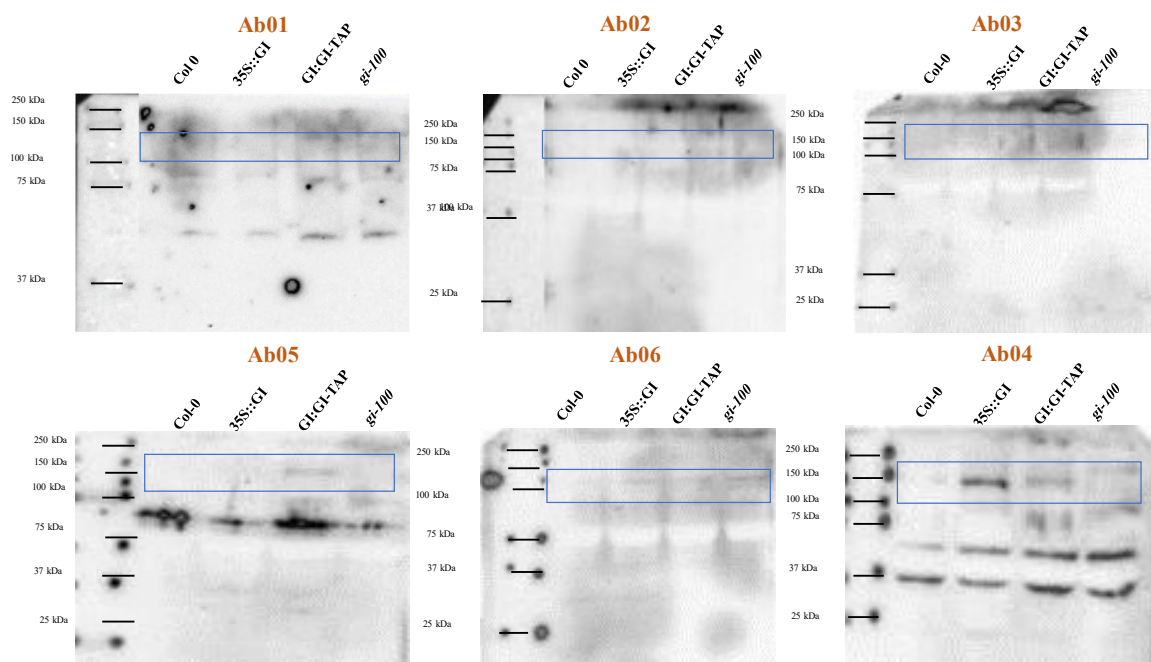


Figure 24. Characterization of all the probable GI antibodies. The PVDF membrane was blotted against anti-GI primary antibodies (Ab01, Ab02, Ab03, Ab04, Ab05, and Ab06) raised in rabbits and further incubated with secondary antibody anti-rabbit polyclonal HRP for 1 h at room temperature. Detection was done using an ECL substrate. The total protein was extracted from Col-0, 35S::GI, GI::GI-TAP, and *gi-100*, and a western blot was performed.

To enhance the signal intensity, we optimized the Western blotting protocol by extending the incubation period of the secondary antibody by an additional 1 hour, resulting in the desired band visualization at 127 kDa (Figure 25).

To investigate the presence of functional GI protein in *gi-C27*, the CRISPR mutant line of GI, Western blot analysis was conducted using protein extracts from Col-0, 35S::GI, GI: GI-TAP, *gi-100*, and *gi-C27* lines. The results revealed the absence of a functional protein band at 127 kDa in the *gi-C27* lane (Figure 25). This observation provides conclusive evidence that the newly developed CRISPR mutant line of GI, *gi-C27*, does not produce any functional GI protein. Consequently, this finding eliminates the possibility of off-target effects associated with GI in the *gi-C27* mutant line.

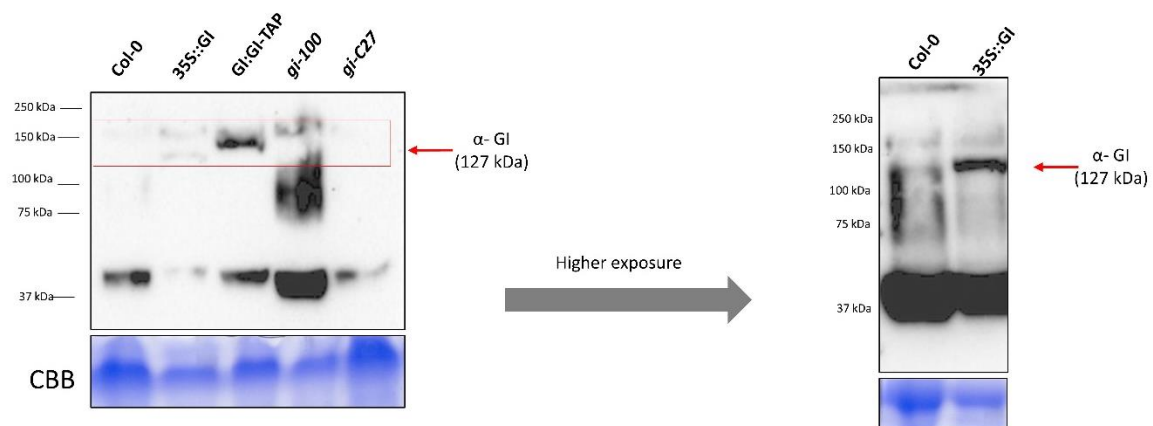


Figure 25. Specific binding of Ab04 to endogenous GI of *Arabidopsis thaliana*. The PVDF membrane was blotted against Ab04 anti-GI primary antibody raised in rabbits and further incubated with secondary antibody anti-rabbit polyclonal HRP for 2 hours at room temperature. Detection was done using an ECL substrate. The total protein was extracted from Col-0, 35S::GI, GI: GI-TAP, *gi-100*, and *gi-C27*, and a western blot was performed. Corresponding loading control is shown by SDS-PAGE gel stained with Coomassie Brilliant Blue (CBB).

Whole genome sequencing was performed to validate the newly developed CRISPR mutant line of GI. The DNA extracted from *gi-C27* seedlings grown under LD conditions at 22 °C was sent to a Genotypic company for whole genome sequencing. The results showed that two frameshift mutations have occurred in the *gi-C27* line. There is the addition of a Cytosine (C) and a Thymine (T) in the NC_003070.9 chromosome at 8062469 (Exon 2) and 8063810 (Exon 7) position respectively. To investigate if the frameshift mutation in the *gi-C27* line can translate any protein, the CDS sequence of *gi-C27* was taken and translated using Snap gene software. Surprisingly, it was found that upon translation, the two stop codons are produced from exon-2 and exon-7 (Figure 26). Therefore, the above results convincingly suggest that *gi-C27* is a

complete null mutant that does not produce any functional protein. In addition, it is also shown here that the Ab04 can bind to endogenous GI in *A. thaliana*.

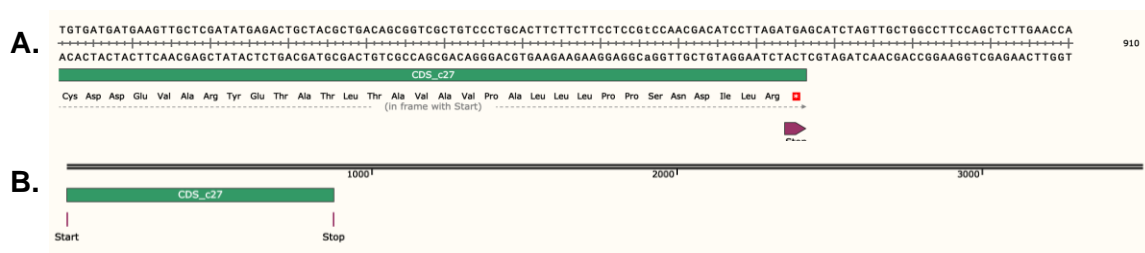


Figure 26. CDS sequence of GI translating the GI protein at Exon-2 (A) and Exon-7 (B)

5.1.2.3. Re-evaluating the role of GIGANTEA using CRISPR Cas9 technology

In the current study, the probable role of GI was re-investigated in seedlings and adult plants of *Arabidopsis thaliana* in response to different lights, sugar, low temperature, drought stress, and salinity stress. We conducted the study by comparing the traditionally present T-DNA insertional mutant i.e., *gi-100*, and CRISPR mutant lines of *gi* i.e., *gi-C27* in Col-0 background.

5.1.2.3.1 Characterizing hypocotyl and root development in CRISPR edited *gi* mutants of *Arabidopsis thaliana*

Hypocotyl and root development of *gi-C27*, *gi-100*, 35S::GI, and Col-0 were studied in response to different light and sugar. Dark (D), White (W), Red (R), Far Red (FR), and Blue (B) were used for the study.

Under dark conditions, the hypocotyl lengths of 35S::GI, *gi-100*, and *gi-C27* mutants were notably reduced by 2.87, 2.53, and 1.55-fold respectively compared to the Col-0 wildtype. In the absence of sucrose supplementation, all *gi* mutants including overexpressing GI lines displayed significantly shorter hypocotyl lengths compared to the wild type. However, upon supplementation with 1% sucrose in the MS media, the hypocotyl lengths of 35S::GI, *gi-100*, and *gi-C27* mutants were comparable to those of Col-0 wildtype seedlings (Figure 27).

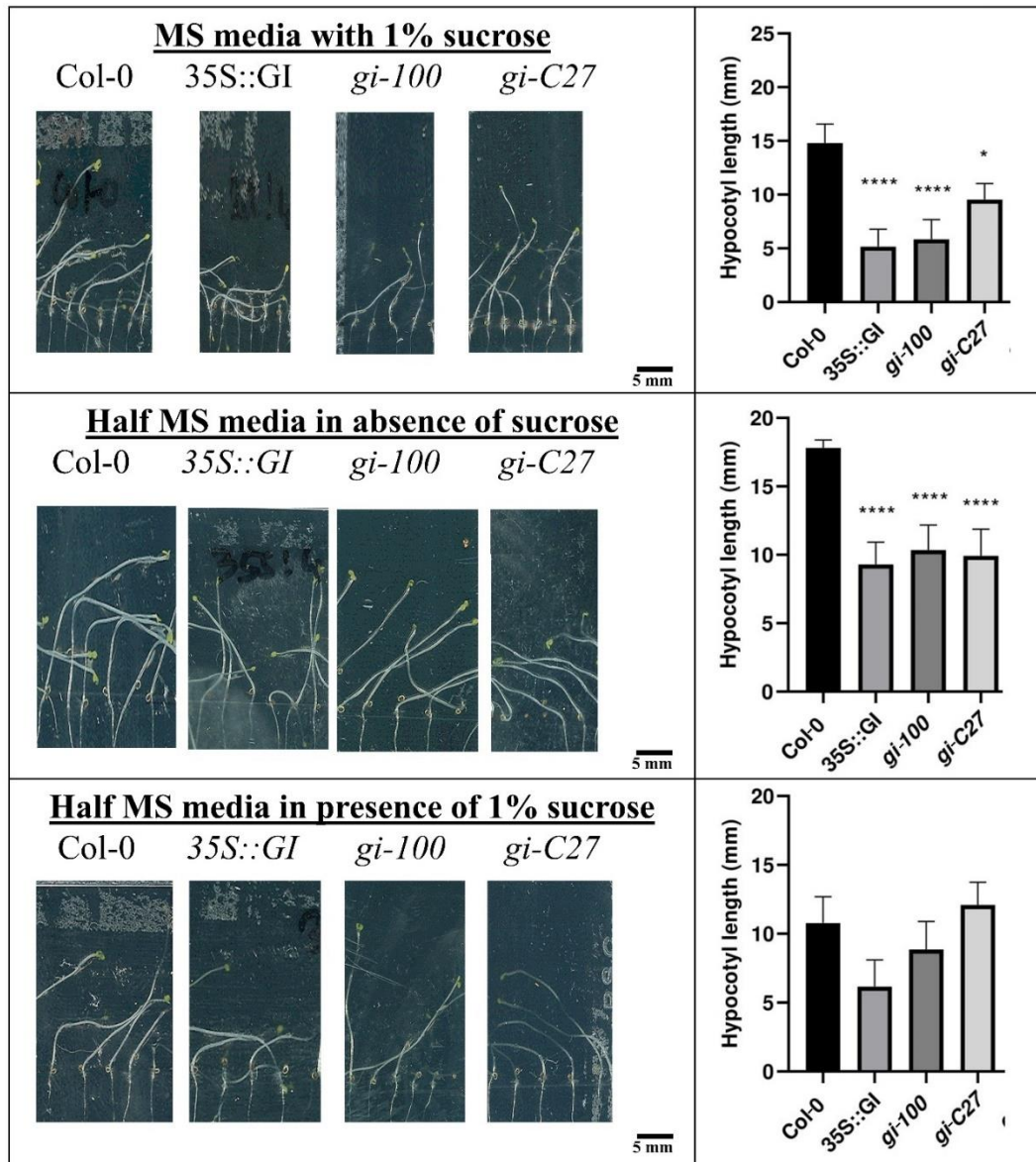


Figure 27. Comparison of *A. thaliana* hypocotyl development between wild-type Col-0 ecotype, 35S::GI, *gi-100* and *gi-C27* mutants under dark in MS, half MS without sucrose and half MS with 1% sucrose growth media.

The root lengths of *gi-C27* were significantly shorter by 1.46-fold than Col-0. Whereas, 35S::GI and *gi-100* remained indistinguishable from Col-0 WT. Surprisingly, in the absence of sucrose in the MS media, the root lengths of all the mutants and 35S::GI were significantly shorter as compared to the wild type. However, upon the addition of 1 % sucrose in the MS media, the root lengths rescued the phenotype and were indistinguishable from the Col-0 (Figure 28).

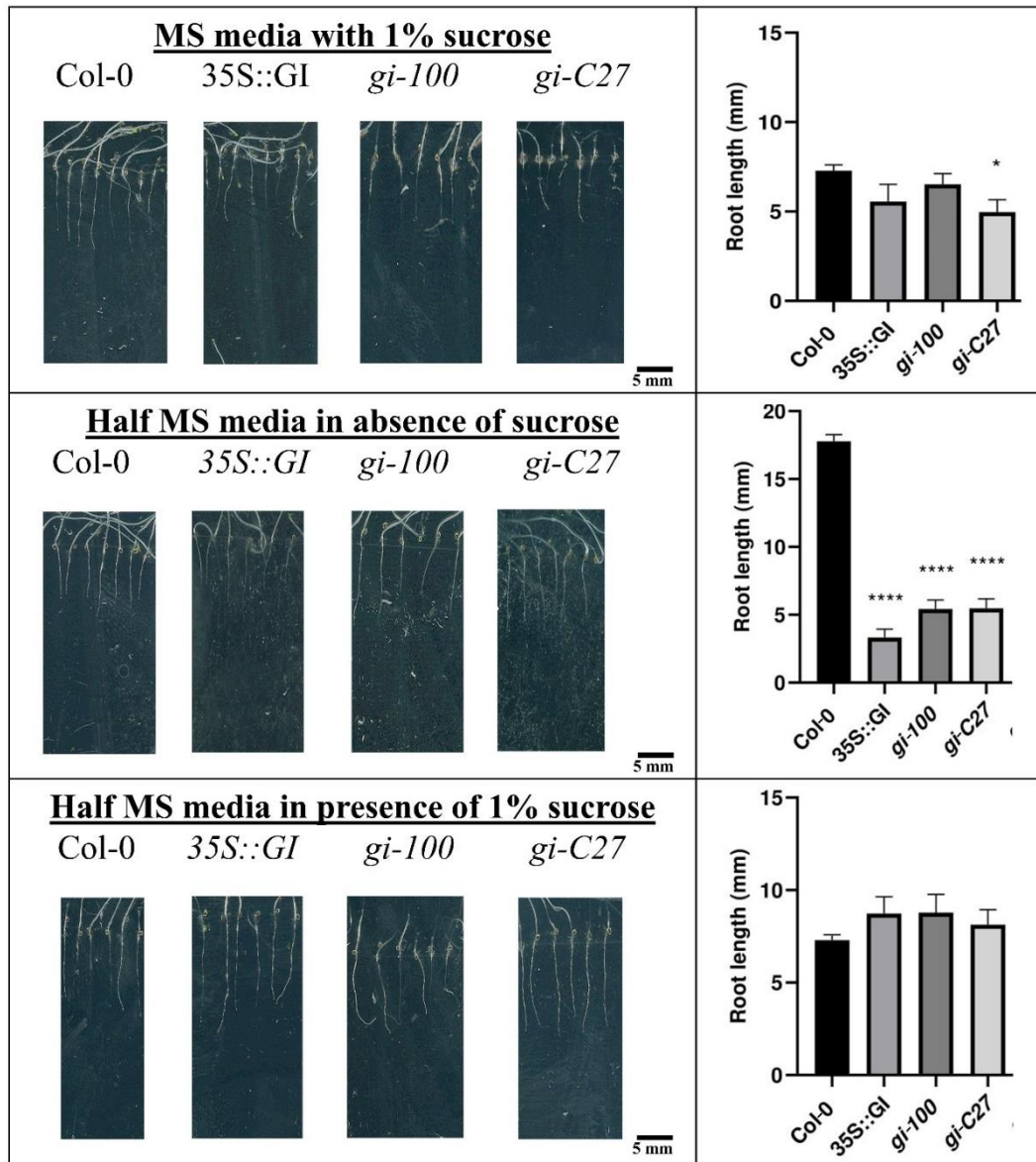


Figure 28. Comparison of *A. thaliana* root development between wild-type Col-0 ecotype, 35S::GI, *gi-100* and *gi-C27* mutants under dark in MS, half MS without sucrose and half MS with 1% sucrose growth media.

Under white light conditions, the hypocotyl length of 35S::GI was significantly shorter than the wildtype seedlings by nearly 2-fold. However, the hypocotyl lengths of *gi-100* and *gi-C27* were longer by ~1.5-fold and ~1.8-fold respectively as compared to Col-0. A similar trend in the hypocotyl development was observed in the absence and presence of sucrose in the MS media (Figure 29).

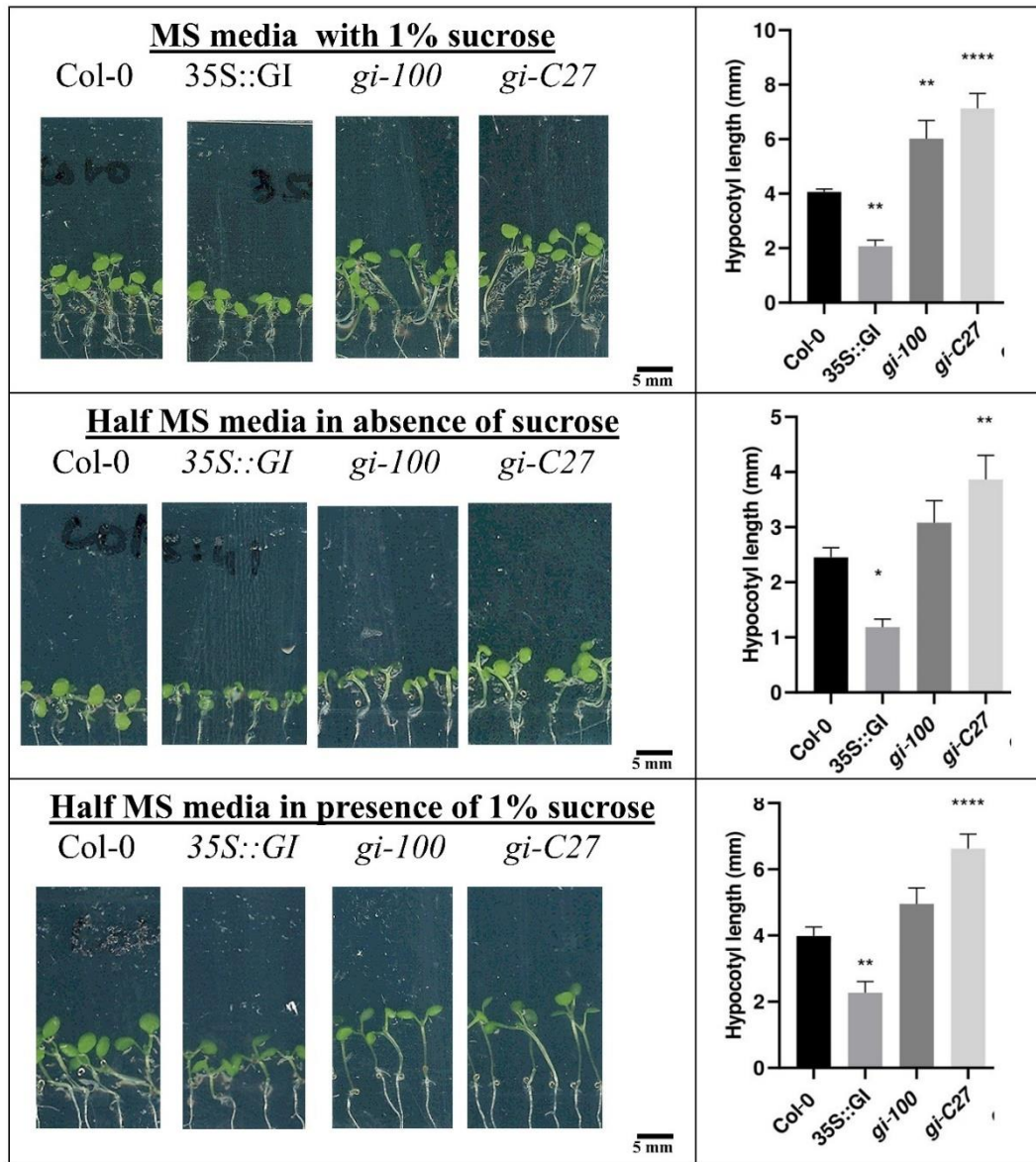


Figure 29. Comparison of *A. thaliana* hypocotyl development between wild-type Col-0 ecotype, 35S::GI, *gi-100* and *gi-C27* mutants under white light in MS, half MS without sucrose and half MS with 1% sucrose growth media.

The root lengths in 35S::GI and *gi-100* were similar while *gi-C27* was significantly shorter by ~1.2-fold as compared to Col-0. The effect of sucrose was not seen in the root lengths of *gi* mutants as well as 35S::GI as there was no significant change in the root lengths of these lines as compared to Col-0 in the presence and absence of sucrose in the MS media (Figure 30).

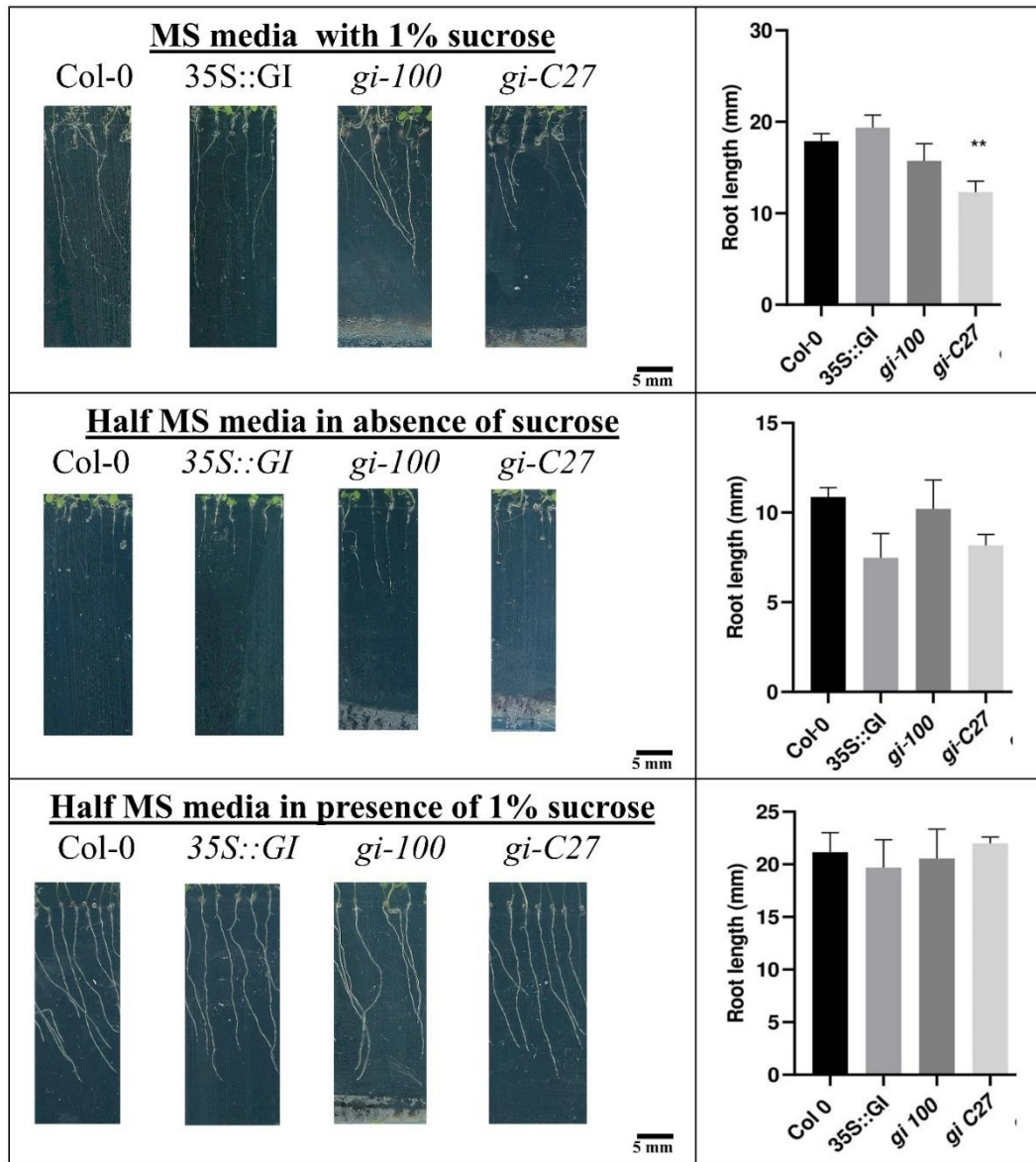


Figure 30. Comparison of *A. thaliana* root development between wild-type Col-0 ecotype, 35S::GI, *gi-100* and *gi-C27* mutants under white light in MS, half MS without sucrose and half MS with 1% sucrose growth media.

Under red light, the hypocotyl length of 35S::GI was significantly shorter as compared to Col-0 wildtype. Whereas, the hypocotyl lengths of *gi* mutants like *gi-100* and *gi-C27* were similar to Col-0 and were non-significant. The phenotype remained similar in the presence and absence of 1 % sucrose in the MS media (Figure 31).

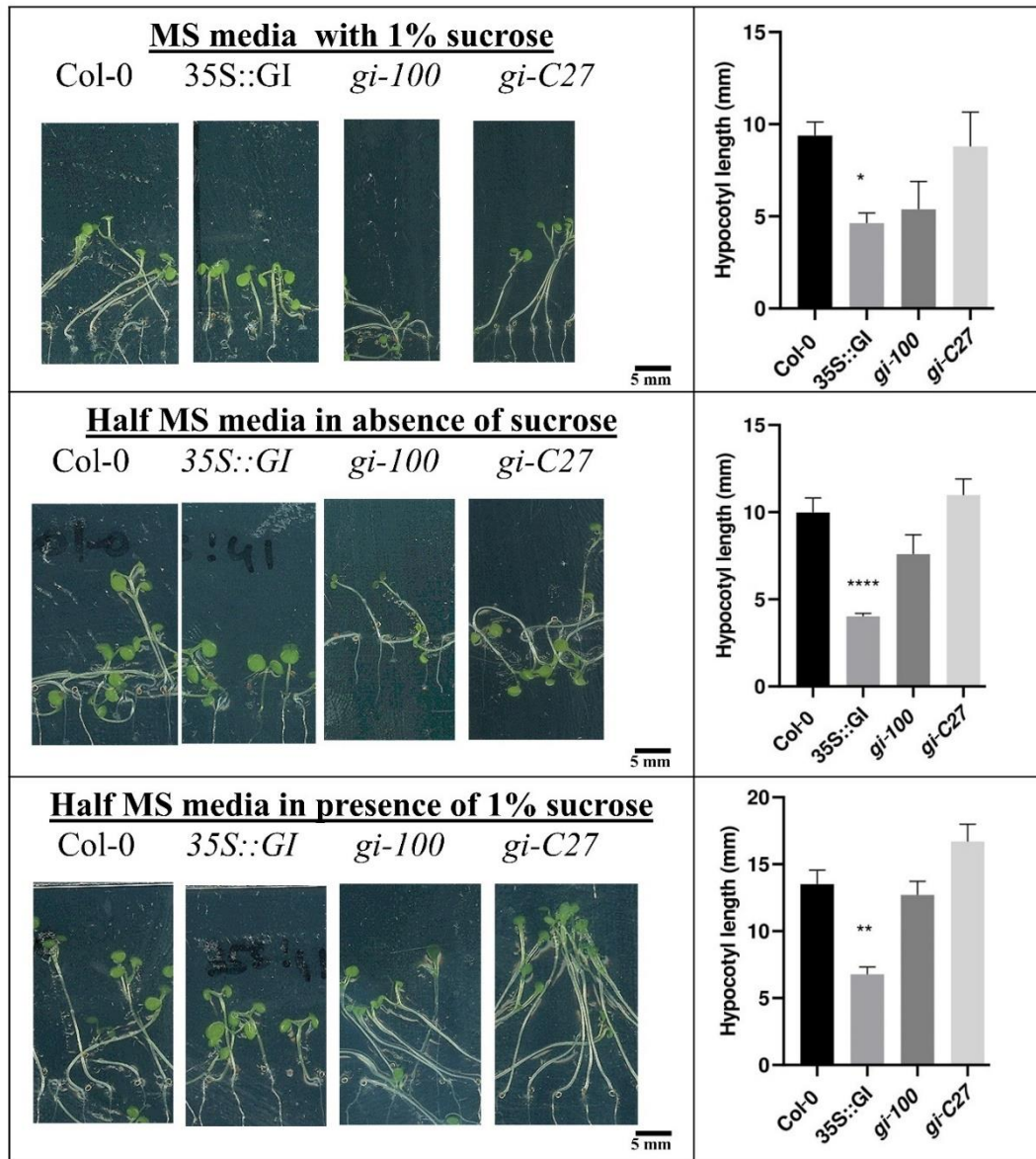


Figure 31. Comparison of *A. thaliana* hypocotyl development between wild-type Col-0 ecotype, 35S::GI, *gi-100* and *gi-C27* mutants under red light in MS, half MS without sucrose and half MS with 1% sucrose growth media.

The root lengths of *gi-100* (~4.8-fold) and *gi-C27* (~1.6-fold) were significantly shorter than the Col-0 under red light. This trend remained similar with the presence and absence of 1 % sucrose in the MS media (Figure 31).

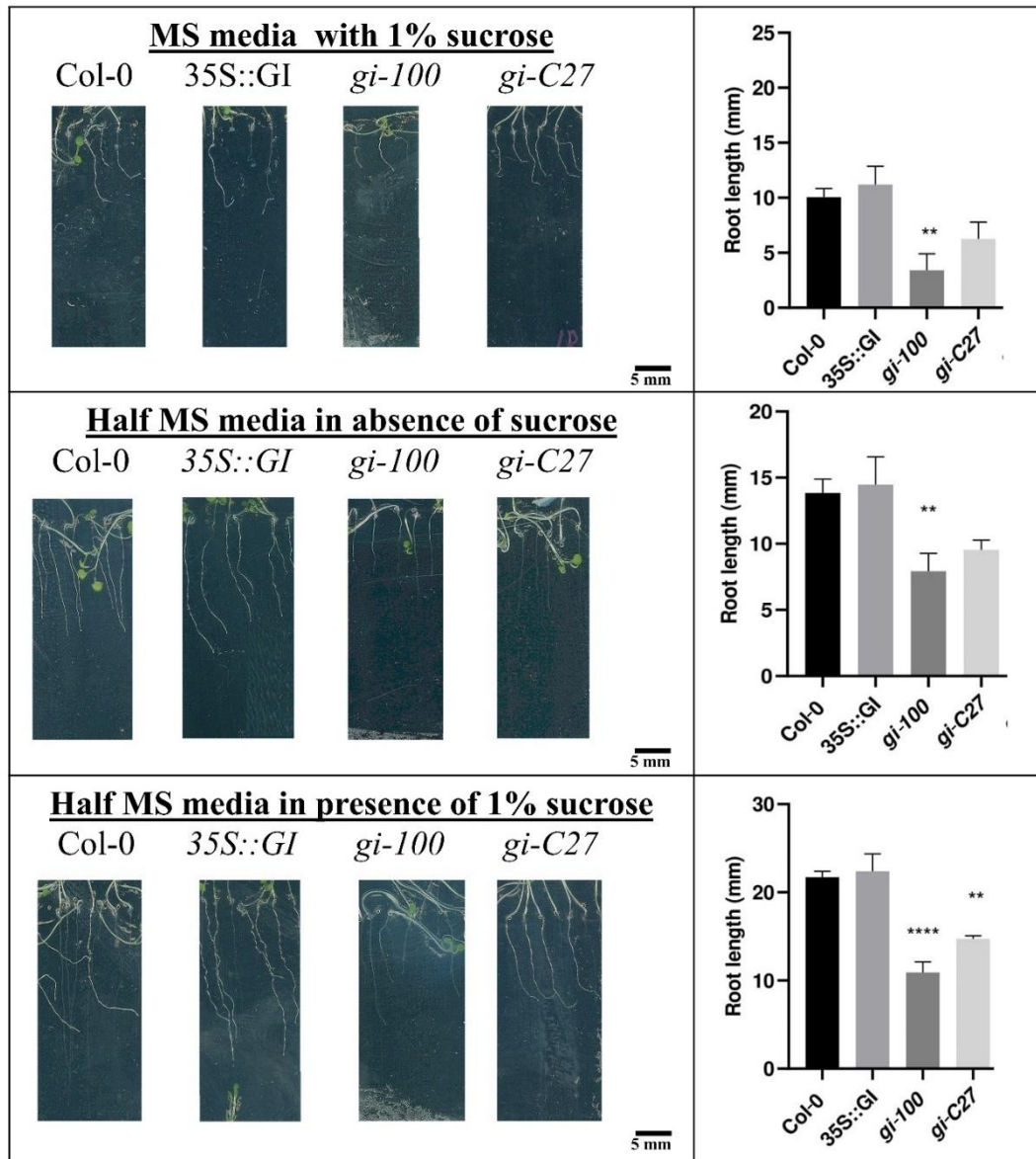


Figure 32. Comparison of *A. thaliana* root development between wild-type Col-0 ecotype, 35S::GI, *gi-100* and *gi-C27* mutants under red light in MS, half MS without sucrose and half MS with 1% sucrose growth media.

The hypocotyl lengths of *gi-100* (~1.8-fold) and *gi-C27* (~1.18) were significantly longer than the Col-0 and 35S::GI under far red light. The Hypocotyl length of 35S::GI (~1.9-fold) is significantly shorter than the Col-0. However, a similar pattern of hypocotyl length was retained in the presence and absence of 1 % sucrose in the MS media (Figure 33).

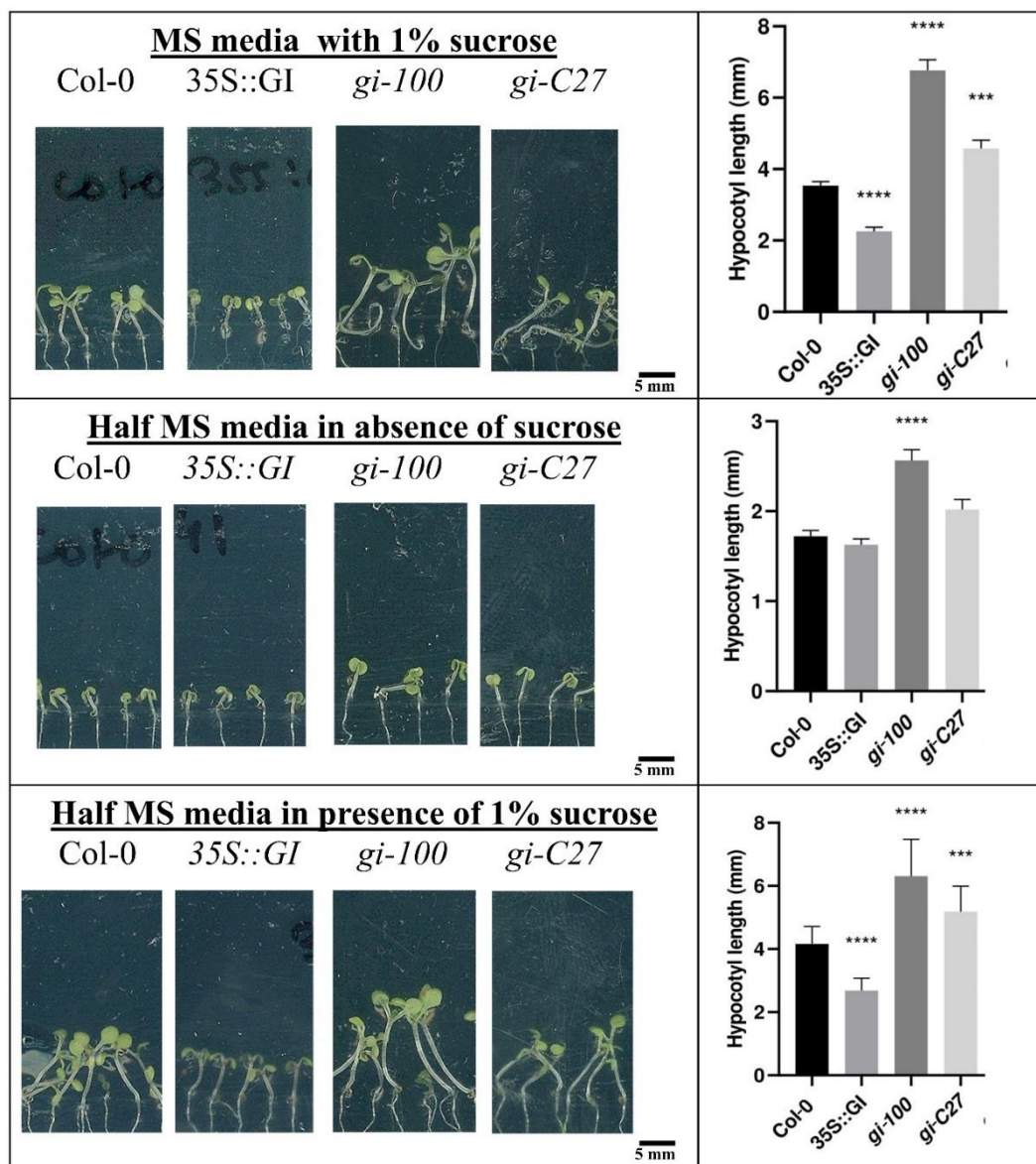


Figure 33. Comparison of *A. thaliana* hypocotyl development between wild-type Col-0 ecotype, 35S::GI, *gi-100* and *gi-C27* mutants under far-red light in MS, half MS without sucrose and half MS with 1% sucrose growth media.

The root length of 35S::GI, *gi-100*, and *gi-C27* was indistinguishable from Col-0 wild type under far-red light. However, in the absence of sucrose in the MS media, *gi-100* showed longer hypocotyl than Col-0. The phenotype of the mutants and 35S::GI was not rescued on the addition of 1 % sucrose in the MS media (Figure 34).

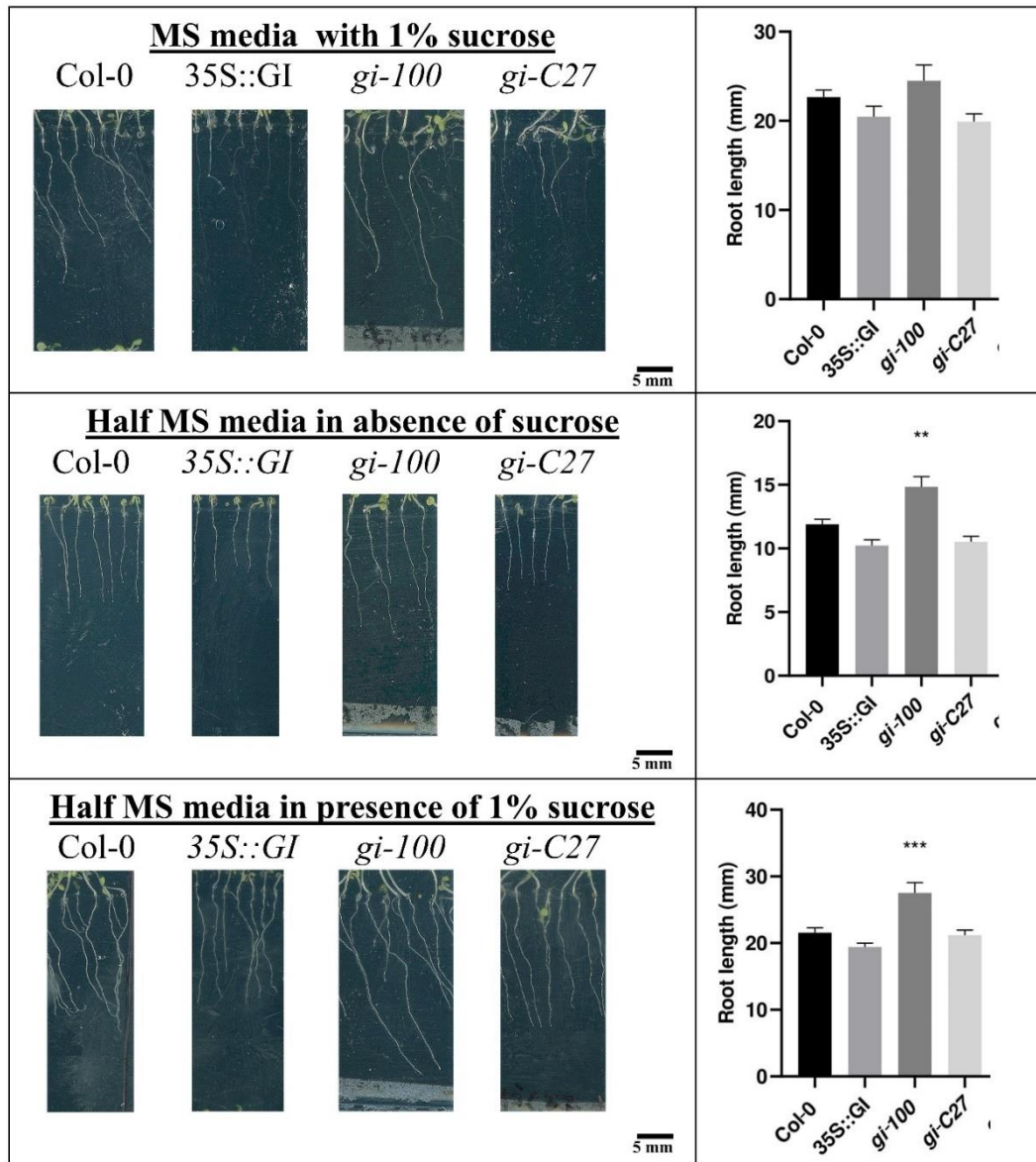


Figure 34. Comparison of *A. thaliana* root development between wild-type Col-0 ecotype, 35S::GI, *gi-100* and *gi-C27* mutants under far-red light in MS, half MS without sucrose and half MS with 1% sucrose growth media.

Under blue light, the hypocotyl lengths of *gi-100* (~1.4-fold) and *gi-C27* (~1.4-fold) were significantly longer as compared to Col-0. While the over-expressing line of GI i.e., 35S::GI (~1.3-fold) was significantly shorter than the wildtype. Here, it was also observed that the hypocotyl length pattern in the presence and absence of 1 % sucrose remained similar to that of the normal condition i.e., full MS with 1 % sucrose (Figure 35).

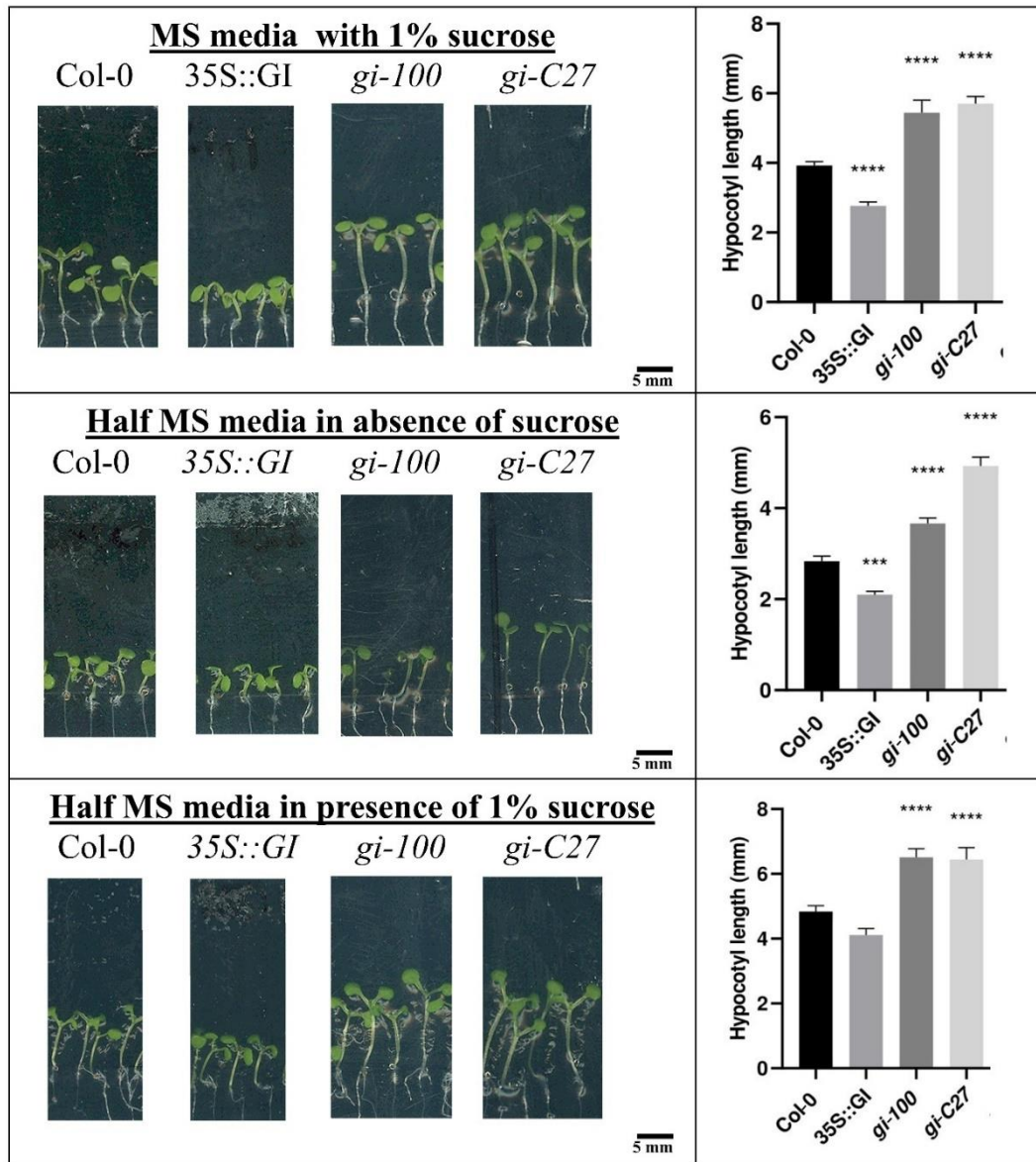


Figure 35. Comparison of *A. thaliana* hypocotyl development between wild-type Col-0 ecotype, 35S::GI, *gi-100* and *gi-C27* mutants under blue light in MS, half MS without sucrose and half MS with 1% sucrose growth media.

Unlike the hypocotyl, root lengths in 35S::GI, *gi-100*, and *gi-C27* were indistinguishable from the Col-0 wildtype. The hypocotyl lengths were similar irrespective of the presence and absence of 1 % sucrose in the MS media (Figure 36).

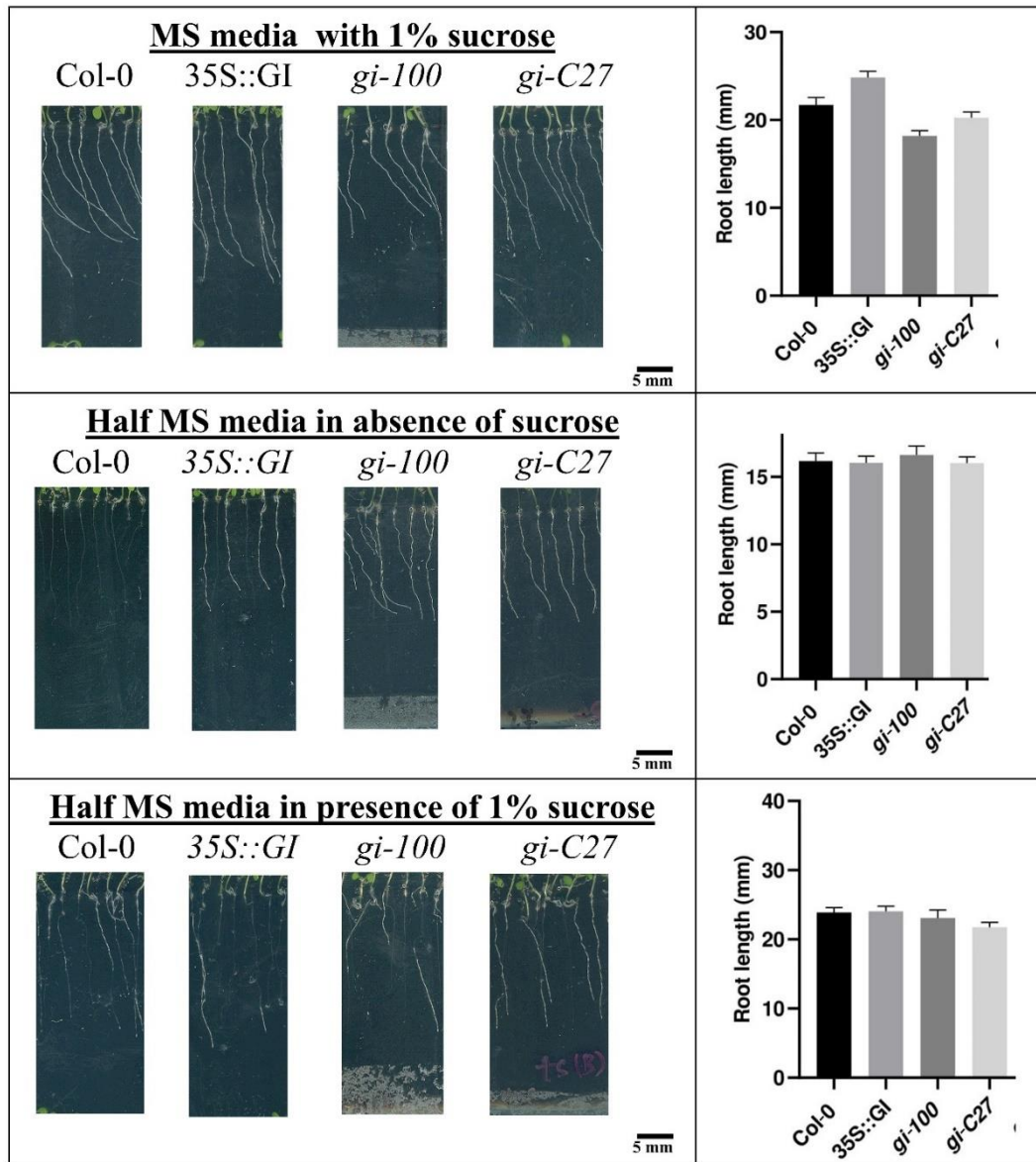


Figure 36. Comparison of *A. thaliana* root development between wild-type Col-0 ecotype, 35S::GI, *gi-100* and *gi-C27* mutants under blue light in MS, half MS without sucrose and half MS with 1% sucrose growth media.

5.1.2.3.2. Photoperiodic Flowering of CRISPR mutant of GI in *Arabidopsis thaliana*

Previously it has been reported that *gi* T-DNA insertional mutants exhibited delayed flowering phenotype in Long Day (LD) as well as Short Day (SD) conditions. To validate the retention of delayed flowering phenotype response in CRISPR mutant of *GI*, an assessment of photoperiodic flowering was done under LD and SD conditions. Col-0 wildtype, T-DNA insertional mutant i.e., *gi-100* along with CRISPR mutant i.e., *gi-C27* was used for the study. Flowering time is reciprocally related to the total number of rosette leaves as well as the number

of days to bolting in *A. thaliana* (Mishra and Panigrahi, 2015). The above seed lines were allowed to grow in soil pots under LD and SD conditions at 22 °C.

Under LD conditions, the photoperiodic flowering in *gi-100* (62 ± 2 days) and *gi-C27* (65 ± 2 days) was significantly later as compared to Col-0 (22 ± 2 days). Similarly, the number of rosette leaves was higher in *gi-100* which had (50 ± 2 leaves) and *gi-C27* (38 ± 2 leaves) than in the Col-0 wild type (12 ± 2 leaves). However, the difference in the flowering time between *gi-100* and *gi-C27* was not prominent. Interestingly, the number of rosette leaves in *gi-100* was more than the *gi-C27* (Figure 37).

Under SD conditions, the photoperiodic flowering in *gi-100* was significantly later with 110 ± 2 days of flowering as compared to Col-0 (80 ± 2 days). However, the flowering time of *gi-C27* was very similar to Col-0 with 80 ± 2 days. Similarly, the number of rosette leaves was higher in *gi-100* with 62 ± 2 leaves and lower in *gi-C27* with 40 ± 2 leaves than in the Col-0 wild type with 55 ± 2 leaves. However, the difference in the flowering time between *gi-100* and *gi-C27* was not prominent. Interestingly, the number of rosette leaves in *gi-100* was more than the *gi-C27* (Figure 37).

The effect of low temperature on photoperiodic flowering is also investigated in this study. Under LD conditions, the flowering time was delayed significantly in *gi-100* and *gi-C27* than in Col-0. The delay in the flowering time in *gi* mutants induced by low temperature was also validated with the number of rosette leaves. The rosette leaves were significantly more in *gi* mutants than the wild type. However, under SD conditions, low temperature induced early flowering in both the *gi* mutants. Despite, *gi-100* showed early flowering under SD conditions at 18 °C, the number of rosette leaves was more than that of Col-0 which leads to an indication that there might be an off-target effect of T-DNA insertional mutant which is playing a role in the flowering time in *gi-100*. The increased number of rosette leaves of *gi-100* The rosette

leaves of *gi-C27* were significantly less than that of Col-0, which validates the fact that *gi-C27* shows early flowering under SD conditions at 18 °C (Figure 37).

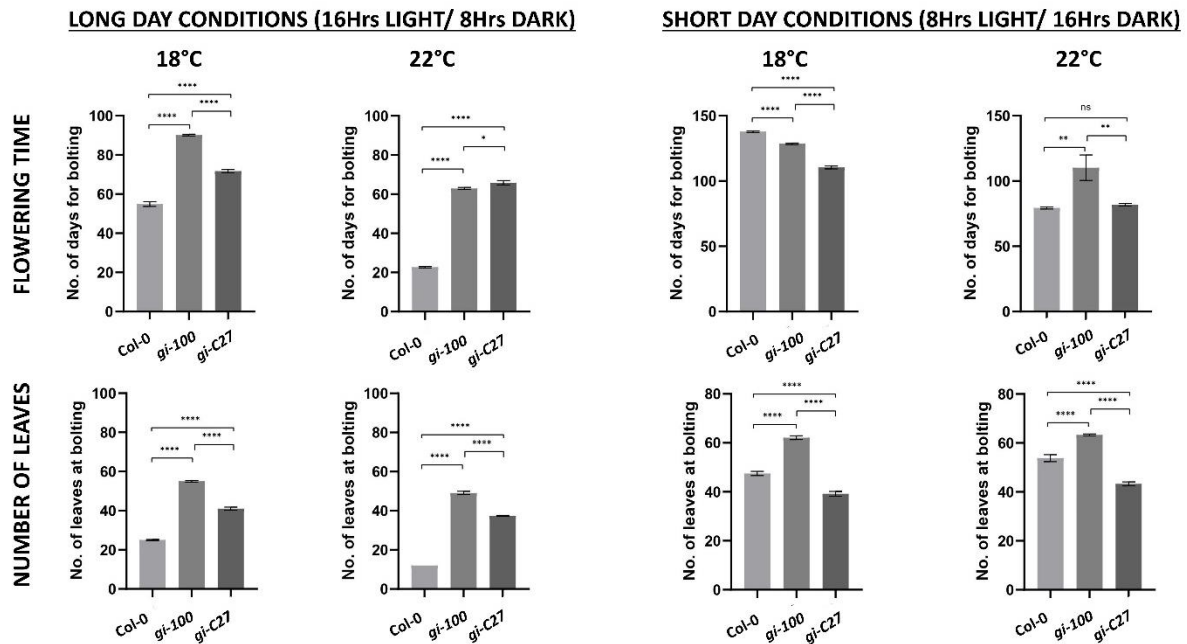


Figure 37. Analysis of flowering time phenotype in Col-0, *gi-100*, and *gi-C27* under long day (LD) and short day (SD) conditions at 18 °C and 22 °C. Graphical representation of number of days to bolting (upper panel) and number of rosette leaves (bottom panel). The plants were allowed to grow on soil at 18 °C and 22 °C under LD and SD conditions. Two-way analysis of variance (ANOVA) using Tukey's multiple comparisons test was performed with the help of GraphPad prism to test for significance among the dataset, * $p < 0.05$, ** $p < 0.01$, *** $p < 0.001$, ns- non significant.

5.1.2.3.3. Effect of drought stress on CRISPR mutant of GI in *Arabidopsis thaliana*.

GI has been observed to play an important role in abiotic stress like drought stress in *Arabidopsis thaliana* (Mishra and Panigrahi, 2015). To validate the function role of GI in drought response is persistent in CRISPR mutant of *gi* i.e., *gi-C27*, drought stress was imposed on Col-0, *gi-100* (T-DNA insertional mutant), and *gi-C27*. Drought stress for 10 days was imposed on the adult plants 10 days before their bolting. The experiment was carried out under long day (LD, 16 hours light/ 8 hours dark) and short day (SD, 8 hours light/ 16 hours dark) conditions at 22 °C.

It was observed that under LD conditions, both the mutants of *gi* i.e., *gi-100* and *gi-C27* were drought resistant as compared to Col-0. The leaves of *gi-100* and *gi-C27* were greener than the leaves of Col-0 (Figure 38, upper panel). The *gi* mutants also exhibited higher endogenous

temperature after 10 days of stress period than Col-0. This indicates that the leaves of *gi* mutants are more metabolically active than the Col-0 wildtype (Figure 38, lower panel).

These findings underscore the significant role of GI in conferring drought resistance in *Arabidopsis thaliana*, as evidenced by distinct phenotypic and physiological responses observed in *gi* mutants under drought stress conditions, particularly under LD photoperiods.

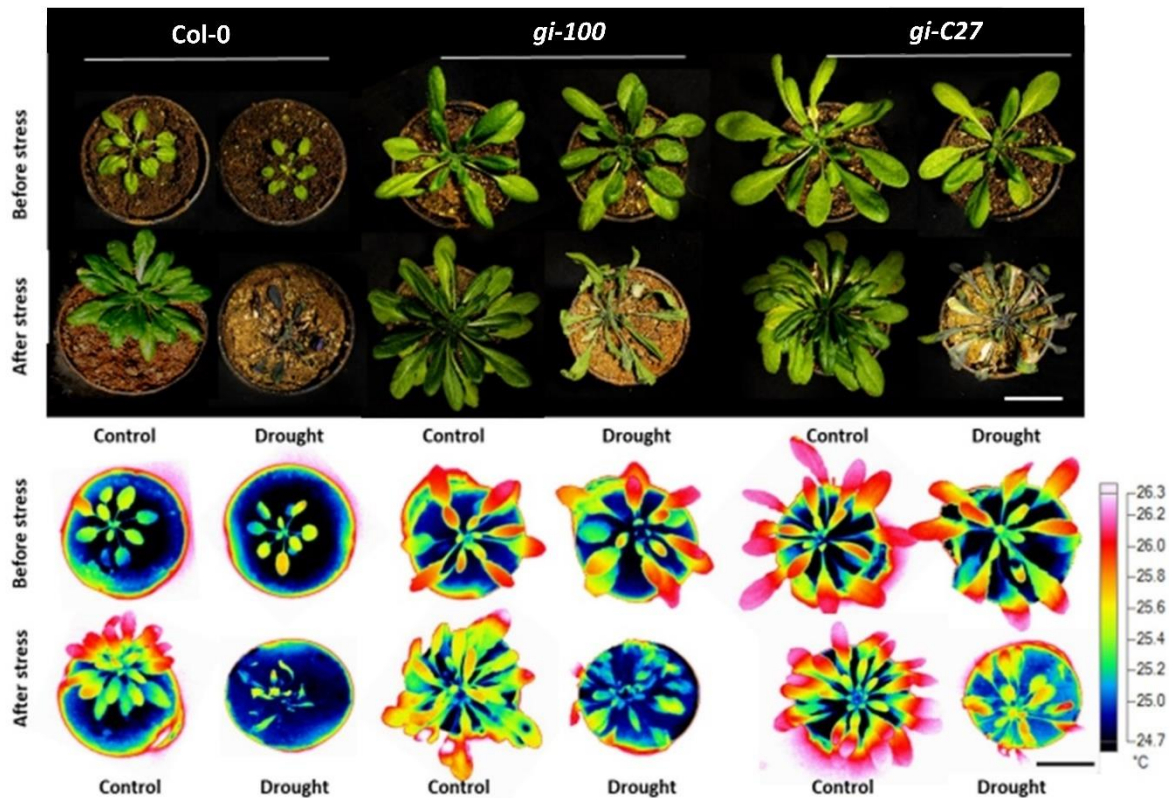


Figure 38. Effect of drought stress under long-day conditions on the *gi* mutants in *Arabidopsis thaliana*. Plants of Col-0, *gi-100*, and *gi-C27* genotypes were grown on soil in pots under LD conditions at 22 °C till the bolting stage. Plants were either well-watered or imposed water withheld for 10 days (drought stress) as described in materials and methods. The leaf temperature of the plants grown in water withheld conditions at 22 °C (lower panel) was measured from thermal pictures that were taken with a FLUKE infrared camera and analyzed using the SMART VIEW software. Leaf surface temperatures showing the highest temperatures were selectively chosen from at least ten individual plants. Three individual biological replicates were performed. Data presented as mean \pm SE. One-way analysis of variance (ANOVA) using Tukey's multiple comparisons test was performed with the help of GraphPad Prism to test for significance among the dataset, * $p < 0.05$, ** $p < 0.01$, *** $p < 0.001$ and ns represent non-significant differences—scale bar: 1 cm.

Under short-day (SD) conditions, the response of *gi-100* and *gi-C27* mutants to drought stress exhibited notable differences. Specifically, *gi-100* displayed drought resistance characterized by greener and turgid leaves compared to the stressed Col-0 plants. Conversely, *gi-C27*

exhibited drought susceptibility, evidenced by the presence of dried leaves, contrasting with the phenotype of Col-0 under drought stress conditions (refer to Figure 39, upper panel).

Moreover, the *gi-100* mutant displayed higher endogenous temperatures following the 10-day stress period compared to Col-0, indicating heightened metabolic activity in *gi-100* leaves relative to the Col-0 wild type. In contrast, both Col-0 and *gi-C27* exhibited lower endogenous temperatures, suggesting cooler temperatures and reduced metabolic activity in their leaves (refer to Figure 39, lower panel).

These observations highlight the divergent responses of *gi-100* and *gi-C27* mutants under SD conditions to drought stress. While *gi-100* demonstrates enhanced drought resistance with elevated metabolic activity, *gi-C27* exhibits increased susceptibility to drought stress, resulting in compromised leaf conditions compared to Col-0.

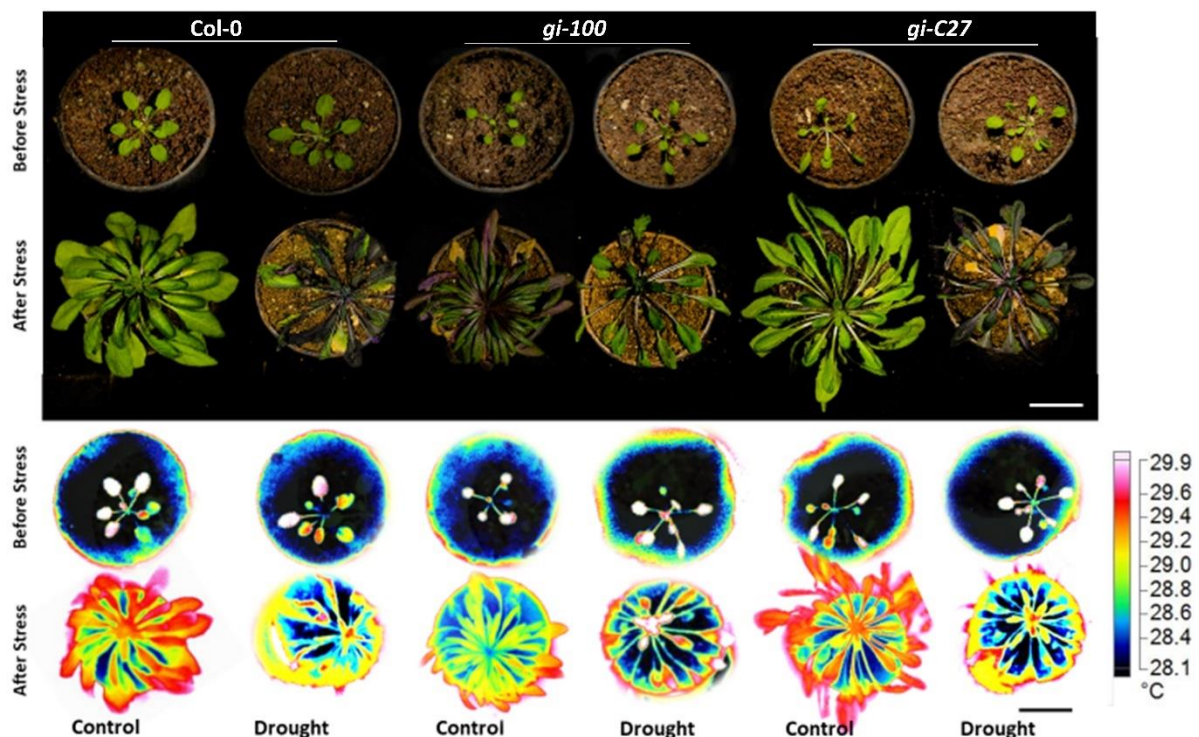


Figure 39. Effect of drought stress under short-day conditions on the *gi* mutants in *Arabidopsis thaliana*. Plants of Col-0, *gi-100*, and *gi-C27* genotypes were grown on soil in pots under LD conditions at 22 °C till the bolting stage. Plants were either well-watered or imposed water withheld for 10 days (drought stress) as described in materials and methods. The leaf temperature of the plants grown in water withheld conditions at 22 °C (lower panel) was measured from thermal pictures that were taken with a FLUKE infrared camera and analyzed using the SMART VIEW software. —scale bar: 1 cm

To quantify the endogenous temperature of the drought-stressed leaves as compared to the control leaves which were well watered, the leaf surface temperatures showing the highest temperatures were selectively chosen from at least ten individual plants. The observations were recorded using a FLUKE infrared camera which was further quantified in the SMART VIEW software as described in the Materials and Methods. It was observed that the endogenous temperature in drought-treated plants decreased by 1.09, 1.12, and 1.13-fold as compared to their respective controls in Col-0, *gi-100*, and *gi-C27* respectively. It was also found that under LD conditions the average temperature in Col-0 stressed plants reduced to 21.02 °C as compared to Col-0 in control plants with 23.06 °C. In the case of *gi* mutants drought-stressed plants, the average temperature of leaves was higher than the wild type. The average temperatures of *gi-100* and *gi-C27* were found to be 22.24 °C and 22.98 °C respectively after drought stress (Figure 40). Under SD conditions, there was a reduction of endogenous temperature in the leaves of Col-0 and *gi-C27* by 1.04 and 1.02-fold as compared to their respective controls. However, the endogenous temperature of *gi-100* drought-stressed plants increased by 1.03-fold as compared to its control. The results thus indicated that Col-0 and *gi-C27* had less metabolic activity, whereas, *gi-C27* had more metabolic activity after drought stress (Figure 40).

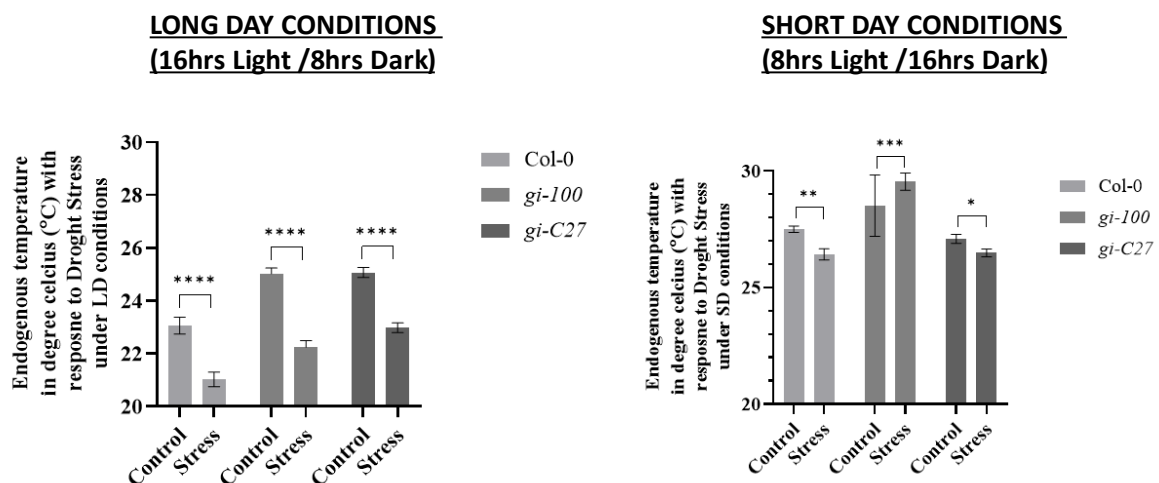


Figure 40. Effect of drought stress on the endogenous temperature on leaves under short-day conditions on the *gi* mutants in *Arabidopsis thaliana*. Plants of Col-0, *gi-100*, and *gi-C27* genotypes were grown on soil in pots under either LD or SD conditions at 22 °C till the bolting stage. Plants were either well-watered or imposed water withheld for 10 days (drought stress) as described in materials and methods. The leaf temperature of the plants grown in water withheld conditions at 22 °C was measured from thermal pictures that were taken with a FLUKE infrared camera and analyzed using the SMART VIEW software. Leaf surface temperatures showing the highest temperatures were selectively chosen from at least ten individual plants. Three individual biological replicates

were performed. Data presented as mean \pm SE. One-way analysis of variance (ANOVA) using Tukey's multiple comparisons test was performed with the help of GraphPad Prism to test for significance among the dataset, * $p < 0.05$, ** $p < 0.01$, *** $p < 0.001$ and ns represent non-significant differences.

Dehydration due to drought is associated with characteristic physiological changes including accumulation of stress pigments such as carotenoids and flavonoids, reduction of photosynthetic efficiency, generation of reactive oxygen species, and increased ROS scavenging due to various ROS scavenging enzyme activity intolerant species, which have been well documented in previous studies (Panigrahy *et al.*, 2011; Tomanek *et al.*, 2012; Manasa *et al.*, 2022; Panigrahy *et al.*, 2022). Dehydration tolerance in *gi* mutant lines i.e., *gi-100* and *gi-C27* was validated after inducing drought stress by studying various biochemical parameters such as oxygen free radicals (O_2^-), relative water content (RWC), chlorophyll, carotenoids, malondialdehyde (MDA), enzyme activity of superoxide dismutase catalase (CAT) and peroxidase (POX) in comparison with those of Col-0 as well as with their respective controls without WW.

Col-0 lines showed a sharp increase in O_2^- (visible due to histochemical NBT staining in the leaves) due to drought stress at 22 °C under LD and SD conditions. Before WW, both the *gi* mutant lines had a comparable amount of O_2^- as that of the Col-0 under LD and SD conditions at 22 °C. Under LD conditions, the accumulation of O_2^- in *gi-100* (~2.2-fold) and *gi-C27* (~1.45-fold) was higher as compared to Col-0 after the induction of drought stress. However, under SD conditions, the accumulation of O_2^- was significantly higher (~0.6-fold) and lower (~1.5-fold) in *gi-100* and *gi-C27* respectively as compared to Col-0 after drought stress (Figures 41 and 42).

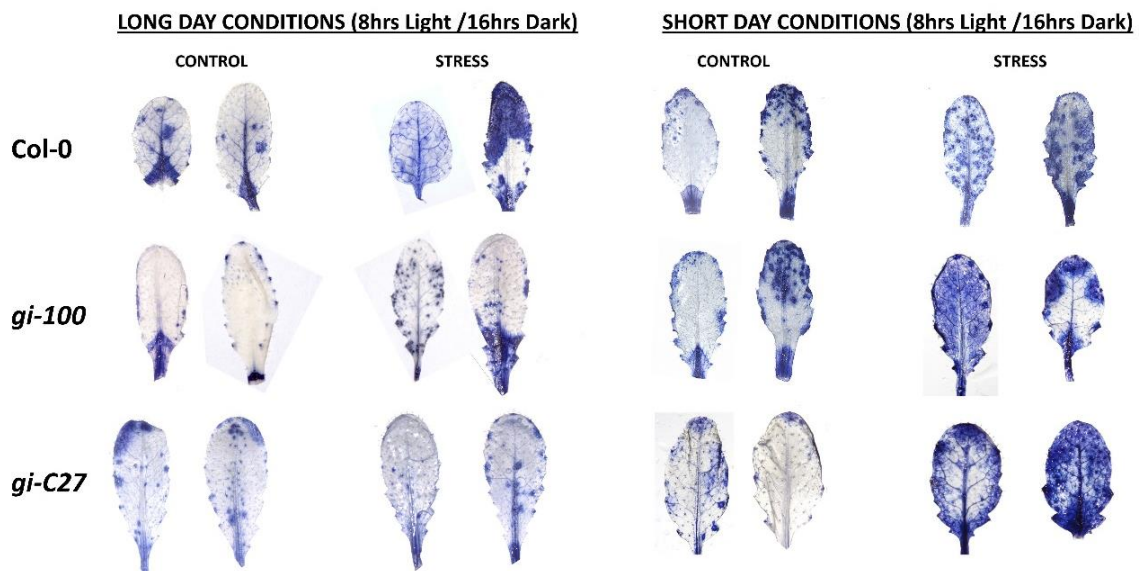


Figure 41. Histochemical detection of oxygen radical during dehydration stress. Plants of Col-0, *gi-100*, and *gi-C27* genotypes were grown on soil in pots under either LD or SD conditions at 22 °C till the bolting stage. Plants were either well-watered or imposed water withheld for 10 days (drought stress) as described in materials and methods. Histochemical detection of oxygen radicals was done using NBT staining.

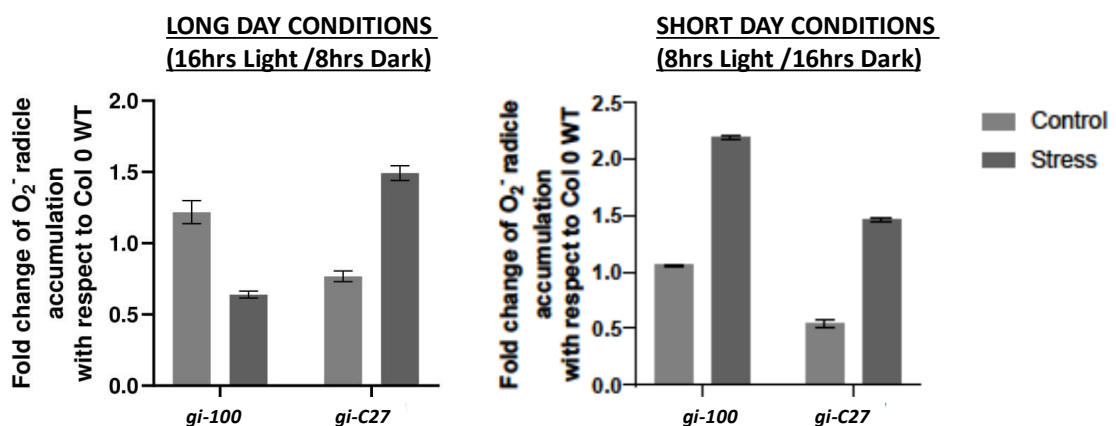


Figure 42. Histochemical detection of oxygen radical during dehydration stress. Plants of Col-0, *gi-100*, and *gi-C27* genotypes were grown on soil in pots under either LD or SD conditions at 22 °C till the bolting stage. Plants were either well-watered or imposed water withheld for 10 days (drought stress) as described in materials and methods. Histochemical detection of oxygen radicals was done using NBT staining and the percentage of oxygen radical (O_2^-) accumulation in the leaves was by calculating the stained area to the total area of the leaves using ImageJ software. Three individual biological replicates were performed for each experiment with 3 plants in each sample. Data presented as mean \pm SE.

Under LD conditions, the relative water content (RWC) in Col-0 decreased by ~3.6-fold compared to its control, whereas, the decrease in *gi-100* and *gi-C27* was nearly half of its starting value due to water withheld (Figure 43A). The reduction in the percentage of RWC was significantly lower in the *gi* mutants (~38-40 %) as compared to Col-0 (~20 %) in response to drought stress. The chlorophyll content in Col-0 decreased significantly (~3.05-fold) after drought stress. However, the chlorophyll content in drought-stressed plants of *gi-100* and *gi-*

C27 increased by ~2-fold and ~2-fold respectively as compared to their controls (Figure 43B). Carotenoid content accumulation with the effect of drought stress under LD conditions was negligible in the Col-0 line. Whereas, both the *gi* lines showed higher carotenoid accumulation after drought stress i.e., ~6.5-fold and 5.5-fold higher carotenoids in the *gi-100* and *gi-C27* line respectively (Figure 43C). Malondialdehyde (MDA) accumulation due to lipid peroxidation in plant leaves serves as an indicator of abiotic stress response (Singh *et al.*, 2009). Col-0 plants showed a significant increase of MDA content after drought stress i.e., ~8-fold as compared to its respective control (Figure 43D). MDA accumulation after drought stress in *gi* lines was significantly less than that of Col-0. Moreover, both *gi-100* and *gi-C27* showed similar patterns of MDA accumulation, i.e., nearly 1.5-fold and 1.4-fold increase than their respective control plants (Figure 43D). The enzymatic activity like catalase (CAT) and peroxidase (POX) in response to drought stress was also studied to validate the drought resistance in *gi* mutant plants. Drought stress resulted in a significant increase in CAT and POX activity within Col-0 plants. There was a notable increase of ~2.3 and ~25-fold in the CAT and POX activity in the drought-stressed plants of Col-0 plants (Figure 43E & 43F). The increase in CAT activity in drought-stressed plants of *gi* mutants was significantly less than in the wild type. These results indicate that the *gi* mutants are drought-resistant under LD conditions.

Under SD conditions, the relative water content (RWC) in Col-0 and *gi-C27* decreased by ~2- and 2-fold as compared to its control, whereas, the decrease in *gi-100* was nearly only 1.3-fold from its starting value due to water withheld (Figure 43G). The reduction in the percentage of RWC was significantly lower in the *gi-100* plants (~60 %) as compared to Col-0 (~30 %) in response to drought stress. There was a significant reduction in the water withholding capacity in the *gi-C27* mutant (~35 %) as well as the wild type i.e., Col-0 (~30 %) after drought stress. The chlorophyll content in Col-0 and *gi-C27* decreased significantly by ~2-fold and ~2-fold after drought stress. However, the chlorophyll content in drought-stressed plants of *gi-100* remained unchanged as compared to their controls (Figure 43H). Carotenoid content

accumulation with the effect of drought stress under SD conditions was negligible in the *gi-100* line. Whereas, both the Col-0 and *gi-C27* lines showed higher carotenoid accumulation after drought stress i.e., ~1.6-fold and 2.5-fold higher carotenoids in the Col-0 and *gi-C27* lines respectively (Figure 43I). Malondialdehyde (MDA) accumulation due to lipid peroxidation in plant leaves serves as an indicator of abiotic stress response (Singh *et al.*, 2009). Col-0 and *gi-C27* plants showed a significant increase of MDA content after drought stress i.e., ~12-fold and 1.7-fold respectively as compared to their respective control (Figure 43J). MDA accumulation after drought stress in *gi-100* lines was significantly less than that of Col-0 and *gi-C27*. Moreover, both Col-0 and *gi-C27* showed similar patterns of MDA accumulation to their respective control plants (Figure 43J). The enzymatic activity like catalase (CAT) and peroxidase (POX) in response to drought stress was also studied to validate the drought resistance in *gi* mutant plants. Drought stress resulted in a significant increase in CAT and POX activity within Col-0 and *gi-C27* plants. There was a notable increase of ~3.1 and ~12-fold in the CAT and POX activity in the drought-stressed plants of Col-0 plants (Figure 43K & 43L). Unlike Col-0, a similar trend was also observed in *gi-C27* lines after drought stress. The CAT and POX activity increased nearly 4-fold and 16-fold in *gi-C27* lines as compared to their respective controls. However, the increase in CAT and POX activity in drought-stressed plants of the *gi-100* mutant was significantly less than in the wild type. These results indicate that the *gi-100* is drought-resistant and *gi-C27* is drought-intolerant under SD conditions.

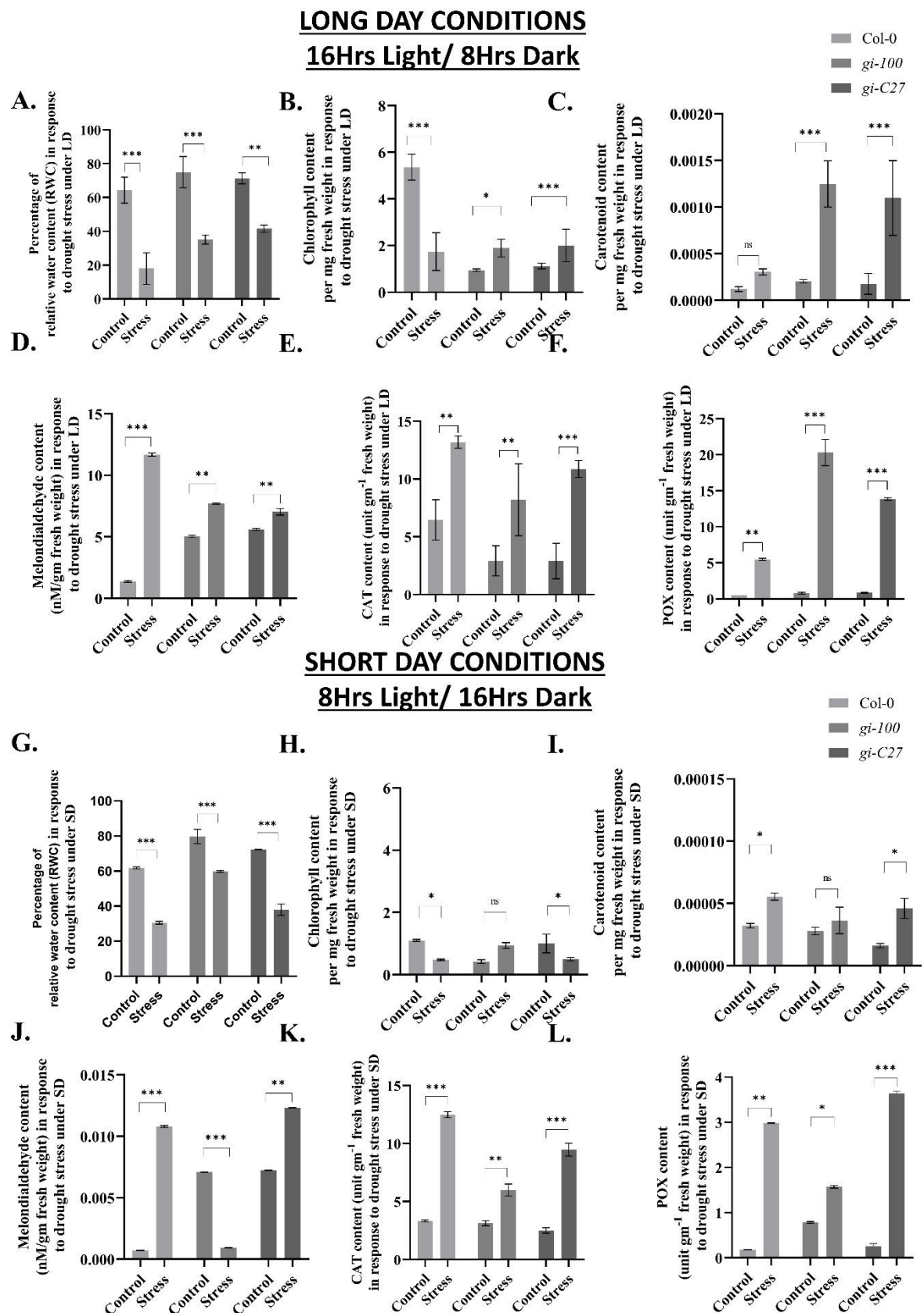


Figure 43. Test of physiological and biochemical parameters during dehydration stress. Plants of Col-0, *gi-100*, and *gi-C27* genotypes were grown on soil in pots under either LD (A-F) or SD (G-L) conditions at 22 °C till 10 days before bolting. Drought stress was imposed for 10 days at 22 °C under LD and SD conditions. Physiological parameters including relative water content (RWC) (A, G), total chlorophyll (B, H) and carotenoid (C, I) content, malondialdehyde content (MDA) (D, J), determination of ROS scavenging enzyme activity including catalase (CAT) (E, K) and Guaiacol peroxidase (POX) (F, L) activity under control and drought stress were done using spectrophotometric assays. Three individual biological replicates were performed for each

experiment with 3 plants in each sample. Data presented as mean \pm SE. One-way analysis of variance (ANOVA) using Tukey's multiple comparisons test was performed with the help of GraphPad Prism to test for significance among the dataset, * $p < 0.05$, ** $p < 0.01$, *** $p < 0.001$, ns: non-significant.

5.1.2.3.4. Role of GI in salt stress

GIGANTEA (GI) has been identified as a crucial player in response to abiotic stresses, particularly salinity stress, in *Arabidopsis thaliana* (Mishra and Panigrahi, 2015). To ascertain the persistent role of GI in salinity response, a CRISPR mutant of GI, specifically *gi-C27*, was used alongside Col-0 (wildtype) and *gi-100* (T-DNA insertional mutant) in a drought stress experiment. The plants grown in soil pots were supplemented with 200 mM NaCl in the roots approximately 10 days before their bolting stage. The experiment was conducted under both long day (LD, 16 hours light/8 hours dark) and short day (SD, 8 hours light/16 hours dark) conditions maintained at 22 °C.

Under LD conditions, both *gi-100* and *gi-C27* mutants exhibited enhanced salinity resistance compared to Col-0. Notably, the leaves of *gi-100* and *gi-C27* mutants displayed a greener and turgid phenotype relative to Col-0 which dried and turbid (refer to Figure 44, upper panel). Additionally, *gi* mutants demonstrated a higher endogenous temperature following the 10-day stress period in comparison to Col-0. This observation suggests that the leaves of *gi* mutants had greater metabolic activity compared to the Col-0 wildtype (refer to Figure 44, lower panel).

These findings underscore the significant role of GI in conferring salinity resistance in *Arabidopsis thaliana*, as evidenced by distinct phenotypic and physiological responses observed in *gi* mutants under drought stress conditions, particularly under LD photoperiods.

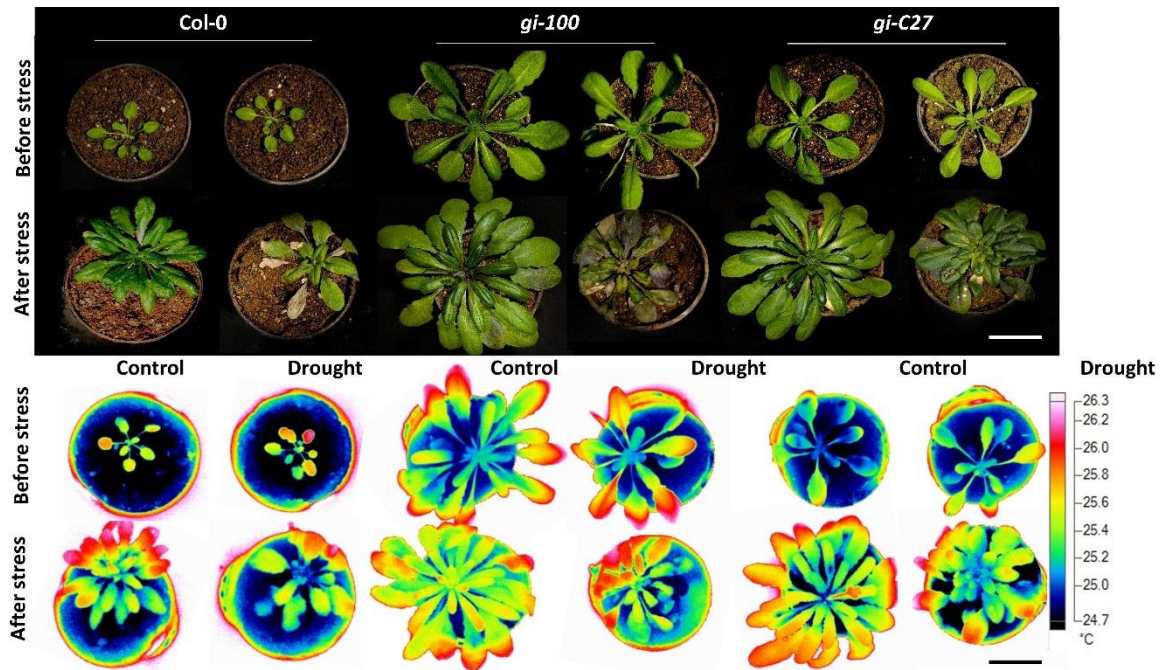


Figure 44. Effect of salinity stress under long-day conditions on the *gi* mutants in *Arabidopsis thaliana*. Plants of Col-0, *gi-100*, and *gi-C27* genotypes were grown on soil in pots under LD conditions at 22 °C till the bolting stage. Plants were either well-watered or supplemented with 200 mM NaCl for 10 days (salinity stress) as described in materials and methods. The leaf temperature of the plants grown in water withheld conditions at 22 °C (lower panel) was measured from thermal pictures that were taken with a FLUKE infrared camera and analyzed using the SMART VIEW software. Leaf surface temperatures showing the highest temperatures were selectively chosen from at least ten individual plants. Three individual biological replicates were performed. Data presented as mean \pm SE. One-way analysis of variance (ANOVA) using Tukey's multiple comparisons test was performed with the help of GraphPad Prism to test for significance among the dataset, * $p < 0.05$, ** $p < 0.01$, *** $p < 0.001$ and ns represent non-significant differences—scale bar: 1 cm.

Under short-day (SD) conditions, the response of *gi-100* and *gi-C27* mutants to salinity stress exhibited notable differences. Specifically, *gi-100* displayed drought resistance characterized by greener and turgid leaves compared to the stressed Col-0 plants. Conversely, *gi-C27* exhibited salinity susceptibility, evidenced by the presence of turbid leaves, similar to the phenotype of Col-0 under salinity stress conditions (refer to Figure 45, upper panel). Moreover, the *gi-100* mutant displayed higher endogenous temperatures following the 10-day stress period compared to Col-0, indicating more metabolic activity in *gi-100* leaves relative to the Col-0 wild type. In contrast, both Col-0 and *gi-C27* exhibited lower endogenous temperatures, suggesting cooler temperatures and reduced metabolic activity in their leaves (refer to Figure 45, lower panel).

These observations highlight the divergent responses of *gi-100* and *gi-C27* mutants under SD conditions to salinity stress. While *gi-100* demonstrates enhanced salinity resistance with

elevated metabolic activity, *gi-C27* exhibits increased susceptibility to salinity stress similar to Col-0.

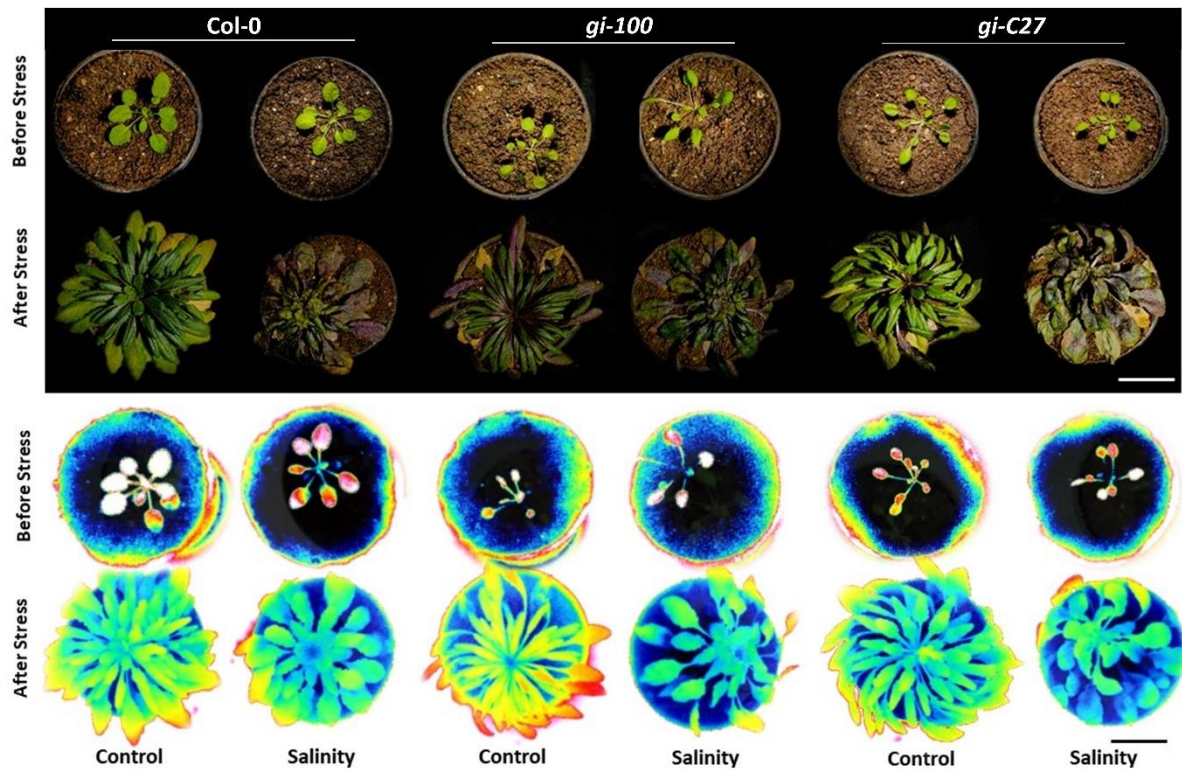


Figure 45. Effect of salinity stress under short-day conditions on the *gi* mutants in *Arabidopsis thaliana*. Plants of Col-0, *gi-100*, and *gi-C27* genotypes were grown on soil in pots under SD conditions at 22 °C till the bolting stage. Plants were either well-watered or supplemented with 200 mM NaCl for 10 days (salinity stress) as described in materials and methods. The leaf temperature of the plants grown in water withheld conditions at 22 °C (lower panel) was measured from thermal pictures that were taken with a FLUKE infrared camera and analyzed using the SMART VIEW software. Leaf surface temperatures showing the highest temperatures were selectively chosen from at least ten individual plants. Three individual biological replicates were performed. Data presented as mean \pm SE. One-way analysis of variance (ANOVA) using Tukey's multiple comparisons test was performed with the help of GraphPad Prism to test for significance among the dataset, * $p < 0.05$, ** $p < 0.01$, *** $p < 0.001$ and ns represent non-significant differences—scale bar: 1 cm.

To assess the impact of salinity stress on leaf temperatures, the highest temperatures were recorded from at least ten individual plants subjected to salinity stress with 200 mM NaCl solution and compared with control plants that were well-watered. These measurements were conducted using a FLUKE infrared camera, and the data were analyzed using SMART VIEW software, following the outlined procedures in the Materials and Methods section. The results indicated under LD conditions, there was a reduction in endogenous temperature by ~ 1.06 -fold, ~ 1.1 -fold, and ~ 1.13 -fold in salt-treated plants compared to their respective well-watered controls in Col-0, *gi-100*, and *gi-C27*, respectively. The average leaf temperatures of salinity-stressed Col-0 plants decreased to 23.94 °C from 25.35 °C observed in control plants.

Conversely, the average leaf temperatures of *gi* mutants following salinity stress were lower than those of the wild type. Specifically, the average temperatures recorded for *gi-100* and *gi-C27* were 22.84 °C and 23.01 °C, respectively, after drought stress (refer to Figure 46). Under SD conditions, the average leaf temperature after salinity stress decreased to 1.04-fold, 1.03-fold, and 1.08-fold in Col-0, *gi-100*, and *gi-C27* as compared to their controls respectively. However, the change in endogenous temperature of leaves in Col-0, *gi-100*, and *gi-C27* in salinity-stressed plants as well as control plants was negligible.

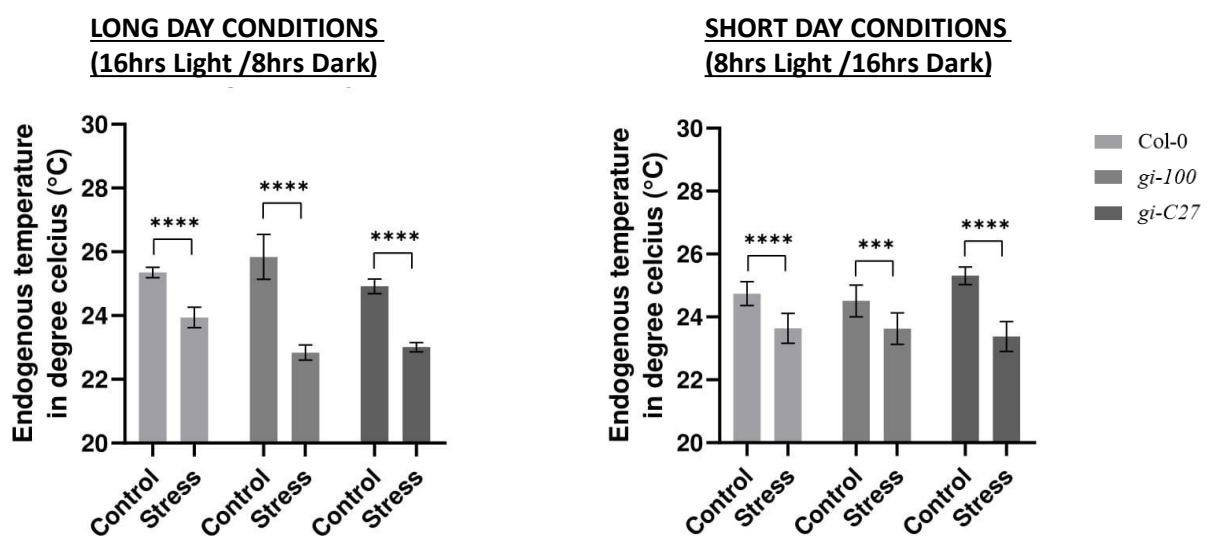


Figure 46. Effect of salinity stress on the endogenous temperature on leaves under short-day conditions on the *gi* mutants in *Arabidopsis thaliana*. Plants of Col-0, *gi-100*, and *gi-C27* genotypes were grown on soil in pots under either LD or SD conditions at 22 °C till the bolting stage. Plants were either well-watered or supplemented with 200 mM NaCl for 10 days (salinity stress) as described in materials and methods. The leaf temperature of the plants grown in water withheld conditions at 22 °C was measured from thermal pictures that were taken with a FLUKE infrared camera and analyzed using the SMART VIEW software. Leaf surface temperatures showing the highest temperatures were selectively chosen from at least ten individual plants. Three individual biological replicates were performed. Data presented as mean \pm SE. One-way analysis of variance (ANOVA) using Tukey's multiple comparisons test was performed with the help of GraphPad Prism to test for significance among the dataset, * $p < 0.05$, ** $p < 0.01$, *** $p < 0.001$ and ns represent non-significant differences.

Dehydration resulting from salinity stress induces various physiological changes, including the accumulation of stress pigments such as carotenoids and flavonoids, reduced photosynthetic efficiency, generation of reactive oxygen species (ROS), and increased ROS scavenging enzyme activity. These changes have been extensively documented in previous studies (Panigrahy *et al.*, 2011; Tomanek *et al.*, 2012; Manasa *et al.*, 2022; Panigrahy *et al.*, 2022).

The dehydration tolerance in *gi* mutant lines, *gi-100* and *gi-C27*, was validated by studying various biochemical parameters such as oxygen free radicals (O_2^-), relative water content (RWC), chlorophyll, carotenoids, malondialdehyde (MDA), and enzyme activity of catalase (CAT), and peroxidase (POX), in comparison with those of Col-0 and their respective well-watered controls.

Under LD and SD conditions at 22 °C, Col-0 lines exhibited a significant increase in O_2^- levels due to salinity stress, visible through histochemical NBT staining in the leaves. Before salinity stress, both *gi* mutant lines displayed comparable O_2^- levels to Col-0 under LD and SD conditions at 22 °C. However, under LD conditions, O_2^- accumulation decreased by ~0.75-fold and ~0.74-fold in *gi-100* and *gi-C27* compared to Col-0 after salinity stress. Conversely, under SD conditions, the accumulation of O_2^- was significantly lower (~0.45-fold) in *gi-100* as compared to Col-0 after drought stress. However, the accumulation of O_2^- was nearly similar to Col-0 in *gi-C27* after salinity stress (refer to Figure 47 and Figure 48).

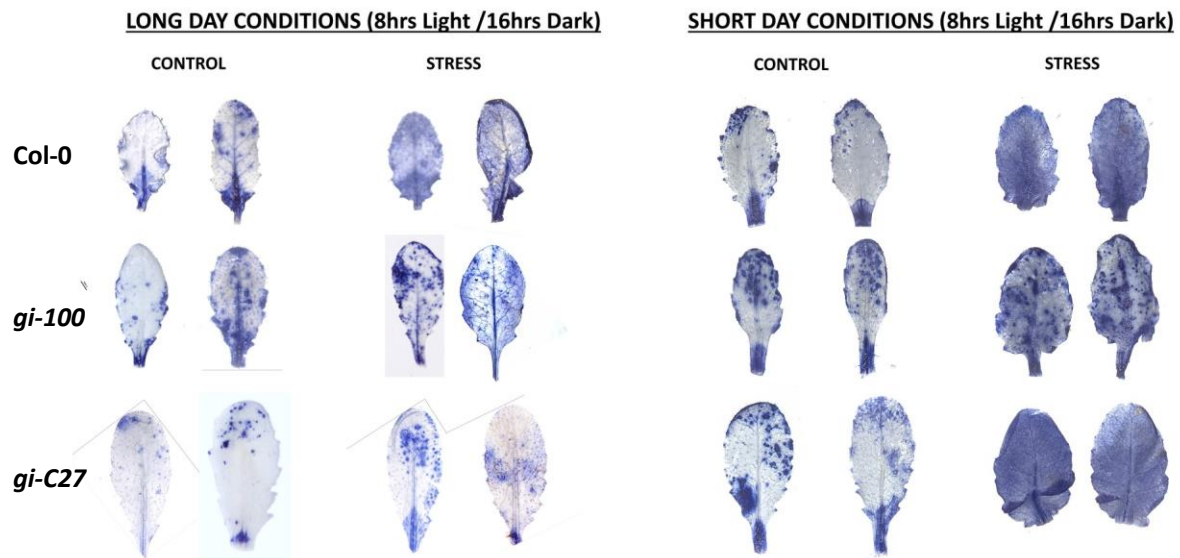


Figure 47. Histochemical detection of oxygen radical during salinity stress. Plants of Col-0, *gi-100*, and *gi-C27* genotypes were grown on soil in pots under either LD or SD conditions at 22 °C till the bolting stage. Plants were either well-watered or supplemented with 200 mM NaCl for 10 days (salinity stress) as described in materials and methods. Histochemical detection of oxygen radicals was done using NBT staining.

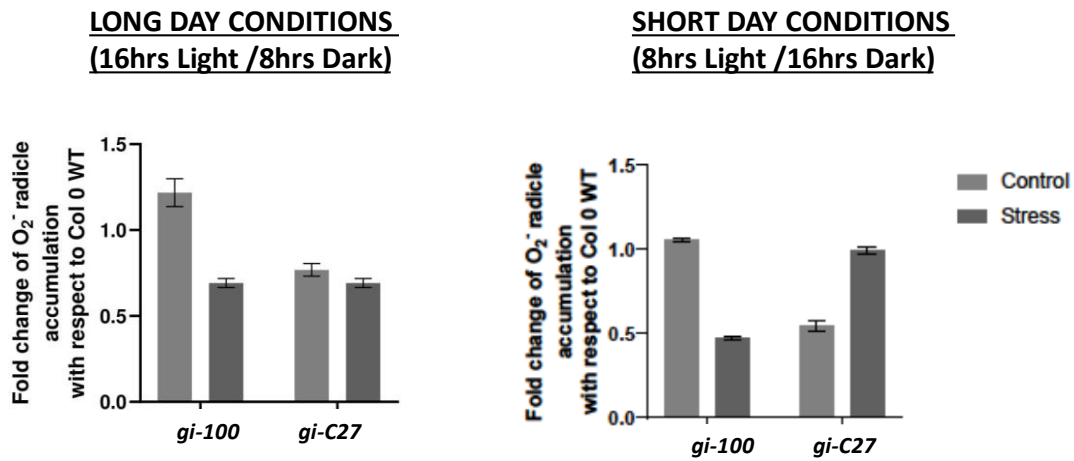


Figure 48. Histochemical detection of oxygen radical during salinity stress. Plants of Col-0, *gi-100*, and *gi-C27* genotypes were grown on soil in pots under either LD or SD conditions at 22 °C till the bolting stage. Plants were either well-watered or supplemented with 200 mM NaCl for 10 days (salinity stress) as described in materials and methods. Histochemical detection of oxygen radicals was done using NBT staining and the percentage of oxygen radical (O₂⁻) accumulation in the leaves by calculating the stained area to the total area of the leaves using ImageJ software. Three individual biological replicates were performed for each experiment with 3 plants in each sample. Data presented as mean ± SE. One-way analysis of variance (ANOVA) using Tukey's multiple comparisons test was performed with the help of GraphPad Prism to test for significance among the dataset, **p* < 0.05, ***p* < 0.01, ****p* < 0.001, ns: non-significant—scale bar: 2 mm.

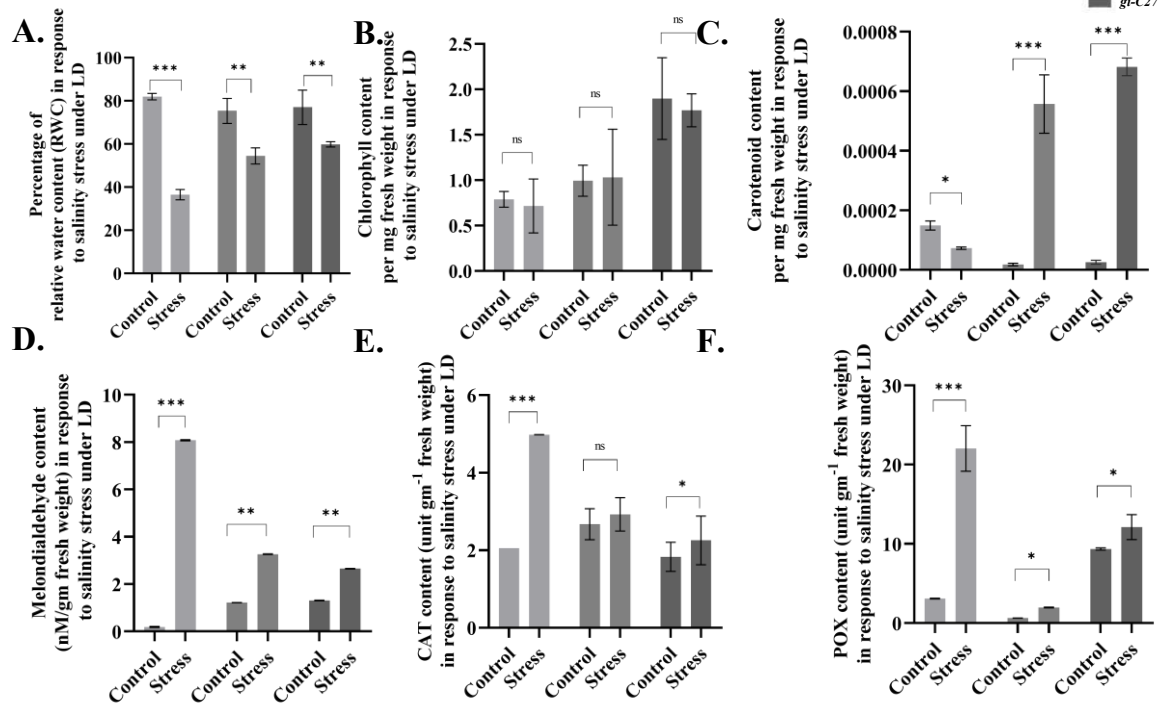
Under LD conditions, the relative water content (RWC) in Col-0 decreased by ~2.1-fold as compared to its control, whereas, the decrease in *gi-100* and *gi-C27* was less i.e., 58 % and 60 % respectively due to salinity stress (Figure 49A). The reduction in the percentage of RWC was significantly lower in the *gi* mutants (~1.3-fold in *gi-100* and 1.3-fold in *gi-C27*) as compared to Col-0 (~20 %) in response to salinity stress. The chlorophyll content in Col-0 as well as *gi* mutants was indistinguishable from the control after drought stress (Figure 49B). Carotenoid accumulation with the effect of salinity stress under LD conditions was significantly low (~3.4-fold) in the Col-0 line as compared to its control. Whereas, both the *gi* lines showed higher carotenoid accumulation after salinity stress i.e., ~12-fold and 14-fold higher carotenoids in the *gi-100* and *gi-C27* lines respectively (Figure 49C). Malondialdehyde (MDA) accumulation due to lipid peroxidation in plant leaves serves as an indicator of abiotic stress response (Singh *et al.*, 2009). Col-0 plants showed a significant increase of MDA content after salinity stress i.e., ~8-fold compared to its respective control (Figure 49D). MDA accumulation after drought stress in *gi* lines was significantly less than that of Col-0. Moreover, both *gi-100* and *gi-C27* showed similar patterns of MDA accumulation, i.e., nearly 3.2-fold and 2.4-fold increases than

their respective control plants (Figure 49D). The enzymatic activity like catalase (CAT) and peroxidase (POX) in response to salinity stress was also studied to validate the salinity resistance in *gi* mutant plants. Salinity stress resulted in a significant increase in CAT and POX activity within Col-0 plants. There was a notable increase of ~2.5 and ~ 5.5-fold in the CAT and POX activity in the salinity-stressed plants of Col-0 plants (Figure 49E & Figure 49F). The increase in CAT activity in salt-treated plants of *gi* mutants was significantly less than in the wild type. These results indicate that the *gi* mutants are salinity-resistant under LD conditions.

Under SD conditions, the relative water content (RWC) in Col-0 and *gi-C27* decreased significantly by ~1.1-fold and 1.3-fold respectively as compared to its control, whereas, the decrease in *gi-100* was nearly only 1.05-fold from its starting value due to salinity stress (Figure 49G). The reduction in the percentage of RWC was observed in Col-0 (~52 %) and *gi-C27* (~58 %) in response to salinity stress. The water withholding capacity in *gi-100* was reduced to only ~75 % after salinity stress from control plants with ~80 % RWC (Figure 49G). The chlorophyll content in Col-0 and *gi-C27* was indistinguishable after salinity stress from their respective controls. However, the chlorophyll content in salinity-stressed plants of *gi-100* increased significantly by ~2-fold as compared to their controls (Figure 54H). Carotenoid content with the effect of salinity stress under SD conditions was negligible in the Col-0, *gi-100*, and *gi-C27* lines (Figure 49I). Malondialdehyde (MDA) accumulation due to lipid peroxidation in plant leaves serves as an indicator of abiotic stress response (Singh *et al.*, 2009). Col-0 and *gi-C27* plants showed a significant increase in MDA content after salinity stress i.e., ~1.3-fold and 1.6-fold respectively as compared to their respective control (Figure 49J). MDA accumulation after salinity stress in *gi-100* lines was significantly less than that of Col-0 and *gi-C27* (Figure 49J). Moreover, both Col-0 and *gi-C27* showed similar patterns of MDA accumulation to their respective control plants (Figure 49J). The enzymatic activity like catalase (CAT) and peroxidase (POX) in response to salinity stress was also studied to validate the salinity resistance in *gi* mutant plants. Salinity stress resulted in a significant decrease in CAT activity

within Col-0 (~2.1-fold), *gi-100* (~1.3-fold), and *gi-C27* (~1.2-fold) plants (Figure 52K). There was a notable increase of ~8.6 and ~ 6.5-fold in the POX activity in the salinity-stressed plants of Col-0 plants and *gi-C27* plants (Figure 49L). These results indicate that the *gi-100* is salinity-resistant and *gi-C27* is salinity-intolerant under SD conditions.

LONG DAY CONDITIONS 16Hrs Light/ 8Hrs Dark



SHORT DAY CONDITIONS 8Hrs Light/ 16Hrs Dark

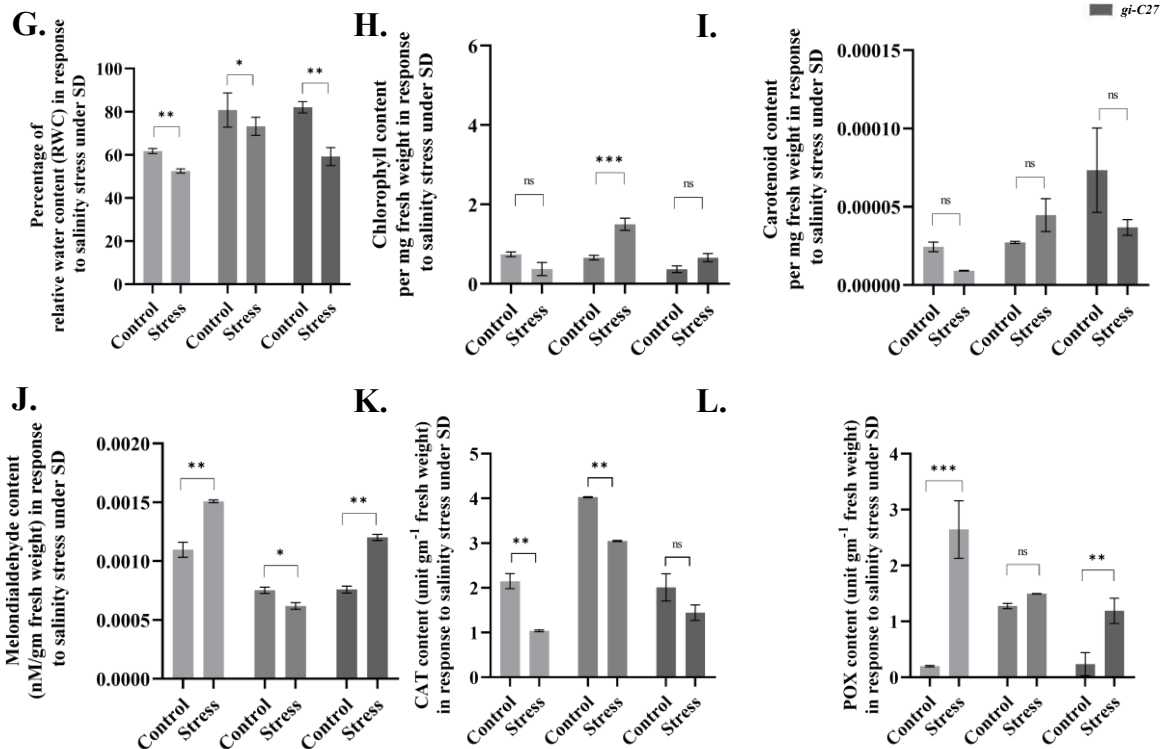


Figure 49. Test of physiological and biochemical parameters during salinity stress. Plants of Col-0, *gi-100*, and *gi-C27* genotypes were grown on soil in pots under either LD (A-F) or SD (G-L) conditions at 22 °C till 10 days before bolting. Salinity stress was imposed for 10 days with supplementing 200 mM NaCl in the soil at 22 °C under LD and SD conditions. Physiological parameters including relative water content (RWC) (A, G), total chlorophyll (B, H) and carotenoid (C, I) content, malondialdehyde content (MDA) (D, J), determination of ROS scavenging enzyme activity including catalase (CAT) (E, K) and Guaiacol peroxidase (POX) (F, L) activity under control and drought stress were done using spectrophotometric assays. Three individual biological replicates were performed for each experiment with 3 plants in each sample. Data presented as mean \pm SE. One-way analysis of

variance (ANOVA) using Tukey's multiple comparisons test was performed with the help of GraphPad Prism to test for significance among the dataset, $*p < 0.05$, $**p < 0.01$, $***p < 0.001$, ns: non-significant.

4.1.3. DISCUSSION

T-DNA insertion mutants, which were initially groundbreaking in plant molecular research, have shown the likelihood of off-target effects. Adjacent genes, situated either upstream or downstream of the insertion site, often undergo alterations in expression levels due to the T-DNA insertion event. This phenomenon is likely caused by the disruption of cis-acting regulatory elements within the genomic locus, which may affect neighboring genes. Furthermore, genes that share genomic sequences with adjacent loci are vulnerable to disruption if T-DNA integrates within these shared regions. As a result, the phenotypic consequences of such gene mutations or modifications may appear as off-target effects. The CRISPR mutant of *GI* i.e., *gi-C27* that was selected through genotyping exhibited a late flowering phenotype under LD conditions. It exhibited a flowering phenotype similar to Col-0 wild-type under SD conditions. A similar exponential shoot-up of the rosette leaf number was also observed in *gi-C27* and *gi-100* under LD conditions. However, the *gi-C27* and the wildtype had similar rosette leaves under SD conditions. The study further investigated the presence of functional GI protein in *gi-C27*, a CRISPR mutant line of GI. Western blot analysis revealed the absence of a functional protein band at 127 kDa in the *gi-C27* lane, indicating that *gi-C27* does not produce any functional GI protein. Ab04 can effectively bind to endogenous GI in *Arabidopsis thaliana*, providing a valuable tool for future research on GI protein function and regulation. Whole-genome sequencing confirmed two frameshift mutations in the *gi-C27* line, producing stop codons in exon 2 and exon 7. Consequently, *gi-C27* was identified as a complete null mutant that lacks functional GI protein.

The observed variations in hypocotyl and root lengths suggest that GI plays distinct roles in light-dependent growth responses and sucrose modulation. The contrasting responses in hypocotyl lengths under different light conditions highlight the complexity of GI's regulatory functions. The differential effects of sucrose supplementation indicate an interplay between GI and sugar signaling pathways in modulating plant growth. The shorter root lengths in *gi-C27*

under dark conditions and red light suggest specific roles for GI in root development, possibly linked to light perception mechanisms. Rescuing root lengths by sucrose supplementation in some conditions implies interactions between sugar availability and root development pathways. The significant increase in hypocotyl lengths in *gi-100* and *gi-C27* under far-red light suggests a role for GI in light signal transduction pathways. The absence of rescue by sucrose indicates that sugar availability may not counteract the effects of far-red light on hypocotyl elongation. The response to blue light reveals a distinct influence of GI and its mutants on hypocotyl development. Regardless of sucrose, the consistency in root lengths suggests that GI's role in root development may be less influenced by sugar availability under blue light conditions. Finally, the study demonstrates the multifaceted roles of GI in *Arabidopsis thaliana* growth responses to various light conditions and sucrose availability. The findings highlight the complex interaction of GI, light signalling pathways, and sugar modulation in regulating hypocotyl and root development. The differences in responses observed in various mutants highlight the specificity of GI functions in different environmental and nutritional contexts. Further research is needed to understand the molecular mechanisms underlying these responses, as well as the implications for overall plant growth and development.

The study also aimed to investigate the role of GI in drought and salinity response in *Arabidopsis thaliana* under both long-day (LD) and short-day (SD) conditions. Two mutants, *gi-100* (T-DNA insertional mutant) and *gi-C27* (CRISPR mutant), along with the wild type (Col-0), were subjected to drought stress, and various physiological and biochemical parameters were assessed. Under LD conditions, both *gi-100* and *gi-C27* mutants exhibited drought and salinity resistance compared to Col-0, as evidenced by greener leaves and higher endogenous temperatures. The elevated metabolic activity observed in *gi* mutants indicates their ability to withstand drought stress. These findings support the notion that GI plays a crucial role in drought response under LD photoperiods. In contrast, under SD conditions, the response of *gi-100* and *gi-C27* mutants to drought and salinity stress differed significantly. While *gi-100*

displayed drought and salinity resistance with greener and turgid leaves, *gi-C27* showed susceptibility to drought and salinity stress, resulting in dried and turbid leaves akin to Col-0 under stress conditions. The differential response of *gi* CRISPR mutant under LD and SD conditions suggests that the role of GI in drought and salinity response may be influenced by the photoperiod. In conclusion, the study highlights the significant role of GI in conferring drought and salinity resistance in *Arabidopsis thaliana*, particularly under LD conditions. The contrasting responses of *gi* mutants under SD conditions underscore the influence of photoperiod on GI-mediated drought and salinity response mechanisms. The study reveals that GI does not have a role in photoperiodic flowering, drought, and salinity resistance under SD conditions. The findings contribute to our understanding of the molecular mechanisms underlying plant responses to abiotic stress and may inform strategies for developing stress-tolerant crop varieties in the future. Further investigations into the signaling pathways and gene networks regulated by GI in response to photoperiodic flowering, drought and salinity stress will help us to understand the intricacies of GI-mediated or GI-independent response in plants under SD conditions.

5.2. To evaluate the role of GIGANTEA in biotic stress i.e., *Fusarium oxysporum* infection.

5.2.1. BACKGROUND

The transition from the vegetative to the reproductive phase in plants is influenced by several factors including light, temperature, age, and hormones. Photoperiodic flowering occurs when this transition is influenced by light and fine-tuned by diurnal and circadian regulatory mechanisms (de Montaigu *et al.*, 2010; Sanchez and Kay, 2016). GIGANTEA (GI) is one of the crucial circadian clock output components in plants (Fowler *et al.*, 1999; Kim *et al.*, 2013b). GI gene was first discovered in *Arabidopsis* because mutations in it delayed flowering response to inductive photoperiods with little variation in short days (SDs) (Rédei, 1962; Fowler *et al.*, 1999). In *Arabidopsis thaliana*, a single copy of GI contains 14 exons that code for a 127 kDa protein with 1173 amino acids (Park *et al.*, 1999). GI is reported to be a nuclear protein with a nuclear localization sequence between residues 543 and 783 in the core 241 amino acid region (Huq *et al.*, 2000). GIGANTEA structural homology reveals that it lacks any conserved protein domains (David *et al.*, 2006; Mishra and Panigrahi, 2015). GI is diurnally regulated, and its transcript and protein levels are strictly controlled by the circadian clock (Patnaik *et al.*, 2022). Any change in the components of the circadian clock has been demonstrated to alter the transcription of GI. Furthermore, despite overexpressing the GI protein with a constitutive promoter, its abundance follows a cyclic pattern of aggregation under long-day (LD) and SDs indicating an additional layer regulation on the protein expression at the post-transcriptional level (David *et al.*, 2006; Yu *et al.*, 2008). The ubiquitin E3 ligase activity of CONSTITUTIVE PHOTOMORPHOGENIC 1 (COP1) controls the post-transcriptional regulation of GI protein, which leads to its degradation by the 26S proteasome machinery.

In vascular plants, GI is evolutionarily conserved and plays an important role in a variety of physiological responses. The role of GI in photoperiodic flowering has been thoroughly studied, where it is required to increase the transcription of *CONSTANS* (*CO*) and *FLOWERING LOCUS*

T (FT) (Fornara *et al.*, 2009). The degradation of repressors from the DOF family of transcriptional regulators, known as CYCLING DOF FACTORS (CDFs), is necessary for the stimulation of CO and FT expression under LD conditions. In the afternoon, GIGANTEA forms a complex with the blue light-absorbing FLAVIN-BINDING KELCH REPEAT F-BOX 1 (FKF1), an F-box protein, which degrades the DOF transcriptional repressors, allowing CO transcription leading to flowering under long-day conditions (Sawa Mariko *et al.*, 2007; Imaizumi *et al.*, 2005; Kim *et al.*, 2013). Other blue light circadian photoreceptors like LOV KELCH protein 2 (LKP2) and ZEITLUPE (ZTL) interact and stabilize GI (Kim *et al.*, 2007). This regulates the appropriate development and resilience of the circadian clock in plants (Somers *et al.*, 2000; Kim *et al.*, 2007; Fornara *et al.*, 2009; Baudry *et al.*, 2010). In recent times, GI has been shown to act as a co-chaperone in the *Arabidopsis thaliana*'s circadian clock, facilitating the maturation of ZTL (Cha *et al.*, 2017).

Different abiotic stresses, such as cold, drought, salt, and oxidative stress, are regulated by GI in the plants. The level of GI transcript is increased during cold stress, inducing cold acclimation in *A. thaliana* via a C-repeat Binding proteins (CBFs)-independent route (Fowler and Thomashow, 2002). On the contrary, another finding states that cold-responsive gene (COR) mRNA expression is higher in *gi* mutants than in Col-0 WT, and this is likely to be responsible for promoting freezing tolerance in *gi* mutant plants, implying an additional overlay in regulating transcription of cold response pathway in *gi* mutant plants (Fornara *et al.*, 2015). GI is shown to play a crucial role in drought tolerance too. Drought resistance is improved by GI via the abscisic acid (ABA) dependent drought escape mechanism (Riboni *et al.*, 2013) besides its inhibitory role in salinity stress tolerance. It inhibits Salt Overly Sensitive (SOS1) and Na^+/H^+ anti-porter channels by binding directly to SOS2. Furthermore, while salt stress does not affect GI transcription, it reduces protein stability (Kim *et al.*, 2013a). When it comes to oxidative stress tolerance, the GI plays a function as an inhibitor (Riboni *et al.*, 2013). The absence of GI promotes the constitutive production of *SUPEROXIDE DISMUTASE (SOD)* and

ASCORBATE PEROXIDASE (APX) genes and therefore, *gi* mutants are resistant to oxidative stress caused by H₂O₂ (Riboni *et al.*, 2013). Although, *gi* mutants have been reported to provide resistance to *Fusarium oxysporum* (*F. oxysporum*) infection than wild-type plants in *A. thaliana* (Lyons *et al.*, 2015a), the molecular mechanism is yet unknown.

F. oxysporum is a soil-borne hemibiotrophic fungal pathogen, which is the causative pathogen for vascular wilt disease in plants (Michielse and Rep, 2009; Lyons *et al.*, 2015a). It begins its disease cycle as a biotroph, infecting the root system which gradually spreads up to the vasculature, where it secretes phototoxic chemicals, causing wilting. This necrotrophic pathogen eventually causes necrosis, plant senescence, and death (Czymmek *et al.*, 2007; Cole *et al.*, 2014; Lyons *et al.*, 2015a). To combat pathogen invasion, plants use a variety of defense mechanisms. The host response to *Fusarium* infection is regulated by ABA, ethylene, and auxin to improve vulnerability to this disease, while gibberellic acid (GA) is thought to influence jasmonic acid (JA)/salicylic acid (SA) signalling (Anderson *et al.*, 2004; Kidd *et al.*, 2011; Pantelides *et al.*, 2013). In *A. thaliana*, the jasmonate (JA) signalling pathway contributes both positively and negatively to resistance against *F. oxysporum*. JA receptor mutants like *coil* have evoked resistance to *F. oxysporum* (Thatcher *et al.*, 2009), but bioactive jasmonates produced during infection have been found to cause senescence of the host (Cole *et al.*, 2014). Salicylic acid (SA) improves resistance to *F. oxysporum* during the biotrophic phase of infection (Edgar *et al.*, 2006; Cole *et al.*, 2014). Salicylic acid deficient *sid2* mutant is more susceptible to *Fusarium* wilt than the WT (Diener and Ausubel, 2005). Late flowering mutants such as *gi-1*, *mediator 8 (med8)*, *phytochrome and flowering time 1 (pft1)*, *auxin response factor 2 (arf2)*, and *myc2*, have also been found to promote resistance to *F. oxysporum* in plants (Kidd *et al.*, 2009; Gangappa and Chattopadhyay, 2010; Lyons, *et al.*, 2015a, b), implying the role of *flowering genes in modulating the defense pathways in plants*. Despite plenty of studies that describe the possible functions of GI in abiotic stress response, little is known about its involvement in biotic stress tolerance (Lyons *et al.*, 2015a; Kundu and Sahu, 2021; Singh, 2022).

Biotic stress is also reported to be important in modulating the flowering transition (Kazan and Lyons, 2016), pointing to a possible link between GI and biotic stress tolerance. Thus, exploration of the role of GI on the disease defense mechanism of plants is very important in a global climate-changing scenario. We demonstrated the role of GI in *F. oxysporum-induced* biotic stress tolerance of *A. thaliana* through transcript expression analysis of JA and SA pathway genes in *gi-100* mutants, confocal microscopy of root cortical cell morphology, stomatal anomalies during fungal progression, disease severity, PS II activity changes in relation to Chl *a* fluorescence, and thermal imaging of internal leaf temperature behaviors in presence and absence of GI.

5.2.2. RESULTS

5.2.2.1. Severity of wilt disease due to *F. oxysporum* in Col-0 and *gi-100* plants

The report of GIGANTEA (GI)'s involvement in the susceptibility of *Arabidopsis* to the hemibiotrophic fungus *Bipolaris sorokiniana* (Kundu and Sahu, 2021) prompted us to investigate GI function in plant defense against other pathogens, particularly the soilborne fungus *F. oxysporum*, which infects *Arabidopsis* at the vegetative stage. In this study, the probable role of GIGANTEA in plant defense during the *Fusarium-Arabidopsis* association was investigated using a T-DNA insertion mutant of GIGANTEA (GI), i.e., *gi-100* (Huq *et al.*, 2000).

At 9-DPI, the *gi-100* mutant plants were found to be more resistant to wilt disease infection with greener and expanded leaves as compared to the Col-0 plants. The effect of *F. oxysporum* on another *gi* mutant such as *gi-1* has been carried out and similar results were obtained. The plants showed disease resistivity upon *F. oxysporum* infection (Figure 50B). Whereas, the line overexpressing GI i.e., 35S::GI showed susceptibility to the wilt disease with less expanded and turgid leaves (Figure 50B). The disease severity percentage indicating the disease progression in the *gi-100* and *gi-1* mutants was significantly ($p \leq 0.05$) slower than in the Col-0 plants, with the area of necrotic lesions (red arrows) in the Col-0 plants being significantly higher (nearly double) than (in the *gi-100* mutants after 9-DPI (Figure 50C and 50D). Following 9-DPI, necrosis was also apparent on the leaves of the *gi-100*, *gi-1*, and Col-0 plants. Hence, all further analyses were carried out with *gi-100* plants. Trypan blue staining in leaf mesophyll cells of Col-0 (Figure 50F, upper panel) and *gi-100* (Figure 50F, lower panel) showed that non-viable cells are significantly higher in Col-0 than in *gi-100*. Here, we showed that the invasion of this root-borne fungus even through the stomata confirmed the infection through the leaf. The fungal progression in Col-0 (Figure 50G, upper panel, right to left) and *gi-100* (Figure 50G, lower panel, right to left) roots from lateral root hair cells through the epidermal cells tap root cells

could visualize the gradual spread of the disease. These results indicated that the progression of the disease was significantly less in *gi-100* compared to the wild type.

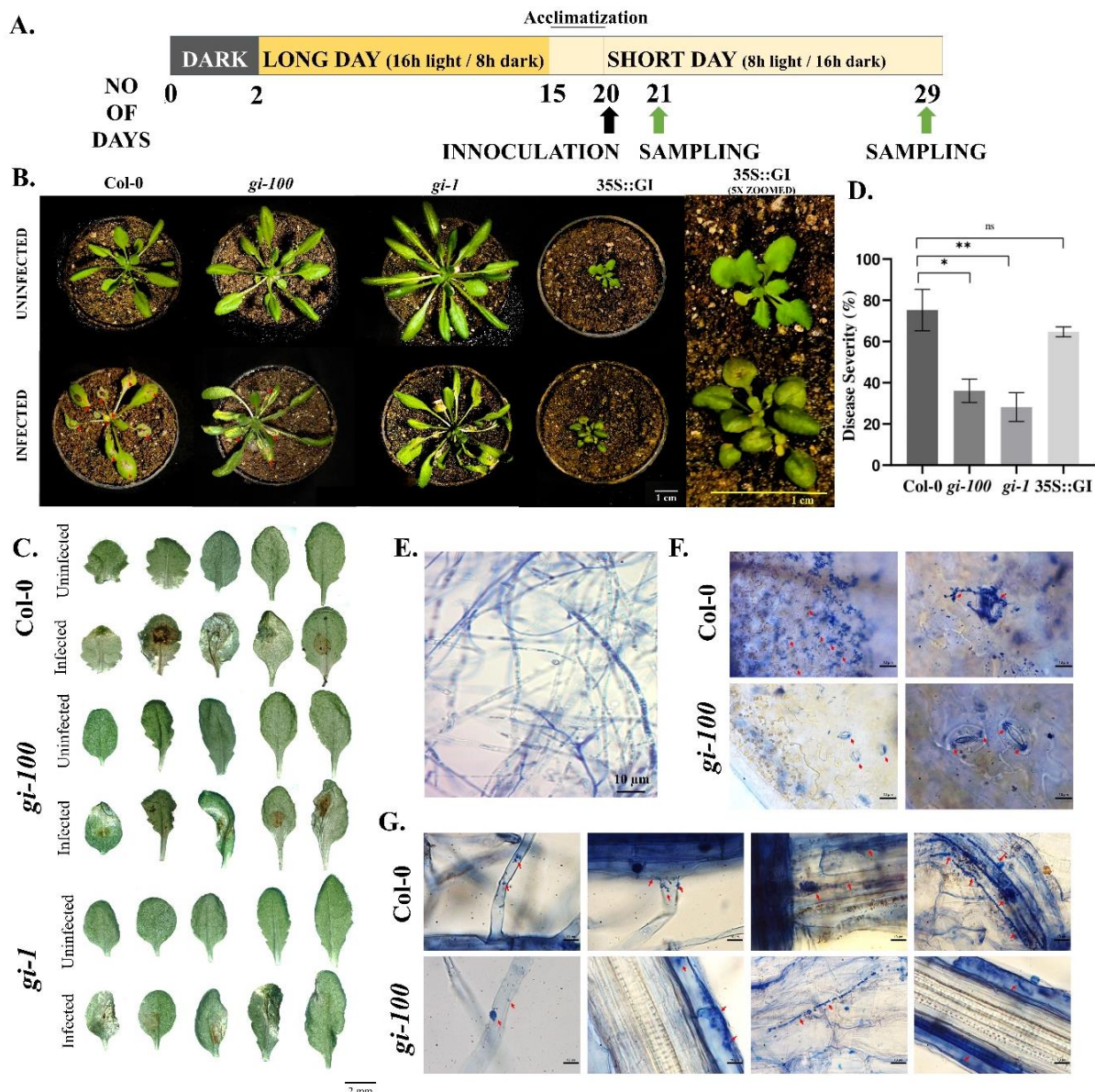


Figure 50. Effect of *F. oxysporum* infection on GIGANTEA (GI) in *Arabidopsis thaliana*. (A) Schematic representation of light treatment, plant growth conditions, and sample harvest. (B) Plants in pots infected with wilt disease caused due to *F. oxysporum*. Columbia-0 (Col-0), *gigantea* mutant (*gi-100*, *gi-1*), and overexpressed GI (35S::GI) plants after 9 and 5 days post-inoculation (DPI) respectively. (C) Leaf morphology of Col-0, *gi-100*, and *gi-1* mutant plants after 9-DPI infected with *F. oxysporum*. The leaves of infected and uninfected plants were excised 9-DPI and were photographed using a Carl Zeiss stereo microscope. (D) Disease progression after *F. oxysporum* inoculation in Col-0 and *gi-100* was interpreted as in disease severity percentage (area in square meters of necrosis). The disease severity was analyzed using ImageJ software as described in materials and methods. (E) The viability of fungal hyphae of *F. oxysporum* was reclaimed by staining with trypan blue before infection. (F) Fungal invasion in Col-0 and *gi-100* stained with trypan blue in leaf mesophyll cells in the upper and lower row respectively. Magnification is indicated at the top right of each figure. (G) Progression of fungal hyphae from lateral hair cells to tap root cells (left to right) in Col-0: upper row and *gi-100*: lower row visualized at 100X. Data represented as Mean \pm SE. Student's paired T-test was used to evaluate significant differences and compare between Col-0 and *gi-100* plants. * $p < 0.05$, ** $p < 0.01$, *** $p < 0.001$

5.2.2.2. Effect of *F. oxysporum* infection on GIGANTEA transcript and protein levels

As the absence of GI affected the severity of wilt disease, the transcript abundance and protein accumulation of GI before and after *F. oxysporum* infection at 24-HPI were studied to investigate the scenario at the molecular level. After 24-HPI, nearly a 2-fold rise in the level of GI transcript was observed in Col-0 leaf samples (Figure 51A). For protein levels, GI::GI-TAP was used to mimic the GI levels in Col-0 WT. In the immune-blot analysis of GI at 24-HPI following *F. oxysporum* infection, the protein abundance of GI was nearly double that of the uninfected samples (Figure 51B, 51C). These results confirmed that *F. oxysporum* infection causes an increase of GIGANTEA protein, which may lead to susceptibility in *Arabidopsis thaliana*.

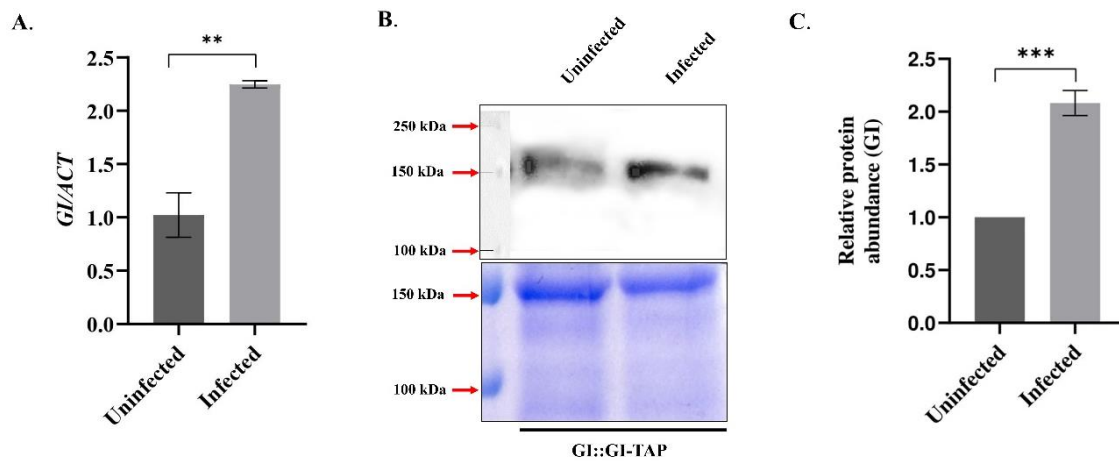


Figure 51. Transcript and protein levels of GIGANTEA after *F. oxysporum* infection Quantitative RT-PCR results showing *GI* transcript abundance in uninfected (0-HPI) and 24-HPI in Col-0 leaf samples. Transcript abundance in Col-0 uninfected at 24-HPI was taken as 1 to calculate the relative transcript level of *GI*. ACTIN was used to normalize transcript levels. (B) Immuno-blot detection and (C) relative protein levels of GI in the uninfected and infected GI::GI-TAP leaf samples. (B) The bottom panels show SDS-PAGE stained with Coomassie Brilliant Blue (CBB). The top panel shows the PVDF membrane blotted against anti-GI monoclonal primary antibody raised in rabbits (Unpublished data) and further incubated with secondary antibody anti-rabbit polyclonal HRP for 2 h at room temperature. Detection was done using an ECL substrate. Corresponding loading control is shown by Coomassie Brilliant Blue (CBB) stained gel. (C) For relative protein levels, ImageJ software was used for densitometric quantification of western blot and normalization with the loading controls against Coomassie brilliant blue staining. Calculations were done by taking protein abundance in uninfected conditions at 0-HPI as 100 %. The qRT-PCR reactions were done in triplicates from three biological replicates. Data is represented as Mean \pm SE. To evaluate significant differences, students' unpaired T-test was used to compare between uninfected and infected Col-0 plants. * $p < 0.05$, ** $p < 0.01$, *** $p < 0.001$.

5.2.2.3. Effect of *Fusarium* infection on flowering time

As any kind of biotic or abiotic stress alters the flowering and reproductive ability of a plant, the flowering phenotype of Col-0 plants was studied with or without *F. oxysporum* infection. Flowering time is reciprocally related to the total number of rosette leaves in *A. thaliana* (Mishra and Panigrahi, 2015). Moreover, GI has been demonstrated to control and regulate photoperiodic flowering in *Arabidopsis thaliana* by upregulating the expression of the *FT* gene (Wang *et al.*, 2011). Col-0 plants flowers with $\sim 17 \pm 2$ leaves at the time of bolting (Figure 52A, 52B & 52C). Col-0 plants could not survive the infection with 70 % lethality by 15-DPI. However, the Col-0 plants that could survive showed early flowering phenotype with $\sim 12 \pm 3$ leaves at the time of bolting (Figure 52A, 52B & 52C). The uninfected *gi-100* plants show delayed flowering with 50 ± 2 rosette leaves at the time of bolting. Even in the *gi-100* plants, *F. oxysporum* infection induced 30 % of lethality. However, in *gi-100* infected plants, the flowering time was unaltered with a similar number of rosette leaves as compared to their respective uninfected plants. These results indicated that during *F. oxysporum* infection GI had minimal or no role in flowering time regulation. During plant-pathogen interactions, the expression of flowering regulatory genes including *FLOWERING LOCUS T (FT)* and *FLC* is known to be altered (Wang *et al.*, 2011). Hence, the transcript expression of *FT* at 0-HPI and 24-HPI in Col-0 and *gi-100* were studied using the qRT-PCR approach. After infection, *FT* expression in Col-0 plants suddenly increased to > 2 -fold at 24-HPI. The expression of *FT* in *gi-100* was 0.79-fold lower than that of Col-0 plants under uninfected conditions (Figure 52D). At 24-HPI, the *FT* expression in *gi-100* plants was further reduced to ~ 2.9 fold. Together these results indicated that the flowering time phenotype in *gi-100* might be regulated by several factors in addition to *FT* expression.

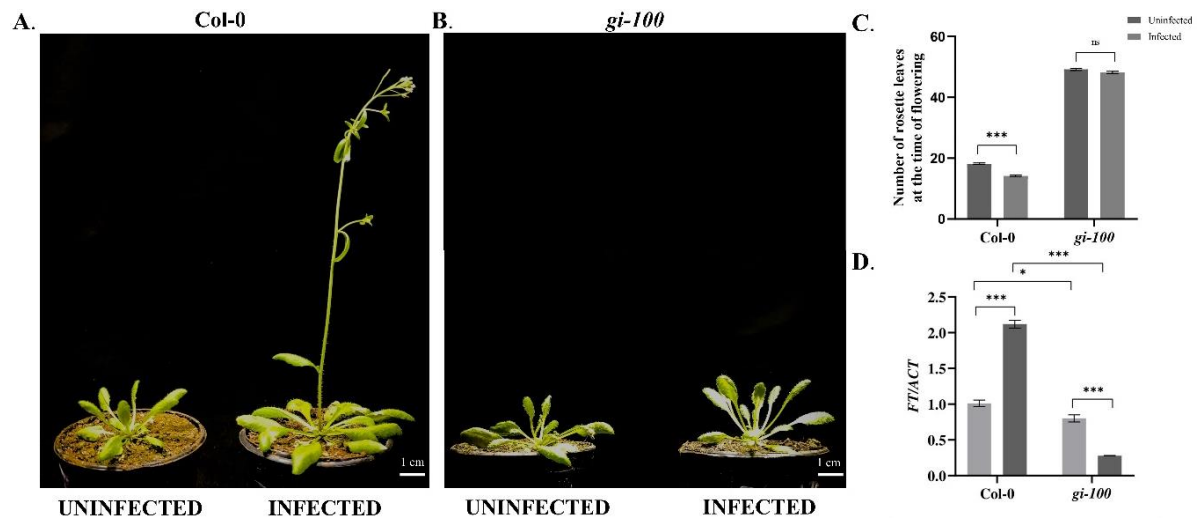


Figure 52. Analysis of flowering time phenotype in the *F. oxysporum* infected Col-0 plants (A) Phenotype of 29d mature Col-0 and (B) *gi-100* plants, that were infected with *F. oxysporum* (9-DPI) and uninfected plant as control. (C) Number of rosette leaves in Col-0 and *gi-100* at the time of flowering (D) Transcript expression analysis of *FT* gene using RT-qPCR after 24-HPI in Col-0 and *gi-100*. ACTIN was used to normalize transcript levels. The qRT-PCR reactions were done in triplicates from three biological replicates. Two-way analysis of variance (ANOVA) using Tukeys's multiple comparisons test was performed with the help of GraphPad prism to test for significance among the dataset, * $p < 0.05$, ** $p < 0.01$, *** $p < 0.001$, **** $p < 0.001$.

5.2.2.4. Involvement of salicylic acid (SA) and jasmonic acid (JA) pathway during *F. oxysporum* infection in *gi-100* plants

To understand the molecular basis of resistance of *gi-100* plants to *F. oxysporum* infection, transcript expressions of genes of jasmonic acid (JA) and salicylic acid (SA) signalling pathways were studied. As JA and SA signalling are the primary respondents for conferring resistance to wilt disease during the biotrophic and necrotic phases of infection respectively with *F. oxysporum* (Cole *et al.*, 2014; Edgar *et al.*, 2006). Under the uninfected condition, the levels of *ISOCHORISMATE SYNTHASE 1 (ICS1)* are low in Col-0 whereas it was ~2.3-fold induced in the *gi* mutant. While there was a negligible increase in the transcript levels of *ICS1*, the SA biosynthesis gene in Col-0 plants after 24-HPI, it was drastically down (~6-fold) in the *gi-100* (Figure 53A) at the same time point. *NON-EXPRESSOR OF PATHOGENESIS-RELATED GENES 1 (NPR1)* is involved in SA-mediated growth regulation by controlling cell division and expansion (Vanacker *et al.*, 2001; Wang *et al.*, 2020; Fuzikura *et al.*, 2020; Li *et al.*, 2022). The transcript expression of *NPR1* showed a ~0.6-fold increase in the Col-0 and a significant reduction of ~2-fold in the *gi-100* plant samples with infection (Figure 53B).

PATHOGEN RESPONSIVE GENE 1 (PR1) is a well-known pathogenesis-related protein family, and its accumulation is SA-dependent and linked to SAR (van Loon and van Strien, 1999; van Loon *et al.*, 2006; Yang *et al.*, 2018). In general, PR1 is associated with defense against biotrophs or hemi-biotrophs (Glazebrook, 2005; Yang *et al.*, 2018). *PATHOGEN RESPONSIVE GENE 1 (PR1)* transcript levels were decreased to ~4-fold in Col-0 after *F. oxysporum* infection (Figure 53C). To identify the downstream regulatory components that might be involved in controlling the expression of *PR1* upon *Fusarium* infection, transcript accumulation of transcription factor, *TGACG SEQUENCE-SPECIFIC BINDING PROTEIN 2 (TGA2)* was investigated. The endogenous levels of *TGA2* in *gi-100* were found to be ~7.3-fold less than that of the Col-0 plants in uninfected conditions. However, 24-HPI, *TGA2* transcript expression levels reduced to 79 % in the Col-0 samples. Contrastingly, in the *gi-100* samples it increased by ~1.8-fold of its corresponding starting amounts (Figure 53D). These results indicated an opposite trend of gene regulation of *TGA2* in the *gi-100* as compared to the Col-0. *PHYTOALEXIN DEFICIENT 4 (PAD4)* is an essential component in the modulation of phytoalexin biosynthesis in response to a range of bacterial and fungal diseases, hence, is widely used to ameliorate plant resistance against pathogen infections (Cui *et al.*, 2017). Similar to *TGA2*, the *PAD4* endogenous transcript levels were also significantly less in the *gi-100* plants before infection. While the *PAD4* transcript levels increased to ~1.15-fold in Col-0 at 24-HPI, it showed a minimal decrease in the *gi-100* leaves, nearly ~1-fold (Figure 53E). Hence, *PAD4* regulation also seemed to be contrasting in *gi-100* to the Col-0. These results indicated that SA pathway genes were contrastingly regulated in the *gi-100* samples post-infection as compared with their Col-0 counterparts. Moreover, the SA pathway was found to be positively regulated in the *gi-100* post-infection period. Quantification of salicylic acid hormone in *gi-100* and Col-0 plants after 24-HPI was carried out to further investigate the basis of these results. Endogenous SA amount was found to be ~2.1-fold higher in the *gi-100* plants compared to the Col-0 plants before infection. However, after *F. oxysporum* infection, while the SA amounts

increased significantly to 0.5-fold in Col-0 plants, it was decreased to nearly half i.e., ~2.2-fold in the *gi-100* plant samples (Figure 53F). These results further confirmed that GI positively regulates the SA pathway genes during response to *F. oxysporum* infection.

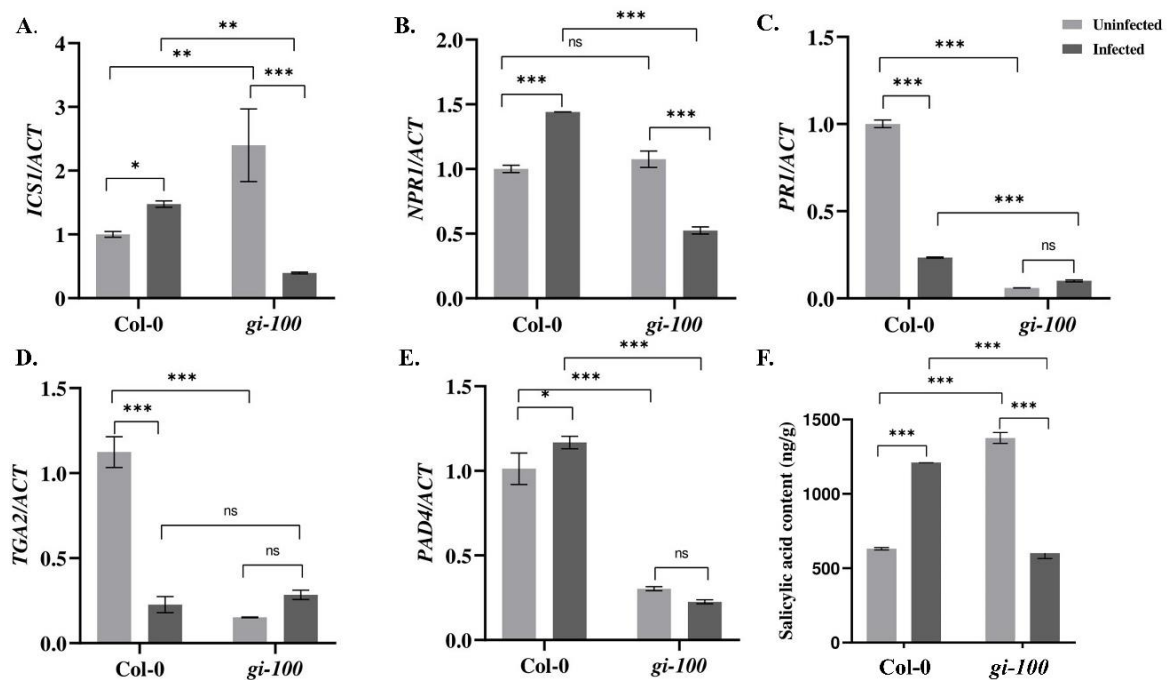


Figure 53. Involvement of salicylic acid pathway during *F. oxysporum* infection in *gi-100* plants infection. (A-E) Transcript expression validation using RT-qPCR and (F) Quantitative profiling of salicylic acid amount at 24-DPI by *F. oxysporum* was done in *gi-100* and Col-0 lines of *A. thaliana*.; (A) *ISOCHORISMATE SYNTHASE 1* (*ICSI*), (B) *NON-EXPRESSOR OF PATHOGENESIS-RELATED GENES 1* (*NPR1*), (C) *PATHOGEN RESPONSIVE GENE 1* (*PRI*), (D) *TGACG SEQUENCE-SPECIFIC BINDING PROTEIN 2* (*TGA2*), (E) *PAD4*. ACTIN was used to normalize transcript levels. Determination of (F) Salicylic acid (SA) amount. For SA quantification, D4-salicylic acid was taken as standard. Values represented are mean \pm SE. The qRT-PCR reactions were done in triplicates from three biological replicates. Two-way analysis of variance (ANOVA) using Sidak's multiple comparisons test was performed with the help of GraphPad prism to test for significance among the dataset, * $p < 0.05$, ** $p < 0.01$, *** $p < 0.001$, **** $p < 0.001$.

Having known about the regulation of the SA pathway genes, JA pathway genes were also investigated. *CORONATINE INSENSITIVE 1* (*COI1*) act as the co-receptor in the perception of jasmonyl-(L)-isoleucine (JA-Ile) (Ruan *et al.*, 2019). Though the amounts of JA were comparable between the Col-0 and *gi-100* plants before infection, its regulation was contrasted 24-HPI. There was not much difference in the expression of *COI1* in Col-0 samples; however, it showed a ~3.4-fold increase in *gi-100* after infection (Figure 54A). The *PLANT DEFENSIN1.2* (*PDF1.2*) is known as an important regulator of the JA signaling pathway (Ruan *et al.*, 2019). Relative expression levels of *PDF1.2* were significantly increased in both the Col-0 and *gi-100* samples by ~10-fold and ~7-fold respectively (Figure 54B), indicating a probable

inhibition due to GI in the JA pathway. Further confirmation of the above results was done by quantification of JA and jasmonic acid isoleucine (JA-ile) in *gi-100* and Col-0 leaf samples 24-HPI. After *F. oxysporum* infection, both the JA and the JA-ile plant hormone amounts showed opposite trends in Col-0 compared to the *gi-100* samples, i.e., while Col-0 samples showed ~4-fold and ~1.5-fold decrease, *gi-100* samples had ~6.5 and ~2.3-fold increase respectively (Figure 54C and Figure 54D). These results confirmed that GI negatively regulates JA pathway genes to confer resistance against *F. oxysporum* infection.

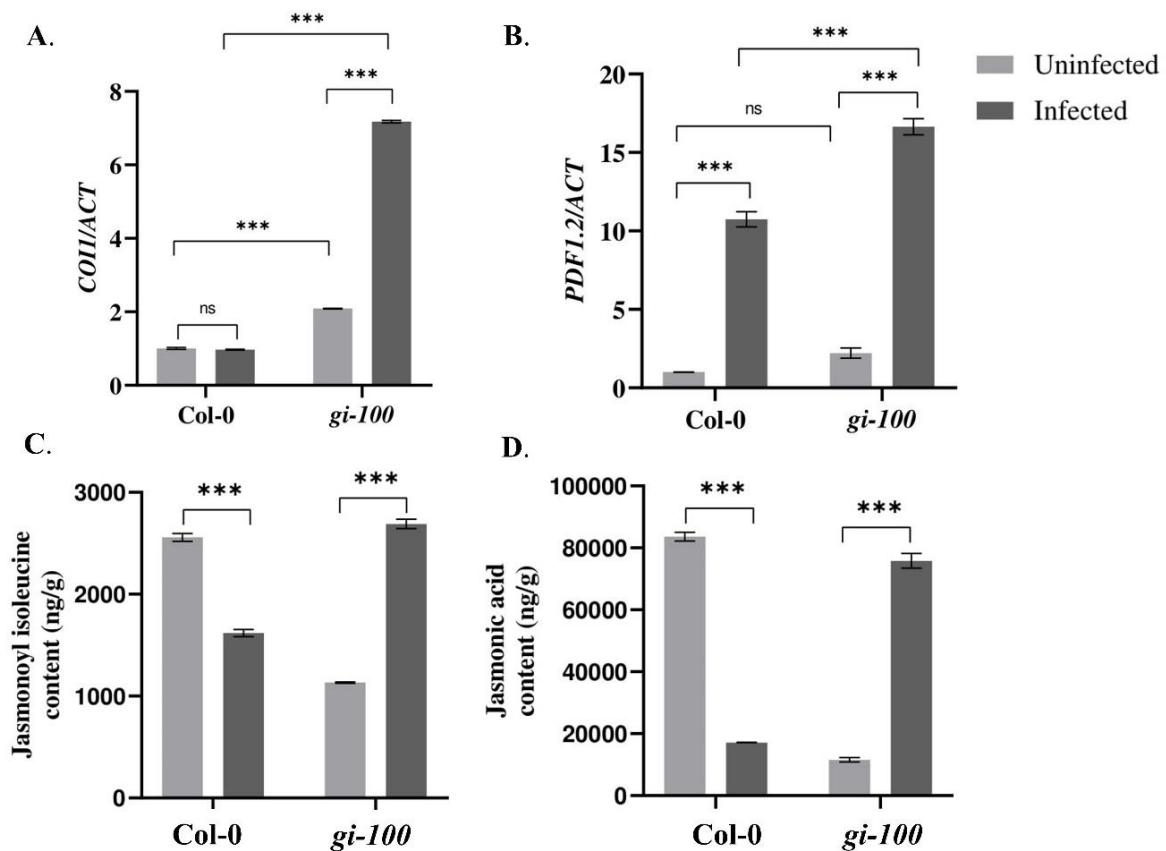


Figure 54. Involvement of jasmonic acid pathway during *F. oxysporum* infection in *gi-100* plants. (A-B) Transcript expression validation using RT-qPCR and (C-D) Quantitative profiling of jasmonic acid and jasmonoyl-(L)-isoleucine amount at 24-DPI by *F. oxysporum* was done in *gi-100* and Col-0 leaf samples. (A-B) Relative Transcript levels of (A) *CORONATINE INSENSITIVE 1 (COI1)* and (B) *PLANT DEFENSIN1.2 (PDF1.2)*. ACTIN was used to normalize transcript levels. Determination of (C) Jasmonic Acid hormone and (D) jasmonoyl-(L)-isoleucine JA-ile amounts. For JA and JA-ile quantification, D6-jasmonic acid and jasmonic acid- [13C6] isoleucine conjugate were taken as standard. The qRT-PCR reactions were done in triplicates from three biological replicates. Values are expressed as mean \pm SD. Two-way analysis of variance (ANOVA) using Sidak's multiple comparisons test was performed with the help of GraphPad prism to test for significance among the dataset, * $p < 0.05$, ** $p < 0.01$, *** $p < 0.001$.

Moreover, it was also found that the ABA content was also ~1.6-fold higher in *gi-100* plants than the minimal change observed in the Col-0 plants 24-HPI (Figure 55A). Oxylipins are a

new class of signals that enhance virulence in plants under biotic stress tolerance (Reverberi *et al.*, 2012). The endogenous oxylipin amount was less in the *gi-100* samples before infection, however, increased 24-HPI in both the Col-0 and *gi-100* plant samples irrespective of the genotype (Figure 55B). This result suggested that *gi-100* mutants were highly resistant to *F. oxysporum* infection, probably due to lower oxylipin synthesis in *gi-100* mutants. The increase in oxylipin content in Col-0 plants suggests that having GI in the host increased vulnerability by increasing oxylipin content in plants following *F. oxysporum* infection.

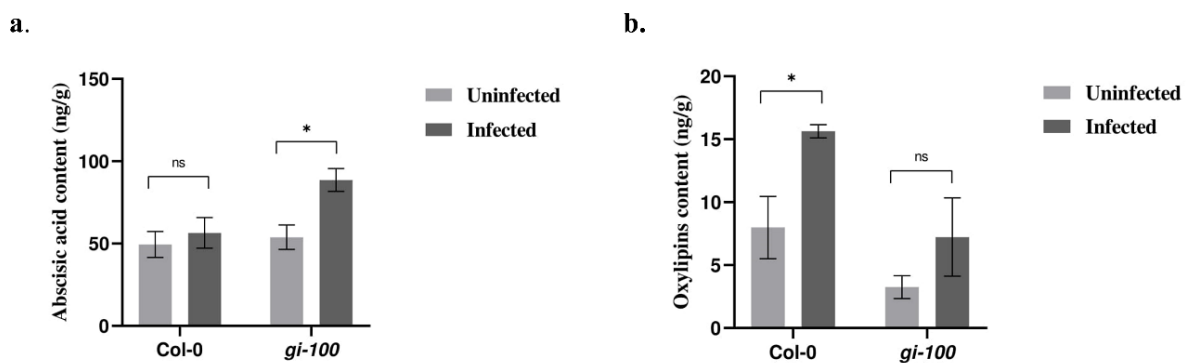


Figure 55. Determination of Absciscic acid and Oxylipins after *F. oxysporum* in Col 0 and *gi-100* plants. Determination of endogenous ABA (A) and oxylipins (B) amount at 9-DPI by *F. oxysporum* in *gi-100* as well as Col-0 leaf samples. Data points represent mean \pm SD. Two-way analysis of variance (ANOVA) using Sidak's multiple comparisons test was performed with the help of GraphPad prism * $p < 0.05$. ** $p < 0.01$, *** $p < 0.001$.

5.2.2.5. Comparative anatomy of the effect of *F. oxysporum* infection on root cell structure in Col-0 and *gi-100* plants

To further investigate the extent of *F. oxysporum* infection under our experimental regime and to determine changes caused due to the pathogen infection and its colonisation strategy, confocal microscopy was done in the root cells of Col-0 and *gi-100* at 9-DPI. Roots inoculated with *F. oxysporum* strain revealed several deformities in the epidermal cell walls in both Col-0 and *gi-100* both in the confocal microscopy (Figure 57A-B, E-F) and after trypan blue staining (Figure 56).

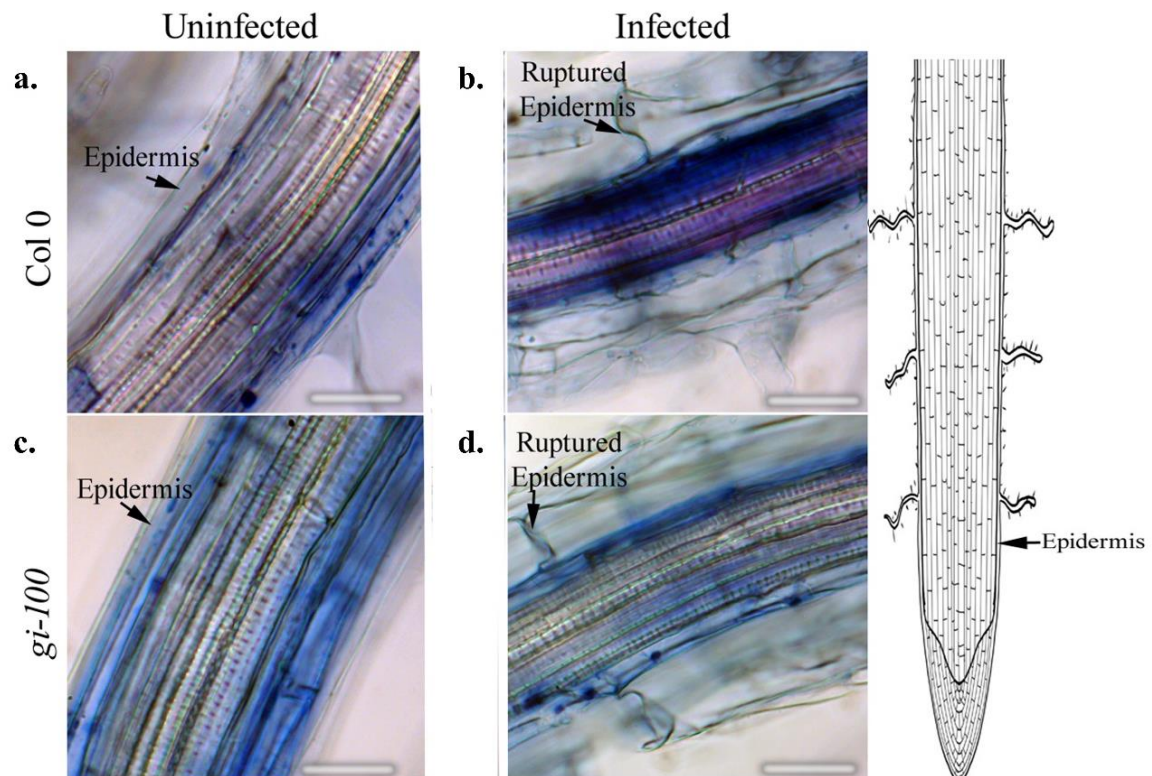


Figure 56. Effect of *F. oxysporum* infection on root cell morphology. Longitudinal root tissue sections from uninfected and 9-DPI were stained with trypan blue for epidermal cell wall morphology. The epidermal cell wall of vascular cells showed structural changes in infected Col-0 and *gi-100* root cells. Arrow pointing to ruptured epidermis in B, D. Scale bar 100 μ m.

The damage in the epidermal root cells of the *gi* mutant was the least as compared to Col-0 (Figure 57B & Figure 57F). The root cap cells (Columella cells, Wachsman *et al.*, 2015) showed structural irregularities in the cell shape of infected root tissues in both the genotypes, which were less in number in *gi-100* as compared to Col-0 (Figure 57C-D & Figure 57G-H). These results indicated that the damage in the root cap cells induced due to *F. oxysporum* infection was less in *gi-100* plants than in the Col-0 plants. This structural disorganization could be due to the mycotoxins produced by the fungus after infection (Perincherry *et al.*, 2019).

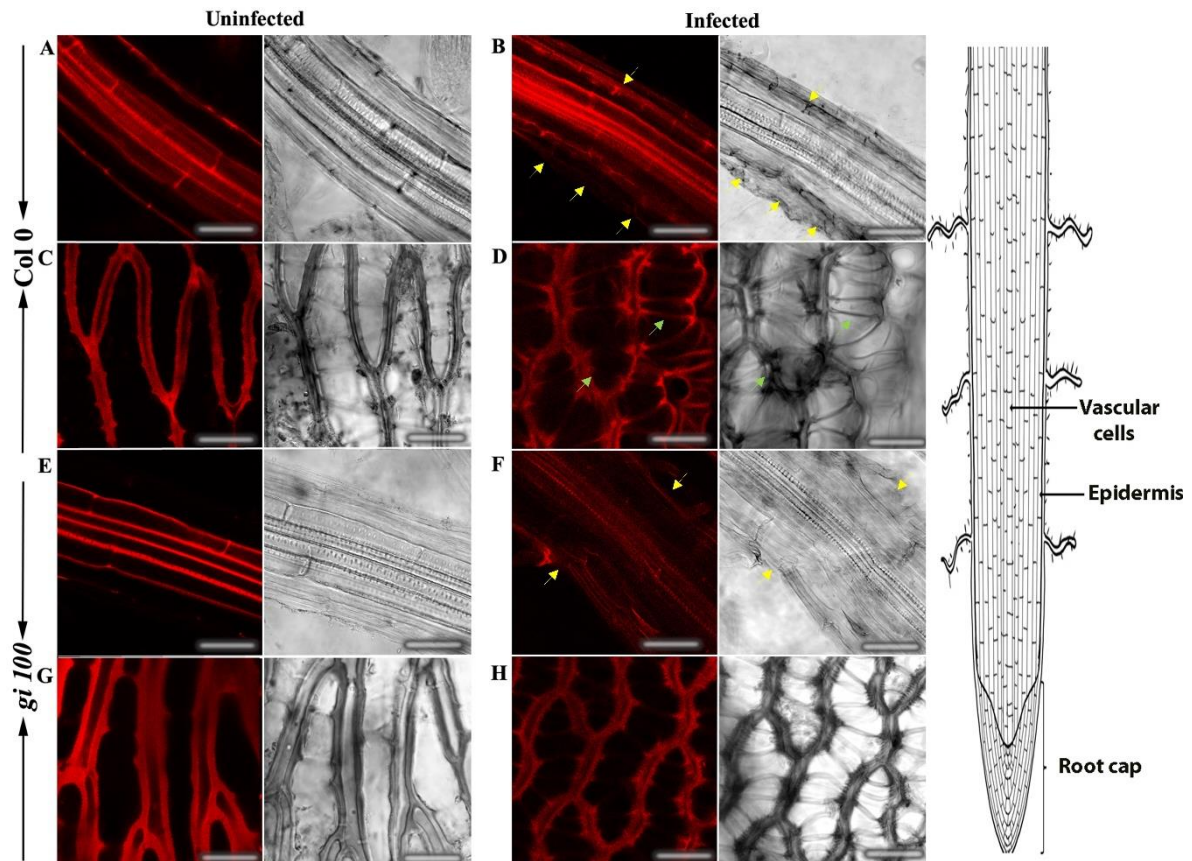


Figure 57. Effect of *F. oxysporum* infection on root cells in *Arabidopsis thaliana* using propidium iodide. Concurrent confocal fluorescence and transmitted light images of uninfected and infected roots from Col-0 and *gi-100* at 9-DPI stained with propidium iodide. Epidermal cell wall showed structural deformities in infected Col-0 and *gi-100* (yellow arrows in B, F). Columella cells showed structural irregularities in the cell shape of infected Col-0 (green arrows in D). Scale bar 100 μ m.

5.2.2.6. Effect of *F. oxysporum* infection on stomatal density and integrity in

Col-0 and *gi-100* plants

The number of stomata was higher in the *gi-100* than in the Col-0 uninfected leaf cells. However, the stomatal density was reduced both in cases of Col-0 as well as in *gi-100* upon *F. oxysporum* infection (Figure 58). The structural changes in the cell wall of stomata guard cells and disintegration of nuclei were observed in the guard cell of Col-0 infected leaves as an indication of cell death (Figure 58). Nevertheless, intact guard cells with nuclei could be visualized in the *gi-100* infected leaves (Figure 58). These observations in the stomatal guard cells were reclaimed with Acridine Orange staining which stains the cell wall of stomatal guard cells (Figure 59).

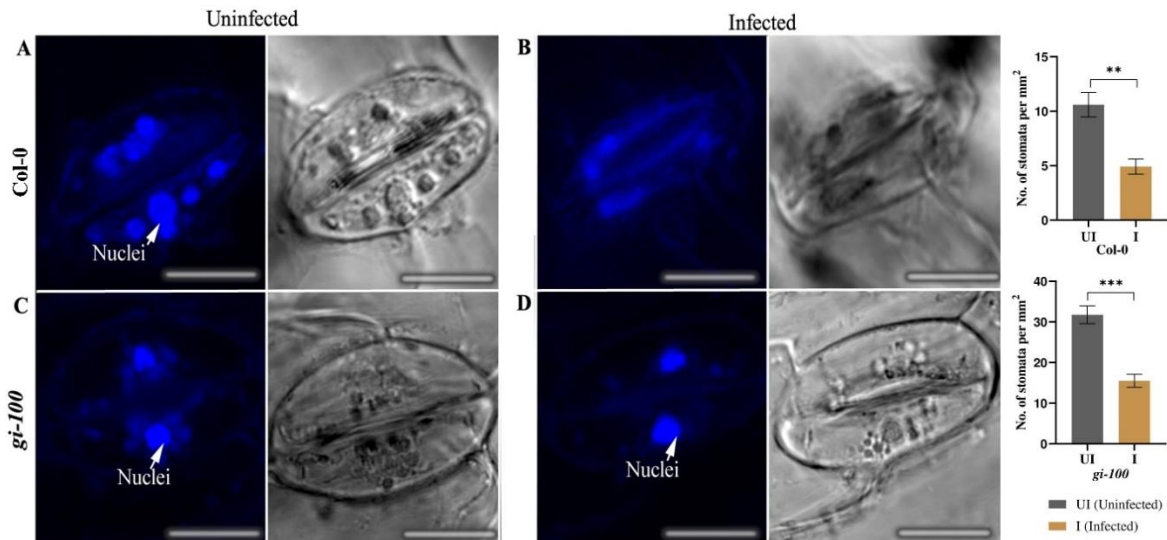


Figure 58. Effect of *F. oxysporum* infection on stomatal density and integrity in *Col-0* and *gi-100* plants. Concurrent confocal fluorescence and transmitted light images of uninfected (A, C) and infected (B, D) *Arabidopsis* leaves at 9-DPI and labeled with DAPI stain for visualizing the nuclei. Nuclei are marked with arrows. The number of stomata was counted from the images taken during microscopy and calculated per unit area. Scale bar 100 μ m.

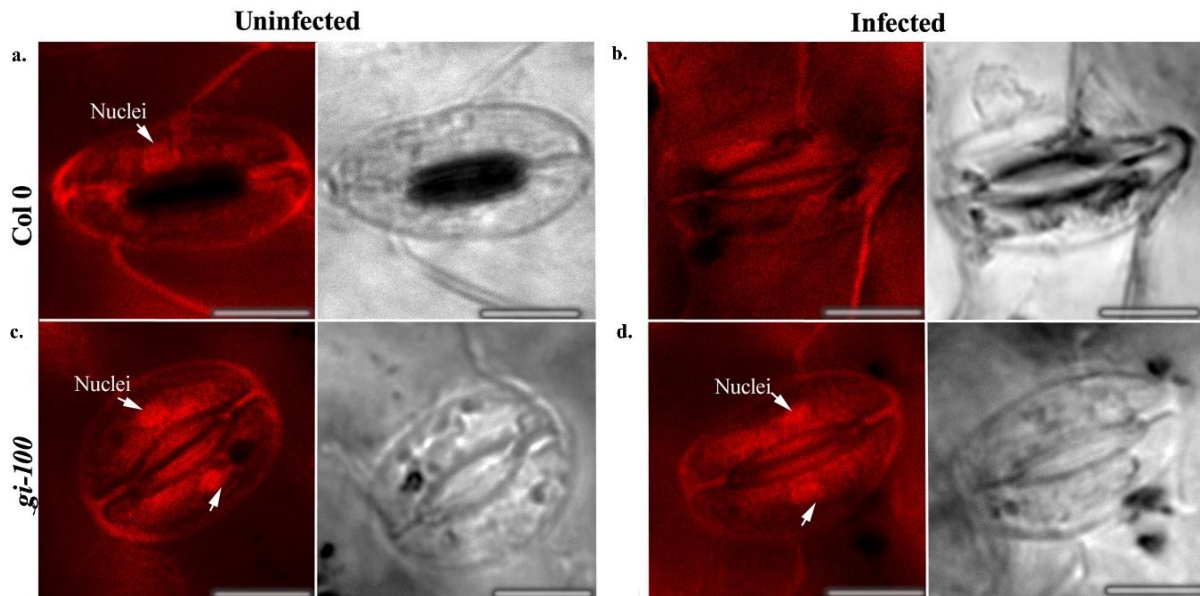


Figure 59. Effect of *F. oxysporum* infection on stomatal number and integrity in *Col-0* and *gi-100* plants. Concurrent confocal fluorescence and transmitted light images of uninfected and infected *Arabidopsis* leaves were taken which were labeled with Acridine orange. The arrow points to the nuclei of guard cells in uninfected *Col-0* and infected *gi-100* lines. Scale bar 100 μ m.

5.2.2.7. Effect of *F. oxysporum* infection on Chlorophyll A fluorescence and photosynthetic electron transport

To attain a deeper understanding of photosynthetic parameters, Chl *a* fluorescent transient curve was generated from *Col-0* and *gi-100* lines, 24 HPI with *F. oxysporum*. In the J-I phase, a significant decrease was observed in infected *Col-0* and *gi-100* lines where *Col-0* showed

minimum fluorescent signals which was also continued in the I-P phase. However, *gi-100* showed a steady increase of *Chl a* fluorescence from J-P and reached to level of uninfected plants (Figure 60A). Infection of plants with *F. oxysporum* significantly decreased Chl F levels at J-step (Vj) in Col-0 and *gi-100* lines as compared to their respective control (untreated) but slightly higher in *gi-100* than Col-0 plants. A significant increase of Chl F in I (Vi) with the infected *gi-100* plants was recorded as compared to Col-0 infected plants at P (Vp) phases (Figure 60B).

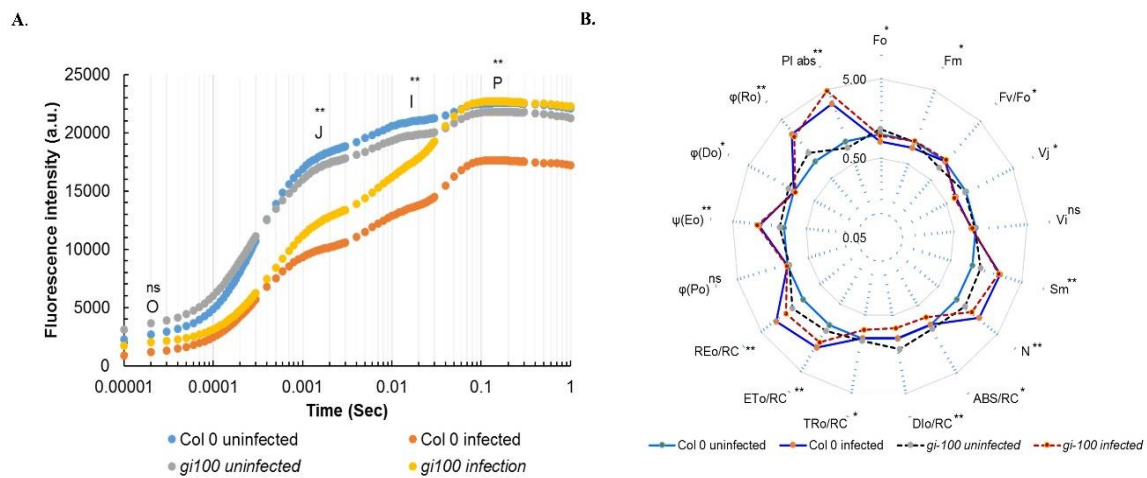


Figure 60. Effect of *F. oxysporum* on Chl a fluorescence Col-0 WT and *gi-100* leaves were incubated at 24-DPI with Multifunction Plant Efficiency Analyzer (M-PEA) (Hansatech Instruments Ltd, UK) for obtaining chlorophyll. (A) Fluorescence intensity on OJIP transient curve. (B) Spider plot for Col-0 and *gi-100* lines of *A. thaliana* plants 24-DPI with *F. oxysporum* with their respective control. Values are expressed as mean \pm SD. Two-way analysis of variance (ANOVA) using Sidak's multiple comparisons test was performed with the help of GraphPad prism * $p < 0.05$. ** $p < 0.01$, *** $p < 0.001$.

5.2.2.8. Leaf internal temperature after *F. oxysporum* infection

As Phytochrome B has been shown to act as a thermosensor (Legris *et al.*, 2016), and GI is involved in the phytochrome signalling responses, (Huq *et al.*, 2000). the involvement of GI in controlling a plant's internal temperature was investigated and compared among the infected and uninfected plants to determine the effect of *F. oxysporum* infection. The average leaf temperature of *gi-100* plants was ~ 1.1 °C ($p < 0.05$) higher than the Col-0 (Figure 61). The average leaf temperature of both Col-0 and *gi-100* plants decreased insignificantly due to *F. oxysporum*. This result indicated that GI probably has a role in maintaining lower internal

temperature in Col-0 plants.

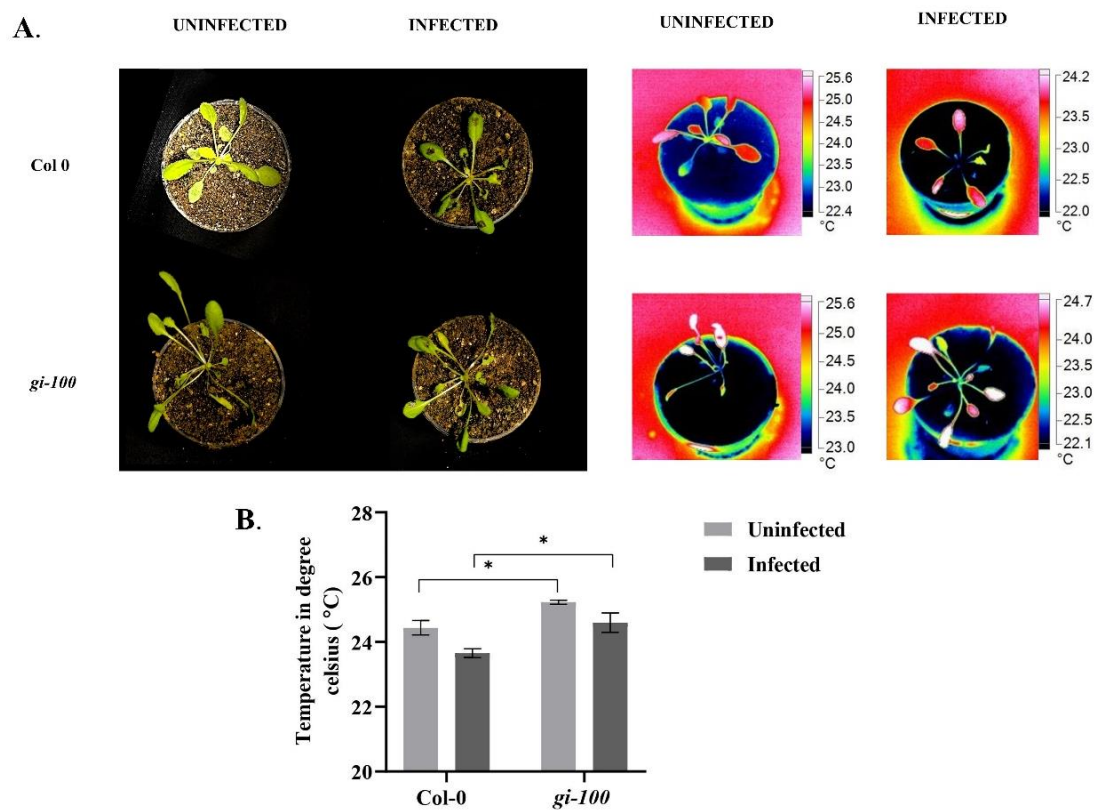


Figure 61. Leaf internal temperature analysis in Col-0 and *gi-100*. (A) Representative and images of Col-0 and *gi-100* plants without and with *F. oxysporum* infection at 9-DPI. The pictures were taken with a FLUKE Infra-red Camera and analyzed using the SMART VIEW software as described in the material and method section. (B) Leaf internal temperatures from a minimum of at least 10 plants of Col-0 and *gi-100* were taken. Leaf surfaces showing the highest temperatures were selectively chosen. Values are expressed as mean \pm SD. Two-way analysis of variance (ANOVA) using Sidak's multiple comparisons test was performed with the help of GraphPad Prism.

5.2.3. DISCUSSION

GI is ubiquitously present in plants at all stages of development (Mishra and Panigrahi, 2015), suggesting that it is involved in various physiological activities including flowering time regulation (Park *et al.*, 1999), light signalling (Martin-Tryon *et al.*, 2007), starch accumulation (Eimert *et al.*, 1995), circadian clock control (Park *et al.*, 1999), transpiration (Sothorn *et al.*, 2002; Tseng *et al.*, 2004), chlorophyll accumulation (Kurepa *et al.*, 1998a), and miRNA processing (Jung *et al.*, 2007). In plants, GIGANTEA has also been demonstrated to regulate abiotic stressors such as drought (Riboni *et al.*, 2013), cold (Cao *et al.*, 2005; Fornara *et al.*, 2015), salt (W., Y., Kim, *et al.*, 2013) and oxidative stress (Kurepa *et al.*, 1998), although its involvement in pathogen attack is yet unknown. Recent research reveals that during a fungal pathogen infection, *Bipolaris sorokiniana*, GI targets the salicylic acid pathway in *Arabidopsis* and wheat, making the plant more susceptible to the disease (Kundu and Sahu, 2021). GIGANTEA, a photoperiodic pathway regulator, also improves susceptibility to *F. oxysporum*, according to RNA-seq data analysis (Lyons *et al.*, 2015a, 2015b). The *Atgi-1* and *Atgi-2* mutants are resistant to *F. oxysporum* infection (Lyons, Rusu, *et al.*, 2015; Lyons, Stiller, *et al.*, 2015), however, the mechanism behind this is yet unknown.

In this study, we have demonstrated the causative mechanism of the involvement of GIGANTEA in *F. oxysporum*-induced wilt disease. Progression of the disease was confirmed by the visible disease symptoms on the leaves at 6-DPI which is also supported by previous findings (Lyons *et al.*, 2015a). Our study reclaimed that although the infection mode in *F. oxysporum* is commonly known to be root-borne (Jones and Dangl, 2006), it can also induce pathogenicity through leaf infections in laboratory conditions. The integrative growth approach of an initial 15 day of LD conditions followed by the rest of the entire study under SD conditions was done to attain a synchronized growth morphology with a comparable number of rosette leaves in all three genotypes used in the study. Following *F. oxysporum* inoculation, we noticed an increase in the expression of GI and FT in Col-0. Our findings showed that *F. oxysporum*

infection causes early flowering in Col-0 plants and unaltered flowering in *gi-100* plants. These results suggested that GI may not play a primary role in flowering time regulation during infection. Despite the decrease in FT expression to nearly half at 24-HPI, the flowering time was unaltered in *gi-100* plants. This observation indicated that the flowering time could be regulated by other factors in *gi-100* plants, and warrants the study of the expression of FT and other related factors at the time of bolting post-pathogen infection. Nevertheless, our observation of a decrease in FT expression in *gi-100* uninfected plants is supported by a similar observation in *gi-1* (Kim *et al.*, 2013).

We hypothesized that the GI-mediated disease mechanism is blue light-dependent since GI is related to blue light receptors such as ZEITLUPE (ZTL), FLAVIN-BINDING, KELCH REPEAT, F-BOX 1 (FKF1), and LOV KELCH PROTEIN 2 (LKP2) for its function (Cha *et al.*, 2017). G-BOX BINDING FACTOR 1 (GBF1), a blue light-induced transcription factor has been recently found to have a positive effect on disease tolerance in recent studies (Giri *et al.*, 2017). To further study the mechanism by which GI induces susceptibility during *F. oxysporum* infection we have checked the accumulation of SA, JA, and ABA phytohormones. Our finding suggests that during *F. oxysporum* infection, GI inhibits the JA pathway and ABA accumulation while stimulating the SA pathway. DELLA protein regulates plant pathogen defense in *Arabidopsis*, according to recent research. Further, GI protein has been demonstrated to regulate gibberellic acid signalling by stabilizing the DELLA protein (Nohales and Kay, 2019). More studies can shed light on the GI-DELLA interaction and its involvement in plant pathogen response.

F. oxysporum being a hemi-biotrophic pathogen, expands its hyphae in the host cells during the initial days of infection, and subsequently produces mycotoxins which kill the host plant (Lagopodi *et al.*, 2002). Hence, any kind of lesions or aberrations macroscopically are not visible on the plant during the initial phase of infection. Concurrently, we didn't observe any phenotypic changes in *A. thaliana* during the initial phase of infection i.e., 1 to 4-DPI. However,

at 9-DPI the Col-0 WT plants displayed a susceptible phenotype to the disease with at least 60 % of the leaf area under necrosis. Since the fungal hyphae are known to invade the plant's root system through the root hairs (Lagopodi *et al.*, 2002; Banhara *et al.*, 2015) and block the vascular bundles of the plant, we investigated the root cells of the infected and uninfected plants using confocal microscopy. Propidium iodide (PI) followed by trypan blue stain was used to stain the plant cell walls to determine the extent of fungal infection in the root cells. Noticeable structural changes could be observed in the infected epidermal cells as compared with the uninfected epidermal root cells in both Col-0 and *gi-100* plants at 9-DPI. The epidermal cells of Col-0 were found to be ruptured to a greater extent than the *gi* mutant. This could be due to the mycotoxins produced by the pathogen. However, staining the fungal hyphae with trypan blue at a later stage of infection could not be done due to the ruptured cells and overlapping of vascular root cells on the root cap cells. Moreover, plugging in the vascular bundles was found specifically in the Col-0 plants which probably became the primary reason for the Col-0 plant's susceptibility to the disease. The nuclei in stomatal guard cells were also observed to be disintegrated in Col-0 indicating cell death whereas, the nuclei in guard cells were intact even after infection confirming the resistivity of the plant towards *F. oxysporum* infection.

Phytochrome B was recently reported to act as a thermosensor due to its temperature-sensing property in plants (Legris *et al.*, 2016). We presume the interplay of Phy-B signalling and involvement of PHYTOCHROME INTERACTING FACTORS (PIF-4, PIF-7) module in this process. GIGANTEA is known to control phytochrome signalling during hypocotyl elongation in *Arabidopsis thaliana* (Huq *et al.*, 2000). This prompted us to investigate the plant's internal temperature during *F. oxysporum* infection in the presence and absence of GI. The noble finding of higher temperature in the *gi-100* plants regardless of *F. oxysporum* infection indicated that GI plays a function in controlling a plant's internal temperature. A similar report of weakened plant immune defense during the temperature rise has been shown (Kim *et al.*, 2022). Hence, integrating both the results it could be suggested that the influence of light and temperature on

the host-pathogen association in plants may be mediated by GI. Based on the findings of the present study, we propose a model in which GI acts as a negative regulator of defense signalling in *Arabidopsis* and can contribute to the susceptibility to wilt disease (Figure 62). Explicitly, *Fusarium* infection in Col-0 induces GI expression and accumulation resulting in reduced endogenous JA amount followed by reduced JA-ile (active form) amount. Consequently, a decrease in the accumulation of *COII* transcript level, which is unable to bind to JA-ile, forms a complex with JAZs. The JAZs act as a repressor to inhibit the *PDF 1.2*. This eventually leads the plant to become susceptible to *Fusarium* infection. On the other hand, the susceptibility of Col-0 to the vascular wilt disease caused by *F. oxysporum* was found to be positively regulated by the SA pathway. Therefore, in the *gi* mutant, the SA content, as well as the *ICS1* transcript levels, are high under uninfected conditions. After the plant was attacked by the pathogen there was an increased transcript expression of *PAD4* which corroborated the fact that GI binds with *PAD4* intronic region upon pathogen infection (Singh, 2022). The level of *ICS1* transcript increased as a result of which, the amount of SA metabolites also increased in the plant. The *NPR1* transcript levels were also elevated after the pathogen infection. However, the transcript levels of *TGA2*, a transcription factor decreased in the presence of GI in Col-0 after infection. TGA bZIP factors can function as either repressors or activators, or both. In the absence of SA stimulation, TGA2 binds to the PR-1 promoter and inhibits transcription. NPR1 binds to TGA2 at the promoter in SA-stimulated cells, masking TGA2's repressor domain. In an SA-dependent manner, the protein complex activates transcription. TGA2 thus acts as a repressor or a coactivator in this context (Rochon *et al.*, 2006). However, in our case, the transcription level of TGA2 was low after pathogen infection. As a result of which the complex formation of NPR1 and TGA2 is hindered. This might be due to some fungal toxins secreted by the pathogen and it is preventing the NPR1 from masking the TGA's repressor domain. It was also observed that *PR1* transcript (SA defense responsive gene) significantly decreased in Col-0 WT. In contrast, *gi* mutation, on the other hand, causes the release of this positive suppression of pathogen-

induced SA signalling, resulting in increased resistance of *gi-100* plants. As a result, we conclude that the GIGANTEA module promotes susceptibility to *F. oxysporum* infection by promoting the salicylic acid pathway and inhibiting the jasmonic acid pathway in *Arabidopsis thaliana*.

The present study makes a significant increment in understanding the involvement of the circadian clock component GIGANTEA in controlling biotic stress response during the pathogen infection by *F. oxysporum* in *Arabidopsis thaliana*. This is one of the few reports known for molecular mechanisms of involvement of GI for biotic stress tolerance (specifically against *F. oxysporum* infection, which causes vascular wilt disease in Columbia-0 wild-type plants). Disease resistance in *gi-100* for the said disease is positively regulated by modulating jasmonic acid pathway genes (i.e., *CORONATINE INSENSITIVE 1 (COI1)* and *PLANT DEFENSIN 1.2 (PDF1.2)*). In addition, our report also reveals the involvement of ABA, SA pathways genes, and oxylipins in this response. Though GI promotes early flowering under controlled conditions, our report also showed that it is not involved in flowering time regulation during *F. oxysporum* infection. This is the first study to report that GI is involved in maintaining the lower temperature of plants, as *gi-100* plants maintained higher temperatures irrespective of the pathogen infection. The finding of this study can be useful to build stronger strategies for improving crop yield in fields in case of *F. oxysporum* infection by manipulating the genes of jasmonic acid and salicylic pathway.

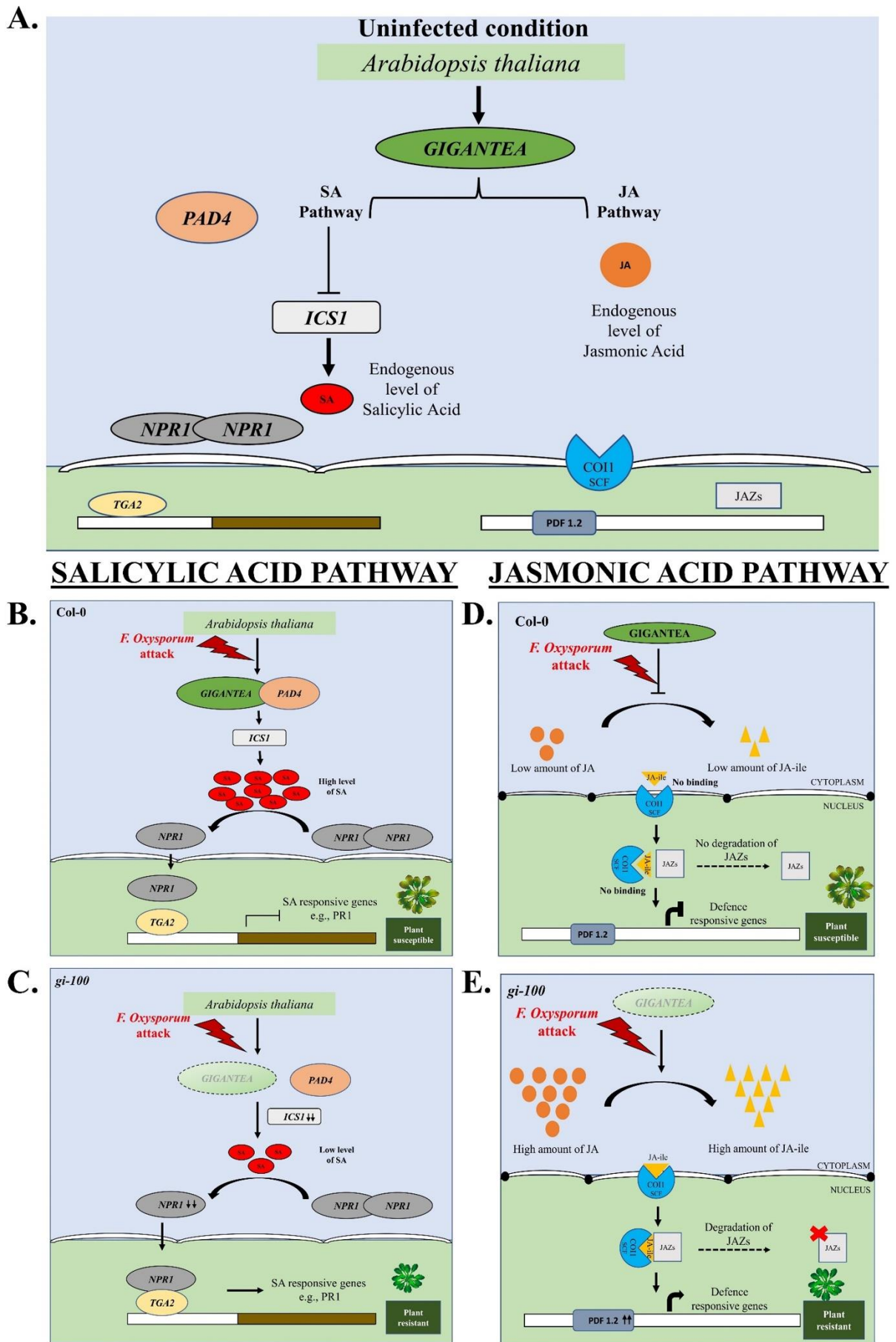


Figure 62. Diagrammatic representation of involvement of GIGANTEA, jasmonic acid, and salicylic acid pathway genes for eliciting pathogen response to *F. oxysporum* infection in *Arabidopsis thaliana*. (A) Under

uninfected conditions, Jasmonic and salicylic acid levels and GI are at endogenous levels. The levels of ICS1 are low due to its inhibition. The dimerized form of NPR1 is unable to move into the nucleus and bind to any TF for defense response. Similarly, the JA pathway is also uninduced. (B) Salicylic acid pathway: When *F. oxysporum* infects wild-type Col-0 plants, increased GIGANTEA (GI) accumulation results in GI binding to PAD4, followed by increased SA accumulation. However, when infected, NPR1 is unable to bind to the transcription factor TGA2, limiting the expression of defense-related genes i.e., PR1. (D) In the absence of GI, the SA pathway is reversed upon *F. oxysporum* infection, making the plant more resistant to the disease. (C) Jasmonic acid pathway: Increased GI expression and accumulation, on the other hand, results in less JA-ile in Col-0 (active form). Followingly, there is a reduction in the transcript level of *COI1*, which does not bind to JA-ile and thus cannot form a complex with JAZs. JAZs function as a repressor, inhibiting PDF 1.2. This eventually makes the plant vulnerable to *Fusarium* infection. (E) On the contrary, in the absence of GI, the accumulation of JA-ile is high and it provides resistance to the plant upon *F. oxysporum* infection.

CHAPTER-5

NOVEL ROLE OF AUXIN BINDING PROTEIN1 (ABP1) IN PLANT DEVELOPMENT AND ABIOTIC STRESS TOLERANCE

CHAPTER-5: Novel Role of Auxin Binding Protein1 (ABP1) in Plant Development and Abiotic Stress Tolerance

5.1. BACKGROUND

Auxin Binding Protein 1 (ABP1) has been a protein of mystery with its undulating confusions pertaining to its history (Hertel *et al.*, 1972), and structural properties of having C-terminal KDEL as an ER retention sequence (Tian *et al.*, 1995). ABP1 stood for its name for being crystalized with bound auxin in affinity chromatography assays in many species including maize (Hesse *et al.*, 1986) and tobacco (Shimomura *et al.*, 1999) showing high binding affinities with a synthetic auxin 1-naphthalene acetic acid (NAA) or endogenous auxin (IAA) respectively. Though it has an auxin binding site, neither any conformational change was observed due to bound or unbound auxin nor any response in its transcripts levels due to auxin treatment could be detected. Furthermore, ABP1 was found to be outstandingly stable, not affected by any stimulus, hormone, or stress treatment other than heat stress, which leads to its degradation. Notwithstanding, an inconsistent and mild-hiked response of ABP1 to some pathogens was also found (Oliver *et al.*, 1995). Extensive gene expression studies could scarcely find any distinctive profiles of ABP1 except some tissue-specific expressions in the active cambium, embryo tissue, germinating endosperm, stele, hydathodes, and trichomes which could hardly explain its dedicated role in auxin perception in plants. ABP1 is speculated with several auxin-induced signalling events that require its expression in the apoplast. However, its ER retention signal sequence which confirms more than 80 % of its presence in the ER. Even, ABP1-like sequences with or without the KDEL ER retention sequences have also been detected in lower plants (Tomas *et al.*, 2010; Panigrahi *et al.*, 2009). These discrepancies have been explained by the findings that the TIR1 or AFB1, the bonafide auxin receptor is necessarily involved in the rapid polarization events at the plasma membrane and it requires intracellular auxin reinforcing the physiological non-relevance of the ABP1's auxin

binding for these rapid responses. Despite the non-sigmoidal kinetics of auxin binding to ABP, it has a higher and specific binding affinity to the synthetic auxin 1-NAA (more than two-fold) compared to the endogenous auxin (IAA) (Hesse *et al.*, 1989). Further to demonstrate ABP1's role in plants, several overexpression lines of ABP1 were studied in different instances by Baulry *et al.*, (2000); Čovanová *et al.*, (2013); Grones *et al.*, (2015a); Robert *et al.*, (2010); Chen *et al.*, (2014), which linked its role to activities at plasma membrane such as K⁺ influx to applied auxin, promotion of clathrin-mediated endocytosis of the PIN efflux carriers at the plasma membrane and its definite non-involvement in auxin signalling via the TIR1-Aux/IAA coreceptor complex, thus splitting ABP1 from auxin action. Grones *et al.*, (2015a) showed the essential role of auxin binding pocket of ABP1 in mediating clathrin association with membranes for endocytosis regulation suggesting that auxin binding is central to the function of ABP1 (Grones *et al.*, 2015a). Thus, ABP1 could act as a receptor for rapid auxin responses, such as the activation of plasma membrane H⁺-ATPases, modulation of cytosolic Ca²⁺ concentrations, TMK1-based cell-surface signalling and auxin canalization (Dahlke *et al.*, 2010; Friml *et al.*, 2022). Concerning the physiological response linked to this interaction, the calcium influx with the auxin-induced calcium-binding interactors of ROPs is associated with root growth (Hazak *et al.*, 2019). The Major bottleneck in understanding its biological function was hindered due to the embryo-lethal effect of existing T-DNA insertional mutants. Relatively recent observation using CRISPR/Cas9 technology that the *abp1* null mutants do not affect plant development was intriguing. Furthermore, a follow-up work attributed to the second site mutation of the adjacent BSM gene (Michalko *et al.*, 2016; Gao *et al.*, 2015). Moreover, ABP1 was also shown to be directly or indirectly involved in auxin and light signalling, as the application of auxin inhibitor inhibited hypocotyl elongation and gravitropism under R and FR-enriched light in *abp1* mutants but not in wild type (Effendi *et al.*, 2013). ABP1-mediated auxin response was shown to positively affect PhyB signalling for shade (FR-enriched) induced hypocotyl growth inhibition. ABP1 was shown to promote the accumulation of the

dephosphorylated form of PhyB required for repressing the gene expression along with the positive regulation of the SCF^{TIR1/AFB} pathway (Grones *et al.*, 2015b). The key role of ABP1 was also shown for shoot growth, leaf venation, cell expansion, and division in *Boehmeria nivea* L. (Braun *et al.*, 2008). To explore more on functional and divergent roles of ABP1 in plant development, we conducted scrupulous investigations using two independent CRISPR/Cas9 generated knockout lines of ABP1, namely *abp1-C1* (Gao *et al.*, 2015) and *abp1-C2* (unpublished). Single or combinatorial abiotic stresses were imposed under different monochromatic light and plant phenotypes such as seedling development, flowering time, and components of circadian clock genes were studied. We observed the effect of *abp1* mutation under low-temperature, dehydration stress, and /or under different monochromatic light sources including red, far-red, and blue in particular. Here, we discovered a distinct role of ABP1 in establishing a link between photoperiod sensing and circadian clock signalling at lower temperatures and also for dehydration tolerance in *Arabidopsis*.

5.2. RESULTS

The current study investigated the probable role of ABP1 in response to different monochromatic lights, low temperature, and water withdrawal (WW) in seedlings and adult plants of *Arabidopsis thaliana*. We conducted the study using two independent CRISPR mutant lines of *abp1* i.e., *abp1-C1* (Gao et al., 2015) and *abp1-C2* (unpublished) in Col-0 background. The null expression of *ABP1* in the above mutant lines was confirmed using q-RT PCR and sequencing analysis (data not shown).

5.2.1. ABP1 affects seedling root phenotype under red and blue light

Hypocotyl, primary, secondary and lateral root numbers and lengths were measured as described in materials and method at 22 °C under diurnal LD conditions with Red (R, 30 $\mu\text{mol m}^{-2} \text{s}^{-1}$ 660 nm)/ far-red (FR, 30 $\mu\text{mol m}^{-2} \text{s}^{-1}$, 730 nm)/ blue (B, 30 $\mu\text{mol m}^{-2} \text{s}^{-1}$, 460 nm)/ white light (W, 50 $\mu\text{mol m}^{-2} \text{s}^{-1}$) or in Dark (D, 0 $\mu\text{mol m}^{-2} \text{s}^{-1}$). Among all the light qualities, hypocotyl length and root patterning in *abp1* mutants (i.e., *abp1-C1* and *abp1-C2*) showed a distinct difference compared to Col-0 when grown at 22 °C under R and B. The *abp1-C1* and *abp1-C2* had considerably shorter hypocotyls (2.8-fold) and roots (1.2-fold) as compared to Col-0 specifically under R light (Figure 64A & 64B), with no significant differences under the rest of the monochromatic lights including FR, B and W light or D (Figure 63).

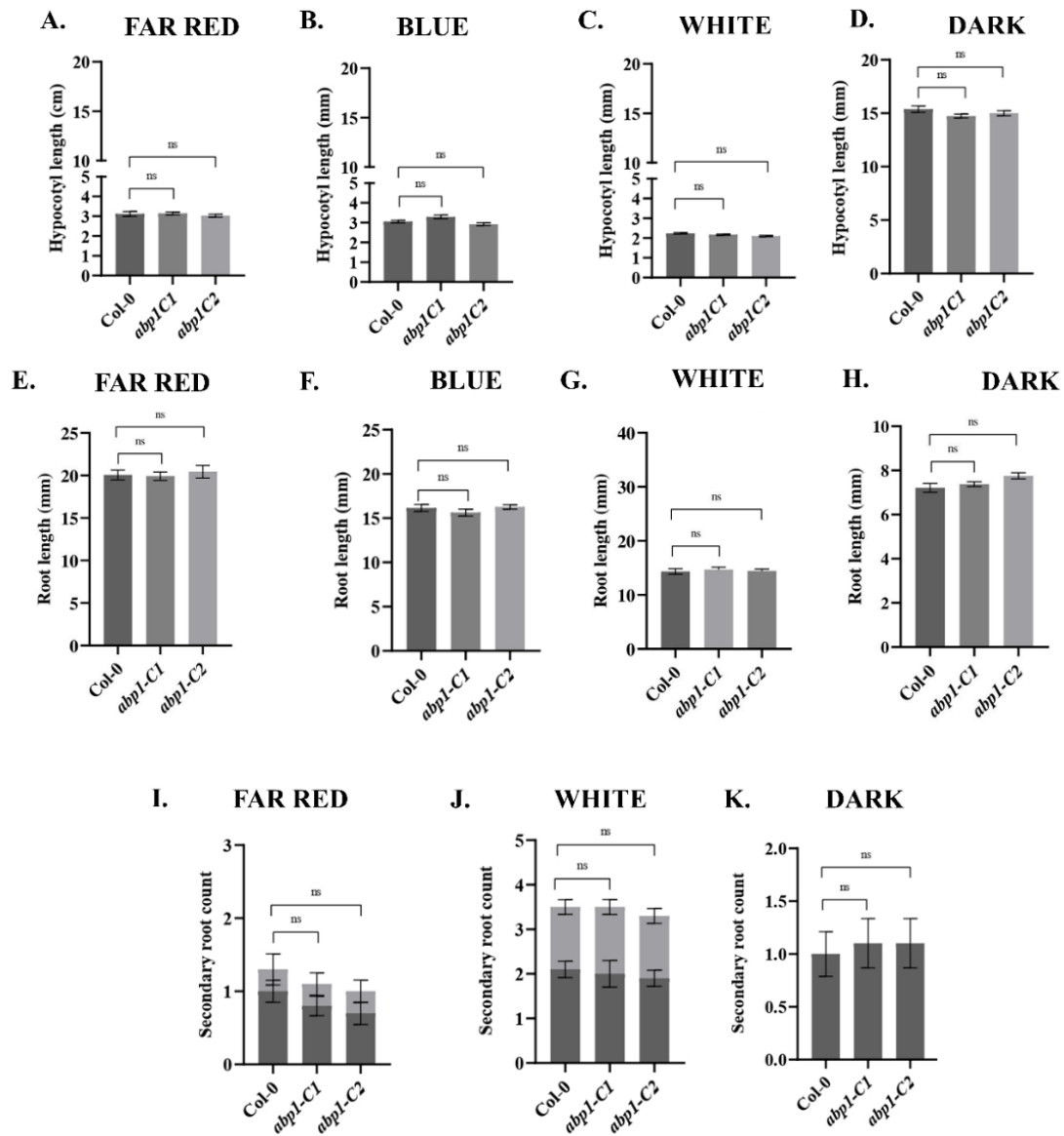


Figure 63. Seedling growth parameters were non-significant under different monochromatic lights at 22 °C. Seedlings of Col-0, *abp1-C1*, and *abp1-C2* lines were grown on MS media under LD conditions and different monochromatic lights of Far-red (A, E, I), Blue (B, F), White (C, G, J) or in darkness (D, H, K) till 7-days, after which hypocotyl growth (A-D) or root length (E-H) and secondary root counts (I-K) were measured using ImageJ software from the scanned images. Nearly 300 seedlings were grown in 3 biological replicates with 100 seedlings each time. Data presented as mean \pm SE. One-way analysis of variance (ANOVA) using Tukey's multiple comparisons test was performed with the help of GraphPad Prism to test for significance among the dataset, * $p < 0.05$, ** < 0.01 , ns – non-significant.

Hypocotyl and root lengths under W light were exactly similar to that shown by Gao *et al.*, (2015). Further, the secondary root phenotype (i.e., number of lateral and adventitious roots) in *abp1* mutants under monochromatic R (Figure 64C) or B (Figure 64D) or simultaneous irradiations of R and B (R+B) (Figure 64E) lights were noted. Under R, the secondary root counts were insignificant in all three lines (Figure 64E). In contrast, under diurnal B, the secondary root counts in *abp1* mutants were significantly decreased in the ABP1 mutants (~70

% in *abp1-C1* and ~65 % in *abp1-C2*) as compared to the Col-0 ecotype (Figure 64D). lateral root number. However, the secondary root counts under diurnal R+B light showed marginally significant differences when compared between WT and mutants (Figure 64E), leading to the inference that the decreased secondary root number under B could be effectively overridden by the simultaneous irradiation of B with the R light (i.e., B+R lights). To understand more about R light signalling and the circadian clock, the relative transcript levels of *PHYTOCHROME B* (*PHYB*) and *GIGANTEA* (*GI*) were examined under R light irradiations. There were ~26-fold and 20-fold increases in the *PhyB* transcript levels in *abp1-C1* and *abp1-C2* mutants respectively as compared to Col-0 (Figure 64F). The relative transcript levels of *GI* in *abp1-C1* and *abp1-C2* were ~3.8-fold and 4-fold lower than Col-0 respectively (Figure 64G). These results indicated that ABP1 most likely has a role in root development under R light and secondary root growth under B light, with the former role being mediated by phytochrome B and/ or GI.

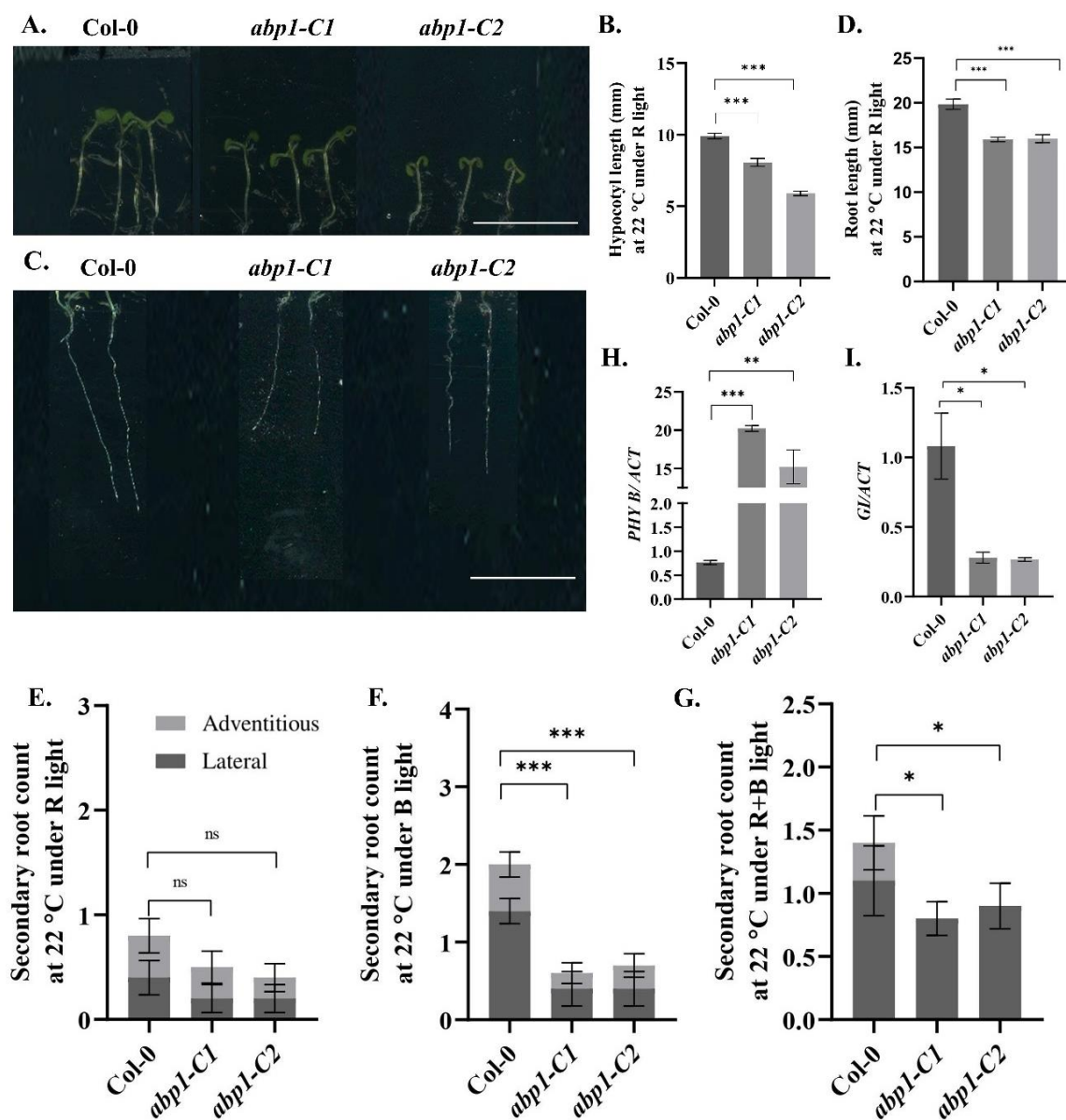


Figure 64. Seedlings under diurnal monochromatic red light at 22 °C. Seedlings of Col-0, *abp1-C1*, and *abp1-C2* lines were grown on MS media under monochromatic red light at 22 °C in long-day conditions for 7 d (A-C), after which the phenotype was noted for hypocotyl lengths (B) root lengths (D) and the number of secondary roots (lateral and adventitious roots) (E). Secondary root count was also noted for seedlings grown under diurnal monochromatic blue (F), or under a simultaneous irradiation of red and blue light (G). Roots from the seedlings grown under red were analyzed for transcript expression of Phytochrome B (*PHYB*) (H) and *GIGANTEA* (*GI*) (I). For the hypocotyl and root phenotype, 300 seedlings were grown in 3 biological replicates with 100 seedlings each time. The qRT-PCR reactions were done in triplicates from three biological replicates. *ACTIN* was used to normalize transcript levels. Data presented as mean \pm SE. One-way analysis of variance (ANOVA) using Tukey's multiple comparisons test was performed with the help of GraphPad Prism to test for significance among the dataset, * $p < 0.05$, ** $p < 0.01$, *** $p < 0.001$ and ns represent non-significant differences. Scale bar: 1 cm.

5.2.2. ABP1 mediates hypocotyl elongation under diurnal red rhythm along with low temperature

In addition to the hypocotyl and root phenotype at the seedling stage at 22 °C, it was of interest to check the seedling phenotype if any with effect to low temperature (i.e., 18 °C). Congruent

with the data of Gao *et al.*, (2015), no remarkable difference in the hypocotyl and root length was observed under 22 °C under W light (Figure 63). Similarly, no phenotypic difference was observed at 18 °C in *abp1* mutants compared to Col-0 under W light irrespective of photoperiod i.e., LD (Figure 65A-65C) or SD (Figure 65D-65F) conditions.

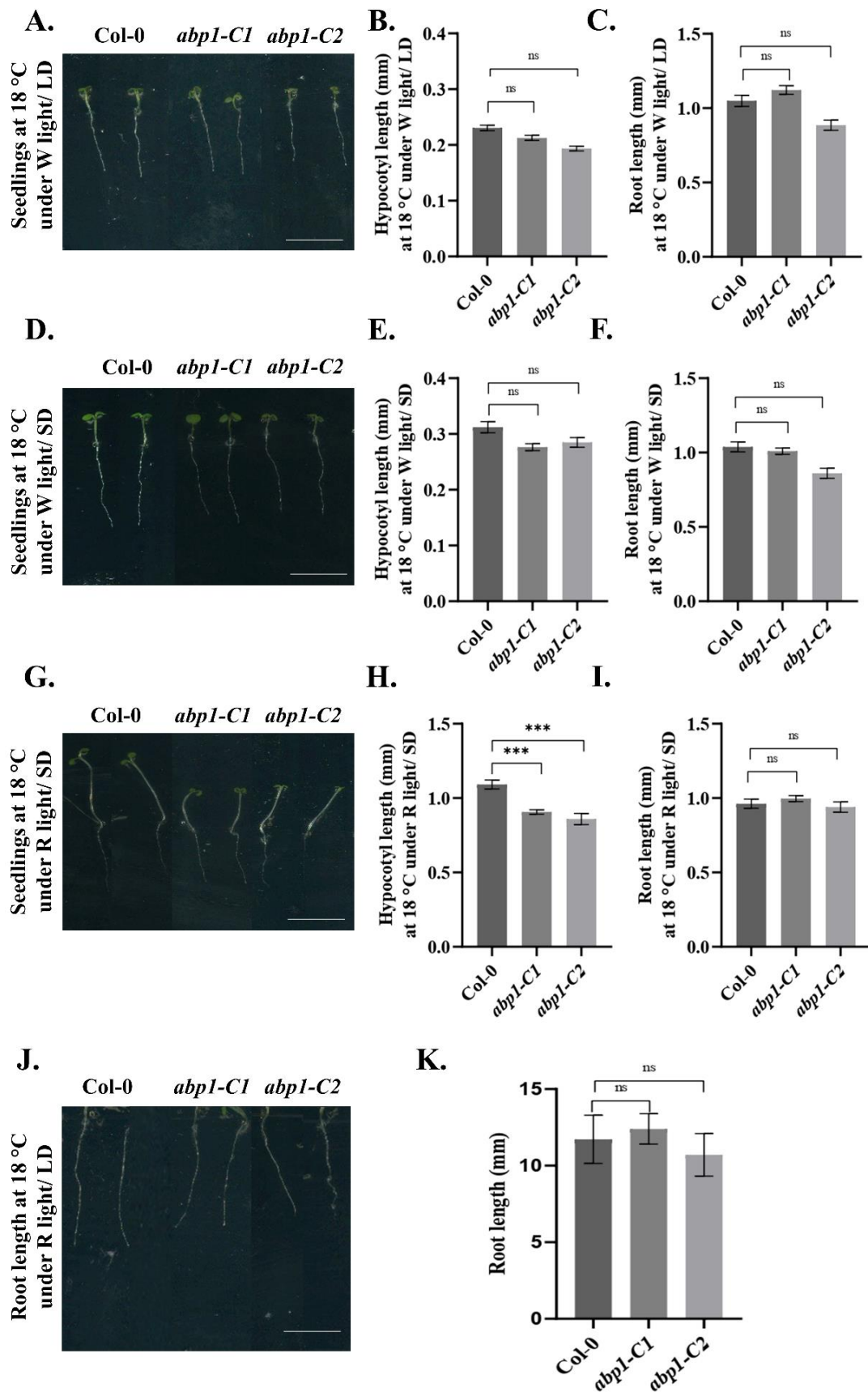


Figure 65. The seedling phenotype at low temperature i.e., 18 °C. Seedlings of Col-0, *abp1-C1*, and *abp1-C2* lines were grown on MS media under LD (A-C), SD (D-F) conditions under W light, and SD (G-I), LD (J-K) under R light at 18 °C. Hypocotyl and root length were measured using ImageJ software from the scanned images. Nearly 300 seedlings were grown in 3 biological replicates with 100 seedlings each time. Data presented as mean \pm SE. One-way analysis of variance (ANOVA) using Tukey's multiple comparisons test was performed with the

help of GraphPad Prism to test for significance among the dataset, * $p < 0.05$, ** < 0.01 , ns – non-significant. The scale bar indicates 5 mm.

However, the hypocotyl lengths of *abp1* mutants were significantly different at 18 °C under diurnal R light both under LD (Figure 66A) and SD (Figure 65D-65F) photoperiod. The hypocotyl length of 7-d-old *abp1* mutant seedlings grown in LD conditions was significantly shorter (1.36-fold in *abp1-C1* and 2.08-fold in *abp1-C2*) than Col-0 wild type (Figure 66E & 66F). Similarly, the *abp1* mutants (1.2-fold in *abp1-C1* and 1.2-fold in *abp1-C2*) showed shorter hypocotyl concerning Col-0 lines under SD conditions at 18 °C (Figure 65G-65I). In addition, the root lengths of *abp1* mutants were marginally shorter than the Col-0 under R light at 18 °C irrespective of the LD or SD photoperiods (Figure 65K & 65L). The transcript levels of *PHY B* were 1.39-fold and 1.58-fold higher in *abp1-C1* and *abp1-C2* mutants respectively than that of Col-0 at 18 °C (Figure 66G). The transcript level of *GI* was significantly decreased (i.e., 2.48-fold) in the *abp1-C1* than in Col-0 wild-type plants. Though the decrease in *GI* transcript level in *abp1-C2* was not as severe as in *abp1-C1* still it was significant ($p \leq 0.05$) (Figure 66H). These results indicated that ABP1 is involved in hypocotyl growth inhibition under monochromatic R light at lower temperatures. Downregulation in *GI* gene expression also suggested that these seedling phenotypic changes in *abp1* mutants are directly or indirectly GI-mediated. Moreover, the role of ABP1 in controlling the seedling phenotype (hypocotyl length and root growth) under low temperature appears to have a conserved yet unidentified mechanistic function to that of ambient temperature (i.e., 22 °C).

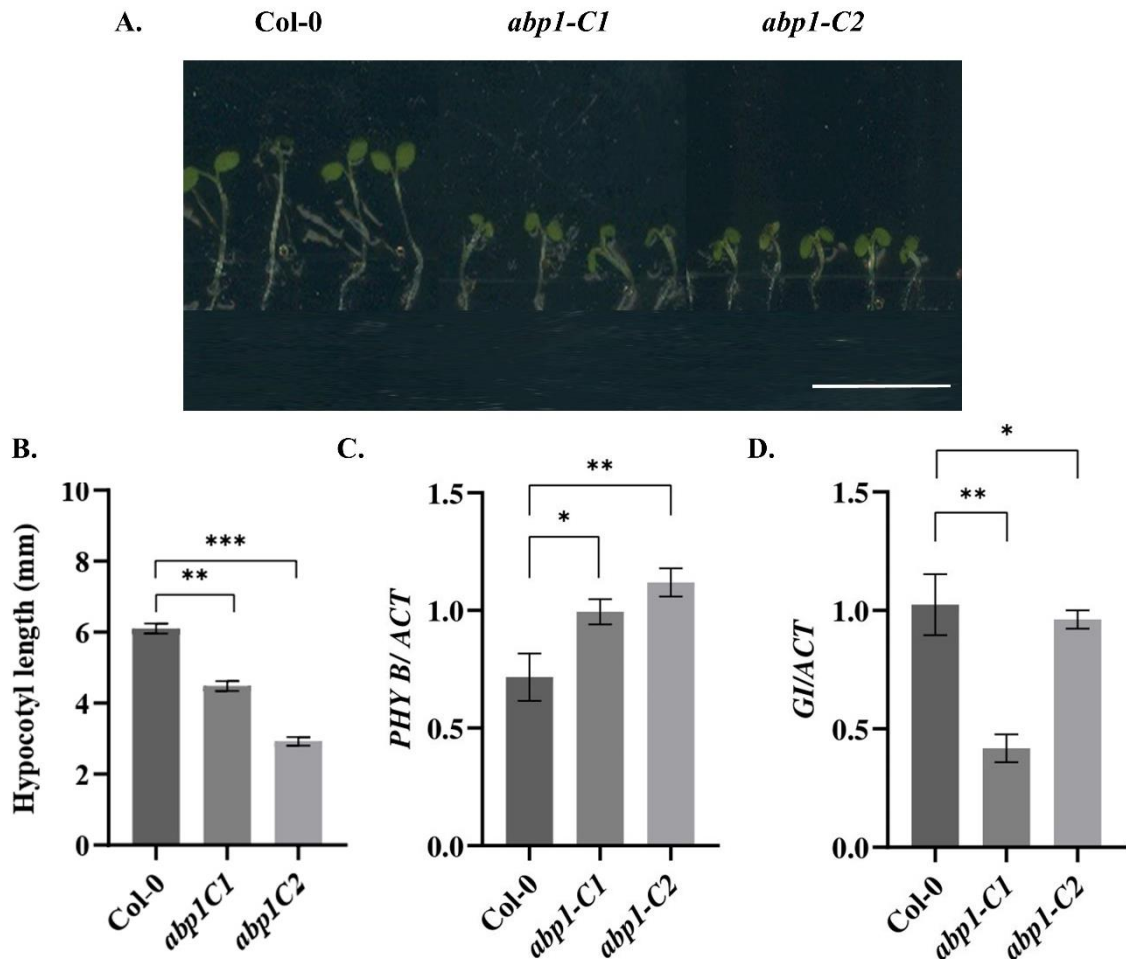


Figure 66. Hypocotyl growth inhibition under monochromatic red light and lower temperature (18 °C). A. Seedlings of Col-0, *abp1-C1*, and *abp1-C2* genotypes were grown on MS media under monochromatic red light at 22 °C and long-day conditions for 7-days (A), after which hypocotyl length was measured (B). Hypocotyl from the seedlings grown under red was analyzed for transcript expression of Phytochrome B (*PHYB*) (C) and *GIGANTEA* (*GI*) (D). The hypocotyl lengths were measured using ImageJ software. Data presented as mean \pm SE. The qRT-PCR reactions were done in triplicate from three biological replicates. *ACTIN* was used to normalize transcript levels. One-way analysis of variance (ANOVA) using Tukey's multiple comparisons test was performed with the help of GraphPad Prism to test for significance among the dataset, * $p < 0.05$, ** $p < 0.01$, *** $p < 0.001$ and ns represent non-significant differences. Scale bar: 1 cm.

5.2.3. Synthetic auxin 1-NAA can rescue *abp1* mutant root phenotype under red light

Since *abp1-C1* and *abp1-C2* mutants showed R light-specific root phenotype strikingly under 22 °C (Figure 64) and marginally under 18 °C (Figure 65K & 65L), a rescue assay was performed using synthetic auxins i.e., 1-NAA (active form of auxin) and 2-NAA (inactive form of auxin). Col-0 lines showed a 51-57 % decrease in root length with 10 mM 1-NAA supplement in the growth medium (Figure 67A & 67C). In both the *abp1-C1* and *abp1-C2* lines, the root length attained to those of their respective controls with 10 mM of 2-NAA in the media (Figure 67B & 67C). A similar but less dramatic observation was also obtained when another synthetic

auxin i.e., 2, 4- dichlorophenoxyacetic acid (2,4-D) was used (data not shown). These results indicated that while exogenous auxin supplement resulted in root length inhibition in Col-0, it could complement the growth inhibition in the absence of ABP1 (in the *abp1* mutant lines). The expression of YUCCA2 was also observed as phytohormone auxin is synthesized mainly through TRYPTOPHAN AMINOTRANSFERASE OF *ARABIDOPSIS* 1 (TAA1) and YUCCA (YUC) (Liu *et al.*, 2016). The levels of YUCCA2 genes in *abp1-C1* and *abp1-C2* increased by 1.5 and 1.5-fold respectively as compared to Col-0 (Figure 67D). Hence, it led to the explanation that the decrease in the root length in Col-0 under R light was very likely due to ABP1 binding to auxin in the roots. These results convincingly suggested that ABP1 has an important role in root development under R light (660 nm) of 30 $\mu\text{mol m}^{-2} \text{s}^{-1}$ fluence and pronounced at 22 °C growth conditions while compared to that of 18 °C.

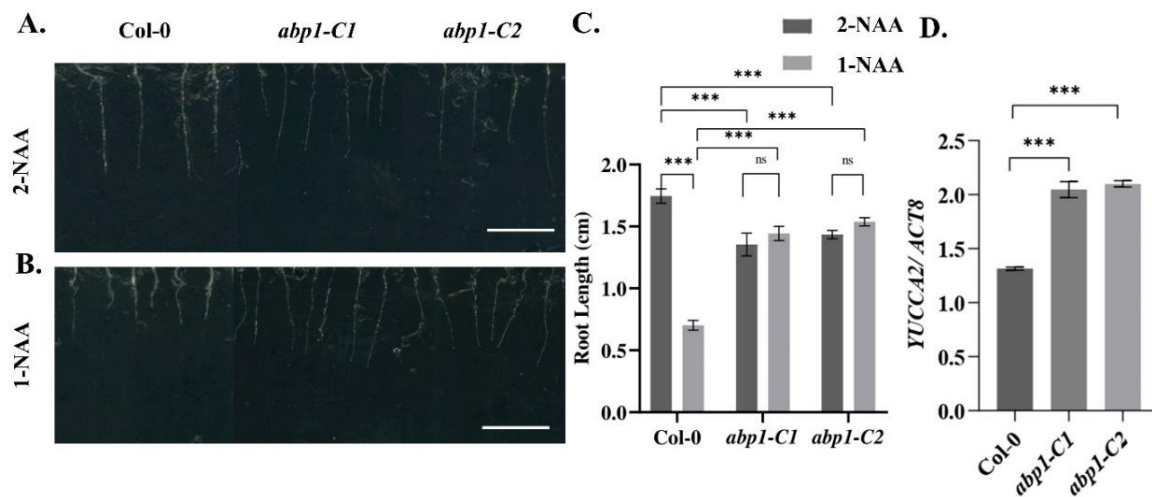


Figure 67. Complementation of root growth phenotype with external application of synthetic auxin. Seedlings of Col-0, *abp1-C1* and *abp1-C2* genotypes were grown on MS media under monochromatic red light, 22 °C and long-day conditions for 7 days, and root phenotype was studied after supplement of 1 mM 1-naphthaleneacetic acid (NAA) active form of auxin (B) and 2-NAA, inactive form of auxin (A) or with 1 mM 1-NAA, after which root length were measured (C). The 3rd and 4th leaves of adult plants (10-d before bolting) were used for analyses of transcript expression of *YUCCA2* (D). 300 seedlings were grown in 3 biological replicates with 100 seedlings each time. The root lengths were measured using ImageJ software. Data presented as mean \pm SE. One-way analysis of variance (ANOVA) using Tukey's multiple comparisons test was performed with the help of GraphPad Prism to test for significance among the dataset, * $p < 0.05$, ** $p < 0.01$, *** $p < 0.001$ and ns represent non-significant differences. Scale bar: 1 cm

5.2.4. ABP1 mutation delayed timing to flower at low temperature irrespective of photoperiod

Since ABP1 mutants showed higher *PHYB* and lower *GI* at lower temperatures (Figure 66), it was of interest to evaluate adult plant phenotypes in these conditions. First, we tested both the CRISPR mutants of ABP1 under W light at 22 °C and were convinced that the result was somewhat similar to as described by Gao *et al.*, (2015) (Figure 68).

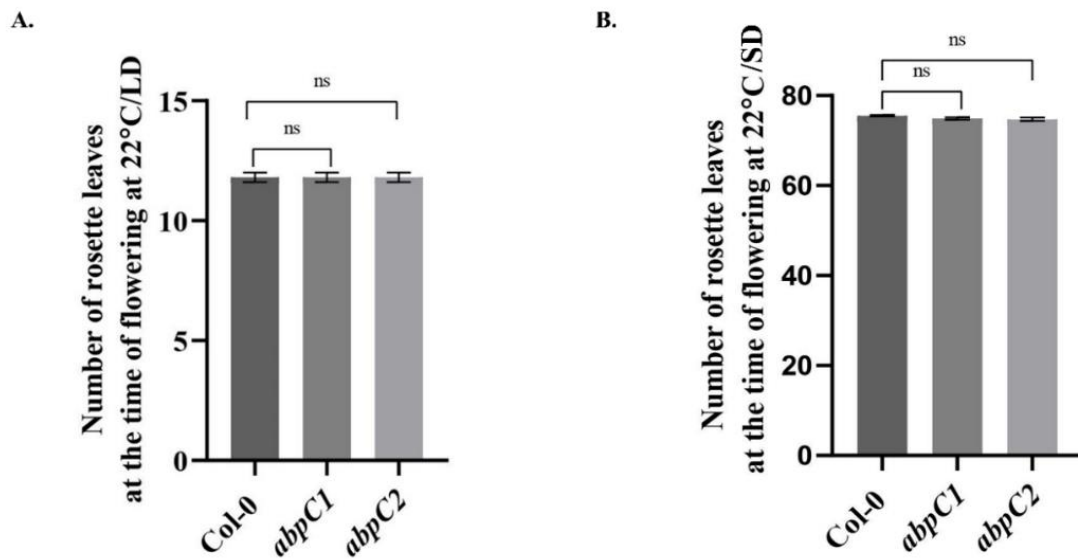


Figure 68. Flowering phenotype under LD and SD conditions at 22 °C. Plants of Col-0, *abp1-C1*, and *abp1-C2* genotypes were grown on soil in pots under LD or SD conditions at 22 °C till bolting. The total number of rosette leaves at the time of bolting grown under 22 °C under LD (A) and SD (B) conditions were noted. Three biological replicates were performed using 10 plants in each replicate. Data presented as mean \pm SE. One-way analysis of variance (ANOVA) using Tukey's multiple comparisons test was performed with the help of GraphPad Prism to test for significance among the dataset, * $p < 0.05$, ** $p < 0.01$, *** $p < 0.001$ and ns represent non-significant differences.

However, both the *abp1-C1* and *abp1-C2* mutants showed delayed flowering with an increased number of rosette leaves at 18 °C under WL irrespective of photoperiod (i.e., under both 16/8 hour, LD and 8/16 hour, SD) (Figure 69A and Figure 69C). The *abp1-C1* and *abp1-C2* mutants had a significantly higher number of rosette leaves, 23 ± 2 and 25 ± 2 respectively than the Col-0 with 16 ± 2 rosette leaves at the time of bolting (Figure 69B). Similarly, the *abp1-C1* and *abp1-C2* mutants had 59 ± 2 and 57.8 ± 2 leaves respectively compared to 45 ± 2 rosette leaves at the time of bolting under SD conditions (Figure 69D). Since the *abp1* mutants showed similar phenotypic as compared to Col-0 wildtype with effect to low temperature in both LD as well as

SD conditions, further experiments were carried out with plants grown under LD conditions. Rosette radius in *abp1-C1* and *abp1-C2* mutants also showed a 1.1-fold and 1.2-fold increase in the rosette radius as compared to the *col-0* lines (Figure 69E). Transcript expression levels of *FT* in *Col-0* in comparison to those of *abp1* mutants grown at 18 °C were investigated to explain the above-mentioned flowering phenotype. The expression levels of *FT* in *abp1-C1* and *abp1-C2* were observed to be 12.5-fold and 1.69-fold lower respectively than *Col-0* (Figure 69F). Since the rosette radius was larger in the mutants, the expression of *GI* in *abp1* mutants was investigated. The quantitative level of *GI* transcript was found to be significantly lower (i.e., 6.48-fold and 3.91-fold) than *Col-0* (Figure 69G).

Another important phenotype we observed is leaf epinasty. The leaves of *ABP1* mutants were found to be more curled towards the abaxial surface (Figure 69H). The leaf flatness is expressed here as the ratio of the straight-line distance between the two leaf edges to the actual leaf width. The leaves of *abp1-C1* and *abp1-C2* are 3.04-fold and 2.56-fold more curled than the *Col-0* leaves at 18 °C (Figure 69I). However, the leaves of *abp1* mutants were found to be completely expanded with a marginal difference at 22 °C (Figure 69I). The above results convincingly showed that *ABP1* mutation delays flowering and causes leaf epinasty at low temperature.

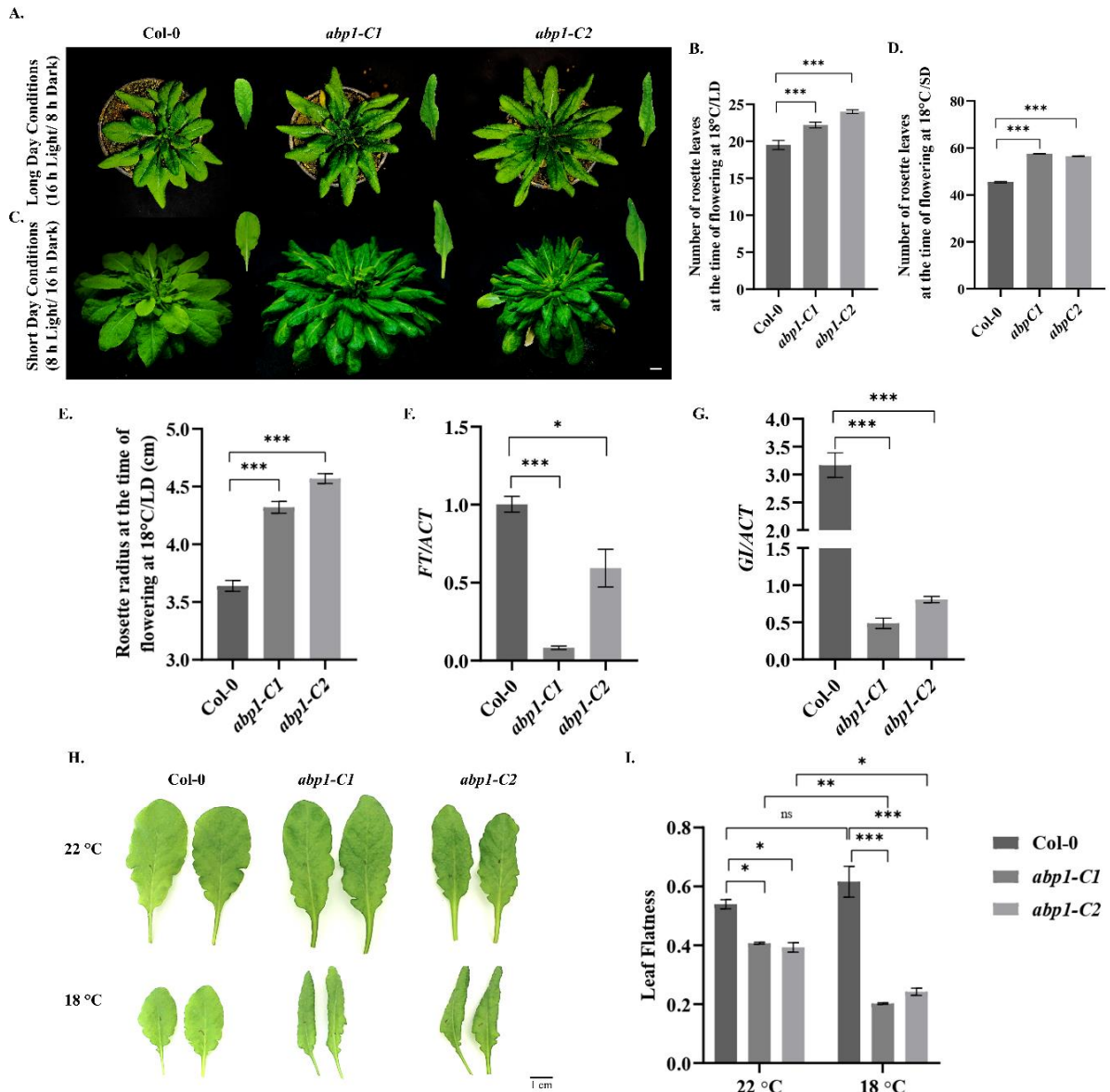


Figure 69. Flowering phenotype at low temperature (18 °C). Plants of Col-0, *abp1-C1*, and *abp1-C2* genotypes were grown on soil in pots under LD (A-B) and SD (C-D) conditions and 18 °C till bolting. Rosette leaves (B & D) and radius at the time of flowering (E) were noted. Three biological replicates were performed using 10 plants in each replicate. Mature leaves were used for analyses of transcript expression of *FLOWERING TIME (FT)* (D) and *GIGANTEA (GI)* (E). Representative leaves from each genotype are shown to show epinasty (H) and histogram representing the leaf flatness in each genotype at 22 and 18 °C. Data presented as mean \pm SE. The qRT-PCR reactions were done in triplicate from three biological replicates. *ACTIN* was used to normalize transcript levels. One-way analysis of variance (ANOVA) using Tukey's multiple comparisons test was performed with the help of GraphPad Prism to test for significance among the dataset, * $p < 0.05$, ** $p < 0.01$, *** $p < 0.001$ and ns represent non-significant differences. Scale bar: 1 cm.

5.2.5. Role of defense hormones in mediating low-temperature response in *abp1* mutant lines.

Cold responses and acclimatization are known to be associated with the dynamic interplay of several hormones including Jasmonic acid (JA) (Wang *et al.*, 2020), abscisic acid (ABA), and salicylic acid (SA) in many plant species (Shi and Yang, 2014; Scott *et al.*, 2004). As *abp1*

mutants showed resistant growth effects with a higher number of leaves and delayed flowering under low temperatures, we analyzed the levels of endogenous defense hormones such as ABA, SA, and JA under low temperatures in *abp1* mutants. Col-0 lines showed a 1.1-fold decrease, whereas *abp1-C1* and *abp1-C2* lines had 1.3-fold and 1.07-fold increase in ABA content respectively in plants grown under 18 °C as compared with their respective control plants grown under 22 °C (Figure 70A). Similarly, Col-0 lines showed a 1.1-fold decrease, whereas *abp1-C1* and *abp1-C2* lines had 1.2-fold and 1.2-fold increase in SA content respectively in plants grown under 18 °C (Figure 70B). However, jasmonic acid (JA) content in Col-0 lines was in a reverse trend with a 2.37-fold increase in response to low temperature. The *abp1-C1* and *abp1-C2* lines showed a 0.23-fold and 4.27-fold decrease in JA content in similar conditions (Figure 70C). These results indicated that the cold resistance response under low temperatures in *abp1* mutants was mediated by the accumulation of several defense hormones including ABA and SA.

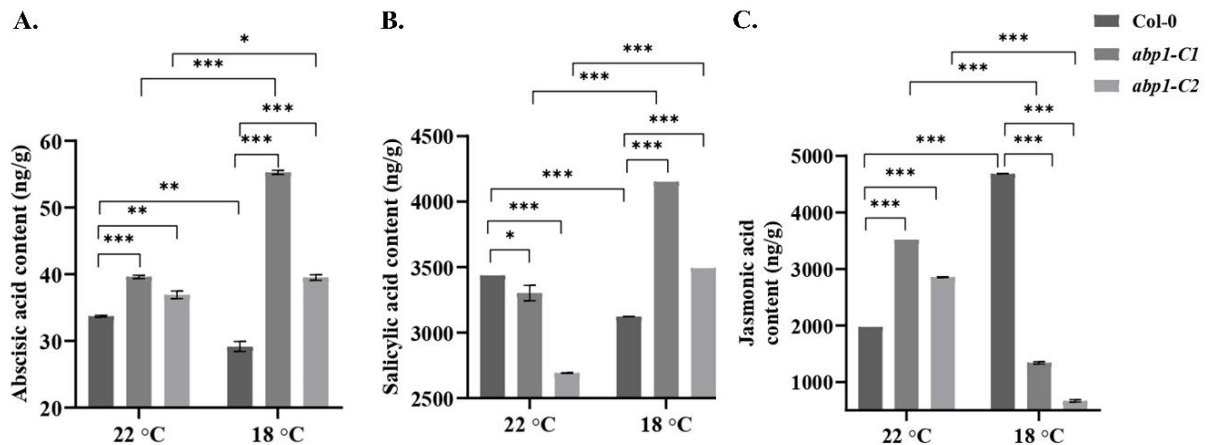


Figure 70. Estimation of endogenous contents of defense hormones (abscisic acid, salicylic acid, and jasmonic acid). Leaf samples from adult plants grown on soil in pots under LD conditions from Col-0, *abp1-C1*, and *abp1-C2* lines grown under either 22 °C or 18 °C were collected at the bolting stage, which were processed for determination of endogenous contents of abscisic acid (ABA) (A), Salicylic acid (SA) (B) and jasmonic acid (JA) (C). D6-ABA, D4-SA, and D6-JA were used as internal standards for ABA, SA, and JA quantification. Three individual biological replicates were performed to obtain the mean \pm SE. One-way analysis of variance (ANOVA) using Tukey's multiple comparisons test was performed with the help of GraphPad Prism to test for significance among the dataset, * $p < 0.05$, ** $p < 0.01$, *** $p < 0.001$.

5.2.6. Altered trichome morphology contributes to cold resistance in *abp1* mutants

Trichomes are known to be involved in several abiotic stresses (Wang *et al.*, 2021) including cold tolerance. As shown in previous studies, low-temperature stress resulted in varied alterations (either lower or higher) in trichome density (Sun *et al.*, 2022; Zhang *et al.*, 2020) across different plant species. In the Col-0 line trichome density was increased by 2.9-fold under low temperature (Figure 71A & 71B). However, in *abp1-C1* and *abp1-C2* lines the trichome density increased insignificantly at 18 °C compared to their respective controls at 22 °C leading to reduced trichome density than those of Col-0 at 18 °C (Figure 71A & 71B). Trichome architecture and branching have also been known to vary in response to abiotic stresses (Ordachescu *et al.*, 2008). A number of proteins regulate secondary branching in trichomes, either positively or negatively (Zhang *et al.*, 2021). Secondary trichome branching was not observed in Col-0 lines both under control conditions and low temperatures. However, 58.3 % and 38.7 % increases in secondary branching (i.e., four branched trichomes) were observed in *abp1-C1* and *abp1-C2* lines respectively at 22 °C as compared to those of Col-0 (Figure 71C & 71D). With the effect of low temperature, 2.75-fold and a non-significant decrease in secondary branching were observed in *abp1-C1* and *abp1-C2* lines (Figure 71C & 71D) compared to their controls at 22 °C respectively. TRIPTYCHON (TRY) acts as a negative regulator of secondary branching of trichomes and its loss of function results in the formation of new branch points (Lescot *et al.*, 2002). CAPRICE (CPC) is a negative regulator of trichome initiation and development (Fambrini *et al.*, 2019). The microscopic observations of the trichomes were validated genetically by analyzing the transcript levels of *CPC* and *TRY* genes in the *abp1* lines in comparison to Col-0. Under control growth conditions, transcript levels of *CPC* were 12.9-fold and 11-fold less in the *abp1-C1* and *abp1-C2* lines than in the Col-0 (Figure 71E). Similarly, transcript levels of *TRY* were 3-fold and 1.4-fold less in *abp1-C1* and *abp1-C2* lines than the Col-0 (Figure 71F). With effect to low-temperature stress, *CPC* transcript levels increased non-significantly, while increased 2-fold and 1.1-fold in the case of the *TRY* transcript

in the *abp1-C1* and *abp1-C2* lines respectively, when compared to their respective controls grown at 22 °C (Figure 71E & 71F). These results showed that cold resistance in *abp1* mutant lines is mediated by decreasing trichome density and increasing branching patterns which in turn are regulated by an increase in transcript levels of negative regulators of trichome branching genes such as *CPC* and *TRY*.

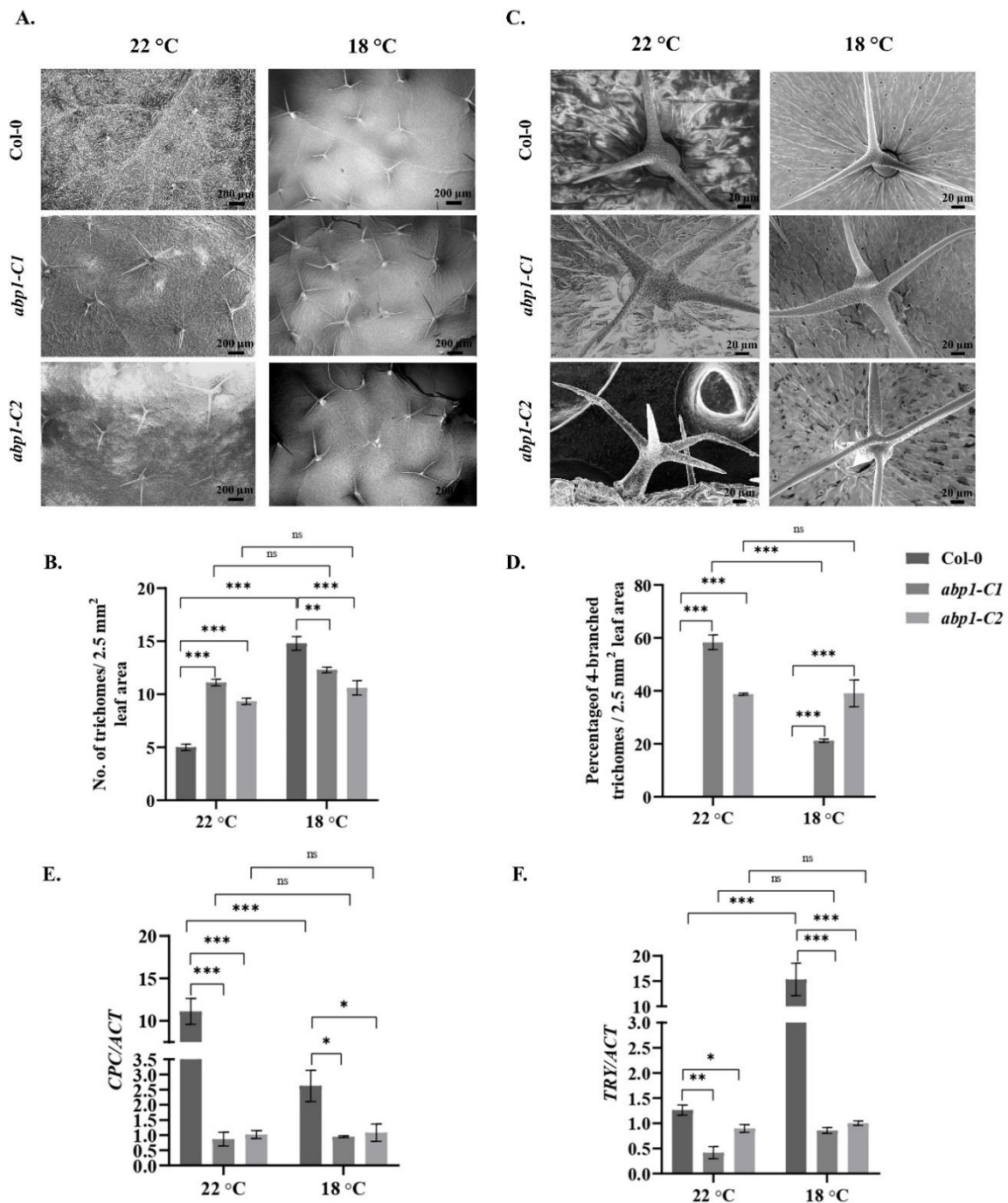


Figure 71. Molecular analysis of trichome morphology. Plants of Col-0, *abp1-C1*, and *abp1-C2* genotypes were grown on soil in pots under LD conditions at 22 °C and 18 °C till bolting followed by sample collection. Leaf samples were studied using scanning electron microscopy (SEM) (A & C). Trichome density (B) and percentage of 4-branched trichomes (D) were analyzed from SEM micrographs. The percentage of 4-branched trichomes was calculated to the total number of trichomes (D). Three individual biological replicates were performed. Data

presented as mean \pm SE. Leaf samples were used for transcript expression analysis of *CPC* (E) or *TRY* (F). Reactions were done in triplicate from three biological replicates. *ACTIN* was used to normalize transcript levels. One-way analysis of variance (ANOVA) using Tukey's multiple comparisons test was performed with the help of GraphPad Prism to test for significance among the dataset, * $p < 0.05$, ** $p < 0.01$, *** $p < 0.001$.

5.2.7. ABP1 mutation positively affects dehydration tolerance

Cold or drought stress induces dehydration, which is well documented in different studies (Bhat *et al.*, 2022; Manasa *et al.*, 2022; Zhang *et al.*, 2018). Divulged of the cold resistance effect due to ABP1 mutation, we investigated the effect of dehydration induced by water withheld (WW) at 22 °C or low temperature (18 °C) in *abp1* mutant lines in comparison with Col-0 (Figure 72A).

5.2.7.1. Physiological parametric confirmation of dehydration tolerance

Relative water content (RWC) decreased to nearly half of its starting value due to WW in Col-0 under both 22 °C (Figure 72B) and low temperature (Figure 72C), whereas in *abp1-C1* there was only minimal change in the RWC percentage (~25.1 % at 22 °C and 5.7 % at 18 °C) after 5 days and 10 days of WW respectively. The *abp1-C2* also showed a similar decrease in RWC as that of *abp1-C1* (Figure 72B & 72C). Malondialdehyde (MDA) accumulation due to lipid peroxidation in plant leaves serves as an indicator of abiotic stress response (Singh *et al.*, 2009). Col-0 plants showed a significant increase of MDA content after WW i.e., 4.1-fold and 5.8-fold as compared to their respective controls at 22 °C and 18 °C respectively (Figure 72D & 72E). MDA accumulation after WW in *abp1* lines was significantly less as compared to that of Col-0. Moreover, both *abp1-C1* and *abp1-C2* showed similar patterns of MDA accumulation, i.e., nearly 2.4-fold and 1.76-fold (at 22 °C) (Figure 72D) as well as 1.5-fold and 1.1-fold (at 18 °C) (Figure 72E) increase than their respective control plants.

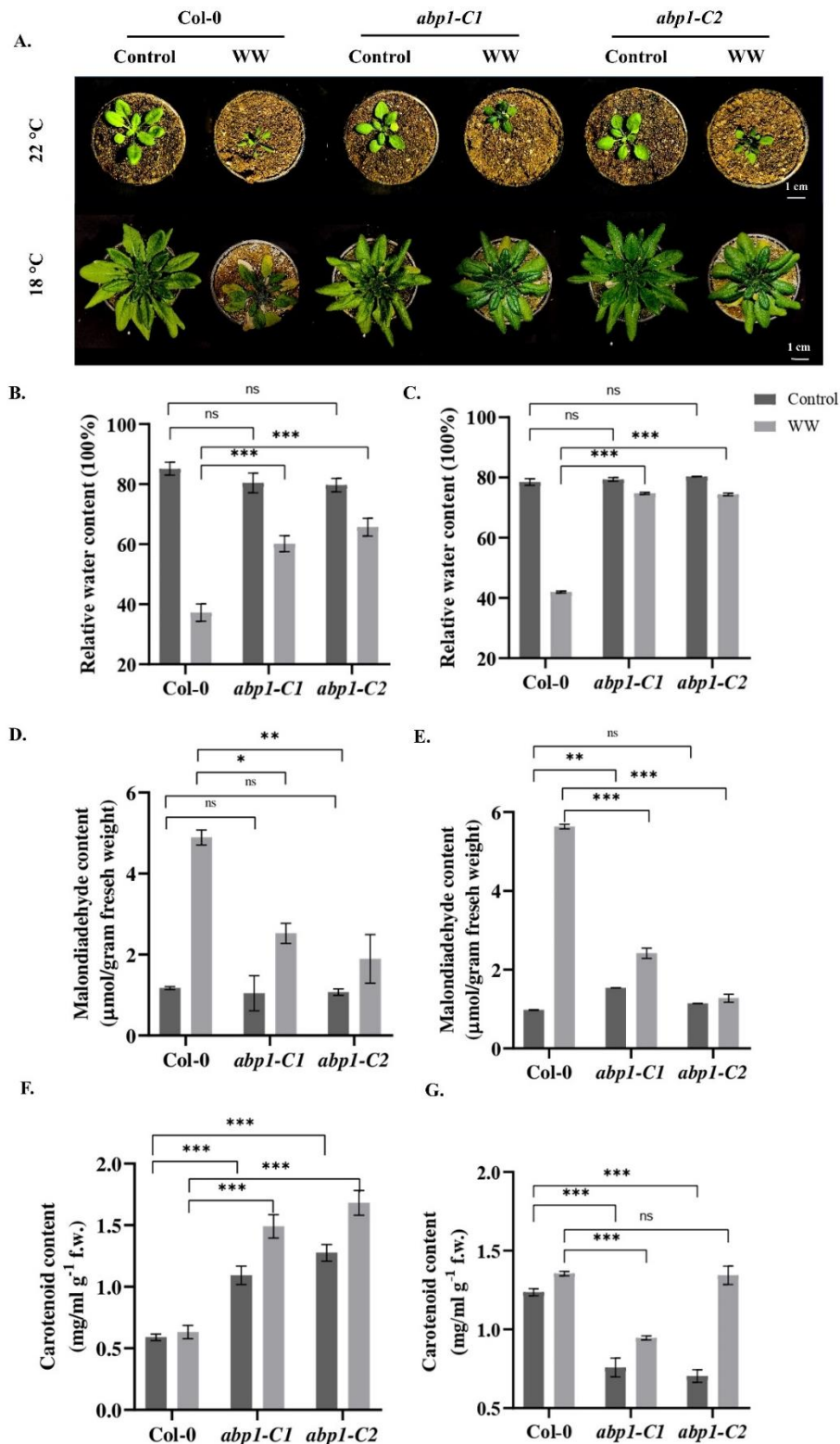


Figure 72. Analysis of dehydration stress tolerance. Plants of Col-0, *abp1-C1*, and *abp1-C2* genotypes were grown on soil in pots under LD conditions at 22 °C or 18 °C till 15-d or 40-d old stage respectively (as described in section 2.1). Water withheld (WW) for 5-d at 22 °C (**A, top row**) or 10-d at low temperature (**A, bottom row**) was imposed to induce dehydration stress. Physiological parameters including relative water content (**B, C**), malondialdehyde content (**D, E**), and total carotenoid content (**F, G**) were studied from the leaf samples subjected to WW at 22 °C and 18 °C respectively. Three individual biological replicates were performed. Data presented as mean \pm SE. One-way analysis of variance (ANOVA) using Tukey's multiple comparisons test was performed with the help of GraphPad Prism to test for significance among the dataset, * $p < 0.05$, ** $p < 0.01$, *** $p < 0.001$, ns: non-significant. Scale bar: 1 cm.

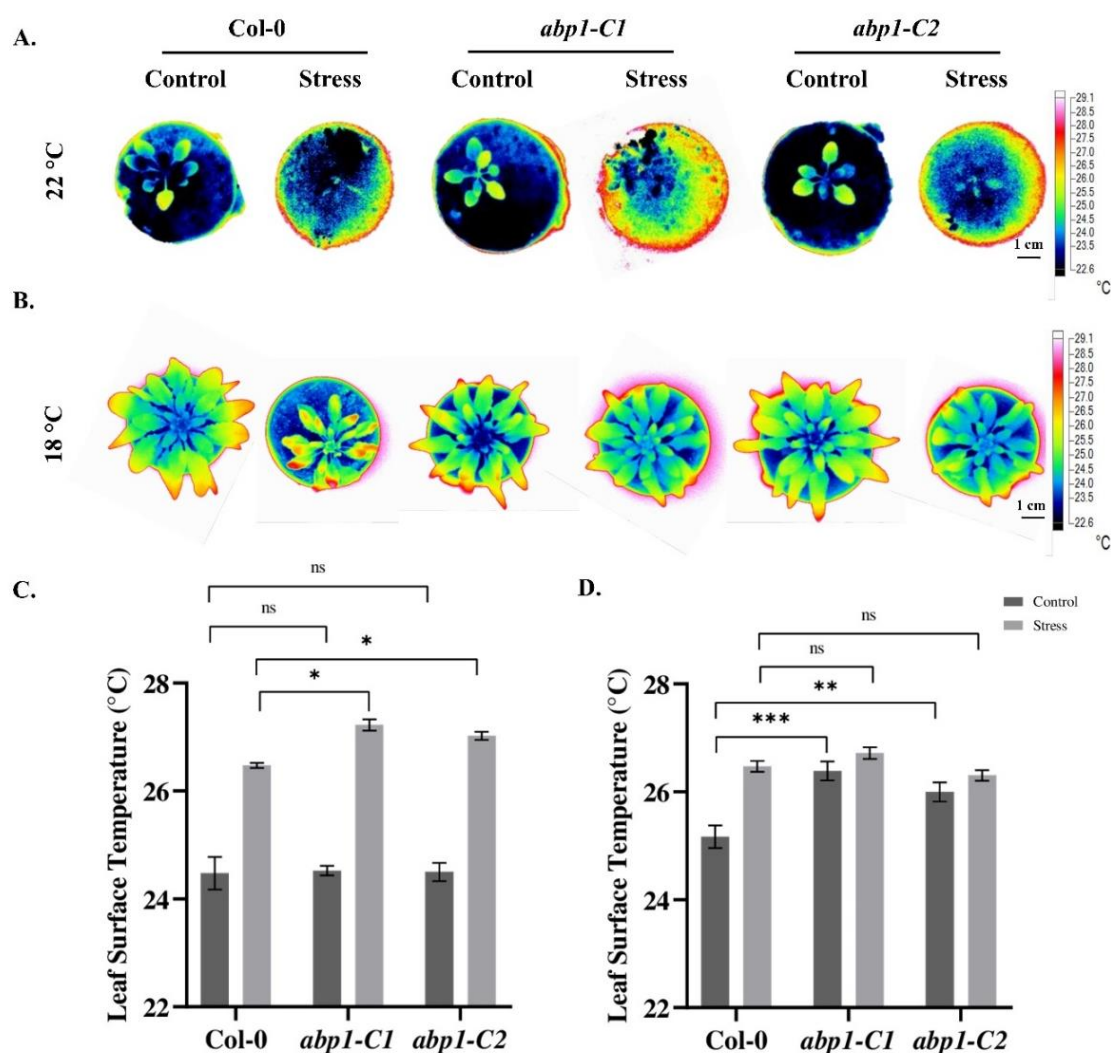


Figure 73. Plant leaf Temperature analysis. **A and B.** Plants of Col-0, *abp1-C1*, and *abp1-C2* genotypes were grown on soil in pots under LD conditions at 22 °C (**A**) or 18 °C (**B**) till the bolting stage. Plants were either well-watered or water withheld for 5-10 days (WW) as described in materials and methods. Leaf temperature of the plants grown in water withheld conditions at 22 °C (**A and C**) or 18 °C (**B and D**) were measured from thermal pictures that were taken with a FLUKE infrared camera and analyzed using the SMART VIEW software. Leaf surface temperatures showing the highest temperatures were selectively chosen from at least ten individual plants. Three individual biological replicates were performed. Data presented as mean \pm SE. One-way analysis of variance (ANOVA) using Tukey's multiple comparisons test was performed with the help of GraphPad Prism to test for significance among the dataset, * $p < 0.05$, ** $p < 0.01$, *** $p < 0.001$ and ns represent non-significant differences. Scale bar: 1 cm.

5.2.7.2. Biochemical parametric confirmation of dehydration tolerance

Dehydration due to drought or cold is associated with characteristic physiological changes including accumulation of stress pigments such as carotenoids and flavonoids, reduction of photosynthetic efficiency, generation of reaction oxygen species, and increased ROS scavenging due to various ROS scavenging enzyme activity intolerant species, which have been well documented in previous studies (Panigrahy *et al.*, 2011; Tomanek *et al.*, 2012; Manasa *et*

al., 2022; Panigrahy *et al.*, 2022). Dehydration tolerance in *abp1* mutant lines was validated after WW by studying various biochemical parameters such as carotenoids, oxygen free radicals (O_2^-), enzyme activity of superoxide dismutase (SOD), catalase (CAT) and peroxidase (POX) in comparison with those of Col-0 as well as with their respective controls without WW.

Carotenoid content accumulation with effect on WW at both 22 °C and 18 °C was negligible in the Col-0 line. Whereas, both the *abp1* lines showed higher carotenoid accumulation after WW (i.e., 1.3-fold, 1.3-fold higher carotenoids at 22 °C (Figure 72) and 1.25-fold, 1.9-fold higher carotenoids at 18 °C (Figure 72G)) in *abp1-C1* and *abp1-C2* line respectively.

Col-0 lines showed a sharp increase in O_2^- (also visible due to histochemical staining in the leaves) due to WW (3.2-fold and 2.5-fold increase) both at 22 °C (Figure 74A & 74B) and 18 °C (Figure 74C & 74D) respectively. Before WW, both the *abp1* lines had a comparable amount of O_2^- as that of the Col-0 at 22 °C (Figure 74B). Notably, *abp1-C1* had 2.6-fold less and *abp1-C2* line had 1.6-fold higher O_2^- than Col-0 at 18 °C before WW (Figure 74D). Dehydration stress due to WW showed significantly less O_2^- accumulation in both the *abp1* lines as compared to that of Col-0 at 22 °C (Figure 74B). Explicitly, while *abp1-C1* showed a 1.7-fold increase, the *abp1-C2* line showed a 1.7-fold increase in O_2^- respectively at 22 °C (Figure 74B). Under 18 °C, both the *abp1* lines showed negligible or non-significant increases in O_2^- as compared to their respective controls (Figure 74D).

WW at both 22 °C and 18 °C resulted in a significant increase in catalase (CAT), peroxidase (POX), and superoxide dismutase (SOD) enzyme activities within Col-0 plants. At 22 °C, the increases were notable, with a 3.2-fold, 3.8-fold, and 2.2-fold rise in CAT, POX, and SOD activities, respectively (Figure 74E, 74G & 74I). Similarly, at 18 °C, the enzyme activities in Col-0 plants exhibited substantial increments of 4.14-fold, 38.6-fold, and 2.3-fold for CAT, POX, and SOD, respectively (Figure 74F, 74H & 74J). However, in comparison to Col-0, the *abp1* mutant lines showed relatively smaller increases in enzyme activities after WW treatment.

Notably, the increases in CAT and SOD activities at 22 °C, as well as CAT activity at 18 °C (for the *abp1-C2* line), were not statistically significant when compared to their respective controls post WW in both *abp1* mutant lines. Furthermore, observing the *abp1* lines in detail, after WW at 22 °C, there was a 1.9-fold and 1.5-fold increase in POX activity in *abp1-C1* and *abp1-C2* lines, respectively. Similarly, at 18 °C, an increase of 1.5-fold, 1.2-fold in CAT activity, 3.8-fold, 1.5-fold in POX activity, and 1.4-fold, 1.4-fold in SOD activity was observed in *abp1-C1* and *abp1-C2* lines, respectively, when compared to their respective control conditions.

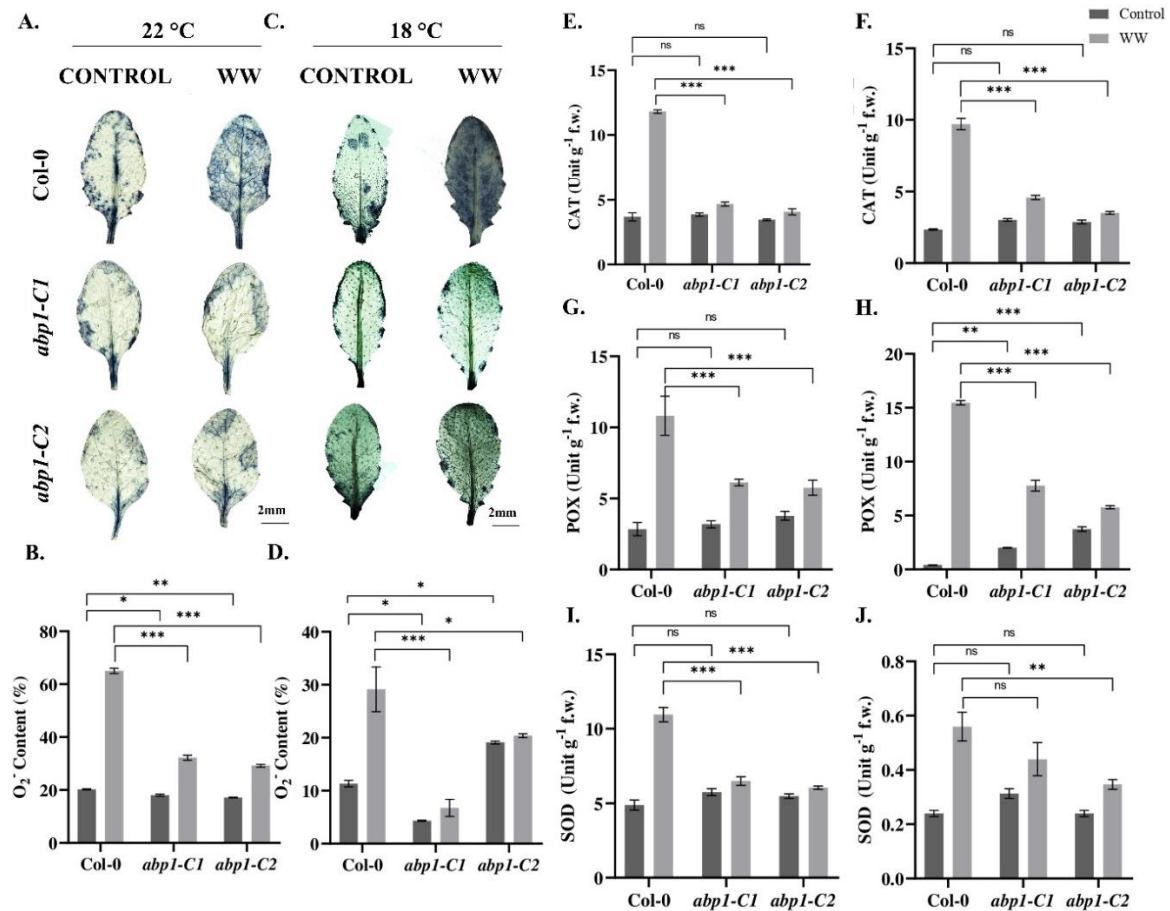


Figure 74. Test of biochemical parameters during dehydration stress. Plants of Col-0, *abp1-C1*, and *abp1-C2* genotypes were grown on soil in pots under LD conditions at 22 °C or 18 °C till 15-d or 40-d old stage respectively (as described in section 2.1). Water withheld (WW) for 5-d at 22 °C or 10-d at low temperature was imposed to induce dehydration stress. Histochemical detection of oxygen radical at control, 22 °C (A, B) and 18 °C (C, D) was done using NBT staining (A, C) and percentage of oxygen radical (O₂⁻) accumulation (B, D) in the leaves by calculating the stained area to the total area of the leaves using ImageJ software. Determination of ROS scavenging enzyme activity including catalase (CAT) (E, F), Guaiacol peroxidase (POX) (G, H), and Superoxide dismutase (SOD) activity (I, J) under control and low temperature was done using spectrophotometric assays. Three individual biological replicates were performed for each experiment with 3 plants in each sample. Data presented as mean ± SE. One-way analysis of variance (ANOVA) using Tukey's multiple comparisons test was performed with the help of GraphPad Prism to test for significance among the dataset, **p* < 0.05, ***p* < 0.01, ****p* < 0.001, ns: non-significant. Scale bar: 2 mm.

5.3. DISCUSSION

Our results demonstrated that ABP1 has a positive role for primary root elongation under R at 22 °C, as the *abp1* mutants showed shorter roots under the said conditions. Auxin at lower concentrations is known to promote root elongation whereas inhibits the same at higher concentrations (Ivanchenko *et al.*, 2010). We could complement the root elongation phenotype in Col-0 with external supplement of auxin in the medium, which was absent in the *abp1* mutant lines indicating that ABP1 binding to auxin is indispensable for root elongation under R at 22 °C. Root-localised phytochromes have implications for root elongation (Stephanie *et al.*, 2011). We also demonstrated the regulation of PhyB in ABP1-auxin-mediated root development under R at 22 °C. This statement was explained by the observations of drastically diminished or elevated transcript levels of *PHYB* in Col-0 and *abp1* lines respectively. The decrease in RL under R light in *abp1* mutant lines could be due to the elevated *PHYB* levels as compared to Col-0. This observation explained that root elongation is negatively affected due to the *PHYB* transcript. Our data indicated that ABP1 is involved in decreasing PhyB levels in roots which exerted a positive effect in root elongation under R at 22 °C. Tissue-specific and pleiotropic developmental role of ABP1 emerged when we observed hypersensitivity concerning hypocotyl length in the *abp1* mutants when compared to Col-0 under R at lower temperature (18 °C). Here again, regulation by photoreceptor was reclaimed due to altered transcript levels of *PHYB* in the *abp1* mutants. ABP1 was again shown to affect by decreasing PhyB levels in hypocotyls to exert a negative effect on hypocotyl growth inhibition under R at 18 °C. Hence, it was concluded that ABP1 was involved in decreasing *PHYB* levels in both roots and hypocotyls to control root and hypocotyl elongation under R at 22 °C and 18 °C respectively. The circadian clock coordinates diurnal carbon allocation and controls root growth following a robust diel oscillation of a minimum after (8-9 hours) dawn and a maximum at the end of the night (Yazdabakhsh *et al.*, 2011). GIGANTEA is not only the component of the night loop of the circadian clock but is also involved in PhyB light

signaling for the regulation of flowering time control (Mishra and Panigrahi, 2015). Altered transcript levels of *GI* in the *abp1* mutants indicated a circadian clock control in the root growth phenotype under R at 22 °C. Depleted GI levels in *abp1* mutants indicated its positive role in ABP1-auxin-mediated root growth under R at 22 °C. Thus, ABP1 acts to elevate GI transcript levels to positively affect root elongation under R at 22 °C. Further, ABP1 affected positively the GI transcript levels to control negative hypocotyl growth inhibition under R at 18 °C. Hence, summatedly it inferred that ABP1 positively affects GI levels to control root and hypocotyl elongation under R light at 22 °C and 18 °C respectively. Moreover, a probable role of ABP1 in controlling secondary root growth was also observed at 22 °C specifically in B light, where FR light was ineffective and R light was found to have a probable antagonistic role for this response. B light is known to exert additive roles for hypocotyl growth inhibition and root elongation under R light at room temperature (Shinkle *et al.*, 1992; Yeh *et al.*, 2020). Auxin is known to promote lateral root initiation (Ivanchenko *et al.*, 2010). However, the ABP-mediated stimulatory effect on secondary root growth under B light requires further experiments including levels of cryptochromes, phototropins, and PhyA. The additive effect of R light to recover the B light phenotype for secondary root growth could already be imagined as known from previous studies (Jeong *et al.*, 2014). ABP1 function at low temperatures was strengthened by observation of delayed flowering phenotype in the *abp1* mutants irrespective of the photoperiod. Corresponding decreased levels of FT and GI further supported the flowering phenotype in *abp1* mutants. Differential auxin accumulation in the adaxial cells results in leaf epinasty. However, ABP1 binding with auxin was not conclusive for leaf epinasty (Sandalio *et al.*, 2016). Leaves of *abp1* mutants grown at low temperature showed a more pronounced leaf epinasty phenotype than that of Col-0 indicating that ABP1 has a negative role in leaf epinasty and again reclaiming its auxin binding at 18 °C. Defense hormones including ABA, JA, and SA orchestrated a newer side of low-temperature tolerance in the *abp1* mutants. An increase of ABA and SA levels in the *abp1* mutants under low

temperature when compared to the corresponding Col-0 samples indicated that ABP1 mutation affects levels of these two defense hormones whether via auxin or any unknown pathway. On the other hand, JA levels decreased and followed a contrasting trend to those of ABA and SA. The interplay of these three defense hormones with auxin and ABP1 requires further experiments. However, the hormonal data suggested that elevated ABA, SA, and alleviated JA levels contributed to the low-temperature tolerance in the *abp1* mutants. Cold stress tolerance in the *abp1* mutants was associated with our observations of a decrease in trichome density and an increase in secondary branching (i.e., four-branched trichomes) compared to those of the Col-0 with effect to low-temperature stress. These data suggested that trichome density was associated negatively and four-branched trichomes were associated positively with the cold stress tolerance in the *abp1* lines. Under low-temperature stress, the reduced JA levels in the *abp1* mutants could explain the reduced trichome density compared to Col-0, as JA significantly promotes trichome development (Fambrini *et al.*, 2019). Under control growth conditions, reduced *CPC* and *TRY* transcript levels explained the dense trichomes in the *abp1* mutants than the Col-0. Moreover, reduced *CPC* transcript levels in Col-0 could correlate to the higher number of trichomes under low temperature. However, the decreased trichome density in the *abp1* mutants under low temperature could be mediated either due to elevated *TRY* transcripts in *abp1-C1* or by the other members involved in trichome development (Fambrini *et al.*, 2019), and needs further study. The upregulation of the negative regulator of branching such as *TRY1* also evidenced in the increased four-branched trichomes, which may mediate cold stress tolerance, as trichome differentiation was shown to mediate cold stress tolerance (Dhawan *et al.*, 2016). Cold stress tolerance was found to be an effect due to dehydration tolerance as a whole which was proved when *abp1* lines showed better tolerance characteristics after 5 days of water withheld when compared to those of Col-0 under both 22 °C as well as low-temperature conditions. The *abp1* mutants showed relatively less water loss, less accumulation of stress metabolite MDA, and less enzyme

activity of SOD, CAT, and POX than the Col-0 lines after WW under both 22 °C as well as low-temperature conditions. The higher dehydration tolerance in the *abp1* mutants could be explained by less ROS (O_2^-) accumulation probably due to higher carotenoid accumulation, which acts as an efficient quencher for singlet oxygen (Ramel *et al.*, 2012). The non-significant increase in the ROS scavenging enzyme activities in the *abp1* lines with an effect on WW may be possible due to the maintenance of higher temperatures in these lines as compared to the Col-0 (Figure 73). Hence, it could represent better resistance to the low temperature of the *abp1* lines than Col-0.

The present study demonstrated the possible roles of ABP1 in different stages of plant development in selective and specific environmental conditions. Major among them which were revealed here are as follows: ABP1 positively regulates root growth under red light, negatively regulates hypocotyl growth inhibition under red light and low temperature (18 °C) regime, and is involved in the regulation of flowering at low temperature irrespective of photoperiod, in a clock-controlled manner and strictly dependent on its binding with auxin. ABP1 bears an antagonistic role in deciphering dehydration tolerance induced due to low temperature or water withdrawal of 5 days. ABP1 mutation alters the defense hormone levels including abscisic acid, jasmonic acid, and salicylic acid. Dehydration tolerance in *abp1-C1* and *abp1-C2* mutant lines was suggestively attained by altered defense hormone levels, trichome density and architecture, and plant temperature. These new findings have opened further roads for functional validations to understand the molecular mechanisms of these processes.

CHAPTER 6

EFFECT OF MONOCHROMATIC LIGHT, PHYTOHORMONES, TEMPERATURE, AND Ca^{2+} ON TUBULIN MODIFICATION AND ORGANISATION IN *Physcomitrella patens*

CHAPTER 6: EFFECT OF MONOCHROMATIC LIGHT, PHYTOHORMONES, TEMPERATURE, AND Ca^{2+} ON TUBULIN MODIFICATION AND ORGANISATION IN *Physcomitrella patens*

6.1. BACKGROUND

About 350 million years ago, aquatic bryophytes, like mosses, transitioned to become land-dwelling plants, and this is thought to be how the evolution of land plants began. Mosses such as *Funaria* and *Physcomitrella* have acquired the status of model plants for studying the evolution of land plants. One of the reasons is their ability to be extremely stress-tolerant. Microtubule organization has quite often been linked to stress. The dynamics and orientation of microtubules is an important aspect of stress adaptation in higher plants. In addition, microtubules are also frequently associated with calcium sensing and homeostasis. Due to different environmental conditions, sessile plants undergo significant morphological changes primarily mediated by the cytoskeleton. Microtubules (MTs), which are frequently referred to as "structural elements" of the cells, are significant parts of the cytoskeletal network in plants (Fosket *et al.*, 1992). The assembly and disassembly of the eukaryotic cytoskeleton is an intricate dynamic process that involves several proteins. Of the several proteins known to be a part of the tubulin-FtsZ family, the α and β tubulin proteins form the $\alpha\beta$ -tubulin dimers (Bera and Gupta Jr, 2022). They constitute the protofilaments that come together to form the MTs. Tread-milling and dynamic instability in MTs are some of the major factors attributing to their dynamic behavior. Tread-milling is a type of directional growth in which a specific addition of tubulin dimers occurs at one end of the MT, and gradual loss occurs at the other end, known as the plus and minus ends (Bisgrove *et al.*, 2004). The term "dynamic instability" refers to the variability of MT plus end dynamics. When the GTP cap is present, steady MT growth is ensured, whereas its stochastic loss destabilizes the end structure, resulting in a phenomenon of rapid shrinkage known as catastrophe. After restoring the GTP cap, the MT grows again, a

process known as rescue (Sedbrook *et al.*, 2004). Plant MT dynamics differ substantially from those of animals. Plant MTs are constantly in motion, and moderately fixed interphase MTs pause for only about 10 % of the time, whereas those of animals pause for 60 % of their MT lifetime (Shaw *et al.*, 2003; Ehrhardt *et al.*, 2006).

According to recent research, MTs appear to serve as sensors for various abiotic stimuli in plants, which raises several questions regarding the exact nature of the involvement of MTs in stress responses (Ma and Liu, 2017; Nick, 2008). Plants are capable of wide functional diversification, which includes constructing a variety of microtubular structures to adapt to different developmental stages and environmental conditions (Ma and Liu, 2017; Nick, 2008). Tubulin heterogeneity results from spatially and temporally coordinated differential gene transcription and post-translational modifications (PTMs) (Janke and Mageira, 2020). The existence of several isoforms of α and β tubulin in various genomes is well-documented (Oakley *et al.*, 2015). Further, once translated, several kinds of modifications are possible on the translated protein, viz. Tubulin PTMs such as acetylation, tyrosination, polyglutamylation, polyglycylation, etc. (Carmona *et al.*, 2023). Tyrosination, acetylation, phosphorylation, polyglutamylation, poly-glycylation, and transamidation, as well as reversed reactions, are all reported in plant systems especially the angiosperms and gymnosperms (Wloga *et al.*, 2017). This diversification of the evolutionarily conserved tubulin is summed up under the umbrella term “tubulin code”. However, the reasons for its existence and its functions are still unclear and need further investigation. These highly specific PTMs are expected to be capable of affecting the stability of microtubules, their biophysical properties, and the kind of surfaces they can interact with. However, their effects seem to be highly understated in the short term as their role seems clearer in complex, long-term cellular functions and homeostasis, which has been difficult to establish (Janke and Mageira, 2020).

Tyrosination is the most common PTM in all higher plants (MacRae *et al.*, 1997). Tyrosine is the last C-terminal amino acid in tubulins and is highly conserved. The removal of this residue

by carboxypeptidases results in stable and long-lived MTs, whereas tyrosinated MTs indicate that the MT is relatively new (Aström *et al.*, 1992; Smertenko *et al.*, 1997). The presence of detyrosinated tubulin is restricted to specific tissues. Auxin deficiency also causes tubulin detyrosination, most likely via a tubulin tyrosine carboxypeptidase activation, influencing tubulin isoform accumulation (Wiesler *et al.*, 2002). Certain glutamic residues within the tail domains undergo poly-modifications like polyglutamylation, which are added onto their γ -carboxyl groups to create peptide side chains of glutamate or glycine (Dijk *et al.*, 2007). Tyrosination and polyglutamylation occur with the help of enzymes belonging to the Tubulin Tyrosine Ligase Like (TTLL) family, which are also involved in other PTMs, such as polyglycylation. They have a Tubulin Tyrosine Ligase (TTL) domain that is conserved (pfam3033). In addition, the TTL domain has a conserved extension in TTLLs. According to recent findings, there are 14 members of the TTLL enzyme family in mammals (Janke *et al.*, 2005; Dijk *et al.*, 2007). Several reports also confer that TTL and TTLL have various roles in the mouse model system. It is observed that in mice, TTL is the key enzyme involved in tyrosination (MacRae, 1997). Moreover, TTLL1, TTLL4, TTLL5, TTLL6, TTLL7, TTLL9, TTLL11 and TTLL13 are involved in polyglutamylation (Gardiner, 2019). Generally, acetylation is considered a marker for the stability of proteins (Ali *et al.*, 2018). In the case of acetylation of Lys-40 residue in alpha-tubulin, proteins like Alpha tubulin N-acetyl transferase (ATAT) and MEC-17 play a major role. Earlier findings confirm that the homologs of MEC-17 are present in most of the eukaryotes except for fungi and plants (Akella *et al.*, 2010).

It has been observed that MTs, along with MAPs and motor proteins, require PTMs triggered by hormonal signals, internal or external stimuli, and developmental stages to perform a specific function (Smertenko *et al.*, 2004; Del Duca *et al.*, 2009). These external stimuli induce ROS formation, followed by an increase in the endogenous calcium ion (Ca^{2+}) in the cell. MT remodeling occurs due to the activation of different MAP kinase signaling pathways that induce several transcription enzymes regulating PTMs (Livanos *et al.*, 2014). The cytoskeleton in

plants acts as a 'low-temperature sensor' (Mazars *et al.*, 1997; Abdrakhamanova *et al.*, 2003). The characteristic feature of plant cellular mechanics is the transmission of an extracellular signal from the cell wall to the plasma membrane and then to the cytoskeleton (Akashi, *et al.*, 1990; Nguema-Ona *et al.*, 2007). Cold stress causes a decrease in membrane fluidity, which causes MT disassembly and reorganization using cell wall proteins such as xyloglycans (Akashi, *et al.*, 1990; Takeda *et al.*, 2002). MT activity mediates Ca^{2+} channel activation, resulting in a transient increase in intracellular Ca^{2+} levels, triggering downstream signaling events and the expression of cold-induced genes, but the relationship is complex, as Ca^{2+} influx induces MT depolymerization (Mazars *et al.*, 1997; Breviario *et al.*, 2000). MAPKs, which phosphorylate either tubulin or MAPs during cold acclimation, also influence cortical MT organization.

Among all the previously identified tubulin PTMs, four PTMs are known to be evolutionarily conserved from protists to humans. These are detyrosination, acetylation, polyglutamylation, and polyglycylation (Joachimciak *et al.*, 2023). However, a similar comprehensive statement cannot be made about the plant kingdom. Reports of various tubulin PTMs in plants are inconsistent, especially in lower plants (mosses, liverworts, hornworts, and ferns), which act as a vital link between protists and higher plants (angiosperms and gymnosperms). Here, using *Physcomitrella patens*, a lower plant lacking GIGANTEA which is an important circadian clock component, we tried to address the functional significance of microtubule dynamics on exposure to temperature stress and varying calcium concentrations. Previous data from our lab shows the presence and distribution of tubulin PTMs in *P. patens* by western blotting. Nuclear-cytoplasmic partitioning of proteins present in protonemal cells of *P. patens* grown in an increasing concentration of calcium at 25 °C was performed. Acetylated, polyglutamylated and tyrosinated tubulin was detected using western blotting. This evidence shows that all three PTMs of tubulin occur in *P. patens* (Figure 100, Annexure 2). The abundance of polyglutamylated and tyrosinated tubulin was higher than the acetylated tubulin in *P. patens*.

It was also seen that these tubulin modifications showed a major dynamic in its distribution between particulate (nuclear) and soluble (cytoplasmic) fractions. These previous data from our lab convincingly suggested that functional post-translationally modified tubulins are present in *P. patens* (Annexure 2).

This gave us a clue for the presence of enzymes responsible for post-translational modifications of tubulin in *P. patens*. Therefore, *In-silco* analysis approach was used to identify the enzymes that are present in *P. patens*. The Insilco approach shows that enzymes like TTLLs, ATAT, and ELP3 involved in post-translational tubulin modifications (tyrosination, acetylation, and polyglutamylation) are present in *P. patens*. Further, we show the presence and distribution of post-translational tubulin modifications and demonstrate the changes in microtubule dynamics due to calcium in *P. patens*. We also show that the flux of endogenous calcium in the cells varies significantly with respect to varying temperatures and exogenous calcium concentrations. Our results demonstrate that increasing calcium concentration decreases the abundance of modified tubulin in cold stress, whereas it varies significantly under heat stress. In conclusion, we find the moss model to be an amazing system for understanding microtubule modification and orientation in stress adaptation. This study is of practical relevance, as it can prevent temperature-induced damage in different crops, contributing to improved modern agricultural practices.

6.2. RESULT

6.2.1. Post-translational modifications of tubulin are likely to occur in *Physcomitrella patens*

Tubulin PTMs such as acetylation, polyglutamylation, and tyrosination have been associated with the stability and dynamic nature of microtubules in eukaryotes. However, little is known about tubulin PTMs in lower plants, such as bryophytes. we investigated the presence of enzymes responsible for catalyzing post-translational modifications of tubulin in plants. The schematic representation of the methodology used in the search process for homologs of enzymes involved in PTMs in *P. patens* and the schematic diagram summarizing the conclusions from the *in-silco* search are shown in Figure 81A & 81B. The organisms used for this *in-silco* approach along with the best hits, max score, total score, query cover, E value and percent identity are summarised in Table 9.

Mouse To <i>Tetrahymena</i>								
Accession Number	no. of hits	Max Score	Total Score	Query Cover	E value	Percent Identity	Accession Length	Best hit
NP_081468.1	43	144	144	0.5	2E-37	0.3756	1559	XP_001007746.2
NP_001344882.1	48	447	447	0.9	3E-156	0.5438	413	XP_001019702.2
NP_849200.2	48	447	447	0.9	3E-156	0.5438	413	XP_001019702.2
NP_001091737.1	53	216	216	0.58	4E-62	0.3584	672	XP_001022009.2
NP_001401283.1	53	216	216	0.58	4E-62	0.3584	672	XP_001022009.2
XP_011244476.1	53	216	216	0.58	4E-62	0.3584	672	XP_001022009.2
XP_011244473.1	53	216	216	0.58	4E-62	0.3584	672	XP_001022009.2
NP_001014974.1	46	290	290	0.46	3E-85	0.331	598	XP_001025259.3
XP_006496287.1	47	290	290	0.46	3E-85	0.331	598	XP_001025259.3
XP_006496288.1	46	290	290	0.46	3E-85	0.331	598	XP_001025259.3
NP_001074892.2	52	321	321	0.32	3E-95	0.3977	672	XP_001022009.2
NP_001334324.1	52	320	320	0.33	4E-95	0.3977	672	XP_001022009.2
NP_001351553.1	52	321	321	0.32	3E-95	0.3977	672	XP_001022009.2

NP_001351554.1	52	320	320	0.33	4E-95	0.3977	672	XP_0010220 09.2
NP_001351555.1	52	321	321	0.34	2E-95	0.3977	672	XP_0010220 09.2
NP_001351556.1	52	308	308	0.35	2E-91	0.4062	672	XP_0010220 09.2
NP_001351557.1	51	225	225	0.26	8E-63	0.4098	598	XP_0010252 59.3
XP_006516052.1	52	321	321	0.32	4E-95	0.3977	672	XP_0010220 09.2
XP_030102634.1	52	321	321	0.32	3E-95	0.3977	672	XP_0010220 09.2
XP_036013391.1	52	320	320	0.33	3E-95	0.3977	672	XP_0010220 09.2
XP_006516058.1	52	320	320	0.33	5E-95	0.3977	672	XP_0010220 09.2
XP_006516059.1	52	320	320	0.33	4E-95	0.3977	672	XP_0010220 09.2
XP_006516055.1	52	321	321	0.32	4E-95	0.3977	672	XP_0010220 09.2
XP_017170598.1	52	320	320	0.33	4E-95	0.3977	672	XP_0010220 09.2
XP_017170599.1	52	320	320	0.34	3E-95	0.3977	672	XP_0010220 09.2
XP_006516057.1	52	321	321	0.32	4E-95	0.3977	672	XP_0010220 09.2
XP_036013393.1	52	320	320	0.33	3E-95	0.3977	672	XP_0010220 09.2
XP_006516053.1	52	321	321	0.32	4E-95	0.3977	672	XP_0010220 09.2
XP_036013388.1	52	321	321	0.32	4E-95	0.3977	672	XP_0010220 09.2
XP_030102633.1	52	321	321	0.32	3E-95	0.3977	672	XP_0010220 09.2
XP_036013389.1	52	321	321	0.32	3E-95	0.3977	672	XP_0010220 09.2
XP_036013394.1	52	318	318	0.61	8E-99	0.3918	672	XP_0010220 09.2
XP_017170603.1	52	318	318	0.76	2E-100	0.3918	672	XP_0010220 09.2
XP_006516062.1	52	308	308	0.33	4E-91	0.4062	672	XP_0010220 09.2
XP_030102635.1	51	225	225	0.26	9E-63	0.4098	598	XP_0010252 59.3
XP_017170601.1	51	225	225	0.26	9E-63	0.4098	598	XP_0010252 59.3
XP_006516054.1	52	321	321	0.32	4E-95	0.3977	672	XP_0010220 09.2
XP_036013390.1	52	321	321	0.32	3E-95	0.3977	672	XP_0010220 09.2
XP_006516064.1	31	93.2	93.2	0.16	4E-19	0.3571	672	XP_0010220 09.2
NP_766387.2	43	377	377	0.47	1E-114	0.4324	1195	XP_0010182 57.2
XP_017170020.1	40	355	355	0.47	4E-108	0.4594	1195	XP_0010182 57.2
XP_017170021.1	42	351	351	0.72	8E-110	0.4594	1195	XP_0010182 57.2
NP_001289886.1	47	334	334	0.46	2E-98	0.4005	1195	XP_0010182 57.2
NP_001289887.1	47	337	337	0.69	2E-102	0.4005	1195	XP_0010182 57.2

NP_001344146.1	47	335	335	0.47	8E-99	0.4005	1195	XP_0010182 57.2
XP_036019207.1	47	334	334	0.48	9E-99	0.4005	1195	XP_0010182 57.2
XP_036019208.1	47	335	335	0.49	4E-99	0.4005	1195	XP_0010182 57.2
XP_036019205.1	47	335	335	0.46	1E-98	0.4005	1195	XP_0010182 57.2
XP_036019206.1	47	335	335	0.47	5E-99	0.4005	1195	XP_0010182 57.2
NP_084050.1	43	246	246	0.45	9E-69	0.4053	1451	XP_0014708 95.2
XP_036018534.1	43	244	244	0.47	2E-68	0.4072	1451	XP_0014708 95.2
NP_898838.2	13	278	278	0.74	6E-83	0.3434	818	XP_0010202 06.1
NP_001382944.1	38	379	379	0.51	1E-115	0.4132	1195	XP_0010182 57.2
NP_808433.2	38	380	380	0.52	3E-116	0.4203	1195	XP_0010182 57.2
XP_006540988.2	38	374	374	0.52	3E-114	0.4279	1195	XP_0010182 57.2
XP_030098479.1	38	374	374	0.52	3E-114	0.4279	1195	XP_0010182 57.2
XP_030098481.1	38	373	373	0.55	1E-114	0.4279	1195	XP_0010182 57.2
XP_006540977.1	38	375	375	0.47	5E-114	0.4279	1195	XP_0010182 57.2
XP_006540978.1	38	375	375	0.47	5E-114	0.4279	1195	XP_0010182 57.2
XP_006540976.1	38	375	375	0.47	5E-114	0.4279	1195	XP_0010182 57.2
XP_006540981.1	38	376	376	0.47	2E-114	0.4356	1195	XP_0010182 57.2
XP_006540983.1	38	375	375	0.52	4E-115	0.4279	1195	XP_0010182 57.2
XP_006540984.1	38	375	375	0.52	4E-115	0.4279	1195	XP_0010182 57.2
XP_006540979.1	38	375	375	0.47	4E-114	0.4279	1195	XP_0010182 57.2
XP_036009035.1	38	376	376	0.47	2E-114	0.4332	1195	XP_0010182 57.2
XP_030098480.1	38	375	375	0.53	4E-115	0.4279	1195	XP_0010182 57.2
XP_006540980.1	38	379	379	0.51	1E-115	0.4155	1195	XP_0010182 57.2
XP_006540985.1	38	374	374	0.53	1E-114	0.4279	1195	XP_0010182 57.2
XP_017177782.1	38	373	373	0.55	1E-114	0.4279	1195	XP_0010182 57.2
NP_001077087.1	50	376	376	0.92	2E-124	0.4329	648	XP_0010315 61.2
NP_001342646.1	50	263	313	0.88	1E-81	0.4508	648	XP_0010315 61.2
NP_001342648.1	50	275	325	0.91	3E-86	0.457	648	XP_0010315 61.2
NP_001342649.1	50	315	315	0.94	2E-102	0.4466	648	XP_0010315 61.2
NP_083340.2	50	365	365	0.9	4E-120	0.4282	648	XP_0010315 61.2
XP_030108020.1	50	315	315	0.94	2E-102	0.4466	648	XP_0010315 61.2

XP_030108016.1	50	353	353	0.95	4E-116	0.4245	648	XP_0010315 61.2
XP_030108013.1	50	364	364	0.92	7E-120	0.4282	648	XP_0010315 61.2
XP_030108015.1	50	353	353	0.95	4E-116	0.4245	648	XP_0010315 61.2
XP_030108021.1	50	274	314	0.97	2E-86	0.457	648	XP_0010315 61.2
XP_030108018.1	50	365	365	0.97	1E-120	0.4292	648	XP_0010315 61.2
XP_030108017.1	50	353	353	0.95	4E-116	0.4245	648	XP_0010315 61.2
XP_030108012.1	50	364	364	0.9	1E-119	0.4282	648	XP_0010315 61.2
XP_006500383.1	50	327	327	0.97	6E-107	0.4518	648	XP_0010315 61.2
XP_030108014.1	50	375	375	0.94	3E-124	0.4329	648	XP_0010315 61.2
XP_030108019.1	50	365	365	0.97	1E-120	0.4292	648	XP_0010315 61.2
NP_001136216.1	1	146	146	0.58	1E-39	0.3472	399	XP_0010104 76.2
NP_001136217.1	1	146	146	0.73	1E-40	0.3472	399	XP_0010104 76.2
NP_001334307.1	1	143	143	0.47	1E-38	0.4072	399	XP_0010104 76.2
NP_001344794.1	1	147	147	0.69	2E-40	0.3472	399	XP_0010104 76.2
NP_082752.3	1	143	143	0.61	1E-39	0.4072	399	XP_0010104 76.2
XP_036016697.1	1	147	147	0.69	2E-40	0.3472	399	XP_0010104 76.2
XP_036016698.1	1	143	143	0.63	1E-39	0.4072	399	XP_0010104 76.2
NP_001240741.1	1	843	843	0.95	0	0.6998	569	XP_0010324 26.3
NP_083087.1	1	843	843	0.99	0	0.6947	569	XP_0010324 26.3
<i>Tetrahymena To Chlamydomonas</i>								
XP_001007746.2	11	141	141	0.11	2E-33	0.3717	1424	XP_0016956 18.2
XP_001019702.2	14	367	367	0.93	5E-123	0.4345	564	XP_0429276 29.1
XP_001022009.2	14	233	233	0.47	5E-65	0.3879	1613	XP_0429277 06.1
XP_001025259.3	12	232	232	0.56	3E-65	0.3618	1613	XP_0429277 06.1
XP_001018257.2	14	303	303	0.33	1E-84	0.3675	1613	XP_0429277 06.1
XP_001031561.2	14	409	409	0.61	2E-137	0.4842	433	XP_0429143 48.1
XP_001470895.2	12	262	262	0.25	3E-71	0.317	1312	XP_0429288 65.1
XP_001020206.1	4	57.4	57.4	0.28	2E-08	0.2319	427	BAI67941.1
XP_001018257.2	14	303	303	0.33	1E-84	0.3675	1613	XP_0429277 06.1
XP_001031561.2	14	409	409	0.61	2E-137	0.4842	433	XP_0429143 48.1
XP_001026474.2	14	300	300	0.45	3E-85	0.3588	1613	XP_0429277 06.1

XP_001010476.2	1	171	171	0.36	3E-47	0.5203	639	XP_042923011.1
XP_001032426.3	1	827	827	0.93	0	0.7039	649	XP_042923189.1
<i>Chlamydomonas To Physcomitrella patens</i>								
XP_001695618.2	21	122	122	0.16	5E-29	0.3106	443	XP_024394497.1
XP_042927629.1	19	316	316	0.7	7E-101	0.3995	549	XP_024394465.1
XP_042927706.1	19	376	376	0.31	2E-114	0.4087	629	XP_024377741.1
XP_042914348.1	21	436	436	0.92	1E-149	0.5201	549	XP_024394465.1
XP_042928865.1	19	271	271	0.32	6E-80	0.3471	448	XP_024377747.1
BAI67941.1	21	435	435	0.93	4E-149	0.5167	549	XP_024394465.1
XP_042923011.1	2	149	149	0.25	7E-39	0.4438	450	XP_024381641.1
XP_042923189.1	3	881	881	0.84	0	0.777	569	XP_024403246.1
<i>Tetrahymena To Physcomitrella patens</i>								
XP_001007746.2	21	105	105	0.11	9E-23	0.3125	532	XP_024394484.1
XP_001019702.2	21	295	295	0.96	6E-95	0.4005	549	XP_024394465.1
XP_001022009.2	21	228	228	0.48	1E-67	0.3701	416	XP_024377750.1
XP_001025259.3	19	223	223	0.56	1E-66	0.3761	403	PNR53094.1
XP_001018257.2	19	320	320	0.38	6E-96	0.375	629	XP_024377741.1
XP_001031561.2	19	410	410	0.6	4E-136	0.4817	549	XP_024394465.1
XP_001470895.2	21	262	262	0.29	2E-74	0.3573	646	XP_024377740.1
XP_001020206.1	8	427	427	0.97	5E-137	0.3052	857	XP_024379358.1
XP_001018257.2	19	320	320	0.38	6E-96	0.375	629	XP_024377741.1
XP_001031561.2	19	410	410	0.6	4E-136	0.4817	549	XP_024394465.1
XP_001026474.2	19	327	327	0.48	5E-100	0.39	646	XP_024377740.1
the presence of a ttl13-like (XP_024377742.1) is also noted in NCBI(from TTLL6 gene) but not in phytozome								
XP_001010476.2		149	149	0.38	2E-40	0.4843	450	XP_024381641.1
XP_001032426.3		852	852	0.96	0	0.7094	569	XP_024403246.1

Table 9. ID numbers, best hit, max score, total score, query cover, E value, and percent identity of organisms used in the phylogenetic tree construction of ELP3, TTLL6, TTLL9, TTLL12, and ATAT.

In mammals, 14 enzymes have been identified which belong to the TTLL family (i.e., TTL and TTLLs). These enzymes have a conserved TTL domain and are involved in several PTMs, including tyrosination and polyglutamylation. Besides, TTLLs have a conserved extension to the TTL domain. In *Mus musculus*, TTL is responsible for tyrosination, while along with the

other reported (Ruse *et al.*, 2022) TTLLs like TTLL1, TTLL4, TTLL5, TTLL6, TTLL7, TTLL9, TLL11, and TTLL13, TTLL2 might also be involved in polyglutamylation as per data extracted from Uniport database. Moreover, TTLL12 is involved in regulating several PTMs, such as tyrosination-detyrosination and polyglutamylation. From the BLASTP searches, out of 14 TTLL proteins present in mammals, three TTLLs (Table 9) were found in lower plants, i.e., *P. patens*, which were sparsely characterized in different databases like Phytozome 13, NCBI, and UniProt. The cladogram suggests that homologs of TTLL12 are widely distributed throughout the plant kingdom and eukaryotes (Janke *et al.*, 2005) except in algae (Figure 75C). Surprisingly, homologs of TTLL6 and TTLL9 were found in the lower plants (e.g., *P. patens*) and algae (e.g., *Dunaliella salina*) but not in higher plants (Figure 75D & 75E).

Similarly, ATAT (alpha-tubulin acetyltransferase1) is known to acetylated tubulin at the Lys-40 residue in mammals. The BLASTP searches of ATAT from *Mus musculus* yielded an ATAT homolog in *P. patens* (Table 10). Further, the Alpha-tubulin acetyltransferase (ATAT) protein was found to be absent in higher plants but present in lower plants like *P. patens* (Figure 80F). In higher plants that seem to lack the ATAT homolog, Elongator Protein 3 (ELP3) emerges as a key player in acetylating multiple substrates and might become the perfect candidate for the function of ATAT, contributing significantly to plant cellular processes. ELP3 is a pleiotropic protein that is involved in histone acetylation and transcriptional elongation among other functions (Creppe *et al.*, 2009; Pereira *et al.*, 2018). It is present in lower as well as higher plants like *Physcomitrella patens*, *Marchantia polymorpha*, *Arabidopsis thaliana*, *Glycine max*, and *Solanum tuberosum* (Figure 75G).

Our results illustrate the relatedness among various plant species, where a range of enzymes is responsible for PTMs of tubulin, such as tyrosination, acetylation, and polyglutamylation, which indicates their occurrence in *Physcomitrella patens* as well.

Name of the protein	Protein IDs derived from PHYTOZOME
ATAT	<i>P. patens</i> v3.3 Pp3c1_13990V3.1.p
ELP3	<i>P. patens</i> v3.3 Pp3c18_6090V3.1.p
TTLL6	<i>P. patens</i> v3.3 Pp3c6_25370V3.1.p
TTLL9	<i>P. patens</i> v3.3 Pp3c1_16240V3.1.p
TTLL12	<i>P. patens</i> v3.3 Pp3c6_19960V3.1.p

Table 10. List of proteins identified in PHYTOZOME and sorted in alphabetical order by protein name.

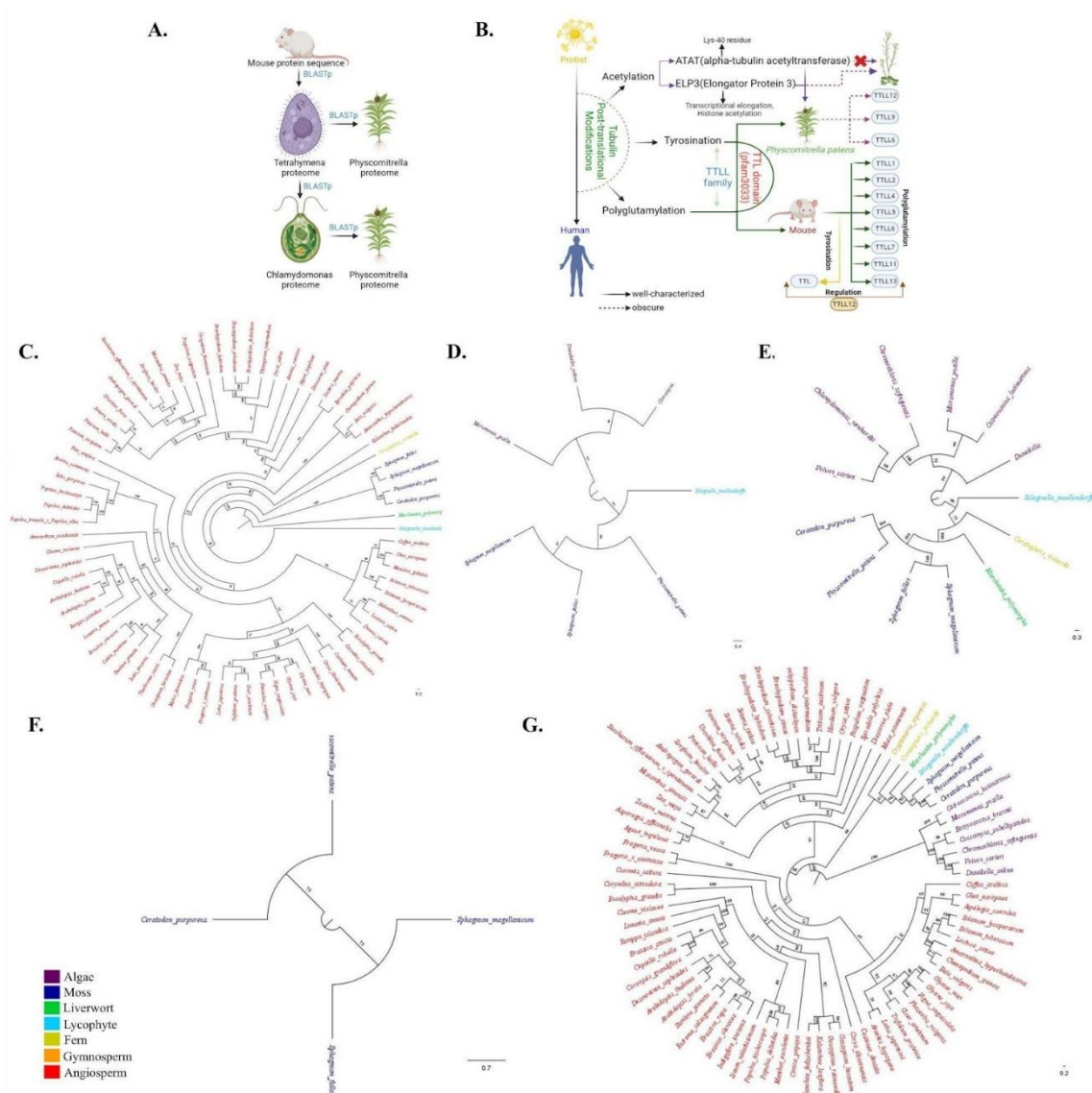


Figure 75. *In-silico* analysis of enzymes involved in PTMs of tubulin in *P. patens*. Schematic diagram representing the methodology of the search process for homologs of enzymes involved in PTMs in *P. patens* (A), Schematic diagram summarizing the conclusions from the *in-silico* search (B), Cladograms of TTLL12 (C), TTLL6 (D), TTLL9 (E), ATAT (F), and ELP3 (G)

6.2.2. Validation of the presence of post-translational modifications of tubulin in *Physcomitrella patens*.

Further, to validate the presence of PTMS of tubulin in the cytoplasmic and nucleoplasmic regions at the cellular level, super-resolution microscopy was performed. The super-resolution microscopy showed that the post-translational modifications of tubulin are present in the cytoplasm as well as the nucleus of the cell (Figure 76).

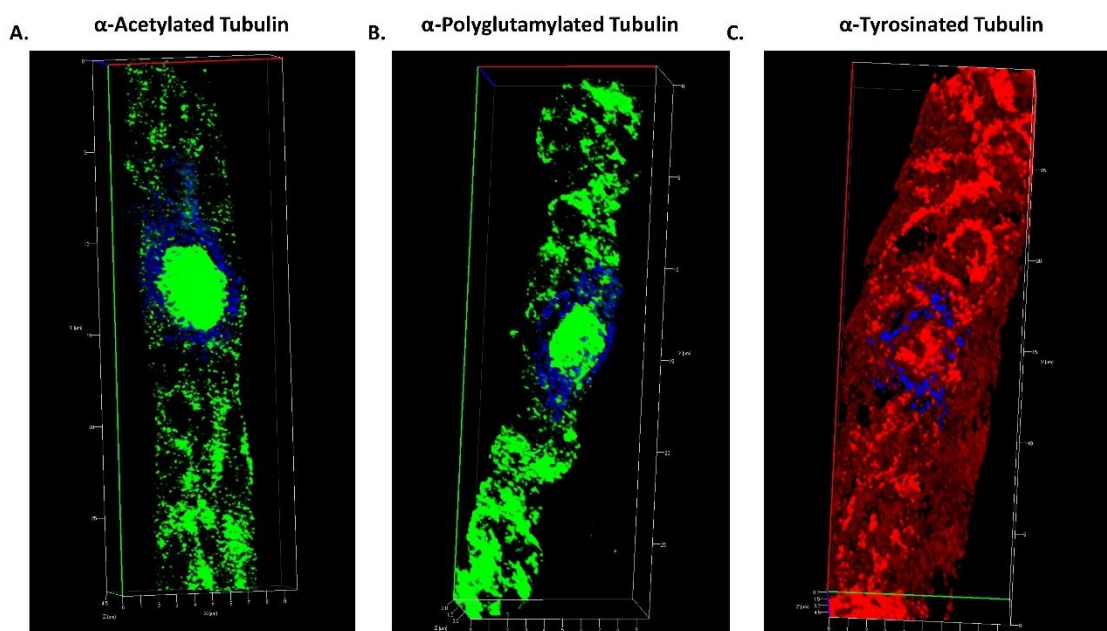


Figure 76. Presence of post-translationally modified tubulins in *P. patens* at the cellular level. Shown are the super resolution images of 7-d old protonema cells of *P. patens* and double immunostained for acetylated/ DAPI (A, Green/ Blue), polyglutamylated/ DAPI (B, Green/ Blue) and tyrosinated tubulin/ DAPI (C, Red/ Blue). The experiment was conducted three times with different biological replicates.

6.2.3. Light-dependent post-translation modifications in *Physcomitrella patens*.

Light plays an important role in the growth and development of plants. Insilco analysis of tubulin modifying enzymes in *P. patens* by PLANTCARE web server showed the presence of light responsive elements (31 in ELP3, 15 in ATAT, 13 in TTLL6, 36 in TTLL9 and 44 in TTLL12) indicating that light might have a role in modulating PTMs of tubulin (Table 11). To check the effect of light, *P. patens* protonema cultures were grown and treated under four different light conditions, i.e., white, red, far-red, and blue, for 7 days at 25 °C. The intensity of tyrosinated (Figure 77A) and acetylated (Figure 77B) tubulin were non-significant under

red, far-red, and blue as compared to white light (Figure 77B & 77D). Meanwhile, the intensity of polyglutamylated tubulin is increased 2.9-fold under red-light treatment and increased 3.3-fold when treated with far-red light (Figure 77E & 77F) in comparison to white light. However, there is no significant effect in polyglutamylated tubulin upon blue light treatment (Figure 77E & 77F).

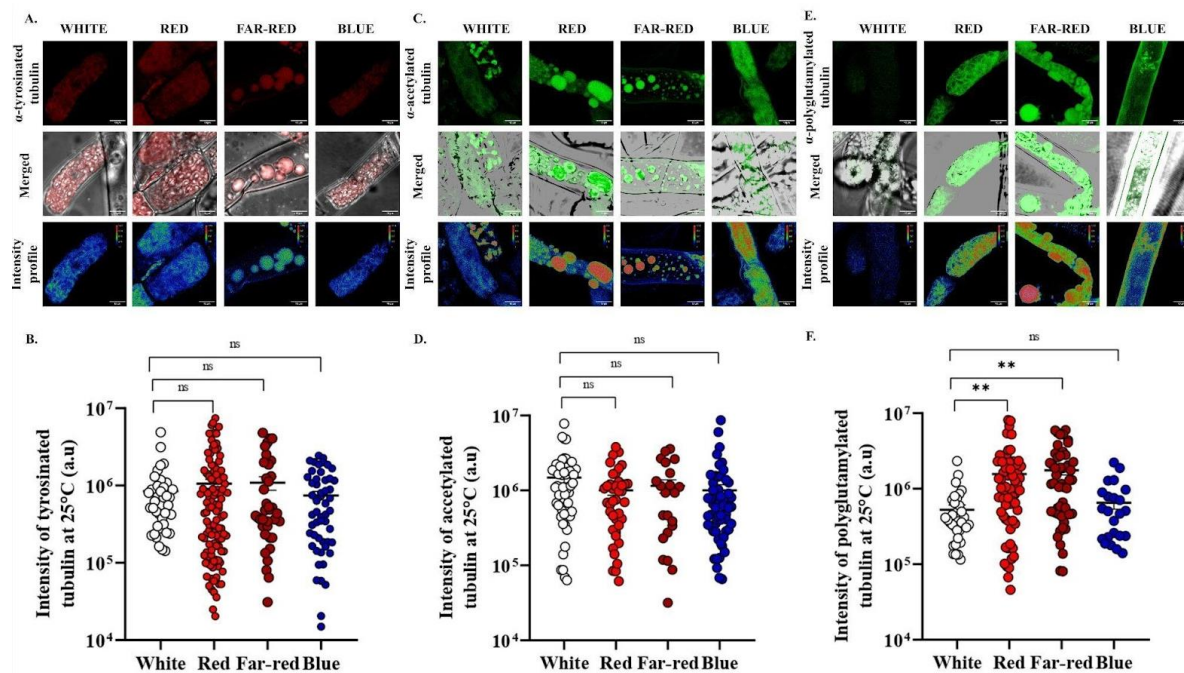


Figure 77. Effect of different lights on the post-translationally modified tubulins in *P. patens*. Concurrent confocal images of 7-d old protonemal culture of *Physcomitrella patens* treated with white, red, far-red, and blue light conditions at 25 °C. Representative immunofluorescence images and graphical representation of tyrosinated (A, B), acetylated (C, D), and polyglutamylated (E, F) tubulin modifications. The experiments were performed three times with different biological replicates. Scale bar- 10 μ m. Values in the graphs are expressed as mean \pm SE. Two-way analysis of variance (ANOVA) using Tukey's multiple comparisons test was performed with the help of GraphPad Prism to test for significance among the dataset, **p < 0.01, ns- non-significant.

Site Name	Organism	Position	Strand	Matrix Score	Sequence	Function
ATAT						
ABRE	<i>Arabidopsis thaliana</i>	372	+	6	CACGTG	cis-acting element involved in the abscisic acid responsiveness
ABRE	<i>Arabidopsis thaliana</i>	2882	+	5	ACGTG	cis-acting element involved in the abscisic acid responsiveness
ABRE	<i>Arabidopsis thaliana</i>	677	-	5	ACGTG	cis-acting element involved in the abscisic acid responsiveness

ABRE	<i>Arabidopsis thaliana</i>	4364	+	7	AACCCGG	cis-acting element involved in the abscisic acid responsiveness
ABRE	<i>Arabidopsis thaliana</i>	373	+	5	ACGTG	cis-acting element involved in the abscisic acid responsiveness
ABRE	<i>Arabidopsis thaliana</i>	4092	+	7	AACCCGG	cis-acting element involved in the abscisic acid responsiveness
ABRE	<i>Arabidopsis thaliana</i>	1664	-	5	ACGTG	cis-acting element involved in the abscisic acid responsiveness
AE-box	<i>Arabidopsis thaliana</i>	3507	+	8	AGAAACAA	part of a module for light response
ATCT-motif	<i>Pisum sativum</i>	2337	-	9	AATCTAATCC	part of a conserved DNA module involved in light responsiveness
AuxRR-core	<i>Nicotiana tabacum</i>	3043	+	7	GGTCCAT	cis-acting regulatory element involved in auxin responsiveness
Box 4	<i>Petroselinum crispum</i>	4619	-	6	ATTAAT	part of a conserved DNA module involved in light responsiveness
CGTCA-motif	<i>Hordeum vulgare</i>	679	+	5	CGTCA	cis-acting regulatory element involved in the MeJA-responsiveness
CGTCA-motif	<i>Hordeum vulgare</i>	4099	+	5	CGTCA	cis-acting regulatory element involved in the MeJA-responsiveness
CGTCA-motif	<i>Hordeum vulgare</i>	2012	-	5	CGTCA	cis-acting regulatory element involved in the MeJA-responsiveness
CGTCA-motif	<i>Hordeum vulgare</i>	4954	-	5	CGTCA	cis-acting regulatory element involved in the MeJA-responsiveness
CGTCA-motif	<i>Hordeum vulgare</i>	1789	+	5	CGTCA	cis-acting regulatory element involved in the MeJA-responsiveness
CGTCA-motif	<i>Hordeum vulgare</i>	4899	-	5	CGTCA	cis-acting regulatory element involved in the MeJA-responsiveness
CGTCA-motif	<i>Hordeum vulgare</i>	3549	+	5	CGTCA	cis-acting regulatory element involved in

						the MeJA-responsiveness
G-Box	<i>Pisum sativum</i>	372	+	6	CACGTG	cis-acting regulatory element involved in light responsiveness
G-Box	<i>Pisum sativum</i>	1664	+	6	CACGTT	cis-acting regulatory element involved in light responsiveness
G-box	<i>Arabidopsis thaliana</i>	372	+	6	CACGTG	cis-acting regulatory element involved in light responsiveness
G-box	<i>Nicotiana plumbaginifolia</i>	2228	-	10	CAGACGTGGCA	cis-acting regulatory element involved in light responsiveness
G-box	<i>Zea mays</i>	677	+	6	CACGTC	cis-acting regulatory element involved in light responsiveness
G-box	<i>Zea mays</i>	4236	+	6	CACGAC	cis-acting regulatory element involved in light responsiveness
G-box	<i>Zea mays</i>	481	-	6	CACGAC	cis-acting regulatory element involved in light responsiveness
G-box	<i>Arabidopsis thaliana</i>	2881	+	6	TACGTG	cis-acting regulatory element involved in light responsiveness
G-box	<i>Zea mays</i>	1020	-	6	CACGAC	cis-acting regulatory element involved in light responsiveness
G-box	<i>Zea mays</i>	4303	-	6	CACGAC	cis-acting regulatory element involved in light responsiveness
GARE-motif	<i>Brassica oleracea</i>	4395	+	7	TCTGTTG	gibberellin-responsive element
GATA-motif	<i>Solanum tuberosum</i>	3617	+	9	AAGGATAAGG	part of a light responsive element
LTR	<i>Hordeum vulgare</i>	514	+	6	CCGAAA	cis-acting element involved in low-temperature responsiveness
LTR	<i>Hordeum vulgare</i>	3476	+	6	CCGAAA	cis-acting element involved in low-temperature responsiveness
LTR	<i>Hordeum vulgare</i>	2271	-	6	CCGAAA	cis-acting element involved in low-temperature responsiveness
LTR	<i>Hordeum vulgare</i>	4049	+	6	CCGAAA	cis-acting element involved in low-temperature responsiveness
P-box	<i>Oryza sativa</i>	4286	-	7	CCTTTTG	gibberellin-responsive element
Sp1	<i>Oryza sativa</i>	4677	+	6	GGGCGG	light responsive element

TC-rich repeats	<i>Nicotiana tabacum</i>	2474	-	9	GTTTTCTTAC	cis-acting element involved in defense and stress responsiveness
TCA-element	<i>Nicotiana tabacum</i>	303	-	9	CCATCTTTTT	cis-acting element involved in salicylic acid responsiveness
TGA-element	<i>Brassica oleracea</i>	3404	+	6	AACGAC	auxin-responsive element
TGA-element	<i>Brassica oleracea</i>	4412	+	6	AACGAC	auxin-responsive element
TGA-element	<i>Brassica oleracea</i>	3581	+	6	AACGAC	auxin-responsive element
TGACG-motif	<i>Hordeum vulgare</i>	679	-	5	TGACG	cis-acting regulatory element involved in the MeJA-responsiveness
TGACG-motif	<i>Hordeum vulgare</i>	4099	-	5	TGACG	cis-acting regulatory element involved in the MeJA-responsiveness
TGACG-motif	<i>Hordeum vulgare</i>	2012	+	5	TGACG	cis-acting regulatory element involved in the MeJA-responsiveness
TGACG-motif	<i>Hordeum vulgare</i>	4954	+	5	TGACG	cis-acting regulatory element involved in the MeJA-responsiveness
TGACG-motif	<i>Hordeum vulgare</i>	1789	-	5	TGACG	cis-acting regulatory element involved in the MeJA-responsiveness
TGACG-motif	<i>Hordeum vulgare</i>	4899	+	5	TGACG	cis-acting regulatory element involved in the MeJA-responsiveness
TGACG-motif	<i>Hordeum vulgare</i>	3549	-	5	TGACG	cis-acting regulatory element involved in the MeJA-responsiveness
ELP3						
ABRE	<i>Arabidopsis thaliana</i>	1522	+	6	CACGTG	cis-acting element involved in the abscisic acid responsiveness
ABRE	<i>Arabidopsis thaliana</i>	3843	+	5	ACGTG	cis-acting element involved in the abscisic acid responsiveness
ABRE	<i>Arabidopsis thaliana</i>	2743	+	5	ACGTG	cis-acting element involved in the abscisic acid responsiveness
ABRE	<i>Arabidopsis thaliana</i>	1523	+	5	ACGTG	cis-acting element involved in the

						abscisic acid responsiveness
ABRE	<i>Arabidopsis thaliana</i>	3243	+	5	ACGTG	cis-acting element involved in the abscisic acid responsiveness
ACE	<i>Petroselinum crispum</i>	5673	-	9	GCGACGTACC	cis-acting element involved in light responsiveness
AE-box	<i>Arabidopsis thaliana</i>	716	+	8	AGAAACAA	part of a module for light response
AE-box	<i>Arabidopsis thaliana</i>	6327	-	8	AGAAACAA	part of a module for light response
AE-box	<i>Arabidopsis thaliana</i>	1538	-	8	AGAAACAA	part of a module for light response
ATCT- motif	<i>Pisum sativum</i>	6071	+	9	AATCTAATCC	part of a conserved DNA module involved in light responsiveness
AuxRR- core	<i>Nicotiana tabacum</i>	5796	+	7	GGTCCAT	cis-acting regulatory element involved in auxin responsiveness
Box 4	<i>Petroselinum crispum</i>	123	+	6	ATTAAT	part of a conserved DNA module involved in light responsiveness
Box 4	<i>Petroselinum crispum</i>	419	+	6	ATTAAT	part of a conserved DNA module involved in light responsiveness
Box 4	<i>Petroselinum crispum</i>	230	+	6	ATTAAT	part of a conserved DNA module involved in light responsiveness
Box 4	<i>Petroselinum crispum</i>	795	+	6	ATTAAT	part of a conserved DNA module involved in light responsiveness
Box 4	<i>Petroselinum crispum</i>	154	+	6	ATTAAT	part of a conserved DNA module involved in light responsiveness
Box 4	<i>Petroselinum crispum</i>	624	+	6	ATTAAT	part of a conserved DNA module involved in light responsiveness
Box 4	<i>Petroselinum crispum</i>	291	+	6	ATTAAT	part of a conserved DNA module involved in light responsiveness
Box 4	<i>Petroselinum crispum</i>	4681	-	6	ATTAAT	part of a conserved DNA module involved in light responsiveness
CGTCA- motif	<i>Hordeum vulgare</i>	5965	-	5	CGTCA	cis-acting regulatory element involved in

						the MeJA-responsiveness
CGTCA-motif	<i>Hordeum vulgare</i>	4436	-	5	CGTCA	cis-acting regulatory element involved in the MeJA-responsiveness
CGTCA-motif	<i>Hordeum vulgare</i>	3792	-	5	CGTCA	cis-acting regulatory element involved in the MeJA-responsiveness
CGTCA-motif	<i>Hordeum vulgare</i>	3782	+	5	CGTCA	cis-acting regulatory element involved in the MeJA-responsiveness
CGTCA-motif	<i>Hordeum vulgare</i>	3241	-	5	CGTCA	cis-acting regulatory element involved in the MeJA-responsiveness
CGTCA-motif	<i>Hordeum vulgare</i>	2741	-	5	CGTCA	cis-acting regulatory element involved in the MeJA-responsiveness
CGTCA-motif	<i>Hordeum vulgare</i>	2569	-	5	CGTCA	cis-acting regulatory element involved in the MeJA-responsiveness
CGTCA-motif	<i>Hordeum vulgare</i>	2332	+	5	CGTCA	cis-acting regulatory element involved in the MeJA-responsiveness
G-Box	<i>Pisum sativum</i>	1522	+	6	CACGTG	cis-acting regulatory element involved in light responsiveness
G-box	<i>Arabidopsis thaliana</i>	1522	+	6	CACGTG	cis-acting regulatory element involved in light responsiveness
G-box	<i>Nicotiana glauca</i>	3840	+	10	CAGACGTGGCA	cis-acting regulatory element involved in light responsiveness
G-box	<i>Zea mays</i>	2742	-	6	CACGTC	cis-acting regulatory element involved in light responsiveness
G-box	<i>Brassica oleracea</i>	85	+	9	TAACACGTAG	cis-acting regulatory element involved in light responsiveness
G-box	<i>Zea mays</i>	3842	-	6	CACGTC	cis-acting regulatory element involved in light responsiveness
G-box	<i>Zea mays</i>	3242	-	6	CACGTC	cis-acting regulatory element involved in light responsiveness
GT1-motif	<i>Arabidopsis thaliana</i>	4609	+	6	GGTTAA	light responsive element
GT1-motif	<i>Avena sativa</i>	2926	+	7	GGTTAAT	light responsive element

GT1-motif	<i>Arabidopsis thaliana</i>	1619	-	6	GGTTAA	light responsive element
GT1-motif	<i>Avena sativa</i>	1618	-	7	GGTTAAT	light responsive element
GT1-motif	<i>Arabidopsis thaliana</i>	1101	+	6	GGTTAA	light responsive element
GT1-motif	<i>Arabidopsis thaliana</i>	1065	+	6	GGTTAA	light responsive element
I-box	<i>Larix laricina</i>	4648	+	9	GTATAAGGCC	part of a light responsive element
I-box	<i>Triticum aestivum</i>	2920	+	8	AGATAAGG	part of a light responsive element
LAMP-element	<i>Pisum sativum</i>	5024	+	8	CTTTATCA	part of a light responsive element
LTR	<i>Hordeum vulgare</i>	5237	-	6	CCGAAA	cis-acting element involved in low-temperature responsiveness
P-box	<i>Oryza sativa</i>	856	+	7	CCTTTTG	gibberellin-responsive element
TC-rich repeats	<i>Nicotiana tabacum</i>	273	-	9	ATTCTCTAAC	cis-acting element involved in defense and stress responsiveness
TC-rich repeats	<i>Nicotiana tabacum</i>	4598	+	9	GTTTTCTTAC	cis-acting element involved in defense and stress responsiveness
TCA-element	<i>Nicotiana tabacum</i>	2944	+	9	CCATCTTTTT	cis-acting element involved in salicylic acid responsiveness
TCCC-motif	<i>Spinacia oleracea</i>	2130	-	7	TCTCCCT	part of a light responsive element
TGA-box	<i>Glycine max</i>	3779	-	8	TGACGTAA	part of an auxin-responsive element
TGA-element	<i>Brassica oleracea</i>	6401	+	6	AACGAC	auxin-responsive element
TGA-element	<i>Brassica oleracea</i>	2762	+	6	AACGAC	auxin-responsive element
TGA-element	<i>Brassica oleracea</i>	2390	+	6	AACGAC	auxin-responsive element
TGACG-motif	<i>Hordeum vulgare</i>	3792	+	5	TGACG	cis-acting regulatory element involved in the MeJA-responsiveness
TGACG-motif	<i>Hordeum vulgare</i>	3241	+	5	TGACG	cis-acting regulatory element involved in the MeJA-responsiveness
TGACG-motif	<i>Hordeum vulgare</i>	2741	+	5	TGACG	cis-acting regulatory element involved in the MeJA-responsiveness
TGACG-motif	<i>Hordeum vulgare</i>	3782	-	5	TGACG	cis-acting regulatory element involved in

						the MeJA-responsiveness
TGACG-motif	<i>Hordeum vulgare</i>	2569	+	5	TGACG	cis-acting regulatory element involved in the MeJA-responsiveness
TGACG-motif	<i>Hordeum vulgare</i>	5965	+	5	TGACG	cis-acting regulatory element involved in the MeJA-responsiveness
TGACG-motif	<i>Hordeum vulgare</i>	2332	-	5	TGACG	cis-acting regulatory element involved in the MeJA-responsiveness
TGACG-motif	<i>Hordeum vulgare</i>	4436	+	5	TGACG	cis-acting regulatory element involved in the MeJA-responsiveness
chs-CMA2a	<i>Petroselinum crispum</i>	1270	-	8	TCACTTGA	part of a light responsive element
circadian	<i>Lycopersicon esculentum</i>	5366	-	9	CAAAGATATC	cis-acting regulatory element involved in circadian control
TTL6						
3-AF1 binding site	<i>Solanum tuberosum</i>	1864	+	10	TAAGAGAGGAA	light responsive element
ABRE	<i>Arabidopsis thaliana</i>	3607	-	5	ACGTG	cis-acting element involved in the abscisic acid responsiveness
ABRE	<i>Arabidopsis thaliana</i>	3167	+	5	ACGTG	cis-acting element involved in the abscisic acid responsiveness
ABRE	<i>Arabidopsis thaliana</i>	2048	+	5	ACGTG	cis-acting element involved in the abscisic acid responsiveness
Box 4	<i>Petroselinum crispum</i>	522	+	6	ATTAAT	part of a conserved DNA module involved in light responsiveness
Box 4	<i>Petroselinum crispum</i>	4232	-	6	ATTAAT	part of a conserved DNA module involved in light responsiveness
Box 4	<i>Petroselinum crispum</i>	2129	+	6	ATTAAT	part of a conserved DNA module involved in light responsiveness
Box 4	<i>Petroselinum crispum</i>	4260	-	6	ATTAAT	part of a conserved DNA module involved in light responsiveness
CGTCA-motif	<i>Hordeum vulgare</i>	4118	-	5	CGTCA	cis-acting regulatory element involved in

						the MeJA-responsiveness
G-Box	<i>Pisum sativum</i>	3607	+	6	CACGTT	cis-acting regulatory element involved in light responsiveness
G-box	<i>Arabidopsis thaliana</i>	3166	+	6	TACGTG	cis-acting regulatory element involved in light responsiveness
G-box	<i>Arabidopsis thaliana</i>	2047	+	6	TACGTG	cis-acting regulatory element involved in light responsiveness
GARE-motif	<i>Brassica oleracea</i>	1546	-	7	TCTGTTG	gibberellin-responsive element
GT1-motif	<i>Solanum tuberosum</i>	2550	-	9	GTGTGTGAA	light responsive element
GT1-motif	<i>Solanum tuberosum</i>	4203	+	9	GTGTGTGAA	light responsive element
Gap-box	<i>Arabidopsis thaliana</i>	3721	+	9.5	CAAATGAA(A/G)A	part of a light responsive element
TC-rich repeats	<i>Nicotiana tabacum</i>	1376	+	9	ATTCTCTAAC	cis-acting element involved in defense and stress responsiveness
TC-rich repeats	<i>Nicotiana tabacum</i>	2271	+	9	GTTTTCTTAC	cis-acting element involved in defense and stress responsiveness
TC-rich repeats	<i>Nicotiana tabacum</i>	2187	+	9	GTTTTCTTAC	cis-acting element involved in defense and stress responsiveness
TCA-element	<i>Nicotiana tabacum</i>	386	-	9	CCATCTTTTT	cis-acting element involved in salicylic acid responsiveness
TCA-element	<i>Nicotiana tabacum</i>	4302	+	10	CCATCTTTTT	cis-acting element involved in salicylic acid responsiveness
TCT-motif	<i>Arabidopsis thaliana</i>	2313	+	6	TCTTAC	part of a light responsive element
TCT-motif	<i>Arabidopsis thaliana</i>	1863	-	6	TCTTAC	part of a light responsive element
TCT-motif	<i>Arabidopsis thaliana</i>	2191	+	6	TCTTAC	part of a light responsive element
TGACG-motif	<i>Hordeum vulgare</i>	4118	+	5	TGACG	cis-acting regulatory element involved in the MeJA-responsiveness
TTLL9						
AAAC-motif	<i>Spinacia oleracea</i>	5748	+	11	CAATCAAAACCT	light responsive element
ABRE	<i>Oryza sativa</i>	459	+	9	GCCGCGTGGC	cis-acting element involved in the abscisic acid responsiveness
ABRE	<i>Arabidopsis thaliana</i>	2580	-	5	ACGTG	cis-acting element involved in the

						abscisic acid responsiveness
ABRE	<i>Arabidopsis thaliana</i>	1569	+	5	ACGTG	cis-acting element involved in the abscisic acid responsiveness
ABRE	<i>Arabidopsis thaliana</i>	4844	+	5	ACGTG	cis-acting element involved in the abscisic acid responsiveness
ABRE	<i>Arabidopsis thaliana</i>	461	+	6	CACGTG	cis-acting element involved in the abscisic acid responsiveness
ABRE	<i>Arabidopsis thaliana</i>	1837	+	5	ACGTG	cis-acting element involved in the abscisic acid responsiveness
ABRE	<i>Arabidopsis thaliana</i>	462	+	5	ACGTG	cis-acting element involved in the abscisic acid responsiveness
ACE	<i>Petroselinum crispum</i>	3364	-	9	CTAACGTATT	cis-acting element involved in light responsiveness
AE-box	<i>Arabidopsis thaliana</i>	308	+	8	AGAAACTT	part of a module for light response
AE-box	<i>Arabidopsis thaliana</i>	3729	-	8	AGAAACTT	part of a module for light response
AE-box	<i>Arabidopsis thaliana</i>	2698	-	8	AGAAACAA	part of a module for light response
ATCT- motif	<i>Pisum sativum</i>	3558	+	10	AATCTAATCC	part of a conserved DNA module involved in light responsiveness
AuxRR- core	<i>Nicotiana tabacum</i>	376	+	7	GGTCCAT	cis-acting regulatory element involved in auxin responsiveness
Box 4	<i>Petroselinum crispum</i>	4583	-	6	ATTAAT	part of a conserved DNA module involved in light responsiveness
Box 4	<i>Petroselinum crispum</i>	6337	-	6	ATTAAT	part of a conserved DNA module involved in light responsiveness
Box II	<i>Petroselinum crispum</i>	459	-	9	CCACGTGGC	part of a light responsive element
Box II	<i>Arabidopsis thaliana</i>	4841	-	9	ACACGTAGA	part of a light responsive element
Box II	<i>Petroselinum crispum</i>	460	+	9	CCACGTGGC	part of a light responsive element
CGTCA- motif	<i>Hordeum vulgare</i>	5373	+	5	CGTCA	cis-acting regulatory element involved in

						the MeJA-responsiveness
CGTCA-motif	<i>Hordeum vulgare</i>	4909	-	5	CGTCA	cis-acting regulatory element involved in the MeJA-responsiveness
CGTCA-motif	<i>Hordeum vulgare</i>	3902	+	5	CGTCA	cis-acting regulatory element involved in the MeJA-responsiveness
CGTCA-motif	<i>Hordeum vulgare</i>	3247	+	5	CGTCA	cis-acting regulatory element involved in the MeJA-responsiveness
CGTCA-motif	<i>Hordeum vulgare</i>	3202	+	5	CGTCA	cis-acting regulatory element involved in the MeJA-responsiveness
CGTCA-motif	<i>Hordeum vulgare</i>	2690	+	5	CGTCA	cis-acting regulatory element involved in the MeJA-responsiveness
CGTCA-motif	<i>Hordeum vulgare</i>	2108	+	5	CGTCA	cis-acting regulatory element involved in the MeJA-responsiveness
CGTCA-motif	<i>Hordeum vulgare</i>	2433	-	5	CGTCA	cis-acting regulatory element involved in the MeJA-responsiveness
G-Box	<i>Pisum sativum</i>	461	+	6	CACGTG	cis-acting regulatory element involved in light responsiveness
G-box	<i>Arabidopsis thaliana</i>	4843	+	6	TACGTG	cis-acting regulatory element involved in light responsiveness
G-box	<i>Arabidopsis thaliana</i>	2580	-	6	TACGTG	cis-acting regulatory element involved in light responsiveness
G-box	<i>Arabidopsis thaliana</i>	1836	+	6	TACGTG	cis-acting regulatory element involved in light responsiveness
G-box	<i>Arabidopsis thaliana</i>	1568	+	6	TACGTG	cis-acting regulatory element involved in light responsiveness
G-box	<i>Arabidopsis thaliana</i>	461	+	6	CACGTG	cis-acting regulatory element involved in light responsiveness
G-box	<i>Arabidopsis thaliana</i>	459	+	9	GCCACGTGGA	cis-acting regulatory element involved in light responsiveness
GA-motif	<i>Arabidopsis thaliana</i>	193	+	8	ATAGATAA	part of a light responsive element
GARE-motif	<i>Brassica oleracea</i>	1903	-	7	TCTGTTG	gibberellin-responsive element

GARE-motif	<i>Brassica oleracea</i>	3699	-	7	TCTGTTG	gibberellin-responsive element
GATA-motif	<i>Arabidopsis thaliana</i>	2505	+	7	GATAGGA	part of a light responsive element
GATA-motif	<i>Solanum tuberosum</i>	677	-	9	AAGGATAAGG	part of a light responsive element
GT1-motif	<i>Arabidopsis thaliana</i>	3028	-	6	GGTTAA	light responsive element
GT1-motif	<i>Avena sativa</i>	3027	-	7	GGTTAAT	light responsive element
GT1-motif	<i>Avena sativa</i>	216	+	7	GGTTAAT	light responsive element
GTGGC-motif	<i>Hordeum vulgare</i>	1757	-	10	CAGCGTGTGGC	part of a light responsive element
GTGGC-motif	<i>Spinacia oleracea</i>	3112	-	10	GATTCTGTGGC	part of a light responsive element
I-box	<i>Larix laricina</i>	1107	+	9	GTATAAGGCC	part of a light responsive element
L-box	<i>Petroselinum crispum</i>	2116	+	10	ATCCCACCTAC	part of a light responsive element
LTR	<i>Hordeum vulgare</i>	4292	+	6	CCGAAA	cis-acting element involved in low-temperature responsiveness
MRE	<i>Petroselinum crispum</i>	301	-	7	AACCTAA	MYB binding site involved in light responsiveness
P-box	<i>Oryza sativa</i>	647	+	7	CCTTTTG	gibberellin-responsive element
TATC-box	<i>Oryza sativa</i>	4750	-	7	TATCCCA	cis-acting element involved in gibberellin-responsiveness
TCA-element	<i>Brassica oleracea</i>	1609	+	9	TCAGAAGAGG	cis-acting element involved in salicylic acid responsiveness
TCA-element	<i>Nicotiana tabacum</i>	2849	-	9	CCATCTTTTT	cis-acting element involved in salicylic acid responsiveness
TCA-element	<i>Nicotiana tabacum</i>	2661	-	9	CCATCTTTTT	cis-acting element involved in salicylic acid responsiveness
TCA-element	<i>Nicotiana tabacum</i>	6157	+	9	CCATCTTTTT	cis-acting element involved in salicylic acid responsiveness
TCT-motif	<i>Arabidopsis thaliana</i>	1623	-	6	TCTTAC	part of a light responsive element
TCT-motif	<i>Arabidopsis thaliana</i>	4648	-	6	TCTTAC	part of a light responsive element
TCT-motif	<i>Arabidopsis thaliana</i>	3693	+	6	TCTTAC	part of a light responsive element
TCT-motif	<i>Arabidopsis thaliana</i>	5080	+	6	TCTTAC	part of a light responsive element
TCT-motif	<i>Arabidopsis thaliana</i>	731	-	6	TCTTAC	part of a light responsive element

TCT-motif	<i>Arabidopsis thaliana</i>	4637	-	6	TCTTAC	part of a light responsive element
TGA-element	<i>Brassica oleracea</i>	6207	+	6	AACGAC	auxin-responsive element
TGACG-motif	<i>Hordeum vulgare</i>	2433	+	5	TGACG	cis-acting regulatory element involved in the MeJA-responsiveness
TGACG-motif	<i>Hordeum vulgare</i>	3247	-	5	TGACG	cis-acting regulatory element involved in the MeJA-responsiveness
TGACG-motif	<i>Hordeum vulgare</i>	2690	-	5	TGACG	cis-acting regulatory element involved in the MeJA-responsiveness
TGACG-motif	<i>Hordeum vulgare</i>	4909	+	5	TGACG	cis-acting regulatory element involved in the MeJA-responsiveness
TGACG-motif	<i>Hordeum vulgare</i>	2108	-	5	TGACG	cis-acting regulatory element involved in the MeJA-responsiveness
TGACG-motif	<i>Hordeum vulgare</i>	3902	-	5	TGACG	cis-acting regulatory element involved in the MeJA-responsiveness
TGACG-motif	<i>Hordeum vulgare</i>	5373	-	5	TGACG	cis-acting regulatory element involved in the MeJA-responsiveness
TGACG-motif	<i>Hordeum vulgare</i>	3202	-	5	TGACG	cis-acting regulatory element involved in the MeJA-responsiveness
chs-CMA1a	<i>Daucus carota</i>	1671	-	8	TTACTTAA	part of a light responsive element
circadian	<i>Lycopersicon esculentum</i>	761	-	9	CAAAGATATC	cis-acting regulatory element involved in circadian control
TTL12						
ABRE	<i>Arabidopsis thaliana</i>	1428	+	5	ACGTG	cis-acting element involved in the abscisic acid responsiveness
ABRE	<i>Arabidopsis thaliana</i>	2032	+	5	ACGTG	cis-acting element involved in the abscisic acid responsiveness
ABRE	<i>Arabidopsis thaliana</i>	2386	-	5	ACGTG	cis-acting element involved in the abscisic acid responsiveness
ABRE	<i>Arabidopsis thaliana</i>	2527	+	5	ACGTG	cis-acting element involved in the

						abscisic acid responsiveness
ABRE	<i>Arabidopsis thaliana</i>	3289	+	5	ACGTG	cis-acting element involved in the abscisic acid responsiveness
ABRE	<i>Arabidopsis thaliana</i>	4192	-	6	CACGTG	cis-acting element involved in the abscisic acid responsiveness
ABRE	<i>Arabidopsis thaliana</i>	4193	+	5	ACGTG	cis-acting element involved in the abscisic acid responsiveness
ABRE	<i>Arabidopsis thaliana</i>	4300	-	5	ACGTG	cis-acting element involved in the abscisic acid responsiveness
ABRE	<i>Arabidopsis thaliana</i>	4793	-	5	ACGTG	cis-acting element involved in the abscisic acid responsiveness
ABRE	<i>Arabidopsis thaliana</i>	5608	-	5	ACGTG	cis-acting element involved in the abscisic acid responsiveness
ABRE	<i>Arabidopsis thaliana</i>	439	-	5	ACGTG	cis-acting element involved in the abscisic acid responsiveness
ABRE	<i>Arabidopsis thaliana</i>	1251	+	5	ACGTG	cis-acting element involved in the abscisic acid responsiveness
ABRE	<i>Arabidopsis thaliana</i>	5819	+	5	ACGTG	cis-acting element involved in the abscisic acid responsiveness
ABRE	<i>Arabidopsis thaliana</i>	5985	-	5	ACGTG	cis-acting element involved in the abscisic acid responsiveness
ABRE	<i>Arabidopsis thaliana</i>	6070	-	5	ACGTG	cis-acting element involved in the abscisic acid responsiveness
ABRE	<i>Arabidopsis thaliana</i>	6858	+	5	ACGTG	cis-acting element involved in the abscisic acid responsiveness
ABRE	<i>Arabidopsis thaliana</i>	6994	+	5	ACGTG	cis-acting element involved in the abscisic acid responsiveness
ABRE	<i>Arabidopsis thaliana</i>	7380	-	5	ACGTG	cis-acting element involved in the

						abscisic acid responsiveness
ACE	<i>Petroselinum crispum</i>	6078	-	9	CTAACGTATT	cis-acting element involved in light responsiveness
AE-box	<i>Arabidopsis thaliana</i>	7604	-	8	AGAAACTT	part of a module for light response
AE-box	<i>Arabidopsis thaliana</i>	3605	-	8	AGAAACTT	part of a module for light response
AE-box	<i>Arabidopsis thaliana</i>	5991	+	8	AGAAACAA	part of a module for light response
ATC-motif	<i>Zea mays</i>	55	+	9	TGCTATCCG	part of a conserved DNA module involved in light responsiveness
Box 4	<i>Petroselinum crispum</i>	3870	+	6	ATTAAT	part of a conserved DNA module involved in light responsiveness
Box 4	<i>Petroselinum crispum</i>	8092	-	6	ATTAAT	part of a conserved DNA module involved in light responsiveness
CAG-motif	<i>Arabidopsis thaliana</i>	7449	-	10	GAAAGGCAGAC	part of a light response element
CGTCA- motif	<i>Hordeum vulgare</i>	7952	-	5	CGTCA	cis-acting regulatory element involved in the MeJA- responsiveness
CGTCA- motif	<i>Hordeum vulgare</i>	7838	+	5	CGTCA	cis-acting regulatory element involved in the MeJA- responsiveness
CGTCA- motif	<i>Hordeum vulgare</i>	7756	-	5	CGTCA	cis-acting regulatory element involved in the MeJA- responsiveness
CGTCA- motif	<i>Hordeum vulgare</i>	6992	-	5	CGTCA	cis-acting regulatory element involved in the MeJA- responsiveness
CGTCA- motif	<i>Hordeum vulgare</i>	6780	-	5	CGTCA	cis-acting regulatory element involved in the MeJA- responsiveness
CGTCA- motif	<i>Hordeum vulgare</i>	5097	+	5	CGTCA	cis-acting regulatory element involved in the MeJA- responsiveness
CGTCA- motif	<i>Hordeum vulgare</i>	6123	-	5	CGTCA	cis-acting regulatory element involved in the MeJA- responsiveness
CGTCA- motif	<i>Hordeum vulgare</i>	4312	+	5	CGTCA	cis-acting regulatory element involved in the MeJA- responsiveness

CGTCA-motif	<i>Hordeum vulgare</i>	4055	+	5	CGTCA	cis-acting regulatory element involved in the MeJA-responsiveness
CGTCA-motif	<i>Hordeum vulgare</i>	2716	-	5	CGTCA	cis-acting regulatory element involved in the MeJA-responsiveness
CGTCA-motif	<i>Hordeum vulgare</i>	1709	+	5	CGTCA	cis-acting regulatory element involved in the MeJA-responsiveness
G-Box	<i>Pisum sativum</i>	1250	-	6	CACGTT	cis-acting regulatory element involved in light responsiveness
G-Box	<i>Pisum sativum</i>	5985	+	6	CACGTT	cis-acting regulatory element involved in light responsiveness
G-Box	<i>Pisum sativum</i>	4793	+	6	CACGTT	cis-acting regulatory element involved in light responsiveness
G-Box	<i>Pisum sativum</i>	6857	-	6	CACGTT	cis-acting regulatory element involved in light responsiveness
G-Box	<i>Pisum sativum</i>	2386	+	6	CACGTT	cis-acting regulatory element involved in light responsiveness
G-Box	<i>Pisum sativum</i>	6070	+	6	CACGTT	cis-acting regulatory element involved in light responsiveness
G-Box	<i>Pisum sativum</i>	5818	-	6	CACGTT	cis-acting regulatory element involved in light responsiveness
G-Box	<i>Pisum sativum</i>	1427	-	6	CACGTT	cis-acting regulatory element involved in light responsiveness
G-Box	<i>Pisum sativum</i>	4192	-	6	CACGTG	cis-acting regulatory element involved in light responsiveness
G-box	<i>Brassica oleracea</i>	6070	-	8	TAAACGTG	cis-acting regulatory element involved in light responsiveness
G-box	<i>Arabidopsis thaliana</i>	4364	+	9	GCCACGTGGA	cis-acting regulatory element involved in light responsiveness
G-box	<i>Arabidopsis thaliana</i>	4300	-	6	TACGTG	cis-acting regulatory element involved in light responsiveness
G-box	<i>Arabidopsis thaliana</i>	4192	-	6	CACGTG	cis-acting regulatory element involved in light responsiveness
G-box	<i>Brassica napus</i>	4191	-	8	ACACGTGT	cis-acting regulatory element involved in light responsiveness

G-box	<i>Arabidopsis thaliana</i>	2526	+	6	TACGTG	cis-acting regulatory element involved in light responsiveness
G-box	<i>Arabidopsis thaliana</i>	2031	+	6	TACGTG	cis-acting regulatory element involved in light responsiveness
G-box	<i>Zea mays</i>	6993	-	6	CACGTC	cis-acting regulatory element involved in light responsiveness
G-box	<i>Zea mays</i>	439	+	6	CACGTC	cis-acting regulatory element involved in light responsiveness
G-box	<i>Zea mays</i>	5608	+	6	CACGTC	cis-acting regulatory element involved in light responsiveness
G-box	<i>Zea mays</i>	3288	-	6	CACGTC	cis-acting regulatory element involved in light responsiveness
G-box	<i>Zea mays</i>	7380	+	6	CACGTC	cis-acting regulatory element involved in light responsiveness
GARE-motif	<i>Brassica oleracea</i>	226	-	7	TCTGTTG	gibberellin-responsive element
GARE-motif	<i>Brassica oleracea</i>	4504	+	7	TCTGTTG	gibberellin-responsive element
GT1-motif	<i>Arabidopsis thaliana</i>	6668	-	6	GGTTAA	light responsive element
GT1-motif	<i>Arabidopsis thaliana</i>	4493	-	6	GGTTAA	light responsive element
GT1-motif	<i>Avena sativa</i>	4492	-	7	GGTTAAT	light responsive element
GT1-motif	<i>Arabidopsis thaliana</i>	6666	+	6	GGTTAA	light responsive element
GT1-motif	<i>Avena sativa</i>	5933	+	7	GGTTAAT	light responsive element
LTR	<i>Hordeum vulgare</i>	5524	-	6	CCGAAA	cis-acting element involved in low-temperature responsiveness
LTR	<i>Hordeum vulgare</i>	1519	-	6	CCGAAA	cis-acting element involved in low-temperature responsiveness
LTR	<i>Hordeum vulgare</i>	5200	-	6	CCGAAA	cis-acting element involved in low-temperature responsiveness
P-box	<i>Oryza sativa</i>	1028	+	7	CCTTTTG	gibberellin-responsive element
P-box	<i>Oryza sativa</i>	5296	-	7	CCTTTTG	gibberellin-responsive element
Sp1	<i>Oryza sativa</i>	2005	+	6	GGGCGG	light responsive element
Sp1	<i>Oryza sativa</i>	6262	+	6	GGGCGG	light responsive element

TC-rich repeats	<i>Nicotiana tabacum</i>	4404	+	9	GTTTTCTTAC	cis-acting element involved in defense and stress responsiveness
TC-rich repeats	<i>Nicotiana tabacum</i>	5545	-	9	GTTTTCTTAC	cis-acting element involved in defense and stress responsiveness
TCA-element	<i>Brassica oleracea</i>	3668	+	9	TCAGAAGAGG	cis-acting element involved in salicylic acid responsiveness
TCA-element	<i>Nicotiana tabacum</i>	7663	-	9	CCATCTTTTT	cis-acting element involved in salicylic acid responsiveness
TCT-motif	<i>Arabidopsis thaliana</i>	920	-	6	TCTTAC	part of a light responsive element
TCT-motif	<i>Arabidopsis thaliana</i>	5535	+	6	TCTTAC	part of a light responsive element
TCT-motif	<i>Arabidopsis thaliana</i>	2413	+	6	TCTTAC	part of a light responsive element
TCT-motif	<i>Arabidopsis thaliana</i>	7284	-	6	TCTTAC	part of a light responsive element
TCT-motif	<i>Arabidopsis thaliana</i>	1881	+	6	TCTTAC	part of a light responsive element
TCT-motif	<i>Arabidopsis thaliana</i>	4883	-	6	TCTTAC	part of a light responsive element
TGA-element	<i>Brassica oleracea</i>	362	+	6	AACGAC	auxin-responsive element
TGA-element	<i>Brassica oleracea</i>	6576	-	6	AACGAC	auxin-responsive element
TGACG-motif	<i>Hordeum vulgare</i>	6780	+	5	TGACG	cis-acting regulatory element involved in the MeJA-responsiveness
TGACG-motif	<i>Hordeum vulgare</i>	6992	+	5	TGACG	cis-acting regulatory element involved in the MeJA-responsiveness
TGACG-motif	<i>Hordeum vulgare</i>	7756	+	5	TGACG	cis-acting regulatory element involved in the MeJA-responsiveness
TGACG-motif	<i>Hordeum vulgare</i>	7838	-	5	TGACG	cis-acting regulatory element involved in the MeJA-responsiveness
TGACG-motif	<i>Hordeum vulgare</i>	1709	-	5	TGACG	cis-acting regulatory element involved in the MeJA-responsiveness
TGACG-motif	<i>Hordeum vulgare</i>	7952	+	5	TGACG	cis-acting regulatory element involved in the MeJA-responsiveness
TGACG-motif	<i>Hordeum vulgare</i>	5097	-	5	TGACG	cis-acting regulatory element involved in

						the MeJA-responsiveness
TGACG-motif	<i>Hordeum vulgare</i>	4055	-	5	TGACG	cis-acting regulatory element involved in the MeJA-responsiveness
TGACG-motif	<i>Hordeum vulgare</i>	6123	+	5	TGACG	cis-acting regulatory element involved in the MeJA-responsiveness
TGACG-motif	<i>Hordeum vulgare</i>	2716	+	5	TGACG	cis-acting regulatory element involved in the MeJA-responsiveness
TGACG-motif	<i>Hordeum vulgare</i>	4312	-	5	TGACG	cis-acting regulatory element involved in the MeJA-responsiveness
chs-CMA1a	<i>Daucus carota</i>	5106	-	8	TTACTTAA	part of a light responsive element
chs-CMA2a	<i>Petroselinum crispum</i>	2885	+	8	TCACTTGA	part of a light responsive element
circadian	<i>Lycopersicon esculentum</i>	2364	-	9	CAAAGATATC	cis-acting regulatory element involved in circadian control
circadian	<i>Lycopersicon esculentum</i>	5759	-	9	CAAAGATATC	cis-acting regulatory element involved in circadian control
circadian	<i>Lycopersicon esculentum</i>	4717	-	9	CAAAGATATC	cis-acting regulatory element involved in circadian control
circadian	<i>Lycopersicon esculentum</i>	6937	+	9	CAAAGATATC	cis-acting regulatory element involved in circadian control

Table 11. Responsive elements detected in tubulin modifying enzymes using PLANTCARE web server.

6.2.4. Hormone-dependent post-translational modifications.

Insilco analysis of tubulin modifying enzymes in *P. patens* by PLANTCARE web server showed the presence of hormone responsive elements (28 in ELP3, 28 in ATAT, 8 in TTLL6, 33 in TTLL9 and 48 in TTLL12) indicating that hormones might have a role in modulating PTMs of tubulin (Table 11). Tubulin PTMs were examined upon treatment with phytohormones (auxin and cytokinin). The 7-day-old *Physcomitrella patens* protonema culture was treated with auxin (1 nM) and cytokinin (1 nM), taking 0 nM as control. When treated with 1 nM of auxin, the intensity of tyrosinated tubulin increased significantly by 1.8-fold as compared to the control (0 nM) (Figure 78A), there is no significant effect in the acetylated

and polyglutamylated tubulin (Figure 78B & 78C). Interestingly upon treatment with 1 nM cytokinin, the effect is non-significant in the tyrosinated and acetylated (Figure 78D & 78E). Still, there is a significant decrease by 6-fold in the intensity of polyglutamylated tubulin, as compared to control (0 nM) (Figure 78F).

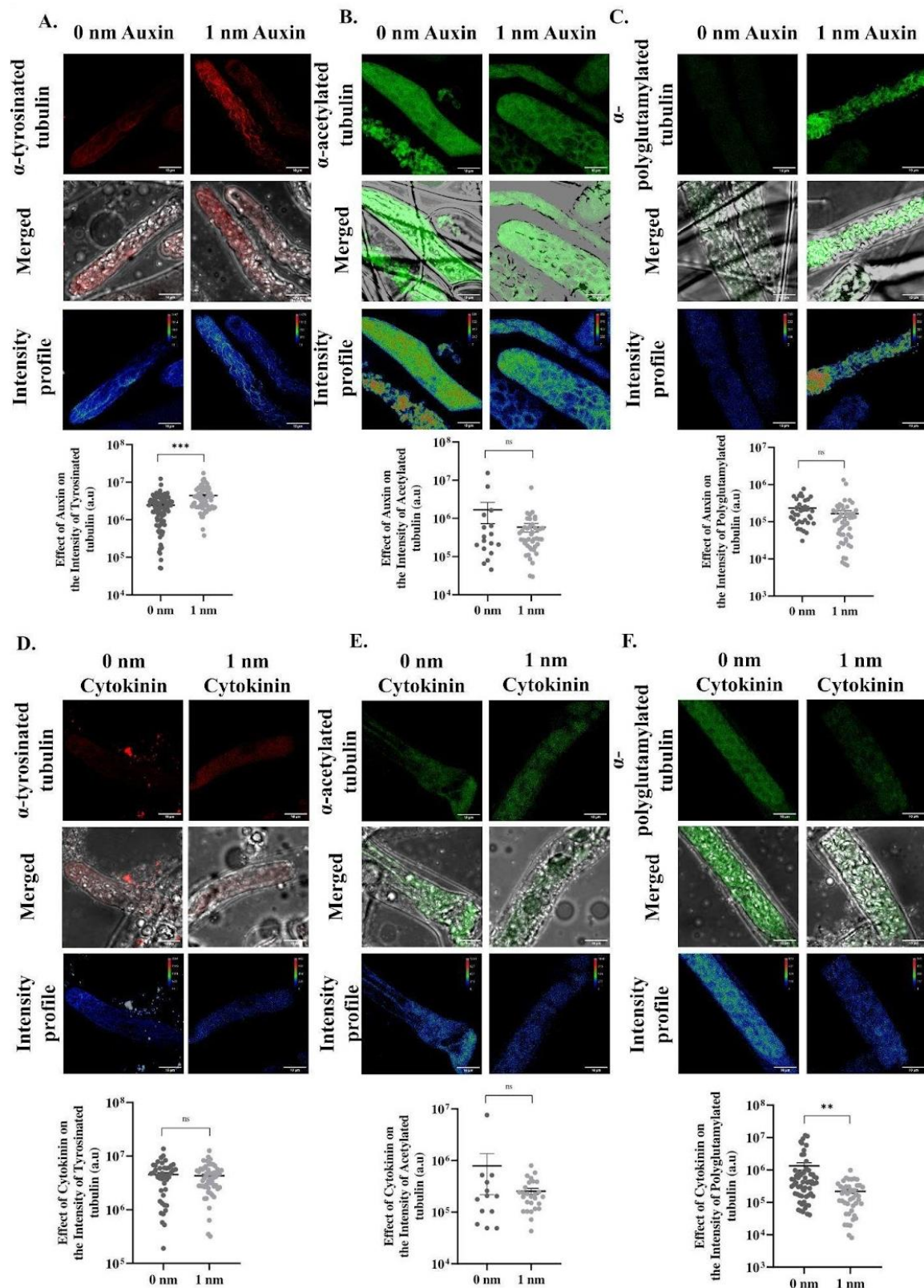


Figure 78. Effect of phytohormones on immunodetection of tubulin modifications in *Physcomitrella patens*. Concurrent confocal images of 7-d old protonema culture of *Physcomitrella patens* treated with phytohormones like 1 nM Auxin (**A-C**) and 1 nM Cytokinin (**D-F**) along with their respective controls without any phytohormones in the growing media grown under white light conditions at 25 °C. Representative immunofluorescence images and graphical representation of tyrosinated (**A, D**), acetylated (**B, E**), and polyglutamylated (**C, F**) tubulin modification. The experiments were performed three times with different biological replicates. Scale bar- 10 µm. Values in the graphs are expressed as mean ± SE. Two-way analysis of variance (ANOVA) using Tukey's multiple comparisons test was performed with the help of GraphPad Prism to test for significance among the dataset, **p < 0.01, ns- non-significant.

To check the effect of phytohormones on the intensity of Ca^{2+} in GcAMP 6f *P. patens*. The 7 days protonema culture of calcium sensor lines was treated with 1 nM of auxin and cytokinin at 25 °C. The intensity of Ca^{2+} significantly increased by 1.5-fold when treated with 1nM of auxin as compared to control (0 nM) (Figure 79A & 79B) but was non-significant upon treatment with cytokinin (Figure 79C & 79D).

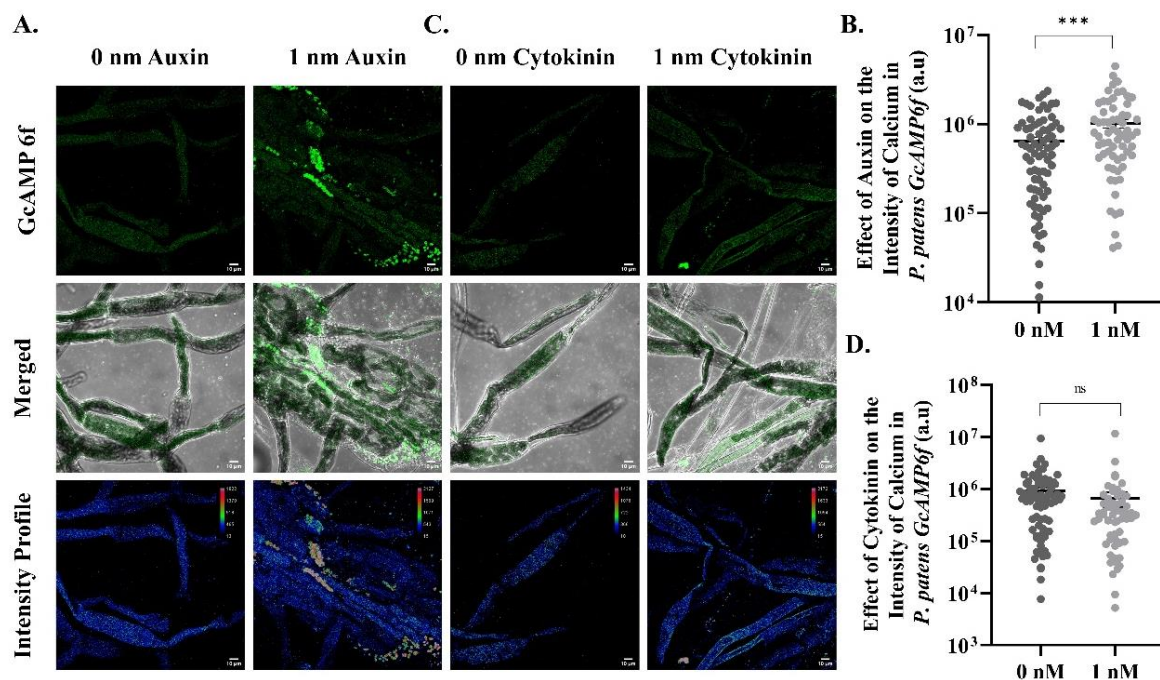


Figure 79. Effect of phytohormones on Ca^{2+} in *Physcomitrella patens*. Representative immunofluorescence images and graphical representation of 7-d old protonema culture of GcAMP 6f line of *Physcomitrella patens* treated with phytohormones like 1 nM Auxin (**A-B**) and 1 nM Cytokinin (**C-D**) along with their respective controls without any phytohormones in the growing media grown under white light conditions at 25 °C. The experiments were performed three times with different biological replicates. Scale bar- 10 µm. Values in the graphs are expressed as mean ± SE. Two-way analysis of variance (ANOVA) using Tukey's multiple comparisons test was performed with the help of GraphPad Prism to test for significance among the dataset, **p < 0.01, ns- non-significant.

6.2.5. Temperature and Calcium-dependent post-translational modifications.

In-silico analysis of tubulin modifying enzymes in *P. patens* by PLANTCARE web server showed the presence of temperature-responsive elements (1 in ELP3, 4 in ATAT, 1 in TTLL9

and 3 in TTLL12) indicating that temperature might have a role in modulating PTMs of tubulin (Table 11). To study the transient nature of temperature and the effect of varying exogenous Ca^{2+} on the post-translation of tubulins, the protonema cultures of *P. patens* were allowed to grow in media containing 0 mM, 10 mM, and 100 mM Ca^{2+} at 18, 25 and 38 °C. At 25 °C, particular trends are observed in the intensities of the modified tubulins in response to extracellular Ca^{2+} in the growing media. The tyrosinated tubulin modifications did not change significantly when treated with 10 mM or 100 mM extracellular Ca^{2+} as compared to the control with 0 mM Ca^{2+} (Figure 80B & 80D). On the other hand, the intensities of acetylated (Figure 80F & 80H) tubulin decreased significantly by 11.6-fold, and polyglutamylated (Figure 80J & 80L) tubulin did not change when treated with high concentrations of Ca^{2+} exogenously i.e., 100 mM as compared to the control with 0 mM of CaCl_2 in the media respectively. Interestingly, the intensities of acetylated (Figure 80F & 80H), as well as polyglutamylated (Figure 80J & 80L) tubulin modifications, did not show any significant change when treated with 10 mM CaCl_2 in the media with respect to their corresponding controls without any extracellular Ca^{2+} in the media. We further examined the effect of varying Ca^{2+} concentrations and cold stress on the PTMs of tubulin in *P. patens*. When protonema was allowed to grow with 10 mM Ca^{2+} , the levels of tyrosinated, acetylated, and polyglutamylated tubulin decreased significantly by 4.1 (Figure 80A & 80D), 1.5 (Figure 80E & 80H) and 5.7-fold (Figure 80I & 80L) as compared to their respective control (0mM of CaCl_2) at 18 °C. Additionally, there was a further decrease in the levels of tyrosinated, acetylated, and polyglutamylated tubulin by 17.2 (Figure 80A & 80D), 2.8 (Figure 80E & 80H) and 3.2-fold (Figure 80I & 80L) in protonema treated with high Ca^{2+} , i.e., 100 mM as compared to their respective control (0 mM) at 18 °C. We further examined the effect of varying Ca^{2+} concentrations and heat stress on the PTMs of tubulin in *P. patens*. At 38 °C, the intensities of tyrosinated tubulin did not change significantly with different concentrations of Ca^{2+} (Figure 80C & 80D). However, the intensities of acetylated tubulin decreased by 2.8 and 11.6-fold when treated with 10 mM and 100 mM of

CaCl₂ externally in the media, respectively, as compared to their control with 0 mM of CaCl₂ at 38 °C (Figure 80G & 80H). The intensities of polyglutamylated tubulin remained unchanged across different concentrations of Ca²⁺ added externally at 38 °C (Figure 80K & 80L). It was also observed that there is a 4.4 and 9.8-fold decrease in the intensities of acetylated tubulin at 38 °C as compared to the intensities of endogenous Ca²⁺ at 25 °C when treated with 0 mM and 10 mM exogenous CaCl₂, respectively (Figure 80L). However, there were no significant changes in the intensities of acetylated tubulin when treated with 100 mM CaCl₂ at 38 °C as compared to its control at 25 °C (Figure 80L). Interestingly, there was no significant difference in the tyrosinated (Figure 80L) and polyglutamylated (Figure 80L) tubulin modifications at 38 °C as compared to their respective controls at 25 °C.

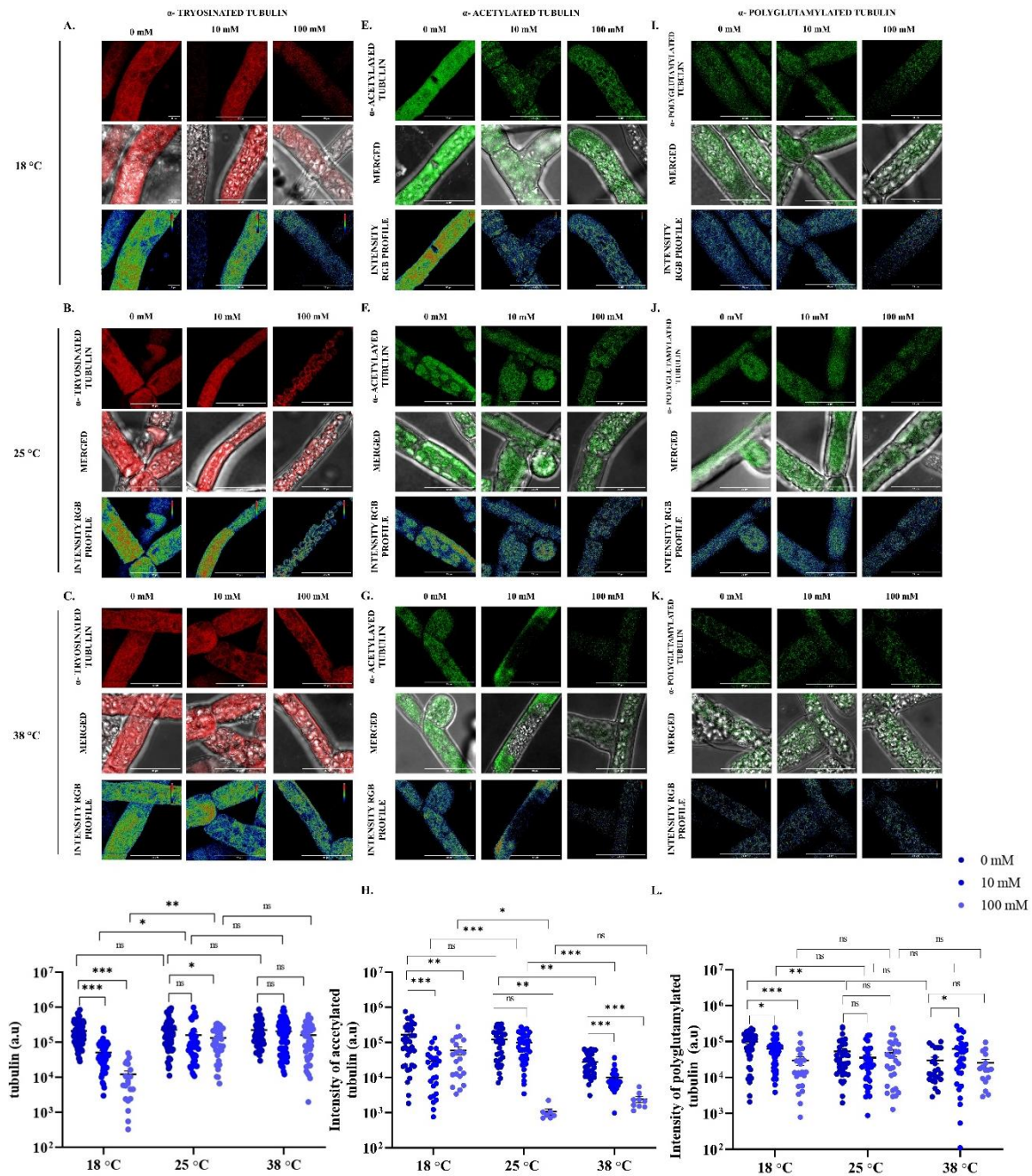


Figure 80. Effect of temperature on immunodetection of tubulin modifications in *Physcomitrella patens*. Representative immunofluorescence images and graphical representation of tyrosinated (A-D), acetylated (E-H), and polyglutamylated (I-L) tubulin modifications in 7-d old protonema culture of *Physcomitrella patens* grown in the presence of 0 mM, 10 mM and 100 mM Ca^{2+} at 25 °C and treated with low (18 °C), ambient (22 °C) and high (38 °C) temperature for 24 h. The experiments were performed three times with different biological replicates. Scale bar- 10 μm . Values in the graphs are expressed as mean \pm SE. Two-way analysis of variance (ANOVA) using Tukey's multiple comparisons test was performed with the help of GraphPad Prism to test for significance among the dataset, * $p < 0.1$, ** $p < 0.01$, *** $p < 0.001$, ns- non-significant.

6.2.6. Validation of a Sensor in *Physcomitrella patens* and Insights into Ca^{2+} and Temperature-Dependent Post-Translational Modifications in GCaMP

To check the sensitivity of the calcium sensor, GCaMP 6f in *P. patens*, ionomycin, and BAPTA AM are used. In the protonema cells, when treated with 5 μM ionomycin (Calcium activator)

for 12 hours at 25 °C, there was a sudden uplift in the intensities of endogenous Ca^{2+} present in the cell as compared to control. However, upon incubation of the protonema tissues with 20 μM BAPTA AM (Calcium chelator), the intensities of endogenous Ca^{2+} significantly decreased as compared to control (Figure 81A). In the case of ionomycin-treated protonema cells, the level of endogenous Ca^{2+} increased significantly by 2.2-fold and decreased by 2.2-fold when treated with BAPTA AM as compared to the control (Figure 81B). These results signify that the calcium sensor GCaMP 6f line is sensitive to extracellular calcium channel-inhibiting and enhancing drugs.

The dynamics of endogenous Ca^{2+} in the protonema cells are also studied when treated with different temperatures using the very efficient calcium sensing GCaMP 6f line of *P. patens*. Additionally, the effect of exogenously supplied CaCl_2 in the growing media is studied on the Ca^{2+} flux *P. patens*. At 25 °C, the intensities of endogenous Ca^{2+} decreased with the increase in Ca^{2+} concentrations in the growing media (Figure 81D). The intensities of endogenous Ca^{2+} decreased by 1.3 and 2.1-fold when treated with 10 mM and 100 mM of CaCl_2 , respectively, at 25 °C (Figure 81F). At 18 °C, the endogenous Ca^{2+} level remained unchanged when treated with low Ca^{2+} concentrations, i.e., 10 mM, but there was a significant upshift by 3.6-fold when exogenously treated with 100 mM of calcium chloride (Figure 81C & 81F). Interestingly, in the absence of any extracellular Ca^{2+} , a 3.3-fold rise in the endogenous Ca^{2+} level was observed with respect to control at 25 °C. However, the level of endogenous Ca^{2+} remained unchanged at 10 mM and subsequently decreased by 2.2-fold at 100 mM with respect to their respective controls at 25 °C (Figure 81C & 81F). Under heat stress conditions i.e., at 38 °C, the endogenous Ca^{2+} remains unchanged with the increase in the exogenous Ca^{2+} supplement in the media (Figure 81E & 81F). However, the endogenously present Ca^{2+} in the protonema cells increased significantly by 2.3-fold at 38 °C when treated with a higher concentration of CaCl_2 in the media, i.e., 100 mM, compared to its control at 25 °C (Figure 81F). On the contrary, the

intensities of endogenous Ca^{2+} remained unchanged when treated with 10 mM CaCl_2 and control at 0 mM as compared to their respective controls at 25 °C (Figure 81F).

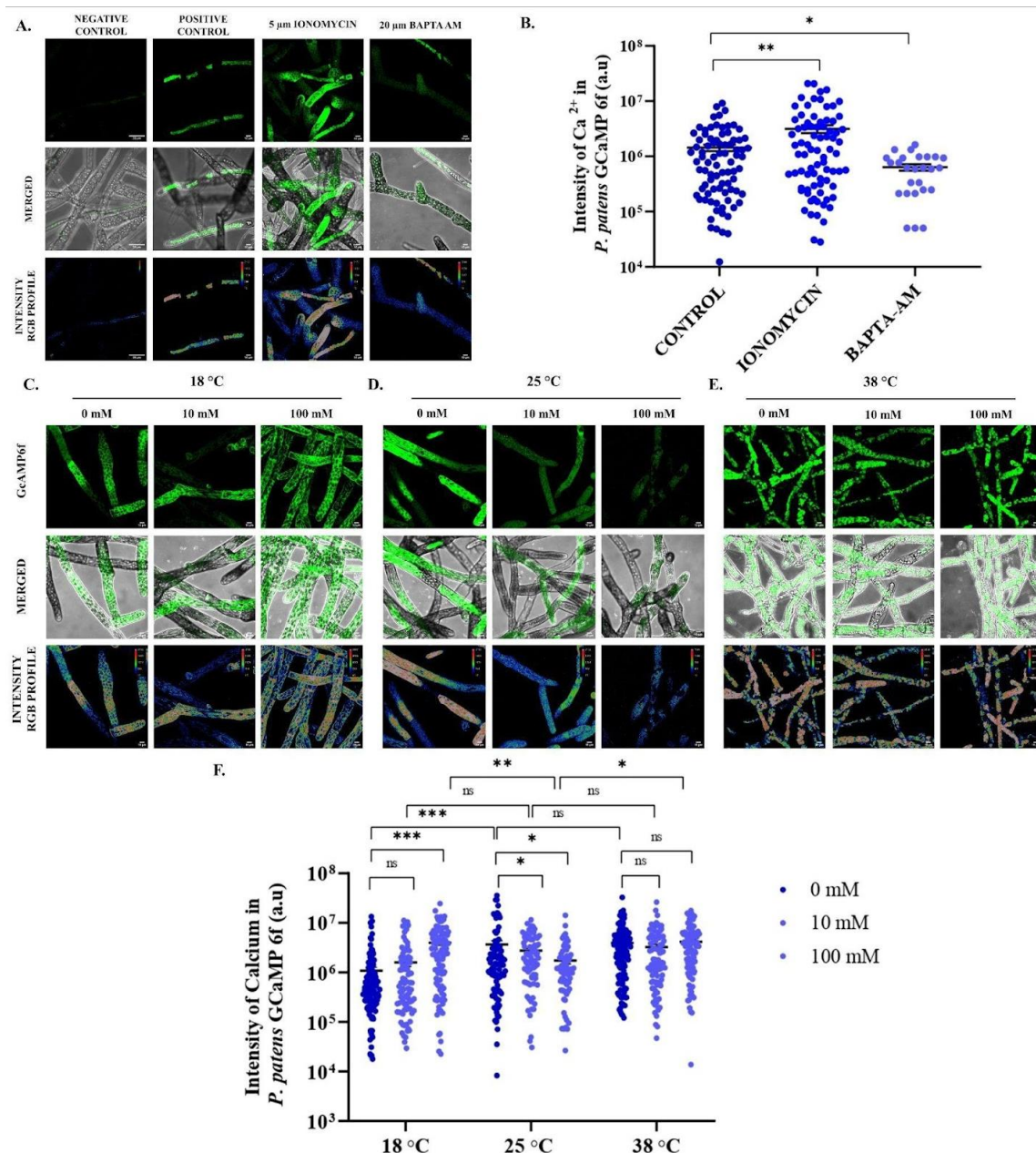


Figure 81. Validation of a Ca^{2+} Sensor and effect of varying exogenous Ca^{2+} and temperatures on Post-Translational Modifications in *Physcomitrella patens*. Representative confocal images (A) and graphical representation (B) of intensities of endogenous Ca^{2+} in the cell of 7-d old GCaMP 6f line in *Physcomitrella patens* treated with 5 μM ionomycin (Calcium activator) and 20 μM BAPTA AM (Calcium inhibitor) for 12 h along with the control at 25 °C. Concurrent confocal images of 7-d old protonema culture of *Physcomitrella patens* grown in the presence of 0 mM, 10 mM, and 100 mM Ca^{2+} at 25 °C and treated with low (18 °C, C), ambient (22 °C, D) and high (38 °C, E) temperature for 24 h. Graphical representation of endogenous Ca^{2+} levels in the cell (F). The experiments were performed three times with different biological replicates. Scale bar- 10 μm . Values in the graphs are expressed as mean \pm SE. Two-way analysis of variance (ANOVA) using Tukey's multiple comparisons test was performed with the help of GraphPad Prism to test for significance among the dataset *p < 0.1, **p < 0.01, ***p < 0.001, ns- non-significant.

6.2.7. Gametophore development is dependent on extracellular Ca^{2+} levels in *P. patens* at ambient and higher temperature

About 5% of the caulonema side branch initials tend to develop into gametophore apical stem cells (Kofuji and Hasebe, 2014). Further, gametophyte development occurs as specific trends in cell division are executed by the developmental program and environmental stimuli of the moss, which involve several hormones and genes (Kofuji and Hasebe, 2014). In this study, the effect of varying temperatures and Ca^{2+} concentrations on the protonema to gametophore transition is observed (Figure 82A). Here, the number of newly developed gametophores is quantified and observed. At 18 °C, the gametophore development was not significant across the different CaCl_2 concentrations (Figure 82B). Whereas the gametophore development was significantly increased by 3.6 and 5.9-fold when treated with 10 mM and 100 mM as compared to the protonema with 0 mM of extracellular Ca^{2+} in the media, respectively, at 25 °C (Figure 82C). Similarly, under high-temperature stress, the gametophore development both increased by 2.5-fold when treated with 10 mM and 100 mM as compared to the protonema with 0 mM of extracellular Ca^{2+} in the media, respectively, at 38 °C (Figure 82D).

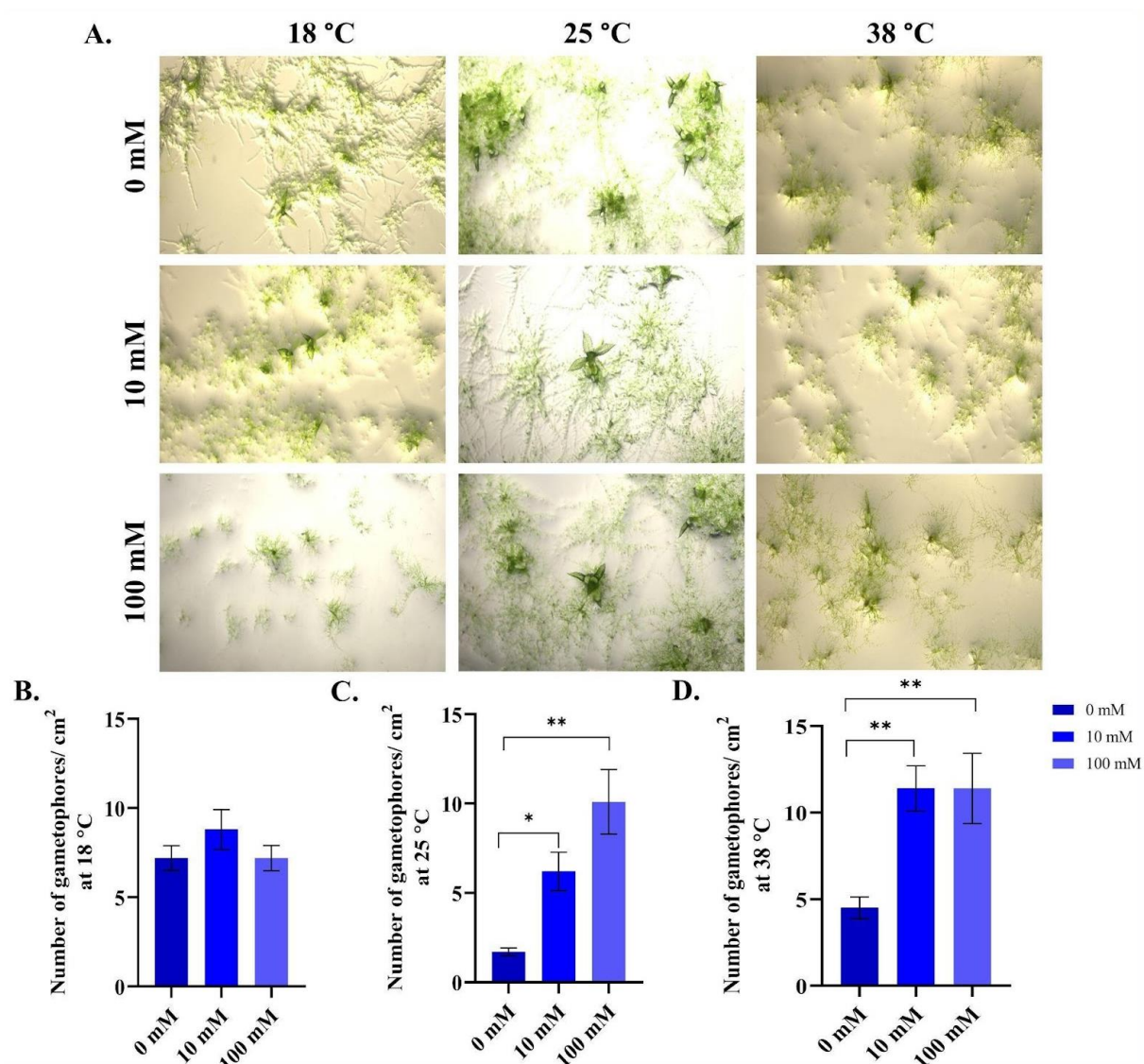


Figure 82. Effect of varying Ca²⁺ concentration and temperature on protonema to gametophyte transition. Representative images (A) and graphical representation (B-D) of newly developed gametophyte in 7-d old protonema culture of *P. patens* grown in the presence of 0 mM, 10 mM, and 100 mM Ca²⁺ at 25 °C (C) and treated to 24 h of cold (18 °C) (B) and heat stress (38 °C) (D). The experiments were performed three times with different biological replicates. Scale bar- 10 μ m. Values in the graphs are expressed as mean \pm SE. Two-way analysis of variance (ANOVA) using Tukey's multiple comparisons test was performed with the help of GraphPad Prism to test for significance among the dataset, *p < 0.1, **p < 0.01.

6.3. DISCUSSION

The study explores the presence and distribution of tubulin post-translational modifications (PTMs) in *Physcomitrella patens*, a lower plant species that lacks a major circadian clock protein i.e., GIGANTEA, and provides insights into the enzymes responsible for catalyzing these modifications. Tubulin PTMs, such as acetylation, polyglutamylation, and tyrosination, are crucial for the stability and dynamics of microtubules in eukaryotes. While these PTMs have been extensively studied in mammals and higher plants, their occurrence and regulation in lower plants like bryophytes remain relatively unexplored. We have identified homologs of TTLL proteins, responsible for polyglutamylation, and ATAT, responsible for tubulin acetylation, in *P. patens*. Interestingly, while some TTLL homologs are widely distributed across plant species and eukaryotes, others are found exclusively in lower plants and algae, suggesting evolutionary divergence in the regulation of tubulin PTMs. The presence of ATAT in *P. patens* but its absence in higher plants highlights evolutionary differences in the regulation of tubulin acetylation. In higher plants lacking ATAT, Elongator Protein 3 (ELP3) behaves as a potential substitute for acetylated tubulin. ELP3, known for its involvement in histone acetylation and transcriptional elongation, is present across lower and higher plants, indicating its conserved role in PTMs. To validate the *in-silico* findings, experimental approaches were employed, demonstrating the presence of acetylated, polyglutamylated, and tyrosinated tubulin modifications in *P. patens* protonema cells through western blotting. The abundance of polyglutamylated and tyrosinated tubulin exceeds that of acetylated tubulin, suggesting differential regulation or functional significance of these PTMs in *P. patens*.

The findings of this study also shed light on the intricate regulation of tubulin post-translational modifications (PTMs) and calcium dynamics in *Physcomitrella patens* in response to various environmental stimuli, including light conditions, phytohormone treatments, temperature fluctuations, and exogenous calcium concentrations. Differential effects of light wavelengths on tubulin PTMs in *P. patens* protonema cultures are demonstrated. Previous studies reveal that

monochromatic lights like red light influence plant development and adaptive responses in *P. patens* through the activation of phytochromes, which regulate various processes including chloroplast movement, side branch formation, and pre-mRNA splicing (Kasahara *et al.*, 2004; Uenaka *et al.*, 2005; Shih *et al.*, 2019). White light appears to have a significant impact on the intensity of tyrosinated and acetylated tubulin, whereas red and far-red light treatments induce a substantial increase in polyglutamylated tubulin levels. This suggests distinct regulatory mechanisms for tubulin PTMs in response to different light spectra, possibly mediated through specific photoreceptors and signalling pathways.

Phytohormones like auxin and cytokinin play a crucial role in plant growth and development by coordinating the signaling cascade components that regulate cell division and differentiation ultimately guiding the transition from the vegetative stage to the reproductive stage in *P. patens*. It has been reported plant microtubules play an important role in signal transduction (Gundersen *et al.*, 1999). Here, we found out that treatment with exogenous auxin leads to a significant increase in tyrosinated tubulin intensity, highlighting the role of auxin signaling in modulating microtubule dynamics. Conversely, the treatment with exogenous cytokinin, majorly responsible for bud formation (Reski *et al.*, 1985) and controlling the developmental stage transition (Xiao *et al.*, 2019), resulted in a marked decrease in polyglutamylated tubulin levels, indicating hormone-specific regulation of tubulin PTMs in bud formation and transition of developmental stages. The involvement of auxin in organ initiation, cell division, and differentiation (Armengot *et al.*, 2016; Thelander *et al.*, 2018) and rhizoid development (Jang *et al.*, 2011) might use tyrosinated tubulin for the signal transduction of these functions. Additionally, changes in calcium levels upon phytohormone treatment further emphasize the intricate crosstalk between hormone signalling and calcium dynamics in *P. patens*.

The study reveals complex interactions between temperature, exogenous calcium levels, and tubulin PTMs in *P. patens* protonema cultures. High calcium concentrations lead to a significant decrease in acetylated tubulin levels at both low and high temperatures, suggesting

a role for calcium signalling in modulating tubulin acetylation. Furthermore, temperature fluctuations influence endogenous calcium levels, with distinct responses observed at different temperatures and calcium concentrations, highlighting the intricate interplay between temperature stress and calcium homeostasis. We also demonstrated the sensitivity of the calcium sensor GCaMP 6f, a reliable tool for studying calcium dynamics in *P. patens* protonema cells, in detecting changes in endogenous calcium levels and tubulin modifications upon treatment with varying temperatures and Ca^{2+} concentrations.

A non-linear regression (Curve fit) and Pearson correlation analysis revealed that tyrosinated tubulin and endogenous Ca^{2+} levels are directly proportional to each other irrespective of extracellular Ca^{2+} present in the growing media (Figure 83A & 83B). This relationship suggests a potential functional or regulatory interaction between tyrosinated tubulin dynamics and intracellular Ca^{2+} signaling pathways. One plausible explanation could be that the presence or dynamics of tyrosinated tubulins influence cellular processes that affect Ca^{2+} homeostasis or signaling mechanisms. The inverse proportionality between polyglutamylated tubulins and endogenous Ca^{2+} levels indicates that as the levels of polyglutamylated tubulins increase, the levels of endogenous Ca^{2+} ions decrease, and vice versa (Figure 83E & 83I). This inverse relationship suggests a different regulatory or functional mechanism compared to the relationship observed with tyrosinated tubulin. Polyglutamylated tubulins may modulate cellular processes or signaling pathways that influence intracellular Ca^{2+} dynamics in an inhibitory or regulatory manner. The direct proportionality between tyrosinated tubulins and endogenous Ca^{2+} levels at 25 °C suggests that there is a positive correlation between the levels of tyrosinated tubulins and intracellular Ca^{2+} ions (Figure 84D). This relationship may indicate that tyrosinated tubulins play a role in regulating or influencing intracellular Ca^{2+} dynamics, possibly through interactions with Ca^{2+} binding proteins or signalling pathways. The negative correlation observed between polyglutamylated tubulins and endogenous Ca^{2+} levels at both lower (18 °C) and higher (38 °C) temperatures suggests a complex regulatory relationship

between polyglutamylated tubulins and intracellular Ca^{2+} dynamics in *Physcomitrella patens* (Figure 84C & 84I). Temperature variations may influence the mechanisms underlying the interplay between polyglutamylated tubulins and intracellular Ca^{2+} signalling pathways, highlighting the sensitivity of these regulatory mechanisms to environmental cues. The observed increase in polyglutamylated tubulins with a rise in tyrosinated tubulin levels at 18 °C (Figure 85A) suggests a potential temperature-dependent regulatory relationship between these two tubulin modifications in *P. patens* and the molecular mechanism involved in such interplay needs further investigation. The consistent increase in acetylated tubulin levels with an increase in tyrosinated tubulin levels (Figure 85B, 85E & 85H), irrespective of temperature, suggests a positive correlation between these two tubulin modifications in *P. patens* which may reflect coordinated regulation or functional interactions between acetylated and tyrosinated tubulins. Whereas, a negative correlation has been found between polyglutamylated tubulins and tyrosinated tubulin in the absence of any extracellular Ca^{2+} (Figure 86A). In the presence of high concentrations of Ca^{2+} in the media, the amount of tyrosinated tubulin decreases with an increase of tyrosinated tubulin, and vice versa (Figure 86H). these changes might reflect the involvement of Ca^{2+} in different modifications of tubulin to happen in the cell. The shift from a positive correlation (Figure 86C) between acetylation and polyglutamylation of tubulin in the absence of extracellular Ca^{2+} to a negative correlation (Figure 86F) in the presence of 10 mM Ca^{2+} ions highlight the regulatory influence of extracellular Ca^{2+} concentrations on tubulin post-translational modifications. This observation suggests that extracellular Ca^{2+} levels may modulate the balance between acetylation and polyglutamylation of tubulin, potentially through Ca^{2+} dependent signaling pathways or regulatory mechanisms.

Overall, these results provide insights into the conservation and divergence of tubulin PTMs across plant species, highlighting the importance of these modifications in regulating microtubule dynamics and cellular processes. The combination of *in-silico* analysis and experimental validation offers a comprehensive understanding of tubulin PTMs in *P. patens*

and sheds light on the evolutionary adaptation of PTM regulation in plants. These results also provide valuable insights into the regulatory mechanisms governing tubulin PTMs and calcium dynamics in *P. patens* in response to environmental cues. Further research elucidating the molecular pathways and signaling components involved in these processes will deepen our understanding of plant adaptation to environmental stress and inform strategies for crop improvement and environmental sustainability.

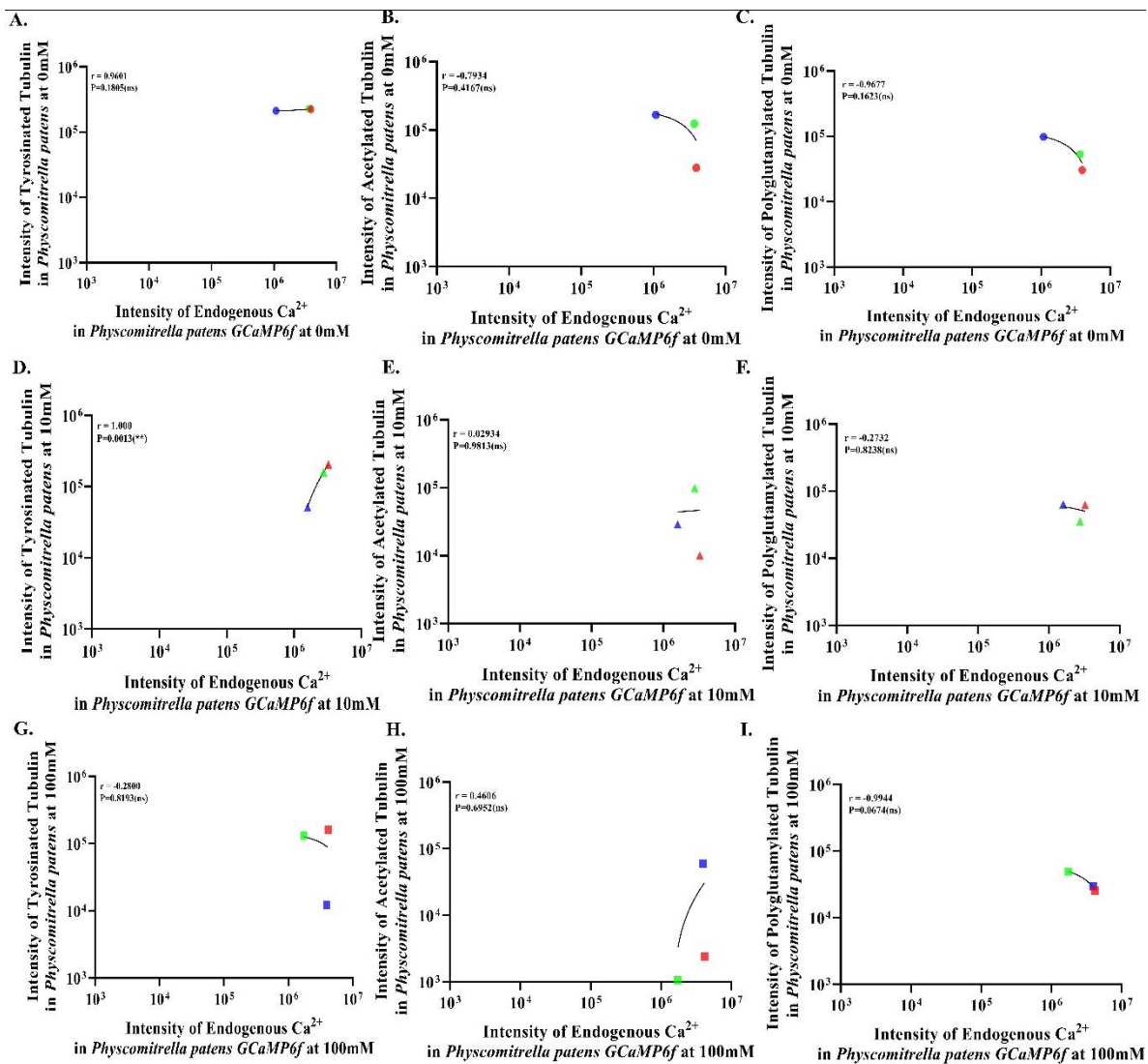


Figure 83. Correlation plot between Endogenous Ca^{2+} levels and tubulin modifications at varying extracellular Ca^{2+} concentrations in *P. patens*. Pearson Correlation (two-tailed P-value) analysis with non-linear regression (curve fit) was done using GraphPad Prism with the highest R-value. Blue, green, and red square indicates 18, 25, and 38 °C respectively. Circle- 0 mM CaCl_2 , triangle-10 mM CaCl_2 and square-100 mM CaCl_2 .

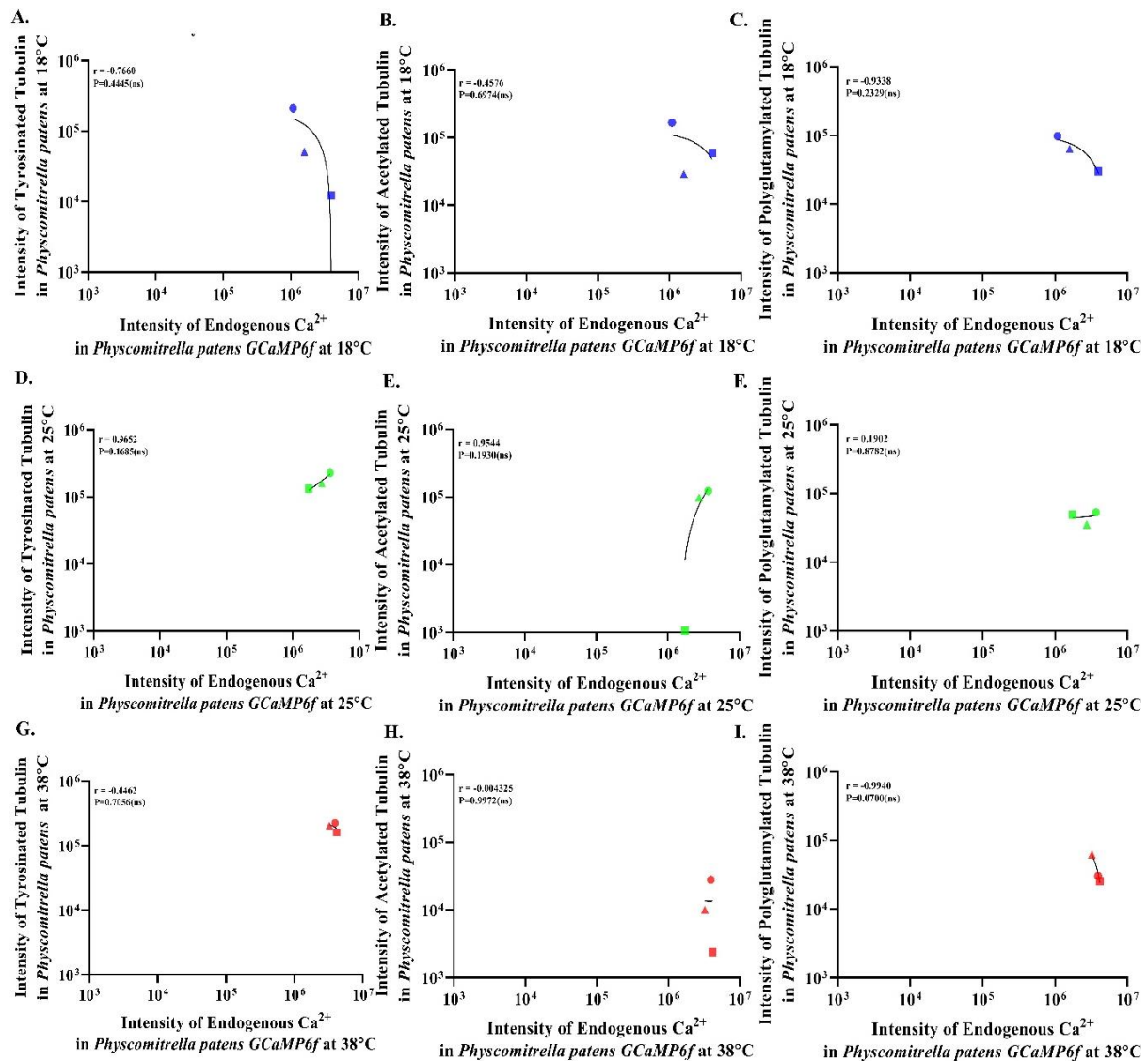


Figure 84. Correlation plot between Endogenous Ca^{2+} levels and tubulin modifications at varying temperatures in *P. patens*. Pearson Correlation (two-tailed P-value) analysis with non-linear regression (curve fit) was done using GraphPad Prism with the highest R-value. Blue, green, and red square indicates 18, 25, and 38 °C respectively. Circle- 0 mM CaCl_2 , triangle-10 mM CaCl_2 and square-100 mM CaCl_2 .

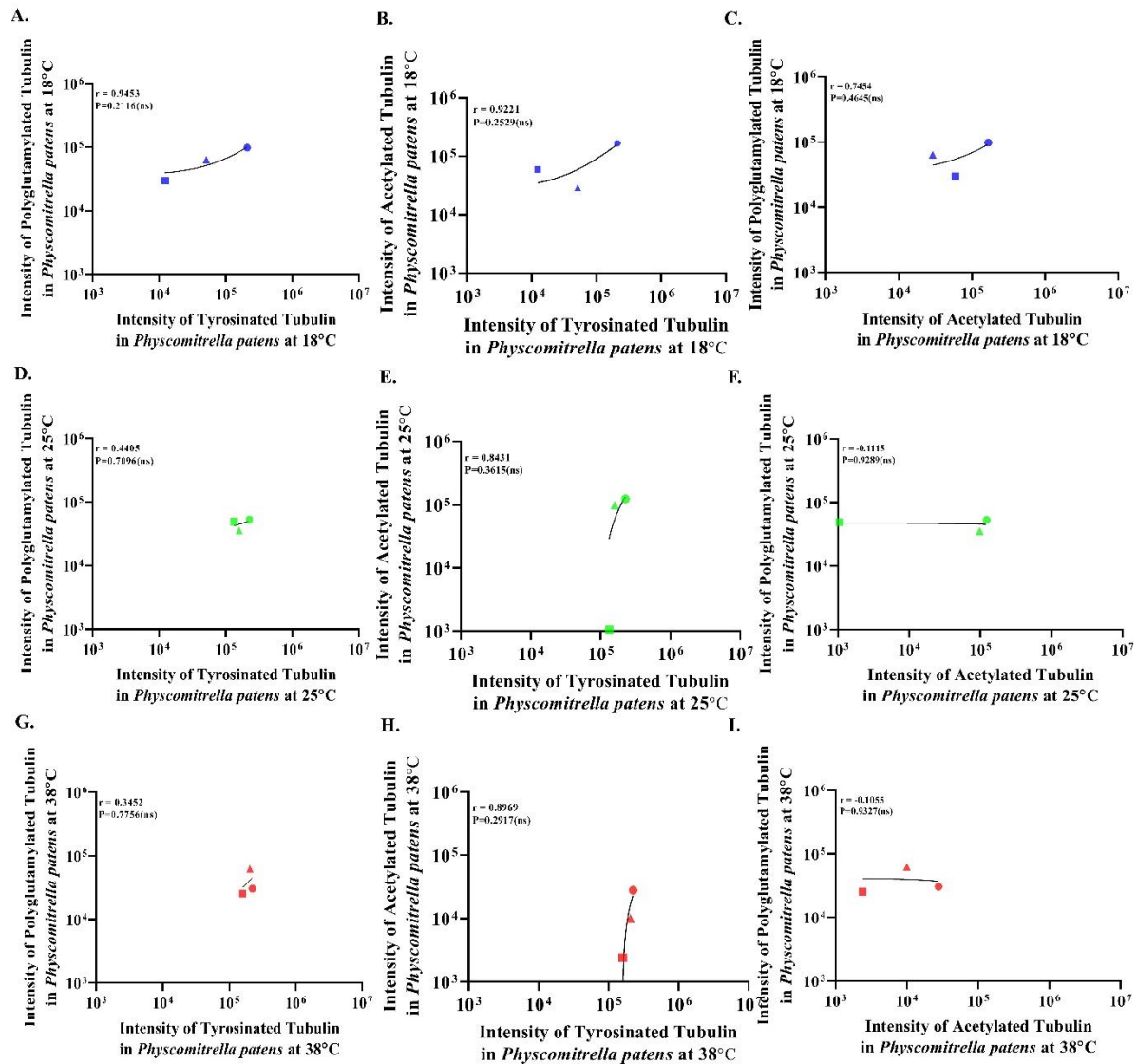


Figure 85. Correlation plot between tubulin modifications at varying temperature treatments in *P. patens*. Pearson Correlation (two-tailed P-value) analysis with non-linear regression (curve fit) was done using GraphPad Prism with the highest R-value. Blue, green, and red square indicates 18, 25, and 38 °C respectively. Circle- 0 mM CaCl_2 , triangle-10 mM CaCl_2 and square-100 mM CaCl_2 .

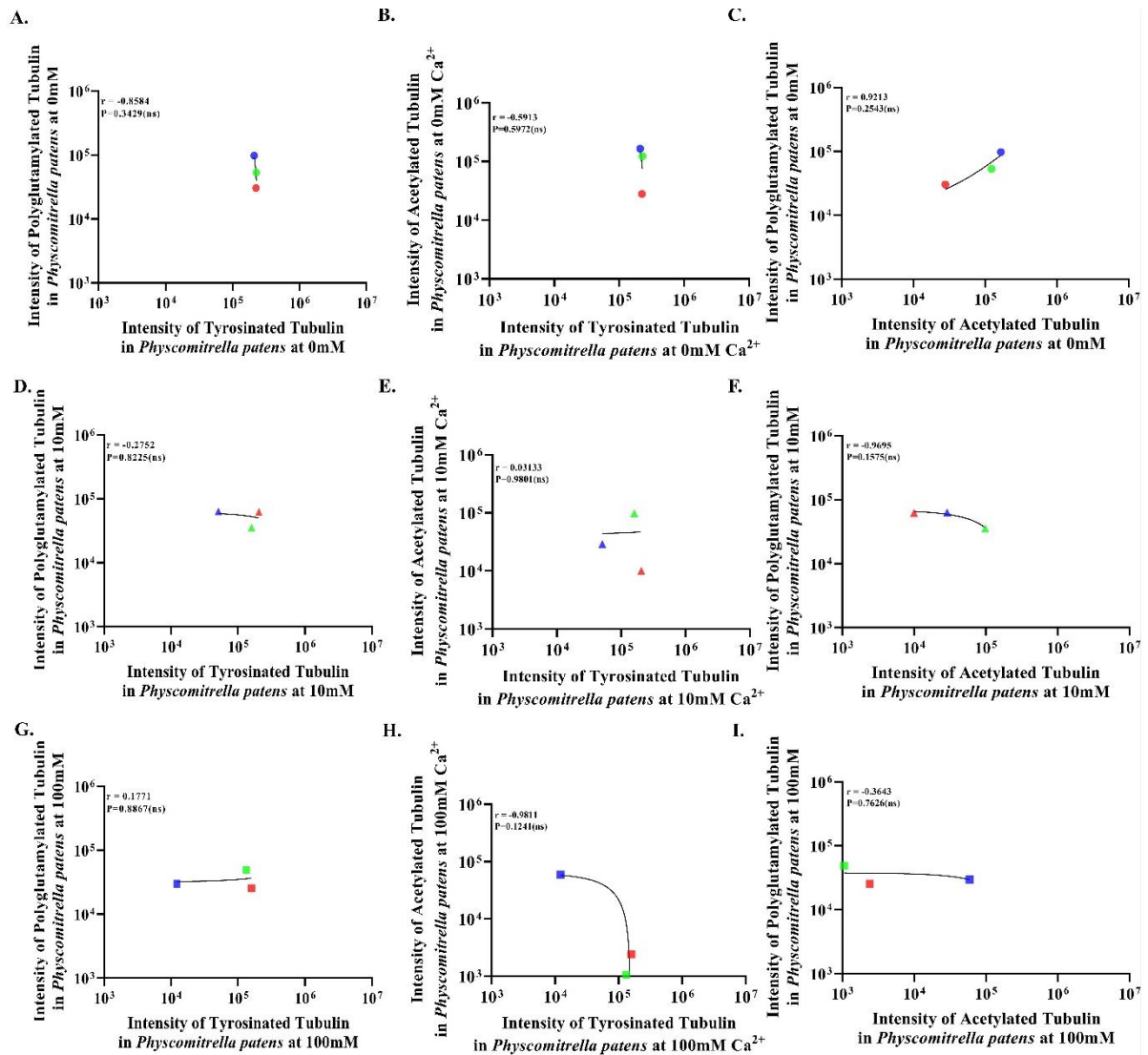


Figure 86. Correlation plot between tubulin modifications at varying extracellular Ca^{2+} treatments in *P. patens*. Pearson Correlation (two-tailed P-value) analysis with non-linear regression (curve fit) was done using GraphPad Prism with the highest R-value. Blue, green, and red square indicates 18, 25, and 38 °C respectively. Circle- 0 mM CaCl_2 , triangle-10 mM CaCl_2 and square-100 mM CaCl_2 .

CHAPTER-7

CORRELATION OF PHYTOCHROME B AND AUXIN IN PATTERNING THE ROOT DEVELOPMENT IN

Arabidopsis thaliana

CHAPTER-7: Correlation of Phytochrome B and Auxin in Patterning the Root

Development in *Arabidopsis thaliana*

7.1. BACKGROUND

The two most significant factors that affect plants at various stages of their lifecycle are light and phytohormones. It has been demonstrated that auxin plays a key role in regulating plant development (Vanneste and Frmil, 2009). In the past years, methods like isotope labeling and GC-MS were used to quantify phytohormones in plants (Petersson *et al.*, 2009; Poefirio *et al.*, 2016). Because these methods involve tissue disruption, it is challenging to study the dynamics of an intact plant. DROUGHT RESISTANT 5 (DR5) is an auxin-based synthetic promoter. DR5::GUS and DR5::GFP consist of -glucuronidase (GUS) and GFP reporters respectively (Chen *et al.*, 2013). They help in monitoring auxin homeostasis and signaling. However, they do not reflect the exact accumulation of the auxin in the cell. It has been demonstrated that a recently developed chemiluminescence-based ratio-metric sensor (the pMIR auxin sensor) offers better and more accurate information pertaining to auxin dynamics. It is made up of various sequences: Renilla - 2A-Firefly Sensor Module. The luciferases Renilla and Firefly are, while the protein sequence 2A helps in stoichiometric co-expression as well and the sequence from DII of AUX/IAA (Wends *et al.*, 2013) makes up the sensor module (SM). When auxin is present in very little or no auxin inside the cell, both the luciferases are expressed and the ratio of firefly to renilla luminescence will be around one. However, when auxin is in excess, it binds to TIR1 and then SM, further degrading SM along with firefly luciferase. Then, the luminescence of firefly will decrease but renilla luminescence will remain constant, as a result, the ratio of firefly to renilla luminescence will decrease and will be less than one (Wends *et al.*, 2013). This ratiometric luminescence signal provides exact and accurate information about the distribution of auxin in specific cells and time. This sensor is highly sensitive and cancels out the effects of cellular surroundings or environment.

T-DNA insertion, site-directed mutagenesis, ethyl methane sulfonate (EMS) mutagenesis, radiation-based mutagenesis, and other techniques have all been used for integrating mutations within the *At* gene (Sikora *et al.*, 2011). T-DNA insertion and EMS mutagenesis are among them, and both have been considered the best possibilities for forward genetic approaches. This method eliminates the need for any preconceived notions by selecting mutants based on discernible phenotypic differences. It is incredibly useful for examining novel elements involved in particular phenomena or signalling pathways as well as for investigating the role of specific genes. Particularly when compared to the T-DNA insertion method, EMS mutagenesis stands out as a frequently used method for generating mutants. It offers the advantage of efficiently producing a substantial number of mutants while saving time. Furthermore, it aids in deciphering the functional roles of individual amino acids in protein activity (Kim *et al.*, 2006). EMS is an alkylating agent known for inducing point mutations, although reports suggest it can also lead to base pair insertions or deletions. Specifically, EMS reacts with guanine, a nucleobase in DNA, forming O6-ethylguanine. This abnormal guanine is perpetuated during DNA replication, where DNA polymerase mistakenly adds thymine instead of cytosine in response to O6-ethylamine. This process results in random mutations, causing AT to GC and GC to AT transition point mutations in 99 % of cases. Moreover, EMS can occasionally generate stop codon and missense mutations (Sega, 1984).

Light signalling mutants like *hy3* and *srll* have been rendered feasible by EMS mutagenesis. EMS mutagenesis was used to generate the PHYB mutant *hy3* by seeking out hypocotyls that were longer than the wild type under W light. This mutant demonstrated early flowering, decreased chlorophyll content, elongated hypocotyls, petioles, and long root hairs (Reed *et al.*, 1993). On the other hand, PHYB over-expressor (PHYB ox) lines were used to mutagenically generate *srll* mutants. Under continuous R (cR) light, these mutants are hypersensitive and have shorter hypocotyls than PHYB ox and wild-type, but not under continuous F (cFR) light. These mutants, which differ from the wild type in having larger cotyledon areas and shorter

petioles, are monogenic, recessive, and extragenic R-light-specific. Following a brief exposure to higher fluence R light irradiation, CHLOROPHYLL A/B BINDING (CAB) expression was upregulated two-fold in *sr11* mutants. PHYB has been specifically attributed to the increased sensitivity of *sr11* mutants to R light. When exposed to low fluences of R and FR light, the phytochrome signalling 2 (*psi2*) mutants, another EMS mutant, exhibit hypersensitivity, shortening hypocotyls. R light exposure greater than $45 \text{ mol m}^{-2} \text{ sec}^{-1}$ causes necrotic lesions that resemble those seen in the hypersensitive response in this mutant. These lesions' induction has been linked to PHYA and PHYB (Genoud *et al.*, 1998).

N651 expressing lines were mutagenized with EMS to examine the function of the N-terminal 651 amino acids in the PHYB domain. Instead of changes in its expression, the generated mutants were hyposensitive as a result of decreased PHYB activity (Oka *et al.*, 2008). This chapter explores the molecular elements involved in the cross-talk between red light and auxin by producing hyposensitive and hypersensitive Col-0 luciferase (Col-0 Luc) and DR5::GFP lines with altered root architecture using EMS mutagenesis.

7.2. RESULTS

7.2.1. Generation and cloning of fluorescent/luciferase-based auxin sensor constructs in gateway cassette

In this current work, the firefly, AUX/IAA, 2A, and renilla have been amplified in a single stretch and then cloned in the pDONR201 vector by BP gateway cloning. After that, it was transformed into the DH5 α strain of *E. coli*, and the selection was performed in kanamycin. The antibiotic-resistant colonies were confirmed by PCR (Figure 87).

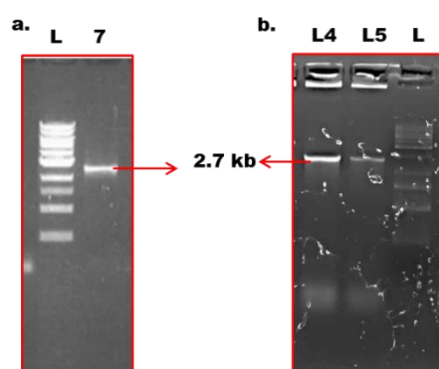


Figure 87. PCR screening after (a) BP and (b) LR reaction for positive cloning with luciferase auxin sensor (Courtesy- Dr. Sony Kumari)

Then, the plasmid of the positive colony was cloned in the pB2GW7 destination vector by LR gateway cloning despite the 35S:CFP:GW vector as mentioned in the materials and method, and further transformation was done in the DH5 α strain of *E. coli*. The selection was performed in spectinomycin antibiotic, the resistant colonies were screened through colony PCR (Figure 88).

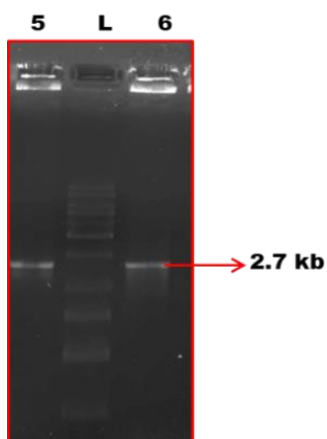


Figure 88. Colony PCR for positive transformed *Agrobacterium* with luciferase auxin sensor (Courtesy: Dr. Sony Kumari)

The plasmid of the positive colony was transformed into *Agrobacterium tumefaciens* by the heat shock method. The selection was done in the presence of spectinomycin and rifampicin, the resistant *Agrobacteria* colonies were further screened by colony PCR (Figure 89). The positive colonies were used to transform Col-0 plants via the floral dip method. The transgenic lines were generated, bulked, and screened through PCR for three generations. and homozygous lines were obtained. The obtained seeds from the above bulking were further checked for positive lines and homozygosity by PCR analysis. The single band at 3 Kb indicated that the lines are homozygous (Figure 90).

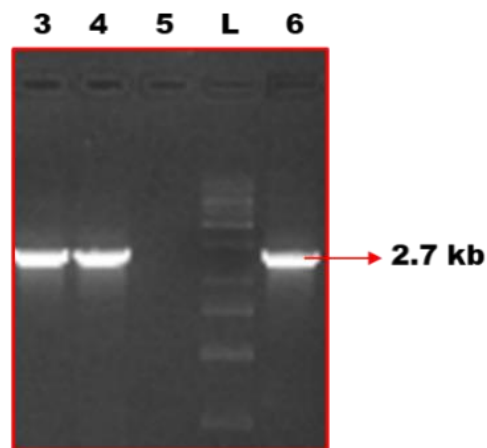


Figure 89. PCR for transgenic Col-0 plants with luciferase auxin sensor (Courtesy: Dr. Sony Kumari)

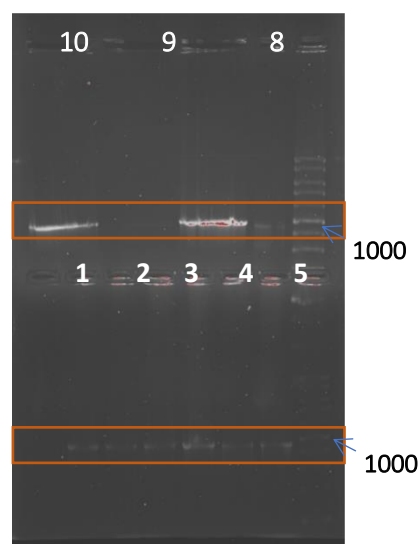


Figure 90. PCR analysis of transformed seeds (F3 generation). Lanes 1 to 10 indicate transformed lines of different pools. (Courtesy: Dr. Sony Kumari)

Further, a transgenic DR5::GFP in the Col-0 line was generated by the floral dip method with a transformed positive culture of *Agrobacterium* with DR5:GFP. The transgenic Col-0 seedlings were screened through microscopy for the presence of GFP in the root tip (Figure 91).

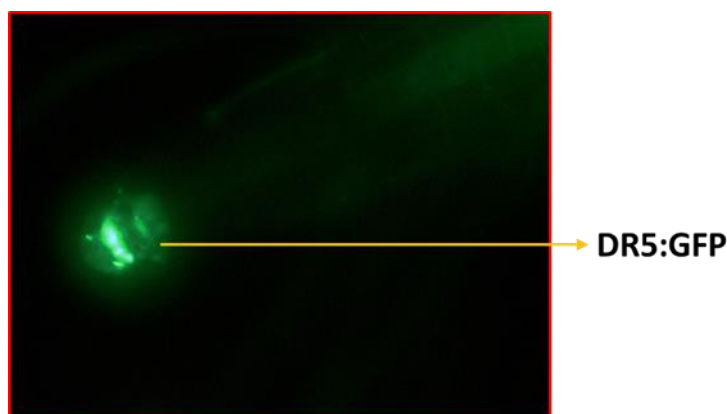


Figure 91. DR5::GFP expression in the root tip of transgenic DR5::GFP plants. (Courtesy: Dr. Sony Kumari)

7.2.2. EMS mutagenesis of auxin sensor and DR5:: GFP expressing Col-0 WT lines and bulking of seeds.

To cancel out any effect due to cloning, both the lines i.e., Col-0 Luc (luciferase-based auxin sensor) and DR5::GFP (fluorescent-based auxin sensor) were used to study the phenotypic difference, if any, under different light conditions. The hypocotyl and root lengths of 7-day-old seedlings were observed under varying light conditions like Red, Far-red, and blue along with positive and negative controls i.e., white light and dark respectively. The hypocotyl and root lengths under all the light conditions were similar as compared to the Col-0 WT (Table 12).

Light Condition	Col-0	Col-0 Luc	DR5::GFP
DARK	1.35±0.2	1.15±0.2	1.25±0.2
WHITE	0.18±0.2	0.15±0.2	0.17±0.2
RED	0.22±0.2	0.18±0.2	0.19±0.2
FAR-RED	0.18±0.2	0.19±0.2	0.18±0.2
BLUE	0.19±0.2	0.20±0.2	0.18±0.2

Table 12. Hypocotyl lengths (average) of 7 day old seedlings of Col-0, Col-0 Luc, and DR5::GFP lines grown under dark, white, red, far-red, and blue light at 22 °C.

Furthermore, these luciferase and fluorescent-based auxin sensor seed lines were EMS mutagenized with 0.2% EMS solution in water. Seeds were soaked in EMS solution for 12 hours and were mutagenized as described in the materials and method. These mutagenized seeds were then sown on soil in different pools (Figure 92).



Figure 92. EMS mutagenesis and bulking of Col-0 Luc and DR5::GFP lines in different pools

The seeds were bulked and collected individually from different pools in separate vials. These vials were further named V 1, V 2, V 3.....V 50 and ED 1, ED 2, ED 3.....ED 50 for EMS mutagenized Col-0 Luc and DR5: GFP lines respectively.

7.2.3. Screening for hypo and hyper-sensitive mutants under saturating RG9 red light field

The obtained seeds from different pools were subsequently screened under continuous red light (saturating RG9 red light) at 22 °C based on the hypocotyl lengths as compared to their respective controls. The initial screening was done from 650 EMS mutagenized Col-0 Luc and 600 EMS mutagenized DR5::GFP lines. The hypocotyls which were longer than the wild type was termed hypersensitive mutants. Similarly, the hypocotyls which were shorter than the wild type were named hyposensitive mutants (Figure 93).

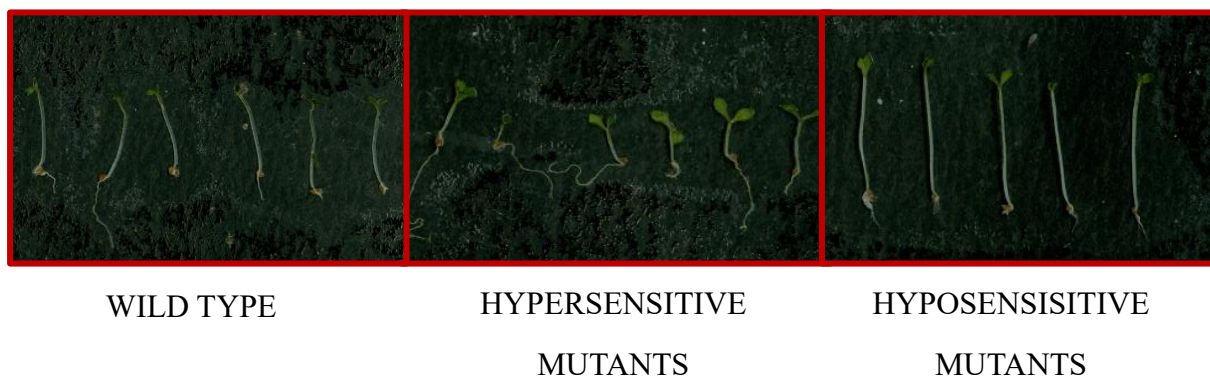


Figure 93. Screening of mutants based on their hypocotyl lengths

In total 211 EMS mutagenized Col-0 Luc lines were screened which showed the above phenotype. Among these, 80 hyposensitive and 131 hypersensitive mutants were obtained. In addition, 307 EMS mutagenized DR5::GFP lines were selected out of which 75 were hyposensitive and 232 were hypersensitive. These mutants were considered as F0 generation. The hypersensitive and hyposensitive mutants which retained the phenotype were further screened under continuous red light till F3 generation. In the F1 generation, 93 EMS mutagenized Col-0 Luc (42 were hyposensitive and 51 were hypersensitive) and 119 EMS mutagenized DR5::GFP (38 were hyposensitive and 81 were hypersensitive) mutants were selected. Similarly, in the F2 generation 38 EMS mutagenized Col-0 Luc (11 were hyposensitive and 27 were hypersensitive) and 63 EMS mutagenized DR5::GFP (23 were hyposensitive and 40 were hypersensitive) mutants were selected. Finally, in the F3 generation, 19 EMS mutagenized Col-0 Luc (6 were hyposensitive and 13 were hypersensitive) and 33 EMS mutagenized DR5::GFP (8 were hyposensitive and 25 were hypersensitive) mutants were selected. The mutants generated are summarised in Figure 94.

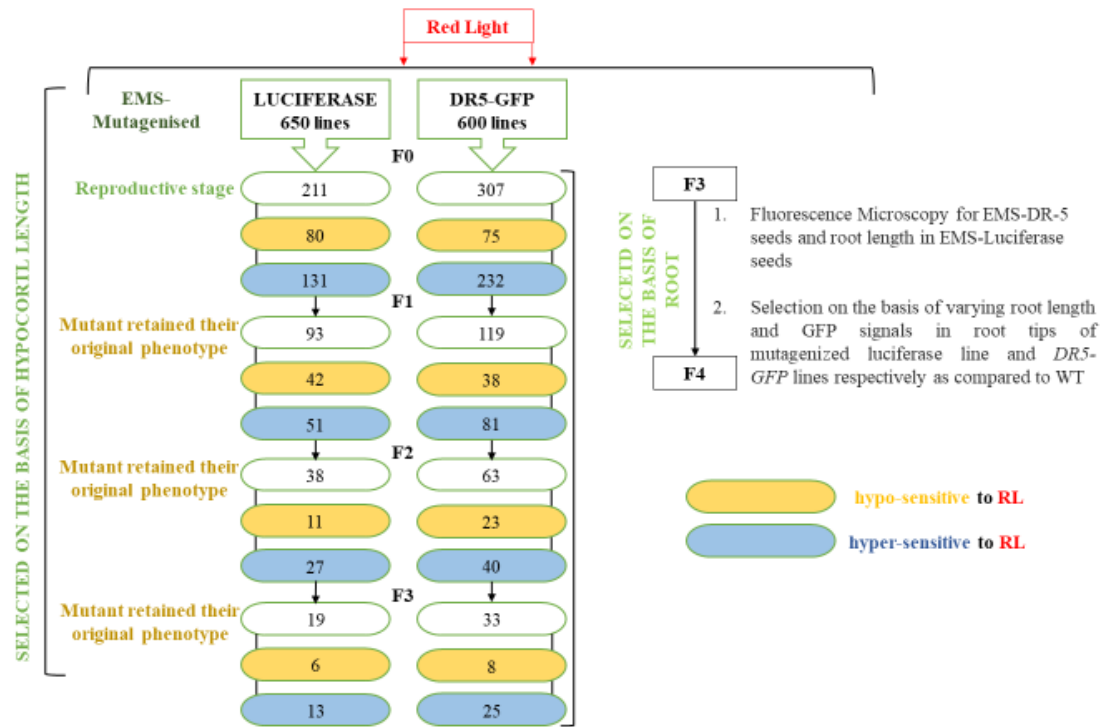


Figure 94. Summary of EMS mutagenized Col-0 Luc and DR5::GFP mutants generated and screened based on hypo and hypersensitive hypocotyl lengths

7.2.4. From the pool of defective in red light, further screening for mutants showing root patterning

Mutant seed lines were further sterilized and sown on MS media. After cold stratification, seeds were grown under diurnal red light (16 hours light/ 8 hours dark) for root patterning study. Seedlings showing altered or defective root architecture were selected and bulked. Seedlings with defective in both red light signalling and root architecture were further checked for alteration in primary root and hypocotyl lengths. The differences in primary root and hypocotyl lengths are listed below in Table 13.

GENOTYPE	ROOT LENGTH (mm)	HYPOCOTYL LENGTH (mm)
DR5::GFP WT	1.6±0.1	0.5±0.1
ED 16 hypo 1-3-2	0.7±0.1	0.1±0.1
ED 91 hypo 1-2-2	0.6±0.1	0.2±0.1
ED 99 hypo 1-2-2	2.2±0.1	0.2±0.1
ED 100 hypo 1-1-1	0.6±0.1	0.2±0.1
ED 118 hypo 1-1-1	0.6±0.1	0.3±0.1
ED 120 hypo 1-2-1	0.9±0.1	0.2±0.1
ED 121 hypo 1-2-2	0.3±0.1	0.2±0.1
ED 127 hypo 1-3-1	3.2±0.1	0.2±0.1
ED 134 hypo 1-2-2	0.3±0.1	0.1±0.1

ED 139 hypo 1-2-3	0.4±0.1	0.1±0.1
ED 143 hypo 1-3-1	0.5±0.1	0.2±0.1
ED 144 hypo 1-2-1	0.6±0.1	0.1±0.1
ED 147 hypo 1-3-2	0.6±0.1	0.2±0.1
ED 160 hypo 1-2-3	0.4±0.1	0.1±0.1
ED 166 hypo 1-2-3	0.2±0.1	0.1±0.1
ED 173 hypo 1-1-1	0.8±0.1	0.5±0.1
ED 176 hypo 1-2-1	0.7±0.1	0.2±0.1
ED 179 hypo 1-1-2	0.3±0.1	0.1±0.1
ED182 hypo 1-1-2	0.6±0.1	0.1±0.1
ED 188 hypo 1-1-2	0.5±0.1	0.1±0.1
ED 196 hypo 1-3-2	2.4±0.1	0.3±0.1
ED 212 hypo 1-3-2	0.9±0.1	0.3±0.1
ED 226 hypo 1-1-1	2.4±0.1	0.3±0.1
ED 251 hypo 1-2-1	0.3±0.1	0.1±0.1
ED 253 hypo 1-3-3	3.1±0.1	0.2±0.1
ED 180 hyper 1-1-3	0.7±0.1	0.2±0.1
ED 184 hyper 1-3-1	0.4±0.1	0.1±0.1
ED 203 hyper 1-1-1	0.9±0.1	0.3±0.1
ED 222 hyper 1-1-1	1.7±0.1	0.5±0.1
ED 235 hyper 1-1-3	0.7±0.1	0.2±0.1
ED 245 hyper 1-3-3	0.9±0.1	0.1±0.1
ED 258 hyper 1-3-1	2.3±0.1	0.3±0.1
ED 268 hyper 1-1-3	1.7±0.1	0.4±0.1
GENOTYPE	ROOT LENGTH (mm)	HYPOCOTYL LENGTH (mm)
COL-0 LUC	1.8±0.1	0.4±0.1
V 3 hypo 1-2-3	1.1±0.1	0.2±0.1
V 36 hypo 1-1-3	0.6±0.1	0.1±0.1
V 37 hypo 1-1-2	0.5±0.1	0.1±0.1
V 53 hypo 1-2-3	0.8±0.1	0.1±0.1
V 64 hypo 1-2-1	1.3±0.1	0.1±0.1
V 66 hypo 1-3-3	0.8±0.1	0.1±0.1
V 128 hypo 1-2-3	1.0±0.1	0.1±0.1
V 143 hypo 1-1-3	1.5±0.1	0.1±0.1
V 144 hypo 1-3-3	1.3±0.1	0.2±0.1
V 145 hypo 1-1-2	0.9±0.1	0.1±0.1
V 152 hypo 1-3-3	0.6±0.1	0.1±0.1
V 161 hypo 1-3-1	1.2±0.1	0.2±0.1
V 163 hypo 1-3-2	0.5±0.1	0.2±0.1
V 188 hyper 1-1-2	1.5±0.1	0.3±0.1
V 198 hypo 1-2-2	0.6±0.1	0.1±0.1
V 10 hyper 1-3-3	2.1±0.1	0.2±0.1
V 20 hyper 1-3-1	1.5±0.1	0.1±0.1
V 27 hyper 1-1-2	1.3±0.1	0.2±0.1
V 129 hyper 1-1-1	2.1±0.1	0.1±0.1

Table 13. Primary root and hypocotyl length measurements of EMS mutagenized DR5::GFP and Col-0 Luc seed lines.

7.3. DISCUSSION

Plants respond to different light qualities and pattern their root architecture. Among them, red light has an important role. Although a microarray experiment has shown changes in a set of auxin-related genes in response to red light, it has been done under sub-optimal light fluence and duration where PhyB does not show High-Irradiance Responses (HIR). Changes in the hypocotyl length and root development have been known for years to be the function of both light and hormones. Among a few phytohormones, auxin has gained much attention for several reasons. Auxin homeostasis is light dependent, and a yet unidentified fairly complicated molecular network perhaps governs this. Many components interact with light and auxin signalling which are yet to be identified. Light-dependent auxin transport mechanism and its signalling have also been studied. A homeodomain leucine-zipper protein encoded by *ATHB2* is involved in auxin signalling, which has been shown to operate downstream to red light photoreceptors. Change in the red: far-red light ratio induces *ATHB2* accumulation, and its over-expression has been shown to inhibit cotyledon expansion and enhance hypocotyl elongation. It also results in reduced secondary growth of vascular tissue and fewer lateral roots. Exogenous auxin treatment can recover *ATHB2*-induced lateral root phenotype suggesting that *ATHB2* is involved both in the shade avoidance response as well as in auxin transport and signalling (Steindler *et al.*, 1999). Although the expression of some of the auxin-responsive genes like *GH3a* is known to be regulated by PhyB, the molecular mechanism of regulation of the auxin abundance by phytochrome is still unclear and is a promising area of research (Mashiguchi *et al.*, 2011). Lateral root emergence is regulated by shoot-localized phytochromes as phytochromes partly control the auxin distribution and play an important role in root development (Halliday *et al.*, 2009). Phytochrome Interacting Factors (PIFs) have been shown to play an important role in plant growth and development through changing responses to auxin signalling and synthesis (Hornitschek *et al.*, 2012; Franklin *et al.*, 2011). Relatively recent studies suggested that PhyB induces shoot branching by suppressing auxin signalling.

(Reddy *et al.*, 2014). Recently, it has been shown that red light causes changes in the activity of auxin-binding Protein 1 (ABP1) and hence ABP1 can be a strong connecting candidate between auxin response and red-light signalling. (Effendi *et al.*, 2013). Furthermore, microarray analysis identifies a group of auxin-related genes induced by red light (Molas *et al.*, 2006). The above-mentioned information is very helpful to explore the involvement of R light in root development where the mechanism behind the role of light-auxin crosstalk in the development of root is not well established. For this, a forward genetics approach is used to identify other novel regulators which may be involved in light and auxin signalling.

In the present work, it has been attempted to identify other candidate genes playing a role apart from PHYB in light and auxin crosstalk in root development. Hence, the EMS mutants of Col-0 Luc and DR5::GFP were generated in this current work. The mutants hypo and hyper-sensitive to R light which had altered hypocotyl morphology were screened and generated. Further, hypo and hyper-sensitive mutants with different root architectures were screened. These mutant lines generated in the current work also displayed developmental defects at the vegetative stage. These hyposensitive mutants of Col-0 Luc and DR5::GFP with altered root architecture can have defects in red light signalling and auxin-associated pathways. These mutants can be further subjected to next-generation sequencing or linkage mapping to know the exact position of the mutation. This study can help in providing information about some novel candidate genes involved in PHYB and auxin cross-talk to regulate root development. It will also help in generating plants having improved root growth with drought resistance, pathogen resistance, and water logging resistance properties.

CHAPTER 8

CONCLUSION AND FUTURE PERSPECTIVE

CHAPTER 8: CONCLUSION AND FUTURE PERSPECTIVE

Combining the findings from various studies provides a comprehensive understanding of the intricate mechanisms governing plant development, stress responses, and environmental adaptations. The ubiquitous expression of GI throughout all stages of plant development underscores its multifaceted pleiotropic roles in diverse physiological processes, ranging from seed dormancy breaking to fruit setting. Many of the above-mentioned outcomes incorporate information from light input and external temperature, making this an intriguing but complex area of plant science. The *in-silico* analyses provide valuable insights into the evolutionary history, conservation patterns, and structural characteristics of the GIGANTEA protein across diverse plant taxa. Despite its large size and pleiotropic functions spanning 14 exons, no conserved domains homologous to any eukaryotic protein have been identified within GI. Utilizing different mutations at putative domains using CRISPR/Cas9 genome editing tools can shed light on the functional roles associated with each exon of GI. Moreover, the absence of GI homologs in most lower plants presents an excellent opportunity to study GI function in naturally occurring *gi* null species, revealing insights into functions lacking or over-presented in lower plants compared to higher plants. To understand this, it would be interesting to investigate the role of GI in *Physomitrella patens* through transformation and study its roles that might evolve, otherwise lost, with particular emphasis on stress tolerance. It would be rather thought provoking to understand the cross-talk between GI and brassinosteroid signaling in lower plants like mosses which are often linked to pathogen response. Furthermore, it would be very intriguing to comprehend if GI acts as a de-glucanase removal enzyme antagonizing spindly function, directly or indirectly. Comparative studies between full-length GI and mutant GI in higher plants can elucidate the significance of GI duplications in different species and offer insights into the evolutionary divergence of GI functions across plant taxa, a phenomenon yet to be explored. Understanding the evolutionary dynamics and functional diversity of GI contributes to our knowledge of plant evolution and adaptation strategies, offering avenues for

further experimental investigations into its biological roles and regulatory mechanisms in plant biology. Further studies on the putative transmembrane loops of GI across various species can be useful in providing profound insights into the structural and functional evolution of GI across various organisms. Furthermore, the conservancy of the GI promoter region and the presence of critical regulatory elements, such as Light-Responsive Elements (LREs), Hormone-Responsive Elements and Stress-Responsive Elements can elucidate the complex regulatory network that governs the mechanistic role of GI in different biological functions in different species. Furthermore, investigating the co-evolutionary dynamics between GI and its interacting partners within regulatory networks can shed light on the molecular basis of trait evolution and phenotypic diversity in plants. Integrating evolutionary genomics, population genetics, and ecological modeling approaches will enable us to reconstruct the evolutionary pathways of GI and its functional adaptations in response to changing environmental conditions. By unraveling the evolutionary mysteries surrounding GI, we not only enhance our understanding of plant evolutionary biology but also pave the way for harnessing its adaptive potential in crop improvement and ecosystem resilience strategies in the face of global environmental change.

Additionally, the study underscores the significant role of GI, using CRISPR mutant of *gi*, in mediating drought and salinity resistance in *Arabidopsis thaliana*, particularly under long-day (LD) conditions. The contrasting responses observed in CRISPR mutant of *gi* under short-day (SD) conditions emphasize the influence of photoperiod on GI-mediated stress responses. Despite its involvement in stress response mechanisms, GI does not regulate photoperiodic flowering, drought, and salinity resistance under SD conditions. These findings advance our understanding of plant responses to abiotic stress and provide insights for developing stress-tolerant crop varieties in the future.

Furthermore, research on the involvement of GI in controlling biotic stress responses during *F. oxysporum* infection in *Arabidopsis thaliana* highlights its role in enhancing disease resistance.

The study elucidates the molecular mechanisms underlying GI's contribution to biotic stress tolerance, particularly against *F. oxysporum*-induced vascular wilt disease. Insights into the modulation of jasmonic acid pathway genes and the involvement of ABA, SA pathways genes, and oxylipins provide valuable information for developing strategies to improve crop yield in the face of pathogen infections.

Moreover, investigations into the roles of ABP1 in plant development and stress responses reveal its multifaceted functions in root growth, flowering regulation, and dehydration tolerance. ABP1's involvement in hormonal regulation and defense mechanisms opens avenues for further research to understand the molecular mechanisms underlying these processes and their implications for plant adaptation and stress resilience.

Additionally, the study on tubulin post-translational modifications (PTMs) across plant species offers insights into the regulatory mechanisms governing microtubule dynamics and cellular processes. The combination of *in-silico* analysis and experimental validation deepens our understanding of PTM regulation and calcium dynamics in response to environmental cues, providing valuable information for crop improvement and environmental sustainability efforts.

Furthermore, efforts to identify candidate genes involved in light and auxin crosstalk in root development highlight the potential for generating plants with improved root growth and stress resistance properties. The generation of mutant lines and subsequent analyses offer opportunities to uncover novel genetic pathways and mechanisms underlying root development and stress responses, paving the way for the development of resilient crop varieties.

Overall, these studies collectively contribute to our understanding of plant biology, stress responses, and environmental adaptations, offering promising avenues for future research and crop improvement strategies.

CHAPTER 9

BIBLIOGRAPHY

CHAPTER 9: BIBLIOGRAPHY

- Abdrakhamanova, A., Wang, Q.Y., Khokhlova, L. and Nick, P., 2003. Is microtubule disassembly a trigger for cold acclimation?. *Plant and Cell Physiology*, 44(7), pp.676-686.
- Adamowski, M. and Friml, J., 2015. PIN-dependent auxin transport: action, regulation, and evolution. *The Plant Cell*, 27(1), pp.20-32.
- Adams, S., Manfield, I., Stockley, P. and Carré, I.A., 2015. Revised morning loops of the *Arabidopsis* circadian clock based on analyses of direct regulatory interactions. *PLoS One*, 10(12), p.e0143943.
- Aebi, H., 1984. [13] Catalase in vitro. In *Methods in enzymology* (Vol. 105, pp. 121-126). Academic press.
- Ahmad, P., Rasool, S., Gul, A., Sheikh, S.A., Akram, N.A., Ashraf, M., Kazi, A.M. and Gucel, S., 2016. Jasmonates: multifunctional roles in stress tolerance. *Frontiers in plant science*, 7, p.813.
- Akashi, T., Kawasaki, S. and Shibaoka, H., 1990. Stabilization of cortical microtubules by the cell wall in cultured tobacco cells: Effects of extensin on the cold-stability of cortical microtubules. *Planta*, 182, pp.363-369.
- Akashi, T., Kawasaki, S. and Shibaoka, H., 1990. Stabilization of cortical microtubules by the cell wall in cultured tobacco cells: Effects of extensin on the cold-stability of cortical microtubules. *Planta*, 182, pp.363-369.
- Akella, J.S., Wloga, D., Kim, J., Starostina, N.G., Lyons-Abbott, S., Morrisette, N.S., Dougan, S.T., Kipreos, E.T. and Gaertig, J., 2010. MEC-17 is an α -tubulin acetyltransferase. *Nature*, 467(7312), pp.218-222.
- Alabadí, D., Gallego-Bartolomé, J., Orlando, L., García-Cárcel, L., Rubio, V., Martínez, C., Frigerio, M., Iglesias-Pedraz, J.M., Espinosa, A., Deng, X.W. and Blázquez, M.A., 2008. Gibberellins modulate light signaling pathways to prevent *Arabidopsis* seedling de-etiolation in darkness. *The Plant Journal*, 53(2), pp.324-335.
- Alabadí, D., Gil, J., Blázquez, M.A. and García-Martínez, J.L., 2004. Gibberellins repress photomorphogenesis in darkness. *Plant physiology*, 134(3), pp.1050-1057.
- Alabadí, D., Oyama, T., Yanovsky, M.J., Harmon, F.G., Más, P. and Kay, S.A., 2001. Reciprocal regulation between TOC1 and LHY/CCA1 within the *Arabidopsis* circadian clock. *Science*, 293(5531), pp.880-883.
- Alloisio, N., Queiroux, C., Fournier, P., Pujic, P., Normand, P., Vallenet, D., Médigue, C., Yamaura, M., Kakoi, K. and Kucho, K.I., 2010. The *Frankia alni* symbiotic transcriptome. *Molecular Plant-Microbe Interactions*, 23(5), pp.593-607.

- Aloni, R., Aloni, E., Langhans, M. and Ullrich, C.I., 2006. Role of auxin in regulating *Arabidopsis* flower development. *Planta*, 223, pp.315-328.
- Aloni, R., Aloni, E., Langhans, M. and Ullrich, C.I., 2006. Role of cytokinin and auxin in shaping root architecture: regulating vascular differentiation, lateral root initiation, root apical dominance and root gravitropism. *Annals of botany*, 97(5), pp.883-893.
- Alonso-Blanco C, Andrade J, Becker C et al (2016) 1,135 genomes reveal the global pattern of polymorphism in *Arabidopsis thaliana*. *Cell* 166(2):481–491
- Anderson, J.P., Badruzsaufari, E., Schenk, P.M., Manners, J.M., Desmond, O.J., Ehlert, C., Maclean, D.J., Ebert, P.R. and Kazan, K., 2004. Antagonistic interaction between abscisic acid and jasmonate-ethylene signaling pathways modulates defense gene expression and disease resistance in *Arabidopsis*. *The Plant Cell*, 16(12), pp.3460-3479.
- Ando, E., Ohnishi, M., Wang, Y., Matsushita, T., Watanabe, A., Hayashi, Y., Fujii, M., Ma, J.F., Inoue, S.I. and Kinoshita, T., 2013. TWIN SISTER OF FT, GIGANTEA, and CONSTANS have a positive but indirect effect on blue light-induced stomatal opening in *Arabidopsis*. *Plant physiology*, 162(3), pp.1529-1538.
- Arieti, R.S. and Staiger, C.J., 2020. Auxin-induced actin cytoskeleton rearrangements require AUX1. *New Phytologist*, 226(2), pp.441-459.
- Armengot, L., Marquès-Bueno, M.M. and Jaillais, Y., 2016. Regulation of polar auxin transport by protein and lipid kinases. *Journal of experimental botany*, 67(14), pp.4015-4037.
- Aström, H., 1992. Acetylated alpha-tubulin in the pollen tube microtubules. *Cell biology international reports*, 16(9), pp.871-881.
- Bader, Z.E., Bae, M.J., Ali, A., Park, J., Baek, D. and Yun, D.J., 2023. GIGANTEA-ENHANCED EM LEVEL complex initiates drought escape response via dual function of ABA synthesis and flowering promotion. *Plant Signaling & Behavior*, 18(1), p.2180056.
- Baek, D., Kim, W.Y., Cha, J.Y., Park, H.J., Shin, G., Park, J., Lim, C.J., Chun, H.J., Li, N., Kim, D.H. and Lee, S.Y., 2020. The GIGANTEA-ENHANCED EM LEVEL complex enhances drought tolerance via regulation of abscisic acid synthesis. *Plant physiology*, 184(1), pp.443-458.
- Baluška, F., Barlow, P.W. and Volkmann, D., 1996. Complete disintegration of the microtubular cytoskeleton precedes its auxin-mediated reconstruction in postmitotic maize root cells. *Plant and cell physiology*, 37(7), pp.1013-1021.
- Baluška, F., Parker, J.S. and Barlow, P.W., 1993. A role for gibberellic acid in orienting microtubules and regulating cell growth polarity in the maize root cortex. *Planta*, 191, pp.149-157.

- Bánfalvi, Z., 2019. Transgenic plants overexpressing trehalose biosynthetic genes and abiotic stress tolerance in plants. *Osmoprotectant-Mediated Abiotic Stress Tolerance in Plants: Recent Advances and Future Perspectives*, pp.225-239.
- Banhara, A., Ding, Y., Kühner, R., Zuccaro, A. and Parniske, M., 2015. Colonization of root cells and plant growth promotion by Piriformospora indica occurs independently of plant common symbiosis genes. *Frontiers in plant science*, 6, p.667.
- Barry, C.S., Fox, E.A., Yen, H.C., Lee, S., Ying, T.J., Grierson, D. and Giovannoni, J.J., 2001. Analysis of the ethylene response in the epinastic mutant of tomato. *Plant Physiology*, 127(1), pp.58-66.
- Baudry, A., Ito, S., Song, Y.H., Strait, A.A., Kiba, T., Lu, S., Henriques, R., Pruneda-Paz, J.L., Chua, N.H., Tobin, E.M. and Kay, S.A., 2010. F-box proteins FKF1 and LKP2 act in concert with ZEITLUPE to control *Arabidopsis* clock progression. *The Plant Cell*, 22(3), pp.606-622.
- Baulry, J.M., Sealy, I.M., Macdonald, H., Brearley, J., Dröge, S., Hillmer, S., Robinson, D.G., Venis, M.A., Blatt, M.R., Lazarus, C.M. and Napier, R.M., 2000. Overexpression of auxin-binding protein enhances the sensitivity of guard cells to auxin. *Plant Physiology*, 124(3), pp.1229-1238.
- Beales J, Turner A, Griffiths S et al (2007) A pseudo-response regulator is misexpressed in the photoperiod insensitive Ppd-D1a mutant of wheat (*Triticum aestivum* L.). *Theor Appl Genet* 115(5):721–733
- Bera, A. and Gupta Jr, M.L., 2022. Microtubules in Microorganisms: How Tubulin Isotypes Contribute to Diverse Cytoskeletal Functions. *Frontiers in Cell and Developmental Biology*, 10, p.913809.
- Berns, M.C., Nordström, K., Cremer, F., Tóth, R., Hartke, M., Simon, S., Klasen, J.R., Bürstel, I. and Coupland, G., 2014. Evening expression of *Arabidopsis* GIGANTEA is controlled by combinatorial interactions among evolutionarily conserved regulatory motifs. *The Plant Cell*, 26(10), pp.3999-4018.
- Bhat, K.A., Mahajan, R., Pakhtoon, M.M., Urwat, U., Bashir, Z., Shah, A.A., Agrawal, A., Bhat, B., Sofi, P.A., Masi, A. and Zargar, S.M., 2022. Low temperature stress tolerance: An insight into the omics approaches for legume crops. *Frontiers in Plant Science*, 13, p.888710.
- Bisgrove, S.R., Hable, W.E. and Kropf, D.L., 2004. + TIPs and microtubule regulation. The beginning of the plus end in plants. *Plant physiology*, 136(4), pp.3855-3863.
- Bisgrove, S.R., Hable, W.E. and Kropf, D.L., 2004. + TIPs and microtubule regulation. The beginning of the plus end in plants. *Plant physiology*, 136(4), pp.3855-3863.

- Blair, E.J., Bonnot, T., Hummel, M., Hay, E., Marzolino, J.M., Quijada, I.A. and Nagel, D.H., 2019. Contribution of time of day and the circadian clock to the heat stress responsive transcriptome in *Arabidopsis*. *Scientific Reports*, 9(1), p.4814.
- Blakeslee, J.J., Peer, W.A. and Murphy, A.S., 2005. Auxin transport. *Current opinion in plant biology*, 8(5), pp.494-500.
- Blau J, Young MW (1999) Cycling vrille expression is required for a functional Drosophila clock. *Cell* 99(6):661–671
- Bowman, J.L., Kohchi, T., Yamato, K.T., Jenkins, J., Shu, S., Ishizaki, K., Yamaoka, S., Nishihama, R., Nakamura, Y., Berger, F. and Adam, C., 2017. Insights into land plant evolution garnered from the *Marchantia polymorpha* genome. *Cell*, 171(2), pp.287-304.
- Brandoli, C., Petri, C., Egea-Cortines, M. and Weiss, J., 2020. Gigantea: uncovering new functions in flower development. *Genes*, 11(10), p.1142.
- Braun, N., Wyrzykowska, J., Muller, P., David, K., Couch, D., Perrot-Rechenmann, C. and Fleming, A.J., 2008. Conditional repression of AUXIN BINDING PROTEIN1 reveals that it coordinates cell division and cell expansion during postembryonic shoot development in *Arabidopsis* and tobacco. *The Plant Cell*, 20(10), pp.2746-2762.
- Breviario, D. and Nick, P., 2000. Plant tubulins: a melting pot for basic questions and promising applications. *Transgenic Research*, 9, pp.383-393.
- Cao S, Jiang L, Song S, Jing R, Xu G (2006) AtGRP7 is involved in the regulation of abscisic acid and stress responses in *Arabidopsis*. *Cell Mol Biol Lett* 11(4):526–535
- Cao SQ, Song YQ, Su L (2007) Freezing sensitivity in the *gigantea* mutant of *Arabidopsis* is associated with sugar deficiency. *Biol Plant* 51(2):359–362
- Cao, S., Ye, M. and Jiang, S., 2005. Involvement of GIGANTEA gene in the regulation of the cold stress response in *Arabidopsis*. *Plant cell reports*, 24, pp.683-690.
- Carmona, B., Marinho, H.S., Matos, C.L., Nolasco, S. and Soares, H., 2023. Tubulin post-translational modifications: The elusive roles of acetylation. *Biology*, 12(4), p.561.
- Carré, I.A., 1996, December. Biological timing in plants. In *Seminars in Cell & Developmental Biology* (Vol. 7, No. 6, pp. 775-780). Academic Press.
- Cha, J.Y., Kim, J., Kim, T.S., Zeng, Q., Wang, L., Lee, S.Y., Kim, W.Y. and Somers, D.E., 2017. GIGANTEA is a co-chaperone which facilitates maturation of ZEITLUPE in the *Arabidopsis* circadian clock. *Nature communications*, 8(1), p.3.
- Cha, J.Y., Lee, D.Y., Ali, I., Jeong, S.Y., Shin, B., Ji, H., Kim, J.S., Kim, M.G. and Kim, W.Y., 2019. *Arabidopsis* GIGANTEA negatively regulates chloroplast biogenesis and resistance to herbicide butafenacil. *Plant cell reports*, 38, pp.793-801.

- Cha, J.Y., Shin, G.I., Ahn, G., Jeong, S.Y., Ji, M.G., Alimzhan, A., Kim, M.G. and Kim, W.Y., 2022. Loss-of-function in GIGANTEA confers resistance to PPO-inhibiting herbicide tiafenacil through transcriptional activation of antioxidant genes in *Arabidopsis*. *Applied Biological Chemistry*, 65(1), pp.1-10.
- Chae, K., Isaacs, C.G., Reeves, P.H., Maloney, G.S., Muday, G.K., Nagpal, P. and Reed, J.W., 2012. *Arabidopsis* SMALL AUXIN UP RNA63 promotes hypocotyl and stamen filament elongation. *The Plant Journal*, 71(4), pp.684-697.
- Chen J, Sonobe K, Ogawa N, Masuda S, Nagatani A, Kobayashi Y, *et al.*, Inhibition of *Arabidopsis* hypocotyl elongation by jasmonates is enhanced under red light in phytochrome B dependent manner. *J Plant Res*. 2013.
- Chen, H., Zhang, J., Neff, M.M., Hong, S.W., Zhang, H., Deng, X.W. and Xiong, L., 2008. Integration of light and abscisic acid signaling during seed germination and early seedling development. *Proceedings of the National Academy of Sciences*, 105(11), pp.4495-4500.
- Chen, J. and Yang, Z., 2014. Novel ABP1-TMK auxin sensing system controls ROP GTPase-mediated interdigitated cell expansion in *Arabidopsis*. *Small GTPases*, p.e29711.
- Chen, J. and Yang, Z., 2014. Novel ABP1-TMK auxin sensing system controls ROP GTPase-mediated interdigitated cell expansion in *Arabidopsis*. *Small GTPases*, p.e29711.
- Chen, J., Sonobe, K., Ogawa, N., Masuda, S., Nagatani, A., Kobayashi, Y. and Ohta, H., 2013. Inhibition of *Arabidopsis* hypocotyl elongation by jasmonates is enhanced under red light in phytochrome B dependent manner. *Journal of plant research*, 126, pp.161-168.
- Chen, J., Tsuda, Y., Stocks, M., Källman, T., Xu, N., Kärkkäinen, K., Huotari, T., Semerikov, V.L., Vendramin, G.G. and Lascoux, M., 2014. Clinal variation at phenology-related genes in spruce: parallel evolution in FTL2 and Gigantea?. *Genetics*, 197(3), pp.1025-1038.
- Chen, J.G., Ullah, H., Young, J.C., Sussman, M.R. and Jones, A.M., 2001. ABP1 is required for organized cell elongation and division in *Arabidopsis* embryogenesis. *Genes & development*, 15(7), pp.902-911.
- Chilley, P.M., Casson, S.A., Tarkowski, P., Hawkins, N., Wang, K.L.C., Hussey, P.J., Beale, M., Ecker, J.R., Sandberg, G.K. and Lindsey, K., 2006. The POLARIS peptide of *Arabidopsis* regulates auxin transport and root growth via effects on ethylene signaling. *The Plant Cell*, 18(11), pp.3058-3072.
- Chinnusamy, V., Zhu, J. and Zhu, J.K., 2007. Cold stress regulation of gene expression in plants. *Trends in plant science*, 12(10), pp.444-451.
- Chow, B.Y., Sanchez, S.E., Breton, G., Pruneda-Paz, J.L., Krogan, N.T. and Kay, S.A., 2014. Transcriptional regulation of LUX by CBF1 mediates cold input to the circadian clock in *Arabidopsis*. *Current Biology*, 24(13), pp.1518-1524.
- clocks. *Nature Reviews Genetics*, 2(9), pp.702-715.

- Coesel S, Mangogna M, Ishikawa T et al (2009) Diatom *PtCPF1* is a new cryptochrome/photolyase family member with DNA repair and transcription regulation activity. *EMBO Rep* 10(6):655–661
- Cole, S.J., Yoon, A.J., Faull, K.F. and Diener, A.C., 2014. Host perception of jasmonates promotes infection by *Fusarium oxysporum* formae speciales that produce isoleucine-and leucine-conjugated jasmonates. *Molecular plant pathology*, 15(6), pp.589-600.
- Corellou F, Schwartz C, Motta JP et al (2009) Clocks in the green lineage: comparative functional analysis of the circadian architecture of the picoeukaryote *Ostreococcus*. *Plant Cell* 21(11):3436–3449
- Corrales, A.R., Nebauer, S.G., Carrillo, L., Fernández-Nohales, P., Marqués, J., Renau-Morata, B., Granell, A., Pollmann, S., Vicente-Carbajosa, J., Molina, R.V. and Medina, J., 2014. Characterization of tomato Cycling Dof Factors reveals conserved and new functions in the control of flowering time and abiotic stress responses. *Journal of experimental botany*, 65(4), pp.995-1012.
- Costigan, S.E., Warnasooriya, S.N., Humphries, B.A. and Montgomery, B.L., 2011. Root-localized phytochrome chromophore synthesis is required for photoregulation of root elongation and impacts root sensitivity to jasmonic acid in *Arabidopsis*. *Plant physiology*, 157(3), pp.1138-1150.
- Čovanová, M., Sauer, M., Rychtář, J., Friml, J., Petrášek, J. and Zažímalová, E., 2013. Overexpression of the auxin binding protein1 modulates PIN-dependent auxin transport in tobacco cells. *PLoS One*, 8(7), p.e70050.
- Covington, M.F. and Harmer, S.L., 2007. The circadian clock regulates auxin signaling and responses in *Arabidopsis*. *PLoS biology*, 5(8), p.e222.
- Creppe, C., Malinouskaya, L., Volvert, M.L., Gillard, M., Close, P., Malaise, O., Laguesse, S., Cornez, I., Rahmouni, S., Ormenese, S. and Belachew, S., 2009. Elongator controls the migration and differentiation of cortical neurons through acetylation of α -tubulin. *Cell*, 136(3), pp.551-564.
- Cui, H., Gobbato, E., Kracher, B., Qiu, J., Bautor, J. and Parker, J.E., 2017. A core function of EDS1 with PAD4 is to protect the salicylic acid defense sector in *Arabidopsis* immunity. *New Phytologist*, 213(4), pp.1802-1817.
- Czymmek, K.J., Fogg, M., Powell, D.H., Sweigard, J., Park, S.Y. and Kang, S., 2007. In vivo time-lapse documentation using confocal and multi-photon microscopy reveals the mechanisms of invasion into the *Arabidopsis* root vascular system by *Fusarium oxysporum*. *Fungal Genetics and Biology*, 44(10), pp.1011-1023.
- Da Silva, E.A., Toorop, P.E., Van Lammeren, A.A. and Hilhorst, H.W., 2008. ABA inhibits embryo cell expansion and early cell division events during coffee (*Coffea arabica* ‘Rubi’) seed germination. *Annals of Botany*, 102(3), pp.425-433.

- Dahlke, R.I., Luethen, H. and Steffens, B., 2010. ABP1: an auxin receptor for fast responses at the plasma membrane. *Plant Signaling & Behavior*, 5(1), pp.1-3.
- Dai, X., Mashiguchi, K., Chen, Q., Kasahara, H., Kamiya, Y., Ojha, S., DuBois, J., Ballou, D. and Zhao, Y., 2013. The biochemical mechanism of auxin biosynthesis by an *Arabidopsis* YUCCA flavin-containing monooxygenase. *Journal of Biological Chemistry*, 288(3), pp.1448-1457.
- Dash, L. Re-evaluating the role of GIGANTEA using CRISPR-Cas9 system. 2018.
- Dattolo E, Ruocco M, Brunet C et al (2014) Response of the seagrass *Posidonia oceanica* to different light environments: Insights from a combined molecular and photo-physiological study. *Mar Environ Res* 101:225–236
- David, K.M., Armbruster, U., Tama, N. and Putterill, J., 2006. Arabidopsis GIGANTEA protein is post-transcriptionally regulated by light and dark. *FEBS letters*, 580(5), pp.1193-1197.
- De Brabander, M., Geuens, G., Nuydens, R., Willebrords, R., Aerts, F., De Mey, J. and McIntosh, J.R., 1986. Microtubule dynamics during the cell cycle: the effects of taxol and nocodazole on the microtubule system of Pt K2 cells at different stages of the mitotic cycle. In *International review of cytology* (Vol. 101, pp. 215-274). Academic Press.
- de Leone, M.J., Hernando, C.E., Mora-García, S. and Yanovsky, M.J., 2020. It's a matter of time: The role of transcriptional regulation in the circadian clock-pathogen crosstalk in plants. *Transcription*, 11(3-4), pp.100-116.
- de Montaigu, A., Tóth, R. and Coupland, G., 2010. Plant development goes like clockwork. *Trends in Genetics*, 26(7), pp.296-306.
- Del Duca, S., Serafini-Fracassini, D., Bonner, P., Cresti, M. and Cai, G., 2009. Effects of post-translational modifications catalysed by pollen transglutaminase on the functional properties of microtubules and actin filaments. *Biochemical Journal*, 418(3), pp.651-664.
- Delwiche, C.F. and Cooper, E.D., 2015. The evolutionary origin of a terrestrial flora. *Current Biology*, 25(19), pp.R899-R910.
- Dhawan, S.S., Shukla, P., Gupta, P. and Lal, R.K., 2016. A cold-tolerant evergreen interspecific hybrid of *Ocimum kilimandscharicum* and *Ocimum basilicum*: analyzing trichomes and molecular variations. *Protoplasma*, 253, pp.845-855.
- Diener, A.C. and Ausubel, F.M., 2005. RESISTANCE TO *FUSARIUM OXYSPORUM* 1, a dominant *Arabidopsis* disease-resistance gene, is not race specific. *Genetics*, 171(1), pp.305-321.
- Dodd, A.N., Salathia, N., Hall, A., Kévei, E., Tóth, R., Nagy, F., Hibberd, J.M., Millar, A.J. and Webb, A.A., 2005. Plant circadian clocks increase photosynthesis, growth, survival, and competitive advantage. *Science*, 309(5734), pp.630-633.

- Doi, K., Izawa, T., Fuse, T., Yamanouchi, U., Kubo, T., Shimatani, Z., Yano, M. and Yoshimura, A., 2004. Ehd1, a B-type response regulator in rice, confers short-day promotion of flowering and controls FT-like gene expression independently of Hd1. *Genes & development*, 18(8), pp.926-936.
- Dong, M.A., Farré, E.M. and Thomashow, M.F., 2011. Circadian clock-associated 1 and late elongated hypocotyl regulate expression of the C-repeat binding factor (CBF) pathway in *Arabidopsis*. *Proceedings of the National Academy of Sciences*, 108(17), pp.7241-7246.
- Durso, N.A. and Cyr, R.J., 1994. A calmodulin-sensitive interaction between microtubules and a higher plant homolog of elongation factor-1 alpha. *The Plant Cell*, 6(6), pp.893-905.
- Edgar, C.I., McGrath, K.C., Dombrecht, B., Manners, J.M., Maclean, D.C., Schenk, P.M. and Kazan, K., 2006. Salicylic acid mediates resistance to the vascular wilt pathogen *Fusarium oxysporum* in the model host *Arabidopsis thaliana*. *Australasian Plant Pathology*, 35, pp.581-591.
- Edwards, K.D., Lynn, J.R., Gyula, P., Nagy, F. and Millar, A.J., 2005. Natural allelic variation in the temperature-compensation mechanisms of the *Arabidopsis thaliana* circadian clock. *Genetics*, 170(1), pp.387-400.
- Effendi, Y., Jones, A.M. and Scherer, G.F., 2013. Auxin-binding-protein1 (ABP1) in phytochrome-B-controlled responses. *Journal of experimental botany*, 64(16), pp.5065-5074.
- Ehrhardt, D.W. and Shaw, S.L., 2006. Microtubule dynamics and organization in the plant cortical array. *Annu. Rev. Plant Biol.*, 57, pp.859-875.
- Eimert, K., Wang, S.M., Lue, W.I. and Chen, J., 1995. Monogenic recessive mutations causing both late floral initiation and excess starch accumulation in *Arabidopsis*. *The Plant Cell*, 7(10), pp.1703-1712.
- Enders, T.A. and Strader, L.C., 2015. Auxin activity: Past, present, and future. *American journal of botany*, 102(2), pp.180-196.
- Enders, T.A., Oh, S., Yang, Z., Montgomery, B.L. and Strader, L.C., 2015. Genome sequencing of *Arabidopsis* abp1-5 reveals second-site mutations that may affect phenotypes. *The Plant Cell*, 27(7), pp.1820-1826.
- Espinoza C, Degenkolbe T, Caldana C et al (2010) Interaction with diurnal and circadian regulation results in dynamic metabolic and transcriptional changes during cold acclimation in *Arabidopsis*. *PLoS ONE* 5(11):e14101
- Espinoza, C., Degenkolbe, T., Caldana, C., Zuther, E., Leisse, A., Willmitzer, L., Hinch, D.K. and Hannah, M.A., 2010. Interaction with diurnal and circadian regulation results in dynamic metabolic and transcriptional changes during cold acclimation in *Arabidopsis*. *PloS one*, 5(11), p.e14101.

- Fabregas, N., Formosa-Jordan, P., Confraria, A., Siligato, R., Alonso, J.M., Swarup, R., Bennett, M.J., Mähönen, A.P., Cano-Delgado, A.I. and Ibanes, M., 2015. Auxin influx carriers control vascular patterning and xylem differentiation in *Arabidopsis thaliana*. *PLoS Genetics*, 11(4), p.e1005183.
- Fambrini, M. and Pugliesi, C., 2019. The dynamic genetic-hormonal regulatory network controlling the trichome development in leaves. *Plants*, 8(8), p.253.
- Farinas B, Mas P (2011) Functional implication of the MYB transcription factor *RVE8/LCL5* in the circadian control of histone acetylation. *Plant J* 66(2):318–329
- Faure S, Turner AS, Gruszka D et al (2012) Mutation at the circadian clock gene *EARLY MATURITY 8* adapts domesticated barley (*Hordeum vulgare*) to short growing seasons. *PNAS USA* 109(21):8328–8333
- Ford, B., Deng, W., Clausen, J., Oliver, S., Boden, S., Hemming, M. and Trevaskis, B., 2016. Barley (*Hordeum vulgare*) circadian clock genes can respond rapidly to temperature in an *EARLY FLOWERING 3*-dependent manner. *Journal of Experimental Botany*, 67(18), pp.5517-5528.
- Fornara, F., de Montaigu, A., Sánchez-Villarreal, A., Takahashi, Y., Ver Loren van Themaat, E., Huettel, B., Davis, S.J. and Coupland, G., 2015. The GI–CDF module of *Arabidopsis* affects freezing tolerance and growth as well as flowering. *The Plant Journal*, 81(5), pp.695-706.
- Fornara, F., Panigrahi, K.C., Gissot, L., Sauerbrunn, N., Rühl, M., Jarillo, J.A. and Coupland, G., 2009. *Arabidopsis* DOF transcription factors act redundantly to reduce *CONSTANS* expression and are essential for a photoperiodic flowering response. *Developmental cell*, 17(1), pp.75-86.
- Fosket *et al.*, *Annu. Rev. Plant Biol.*, 43(1), 201-240 (1992).
- Fowler, S. and Thomashow, M.F., 2002. *Arabidopsis* transcriptome profiling indicates that multiple regulatory pathways are activated during cold acclimation in addition to the CBF cold response pathway. *The Plant Cell*, 14(8), pp.1675-1690.
- Fowler, S., Lee, K., Onouchi, H., Samach, A., Richardson, K., Morris, B., Coupland, G. and Putterill, J., 1999. *GIGANTEA*: a circadian clock-controlled gene that regulates photoperiodic flowering in *Arabidopsis* and encodes a protein with several possible membrane-spanning domains. *The EMBO journal*, 18(17), pp.4679-4688.
- François, L., Bruch, A.A., Utescher, T., Spicer, R.A. and Spicer, T., 2017. Reconstructing Cenozoic vegetation from proxy data and models—A NECLIME synthesis. *Palaeogeography, Palaeoclimatology, Palaeoecology*, 467, pp.1-4.
- Franklin KA, Lee SH, Patel D, Kumar SV, Spartz AK, Gu C, *et al.*, Phytochromeinteracting factor 4 (PIF4) regulates auxin biosynthesis at high temperature. *Proc Natl Acad Sci U S A*. 2011.

- Friml, J., Gallei, M., Gelová, Z., Johnson, A., Mazur, E., Monzer, A., Rodriguez, L., Roosjen, M., Verstraeten, I., Živanović, B.D. and Zou, M., 2022. ABP1–TMK auxin perception for global phosphorylation and auxin canalization. *Nature*, 609(7927), pp.575-581.
- Fujikura, U., Ezaki, K., Horiguchi, G., Seo, M., Kanno, Y., Kamiya, Y., Lenhard, M. and Tsukaya, H., 2020. Suppression of class I compensated cell enlargement by xs2 mutation is mediated by salicylic acid signaling. *PLoS Genetics*, 16(6), p.e1008873.
- Fukuda, H., 2000. Programmed cell death of tracheary elements as a paradigm in plants. *Programmed Cell Death in Higher Plants*, pp.1-9.
- Gangappa, S.N. and Chattopadhyay, S., 2010. MYC2, a bHLH transcription factor, modulates the adult phenotype of SPA1. *Plant signaling & behavior*, 5(12), pp.1650-1652.
- Gao, Y., Zhang, Y., Zhang, D., Dai, X., Estelle, M. and Zhao, Y., 2015. Auxin binding protein 1 (ABP1) is not required for either auxin signaling or *Arabidopsis* development. *Proceedings of the National Academy of Sciences*, 112(7), pp.2275-2280.
- Gardiner, J., 2019. Posttranslational modification of plant microtubules. *Plant signaling & behavior*, 14(10), p.e1654818.
- Gawroński P, Ariyadasa R, Himmelbach A et al (2014) A distorted circadian clock causes early flowering and temperature-dependent variation in spike development in the *Eps-3Am* mutant of einkorn wheat. *Genetics* 196(4):1253–1261
- Genoud, T., Millar, A.J., Nishizawa, N., Kay, S.A., Schäfer, E., Nagatani, A. and Chua, N.H., 1998. An *Arabidopsis* mutant hypersensitive to red and far-red light signals. *The Plant Cell*, 10(6), pp.889-904.
- Giddings Jr, T.H. and Staehelin, L.A., 1991. 7. MICROTUBULE-MEDIATED. *The Cytoskeletal Basis of Plant Growth and Form*, p.85.
- Gil, K.E. and Park, C.M., 2019. Thermal adaptation and plasticity of the plant circadian clock. *New Phytologist*, 221(3), pp.1215-1229.
- Gil, P., Dewey, E., Friml, J., Zhao, Y., Snowden, K.C., Putterill, J., Palme, K., Estelle, M. and Chory, J., 2001. BIG: a calossin-like protein required for polar auxin transport in *Arabidopsis*. *Genes & Development*, 15(15), pp.1985-1997.
- Giri, M.K., Singh, N., Banday, Z.Z., Singh, V., Ram, H., Singh, D., Chattopadhyay, S. and Nandi, A.K., 2017. GBF 1 differentially regulates CAT 2 and PAD 4 transcription to promote pathogen defense in *Arabidopsis thaliana*. *The Plant Journal*, 91(5), pp.802-815.
- Glazebrook, J., 2005. Contrasting mechanisms of defense against biotrophic and necrotrophic pathogens. *Annu. Rev. Phytopathol.*, 43, pp.205-227.
- Gomez, P., Ferrer, M.Á., Fernández-Trujillo, J.P., Calderon, A., Artes, F., Egea-Cortines, M. and Weiss, J., 2009. Structural changes, chemical composition and antioxidant activity of

- cherry tomato fruits (cv. Micro-Tom) stored under optimal and chilling conditions. *Journal of the Science of Food and Agriculture*, 89(9), pp.1543-1551.
- Gould PD, Locke JC, Larue C et al (2006) The molecular basis of temperature compensation in the *Arabidopsis* circadian clock. *Plant Cell* 18(5):1177–1187
- Griffin, Jonathan HC, and Gabriela Toledo-Ortiz. "Plant photoreceptors and their signalling components in chloroplastic anterograde and retrograde communication." *Journal of Experimental Botany* 73, no. 21 (2022): 7126-7138.
- Grones, P. and Friml, J., 2015. ABP1: finally docking. *Molecular Plant*, 8(3), pp.356-358.
- Grones, P., Chen, X., Simon, S., Kaufmann, W.A., De Rycke, R., Nodzyński, T., Zažímalová, E. and Friml, J., 2015. Auxin-binding pocket of ABP1 is crucial for its gain-of-function cellular and developmental roles. *Journal of Experimental Botany*, 66(16), pp.5055-5065.
- Grundy, J., Stoker, C. and Carré, I.A., 2015. Circadian regulation of abiotic stress tolerance in plants. *Frontiers in plant science*, 6, p.648.
- Gundersen, G.G. and Cook, T.A., 1999. Microtubules and signal transduction. *Current opinion in cell biology*, 11(1), pp.81-94.
- Guo, X., Liu, D. and Chong, K., 2018. Cold signaling in plants: Insights into mechanisms and regulation. *Journal of integrative plant biology*, 60(9), pp.745-756.
- Guy, C.L., 1990. Cold acclimation and freezing stress tolerance: role of protein metabolism. *Annual review of plant biology*, 41(1), pp.187-223.
- Guy, C.L., Niemi, K.J. and Brambl, R., 1985. Altered gene expression during cold acclimation of spinach. *Proceedings of the National Academy of Sciences*, 82(11), pp.3673-3677.
- Halliday KJ, Martínez-García JF, Josse EM. Integration of light and auxin signaling. *Cold Spring Harb Perspect Biol*. 2009;1(6):111.
- Han, Y., Zhang, X., Wang, Y. and Ming, F., 2013. The suppression of WRKY44 by GIGANTEA-miR172 pathway is involved in drought response of *Arabidopsis thaliana*. *PLoS One*, 8(11), p.e73541.
- Hanano, S., Domagalska, M.A., Nagy, F. and Davis, S.J., 2006. Multiple phytohormones influence distinct parameters of the plant circadian clock. *Genes to Cells*, 11(12), pp.1381-1392.
- Hardham, A.R., Jones, D.A. and Takemoto, D., 2007. Cytoskeleton and cell wall function in penetration resistance. *Current opinion in plant biology*, 10(4), pp.342-348.
- Hardin PE, Hall JC, Rosbash M (1990) Feedback of the *Drosophila* period gene product on circadian cycling of its messenger RNA levels. *Nature* 343(6258):536–540

- Harding LW Jr, Heinbokel JF (1984) Periodicities of photosynthesis and cell division: Behavior of phase-lagged replicate cultures of *Ditylum brightwellii* a diurnally varying photic regime. *Mar Ecology Progress Ser Oldendorf* 15(3):225–232
- Hazak, O., Mamon, E., Lavy, M., Sternberg, H., Behera, S., Schmitz-Thom, I., Bloch, D., Dementiev, O., Gutman, I., Danziger, T. and Schwarz, N., 2019. A novel Ca²⁺-binding protein that can rapidly transduce auxin responses during root growth. *PLoS biology*, 17(7), p.e3000085.
- Hearn, T.J., Marti Ruiz, M.C., Abdul-Awal, S.M., Wimalasekera, R., Stanton, C.R., Haydon, M.J., Theodoulou, F.L., Hannah, M.A. and Webb, A.A., 2018. BIG regulates dynamic adjustment of circadian period in *Arabidopsis thaliana*. *Plant physiology*, 178(1), pp.358-371.
- Heath, R.L. and Packer, L., 1968. Photoperoxidation in isolated chloroplasts: I. Kinetics and stoichiometry of fatty acid peroxidation. *Archives of biochemistry and biophysics*, 125(1), pp.189-198.
- Hedden, P. and Sponsel, V., 2015. A century of gibberellin research. *Journal of plant growth regulation*, 34, pp.740-760.
- Heinlein, M., Epel, B.L., Padgett, H.S. and Beachy, R.N., 1995. Interaction of tobamovirus movement proteins with the plant cytoskeleton. *Science*, 270(5244), pp.1983-1985.
- Heisler, M.G., Hamant, O., Krupinski, P., Uyttewaal, M., Ohno, C., Jönsson, H., Traas, J. and Meyerowitz, E.M., 2010. Alignment between PIN1 polarity and microtubule orientation in the shoot apical meristem reveals a tight coupling between morphogenesis and auxin transport. *PLoS biology*, 8(10), p.e1000516.
- Hertel, R., Thomson, K.S. and Russo, V.E.A., 1972. In-vitro auxin binding to particulate cell fractions from corn coleoptiles. *Planta*, 107, pp.325-340.
- Hesse, T., Feldwisch, J., Balshüsemann, D., Bauw, G., Puype, M., Vandekerckhove, J., Löbner, M., Klämbt, D., Schell, J. and Palme, K., 1989. Molecular cloning and structural analysis of a gene from *Zea mays* (L.) coding for a putative receptor for the plant hormone auxin. *The EMBO journal*, 8(9), pp.2453-2461.
- Holm K, Källman T, Gyllenstrand N et al (2010) Does the core circadian clock in the moss *Physcomitrella patens* (Bryophyta) comprise a single loop? *BMC Plant Biol* 10(1):1–14
- Hong, L.W., Yan, D.W., Liu, W.C., Chen, H.G. and Lu, Y.T., 2014. TIME FOR COFFEE controls root meristem size by changes in auxin accumulation in *Arabidopsis*. *Journal of experimental botany*, 65(1), pp.275-286.
- Hornitschek, P., Kohnen, M.V., Lorrain, S., Rougemont, J., Ljung, K., López-Vidriero, I., Franco-Zorrilla, J.M., Solano, R., Trevisan, M., Pradervand, S. and Xenarios, I., 2012.

- Phytochrome interacting factors 4 and 5 control seedling growth in changing light conditions by directly controlling auxin signaling. *The Plant Journal*, 71(5), pp.699-711.
- Howes, S.C., Alushin, G.M., Shida, T., Nachury, M.V. and Nogales, E., 2014. Effects of tubulin acetylation and tubulin acetyltransferase binding on microtubule structure. *Molecular biology of the cell*, 25(2), pp.257-266.
- Hsu PY, Devisetty UK, Harmer SL (2013) Accurate timekeeping is controlled by a cycling activator in *Arabidopsis*. *Elife* 2:e00473
- Huang H, Nusinow DA (2016) Into the evening: complex interactions in the *Arabidopsis* circadian clock. *Trends Genet* 32(10):674–686
- Huang, W., Pérez-García, P., Pokhilko, A., Millar, A.J., Antoshechkin, I., Riechmann, J.L. and Mas, P., 2012. Mapping the core of the *Arabidopsis* circadian clock defines the network structure of the oscillator. *Science*, 336(6077), pp.75-79.
- Huq, E., Al-Sady, B., Hudson, M., Kim, C., Apel, K. and Quail, P.H., 2004. Phytochrome-interacting factor 1 is a critical bHLH regulator of chlorophyll biosynthesis. *science*, 305(5692), pp.1937-1941.
- Huq, E., Tepperman, J.M. and Quail, P.H., 2000. GIGANTEA is a nuclear protein involved in phytochrome signaling in *Arabidopsis*. *Proceedings of the National Academy of Sciences*, 97(17), pp.9789-9794.
- Hyten DL, Song Q, Zhu Y et al (2006) Impacts of genetic bottlenecks on soybean genome diversity. *PNAS USA* 103(45):16666–16671
- Imaizumi, T., Schultz, T.F., Harmon, F.G., Ho, L.A. and Kay, S.A., 2005. FKF1 F-box protein mediates cyclic degradation of a repressor of CONSTANS in *Arabidopsis*. *Science*, 309(5732), pp.293-297.
- Imaizumi, T., Tran, H.G., Swartz, T.E., Briggs, W.R. and Kay, S.A., 2003. FKF1 is essential for photoperiodic-specific light signalling in *Arabidopsis*. *Nature*, 426(6964), pp.302-306.
- Iordachescu, M. and Imai, R., 2008. Trehalose biosynthesis in response to abiotic stresses. *Journal of integrative plant biology*, 50(10), pp.1223-1229.
- Iqbal, N., Khan, N.A., Ferrante, A., Trivellini, A., Francini, A. and Khan, M.I.R., 2017. Ethylene role in plant growth, development and senescence: interaction with other phytohormones. *Frontiers in plant science*, 8, p.475.
- Ivanchenko, M.G., Napsucialy-Mendivil, S. and Dubrovsky, J.G., 2010. Auxin-induced inhibition of lateral root initiation contributes to root system shaping in *Arabidopsis thaliana*. *The Plant Journal*, 64(5), pp.740-752.
- Izawa T, Mihara M, Suzuki Y et al (2011) OsGIGANTEA confers robust diurnal rhythms on the global transcriptome of rice in the field. *Plant Cell* 23(5):1741–1755

- Jaglo-Ottosen, K.R., Gilmour, S.J., Zarka, D.G., Schabenberger, O. and Thomashow, M.F., 1998. *Arabidopsis* CBF1 overexpression induces COR genes and enhances freezing tolerance. *Science*, 280(5360), pp.104-106.
- Jang, G. and Dolan, L., 2011. Auxin promotes the transition from chloronema to caulonema in moss protonema by positively regulating PpRSL1 and PpRSL2 in *Physcomitrella patens*. *New Phytologist*, 192(2), pp.319-327.
- Jang, J., Lee, S., Kim, J.I., Lee, S. and Kim, J.A., 2024. The Roles of Circadian Clock Genes in Plant Temperature Stress Responses. *International Journal of Molecular Sciences*, 25(2), p.918.
- Janke, C. and Magiera, M.M., 2020. The tubulin code and its role in controlling microtubule properties and functions. *Nature Reviews Molecular Cell Biology*, 21(6), pp.307-326.
- Janke, C., Rogowski, K., Wloga, D., Regnard, C., Kajava, A.V., Strub, J.M., Temurak, N., van Dijk, J., Boucher, D., van Dorsselaer, A. and Suryavanshi, S., 2005. Tubulin polyglutamylase enzymes are members of the TTL domain protein family. *Science*, 308(5729), pp.1758-1762.
- Jeong, S.W., Hogewoning, S.W. and van Ieperen, W., 2014. Responses of supplemental blue light on flowering and stem extension growth of cut chrysanthemum. *Scientia Horticulturae*, 165, pp.69-74.
- Jiang, B., Shi, Y., Zhang, X., Xin, X., Qi, L., Guo, H., Li, J. and Yang, S., 2017. PIF3 is a negative regulator of the CBF pathway and freezing tolerance in *Arabidopsis*. *Proceedings of the National Academy of Sciences*, 114(32), pp.E6695-E6702.
- Joachimiak, Ewa, and Dorota Wloga. "Tubulin post-translational modifications in protists—Tiny models for solving big questions." In *Seminars in Cell & Developmental Biology*, vol. 137, pp. 3-15. Academic Press, 2023.
- Johnson, C.H., Knight, M.R., Kondo, T., Masson, P., Sedbrook, J., Haley, A. and Trewavas, A., 1995. Circadian oscillations of cytosolic and chloroplastic free calcium in plants. *Science*, 269(5232), pp.1863-1865.
- Jones, J.D. and Dangl, J.L., 2006. The plant immune system. *nature*, 444(7117), pp.323-329.
- Jouve, L., Gaspar, T., Kevers, C., Greppin, H. and Degli Agosti, R., 1999. Involvement of indole-3-acetic acid in the circadian growth of the first internode of *Arabidopsis*. *Planta*, 209, pp.136-142.
- Jung, I., 2015. Aβ-induced degradation of BMAL1 and CBP leads to circadian rhythm
- Jung, J.H., Seo, Y.H., Seo, P.J., Reyes, J.L., Yun, J., Chua, N.H. and Park, C.M., 2007. The GIGANTEA-regulated microRNA172 mediates photoperiodic flowering independent of CONSTANS in *Arabidopsis*. *The Plant Cell*, 19(9), pp.2736-2748.

- Jung, Jae-Hoon, Yeon-Hee Seo, Pil Joon Seo, Jose Luis Reyes, Ju Yun, Nam-Hai Chua, and Chung-Mo Park. "The GIGANTEA-regulated microRNA172 mediates photoperiodic flowering independent of CONSTANS in *Arabidopsis*." *The Plant Cell* 19, no. 9 (2007): 2736-2748.
- Kasahara, M., Kagawa, T., Sato, Y., Kiyosue, T. and Wada, M., 2004. Phototropins mediate blue and red light-induced chloroplast movements in *Physcomitrella patens*. *Plant physiology*, 135(3), pp.1388-1397.
- Kazan, K. and Lyons, R., 2016. The link between flowering time and stress tolerance. *Journal of experimental botany*, 67(1), pp.47-60.
- Ke, M., Gao, Z., Chen, J., Qiu, Y., Zhang, L. and Chen, X., 2018. Auxin controls circadian flower opening and closure in the waterlily. *BMC plant biology*, 18(1), pp.1-21.
- Keily, J., MacGregor, D.R., Smith, R.W., Millar, A.J., Halliday, K.J. and Penfield, S., 2013. Model selection reveals control of cold signalling by evening-phased components of the plant circadian clock. *The Plant Journal*, 76(2), pp.247-257.
- Khaleda, L., Cha, J.Y., Kim, M.G. and Kim, W.Y., 2017. Production and characterization of polyclonal antibody against *Arabidopsis* GIGANTEA, a circadian clock controlled flowering time regulator. *Journal of Plant Biology*, 60, pp.622-629.
- Kidd, B.N., Edgar, C.I., Kumar, K.K., Aitken, E.A., Schenk, P.M., Manners, J.M. and Kazan, K., 2009. The mediator complex subunit PFT1 is a key regulator of jasmonate-dependent defense in *Arabidopsis*. *The Plant Cell*, 21(8), pp.2237-2252.
- Kidd, B.N., Kadoo, N.Y., Dombrecht, B., Tekeoglu, M., Gardiner, D.M., Thatcher, L.F., Aitken, E.A., Schenk, P.M., Manners, J.M. and Kazan, K., 2011. Auxin signaling and transport promote susceptibility to the root-infecting fungal pathogen *Fusarium oxysporum* in *Arabidopsis*. *Molecular Plant-Microbe Interactions*, 24(6), pp.733-748.
- Kieber, J.J. and Schaller, G.E., 2018. Cytokinin signaling in plant development. *Development*, 145(4), p.dev149344.
- Kim WY, Ali Z, Park HJ et al (2013) Release of SOS2 kinase from sequestration with GIGANTEA determines salt tolerance in *Arabidopsis*. *Nat Comm* 4(1):1–13
- Kim Y, Schumaker KS, Zhu JK. EMS mutagenesis of *Arabidopsis*. *Methods Mol Biol*. 2006;323:101-3. doi: 10.1385/1-59745-003-0:101. PMID: 16739570.
- Kim, B., Jeong, Y.J., Corvalan, C., Fujioka, S., Cho, S., Park, T. and Choe, S., 2014. Darkness and gulliver2/phy B mutation decrease the abundance of phosphorylated BZR 1 to activate brassinosteroid signaling in *Arabidopsis*. *The Plant Journal*, 77(5), pp.737-747.
- Kim, C., Kwon, Y., Jeong, J., Kang, M., Lee, G.S., Moon, J.H., Lee, H.J., Park, Y.I. and Choi, G., 2023. Phytochrome B photobodies are comprised of phytochrome B and its primary and secondary interacting proteins. *Nature Communications*, 14(1), p.1708.

- Kim, J., Geng, R., Gallenstein, R.A. and Somers, D.E., 2013. The F-box protein ZEITLUPE controls stability and nucleocytoplasmic partitioning of GIGANTEA. *Development*, 140(19), pp.4060-4069.
- Kim, J.A., Kim, H.S., Choi, S.H., Jang, J.Y., Jeong, M.J. and Lee, S.I., 2017. The importance of the circadian clock in regulating plant metabolism. *International journal of molecular sciences*, 18(12), p.2680.
- Kim, W.Y., Ali, Z., Park, H.J., Park, S.J., Cha, J.Y., Perez-Hormaeche, J., Quintero, F.J., Shin, G., Kim, M.R., Qiang, Z. and Ning, L., 2013. Release of SOS2 kinase from sequestration with GIGANTEA determines salt tolerance in *Arabidopsis*. *Nature communications*, 4(1), p.1352.
- Kim, W.Y., Fujiwara, S., Suh, S.S., Kim, J., Kim, Y., Han, L., David, K., Putterill, J., Nam, H.G. and Somers, D.E., 2007. ZEITLUPE is a circadian photoreceptor stabilized by GIGANTEA in blue light. *Nature*, 449(7160), pp.356-360.
- Kim, Y., Han, S., Yeom, M., Kim, H., Lim, J., Cha, J.Y., Kim, W.Y., Somers, D.E., Putterill, J., Nam, H.G. and Hwang, D., 2013. Balanced nucleocytoplasmic partitioning defines a spatial network to coordinate circadian physiology in plants. *Developmental Cell*, 26(1), pp.73-85.
- Kobayashi, Y., Kobayashi, I., Funaki, Y., Fujimoto, S., Takemoto, T. and Kunoh, H., 1997. Dynamic reorganization of microfilaments and microtubules is necessary for the expression of non-host resistance in barley coleoptile cells. *The Plant Journal*, 11(3), pp.525-537.
- Kofuji, R. and Hasebe, M., 2014. Eight types of stem cells in the life cycle of the moss *Physcomitrella patens*. *Current opinion in plant biology*, 17, pp.13-21.
- Koontz, D.A. and Choi, J.H., 1993. Evidence for phosphorylation of tubulin in carrot suspension cells. *Physiologia Plantarum*, 87(4), pp.576-583.
- Korasick, D.A., Enders, T.A. and Strader, L.C., 2013. Auxin biosynthesis and storage forms. *Journal of experimental botany*, 64(9), pp.2541-2555.
- Kozuka, T., Suetsugu, N., Wada, M. and Nagatani, A., 2013. Antagonistic regulation of leaf flattening by phytochrome B and phototropin in *Arabidopsis thaliana*. *Plant and cell physiology*, 54(1), pp.69-79.
- Krahmer, J., Ganpudi, A., Abbas, A., Romanowski, A. and Halliday, K.J., 2018. Phytochrome, carbon sensing, metabolism, and plant growth plasticity. *Plant physiology*, 176(2), pp.1039-1048.
- Kreps, J.A. and Kay, S.A., 1997. Coordination of plant metabolism and development by the circadian clock. *The Plant Cell*, 9(7), p.1235.
- Krishna Reddy, S. and Finlayson, S.A., 2014. Phytochrome B promotes branching in *Arabidopsis* by suppressing auxin signaling. *Plant physiology*, 164(3), pp.1542-1550.

- Kubota A, Kita S, Ishizaki K et al (2014) Co-option of a photoperiodic growth-phase transition system during land plant evolution. *Nat Comm* 5(1):1–9
- KUMAR, A., PANIGRAHY, M. and PANIGRAHI, K.C., 2018. Optimization of soil parameters and cost effective way of growing *Arabidopsis thaliana* from an Indian perspective. *International Journal of Basic and Applied Agricultural Research*, 16(1), p.54.
- Kumari, S., Yadav, S., Patra, D., Singh, S., Sarkar, A.K. and Panigrahi, K.C., 2019. Uncovering the molecular signature underlying the light intensity-dependent root development in *Arabidopsis thaliana*. *BMC genomics*, 20, pp.1-23.
- Kundu, P. and Sahu, R., 2021. GIGANTEA confers susceptibility to plants during spot blotch attack by regulating salicylic acid signalling pathway. *Plant Physiology and Biochemistry*, 167, pp.349-357.
- Kurepa, J., Smalle, J., Montagu, M.V. and Inzé, D., 1998b Polyamines and paraquat toxicity in *Arabidopsis thaliana*. *Plant and cell physiology*, 39(9), pp.987-992.
- Kurepa, J., Smalle, J., Va, M., Montagu, N. and Inzé, D., 1998. Oxidative stress tolerance and longevity in *Arabidopsis*: the late-flowering mutant gigantea is tolerant to paraquat. *The Plant Journal*, 14(6), pp.759-764.
- Kushwah, S., Jones, A.M. and Laxmi, A., 2011. Cytokinin interplay with ethylene, auxin, and glucose signaling controls *Arabidopsis* seedling root directional growth. *Plant Physiology*, 156(4), pp.1851-1866.
- Lagopodi, A.L., Ram, A.F., Lamers, G.E., Punt, P.J., Van den Hondel, C.A., Lugtenberg, B.J. and Bloemberg, G.V., 2002. Novel aspects of tomato root colonization and infection by *Fusarium oxysporum* f. sp. *radicis-lycopersici* revealed by confocal laser scanning microscopic analysis using the green fluorescent protein as a marker. *Molecular Plant-Microbe Interactions*, 15(2), pp.172-179.
- Larkindale, J. and Huang, B., 2004. Thermotolerance and antioxidant systems in *Agrostis stolonifera*: involvement of salicylic acid, abscisic acid, calcium, hydrogen peroxide, and ethylene. *Journal of plant physiology*, 161(4), pp.405-413.
- Lau, O.S. and Deng, X.W., 2012. The photomorphogenic repressors COP1 and DET1: 20 years later. *Trends in plant science*, 17(10), pp.584-593.
- Ledbetter, M.C. and Porter, K.R., 1963. A "microtubule" in plant cell fine structure. *The Journal of cell biology*, 19(1), pp.239-250.
- LeDizet, M. and Piperno, G., 1986. Cytoplasmic microtubules containing acetylated alpha-tubulin in *Chlamydomonas reinhardtii*: spatial arrangement and properties. *The Journal of cell biology*, 103(1), pp.13-22.
- Lee C, Bae K, Edery I (1998) The drosophila *CLOCK* protein undergoes daily rhythms in abundance, phosphorylation, and interactions with the *PER-TIM* complex. *Neuron* 21(4):857–867

- Legris, M., Klose, C., Burgie, E.S., Rojas, C.C.R., Neme, M., Hiltbrunner, A., Wigge, P.A., Schäfer, E., Vierstra, R.D. and Casal, J.J., 2016. Phytochrome B integrates light and temperature signals in *Arabidopsis*. *Science*, 354(6314), pp.897-900.
- Lescot, M., Déhais, P., Thijs, G., Marchal, K., Moreau, Y., Van de Peer, Y., Rouzé, P. and Rombauts, S., 2002. PlantCARE, a database of plant cis-acting regulatory elements and a portal to tools for *in-silico* analysis of promoter sequences. *Nucleic acids research*, 30(1), pp.325-327.
- Li, A., Sun, X. and Liu, L., 2022. Action of salicylic acid on plant growth. *Frontiers in Plant Science*, 13, p.878076.
- Li, B., Gao, Z., Liu, X., Sun, D. and Tang, W., 2019. Transcriptional profiling reveals a time-of-day-specific role of REVEILLE 4/8 in regulating the first wave of heat shock-induced gene expression in *Arabidopsis*. *The Plant Cell*, 31(10), pp.2353-2369.
- Li, J., Wang, X., Qin, T., Zhang, Y., Liu, X., Sun, J., Zhou, Y., Zhu, L., Zhang, Z., Yuan, M. and Mao, T., 2011. MDP25, a novel calcium regulatory protein, mediates hypocotyl cell elongation by destabilizing cortical microtubules in *Arabidopsis*. *The Plant Cell*, 23(12), pp.4411-4427.
- Li, M., Cao, L., Mwimba, M., Zhou, Y., Li, L., Zhou, M., Schnable, P.S., O'Rourke, J.A., Dong, X. and Wang, W., 2019. Comprehensive mapping of abiotic stress inputs into the soybean circadian clock. *Proceedings of the National Academy of Sciences*, 116(47), pp.23840-23849.
- Liang L, Zhang Z, Cheng N et al (2021) The transcriptional repressor *OsPRR73* links circadian clock and photoperiod pathway to control heading date in rice. *Plant, Cell & Env* 44(3):842–855
- Liew LC, Hecht V, Laurie RE et al (2009) *DIE NEUTRALIS* and *LATE BLOOMER 1* contribute to regulation of the pea circadian clock. *Plant Cell* 21(10):3198–3211
- Liew LC, Hecht V, Sussmilch FC et al (2014) The pea photoperiod response gene *STERILE NODES* is an ortholog of *LUX ARRHYTHMO*. *Plant Physiol* 165(2):648–657
- Lim, C.W., Baek, W., Jung, J., Kim, J.H. and Lee, S.C., 2015. Function of ABA in stomatal defense against biotic and drought stresses. *International journal of molecular sciences*, 16(7), pp.15251-15270.
- McClung, C.R., 2001. Circadian rhythms in plants. *Annual review of plant biology*, 52(1), pp.139-162.
- Lin, C., 2000. Photoreceptors and regulation of flowering time. *Plant physiology*, 123(1), pp.39-50.
- Linde AM, Eklund DM, Kubota A et al (2017) Early evolution of the land plant circadian clock. *New Phytol* 216(2):576–590

- Liu C, Qu X, Zhou Y et al (2018) OsPRR37 confers an expanded regulation of the diurnal rhythms of the transcriptome and photoperiodic flowering pathways in rice. *Plant Cell Environ* 41(3):630–645
- Liu, J., Shi, Y. and Yang, S., 2018. Insights into the regulation of C-repeat binding factors in plant cold signaling. *Journal of integrative plant biology*, 60(9), pp.780-795.
- Liu, Y., Du, M., Deng, L., Shen, J., Fang, M., Chen, Q., Lu, Y., Wang, Q., Li, C. and Zhai, Q., 2019. MYC2 regulates the termination of jasmonate signaling via an autoregulatory negative feedback loop. *The Plant Cell*, 31(1), pp.106-127.
- Livanos, P., Galatis, B. and Apostolakos, P., 2014. The interplay between ROS and tubulin cytoskeleton in plants. *Plant signaling & behavior*, 9(3), p.e28069.
- Locke, J.C., Kozma-Bognár, L., Gould, P.D., Fehér, B., Kevei, E., Nagy, F., Turner, M.S., Hall, A. and Millar, A.J., 2006. Experimental validation of a predicted feedback loop in the multi-oscillator clock of *Arabidopsis thaliana*. *Molecular systems biology*, 2(1), p.59.
- Lu, S., Dong, L., Fang, C., Liu, S., Kong, L., Cheng, Q., Chen, L., Su, T., Nan, H., Zhang, D. and Zhang, L., 2020. Stepwise selection on homeologous PRR genes controlling flowering and maturity during soybean domestication. *Nature Genetics*, 52(4), pp.428-436.
- Lu, T., Ke, M., Lavoie, M., Jin, Y., Fan, X., Zhang, Z., Fu, Z., Sun, L., Gillings, M., Peñuelas, J. and Qian, H., 2018. Rhizosphere microorganisms can influence the timing of plant flowering. *Microbiome*, 6(1), pp.1-12.
- Ludwig-Müller, J., 2011. Auxin conjugates: their role for plant development and in the evolution of land plants. *Journal of experimental botany*, 62(6), pp.1757-1773.
- Luo, X.M., Lin, W.H., Zhu, S., Zhu, J.Y., Sun, Y., Fan, X.Y., Cheng, M., Hao, Y., Oh, E., Tian, M. and Liu, L., 2010. Integration of light-and brassinosteroid-signaling pathways by a GATA transcription factor in *Arabidopsis*. *Developmental cell*, 19(6), pp.872-883.
- Lyons, R., Rusu, A., Stiller, J., Powell, J., Manners, J.M. and Kazan, K., 2015. Investigating the association between flowering time and defense in the *Arabidopsis thaliana*-*Fusarium oxysporum* interaction. *PloS one*, 10(6), p.e0127699.
- Lyons, R., Stiller, J., Powell, J., Rusu, A., Manners, J.M. and Kazan, K., 2015. *Fusarium oxysporum* triggers tissue-specific transcriptional reprogramming in *Arabidopsis thaliana*. *PLoS one*, 10(4), p.e0121902.
- MacRae, T.H., 1997. Tubulin post-translational modifications: enzymes and their mechanisms of action. *European Journal of Biochemistry*, 244(2), pp.265-278.
- Manasa SL, Panigrahy M, Panigrahi KCS, Rout GR (2022) Overview of cold stress regulation in plants. *The Bot Rev* 88:359–387

- Manasa, L.S., Panigrahy, M., Panigrahi, K.C., Mishra, G., Panda, S.K. and Rout, G.R., 2023. Cold Tolerance Mechanisms in Mungbean (*Vigna radiata* L.) Genotypes during Germination. *Agriculture*, 13(2), p.315.
- Mao, J.L., Miao, Z.Q., Wang, Z., Yu, L.H., Cai, X.T. and Xiang, C.B., 2016. *Arabidopsis* ERF1 mediates cross-talk between ethylene and auxin biosynthesis during primary root elongation by regulating ASA1 expression. *PLoS Genetics*, 12(1), p.e1005760.
- Martin-Tryon, E.L., Kreps, J.A. and Harmer, S.L., 2007. GIGANTEA acts in blue light signaling and has biochemically separable roles in circadian clock and flowering time regulation. *Plant physiology*, 143(1), pp.473-486.
- Marzec, M., 2017. Strigolactones and gibberellins: a new couple in the phytohormone world?. *Trends in plant science*, 22(10), pp.813-815.
- Más P, Alabadí D, Yanovsky MJ et al (2003a) Dual role of *TOC1* in the control of circadian and photomorphogenic responses in *Arabidopsis*. *Plant Cell* 15(1):223–236
- Más P, Kim WY, Somers DE, Kay SA (2003b) Targeted degradation of *TOC1* by *ZTL* modulates circadian function in *Arabidopsis thaliana*. *Nature* 426(6966):567–570
- Mashiguchi, K., Tanaka, K., Sakai, T., Sugawara, S., Kawaide, H., Natsume, M., Hanada, A., Yaeno, T., Shirasu, K., Yao, H. and McSteen, P., 2011. The main auxin biosynthesis pathway in *Arabidopsis*. *Proceedings of the National Academy of Sciences*, 108(45), pp.18512-18517.
- Mathews, S. and Donoghue, M.J., 1999. The root of angiosperm phylogeny inferred from duplicate phytochrome genes. *Science*, 286(5441), pp.947-950.
- Matsubara K, Ogiso-Tanaka E, Hori K et al (2012) Natural variation in *Hd17*, a homolog of *Arabidopsis* *ELF3* that is involved in rice photoperiodic flowering. *Plant Cell Physiol* 53(4):709–716
- Mazars, C., Thion, L., Thuleau, P., Graziana, A., Knight, M.R., Moreau, M. and Ranjeva, R., 1997. Organization of cytoskeleton controls the changes in cytosolic calcium of cold-shocked *Nicotiana plumbaginifolia* protoplasts. *Cell Calcium*, 22(5), pp.413-420.
- McBlain BA, Bernard RL (1987) A new gene affecting the time of flowering and maturity in soybeans. *J Hered* 78(3):160–162
- McClung CR (2019) The plant circadian oscillator. *Biology* 8(1):14
- McClung, C.R., 2006. Plant circadian rhythms. *The Plant Cell*, 18(4), pp.792-803.
- Merchant, S.S., Prochnik, S.E., Vallon, O., Harris, E.H., Karpowicz, S.J., Witman, G.B., Terry, A., Salamov, A., Fritz-Laylin, L.K., Maréchal-Drouard, L. and Marshall, W.F., 2007. The *Chlamydomonas* genome reveals the evolution of key animal and plant functions. *Science*, 318(5848), pp.245-250.

- Michalko, J., Glanc, M., Perrot-Rechenmann, C. and Friml, J., 2016. Strong morphological defects in conditional *Arabidopsis* abp1 knock-down mutants generated in absence of functional ABP1 protein. *F1000Research*, 5.
- Michielse, C.B. and Rep, M., 2009. Pathogen profile update: *Fusarium oxysporum*. *Molecular plant pathology*, 10(3), p.311.
- Miquel, M., James Jr, D., Dooner, H. and Browse, J., 1993. *Arabidopsis* requires polyunsaturated lipids for low-temperature survival. *Proceedings of the National Academy of Sciences*, 90(13), pp.6208-6212.
- Mishra, G., Collings, D.A. and Altaner, C.M., 2018. Cell organelles and fluorescence of parenchyma cells in *Eucalyptus bosistoana* sapwood and heartwood investigated by microscopy. *New Zealand Journal of Forestry Science*, 48(1), pp.1-10.
- Mishra, P. and Panigrahi, K.C., 2015. GIGANTEA—an emerging story. *Frontiers in plant science*, 6, p.8.
- Mittal, D., Chakrabarti, S., Sarkar, A., Singh, A. and Grover, A., 2009. Heat shock factor gene family in rice: genomic organization and transcript expression profiling in response to high temperature, low temperature and oxidative stresses. *Plant Physiology and Biochemistry*, 47(9), pp.785-795.
- Mizoguchi, T., Wright, L., Fujiwara, S., Cremer, F., Lee, K., Onouchi, H., Mouradov, A., Fowler, S., Kamada, H., Putterill, J. and Coupland, G., 2005. Distinct roles of GIGANTEA in promoting flowering and regulating circadian rhythms in *Arabidopsis*. *The Plant Cell*, 17(8), pp.2255-2270.
- Mockaitis, K. and Estelle, M., 2008. Auxin receptors and plant development: a new signaling paradigm. *Annual review of cell and developmental biology*, 24, pp.55-80.
- Mockler, T.C., Michael, T.P., Priest, H.D., Shen, R., Sullivan, C.M., Givan, S.A., McEntee, C., Kay, S.A. and Chory, J., 2007, January. The DIURNAL project: DIURNAL and circadian expression profiling, model-based pattern matching, and promoter analysis. In *Cold Spring Harbor symposia on quantitative biology* (Vol. 72, pp. 353-363). Cold Spring Harbor Laboratory Press.
- Molas, M.L., Kiss, J.Z. and Correll, M.J., 2006. Gene profiling of the red light signalling pathways in roots. *Journal of Experimental Botany*, 57(12), pp.3217-3229.
- Moore, T.C. and Moore, T.C., 1974. Roles of Auxins and Cytokinins in Apical Dominance. *Research Experiences in Plant Physiology: A Laboratory Manual*, pp.215-227.
- Morris, K. and Jackson, S.P., 2010. DAY NEUTRAL FLOWERING does not act through GIGANTEA and FKF1 to regulate CONSTANS expression and flowering time. *Plant signaling & behavior*, 5(9), pp.1105-1107.

- Murakami M, Tago Y, Yamashino T, Mizuno T (2007) Comparative overviews of clock-associated genes of *Arabidopsis thaliana* and *Oryza sativa*. *Plant Cell Physiol* 48(1):110–121
- Murphy RL, Klein RR, Morishige DT et al (2011) Coincident light and clock regulation of *PSEUDORESPONSE REGULATOR* protein 37 (PRR37) controls photoperiodic flowering in sorghum. *PNAS USA* 108(39):16469–16474
- Nakamichi, N., Kusano, M., Fukushima, A., Kita, M., Ito, S., Yamashino, T., Saito, K., Sakakibara, H. and Mizuno, T., 2009. Transcript profiling of an *Arabidopsis* PSEUDO RESPONSE REGULATOR arrhythmic triple mutant reveals a role for the circadian clock in cold stress response. *Plant and Cell Physiology*, 50(3), pp.447-462.
- Napier, R., 2021. The story of auxin-binding protein 1 (ABP1). *Cold Spring Harbor Perspectives in Biology*, 13(12), p.a039909.
- Napier, R.M., David, K.M. and Perrot-Rechenmann, C., 2002. A short history of auxin-binding proteins. *Auxin Molecular Biology*, pp.339-348.
- Nguema-Ona, E., Bannigan, A., Chevalier, L., Baskin, T.I. and Driouich, A., 2007. Disruption of arabinogalactan proteins disorganizes cortical microtubules in the root of *Arabidopsis thaliana*. *The Plant Journal*, 52(2), pp.240-251.
- Nick, P., 1998. Signaling to the microtubular cytoskeleton in plants. In *International review of cytology* (Vol. 184, pp. 33-80). Academic Press.
- Nick, P., 2008. Microtubules as sensors for abiotic stimuli. In *Plant Microtubules: Development and Flexibility* (pp. 175-203). Berlin, Heidelberg: Springer Berlin Heidelberg.
- Nishimasu, H., Ran, F.A., Hsu, P.D., Konermann, S., Shehata, S.I., Dohmae, N., Ishitani, R., Zhang, F. and Nureki, O., 2014. Crystal structure of Cas9 in complex with guide RNA and target DNA. *Cell*, 156(5), pp.935-949.
- Nohales, M.A. and Kay, S.A., 2019. GIGANTEA gates gibberellin signaling through stabilization of the DELLA proteins in *Arabidopsis*. *Proceedings of the National Academy of Sciences*, 116(43), pp.21893-21899.
- Nose M, Watanabe A (2014) Clock genes and diurnal transcriptome dynamics in summer and winter in the gymnosperm Japanese cedar (*Cryptomeria japonica* (Lf) D. Don). *BMC Plant Biol* 14(1):1–19
- Oakley, B.R., Paolillo, V. and Zheng, Y., 2015. γ -Tubulin complexes in microtubule nucleation and beyond. *Molecular biology of the cell*, 26(17), pp.2957-2962.
- Oh, E., Zhu, J.Y. and Wang, Z.Y., 2012. Interaction between BZR1 and PIF4 integrates brassinosteroid and environmental responses. *Nature cell biology*, 14(8), pp.802-809.

- Oka, Y., Matsushita, T., Mochizuki, N., Quail, P.H. and Nagatani, A., 2008. Mutant screen distinguishes between residues necessary for light-signal perception and signal transfer by phytochrome B. *PLoS genetics*, 4(8), p.e1000158.
- Oliver, S.C., Venis, M.A., Freedman, R.B. and Napier, R.M., 1995. Regulation of synthesis and turnover of maize auxin-binding protein and observations on its passage to the plasma membrane: comparisons to maize immunoglobulin-binding protein cognate. *Planta*, 197(3), pp.465-474.
- Oliverio, K.A., Crepy, M., Martin-Tryon, E.L., Milich, R., Harmer, S.L., Putterill, J., Yanovsky, M.J. and Casal, J.J., 2007. GIGANTEA regulates phytochrome A-mediated photomorphogenesis independently of its role in the circadian clock. *Plant Physiology*, 144(1), pp.495-502.
- Olsen JL, Rouzé P, Verhelst B et al (2016) The genome of the seagrass *Zostera marina* reveals angiosperm adaptation to the sea. *Nature* 530(7590):331–335.
- Paciorek, T. and Friml, J., 2006. Auxin signaling. *Journal of Cell Science*, 119(7), pp.1199-1202.
- Paik, I. and Huq, E., 2019, August. Plant photoreceptors: Multi-functional sensory proteins and their signaling networks. In *Seminars in Cell & Developmental Biology* (Vol. 92, pp. 114-121). Academic Press.
- Pan, P., Shen, M., Yu, Z., Ge, W., Chen, K., Tian, M., Xiao, F., Wang, Z., Wang, J., Jia, Y. and Wang, W., 2021. SARS-CoV-2 N protein promotes NLRP3 inflammasome activation to induce hyperinflammation. *Nature communications*, 12(1), p.4664.
- Panigrahi, K.C., Panigrahy, M., Vervliet-Scheebaum, M., Lang, D., Reski, R. and Johri, M.M., 2009. Auxin-binding proteins without KDEL sequence in the moss *Funaria hygrometrica*. *Plant cell reports*, 28, pp.1747-1758.
- Panigrahy M, Panigrahi KC, Poli Y, Ranga A, Majeed N (2022) Integrated expression analysis of small RNA, degradome and microarray reveals complex regulatory action of miRNA during prolonged shade in Swarnaprabha rice. *Biology* 11(5):798
- Panigrahy, M., 2004. *Characterisation of mutants involved in Phytochrome A nuclear import and signal transduction* (Doctoral dissertation, Freiburg (Breisgau), Univ., Diss., 2004).
- Panigrahy, M., Neelamraju, S., Rao, D.N. and Ramanan, R., 2011. Heat tolerance in rice mutants is associated with reduced accumulation of reactive oxygen species. *Biologia Plantarum*, 55, pp.721-724.
- Panigrahy, M., Ranga, A., Das, J. and Panigrahi, K.C., 2019. Shade tolerance in Swarnaprabha rice is associated with higher rate of panicle emergence and positively regulated by genes of ethylene and cytokinin pathway. *Scientific Reports*, 9(1), p.6817.

- Pantelides, I.S., Tjamos, S.E., Pappa, S., Kargakis, M. and Paplomatas, E.J., 2013. The ethylene receptor ETR 1 is required for *Fusarium oxysporum* pathogenicity. *Plant Pathology*, 62(6), pp.1302-1309.
- Park Y, Xu ZY, Kim SY et al (2016) Spatial regulation of *ABCG25*, an ABA exporter, is an important component of the mechanism controlling cellular ABA levels. *Plant Cell* 28(10):2528–2544
- Park, D.H., Somers, D.E., Kim, Y.S., Choy, Y.H., Lim, H.K., Soh, M.S., Kim, H.J., Kay, S.A. and Nam, H.G., 1999. Control of circadian rhythms and photoperiodic flowering by the *Arabidopsis* GIGANTEA gene. *Science*, 285(5433), pp.1579-1582.
- Park, H.J., Kim, W.Y. and Yun, D.J., 2013. A role for GIGANTEA: keeping the balance between flowering and salinity stress tolerance. *Plant signaling & behavior*, 8(7), p.e24820.
- Park, H.J., Kim, W.Y. and Yun, D.J., 2016. A new insight of salt stress signaling in plant. *Molecules and cells*, 39(6), p.447.
- Pathan, A.K., Bond, J. and Gaskin, R.E., 2010. Sample preparation for SEM of plant surfaces. *Materials Today*, 12, pp.32-43.
- Patnaik, A., Alavilli, H., Rath, J., Panigrahi, K.C. and Panigrahy, M., 2022. Variations in circadian clock organization & function: A journey from ancient to recent. *Planta*, 256(5), p.91.
- Patnaik, A., Kumar, A., Behera, A., Mishra, G., Dehery, S.K., Panigrahy, M., Das, A.B. and Panigrahi, K.C., 2023. GIGANTEA suppresses wilt disease resistance by down-regulating the jasmonate signaling in *Arabidopsis thaliana*. *Frontiers in Plant Science*, 14, p.1091644.
- Pauwels, L. and Goossens, A., 2011. The JAZ proteins: a crucial interface in the jasmonate signaling cascade. *The Plant Cell*, 23(9), pp.3089-3100.
- Pereira, J.A., Yu, F., Zhang, Y., Jones, J.B. and Mou, Z., 2018. The *Arabidopsis* elongator subunit ELP3 and ELP4 confer resistance to bacterial speck in tomato. *Frontiers in Plant Science*, 9, p.1066.
- Perincherry, L., Lalak-Kańczugowska, J. and Stępień, Ł., 2019. Fusarium-produced mycotoxins in plant-pathogen interactions. *Toxins*, 11(11), p.664.
- Petersen J, Rredhi A, Szyttenholm J, Mittag M (2022) Evolution of circadian clocks along the green lineage. *Plant Physiol.* <https://doi.org/10.1093/plphys/kiac141>
- Petersson, S.V., Johansson, A.I., Kowalczyk, M., Makoveychuk, A., Wang, J.Y., Moritz, T., Grebe, M., Benfey, P.N., Sandberg, G. and Ljung, K., 2009. An auxin gradient and maximum in the *Arabidopsis* root apex shown by high-resolution cell-specific analysis of IAA distribution and synthesis. *The Plant Cell*, 21(6), pp.1659-1668.
- Pfaffl, M.W., 2001. A new mathematical model for relative quantification in real-time RT–PCR. *Nucleic acids research*, 29(9), pp.e45-e45.

- Piechulla B, Brinker M, Wissel K (2001) Circadian gene expression in angiosperms and gymnosperms. *Endocytobiosis Cell Res* 14(1/2):33–44
- Piperno, G., LeDizet, M. and Chang, X.J., 1987. Microtubules containing acetylated alpha-tubulin in mammalian cells in culture. *The Journal of cell biology*, 104(2), pp.289-302.
- Pokhilko A, Fernández AP, Edwards KD et al (2012) The clock gene circuit in *Arabidopsis* includes a repressilator with additional feedback loops. *Mol Syst Biol* 8(1):574
- Porfirio, S., Sonon, R., da Silva, M.D.G., Peixe, A., Cabrita, M.J. and Azadi, P., 2016. Quantification of free auxins in semi-hardwood plant cuttings and microshoots by dispersive liquid–liquid microextraction/microwave derivatization and GC/MS analysis. *Analytical Methods*, 8(31), pp.6089-6098.
- Pua, E.C. and Davey, M.R., 2010. *Plant developmental biology: biotechnological perspectives* (Vol. 1). Heidelberg: Springer.
- Putterill, J., Robson, F., Lee, K., Simon, R. and Coupland, G., 1995. The CONSTANS gene of *Arabidopsis* promotes flowering and encodes a protein showing similarities to zinc finger transcription factors. *cell*, 80(6), pp.847-857.
- Qian, X., Shen, G., Wang, Z., Guo, C., Liu, Y., Lei, Z. and Zhang, Z., 2014. Co-composting of livestock manure with rice straw: characterization and establishment of maturity evaluation system. *Waste management*, 34(2), pp.530-535.
- Rakusová, H., Gallego-Bartolomé, J., Vanstraelen, M., Robert, H.S., Alabadí, D., Blázquez, M.A., Benková, E. and Friml, J., 2011. Polarization of PIN3-dependent auxin transport for hypocotyl gravitropic response in *Arabidopsis thaliana*. *The Plant Journal*, 67(5), pp.817-826.
- Ramel, F., Birtic, S., Cuiñé, S., Triantaphylidès, C., Ravanat, J.L. and Havaux, M., 2012. Chemical quenching of singlet oxygen by carotenoids in plants. *Plant physiology*, 158(3), pp.1267-1278.
- Rao, M.V. and Davis, K.R., 1999. Ozone-induced cell death occurs via two distinct mechanisms in *Arabidopsis*: the role of salicylic acid. *The Plant Journal*, 17(6), pp.603-614.
- Rao, M.V., Paliyath, G. and Ormrod, D.P., 1996. Ultraviolet-B-and ozone-induced biochemical changes in antioxidant enzymes of *Arabidopsis thaliana*. *Plant physiology*, 110(1), pp.125-136.
- Rath, C.C. and Alena Patnaik, A.P., 2018. In-vitro antimycotic activity of selected essential oils and fungicides against *Aspergillus niger* and *fusarium oxysporum*.
- Rawat R, Takahashi N, Hsu PY, Jones MA et al (2011) *REVEILLE8* and *PSEUDO-RESPONSE REGULATOR5* form a negative feedback loop within the *Arabidopsis* circadian clock. *PLoS Genet* 7(3):e1001350

- Rawat, R., Schwartz, J., Jones, M.A., Sairanen, I., Cheng, Y., Andersson, C.R., Zhao, Y., Ljung, K. and Harmer, S.L., 2009. REVEILLE1, a Myb-like transcription factor, integrates the circadian clock and auxin pathways. *Proceedings of the national academy of sciences*, 106(39), pp.16883-16888.
- Rédei, G.P., 1962. Supervital mutants of *Arabidopsis*. *Genetics*, 47(4), p.443.
- Reed, J.W., Nagpal, P., Poole, D.S., Furuya, M. and Chory, J., 1993. Mutations in the gene for the red/far-red light receptor phytochrome B alter cell elongation and physiological responses throughout *Arabidopsis* development. *The Plant Cell*, 5(2), pp.147-157.
- Reski, R. and Abel, W.O., 1985. Induction of budding on chloronemata and caulonemata of the moss, *Physcomitrella patens*, using isopentenyladenine. *Planta*, 165, pp.354-358.
- Reverberi, M., Fabbri, A.A. and Fanelli, C., 2012. Oxidative stress and oxylipins in plant-fungus interaction. In *Biocommunication of Fungi* (pp. 273-290). Dordrecht: Springer Netherlands.
- Riboni, M., Galbiati, M., Tonelli, C. and Conti, L., 2013. GIGANTEA enables drought escape response via abscisic acid-dependent activation of the florigens and SUPPRESSOR OF OVEREXPRESSION OF CONSTANS1. *Plant physiology*, 162(3), pp.1706-1719.
- Riboni, M., Robustelli Test, A., Galbiati, M., Tonelli, C. and Conti, L., 2014. Environmental stress and flowering time: the photoperiodic connection. *Plant signaling & behavior*, 9(7), p.e29036.
- Ristic, Z. and Ashworth, E.N., 1993. Changes in leaf ultrastructure and carbohydrates in *Arabidopsis thaliana* L.(Heyn) cv. Columbia during rapid cold acclimation. *Protoplasma*, 172, pp.111-123.
- Rivas-San Vicente, M. and Plasencia, J., 2011. Salicylic acid beyond defence: its role in plant growth and development. *Journal of experimental botany*, 62(10), pp.3321-3338.
- Robert, S., Kleine-Vehn, J., Barbez, E., Sauer, M., Paciorek, T., Baster, P., Vanneste, S., Zhang, J., Simon, S., Čovanová, M. and Hayashi, K., 2010. ABP1 mediates auxin inhibition of clathrin-dependent endocytosis in *Arabidopsis*. *Cell*, 143(1), pp.111-121.
- Roberts, I.N., Lloyd, C.W. and Roberts, K., 1985. Ethylene-induced microtubule reorientations: mediation by helical arrays. *Planta*, 164, pp.439-447.
- Robson, F., Okamoto, H., Patrick, E., Harris, S.R., Wasternack, C., Brearley, C. and Turner, J.G., 2010. Jasmonate and phytochrome A signaling in *Arabidopsis* wound and shade responses are integrated through JAZ1 stability. *The Plant Cell*, 22(4), pp.1143-1160.
- Rochon, A., Boyle, P., Wignes, T., Fobert, P.R. and Després, C., 2006. The coactivator function of *Arabidopsis* NPR1 requires the core of its BTB/POZ domain and the oxidation of C-terminal cysteines. *The Plant Cell*, 18(12), pp.3670-3685.

- Romani, I., Tadini, L., Rossi, F., Masiero, S., Pribil, M., Jahns, P., Kater, M., Leister, D. and Pesaresi, P., 2012. Versatile roles of *Arabidopsis* plastid ribosomal proteins in plant growth and development. *The Plant Journal*, 72(6), pp.922-934.
- Ruan, J., Zhou, Y., Zhou, M., Yan, J., Khurshid, M., Weng, W., Cheng, J. and Zhang, K., 2019. Jasmonic acid signaling pathway in plants. *International journal of molecular sciences*, 20(10), p.2479.
- Ruse, C.I., Chin, H.G. and Pradhan, S., 2022. Polyglutamylation: biology and analysis. *Amino Acids*, 54(4), pp.529-542.
- Růžicka, K., Ljung, K., Vanneste, S., Podhorská, R., Beeckman, T., Friml, J. and Benková, E., 2007. Ethylene regulates root growth through effects on auxin biosynthesis and transport-dependent auxin distribution. *The Plant Cell*, 19(7), pp.2197-2212.
- Saha, B., Mishra, S., Awasthi, J.P., Sahoo, L. and Panda, S.K., 2016. Enhanced drought and salinity tolerance in transgenic mustard [*Brassica juncea* (L.) Czern & Coss.] overexpressing *Arabidopsis* group 4 late embryogenesis abundant gene (AtLEA4-1). *Environmental and Experimental Botany*, 128, pp.99-111.
- Saito H, Ogiso-Tanaka E, Okumoto Y et al (2012) *Ef7* encodes an *ELF3*-like protein and promotes rice flowering by negatively regulating the floral repressor gene *Ghd7* under both short-and long-day conditions. *Plant Cell Physiol* 53(4):717–728
- Salehi, H., Ransom, C.B., Oraby, H.F., Seddighi, Z. and Sticklen, M.B., 2005. Delay in flowering and increase in biomass of transgenic tobacco expressing the *Arabidopsis* floral repressor gene FLOWERING LOCUS C. *Journal of Plant Physiology*, 162(6), pp.711-717.
- Šamaj, J., Baluška, F. and Hirt, H., 2004. From signal to cell polarity: mitogen-activated protein kinases as sensors and effectors of cytoskeleton dynamicity. *Journal of experimental botany*, 55(395), pp.189-198.
- Sanchez, S.E. and Kay, S.A., 2016. The plant circadian clock: from a simple timekeeper to a complex developmental manager. *Cold Spring Harbor perspectives in biology*, 8(12), p.a027748.
- Sandalio, L.M., Rodríguez-Serrano, M. and Romero-Puertas, M.C., 2016. Leaf epinasty and auxin: A biochemical and molecular overview. *Plant Science*, 253, pp.187-193.
- Sandalio, L.M., Rodríguez-Serrano, M. and Romero-Puertas, M.C., 2016. Leaf epinasty and auxin: A biochemical and molecular overview. *Plant Science*, 253, pp.187-193.
- Sanghera, G.S., Wani, S.H., Hussain, W. and Singh, N.B., 2011. Engineering cold stress tolerance in crop plants. *Current genomics*, 12(1), p.30.
- Sartor F, Eelderink-Chen Z, Aronson B et al (2019) Are there circadian clocks in non-photosynthetic bacteria? *Biology* 8(2):41

- Sawa, M., Nusinow, D.A., Kay, S.A. and Imaizumi, T., 2007. FKF1 and GIGANTEA complex formation is required for day-length measurement in *Arabidopsis*. *Science*, 318(5848), pp.261-265.
- Schaller, G.E., 2012. Ethylene and the regulation of plant development. *BMC biology*, 10(1), pp.1-3.
- Schmidt, S., Dethloff, F., Beine-Golovchuk, O. and Kopka, J., 2013. The REIL1 and REIL2 proteins of *Arabidopsis thaliana* are required for leaf growth in the cold. *Plant physiology*, 163(4), pp.1623-1639.
- Scott, I.M., Clarke, S.M., Wood, J.E. and Mur, L.A., 2004. Salicylate accumulation inhibits growth at chilling temperature in *Arabidopsis*. *Plant Physiology*, 135(2), pp.1040-1049.
- Sedbrook, J.C., Ehrhardt, D.W., Fisher, S.E., Scheible, W.R. and Somerville, C.R., 2004. The *Arabidopsis* SKU6/SPIRAL1 gene encodes a plus end-localized microtubule-interacting protein involved in directional cell expansion. *The Plant Cell*, 16(6), pp.1506-1520.
- Sega, G.A., 1984. A review of the genetic effects of ethyl methanesulfonate. *Mutation Research/Reviews in Genetic Toxicology*, 134(2-3), pp.113-142.
- Serikawa M, Miwa K, Kondo T, Oyama T (2008) Functional conservation of clock-related genes in flowering plants: overexpression and RNA interference analyses of the circadian rhythm in the monocotyledon *Lemna gibba*. *Plant Physiol* 146(4):1952–1963
- Shalit-Kaneh A, Kumimoto RW, Filkov V, Harmer SL (2018) Multiple feedback loops of the *Arabidopsis* circadian clock provide rhythmic robustness across environmental conditions. *PNAS USA* 115(27):7147–7152
- Sharma, M., Irfan, M., Kumar, A., Kumar, P. and Datta, A., 2022. Recent insights into plant circadian clock response against abiotic stress. *Journal of Plant Growth Regulation*, 41(8), pp.3530-3543.
- Sharp, R.E. and LeNoble, M.E., 2002. ABA, ethylene and the control of shoot and root growth under water stress. *Journal of experimental botany*, 53(366), pp.33-37.
- Shaw, S.L., Kamyar, R. and Ehrhardt, D.W., 2003. Sustained microtubule treadmilling in *Arabidopsis* cortical arrays. *Science*, 300(5626), pp.1715-1718.
- Shen-Miller, J., 1973. Rhythmicity in the basipetal transport of indoleacetic acid through coleoptiles. *Plant physiology*, 51(4), pp.615-619.
- Shi, Y. and Yang, S., 2014. ABA regulation of the cold stress response in plants. *Abscisic acid: metabolism, transport and signaling*, pp.337-363.
- Shibaoka, H., 1994. Plant hormone-induced changes in the orientation of cortical microtubules: alterations in the cross-linking between microtubules and the plasma membrane. *Annual review of plant biology*, 45(1), pp.527-544.

- Shih, C.J., Chen, H.W., Hsieh, H.Y., Lai, Y.H., Chiu, F.Y., Chen, Y.R. and Tu, S.L., 2019. Heterogeneous nuclear ribonucleoprotein H1 coordinates with phytochrome and the U1 snRNP complex to regulate alternative splicing in *Physcomitrella patens*. *The Plant Cell*, 31(10), pp.2510-2524.
- Shimomura, S., Watanabe, S. and Ichikawa, H., 1999. Characterization of auxin-binding protein 1 from tobacco: content, localization and auxin-binding activity. *Planta*, 209, pp.118-125.
- Shinkle, J.R., Swoap, S.J., Simon, P. and Jones, R.L., 1992. Cell wall free space of Cucumis hypocotyls contains NAD and a blue light-regulated peroxidase activity. *Plant physiology*, 98(4), pp.1336-1341.
- Siemiatkowska, B., Chiara, M., Badiger, B.G., Riboni, M., D'Avila, F., Braga, D., Salem, M.A.A., Martignago, D., Colanero, S., Galbiati, M. and Giavalisco, P., 2022. GIGANTEA is a negative regulator of abscisic acid transcriptional responses and sensitivity in *Arabidopsis*. *Plant and Cell Physiology*, 63(9), pp.1285-1297.
- Sikora, P., Chawade, A., Larsson, M., Olsson, J. and Olsson, O., 2011. Mutagenesis as a tool in plant genetics, functional genomics, and breeding. *International journal of plant genomics*, 2011.
- Simon NM, Graham CA, Comben NE et al (2020) The circadian clock influences the long-term water use efficiency of *Arabidopsis*. *Plant Physiol* 183(1):317–330
- Singh, A., 2022. GIGANTEA regulates PAD4 transcription to promote pathogen defense against *Hyaloperonospora arabidopsidis* in *Arabidopsis thaliana*. *Plant Signaling & Behavior*, 17(1), p.2058719.
- Singh, B.K., Dawson, L.A., Macdonald, C.A. and Buckland, S.M., 2009. Impact of biotic and abiotic interaction on soil microbial communities and functions: A field study. *applied soil ecology*, 41(3), pp.239-248.
- Singh, H.P., Kaur, S., Mittal, S., Batish, D.R. and Kohli, R.K., 2009. Essential oil of *Artemisia scoparia* inhibits plant growth by generating reactive oxygen species and causing oxidative damage. *Journal of chemical ecology*, 35, pp.154-162.
- Singh. K. Gigantea Antibody Designing And its Characterisation. 2016.
- Slautterback, D.B., 1963. Cytoplasmic microtubules: I. Hydra. *The Journal of cell biology*, 18(2), pp.367-388.
- Smalle, J., Haegman, M., Kurepa, J., Van Montagu, M. and Straeten, D.V.D., 1997. Ethylene can stimulate *Arabidopsis* hypocotyl elongation in the light. *Proceedings of the National Academy of Sciences*, 94(6), pp.2756-2761.
- Smart, R.E. and Bingham, G.E., 1974. Rapid estimates of relative water content. *Plant physiology*, 53(2), pp.258-260.

- Smertenko, A., Blume, Y., Viklický, V., Opatrný, Z. and Dráber, P., 1997. Post-translational modifications and multiple tubulin isoforms in *Nicotiana tabacum* L. cells. *Planta*, 201, pp.349-358.
- Smertenko, A.P., Chang, H.Y., Wagner, V., Kaloriti, D., Fenyk, S., Sonobe, S., Lloyd, C., Hauser, M.T. and Hussey, P.J., 2004. The *Arabidopsis* microtubule-associated protein AtMAP65-1: molecular analysis of its microtubule bundling activity. *The plant cell*, 16(8), pp.2035-2047.
- Somers, D.E., Schultz, T.F., Milnamow, M. and Kay, S.A., 2000. ZEITLUPE encodes a novel clock-associated PAS protein from *Arabidopsis*. *Cell*, 101(3), pp.319-329.
- Song, H., Moon, M., Choe, H.K., Han, D.H., Jang, C., Kim, A., Cho, S., Kim, K. and Mook-Jung, I., 2015. A β -induced degradation of BMAL1 and CBP leads to circadian rhythm disruption in Alzheimer's disease. *Molecular Neurodegeneration*, 10, pp.1-15.
- Song, Y.H., Kubota, A., Kwon, M.S., Covington, M.F., Lee, N., Taagen, E.R., Laboy Cintrón, D., Hwang, D.Y., Akiyama, R., Hodge, S.K. and Huang, H., 2018. Molecular basis of flowering under natural long-day conditions in *Arabidopsis*. *Nat Plants* 4: 824–835. *Plant Cell Physiol*, pp.1-3.
- Stamm, P. and Kumar, P.P., 2013. Auxin and gibberellin responsive *Arabidopsis* SMALL AUXIN UP RNA36 regulates hypocotyl elongation in the light. *Plant Cell Reports*, 32, pp.759-769.
- Staswick, P.E., Serban, B., Rowe, M., Tiriyaki, I., Maldonado, M.T., Maldonado, M.C. and Suza, W., 2005. Characterization of an *Arabidopsis* enzyme family that conjugates amino acids to indole-3-acetic acid. *The Plant Cell*, 17(2), pp.616-627.
- Steindler, C., Matteucci, A., Sessa, G., Weimar, T., Ohgishi, M., Aoyama, T., Morelli, G. and Ruberti, I., 1999. Shade avoidance responses are mediated by the ATHB-2 HD-zip protein, a negative regulator of gene expression. *Development*, 126(19), pp.4235-4245.
- Stepanova, A.N., Yun, J., Robles, L.M., Novak, O., He, W., Guo, H., Ljung, K. and Alonso, J.M., 2011. The *Arabidopsis* YUCCA1 flavin monooxygenase functions in the indole-3-pyruvic acid branch of auxin biosynthesis. *The Plant Cell*, 23(11), pp.3961-3973.
- Stirbet, A., Lazár, D., Kromdijk, J. and Govindjee, 2018. Chlorophyll a fluorescence induction: can just a one-second measurement be used to quantify abiotic stress responses?. *Photosynthetica*, 56(1), pp.86-104.
- Storti, M., Costa, A., Golin, S., Zottini, M., Morosinotto, T. and Alboresi, A., 2018. Systemic calcium wave propagation in *Physcomitrella patens*. *Plant and Cell Physiology*, 59(7), pp.1377-1384.
- Strasser, R.J., Tsimilli-Michael, M. and Srivastava, A., 2004. Analysis of the chlorophyll a fluorescence transient. In *Chlorophyll a fluorescence: a signature of photosynthesis* (pp. 321-362). Dordrecht: Springer Netherlands.

- Sullivan, S., Petersen, J., Blackwood, L., Papanatsiou, M. and Christie, J.M., 2016. Functional characterization of *Ostreococcus tauri* phototropin. *New Phytologist*, 209(2), pp.612-623.
- Sun, P., Huang, C., Zhang, L., Wu, D., Zhang, W., Yu, S., Fu, G., Cheng, S., Wang, Z., Deng, Q. and Zhu, G., 2022. Insight into the effect of low temperature treatment on trichome density and related differentially expressed genes in Chinese cabbage. *Plos one*, 17(9), p.e0274530.
- Swain, S.M., Tseng, T.S. and Olszewski, N.E., 2001. Altered expression of SPINDLY affects gibberellin response and plant development. *Plant Physiology*, 126(3), pp.1174-1185.
- Takata N, Saito S, Saito CT, Uemura M (2010) Phylogenetic footprint of the plant clock system in angiosperms: evolutionary processes of pseudo-response regulators. *BMC Evol Biol* 10(1):1–14
- Takeda, T., Furuta, Y., Awano, T., Mizuno, K., Mitsuishi, Y. and Hayashi, T., 2002. Suppression and acceleration of cell elongation by integration of xyloglucans in pea stem segments. *Proceedings of the National Academy of Sciences*, 99(13), pp.9055-9060.
- Tamura, K., Kawabayashi, T., Shikanai, T. and Hara-Nishimura, I., 2016. Decreased expression of a gene caused by a T-DNA insertion in an adjacent gene in arabidopsis. *Plos one*, 11(2), p.e0147911.
- Tang, R.J., Zhao, F.G., Garcia, V.J., Kleist, T.J., Yang, L., Zhang, H.X. and Luan, S., 2015. Tonoplast CBL–CIPK calcium signaling network regulates magnesium homeostasis in *Arabidopsis*. *Proceedings of the National Academy of Sciences*, 112(10), pp.3134-3139.
- Tax, F.E. and Vernon, D.M., 2001. T-DNA-associated duplication/translocations in *Arabidopsis*. Implications for mutant analysis and functional genomics. *Plant physiology*, 126(4), pp.1527-1538.
- Tessmar-Raible K, Raible F, Arboleda E (2011) Another place, another timer: marine species and the rhythms of life. *BioEssays* 33(3):165–172
- Thatcher, L.F., Manners, J.M. and Kazan, K., 2009. *Fusarium oxysporum* hijacks COI1-mediated jasmonate signaling to promote disease development in *Arabidopsis*. *The Plant Journal*, 58(6), pp.927-939.
- Thelander, M., Landberg, K. and Sundberg, E., 2018. Auxin-mediated developmental control in the moss *Physcomitrella patens*. *Journal of Experimental Botany*, 69(2), pp.277-290.
- Thimann, K.V., 1937. On the nature of inhibitions caused by auxin. *American Journal of Botany*, pp.407-412.
- Thomashow, M.F., 1999. Plant cold acclimation: freezing tolerance genes and regulatory mechanisms. *Annual review of plant biology*, 50(1), pp.571-599.

- Tian, H., Klämbt, D. and Jones, A.M., 1995. Auxin-binding protein 1 does not bind auxin within the endoplasmic reticulum despite this being the predominant subcellular location for this hormone receptor. *Journal of Biological Chemistry*, 270(45), pp.26962-26969.
- Tiller, N., Weingartner, M., Thiele, W., Maximova, E., Schöttler, M.A. and Bock, R., 2012. The plastid-specific ribosomal proteins of *Arabidopsis thaliana* can be divided into non-essential proteins and genuine ribosomal proteins. *The Plant Journal*, 69(2), pp.302-316.
- Tissot, N., Przybyla-Toscano, J., Reyt, G., Castel, B., Duc, C., Boucherez, J., Gaymard, F., Briat, J.F. and Dubos, C., 2014. Iron around the clock. *Plant Science*, 224, pp.112-119.
- Tomanek, L., 2012. Environmental proteomics of the mussel *Mytilus*: implications for tolerance to stress and change in limits of biogeographic ranges in response to climate change.
- Tomas, A., Paponov, I. and Perrot-Rechenmann, C., 2010. AUXIN BINDING PROTEIN 1: functional and evolutionary aspects. *Trends in Plant Science*, 15(8), pp.436-446.
- Tseng, T.S., Salomé, P.A., McClung, C.R. and Olszewski, N.E., 2004. SPINDLY and GIGANTEA interact and act in *Arabidopsis thaliana* pathways involved in light responses, flowering, and rhythms in cotyledon movements. *The Plant Cell*, 16(6), pp.1550-1563.
- Turner A, Beales J, Faure S et al (2005) The pseudo-response regulator Ppd-H1 provides adaptation to photoperiod in barley. *Science* 310(5750):1031–1034
- Uemura, M., Warren, G. and Steponkus, P.L., 2003. Freezing sensitivity in the *sfr4* mutant of *Arabidopsis* is due to low sugar content and is manifested by loss of osmotic responsiveness. *Plant Physiology*, 131(4), pp.1800-1807.
- Uenaka, H., Wada, M. and Kadota, A., 2005. Four distinct photoreceptors contribute to light-induced side branch formation in the moss *Physcomitrella patens*. *Planta*, 222, pp.623-631.
- Vadassery, J., Reichelt, M., Hause, B., Gershenzon, J., Boland, W. and Mithöfer, A., 2012. CML42-mediated calcium signaling coordinates responses to Spodoptera herbivory and abiotic stresses in *Arabidopsis*. *Plant physiology*, 159(3), pp.1159-1175.
- Valverde, F., Mouradov, A., Soppe, W., Ravenscroft, D., Samach, A. and Coupland, G., 2004. Photoreceptor regulation of CONSTANS protein in photoperiodic flowering. *Science*, 303(5660), pp.1003-1006.
- Van Dijk, J., Rogowski, K., Miro, J., Lacroix, B., Eddé, B. and Janke, C., 2007. A targeted multienzyme mechanism for selective microtubule polyglutamylation. *Molecular cell*, 26(3), pp.437-448.
- van Gelderen, K., Kang, C. and Pierik, R., 2018. Light signaling, root development, and plasticity. *Plant physiology*, 176(2), pp.1049-1060.

- Van Loon, L.C. and Van Strien, E.A., 1999. The families of pathogenesis-related proteins, their activities, and comparative analysis of PR-1 type proteins. *Physiological and molecular plant pathology*, 55(2), pp.85-97.
- van Loon, L.C., Rep, M. and Pieterse, C.M., 2006. Significance of inducible defense-related proteins in infected plants. *Annu. Rev. Phytopathol.*, 44, pp.135-162.
- Vanacker, H., Lu, H., Rate, D.N. and Greenberg, J.T., 2001. A role for salicylic acid and NPR1 in regulating cell growth in *Arabidopsis*. *The Plant Journal*, 28(2), pp.209-216.
- Vanneste, S. and Friml, J., 2009. Auxin: a trigger for change in plant development. *Cell*, 136(6), pp.1005-1016.
- Verbelen, J.P., Le, J., Vissenberg, K., De Cnodder, T., Vandenbussche, F., Sugimoto, K. and Van Der Straeten, D., 2008. Microtubules and the control of cell elongation in *Arabidopsis* roots. In *The Plant Cytoskeleton: A Key Tool for Agro-Biotechnology* (pp. 73-90). Springer Netherlands.
- Voß, U., Wilson, M.H., Kenobi, K., Gould, P.D., Robertson, F.C., Peer, W.A., Lucas, M., Swarup, K., Casimiro, I., Holman, T.J. and Wells, D.M., 2015. The circadian clock rephases during lateral root organ initiation in *Arabidopsis thaliana*. *Nature communications*, 6(1), p.7641.
- Wachsman, G., Sparks, E.E. and Benfey, P.N., 2015. Genes and networks regulating root anatomy and architecture. *New Phytologist*, 208(1), pp.26-38.
- Wada, T., Tachibana, T., Shimura, Y. and Okada, K., 1997. Epidermal cell differentiation in *Arabidopsis* determined by a Myb homolog, CPC. *Science*, 277(5329), pp.1113-1116.
- Wang Y, Gu Y, Gao H, Qiu L et al (2016) Molecular and geographic evolutionary support for the essential role of *GIGANTEA* in soybean domestication of flowering time. *BMC Evol Biol* 16(1):1–13. <https://doi.org/10.1186/s12862-016-0653-9>
- Wang, C., Zhang, H., Wang, S. and Mao, S., 2021. Leaf spot of *Hosta ventricosa* caused by *Fusarium oxysporum* in China. *PeerJ*, 9, p.e12581.
- Wang, J., Song, L., Gong, X., Xu, J. and Li, M., 2020. Functions of jasmonic acid in plant regulation and response to abiotic stress. *International journal of molecular sciences*, 21(4), p.1446.
- Wang, L. and Wu, J., 2013. The essential role of jasmonic acid in plant–herbivore interactions—using the wild tobacco *Nicotiana attenuata* as a model. *Journal of Genetics and Genomics*, 40(12), pp.597-606.
- Wang, L., Li, H., Zhao, C., Li, S., Kong, L., Wu, W., Kong, W., Liu, Y., Wei, Y., Zhu, J.K. and Zhang, H., 2017. The inhibition of protein translation mediated by AtGCN1 is essential for cold tolerance in *Arabidopsis thaliana*. *Plant, cell & environment*, 40(1), pp.56-68.

- Wang, M.Y., Zhao, P.M., Cheng, H.Q., Han, L.B., Wu, X.M., Gao, P., Wang, H.Y., Yang, C.L., Zhong, N.Q., Zuo, J.R. and Xia, G.X., 2013. The cotton transcription factor TCP14 functions in auxin-mediated epidermal cell differentiation and elongation. *Plant physiology*, 162(3), pp.1669-1680.
- Wang, W., Withers, J., Li, H., Zwack, P.J., Rusnac, D.V., Shi, H., Liu, L., Yan, S., Hinds, T.R., Guttman, M. and Dong, X., 2020. Structural basis of salicylic acid perception by *Arabidopsis* NPR proteins. *Nature*, 586(7828), pp.311-316.
- Wang, X., Shen, C., Meng, P., Tan, G. and Lv, L., 2021. Analysis and review of trichomes in plants. *BMC plant biology*, 21(1), pp.1-11.
- Wang, Z.Y. and Tobin, E.M., 1998. Constitutive expression of the CIRCADIAN CLOCK ASSOCIATED 1 (CCA1) gene disrupts circadian rhythms and suppresses its own expression. *Cell*, 93(7), pp.1207-1217.
- Wani, S.H., Kumar, V., Shriram, V. and Sah, S.K., 2016. Phytohormones and their metabolic engineering for abiotic stress tolerance in crop plants. *The crop journal*, 4(3), pp.162-176.
- Watanabe S, Xia Z, Hideshima R, Tsubokura Y et al (2011) A map-based cloning strategy employing a residual heterozygous line reveals that the *GIGANTEA* gene is involved in soybean maturity and flowering. *Genetics* 188(2):395–407
- Wei, H., Wang, X., He, Y., Xu, H. and Wang, L., 2021. Clock component OsPRR73 positively regulates rice salt tolerance by modulating OsHKT2; 1-mediated sodium homeostasis. *The EMBO Journal*, 40(3), p.e105086.
- Wei, Z. and Li, J., 2016. Brassinosteroids regulate root growth, development, and symbiosis. *Molecular plant*, 9(1), pp.86-100.
- Weijers, D. and Wagner, D., 2016. Transcriptional responses to the auxin hormone. *Annual review of plant biology*, 67, pp.539-574.
- Weiss, J. and Egea-Cortines, M., 2009. Transcriptomic analysis of cold response in tomato fruits identifies dehydrin as a marker of cold stress. *Journal of applied genetics*, 50, pp.311-319.
- Wend, S., Bosco, C.D., Kämpf, M.M., Ren, F., Palme, K., Weber, W., Dovzhenko, A. and Zurbriggen, M.D., 2013. A quantitative ratiometric sensor for time-resolved analysis of auxin dynamics. *Scientific reports*, 3(1), p.2052.
- Werner, T., Motyka, V., Laucou, V., Smets, R., Van Onckelen, H. and Schmülling, T., 2003. Cytokinin-deficient transgenic *Arabidopsis* plants show multiple developmental alterations indicating opposite functions of cytokinins in the regulation of shoot and root meristem activity. *The Plant Cell*, 15(11), pp.2532-2550.
- Wiesler, B., Wang, Q.Y. and Nick, P., 2002. The stability of cortical microtubules depends on their orientation. *The Plant Journal*, 32(6), pp.1023-1032.

- Wloga, D., Joachimiak, E. and Fabczak, H., 2017. Tubulin post-translational modifications and microtubule dynamics. *International journal of molecular sciences*, 18(10), p.2207.
- Woodward, A.W. and Bartel, B., 2005. Auxin: regulation, action, and interaction. *Annals of botany*, 95(5), pp.707-735.
- Wulund, L. and Reddy, A.B., 2015. A brief history of circadian time: The emergence of redox oscillations as a novel component of biological rhythms. *Perspectives in Science*, 6, pp.27-37.
- Xiao, Y., Liu, D., Zhang, G., Gao, S., Liu, L., Xu, F., Che, R., Wang, Y., Tong, H. and Chu, C., 2019. Big Grain3, encoding a purine permease, regulates grain size via modulating cytokinin transport in rice. *Journal of Integrative Plant Biology*, 61(5), pp.581-597.
- Xie MQ, Wang P, Liu X, Yuan L et al (2014) *LNK1* and *LNK2* are transcriptional coactivators in the *Arabidopsis* circadian oscillator. *Plant Cell* 26(7):2843–2857
- Xin, H., Xianchao, N., Pan, X., Wei, L., Min, Y., Yu, K., Lunwen, Q. and Wei, H., 2019. Comparative transcriptome analyses revealed conserved and novel responses to cold and freezing stress in *Brassica napus* L. *G3: Genes, Genomes, Genetics*, 9(8), pp.2723-2737.
- Xu, H., Zuo, Y., Wei, J. and Wang, L., 2023. The Circadian Clock Coordinates the Tradeoff between Adaptation to Abiotic Stresses and Yield in Crops. *Biology*, 12(11), p.1364.
- Xu, T., Dai, N., Chen, J., Nagawa, S., Cao, M., Li, H., Zhou, Z., Chen, X., De Rycke, R., Rakusová, H. and Wang, W., 2014. Cell surface ABP1-TMK auxin-sensing complex activates ROP GTPase signaling. *Science*, 343(6174), pp.1025-1028.
- Xu, T., Wen, M., Nagawa, S., Fu, Y., Chen, J.G., Wu, M.J., Perrot-Rechenmann, C., Friml, J., Jones, A.M. and Yang, Z., 2010. Cell surface-and rho GTPase-based auxin signaling controls cellular interdigitation in *Arabidopsis*. *Cell*, 143(1), pp.99-110.
- Xue W, Xing Y, Weng X, Zhao Y et al (2008) Natural variation in *Ghd7* is an important regulator of heading date and yield potential in rice. *Nat Genet* 40(6):761–767
- Yang, G., Tang, L., Gong, Y., Xie, J., Fu, Y., Jiang, D., Li, G., Collinge, D.B., Chen, W. and Cheng, J., 2018. A cerato-platanin protein SsCP1 targets plant PR1 and contributes to virulence of *Sclerotinia sclerotiorum*. *New Phytologist*, 217(2), pp.739-755.
- Yazdanbakhsh, N., Sulpice, R., Graf, A., Stitt, M. and Fisahn, J., 2011. Circadian control of root elongation and C partitioning in *Arabidopsis thaliana*. *Plant, Cell & Environment*, 34(6), pp.877-894.
- Yeh, C.M., Kobayashi, K., Fujii, S., Fukaki, H., Mitsuda, N. and Ohme-Takagi, M., 2020. Blue light regulates phosphate deficiency-dependent primary root growth inhibition in *Arabidopsis*. *Frontiers in Plant Science*, 10, p.1803.
- Young, M.W. and Kay, S.A., 2001. Time zones: a comparative genetics of circadian

- Yu, J.W., Rubio, V., Lee, N.Y., Bai, S., Lee, S.Y., Kim, S.S., Liu, L., Zhang, Y., Irigoyen, M.L., Sullivan, J.A. and Zhang, Y., 2008. COP1 and ELF3 control circadian function and photoperiodic flowering by regulating GI stability. *Molecular cell*, 32(5), pp.617-630.
- Yu, Y., Wang, J., Zhang, Z., Quan, R., Zhang, H., Deng, X.W., Ma, L. and Huang, R., 2013. Ethylene promotes hypocotyl growth and HY5 degradation by enhancing the movement of COP1 to the nucleus in the light. *PLoS genetics*, 9(12), p.e1004025.
- Zeng, L., Zhang, Q., Sun, R., Kong, H., Zhang, N. and Ma, H., 2014. Resolution of deep angiosperm phylogeny using conserved nuclear genes and estimates of early divergence times. *Nature communications*, 5(1), p.4956.
- Zha, P., Jing, Y., Xu, G. and Lin, R., 2017. PICKLE chromatin-remodeling factor controls thermosensory hypocotyl growth of *Arabidopsis*. *Plant, cell & environment*, 40(10), pp.2426-2436.
- Zhang B, Liu H, Qi F, Zhang Z et al (2019) Genetic interactions among *Ghd7*, *Ghd8*, *OsPRR37* and *Hd1* contribute to large variation in heading date in rice. *Rice* 12(1):1–13. <https://doi.org/10.1186/s12284-12019-10314-x>
- Zhang, Q. and Bartels, D., 2018. Molecular responses to dehydration and desiccation in desiccation-tolerant angiosperm plants. *Journal of experimental botany*, 69(13), pp.3211-3222.
- Zhang, S.W., Li, C.H., Cao, J., Zhang, Y.C., Zhang, S.Q., Xia, Y.F., Sun, D.Y. and Sun, Y., 2009. Altered architecture and enhanced drought tolerance in rice via the down-regulation of indole-3-acetic acid by TLD1/OsGH3. 13 activation. *Plant physiology*, 151(4), pp.1889-1901.
- Zhang, X., Lyu, J., Zeng, Y., Sun, N., Liu, C. and Yin, S., 2021. Individual effects of trichomes and leaf morphology on PM2. 5 dry deposition velocity: a variable-control approach using species from the same family or genus. *Environmental Pollution*, 272, p.116385.
- Zhang, Y., Song, H., Wang, X., Zhou, X., Zhang, K., Chen, X., Liu, J., Han, J. and Wang, A., 2020. The roles of different types of trichomes in tomato resistance to cold, drought, whiteflies, and botrytis. *Agronomy*, 10(3), p.411.
- Zhang, Y., Yu, J., Xu, X., Wang, R., Liu, Y., Huang, S., Wei, H. and Wei, Z., 2022. Molecular mechanisms of diverse auxin responses during plant growth and development. *International Journal of Molecular Sciences*, 23(20), p.12495.
- Zhao J, Chen H, Ren D, Tang H et al (2015) Genetic interactions between diverged alleles of *EARLY HEADING DATE 1* (*Ehd1*) and *HEADING DATE 3A* (*Hd3a*)/*RICE FLOWERING LOCUS T1* (*RFT 1*) control differential heading and contribute to regional adaptation in rice (*Oryza sativa*). *New Phytol* 208(3):936–948
- Zhao, Y., 2012. Auxin biosynthesis: a simple two-step pathway converts tryptophan to indole-3-acetic acid in plants. *Molecular plant*, 5(2), pp.334-338.

- Zhao, Y., 2018. Essential roles of local auxin biosynthesis in plant development and in adaptation to environmental changes. *Annual Review of Plant Biology*, 69, pp.417-435.
- Zhu, J.K., 2002. Salt and drought stress signal transduction in plants. *Annual review of plant biology*, 53(1), pp.247-273.

ANNEXURE

ANNEXURE 1

To eliminate any off-target effects that are associated with T-DNA mutagenesis in traditionally used *gi* mutants generated from T-DNA insertion from the study, a much-advanced error-free gene editing technique CRISPR Cas9 was used. *GIGANTEA* knock-out mutants were generated using the CRISPR-Cas9 genome editing tool and compared their phenotype with several traditional T-DNA mutants of *GI*. The generation of CRISPR mutants of *GI* was done in collaboration with Dr. Linkan Dash (Dash L., 2018).

a. Transformation and validation of the available plasmid vectors

The pGreen CRISPR binary vector facilitated *Agrobacterium* transformation and Cas9 gene expression in plants. Plasmid vectors were first transformed into *DH5α E. coli* cells using the heat shock method. Colonies were streaked on LB-kanamycin plates and incubated overnight at 37 °C. After selecting a colony, a primary culture was incubated the following day. Plasmid purification and digestion with EcoRI and KpnI confirmed its identity, showing the expected release of ~8.5kbp and 6kbp linearized fragments on a 1% agarose gel (Figure 95).

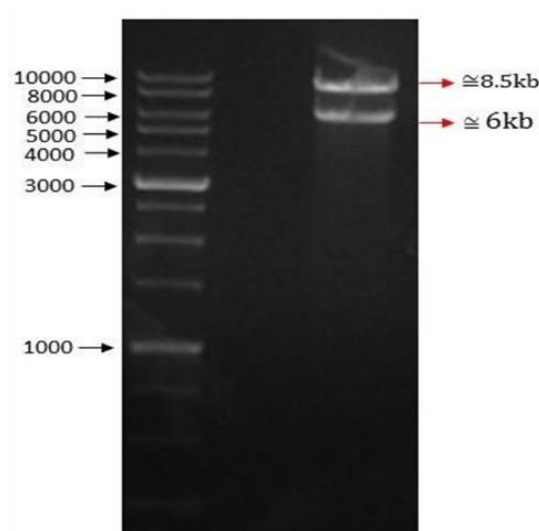


Figure 95. The pGreen CRISPR plasmid was digested with EcoRI and KpnI, then electrophoresed in a 1% gel. Expected release of 8.5kb and 6kb were achieved, confirming its identity. (Adapted from Dash. L., 2018)

b. In-silico designing of guide sequence/spacers

To generate GIGANTEA (GI) knock-out mutants, we focused on multiple sites at the same time to increase the probability of mutagenesis and gene deletion. The CRISPR Cas9 system uses a ~20 base pair RNA guide to form a DNA-Cas9 complex, which cleaves double-stranded DNA at a specific three-base pair PAM (Proto Spacer Adjacent Motif). Using the CHOP-CHOP tool, we carefully identified PAM sites and unique gRNA target sites, ultimately selecting six top-ranked target sites from various exons. Off-target scores were minimal, with predicted efficiencies greater than 70%. The GC content of the targets ranged between 40 and 80 percent, which is ideal for gRNA binding. The guide sequences were double-checked for uniqueness against the *Arabidopsis thaliana* genome using NCBI-Blast. Following *in-silco* design, sequences were synthesized with appropriate 5' additions for cloning into the pBluescript SK (pBSK) vector, enabling gRNA synthesis (Table 14).

Serial No.	Exon No.	Sequence
1	2	TGTTGAGGATCTCGTGGCGG
2	7	TCTAAGGATGTCGTTGGCGG
3	8	GCATCTGGAGCCCACGACGG
4	10	TGAGGCAATTCCTTGGGCAG
5	13	CGGCTGTATTGCTCTTGCCG
6	14	GCAGTGTCGAGAACTGAGT

Table 14. Top six guide sequences that were predicted by CHOP-CHOP for the genomic locus of GI (Adapted from Dash. L., 2018)

c. Cloning of gRNA into the pBSK vector

After synthesizing single-stranded guide sequences, an overnight annealing reaction was performed to create double-stranded guide DNA (gDNA) about 20 base pairs long. As conventional restriction cloning couldn't be applied due to the small size of the gDNA, the

pBSK plasmid with a single BbsI recognition site (5'...GAAGAC...3') was utilized. Upon digestion, BbsI generated overhangs complementary to those intentionally added to the gDNA. Ligation successfully integrated the gDNA into the pBSK vector, which uniquely lost the BbsI site after each insertion, validating the cloning process. Cloned plasmids underwent BbsI restriction digestion and gel electrophoresis, showing bands resembling undigested pBSK plasmid, serving as a control. The cloned plasmids were then transformed into DH5 α cells and allowed to proliferate, followed by plasmid DNA purification (Figure 96).

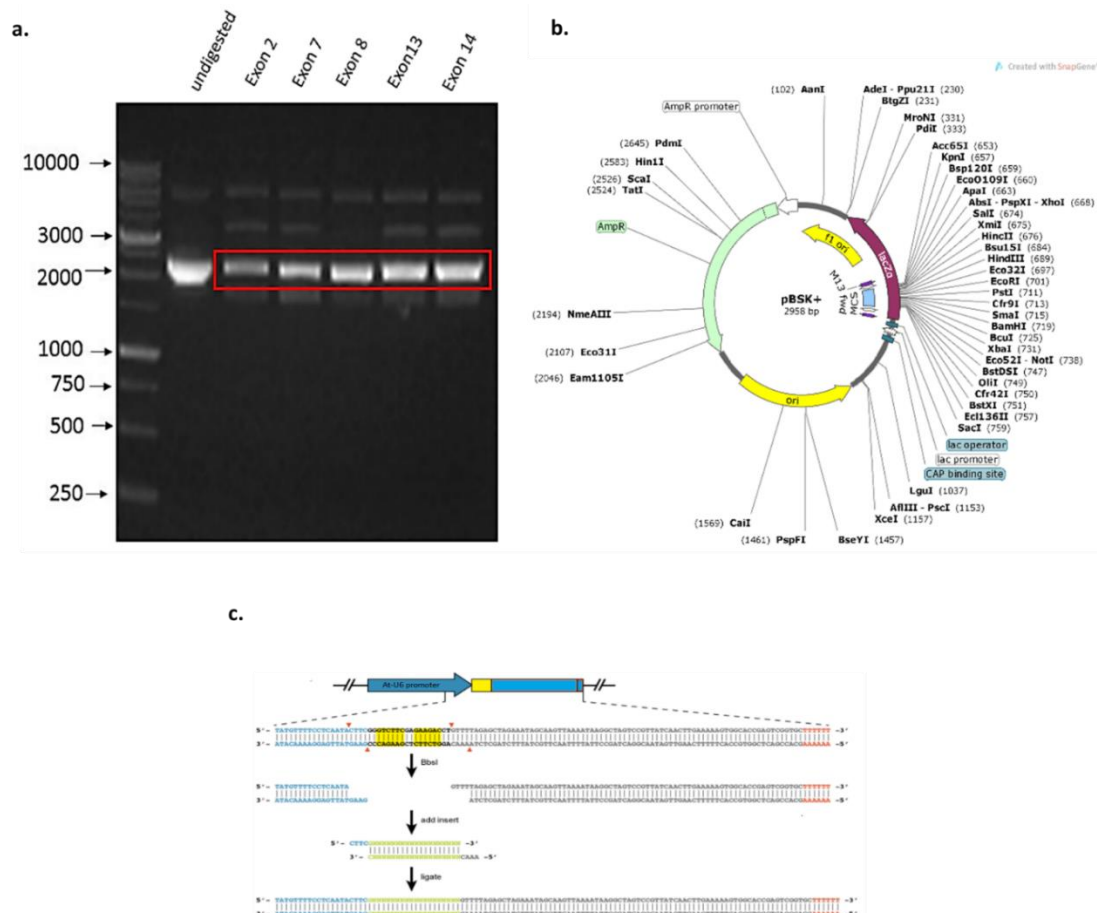


Figure 96. Cloning of gRNA into the pBSK vector. a) After cloning the gDNA into the pBSK vector, it was digested by BbsI followed by gel electrophoresis in 1% gel. An undigested pBSK plasmid was run along the digested products as a control. One can see very similar-looking bands between the control and the digested plasmids. b) Vector map of pBluescript SK+ plasmid (pBSK). c) As shown in the figure the oligo gets cloned between the digested region of the two BbsI sites. But, as a result, the BbsI sites get removed from the plasmid. So, one can expect very similar looking bands between an undigested plasmid and a cloned plasmid being digested by BbsI enzyme (as BbsI sites were removed) under gel electrophoresis (Adapted from Dash. L., 2018).

d. Cloning of multiple guides

To enable multiplexing for targeting two sites in the GI genomic locus, we cloned two gDNAs into separate pBSK vectors before merging them into a single vector. Initially, the six gDNAs

were divided into three pairs and cloned into different plasmid vectors. Using KpnI and SbfI enzymes, we removed the promoter-gDNA-guide backbone cassette from one of each pair and inserted it into the other's vector via restriction clones. Since SpeI and SbfI have compatible overhangs, one guide cassette was cloned upstream of the other, yielding two guide cassettes per vector. The vectors were transformed into DH5 α cells and streak-plated. The following day, three randomly selected colonies from each plate were subjected to colony PCR with primers complementary to the 20-base pair gDNA sequence. The PCR product was expected to be approximately 670 base pairs, similar to a single guide cassette (650 bp). Bacterial colonies showing the expected PCR product size were cultured overnight, and the cloned plasmid was purified after 12 hours (Figure 97).

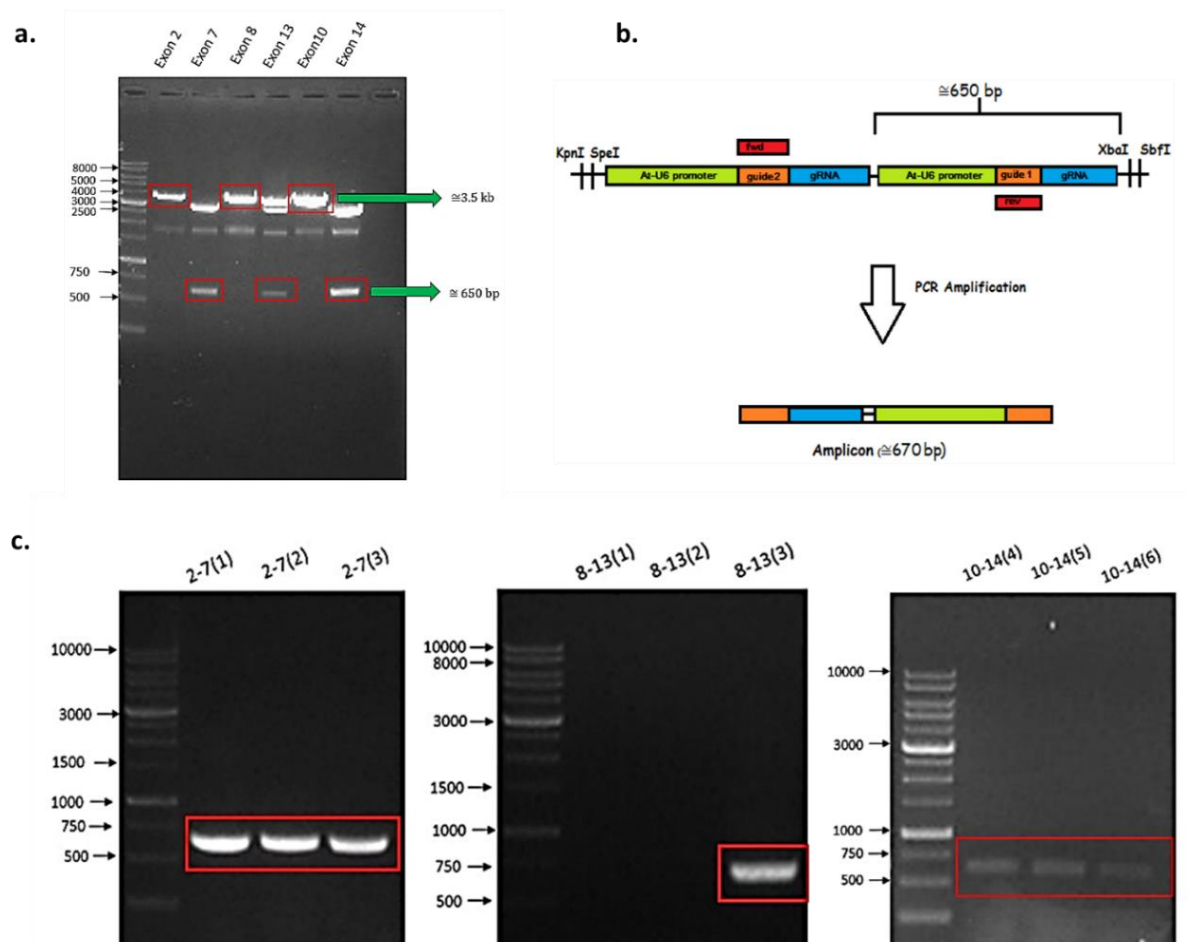


Figure 97. Cloning of multiple guides. a) The gel image illustrates the linearized fragments of plasmid DNA extracted from the gel for subsequent ligation, aiming to clone the guide cassette targeting exon 2 into the vector containing the guide cassette for exon 7 targeting. Similar procedures were carried out for other pairs (8-13, 10-14). b) Schematic representation of the methodology employed for colony PCR to validate the cloning process. c) Gel visualization of the colony PCR conducted on colonies selected from plates streaked the previous night with transformed DH5 α cells. Positive colonies, indicated by the presence of an amplicon of approximately 670 base

pairs in size, were chosen and cultured in LB media. Plasmid DNA was then extracted from these bacterial cultures the following day. (Adapted from Dash, L., 2018)

e. Final ligation of the dual-guide cassette in pGreen CRISPR plasmid

The pGreen CRISPR plasmid, which has a pCAMBIA backbone, is designed to survive in both *E. coli* and *Agrobacterium*. It contains a plant-optimized Cas9 gene controlled by a constitutive CamV promoter, which ensures high expression levels for effective CRISPR targeting. It also includes an eGFP gene driven by the AtS2 promoter, which allows for expression only in seed coats, making it easy to identify under fluorescent microscopy.

To incorporate the dual guide cassette into the pGreen CRISPR plasmid, a two-step restriction cloning process was used. First, the pGreen CRISPR plasmid was digested with ECoRI-KpnI and ECoRI-SbfI enzymes, as well as the isolated plasmid containing the dual guide cassettes digested with KpnI and SbfI. Gel electrophoresis enabled the purification of linearized plasmid DNA fragments.

The dual guide cassettes were ligated together, transformed into DH5 α cells, and streaked onto LB-kanamycin plates for overnight incubation. Colonies were screened using colony PCR, which revealed the expected 670bp bands, indicating successful cloning (Figure 98A).

Positive colonies went through primary culture and plasmid purification. Cas9 integration was confirmed by digesting the purified plasmid with ECoRI and XbaI, resulting in a ~5.5kb linearized plasmid fragment representing the CamV 35S promoter-driven Cas9 gene. This validated the cloning process (Figure 98B).

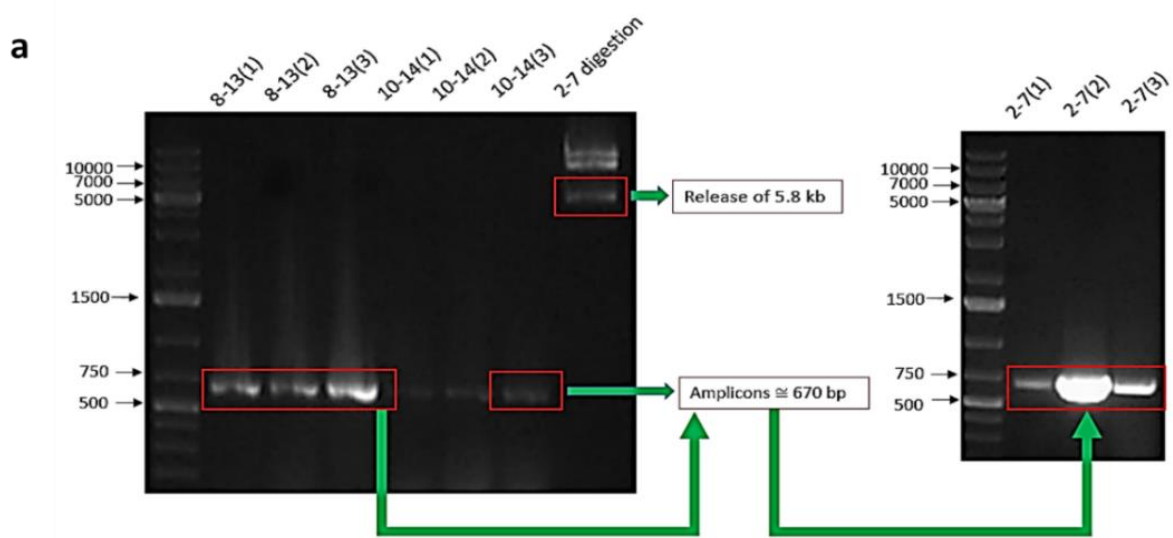


Figure5: Gel image of Colony PCR done after final cloning and restriction digestion of the plasmid cloned with 2-7 dual guide cassette.

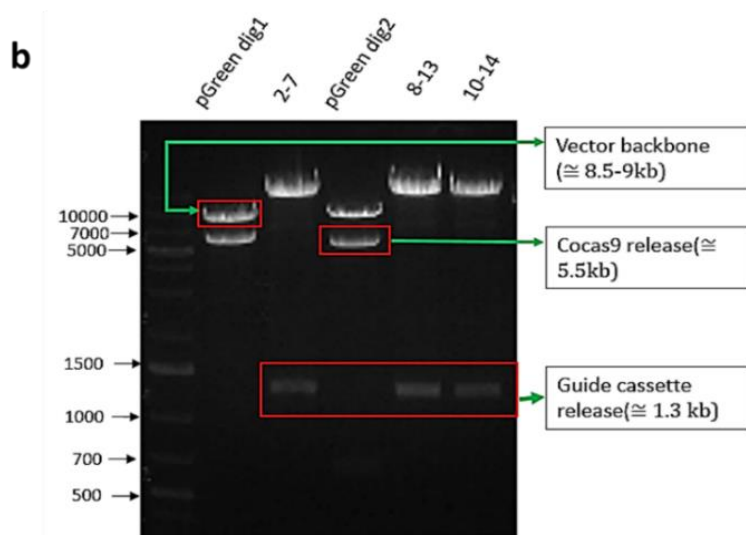


Figure4: Gel image of restriction digestion of pGreen and dual guideRNA plasmids.

Figure 98. Ligation of the dual-guide cassette in pGreen CRISPR plasmid. a) The gel image illustrates the confirmation of cloning via colony PCR and restriction digestion after *Agrobacterium* transformation. The colonies identified as positive during this stage were cultured in YESB media for floral dip in the subsequent step. The validation of construct cloning was achieved through colony PCR, while confirmation of the CamV 35S promoter-driven codon-optimized Cas9 cloning was indicated by the release of 5.5 kbp linearized plasmid DNA observed in the gel. b) The gel image displays the purified linearized plasmid DNA fragments extracted from the gel, which were then subjected to ligation in a single-step process. (Adapted from Dash, L., 2018).

f. *Agrobacterium* transformation

Agrobacterium tumefaciens strain *GV3101* competent cells were transformed with purified plasmids using the freeze-thaw method. The transformed cells were streaked onto LB Kanamycin-Rifampicin plates and incubated at 28 °C for approximately 3 days. Colonies were selected based on their resistance to rifampicin (inherent to *Agrobacterium GV3101*) and

kanamycin (due to the pGreen CRISPR plasmid) (Figure 99A). Random colonies were picked from the plates and subjected to colony PCR for screening (Figure 99B).

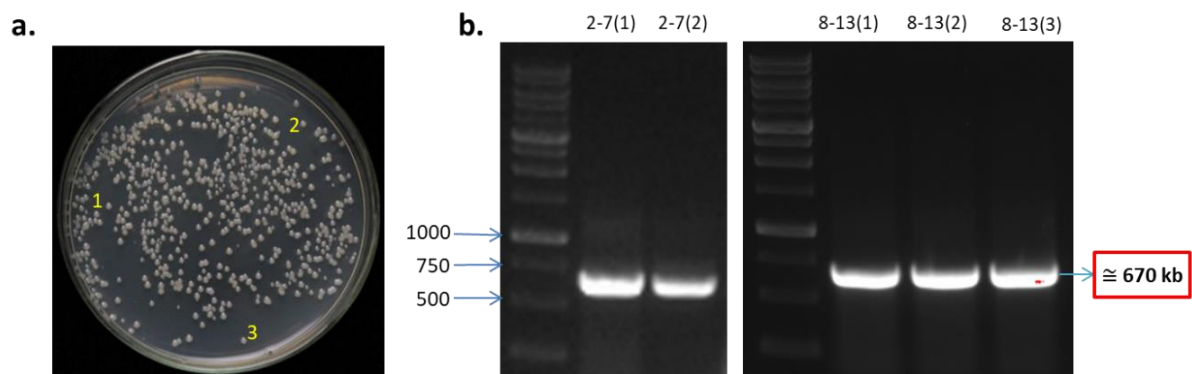


Figure 99. *Agrobacterium* transformation. a) LB Rifampicin-Kanamycin plate post spread plating and incubation. Highlighted colonies were selected and b) ~670 base pair amplicon could be visualized in the gel post-colony PCR reaction. (Adapted from Dash. L., 2018)

g. Floral dip transformation

Positive colonies were inoculated into 100ml of YESB media with 160ul rifampicin and 100 uL kanamycin and grown in a shaker incubator at 28 °C until reaching an OD₆₀₀ of 0.8, typically around 48 hours. Cultures were set in triplicates to prevent overshooting of OD₆₀₀. Upon reaching the desired OD₆₀₀, cultures were mixed with Silwet L-77 surfactant to enhance transformation efficiency.

Healthy *Arabidopsis* Columbia wild-type plants, grown in Long Day conditions, were dipped into the bacterial culture for one minute each to facilitate bacterial transfection. Plants were incubated in darkness for approximately 14 hours to help them recover from the stress induced by *Agrobacterium* infection. Moisture was maintained by wrapping them in poly bags. The following day, plants were transferred back to Long Day conditions and bagged individually to prevent moisture from seed pods and contamination of nearby pots. Plants were allowed to grow under Long Day conditions, and their seeds were eventually harvested.

Reference: Dash. L. Re-evaluating the role of GIGANTEA using CRISPR-Cas9 system. 2018.

ANNEXURE 2

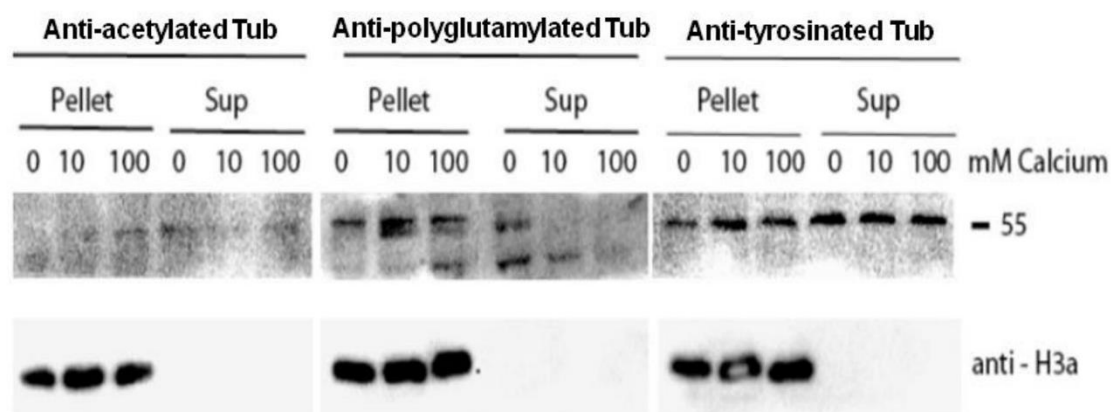


Figure 100. Presence of post-translationally modified tubulins in *P. patens*. Western blot analysis showing the presence and relative levels of acetylated, polyglutamylated, and tyrosinated tubulins in *P. patens* (7-day old liquid protonema culture grown at 25 °C). Western blot was performed using anti-mouse mAbs for respective modified tubulins. Histone is used as a loading control (H3a: Anti-histone antibody). (Courtesy: Dr. Khusbhu Singh)